THE PHYSIOLOGICAL AND PATHOLOGICAL AGGREGATION OF TRANSFORMING GROWTH FACTOR-β-INDUCED AND AMYLOID PRECURSOR PROTEIN IN *DROSOPHILA* SECONDARY CELLS



PREMAN J. SINGH

BALLIOL COLLEGE

UNIVERSITY OF OXFORD

TRINITY TERM 2023

D.PHIL IN PHYSIOLOGY, ANATOMY AND GENETICS

SUPERVISOR: PROFESSOR CLIVE WILSON

DEPARTMENT OF PHYSIOLOGY, ANATOMY AND GENETICS

DECLARATION

The work presented in this thesis is entirely my own, except where collaborative work or ideas are presented. The data in all figures were generated by me.

ACKNOWLEDGEMENTS

All my thanks and everlasting gratitude go to my Supervisor, Professor Clive Wilson, a true pioneer and giant of developmental genetics. To have done my D.Phil under his supervision is an honour I could never have imagined, and for which words fail me now. The depth and breadth of his genius, the profundity of his insight, and above all his unfailing kindness and humanity will always inspire and guide me. My sincerest thanks as well to my Co-Supervisor, Professor Adrian Harris, whose clinical insights as an oncologist, and words of encouragement as a fellow practicing physician who also completed an Oxford D.Phil were invaluable to me. He showed me what was possible as a physician-scientist.

My many and heartfelt thanks to Professor Deborah Goberdhan, Dr. Bhavna Verma, Dr. Mark Wainwright, Adam Wells, Dr. Claudia Mendes, Dr. Pauline Marie, Dr. Aashika Sekar, Dr. John Mason, and Dr. Shih-Jung Fan, who helped and guided me throughout. Their astonishing scholarship, wealth of wisdom, friendship, and encouragement saw me through my work. My profound thanks to Jade Oh, Amy Cording, and Carina Gandy, whose able management made each day in the lab a pleasure. I also thank the wonderfully supportive staff at Micron for their education, help, and guidance with state-of-the-art microscopy. Finally, my thanks to my College, Balliol, and to the Balliol Interdisciplinary Institute. Their generous award of a grant enabled me to work with the Fly Facility at Cambridge University in creating corneal dystrophy transgenic fly lines.

PUBLICATIONS, PRESENTATIONS AND GRANTS FROM THIS WORK

- **Singh, P. J**. 'Probing the Physiology of Amyloidogenesis in the *Drosophila* Reproductive System; A New Model for Alzheimer's and Other Degenerative Disorders'. Talk given at Development and Cell Biology Theme Day, St. Anne's College, Oxford, 29th October 2021.

- **Singh, P. J.,** *et al.* (2022). Homologues of the human disease-associated amyloidogenic proteins APP and TGFBI are required for physiological protein aggregation in *Drosophila* secondary cells. Presentation at the 63rd Annual *Drosophil*a Conference of the Genetics Society of America, San Diego, CA, USA, April 6-10, 2022.

- **Singh, P. J.,** *et al.* (2023). Amyloid Proteins APP and TGFBI have roles in normal protein aggregation (Manuscript in preparation).

- **Singh, P. J.** (2020). 'Modelling Alzheimer's Disease and Amyloid Corneal Dystrophies with Midline Fasciclin, a *Drosophila* Amyloid Protein'. Grant awarded to P. J. Singh by the Balliol Interdisciplinary Institute (BII).

LIST OF ABBREVIATIONS

ABBREVIATION	EXPANSION
Aβ	Beta-amyloid
AD	Alzheimer's Disease
AG	Accessory Gland
AICD	Amyloid Precursor Protein Intracellular Domain
ALS	Amyotrophic Lateral Sclerosis
AMPK	AMP-Activated Protein Kinase
ANCE	Angiotensin Converting Enzyme
APP	Amyloid Precursor Protein
APPL	Amyloid Precursor Protein-Like
BACE	β-Site Amyloid Precursor Protein Cleaving Enzyme
BDSC	Bloomington *Drosophila* Stock Centre
BMP	Bone Morphogenetic Protein
Btl	Breathless
CAA	Cerebral Amyloid Angiopathy
CD	Corneal Dystrophy
CERAD	Consortium to Develop a Registry for Alzheimer's Disease
CFP	Cyan Fluorescent Protein
Chmp2b	Charged Multi Vesicular Body Protein 2b
CJD	Creutzfeldt Jakob Disease
CTF	C-Terminal Fragment
dsx	Doublesex
DGRC	*Drosophila* Genomics Resource Centre
DLB	Dementia with Lewy Bodies
Dpp	Decapentaplegic
DRPLA	Dentatorubral Pallidoluysian Atrophy
EBMD	Epithelial Basement Membrane Dystrophy
ECD	Extracellular Domain

ABBREVIATION	EXPANSION
ESCRT	Endosomal Sorting Complexes Required for Transport
FAD	Familial Alzheimer's Disease
FAS	Fasciclin
FFI	Fatal Familial Insomnia
FTD	Frontotemporal Dementia
GAPDH	Glyceraldehyde-3-Phosphate Dehydrogenase
GCD	Granular Corneal Dystrophy
GFP	Green Fluorescent Protein
GSSS	Gerstmann-Strȁussler-Scheinker Syndrome
HD	Huntington's Disease
ICD	Intracellular Domain
ILV	Intraluminal Vesicle
LB	Luria Broth
LCD	Lattice Corneal Dystrophy
LOAD	Late Onset Alzheimer's Disease
MFAS	Midline Fasciclin
MVB	Multivesicular Body
MVE	Multivesicular Endosome
NFT	Neurofibrillary Tangles
NTF	N-Terminal Fragment
PD	Parkinson's Disease
PMEL17	Premelanosomal Protein-17
PrP	Prion Protein
PS	Presenilin
PSP	Progressive Supranuclear Palsy
RBCD	Reis-Bückler Corneal Dystrophy
RNAi	RNA Interference
sAPP	Soluble Amyloid Precursor Protein

ABBREVIATION	EXPANSION
TBCD	Thiel-Behnke Corneal Dystrophy
TDP-43	Transactive Response DNA-Binding Protein 43
TGFBI	Transforming Growth Factor Beta-Induced
TMD	Transmembrane Domain
UAS	Upstream Activating Sequence
Vps	Vacuolar Protein Sorting
VDRC	Vienna *Drosophila* Resource Centre
SAD	Sporadic Alzheimer's Disease
YFP	Yellow Fluorescent Protein

ABSTRACT

Amyloid proteins abound in nature, share several familial commonalities, and more often than not, play important physiological roles. The same is true of human amyloids, which similarly serve crucial functions, and whose potential aberrancy only come to light with the manifestation of disease. Thus in humans, amyloid or pre-amyloid proteins function normally as peptide hormones, are required for nervous system development, are part of the coagulation cascade, provide a scaffolding for melanin in melanocytes, and are essential for the transparency of the cornea, to name but a few of their known roles.

Drosophila secondary cells located in the male fly's prostate-like accessory glands are unique as a genetically tractable system in containing very large secretory compartments, which are easily visualized *ex vivo*, making them invaluable in the study of secretory processes in living cells. Secondary cells contain a single large dense-core granule (DCG) in each compartment, which I show is comprised of high levels of Midline Fasciclin (MFAS), an amyloid which is the homologue of the human structural and potentially amyloidogenic corneal protein Transforming Growth Factor Beta-Induced (TGFBI).

The biogenesis of DCGs is a robust physiological process, and their secretion has been found by the Wilson laboratory to be crucial in reproduction. This earlier work also presciently suggested links to neurodegeneration, cancer and diabetes. Here, I show that DCG formation is impacted by specific manipulations, chief among these being *mfas* knockdown, which completely blocks the aggregation of proteins into DCGs. Furthermore, knockdown of the *Drosophila* homologue of Amyloid Precursor Protein (APP) called APP-like (APPL), leads to the formation of multiple mini-cores in each compartment, which fail to fuse together. Intriguingly, DCG formation is also impacted by expression of mutations in related human and *Drosophila* amyloid proteins containing amyloidogenic mutations. Thus, amyloidogenic mutations in MFAS' homologue TGFBI, as well as mutations in human APP or its cleaved amyloidogenic amyloid-β peptides, which cause Familial Alzheimer's Disease, when expressed in secondary cells, affect the coalescence of MFAS. When different mutant forms of human *TGFBI* and *APP* were combined with mini-core-inducing mutations (knockdowns of *Drosophila Appl* and $GAPDH_2$), a spectrum of outcomes was produced, ranging from intermediate phenotypes to near-complete rescues.

My work shows that amyloids interact with other amyloid proteins to influence each other's aggregation both physiologically and pathologically, a long-suspected but experimentally undemonstrated conjecture, at least in amyloid pathology. The impossibility of providing proof lay in the fact that amyloidogenesis is an inscrutable, decades-long process, combined with the obvious unethicality of performing brain biopsies on living patients. My work proves this Grail-like surmise and demonstrates a physiological role for APP proteins that is inhibited by amyloidogenic versions of this molecule. It also showcases the depth and power of this system in modelling amyloid diseases of the brain and cornea, which is now leading to the development of a new model explaining the precise molecular function of APP in secretion and the likely route by which this role is compromised in disease.

Table of Contents

CHAPTER 1 ..... **1**

1. INTRODUCTION **2**

1.1 AMYLOID PROTEINS 2

1.1.1 PHYSICAL CHARACTERISTICS OF AMYLOID PROTEINS 2

1.1.2 PHYSIOLOGICAL AMYLOIDS IN NATURE 3

1.1.3 AMYLOID PRECURSOR PROTEINS AS PROGENITORS OF AMYLOID 5

1.2 HUMAN NEURODEGENERATIVE DISEASES ASSOCIATED WITH AMYLOID 7

1.2.1 ALZHEIMER'S DISEASE 7

1.2.2 THE PRODUCTION OF Aβ 9

1.2.3 THE TWO SUBTYPES OF ALZHEIMER'S DISEASE 11

1.2.4 MUTATIONS CAUSING FAMILIAL ALZHEIMER'S DISEASE 12

1.2.5 APP IS THE HOMOLOGUE OF *DROSOPHILA* APPL 14

1.3 AMYLOID CORNEAL DYSTROPHIES 15

1.3.1 THE STRUCTURE OF THE CORNEA AND THE ROLE OF TGFBI 15

1.3.2 TGFBI MUTATIONS AND AMYLOID CORNEAL DYSTROPHIES 16

1.3.3 TGFBI IS THE HOMOLOGUE OF *DROSOPHILA* MFAS 19

1.4 OTHER CLINICAL ISSUES ADDRESSED IN THIS STUDY 20

1.4.1 THE SPREAD OF AMYLOID IN NEURODEGENERATIVE DISEASES 20

1.4.2 EXAMINING THE SIMILARITIES BETWEEN AMYLOIDS AND PRIONS 23

1.4.3 EXAMINING THE 'RESCUE' PROPERTIES OF AMYLOID PROTEINS 24

1.5 THE *DROSOPHILA* ACCESSORY GLAND (AG) AND IT'S RELEVANCE TO SECRETORY BIOLOGY 27

1.5.1 AN OVERVIEW OF THE AG AND IT'S CELL TYPES 27

1.5.2 THE SPECIALIZED FUNCTION OF SECONDARY CELLS (SCs) AND THEIR PRODUCTION OF DCGs 28

1.6 OVERALL AIMS OF THIS STUDY 29

CHAPTER 2 ..... **31**

2. MATERIALS AND METHODS **32**

2.1 DROSOPHILA STOCKS 32

2.1.1 GAL4 AND GAL80 COMBINATION LINES 32

2.1.2 OVEREXRESSION LINES 32

2.1.3 RNAi LINES 33

2.1.4 FLUORESCENTLY TAGGED GENE TRAP DRIVER LINES 33

2.1.5 TRANSGENIC TGFBI LINES 34

2.1.6 MISCELLANEOUS LINES 34
2.2 DESIGN OF GENETIC CONSTRUCTS 35
2.3 CREATION OF GENETIC CONSTRUCTS 36
2.3.1 TRANSFORMATION OF COMPETENT *E. COLI* WITH pUASTattB 36
2.3.2 PREPARATION OF LURIA BROTH AGAR PLATES 36
2.3.4 PREPAPARATION OF SUPERBROTH 37
2.3.5 GROWING TRANSFORMED *E.COLI* IN SUPERBROTH 37
2.3.6 MIDIPREP™ EXTRACTION OF CONSTRUCT-BEARING pUASTattB 37
2.3.7 PRECIPITATION OF pUASattB AND TITRATION OF CONCENTRATION 38
2.3.8 SUMMARY OF GENETIC CONSTRUCTS PREPARED FOR EMBRYO MICROINJECTION 39
2.3.9 RESTRICTION DIGESTION TO CONFIRM FINAL IDENTITY 43
2.3.10 MICROINJECTION OF EMBRYOS TO CREATE TRANSGENIC LINES CARRYING THE DESIRED CONSTRUCTS 44
2.4 *DROSOPHILA* HUSBANDRY 45
2.5 CONTROL OF TRANSGENE EXPRESSION IN SECONDARY CELLS 46
2.6 MICRO-DISSECTION OF ACCESSORY GLANDS 48
2.7 LYSOTRACKER™ STAINING OF LIVE ACCESSORY GLANDS 49
2.8 MOUNTING OF LIVE ACCESSSORY GLANDS 49
2.9 FIXATION OF ACCESSORY GLANDS FOR CONFOCAL MICROSCOPY 49
2.10 MOUNTING OF FIXED ACCESSORY GLANDS FOR CONFOCAL MICROSCOPY 50
2.11 WIDE-FIELD MICROSCOPY 50
2.12 CONFOCAL MICROSCOPY 51
2.13 IMAGE ANALYSIS AND FIGURE PRESENTATION 51
2.14 SUBCELLULAR COMPARTMENT ANALYSIS 51
2.15 CHARACTERISATION OF SECONDARY CELLS BY LIGHT MICROSCOPY 52
2.16 EXOSOME SECRETION ASSAY 52
2.17 STATISTICAL ANALYSIS 53
CHAPTER 3 54
3. THE ESTABLISHMENT OF CONTROLS AND THE BIOLOGY OF MIDLINE FASCICLIN 55
3.1 INTRODUCTION 55
3.1.1 EXPERIMENTAL APPROACH 56
3.2 RESULTS 58

3.2.1 THE N-TERMINALLY TAGGED *GFP-mfas* GENE TRAP LINE DOES NOT AFFECT DCGs 58

3.2.2 C-TERMINALLY GFP-TAGGED *mfas-GFP* AND TGFBI DISRUPT DCG BIOGENESIS 65

3.2.3 RESULTS REGARDING THE BIOLOGY OF MIDLINE FASCICLIN 67

3.2.4 THE RAB6 AND RAB11 IDENTITIES OF LARGE NON-ACIDIC COMPARTMENTS ARE UNAFFECTED BY *mfas* KNOCKDOWN 71

3.3 DISCUSSION 78

3.3.1 THE DIFFERENCE BETWEEN N-TERMINAL-TAGGED VERSUS C-TERMINAL TAGGED MFAS IN INFLUENCING DCG BIOGENESIS 78

3.3.2 THE SIGNIFICANCE OF THE NECESSITY OF MFAS FOR DCG FORMATION 79

3.3.3 THE SIGNIFICANCE OF THE PRESERVATION OF RAB6 AND RAB11 COMPARTMENT IDENTITIES DESPITE THE KNOCKDOWN OF *mfas* 81

3.3.4 SUMMARY OF SIGNIFICANT POINTS 82

CHAPTER 4 84

4. OTHER FACTORS INFLUENCING DCG FORMATION 85

4.1 INTRODUCTION 85

4.1.1 GAPDH AND NEURODEGENERATION 85

4.1.2 THE LINK BETWEEN RAB11, RAB6, APP AND NEURODEGENERATION 87

4.1.3 *APPL*, THE *DROSOPHILA* HOMOLOGUE OF *APP*, IS REQUIRED FOR DCG BIOGENESIS, SUGGESTING LINKS TO NEURODEGENERATION 90

4.1.4 AIMS 95

4.2 RESULTS 95

4.2.1 DROSOPHILA GAPDH2 IS REQUIRED FOR NORMAL DCG ASSEMBLY IN SCs 95

4.2.2 *APPL*, THE *DROSOPHILA* HOMOLOGUE OF *APP*, IS REQUIRED FOR NORMAL DCG ASSEMBLY IN SCs 99

4.2.3 THE RAB6 AND RAB11 IDENTITIES OF LARGE NON-ACIDIC COMPARTMENTS ARE NOT AFFECTED BY *APPL*-KNOCKDOWN 104

4.2.4 NEITHER *mfas* OR *APPL*-KNOCKDOWNS AFFECT ILVs OR EXOSOMES 109

4.2.5 THE RELATIONSHIP BETWEEN VARIOUS SEGMENTS OF APP/APPL AND DCGs 115

4.2.5.1 THE EFFECTS OF DROSOPHILA α-AND γ-SECRETASE KDs ON DCGs….. 118

4.2.5.2 THE EFFECTS OF *DROSOPHILA* APPL EXTRA- AND INTRACELLULAR DOMAIN DELETIONS ON DCGs 120

4.2.5.3 EFFECTS OF FULL-LENGTH AND β-SECRETASE CLEAVED HUMAN APP ON DCGs……124

4.3 DISCUSSION 127
4.3.1 *GAPDH2* IS REQUIRED FOR DCG FORMATION 127
4.3.2 *APPL* IS REQUIRED FOR DCG FORMATION 129
4.3.3 THE RAB6 AND RAB11 IDENTITIES OF LARGE NON-ACIDIC COMPARTMENTS ARE UNAFFECTED BY *APPL*-KNOCKDOWN 132
4.3.4 THE EFFECTS OF *mfas*- AND *APPL*-KDS ON LARGE NON-ACIDIC COMPARTMENTS 134
4.3.5 EFFECTS OF MANIPULATING VARIOUS SEGMENTS OF APP/APPL ON DCG FORMATION 135
CHAPTER 5 141
5. MUTATIONS IN *DROSOPHILA mfas* AND ITS HUMAN HOMOLOGUE *TGFBI* AFFECT DCG FORMATION……...……..142
5.1 INTRODUCTION 142
5.1.1 *TGFBI*-ASSOCIATED CORNEAL DSYTROPHIES 145
5.1.1.1 LATTICE CORNEAL DYSTROPHY……145
5.1.1.2 THIEL-BEHNKE CORNEAL DYSTROPHY……146
5.1.1.3 RIES-BUCKLER CORNEAL DYSTROPHY……147
5.1.1.4 GRANULAR CORNEAL DYSTROPHY……..147
5.1.2 AIMS 149
5.2 RESULTS 149
5.2.1 THE EFFECTS OF *mfas-WT* AND *TGFBI-WT* ON DCG FORMATION 149
5.2.2 THE EFFECTS OF CONSERVED *TGFBI* MUTATIONS *G623D* AND *H626R* ON DCG FORMATION 152
5.2.3 THE EFFECTS OF NON-CONSERVED *TGFBI* MUTATIONS *R555Q* AND *R124C* ON DCG FORMATION 155
5.2.4 INTERACTIONS BETWEEN HUMAN *TGFBI* MUTANTS AND *DROSOPHILA APPL*-RNAi 157
5.3 DISCUSSION 174
5.3.1 AN OVERVIEW OF THE DCG EFFECTS OF *TGFBI* AMYLOIDOGENIC MUTATIONS ON DCGs 174
5.3.2 CONCLUDING REMARKS ON DCG EFFECTS OF TGFBI MUTATIONS 177
5.3.3 OVERVIEW OF INTERACTIONS BETWEEN *TGFBI* MUTANTS AND *APPL-RNAi* 179
CHAPTER 6 182
6. THE EFFECTS OF FAD MUTATIONS ON DCGs, AND DCG AGEING CHARACTERISTICS IN AMYLOIDOGENIC GENETIC BACKGROUNDS ... 183

6.1 INTRODUCTION 183
6.1.1 FAD MUTATIONS IN AND AROUND APP'S Aβ SEQUENCE 185
6.1.2 RETROMER DYSFUNCTION AND NEURODEGENERATIVE DISEASES..... 188
6.1.3 AIMS 194
6.2 RESULTS 194
6.2.1 THE EFFECTS OF *$A\beta_{42}$-WT* AND *$A\beta_{42}$-ARCTIC* ON DCG MORPHOLOGY..... 194
6.2.2 THE EFFECTS OF *$A\beta_{42}$-DUTCH* AND *$A\beta_{42}$-IOWA* ON DCG MORPHOLOGY.... 198
6.2.3 THE EFFECT OF *APP-K595N/M596L-SWEDISH* ON DCG MORPHOLOGY..... 201
6.2.4 THE EFFECTS OF *$GAPDH_2$-RNAi*, *APPL-RNAi*, *$A\beta_{42}$-WT*, *$A\beta_{42}$-ARCTIC* AND *APP-SWEDISH* ON EXOSOME SECRETION 204
6.2.5 THE EFFECTS OF KNOCKDOWN OF RETROMER COMPONENTS VPS26 AND VPS39 ON DCGs 209
6.2.6 RESULTS REGARDING INTERACTIONS BETWEEN ALZHEIMER'S GENES AND 'MINI-CORE' PRODUCING GENOTYPES 212
6.2.6.1 INTERACTION BETWEEN HUMAN APP AND FLY APPL-RNAi……..211
6.2.6.2 INTERACTION BETWEEN HUMAN Aβ-WT AND FLY APPL-RNAi…….214
6.2.6.3 INTERACTION BETWEEN Aβ-ARCTIC AND FLY APPL-RNAi……217
6.2.6.4 INTERACTION BETWEEN Aβ-WT AND FLY GAPDH2-RNAi……..221
6.2.6.5 INTERACTION BETWEEN Aβ-ARCTIC AND FLY GAPDH2-RNAi…….225
6.2.7 DCG AGEING IN Aβ-WT, Aβ-ARCTIC AND TGFBI MUTANTS……...233
6.2.7.1 NORMAL DCG AGEING IN CONTROL FLIES……233
6.2.7.2 DCG AGEING IN Aβ-WT AND Aβ-ARCTIC FLIES…….236
6.2.7.3 DCG AGEING IN MFAS-WT AND TGFBI-WT FLIES…….242
6.2.7.4 DCG AGEING IN TGFBI-G623D & -H626R CONSERVED MUTANTS….246
6.2.7.5 DCG AGEING IN R555Q & R124C NON-CONSERVED MUTANTS……..250
6.2.7.6 AGE-RELATED FATE OF MFAS IN THE AG LUMEN……...252
6.3 DISCUSSION 260
6.3.1 THE INFLUENCE OF *APP* AND *$A\beta_{42}$-WT* ON DCGs..... 260
6.3.2 THE EFFECTS OF *APP-ARCTIC, DUTCH, IOWA,* AND *SWEDISH* MUTATIONS ON DCGs 262
6.3.3 THE EFFECTS OF *$GAPDH_2$-RNAi*, *APPL-RNAi*, *$A\beta_{42}$-WT*, *$A\beta_{42}$-ARCTIC* AND *APP-SWEDISH* ON EXOSOME SECRETION 266
6.3.4 THE EFFECTS OF KNOCKDOWN OF RETROMER COMPONENTS VPS26 AND VPS39 ON DCGs 268

6.3.5 INTERACTIONS BETWEEN ALZHEIMER'S GENES AND 'MINI-CORE' PRODUCING GENOTYPES 271

6.3.5.1 INTERACTIONS BETWEEN HUMAN *APP*, HUMAN *Aβ42-WILD TYPE* AND *DROSOPHILA APPL RNAi*……272

6.3.5.2 INTERACTION BETWEEN *$Aβ_{42}$-E693G-ARCTIC* AND *APPL-RNAi*……..276

6.3.5.3 INTERACTION BETWEEN *$Aβ_{42}$-WILD TYPE* AND *GAPDH2-RNAi*…….,…278

6.3.5.4 INTERACTION BETWEEN *$Aβ_{42}$-E693G-ARCTIC* AND *GAPDH2-RNAi*…….279

6.3.6 THE DURABILITY OF *$Aβ_{42}$-WT*, *$Aβ_{42}$-ARCTIC* AND *TGFBI* MUTANT DCGS AS SHOWN BY AGEING EXPERIMENTS 280

6.3.6.1 THE NORMAL AGEING OF DCGs IN CONTROL FLIES……..282

6.3.6.2 THE AGEING OF DCGs IN *$Aβ_{42}$-WT* AND *$Aβ_{42}$-E693G*-ARCTIC FLIES……..282

6.3.6.3 THE AGEING OF DCGs IN *mfas-WT* AND *TGFBI-WT* FLIES……...283

6.3.6.4 DCG AGEING IN CONSERVED *TGFBI-G623D* AND *-H626R* MUTANTS….284

6.3.6.5 DCG AGEING IN NON-CONSERVED TGFBI-R555Q & R124C MUTANTS...285

6.3.7 THE AGE-RELATED FATE OF MFAS IN THE AG LUMEN 286

CHAPTER 7 289

7. FINAL DISCUSSION 290

7.1 INTRODUCTION 290

7.2 THE DISCOVERY OF A PHYSIOLOGICAL ROLE FOR THE *DROSOPHILA* 'AMYLOID' MFAS 294

PHYSIOLOGICAL AMYLOIDS IN MICROBES 297

PHYSIOLOGICAL AMYLOIDS IN HIGHER ORGANISMS 298

7.3 EVIDENCE THAT AMYLOIDS INFLUENCE EACH OTHER 298

NEURODEGENERATIVE DISEASES IN WHICH THE CONTIGUOUS PROGRESSION OF MISFOLDED AMYLOID IS HISTOLOGICALLY EVIDENT 300

7.4 HUMAN AND *DROSOPHILA* AMYLOIDS AND AMYLOID-ASSOCIATED PROTEINS INTERACT 305

7.4.1 GAPDH/GAPDH2 INFLUENCE *DROSOPHILA* MFAS 306

7.4.2 APP/APPL AND THE Aβ42 SEGMENT INFLUENCE *DROSOPHILA* MFAS 308

7.4.3 HUMAN TGFBI INFLUENCES *DROSOPHILA* MFAS 312

7.5 HUMAN APP AND Aβ INFLUENCE MFAS IN RESCUES OF MINI-CORE-PRODUCING GENOTYPES: CONSIDERATIONS AND PERSPECTIVES 314

7.6 CONCLUDING REMARKS 316

7.6.1 LESSONS FROM MFAS 317

7.6.1.1 MFAS' HIGH EXPRESSION IN SCs…….315

7.6.1.2 MFAS IS ORGANISATIONALLY IDENTICAL TO TGFBI…… 316
7.6.1.3 MFAS IS AN AMYLOID PROTEIN…….317
7.6.1.4 MFAS IS CRUCIAL FOR THE FORMATION OF DCGs……318
7.6.1.5 MFAS HAS INSULARITY OF FUNCTION…….318
7.6.1.6 MFAS IS SUSCEPTIBLE TO THE INFLUENCE OF OTHER AMYLOIDS.318
7.6.1.6.1 MFAS IS INFLUENCED BY DROSOPHILA APPL……...318
7.6.1.6.2 MFAS IS INFLUENCED BY HUMAN FAD MUTANTS……...319
7.6.1.6.2 (a) MFAS' RESPONSE TO Aβ-DUTCH AND -IOWA……319
7.6.1.6.2 (b) MFAS' RESPONSE TO Aβ-ARCTIC……..319
7.6.1.6.2 (c) MFAS' RESPONSE TO APP-SWEDISH……320
7.6.1.6.3 MFAS IS INFLUENCED BY ITS HOMOLOGUE TGFBI…….322
7.6.1.7 MFAS IS RESCUABLE BY OTHER AMYLOIDS…….322
7.6.1.8 MFAS' SENSITIVITY AND SUSCEPTIBILITY TO THE MANIPULATION OF AMYLOIDS…….323
7.6.2 FUTURE DIRECTIONS……324
7.6.2.1 CREATING A DATABASE ON DCG MORPHOLOGY……325
7.6.2.2 CREATING A DATABASE SUBSECTION FOR COMPARING RESCUES329
7.6.2.3 EXPLORING NEURODEGENERATION & NEUROREGENERATION….331
7.6.2.4 USING THIS FLY MODEL TO STUDY FUNDAMENTAL AMYLOID BIOLOGY……...332
CHAPTER 8 334
8. BIBLIOGRAPHY 335
CHAPTER 9 390
9. APPENDIX 391
9.1 SEQUENCES FOR CONSTRUCTS 391
9.1.1 *TGFBI*-WILD TYPE 391
9.1.2 *TGFBI-R124C* (CGC→TGT) 393
9.1.3 *TGFBI-R555Q* (CGC→CAA) 395
9.1.4 *TGFBI-G623D* (GGC→GAT) 397
9.1.5 *TGFBI-H626R* (CAT→CGC) 399
9.1.6 *TGFBI*-WT WITH GFP cDNA ADDED BEFORE THE TAG STOP CODON 401
9.1.7 *mfas*-WILD TYPE ISOFORM K 404
9.1.8 *mfas*-WILD TYPE ISOFORM K PLUS GFP 407

9.1.9 *mfas* ISOFORM-K-G623D (GGT→GAT) 410
9.2 SEQUENCE ALIGNMENT OF TGFBI AND MFAS 414

CHAPTER 1

INTRODUCTION

1. INTRODUCTION

Am not I

A fly like thee?

Or art not thou

A man like me?

(William Blake, The Fly, Stanza 2, Songs of Experience, 1794)

1.1 AMYLOID PROTEINS

1.1.1 PHYSICAL CHARACTERISTICS OF AMYLOID PROTEINS

Amyloids are durable forms of protein formed when normally soluble proteins aggregate to form fibrils. They possess a characteristic Pauling-Corey β-sheet conformation of their polypeptide backbones, which when subjected to X-rays produce a cross-β diffraction pattern (Cohen and Calkins, 1959; Eanes and Glenner, 1968) (**Figure 1.1**). This β-sheet conformation is a common theme despite differences in amino acid sequences and native structures, and confers upon them the physical tenacity shared by all amyloids.

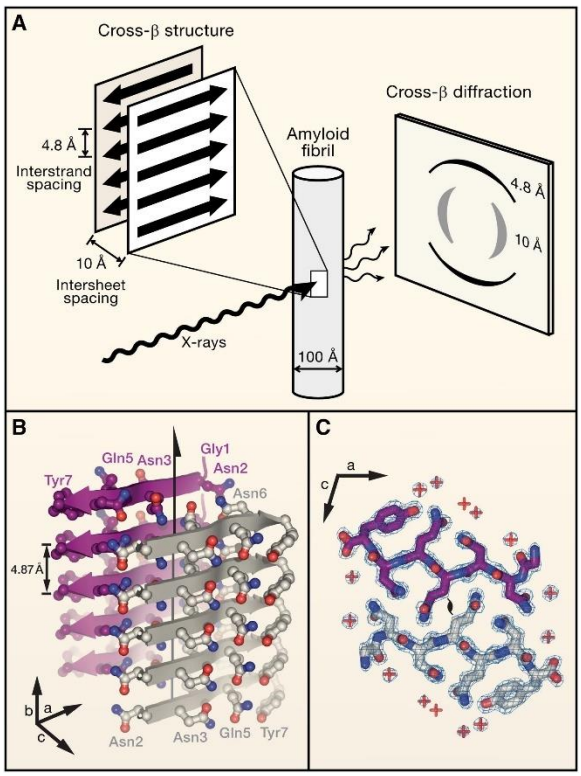

Figure 1.1: The structure of amyloid fibrils. **A)** the cross-β structure as produced by X-rays. **B)** the steric-zipper structure of the yeast prion Sup35, showing 5 layers of β-strands, and the fibril axis marked by the arrow. **C)** Two interdigitating Pauling-Corey β-sheets as viewed looking down the axis. Blue amine and red carbonyl groups form hydrogen bonds between the sheets, while water molecules, shown as red crosses, are excluded from the tight space between the sheets. The polarized hydrogen bonds and the hydrophobic 'dry steric zipper' between the interdigitating β-sheets imparts the durability seen with amyloids and prions. (From Eisenberg and Jucker, Cell 2012, p. 1189).

1.1.2 PHYSIOLOGICAL AMYLOIDS IN NATURE

Amyloids are found widely in nature from bacteria to humans, where they often play physiological roles. Examples of these are the extracellular Curli amyloid fibres in *E. Coli* and *Salmonella* which form physiological biofilms required for adhesion (Chapman *et al.,* 2002), and the amyloid protein Pmel17 produced within mammalian melanocytes which provides the scaffolding for melanin granules (Berson *et al.,* 2003). Amyloid Precursor Protein (APP), the precursor of the Aβ fragments found in

Alzheimer's plaques, while still incompletely understood, has numerous physiological functions. These include synaptogenesis, neurite outgrowth, neuronal migration, neuronal survival, vesicular transport, and synaptic plasticity (Moya *et al.,* 1994; Small *et al.,* 1994; Young-Pearse *et al.,* 2007; Goodman *et al.,* 1994; Koo *et al.,* 1990; Puzzo *et al.,* 2008). Transforming Growth Factor Beta-Induced (TGFBI) is a potentially amyloidogenic human corneal protein which plays a key structural role by anchoring keratocytes to each other, thus ensuring an ordered lattice and thereby corneal transparency (Andersen *et al.,* 2004). Selected examples of physiological amyloids are listed in **Table 1.1.**

SPECIES	AMYLOID PROTEIN	FUNCTION
Escherichia coli	Curli	Biofilms, adhesion
Salmonella species	Curli	Biofilms, adhesion
Streptomyces coelicolor	Chaplins	Surface tension modulation
Podospora anserina	HET-s	Heterokaryon formation
Saccharomyces cerevisiae	URE2p	Nitrogen catabolism
Saccharomyces cerevisiae	Sup35p	Stop codon read-through
Most fungi	Hydrophobins	Fungal coat formation
Insects and fish	Chorion proteins	Eggshell structure
Nephila clavipes	Spidroins	Spider silk structure
Homo sapiens	Pmel17	Melanin scaffolding
Homo sapiens	Amyloid Precursor Protein	Brain development
Homo sapiens	TGFBI	Corneal adhesion
Homo sapiens	Insulin	Glucose metabolism

Table 1.1: Physiological amyloids in nature. (Adapted from Fowler *et al.*, Trends Biochem. Sci. 2007, p. 3).

1.1.3 AMYLOID PRECURSOR PROTEINS AS PROGENITORS OF AMYLOID

The discovery that immunoglobulin light chain precursor protein was digested by lysosome into amyloidogenic fragments led to the understanding that amyloids can be generated by the proteolytic processing of their individual amyloid precursors (Glenner *et al.*, 1971). Prominent amyloids and their precursors are listed in **Table 1.2**.

DISEASE	AMYLOID PRECURSOR	AMYLOID PROTEIN
Alzheimer's Disease	Amyloid Precursor Protein	Aβ peptides
Corneal Dystrophies	TGFBI	TGFBI-Amyloid
Spongiform Encephalopathy	Prion Protein PrPc	PrPsc
Hemodialysis Amyloidosis	β_2-microglobulin	Aβ_2M
Familial Amyloidosis	Fibrinogen αA-chain	AFib
Type II Diabetes	Pro-Islet Amyloid Polypeptide	Islet Amyloid Polypeptide
Finnish Amyloidosis	Gelsolin	AGel
British Familial Dementia	Amyloid Bri Precursor Protein	ABri
Senile Systemic Amyloidosis	Wild-type Transthyretin	ATTR
Prolactinomas	Prolactin	APro
Atrial Amyloidosis	Atrial Natriuretic Factor	Amyloid ANF
Frontotemporal Degeneration	Tau	ATau
Parkinson's Disease	α-synuclein	ASyn
Amyotrophic Lateral Sclerosis	SOD1	SOD1
Myeloma Amyloidosis	Immunoglobulin Light Chains	AL
Organ Amyloidosis	Apolipoprotein A-I and II	AApoA I and II

Table 1.2: Amyloid diseases, associated amyloid proteins, and their corresponding amyloid precursor proteins. Amyloidoses can affect virtually every organ system. There exist differences in processing, however; Aβ, derived from a parent precursor protein requires a series of proteolytic cleavages for it's production, whereas TGFBI and Tau do not.

1.2 HUMAN NEURODEGENERATIVE DISEASES ASSOCIATED WITH AMYLOID

While amyloid deposits affect numerous organs and organ-systems, the most widely-known amyloidoses involve the brain. Prominent among these are Aβ in Alzheimer's disease, α-synuclein in Parkinson's disease, PrPsc in Prion diseases, Tau in Frontotemporal Dementia and Alzheimer's disease, SOD-1 and TDP-43 in Amyotrophic Lateral Sclerosis, Huntingtin in Huntington's disease, and Ataxin in Spinocerebellar Ataxia (reviewed in Wells *et al.,* 2021). These amyloid neurodegenerative diseases have genetic subsets, wherein mutations in the genes encoding the corresponding proteins accelerate the production of abnormal amyloid (reviewed in Philstrøm *et al.*, 2018).

1.2.1 ALZHEIMER'S DISEASE

1.2.1.1 OVERVIEW AND PREVALENCE

Alzheimer's Disease (AD), the commonest form of dementia, has been examined as the prototypical amyloid neurodegenerative disease in this work. Globally, individuals with AD dementia, Prodromal AD, and Preclinical AD are currently estimated at 32, 69, and 315 million respectively, totalling 416 million in all, and constituting 22 % of the population aged 50 and over (Gustavsson *et al.*, 2022).

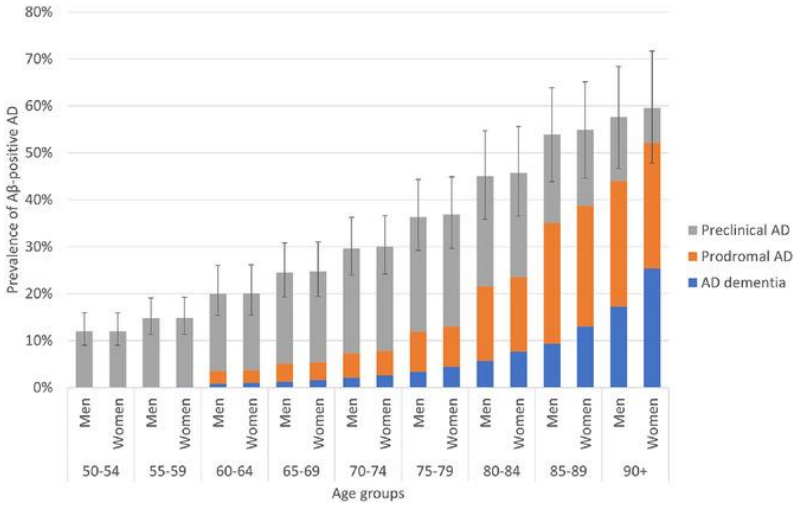

Figure 1.2: The prevalence of the AD spectrum. Rising longevity, the commonest risk factor, has made AD a growing health concern. This is because scientific advances and wider access to healthcare have resulted in the rise of ageing populations worldwide. (Gustavsson *et al.*, Alzheimer's and Dementia 2022, p. 7).

1.2.1.2 THE NEUROPATHOLOGY OF ALZHEIMER'S DISEASE

The signature neuropathological findings in AD are extraneuronal β-amyloid (Aβ) plaques and intraneuronal Neurofibrillary Tau Tangles (NFTs).

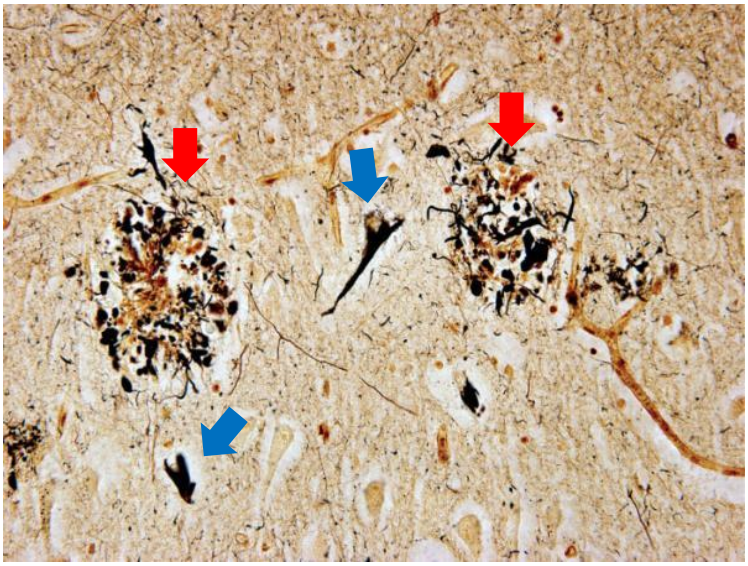

Figure 1.3: Alzheimer's Aβ plaques (red arrows) and Neurofibrillary tangles (NFTs, blue arrows). Modified Bielschowski stain, 400X. (Perl, Mt. Sinai J. Med. 2010, p. 36).

The extent and distribution of NFTs correlate with the degree of dementia and duration of illness (Arriagada *et al.,* 1992, Hof *et al.,* 1995), a neuropathological progression which underscores the relevance of the NFT Braak and Braak staging system (Braak and Braak, 1991). In contrast, β-amyloid deposition, as defined by the Thal staging system (Thal *et al.,* 2002) is less tightly linked with clinical AD. However,when the Thal and Braak and Braak staging systems are combined with the CERAD (Consortium to Establish a Registry for Alzheimer's Disease) score of neuritic plaques (Mirra *et al.,* 1991) the clinicopathological correlation improves significantly (Hyman *et al.,* 2012).

1.2.2 THE PRODUCTION OF Aβ

Aβ oligomers which make up Aβ plaques, like many amyloids, are produced by the proteolytic processing of a precursor protein (**Table 1.2**). In Aβ's case, this parent molecule is known as Amyloid Precursor Protein (APP) and is processed by α-, β- and γ-secretase cleavages. Depending on these cleavages, APP follows two alternate processing pathways, leading to either amyloidogenic or non-amyloidogenic fates. Cleavage by the α-secretase disrupts the Aβ sequence, thereby precluding the formation of Aβ oligomers (the non-amyloidogenic pathway). If α-cleavage is escaped, however, APP is cleaved by β- and γ-cleavages, which release the Aβ segment (usually 42 or 40 amino acids in length) **(Figure 1.4).**

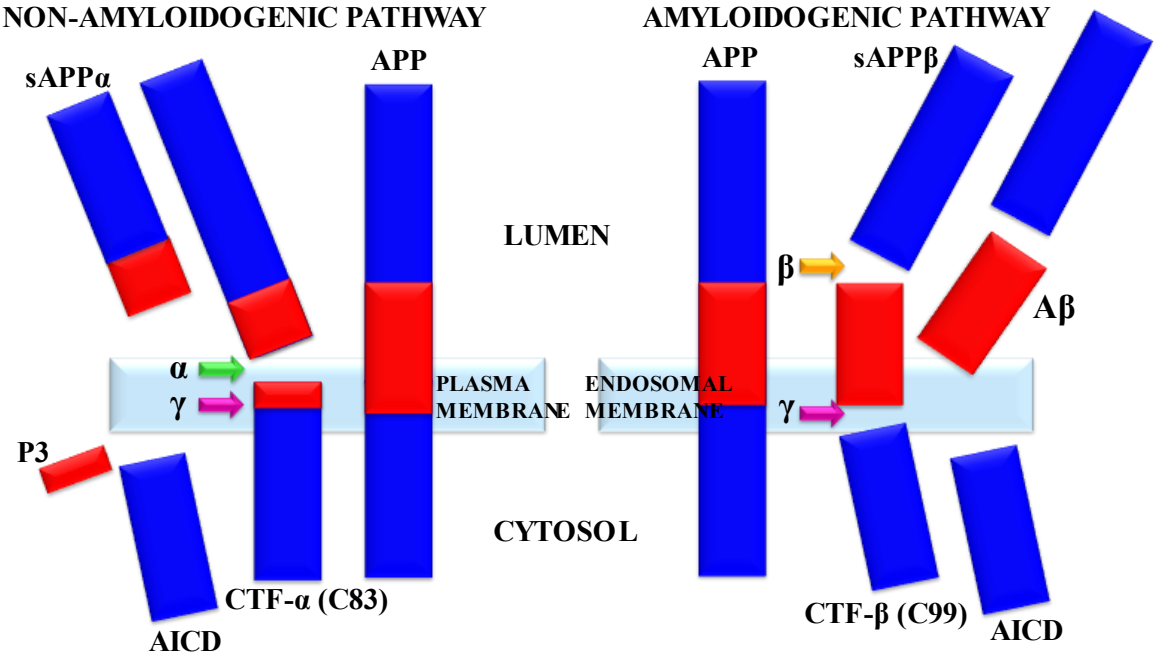

Figure 1.4: Amyloidogenic and non-amyloidogenic processing pathways of APP. The α-secretase cleavage of the non-amyloidogenic pathway precludes the formation of Aβ by disrupting the Aβ segment. Subsequent cleavage by γ-secretase releases the P3 fragment and sAPPα. If APP escapes α-cleavage, the internal Aβ segment is released by β- and γ-secretase cleavages. Several mutations either in the substrate (APP) or in its processing enzyme (γ-secretase, or presenilin) result in FAD. **AICD:** APP Intracellular domain; **CTF:** C-terminal fragment; **sAPP:** soluble APP.

Furthermore, due to the presence of secondary intramembranous γ-secretase cleavage sites (ζ and ε), minor subspecies of the Aβ peptide, occasionally extending up to 49 amino acids, could be released. Depending on the length of Aβ species and their relative proportions, their propensity to fibrillate and to aggregate into Aβ plaques varies. The Aβ sequence with its various cleavage sites is shown in **Figure 1.5**.

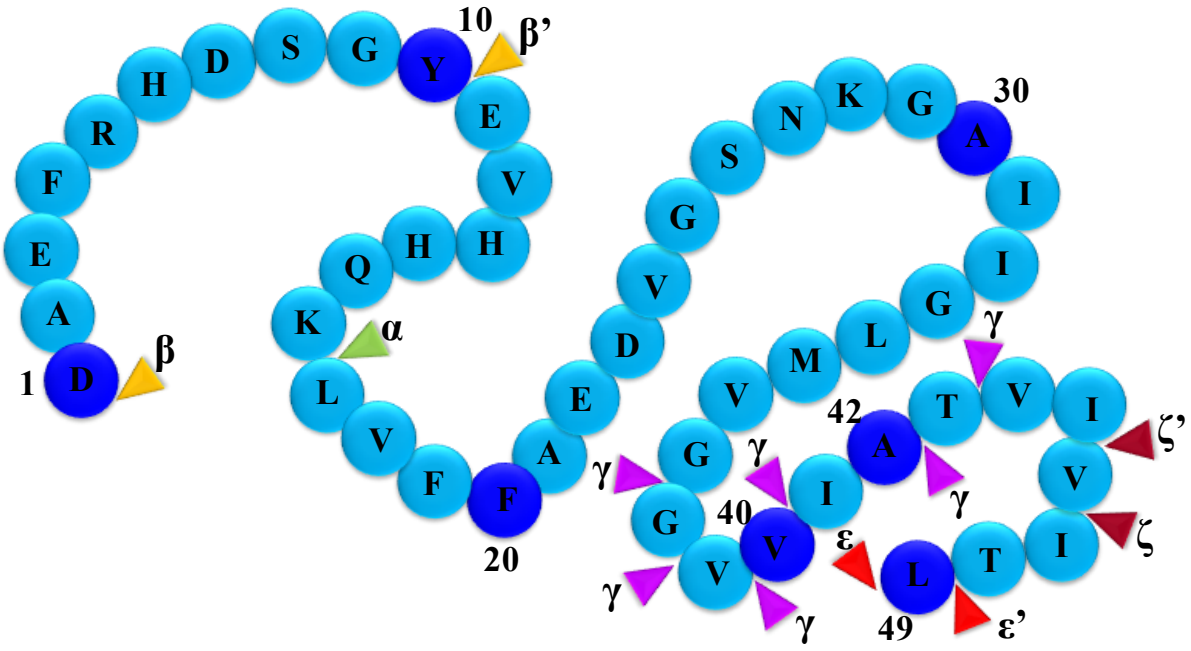

Figure 1.5: APP's secretase cleavage sites. The sequence of wild type $A\beta_{49}$ is shown, together with the cleavage sites of its secretases. **Orange:** β- and β'-cleavage sites. **Green:** α-cleavage site. **Magenta, brown, and red:** γ-, ζ-, and ε- cleavage sites, where cleavages occur by the action of the γ-secretase. The main cleavage products of γ-secretase are $A\beta_{40}$ and $A\beta_{42}$. However, cleavage at ancillary sites releases a variety of Aβ oligomers, including $A\beta_{46}$ (ζ-site), $A\beta_{45}$ (ζ'-site), $A\beta_{49}$ (ε-site) and $A\beta_{48}$ (ε'-site). (Figure drawn and and compiled with information from the following sources: Alzforum.org 2023; Selkoe and Hardy, EMBO Mol. Med. 2016; Li *et al.*, Mol. Neurodegen. 2014; Zhao *et al.*, J. Biol. Chem. 2004).

1.2.3 THE TWO SUBTYPES OF ALZHEIMER'S DISEASE

AD exists in two forms : the commoner, Sporadic or Late-Onset version (SAD or LOAD), and the rarer Familial version (FAD), which is caused by autosomal dominant mutations in various genes (**Figure 1.6**).

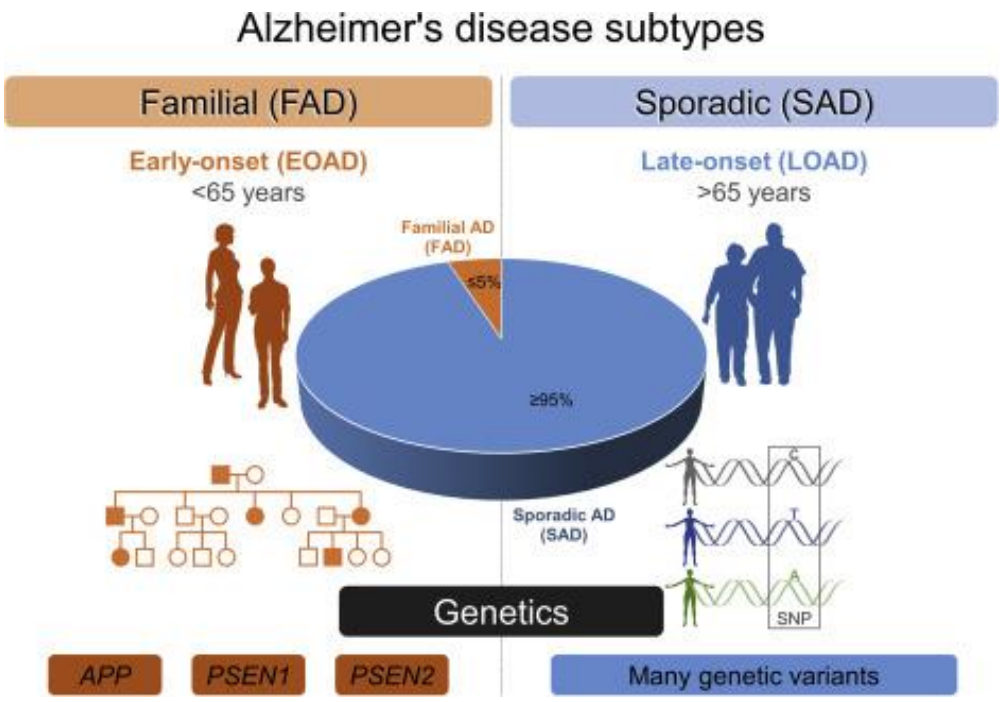

Figure 1.6: Familial and Sporadic subtypes of AD. FAD is caused by almost 400 identified autosomal dominant mutations in the genes for APP and it's γ-secretase, Presenilin (PSEN). FAD and SAD (with rare exceptions which will be seen later) both produce identical disease outcomes. (Adapted from Castanho and Lunnon, Epigenetic processes in Alzheimer's Disease 2019, p. 155).

1.2.4 MUTATIONS CAUSING FAMILIAL ALZHEIMER'S DISEASE

Mutations in either APP (the substrate, **Figure 1.7**), or γ-secretase (the processing enzyme, **Figure 1.8**) cause FAD by producing varyingly fibrillogenic and aggregable Aβ species. Almost 400 of these autosomal dominant mutations have been identified so far (www.alzforum.org). Fortuitously, the neuropathological lesions seen in FAD and SAD are identical. This affords a rare window into the pathophysiology of a widespread disease through the lens of it's uncommoner genetic counterpart.

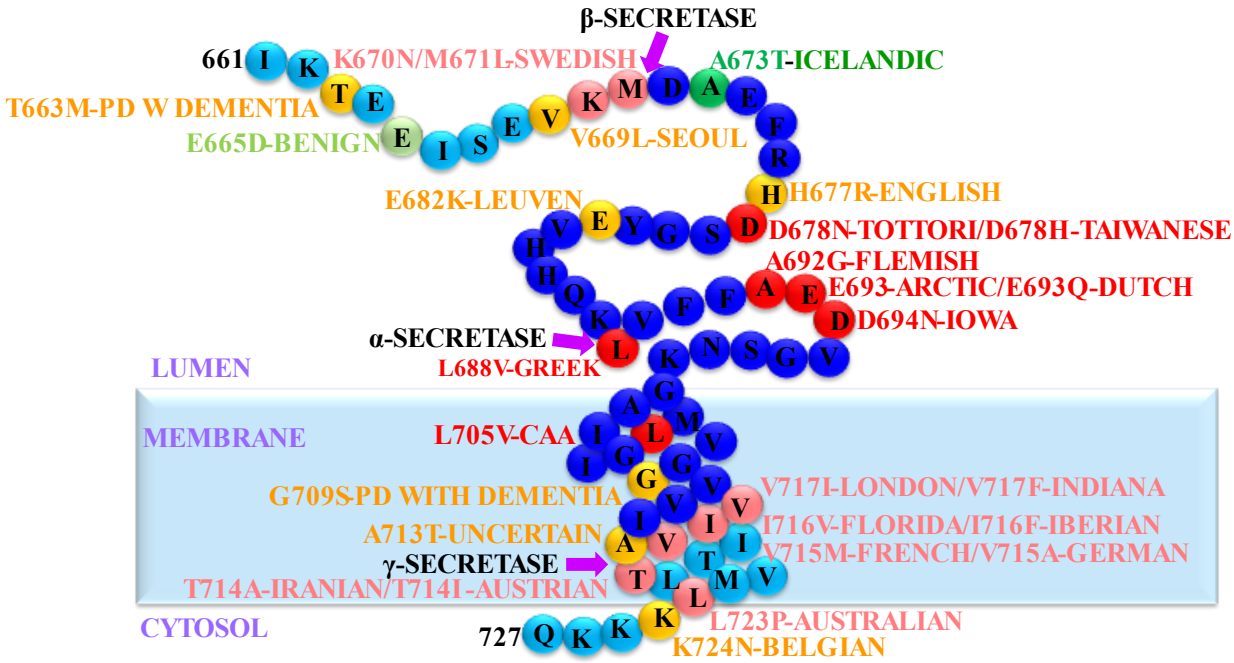

Figure 1.7: FAD mutations in APP, the substrate of Presenilin. Residues 661 to 727 of the 770 amino acid isoform are shown. The $A\beta_{42}$ sequence starts at D672 and ends at A713. Cleavages by β-secretase (extracellularly, between M671 and D672) and γ-secretase (intramembranously, between A713 and T714 release the 42-amino acid Aβ oligomer from the membrane. The sequence of wild type $A\beta_{42}$ is as follows: DAEFRHDSGYEVHHQKLVFFAEDVGSNKGAIIGLMVGGVVIA. **Colour scheme: light blue:** wild type APP residues. **Dark blue:** wild type $A\beta_{42}$ residues. **Bright red:** FAD mutations within the Aβ42 sequence. **Pink:** APP-FAD mutations outside the $A\beta_{42}$ sequence. **Orange:** Mutations of uncertain significance or otherwise unclassified. **Light green:** benign mutations. **Dark green:** protective mutations. **Abbreviations: CAA:** cerebral amyloid angiopathy. **PD:** Parkinson's disease. (Figure drawn and compiled with information from Alzforum.org, 2023).

In this study, I examined the effects of four APP mutations: three of them were within APP's $A\beta_{42}$ segment (the *E693G-Arctic, E693Q-Dutch* and *D694N-Iowa* mutations), while one lay just outside it, towards the N-terminal end of the APP molecule (the *K670N/M671L-Swedish* mutation).

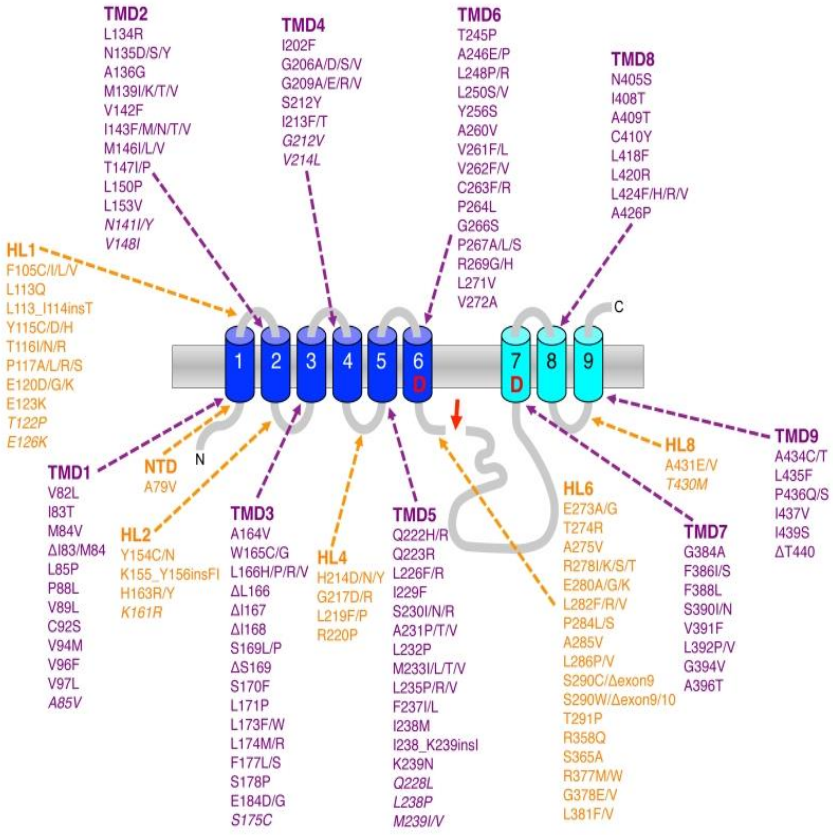

Figure 1.8: FAD mutations in APP's γ-secretase (Presenilin). (Adapted from Alzforum.org and Steiner *et al.*, Cell Stress 2018, p. 298).

1.2.5 APP IS THE HOMOLOGUE OF *DROSOPHILA* APPL

APPL (APP-like), the *Drosophila* homologue of APP, is similarly organized **(Figure 1.9)** and has similar functions in the development of the nervous system (Swanson *et al.*, 2005). Though sharing only about 37-47 % homology overall (Rosen *et al.*, 1989), a much higher degree of conservation is found in the E1 and E2 regions, and particularly in the intracellular domain (Rosen *et al.*, 1989; Swanson *et al.*, 2005). Unlike APP, however, APPL is only expressed in neurons (Luo *et al.*, 1990; Martin-Morris and White, 1990). Pursuant to processing by secretases, where another distinction from mammalian APP is found in the reversal of the α- and β-sites

(Carmine-Simmen *et al.*, 2009; Stempfle *et al.*, 2010), APPL releases a neurotoxic Aβ fragment (Luo *et al.*, 1990; Carmine-Simmen *et al.*, 2009; Bolkan *et al.*, 2012). Given the previously alluded to relatedness of amyloid proteins across species, in this thesis, experimental manipulations of APPL were designed and carried out with the specific aim of observing it's effect on MFAS in *Drosophila* dense-core granules (DCGs) (detailed in **Chapter 4** onwards).

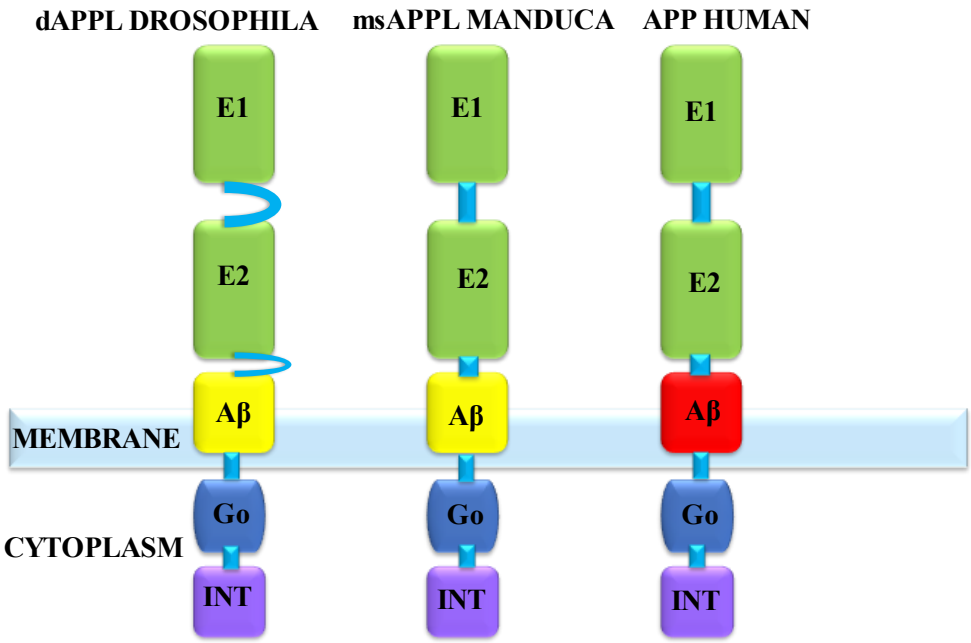

Figure 1.9: Organizational similarities between *Drosophila* and *Manduca* (insect) APPL, and human APP. E1 and **E2:** extracellular domains 1 and 2; **Go:** Goα-binding site; **Int:** internalization domain. (Figure drawn based on data from Cassar and Kretzschmar, Frontiers in Mol. Neurosci., 2016).

1.3 AMYLOID CORNEAL DYSTROPHIES

1.3.1 THE STRUCTURE OF THE CORNEA AND THE ROLE OF TGFBI

The stromal layer of the cornea is comprised of keratocytes held together in tight lattice formation. The highly ordered arrangement of keratocytes is crucial for the transparency

of the cornea, and this adhesion is brought about by the structural protein Transforming Growth Factor Beta-Induced (TGFBI).

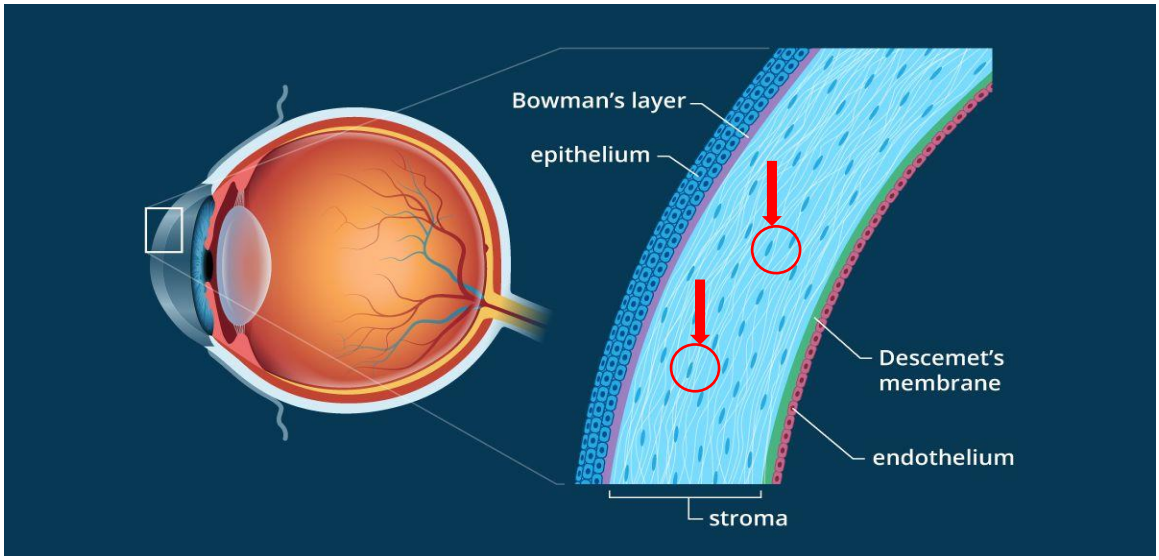

Figure 1.10: Keratocytes in the transparent corneal stroma are arranged in a highly ordered lattice. This tight organization is ensured by the corneal structural protein Transforming Growth Factor Beta-Induced (TGFBI). **Red arrows and circles:** nucleated keratocytes which are held together by TGFBI. (Adapted from allaboutvision.com/resources/cornea/2019).

1.3.2 TGFBI MUTATIONS AND AMYLOID CORNEAL DYSTROPHIES

While the adhesive and organizing influences of wild type-TGFBI are imperative for corneal transparency, mutations in TGFBI direct the protein towards amyloidogenic transformation, resulting in amyloid Corneal Dystrophies (CDs) (Chau *et al.*, 2003; Afshari *et al.*, 2004; Aldave *et al.*, 2005; Chakravarti *et al.*, 2005; Kannabiran and Klintworth, 2006) **(Figure 1.11).** This processing cleavage is effected by the serine protease high-temperature requirement protein A1 (HtrA1), which while being able to cleave wild type-TGFBIp, is far more efficient in cleaving mutated TGFBIp variants, particularly those with amyloidogenic mutations in domain-4 (Poulsen *et al.*, 2019).

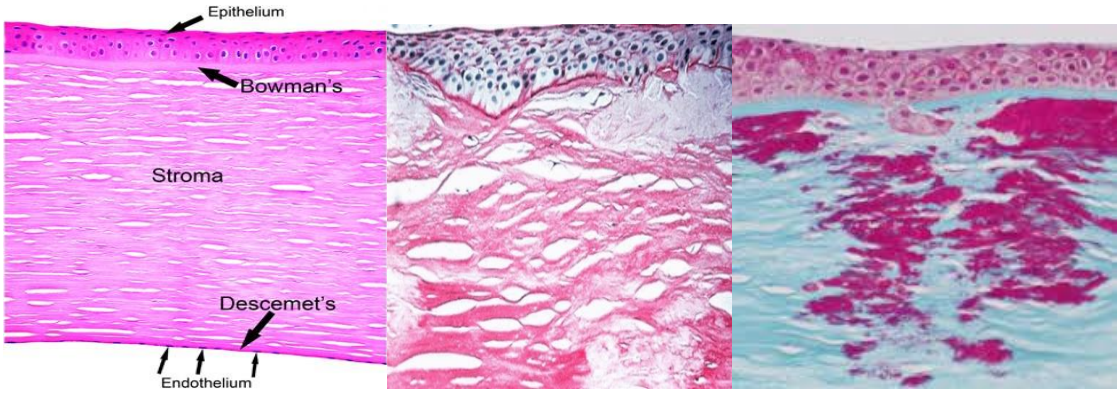

Figure 1.11: Amyloid Corneal Dystrophies. Left panel: Normal cornea showing a well-organized stroma (haematoxylin and eosin). **Middle panel:** Amyloid infiltration showing stromal disruption (haematoxylin and eosin). **Right panel:** Amyloid deposits in the stroma (Masson's Trichrome stain). (From Spalton *et al*., Atlas of Clinical Ophthalmology 2004, used with permission).

In this work, I created flies transgenic for four TGFBI's CD-causing amyloidogenic mutations. Two of these were conserved between TGFBI and MFAS (TGFBI's *Drosophila* homologue) (**Figure 1.13**), while two were not. All four mutations lay within mutation hotspots; three of them in TGFBI's domain-4, and one of them in domain-1 (**Figure 5.8**). These mutations caused a variety of human CDs with a spectrum of clinical characteristics, and included Granular CD, Lattice CD, Reis-Bückler CD, and Thiel-Behnke CD (**Figure 1.12**).

However, a recognised problem with this group of genetic amyloid keratopathies is that there exists considerable genotype/phenotype discrepancy, with some studies showing a disconcordance of as high as 35 % (Han *et al.,* 2021). As will be shown, this work clarified at the molecular level some of the uncertainty surrounding this relatively newly-described group of diseases.

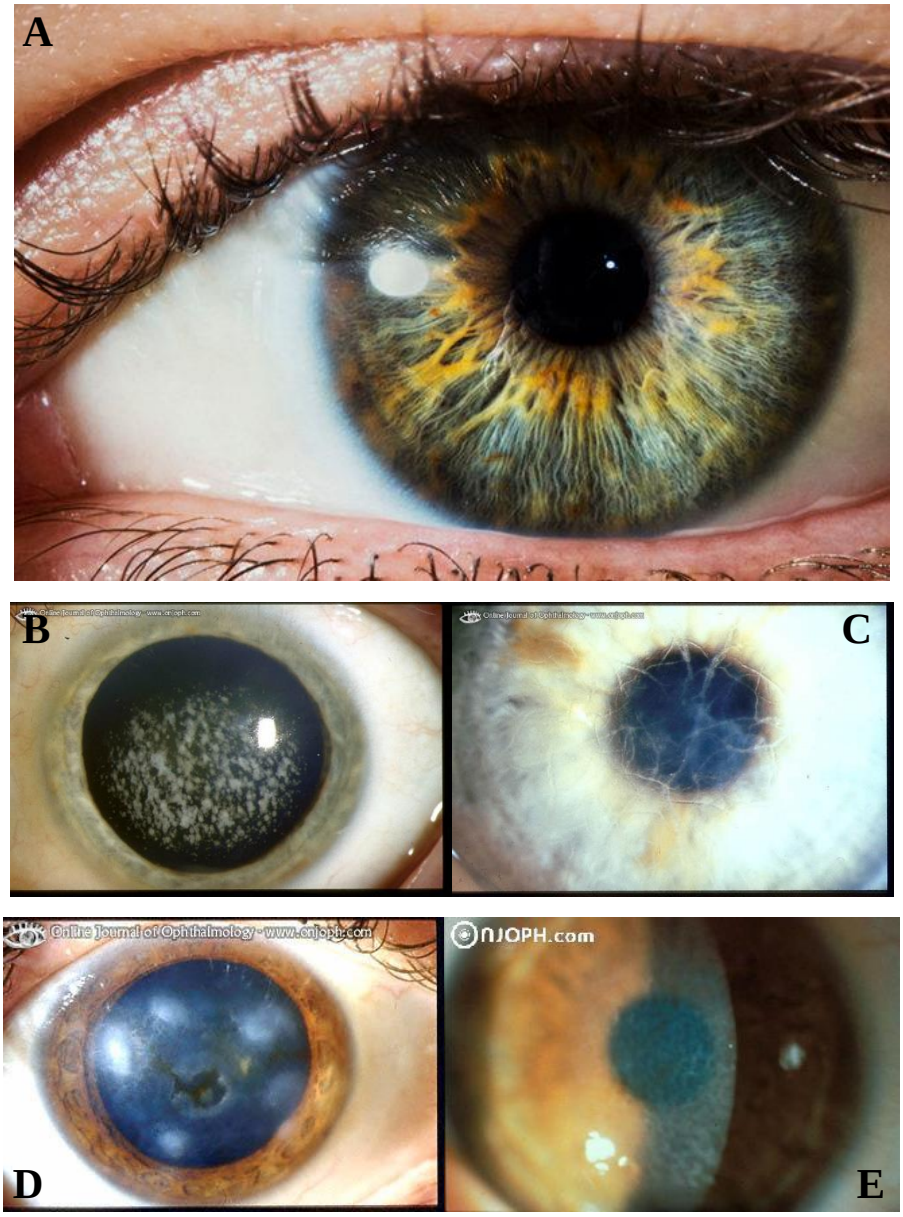

Figure 1.12: The cornea in health and disease. A: Normal eye showing a healthy, transparent cornea. (Used with permission from health.clevelandclinic.org). **B:** Granular CD; **C:** Lattice CD; **D:** Reis-Bückler CD; **E:** Thiel-Behnke CD. (Images **B, C, D** and **E** were used with permission from the Atlas of Ophthalmology; atlasophthalmology.net).

NAME	PHENOTYPE	MUTATION
Granular CD	Progressive snowflake-like central opacities	R555W, R124C
Lattice CD	Bilaterally symmetric lattice-like opacities	H626R, R124C
Reis-Bückler CD	Superficial map-like opacities	G623D
Thiel-Behnke CD	Honeycomb opacities in Bowman's layer	R555Q

Table 1.3: Phenotypes and frequently encountered *TGFBI* mutations of the principal amyloid corneal dystrophies. Most of the major CD mutations were studied in this work, and will be discussed in greater detail in **§ 5** which deals with the manifestations of individual *TGFBI* mutations in flies.

1.3.3 TGFBI IS THE HOMOLOGUE OF *DROSOPHILA* MFAS

TGFBI is the human homologue of *Drosophila* Midline Fasciclin (MFAS) **(Figure 1.13)** a protein highly expressed in the male fly's equivalent of the prostate gland and seminal vesicles (reviewed in Wilson *et al.*, 2017). As discussed in **Chapter 3**, I analysed MFAS and its functions in the AG, where its assembly properties also emerged as important.

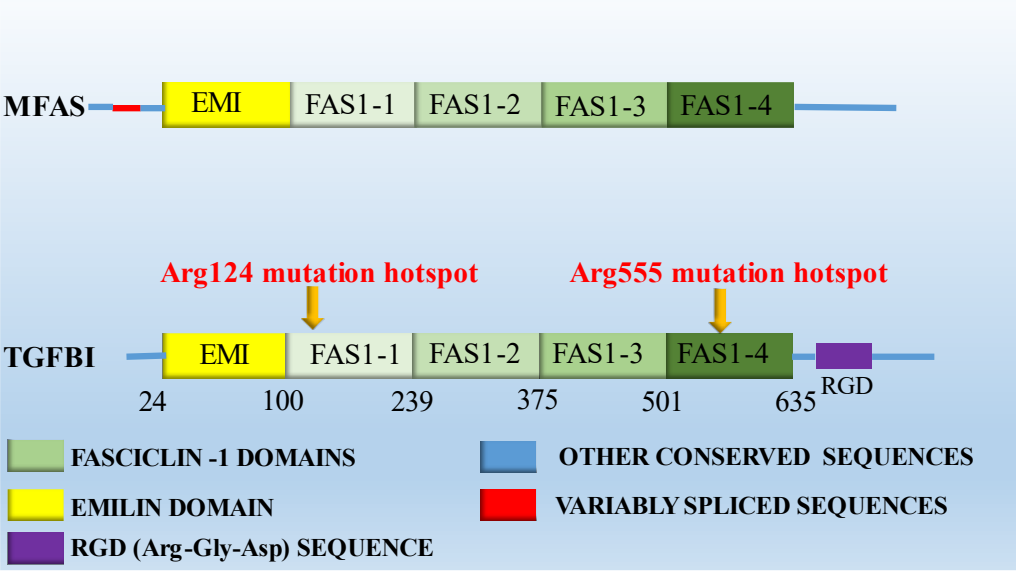

Figure 1.13: TGFBI is the homologue of *Drosophila* MFAS. They belong to the same gene family and are identical in their organization.

Midline Fasciclin (MFAS) is a *Drosophila* amyloid protein which belongs to the ancient and extensive Fasciclin1 (FAS1) family of vertebrate and invertebrate proteins, members of which mediate cell adhesion and signalling. FAS1 proteins have been found in both *eubacteria* and *archaea*, suggesting their provenance preceded the existence of the Last Universal Common Ancestor (LUCA) (Burroughs *et al.,* 2007). FAS1 was first identified in the grasshopper *Schistocerca americana* (Bastiani *et al*., 1987; Snow *et al*., 1988) and in *Drosophila* (Zinn *et al.,* 1988) and belongs to a superfamily of adhesion molecules which includes Cadherin, Integrin, and Leucine-rich repeats (Hu *et al.,* 1998). FAS1 proteins characteristically have repeat fasciclin domains, each approximately 150 amino acids long, and using these as templates, several homologous proteins were identified. These include human Transforming Growth Factor β-Induced (Skonier *et al.,* 1992), human Periostin (Takeshita *et al.,* 1993), human Stabilin-1 and Stabilin-2 (Politz *et al.,* 2002), the alga *Volvox carteri* Cell Adhesion Molecule (CAM) (Huber *et al.,* 1994), the bacterium *Mycobacterium bovis* molecules Mbp70 and Mbp83 (Ulstrup *et al.,* 1995), the plant *Arabidopsis thaliana* arabinogalactan proteins (AGPs) (Schultz *et al.,* 2000), the Shiitake mushroom *Lentinula edodes* FAS1 proteins (Miyazaki *et al.,* 2007), and the fission yeast *Schizosaccharomyces pombe* protein SpFsc1 (Sun *et al.,* 2013). Fortuitously, *Drosophila* MFAS is the seventh-highest most highly expressed protein transcript expressed in fly SCs (Immarigeon *et al.,* 2020), and is readily visualized in DCGs (**Figure 2.12**).

1.4 OTHER CLINICALLY RELEVANT ISSUES ADDRESSED IN THIS STUDY

1.4.1 THE SPREAD OF AMYLOIDS IN NEURODEGENERATIVE DISEASES

The relentless propogation of misfolded amyloid in the brains of patients with neurodegenerative dementias has long been a scientific mystery and clinical concern. Early

studies relied solely on autopsy reports; however the advent of sophisticated imaging techniques combined with the use of β-amyloid dyes made the spread of amyloid trackable in living patients (**Figure 1.14**).

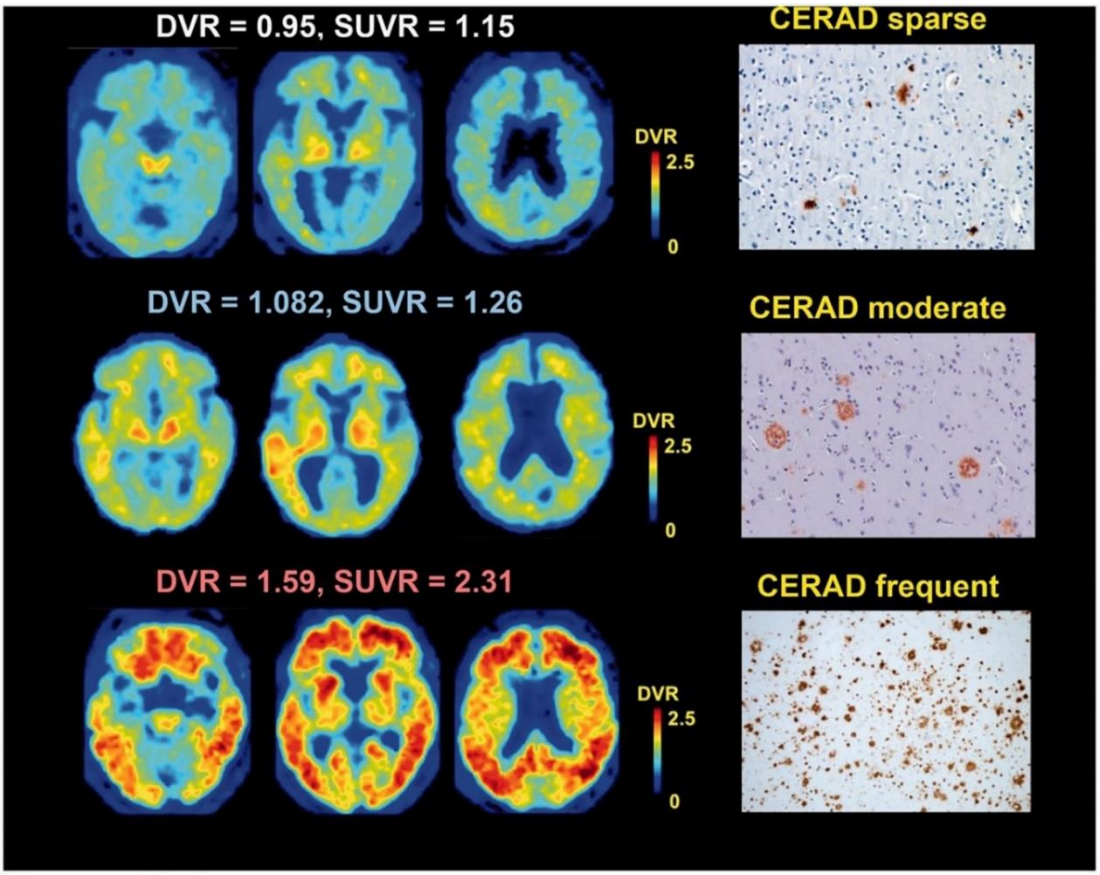

Figure 1.14: Modern amyloid imaging modalities, demonstrating the strong correlation between ante-mortem and post-mortem amyloid burden. PET scans on the left: PET scans using the β-amyloid dye Pittsburgh Compound-B in ante-mortem brains of AD patients. **Histology on the right:** post-mortem histology of the same brains, showing excellent radiological and histological correlation of Aβ burden. **CERAD:** Consortium to Establish a Registry for Alzheimer's Disease; **DVR:** distribution volume ratios; **SUVR:** standardized uptake value ratios. (Villeneuve *et al.*, Brain 2015, p. 2028).

These state-of-the-art live imaging techniques confirmed century-old post-mortem observations that amyloid proteins advanced in a contiguous fashion. Based on these combined post-mortem and radiological studies, it seemed that misfolded amyloids influenced their nearest neighbours to misfold, thus causing an inexorable march forward.

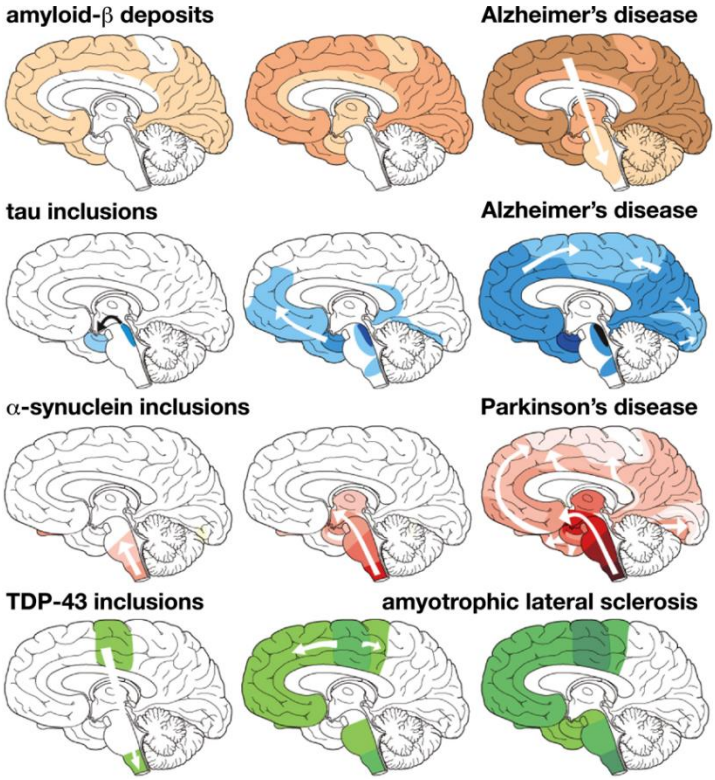

Figure 1.15: Stages of amyloid progression in Alzheimer's, Parkinson's and Amyotrophic Lateral Sclerosis, demonstrating contiguous spread. (Adapted from Jucker and Walker, Nature 2013, p. 45).

This contiguous spread of misfolded amyloid is reflected in all canonical classifications of amyloid neurodegenerative diseases. These include the Thal staging of β-amyloid in Alzheimer's Disease (Thal *et al.*, 2002), the Braak and Braak staging of Tau in Alzheimer's Disease and Frontotemporal Dementia (Braak and Braak, 1991), the McKeith staging of α-synuclein in Parkinson's and Lewy Body Dementias (McKeith *et al.*, 1996), the Brettschneider staging of TDP-43 in Amyotrophic Lateral Sclerosis (Brettschneider *et al.*, 2013), the Parchi staging of PrP in Prion Diseases (Parchi *et al.*, 1995; Parchi *et al.*, 1999), and the Vonsattel staging of Huntingtin in Huntington's Disease (Vonsattel *et al.*, 1985). The message from all these historically validated and clinically relevant staging systems was clear: as universally agreed upon, the propogation of amyloid was indeed unique.

Tellingly, the spread of amyloid did not afflict functionally connected parts of the nervous sytem, like the cortico-basilar tracts or the cortico-spinal system. Rather, occurring over years or even decades, it appeared to advance with the menacing crawl of an infection.

1.4.2 EXAMINING THE SIMILARITIES BETWEEN AMYLOIDS AND PRIONS

When Stanley Prusiner suggested that putative proteinaceous infectious particles might cause slowly advancing brain amyloidoses, he was met with mutterings of heresy and cries of derision. However, persistent scientific efforts opened up the field of prions, and with it the acceptance that life forms might exist outside the DNA-RNA paradigm (Prusiner, 1991). Over the ensuing decades, it turned out that the tell-tale signs of prion affliction in the brain are in fact amyloid deposits, and that amyloids themselves do not behave so differently from prions. In the last 30 years, the spectre of prionoid behaviour looming over amyloids has increasingly been pointed out, always supported by circumstantial but never by direct evidence.

This amyloid-prion connection, though compelling in it's logic, has thus never been observed real-time in a living system, until this point. The work presented here was undertaken with an awareness of these historical precedents and controversies. For 125 years, amyloid's unusual properties and the highly distinctive diseases it engenders have captured the interest of clinicians, geneticists, biologists and chemists. However, the observation of amyloid diseases as they happen, an integral part of any clinical investigation, was made impossible by their decades-long disease course, and the fact that all obtainable brain samples were necessarily post-mortem. With the uncovering of a live system in *Drosophila* which allows visualization of the physiological assembly of an

abundantly expressed protein with amyloid properties (MFAS), a solution to these barriers seemed at hand. As a bonus, this *Drosophila* amyloid is the homologue of the human amyloid TGFBI (**Figure 1.13**), a molecule rapidly gaining prominence itself as the link to a new group of degenerative diseases – amyloid corneal dystrophies. Finally, as I will discuss from **Chapter 4** onwards, part of the MFAS assembly process is driven by *Drosophila* APPL, linking these two putative amyloidogenic proteins and providing an association with the lipid bilayer that is potentially critical in the normal and disease-related properties of these proteins. Add to this is the depth and breadth of *Drosophila's* legendary genetic toolbox, and suddenly this system seemed primed to yield unknowable secrets. These discoveries, as revealed by looking into the fly's accessory glands (AGs), the secondary cells (SCs) within them, and finally the dense-core granules (DCGs) within those SCs, are presented in this work.

1.4.3 EXAMINING THE 'RESCUE' PROPERTIES OF AMYLOID PROTEINS

As an additional look at the possible prion-like properties of amyloids, in **Chapter 6**, I studied the interactions between various lengths of APP, a human pre-amyloid protein with known physiological functions, and APPL, it's fly amyloid counterpart. I also examined the effects of APP and its amyloid derivatives on knockdowns of fly amyloid and amyloid-related genes (*APPL* and *GAPDH2*), which which produce highly distinctive phenotypes. These studies were conducted to determine whether amyloids exert influence over other proteins, which in essence is the basis for their suspected prionoid behaviour. They were also undertaken in the hope of better understanding the effects of amyloids on their surroundings in general, a situation briefly described below with reference to APP and Aβ.

Amyloid (Aβ) plaques are tenacious extra-neuronal structures, displaying unique biophysical and molecular properties. Once transformed into amyloid, APP cleavage products assume these unique attributes which interfere with neuronal and synaptic structure and function (**Figure 1.16**).

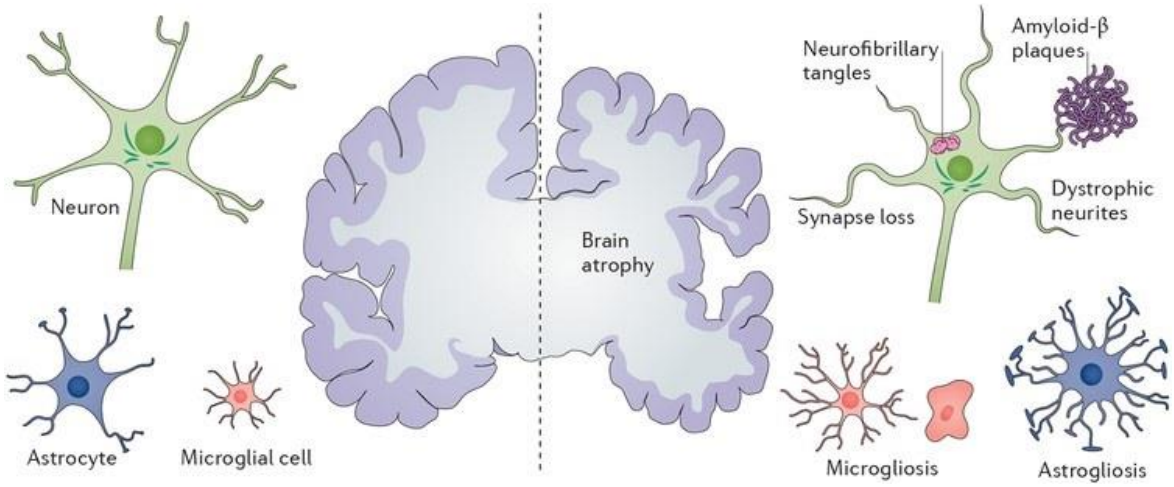

Figure 1.16: Amyloid plaques, their location and overall effects. Amyloid plaques are insoluble extra-neuronal deposits which interfere with the physiological functions of neurons and synapses. (Congdon and Sigurdsson, Nature Reviews Neurology 2018, p. 401).

After they are cleaved from APP and prior to assuming their plaque forms, both mutated and wild type Aβ proteins aggregate into intermediate assembly forms which include monomers, dimers, oligomers, protofibrils, and amyloid fibrils. There remains much uncertainty, however, regarding what exactly the physiological and mutated forms of these various Aβ forms are capable of doing in terms of their precise individual pathological outcomes (reviewed in Chen *et al.*, 2017, and Hampel *et al.*, 2021).

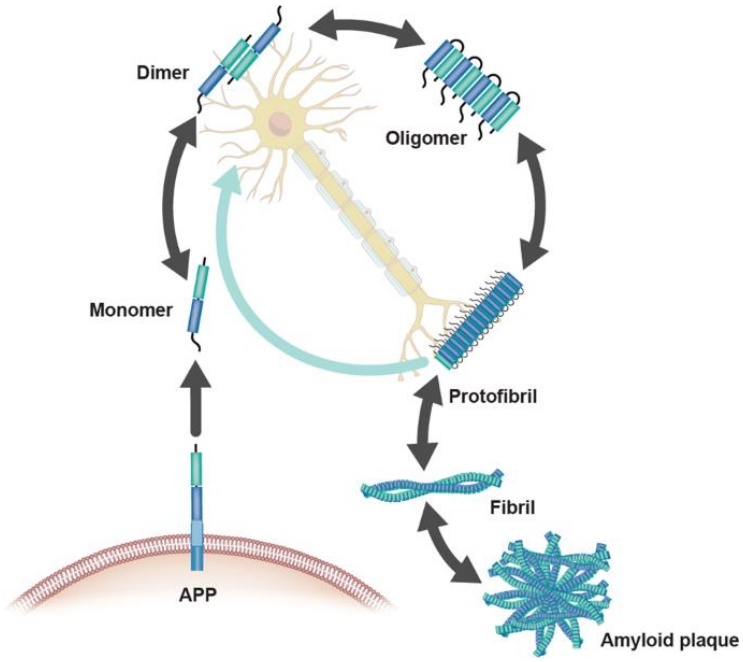

Figure 1.17: The β-amyloid cycle. The aggregation forms of Aβ exist successively in monomer, dimer, oligomer, protofibril, fibril and plaque form, and in their soluble forms can convert from one state to another in a bi-directional fashion. The last two forms (fibrils and plaques) are however insoluble and therefore irreversible. (From Hampel *et al.*, Mol. Psych. 2021, p. 5488).

Aβ monomers, the first released products of APP cleavage at the cell surface, are involved in neuronal cytoprotection, intracellular signalling, and synaptic functions (Rice *et al.*, 2019). As they progress to their oligomer form however, their effects transition from the benign to the malign, as they hinder synaptic functions and structurally disrupt dendritic spines, synapses and neurons (Brinkmalm *et al.*, 2019). These deleterious effects however, vary with their molecular weights, and differing conclusions were reached by different studies, suggesting non-uniformity of Aβ's toxic properties (Hong *et al*., 2018; Yang *et al.*, 2017). In their next iteration as protofibrils, they are still soluble (Walsh *et al.* 1997) but when internalized by microglia, evoke inflammatory and immune responses in addition to causing the previously mentioned functional and structural impediments (Gouwens *et al.*,

2018; Söllvander *et al.,* 2015). Finally, as they progress to their ultimately insoluble forms (amyloid fibrils and plaques), they cause irreversible neuronal and synaptic dysfunction in both animal models and human patients (Petkova *et al.,* 2005; Koffie *et al.,* 2009). In addition, in their insoluble fibril forms they catalyze the formation of their earlier-stage Aβ oligomers, thus setting up a self-perpetuating loop (Cohen *et al.,* 2013). In this thesis, the effects of four species of mutated Aβ proteins, generated by the particularly pernicious FAD *Aβ* mutations *Arctic*, *Dutch*, *Iowa* and *Swedish*, were studied (**Figure 6.3)**. The protein-organising effects discovered in the Arctic mutation were further investigated in rescue experiments in **Chapter 6**, since there are no studies examining individual Aβ mutant's properties, either detrimental or salubrious, when broken down by genotype.

1.5 THE *DROSOPHILA* ACCESSORY GLAND (AG) AND IT'S RELEVANCE TO SECRETORY BIOLOGY

1.5.1 AN OVERVIEW OF THE AG AND IT'S CELL TYPES

Male *Drosophila* have paired AGs, which are analogous to the human prostate and seminal vesicles. As is the case for these mammalian glands, *Drosophila* AGs are the major contributors to seminal fluid. The lining of each AG is comprised of a simple monolayer with two cell types: around 1000 squamous main cells, and, located in the distal third of the gland, about 40 cubdoidal, binucleate secondary cells (SCs) (Wilson *et al.,* 2017). Main cells secrete the 36-amino acid sex peptide (SP), which regulates several aspects of female behavioural reprogramming (Liu and Kubli, 2003; Kubli, 2003; Kubli and Bopp, 2010; Kubli and Bopp, 2012). *SP* mutant or knockdown males fail to induce several normal post-mating behaviours in females, such as a reduction in female receptivity to subsequent mating (Chapman *et al.,* 2003). However, even as prolifically-acting as SP is, several more

complexities have emerged within this paradigm, since other ligands for the SP receptor have been discovered (Kim *et al.*, 2010), and SP-like responses can be evoked in females lacking the SP receptor (Haussmann *et al.*, 2013). Yet other main cell proteins like ovulin (Herndon and Wolfner, 1995), CG33943 (Ravi Ram and Wolfner, 2007), and Acp36DE (Bloch Qazi and Wolfner, 2003) evoke important physiological post-mating responses, comparable to the functions of the myriad seminal fluid proteins in humans.

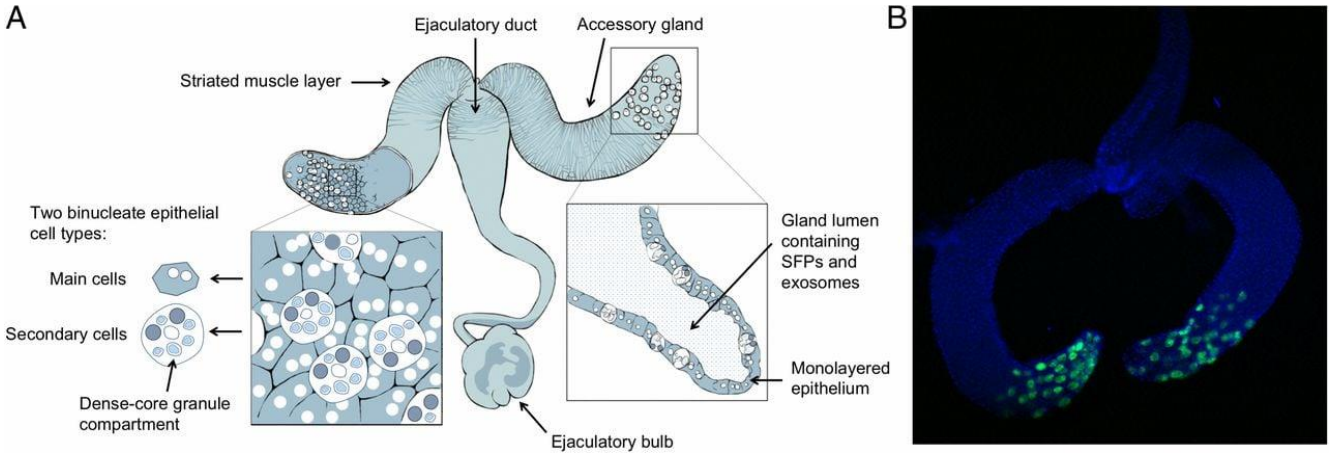

Figure 1.18: The male *Drosophila* reproductive system. A: The paired AGs are lined by a monolayer comprised of main and secondary cells, ensheathed by striated muscle which contracts during ejaculation **B:** Dissected AGs showing SCs which fluoresce due to GFP, with the nuclei stained with DAPI. (From Hopkins *et al.*, Proc. Natl. Acad. Sci. USA 2019, p. 24720).

1.5.2 THE SPECIALIZED FUNCTION OF SECONDARY CELLS (SCs) AND THEIR PRODUCTION OF DENSE-CORE GRANULES (DCGs)

The biological activity of main cells is paralleled by that of the increasingly studied SC, this work having been pioneered by the Wilson group since 2011. These studies found that proteins secreted by SCs are condensed into DCGs, a process regulated by autocrine signalling through the DCG-associated Bone Morphogenetic Protein (BMP) ligand Decapentaplegic (Dpp) (Redhai *et al.*, 2016; Hopkins *et al.*, 2019). The process of

packaging biologically active *Drosophila* proteins into DCGs is remarkably similar to the loading and release of crystalline amyloid insulin hexamers into and from the β-cells of the pancreas. The similarities between *Drosophila* DCGs and a host of other mammalian peptide hormones, which are also stored as amyloids in DCGs in a diverse array of cells, immediately highlights the utility of studying this process in flies. These parallels became particularly relevant with the revelation that *mfas*, encoding the *Drosophila* amyloid MFAS, the homologue of the human amyloidogenic protein TGFBI, is highly expressed in SCs (Immarigeon *et al.*, 2021). Furthermore, as I show in the experimental results, *mfas*-kd completely suppresses DCG formation without altering compartment identity. This demonstrates the unique attributes of DCGs, and as will be seen later, the special place that it's formative protein, MFAS, occupies in biology. Learning these disparate, yet connected facts, and recognising that this *Drosophila* DCG model could be further refined and adapted for their study, I formulated a programme of work which aimed to answer the questions outlined below.

1.6 OVERALL AIMS OF THIS STUDY

1. To standardise and refine the fly SC-DCG model in order to apply it efficiently and consistently to the study of human and *Drosophila* amyloids.

2. To elucidate the role of MFAS in SCs, particularly considering its high expression in these cells.

3. To explore the extent of MFAS' influence, especially on amyloidogenesis-related Rab compartments, DCG formation, exosome generation, and SC nuclear size, the latter being an indication of autocrine activity.

4. To investigate the response of MFAS and DCGs to manipulations of human and fly amyloid and amyloid-related proteins, including GAPDH/GAPDH2, APP/APPL, and TGFBI. These manipulations will include the effects of knockdowns of these genes, as well as effects of the overexpression of their wild type and mutated versions.

5. To test the fidelity of DCGs as indicators of genetic rescues, particularly in settings with varying or opposing effects on their biogenesis.

6. Within the framework of these results, to investigate the veracity of putative amyloid 'crosstalk'. In the setting of this *Drosophila* SC-DCG model, this endeavour will be particularly efficient, since fly genetics would allow the expression of a plurality of amyloid proteins, while the ease of *ex vivo* imaging would allow real-time visualisation of their interactions.

7. Working with results from the above two aims, to attempt to differentiate between pro- and anti-aggregation forces influencing DCGs and amyloid crosstalk.

8. To assess the suitability of DCGs in measuring ageing and other senescence-related changes in flies bearing human amyloidogenic mutations.

9. In unifying all these results, to find commonalities between and learn lessons from the amyloid and amyloid-related proteins MFAS, TGFBI, APP and APPL. I hope that a synthesis of these data will uncover even some small secret of amyloid biology, a quest I think is a timely one, since amyloid pathologies, either through longevity or discovery, are on the rise.

CHAPTER 2

MATERIALS AND METHODS

2. MATERIALS AND METHODS

2.1 DROSOPHILA STOCKS

2.1.1 GAL4 AND GAL80 COMBINATION LINES

GENOTYPE	SOURCE ID	REFERENCE	DESCRIPTION
w^{1118}; tub-GAL80^{ts}/CyO; dsx-GAL4-MFAS-GFP/TM6B	Mark Wainwright, Wilson Lab, Oxford		Composite driver line
w^{1118}; if/CyO; dsxGAL4/TM6B	Stephen Goodwin, Oxford	Rideout *et al.*, 2010	Secondary cell-specific GAL4 line
w^{1118}; tub-GAL80^{ts}/CyO; MKRS/TM6B		McGuire *et al.*, 2003	Ubiquitously expressed temperature-sensitive GAL80
w; ; tubGAL80^{ts}/CyO; dsxGAL4-Btl-GFP	Claudia Mendes, Wilson Lab, Oxford		Driver line with *GFP*-tagged *Breathless*
w^{1118}; tub-GAL80^{ts}/CyO; dsxGAL4-UAS-GFP-GPI	Mark Wainwright, Ben Kroeger, Felix Castellanos, Wilson Lab, Oxford		Composite driver line with GFP-GPI

2.1.2 OVEREXRESSION LINES

GENOTYPE	SOURCE ID	REFERENCE	DESCRIPTION
w^{1118};UAS-$A\beta_{42}$E693G-Arctic	Bloomington 33773	Donated by Vitruvian, LLC	$A\beta_{42}$E693G-Arctic under UAS control
w^{1118}; UAS- $A\beta_{42}$E693Q-Dutch	Bloomington 33775		$A\beta_{42}$E693Q-Dutch under UAS control
w^{1118}; ;UAS- $A\beta_{42}$D694N-Iowa	Bloomington 33779		$A\beta_{42}$D694N-Iowa under UAS control
w^{1118};UAS- $A\beta_{42}$Wild-type	Bloomington 33769		$A\beta_{42}$Wild-type under UAS control
y, w;UAS-APP-YFP	Bloomington 32039		APP under UAS control
w^{1118}; ;UAS-BACE1-APP isoform 695	Bloomington 33797		β-secretase1-APP under UAS control
y, w; ;UAS-Human-GAPDH	Bloomington 79196		Human GAPDH under UAS control
w; ;UAS-K595N/M596L-Swedish	Bloomington 6701		K595N/M596L-Swedish double mutation under UAS control
w^{1118}; ; P{w[+mC}=UAS-sdDeltaE1}3	Bloomington 29866		APPL deleted for the extracellular domain (aa 85-231) under UAS control
y[1] w[*]; P{w[+mC}=UAS-sdDeltaC}2	Bloomington 29865		APPL deleted for the intracellular domain under UAS control

2.1.3 RNAi LINES

GENOTYPE	SOURCE ID	REFERENCE	DESCRIPTION
w^{1118}; ;UAS-APPL-RNAi	Vienna 42673	Singh *et al.*, 2017	RNAi targeting APPL under UAS control
y, v;UAS-APPL-RNAi	Bloomington 39013	Perkins *et al.*, 2015	RNAi targeting APPL under UAS control
y, v; ;UAS-APPL-RNAi	Bloomington 28043	Perkins *et al.*, 2015	RNAi targeting APPL under UAS control
y, sc, v;UAS-MFAS-RNAi	Bloomington 52905	Perkins *et al.*, 2015	RNAi targeting MFAS under UAS control
y, v; ;UAS-MFAS-RNAi	Bloomington 58256	Perkins *et al.*, 2015	RNAi targeting MFAS under UAS control
y, v; ;UAS-GAPDH$_2$-RNAi	Bloomington 26302	Ni *et al.*, 2009	RNAi targeting GAPDH$_2$ under UAS control
y, v;UAS-vps26-RNAi	Bloomington 38937	Ni *et al.*, 2011	RNAi targeting vps26 under UAS control
y, v; ;UAS-vps26-RNAi	Vienna 18396	Pannen *et al.*, 2020	RNAi targeting vps26 under UAS control
w^{1118}; UAS-vps26-RNAi	Vienna 110384	Walsh *et al.*, 2021	RNAi targeting vps26 under UAS control
vps35-RNAi	Bloomington 46200	Lund *et al*., 2018	RNAi targeting vps35 under UAS control
y, sc, v; UAS-vps35-RNAi	Bloomington 38944	Perkins *et a*l., 2015	RNAi targeting vps35 under UAS control
UAS-vps35-RNAi	Bloomington 91645	Perkins *et al.*, 2015	RNAi targeting vps35 under UAS control
UAS-vps35-RNAi	Bloomington 91646	Perkins *et al.*, 2015	RNAi targeting vps35 under UAS control
y, sc, v; UAS-kuz-RNAi	Bloomington 66958	Perkins *et al.*, 2015	RNAi targeting α-secretase under UAS control
y, sc, v; UAS-Nicastrin-RNAi	Bloomington 57497	Perkins *et al.*, 2015	RNAi targeting γ-secretase under UAS control
y, v; UAS-Nicastrin-RNAi	Bloomington 27498	Perkins *et al.*, 2015	RNAi targeting γ-secretase under UAS control
w; UAS-chmp2b-RNAi	Vienna 318679	V. Raghavan	RNAi targeting chmp2b under UAS control

2.1.4 FLUORESCENTLY TAGGED GENE TRAP DRIVER LINES

GENOTYPE	SOURCE ID	REFERENCE	DESCRIPTION
w^{1118}; tub-GAL80^{ts}/CyO; dsx-GAL4-GFP-MFAS/TM6B	Mark Wainwright		Composite driver line with *GFP-mfas* gene trap
w^{1118}; CFP-Rab6, tub-GAL80ts/CyO; dsxGAL4	Claudia Mendes		Composite driver line with *CFP-Rab6* gene trap
w^{1118}; tub-GAL80^{ts}/Xa; YFP-Rab11, dsxGAL4/Xa	Pauline Marie		Composite driver line with *YFP-Rab11* gene trap
w^{1118}; ; GFP-MFAS (MI11275-GFSTF.2)	Bloomington 63204		MFAS-GFP gene trap with N-terminus MFAS

2.1.5 TRANSGENIC TGFBI LINES

GENOTYPE	SOURCE ID	REFERENCE	DESCRIPTION
w; UAS-TGFBI-Wild Type/CyO	Preman Singh		UAS-line with Wild-Type human TGFBI
w; UAS-TGFBI-G623D/CyO	Preman Singh		UAS-line with human TGFBI-G623D
w; UAS-TGFBI-H626R/CyO	Preman Singh		UAS-line with human TGFBI-H626R
w; UAS-TGFBI-R555Q/CyO	Preman Singh		UAS-line with human TGFBI-R555Q
w; UAS-TGFBI-R124C/CyO	Preman Singh		UAS-line with human TGFBI-R124C
w; UAS-MFAS-Wild Type/CyO	Preman Singh		UAS-line with MFAS-Wild Type third copy insertion
w; UAS-MFAS-G623D/CyO	Preman Singh		UAS-line with MFAS-G623D third copy insertion
w; UAS-MFAS-Wild Type-GFP/CyO	Preman Singh		UAS-line with MFAS-Wild Type-GFP insertion
w; UAS-TGFBI-Wild Type-GFP/CyO	Preman Singh		UAS-line with TGFBI-Wild Type-GFP insertion

2.1.6 MISCELLANEOUS LINES

GENOTYPE	SOURCE ID	REFERENCE	DESCRIPTION
w^{1118}	L. Partridge	Redhai *et al*., 2016	Non-transgenic control line
w^{1118}*; if/CyO; MKRS/TM6B*			Balancer line
y, sc, v;UAS- rosy-RNAi	Bloomington 44106	Marie *et al*., 2023	Control line
w^{1118}*; ; MFAS-GFP*	Vienna 37889		MFAS-GFP gene trap with C-terminus MFAS
w; UAS-MFAS-GFP/CyO	Preman Singh		UAS line with MFAS-GFP insertion
w; UAS-TGFBI-GFP/CyO	Preman Singh		UAS line with with TGFBI-GFP insertion

2.2 DESIGN OF GENETIC CONSTRUCTS

As mentioned in the introduction **(§ 1.3.3, Figure 1.13)**, MFAS and TGFBI are identically organized homologues, and TGFBI mutations are increasingly being identified as causing an expanding list of amyloid corneal dystrophies (CDs). However, their sequence homology is only around 30 % (Song *et al.*, 2014). Sequence alignment (**Figure 2.1** and **Appendix 9.2**) revealed conserved and non-conserved regions, and from these, four common CD mutations were selected. Two of these (G623D and H626R) were conserved between TGFBI and MFAS, while two (R555Q and R124C) were not.

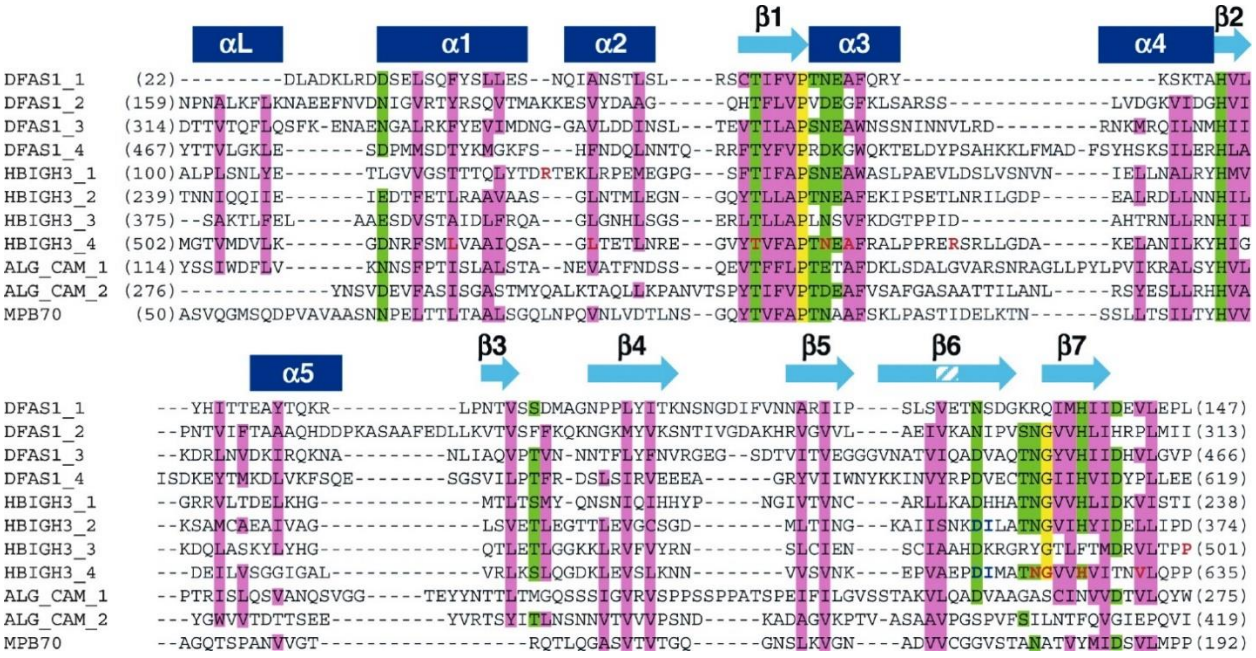

Figure 2.1: Sequence alignment of selected FAS1 domains in *Drosophila* MFAS (shown as DFAS), human TGFBI (HBIG3), *Volvox carteri* Algal-CAM and *Mycobacterium tuberculosis* MPB70. Conserved residues are shaded as follows: pink: apolar; green: polar; yellow: glycine and proline. TGFBI (HBIGH3) residues causing corneal dystrophy mutations are in red. (Taken from Clout *et al.*, Structure 2003, pg. 200).

2.3 CREATION OF GENETIC CONSTRUCTS

The chosen genetic constructs were ordered from Invitrogen (Thermo Fisher Scientific, Waltham, MA, United States), where they were assembled from synthetic oligonucleotides and/or PCR products and inserted into pUASattB_AN230. The plasmid DNA was extracted from transformed bacteria, it's concentration determined by UV spectroscopy, and the final construct was verified by sequencing. The plasmids were received and amplified, as detailed in the following sections.

2.3.1 TRANSFORMATION OF COMPETENT *E. COLI* WITH pUASTattB

NEB® 5-alpha C2987H ultra-competent *E. coli* (New England Biolabs, Ipswich, MA, United States) were removed from a -80°C freezer and hand-thawed. 1-5 µL containing 1 pg-100 ng of plasmid DNA was added to the cell mixture. Without vortexing, the tube was carefully flicked 4-5 times to mix the *E.coli* and the DNA. The mixture then was placed on ice for 2 minutes, avoiding any further mixing. The mixture was then heat-shocked at 42°C for exactly 30 seconds, again with the avoidance of mixing, followed by placement on ice for 2 minutes. 950 µL of room temperature SOC Medium (Merck, Darmstadt, Germany) was then pipetted into the mixture. 50-100 µL was immediately spread onto a selection plate which was then incubated overnight at 37-42°C.

2.3.2 PREPARATION OF LURIA BROTH AGAR PLATES

The following were weighed out into a 1L Erlenmeyer flask: 5 g NaCl, 5 g tryptone, 2.5 g yeast extract, 7.5 g agar. Distilled water was added to make up the volume to 500 mL. The flask was then swirled to mix, covered with aluminum foil, and autoclaved for 20 minutes. After removal from the autoclave, the solution was allowed to cool to 55°C. 500 µL of 1 g Ampicillin (Thermo Fisher Scientific, Waltham, MA, USA) in 10 mL distilled water

(1:1000 concentration) was added, and the solution swirled to mix. Twenty mL of the LB was poured into each 10 cm polystyrene Petri dish. Lids were placed on the plates, and they were allowed to cool for 30-60 minutes until solidified, following which they were inverted. They were then allowed to sit overnight.

2.3.3 PREPAPARATION OF SUPERBROTH

The following were weighed out into a 1L Erlenmeyer flask: 32 g tryptone, 20 g yeast extract, 5 g NaCl, and 5 mL 1 N NaOH. Distilled water was added to make the volume up to 1L, the mixture swirled to dissolve, autoclaved for 20 minutes, and allowed to cool to room temperature.

2.3.4 GROWING TRANSFORMED *E.COLI* IN SUPERBROTH

Superbroth was aliquoted into 3 mL tubes. To each tube, 12 µL of a solution of 1 g Ampicillin (Thermo Fisher Scientific, Waltham, MA, USA) in 10 mL of distilled water was added. A single colony from overnight cultured colonies **(§ 2.15.2)** was carefully inoculated into each 3 mL aliquot of Superbroth. Four such inoculations were done per genetic construct-bearing plasmid.

2.3.5 MIDIPREP™ EXTRACTION OF CONSTRUCT-BEARING pUASTattB

The manufacturer's protocol was followed (PureLink™ HiPure Plasmid Midiprep kit, Invitrogen™, ThermoFisher Scientific, Waltham, MA, USA). Briefly, 10 mL Equilibration Buffer was added to the HiPure Midi Column and the solution allowed to drain by gravity flow. The cells were sedimented by centrifugation at 4000 x *g* for 10 minutes, and all the medium was discarded. 4 ml Resuspension Buffer with RNase A was added to the cell pellet and the pellet resuspended until it was homogenous, but without vortexing. This was incubated at room temperature for 5 minutes, following which 4 mL Precipitation Buffer

was added and mixed by inverting the tube until the mixture was homogenous, but again without vortexing. The lysate was centrifuged at 12000 x *g* for 10 minutes at room temperature. The supernatant was loaded onto the equilibrated column, and the solution allowed to drain by gravity flow. Ten mL Wash Buffer was added to the column. The flow-through after the Wash Buffer drained from the column was discarded, and the wash step was repeated once. A sterile 15 mL centrifuge tube was placed under the column. 5 mL Elution Buffer was added to the column and the solution which contained purified DNA was allowed to drain by gravity flow.

2.3.6 PRECIPITATION OF pUASattB AND TITRATION OF CONCENTRATION

3.5 mL isopropanol was added to the eluate and mixed well. The tube was then centrifuged at 12000 x *g* for 30 minutes at 4°C and the supernatant discarded. The pellet was washed in 3 mL 70 % ethanol and the tube centrifuged at 12000 x g for 5 minutes at 4°C. The supernatant was discarded, the pellet air-dried for 10 minutes, and the plasmid DNA then resuspended in 100 µL distilled water. Using a densitometer, a final concentration of 400 ng/µL was achieved, this being the optimum concentration for embryo microinjection (personal communication, the Fly Facility, University of Cambridge). The plasmid solution was stored at -20°C.

2.3.7 SUMMARY OF GENETIC CONSTRUCTS PREPARED FOR EMBRYO MICROINJECTION

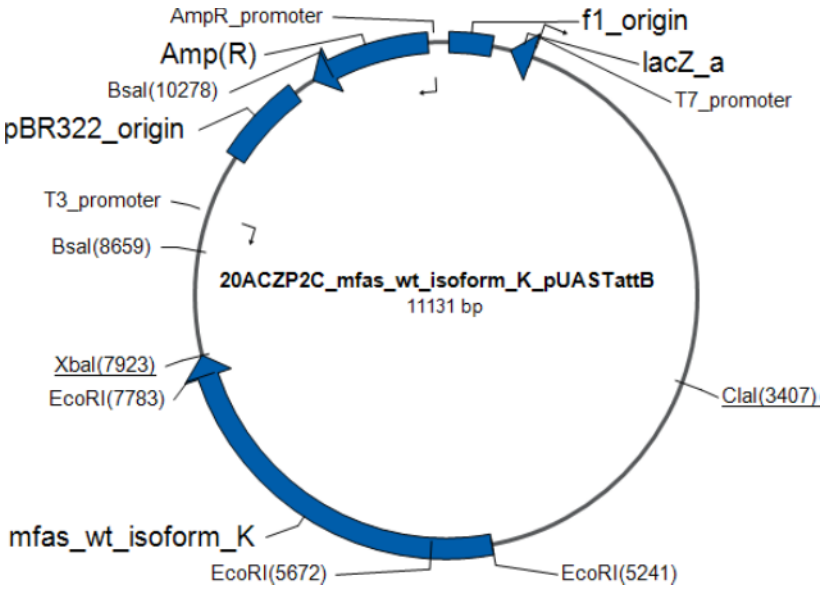

Figure 2.2: *mfas-wild type* isoform K subcloned from plasmid construct 20ACZP2C into *Drosophila*-specific plasmid pUASTattB for embryo microinjection. The sequence is shown in **Appendix 9.1.7.**

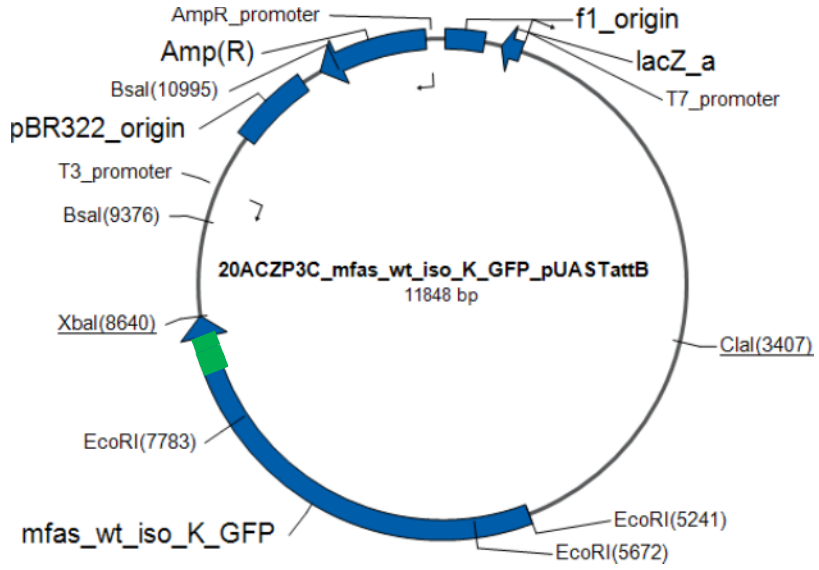

Figure 2.3: *mfas-wild type* isoform K with a C-terminus GFP tag subcloned from plasmid construct 20ACZP3C into *Drosophila*-specific plasmid pUASTattB for embryo microinjection. GFP (shown in green) is inserted into *mfas* just before the TAG stop codon. The sequence is shown in **Appendix 9.1.8.**

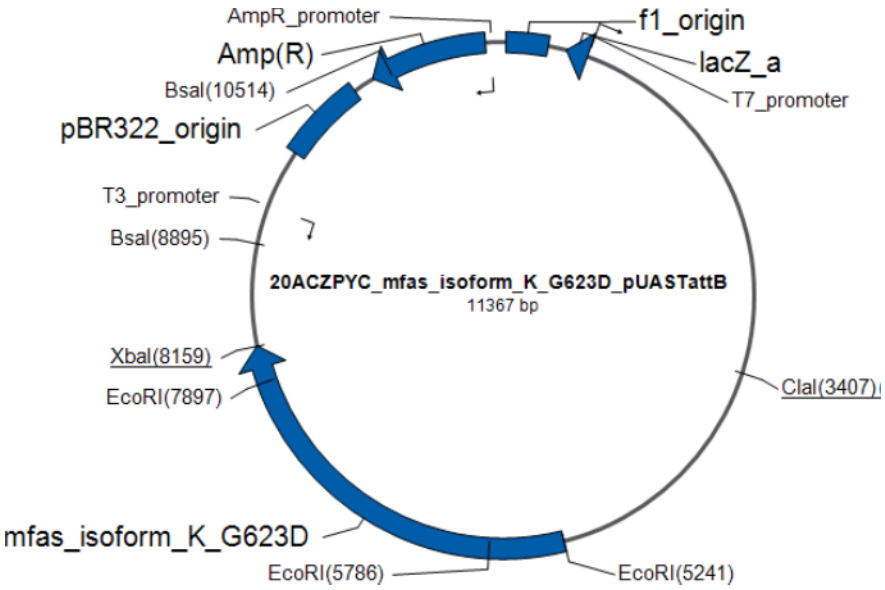

Figure 2.4: *mfas-isoform K-G623D* subcloned from plasmid construct ACZPYC into *Drosophila*-specific plasmid pUASTattB for embryo microinjection. *mfas-G623D* is equivalent to *mfas* wild type except for a single amino acid change. The sequences are shown in **Appendix 9.1.9.**

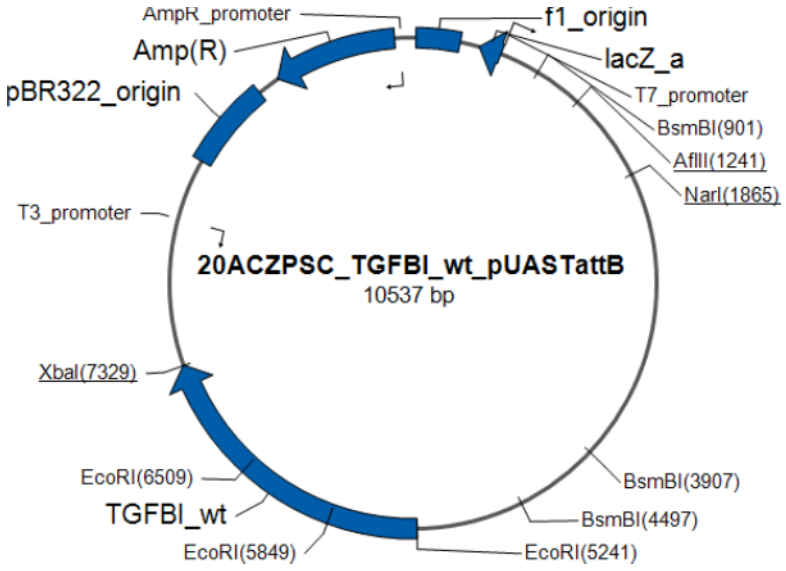

Figure 2.5: *TGFBI-wild type* subcloned from plasmid construct 20ACZPSC into *Drosophila*-specific plasmid pUASTattB for embryo microinjection. The sequence is shown in **Appendix 9.1.1.**

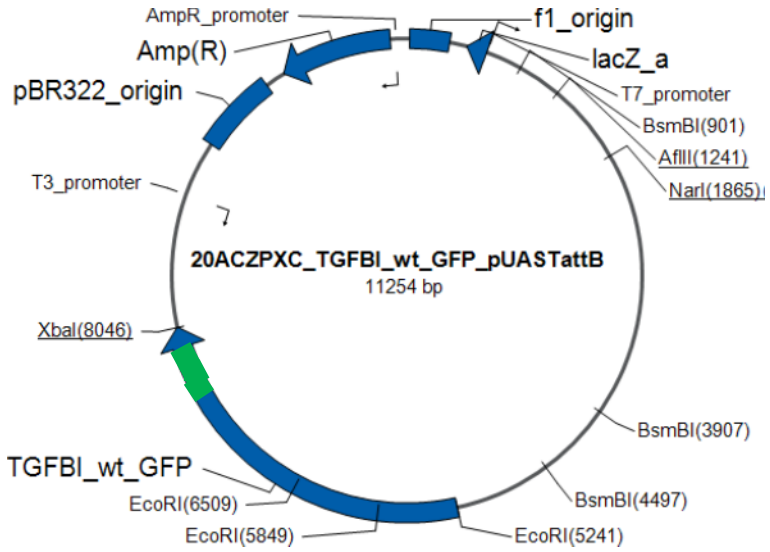

Figure 2.6: *TGFBI-wild type* with a C-terminus GFP tag subcloned from plasmid construct 20ACZPXC into *Drosophila*-specific plasmid pUASTattB for embryo microinjection. GFP (shown in green) is inserted into *TGFBI* just before the TAG stop codon. The sequence is shown in **Appendix 9.1.6.**

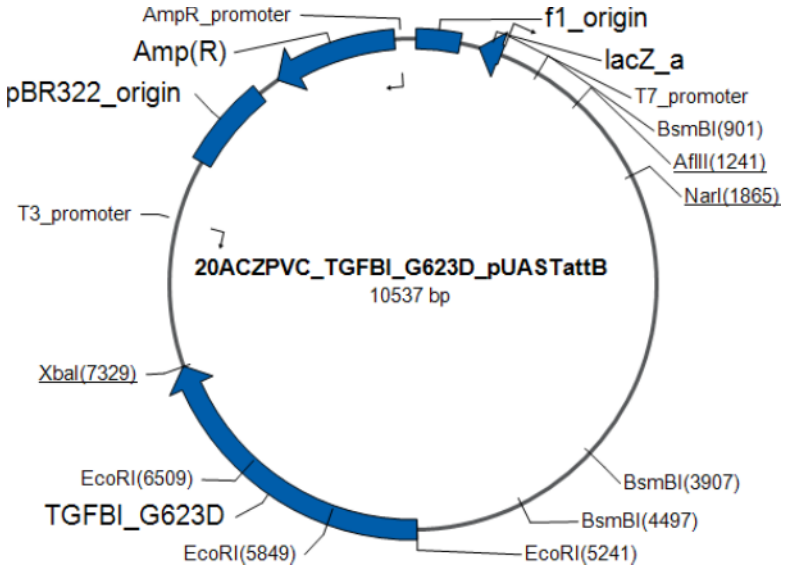

Figure 2.7: *TGFBI-G623D* subcloned from plasmid construct 20ACZPVC into *Drosophila*-specific plasmid pUASTattB for embryo microinjection. *TGFBI-G623D* is equivalent to wild type except for a single amino acid change. The sequences are shown in **Appendix 9.1.4.**

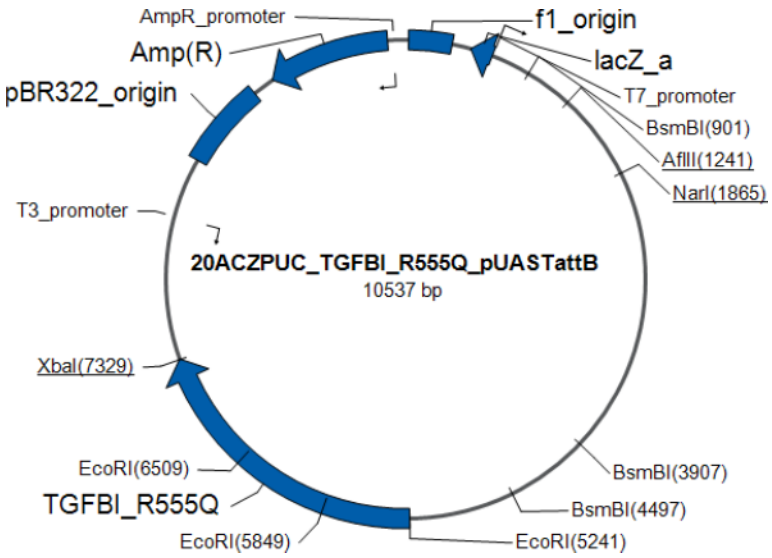

Figure 2.8: *TGFBI-R555Q* subcloned from plasmid construct 20ACZPUC into *Drosophila*-specific plasmid pUASTattB for embryo microinjection. *TGFBI-R555Q* is equivalent to *TGFBI*-wild type except for a single amino acid change. The sequences are shown in **Appendix 9.1.3.**

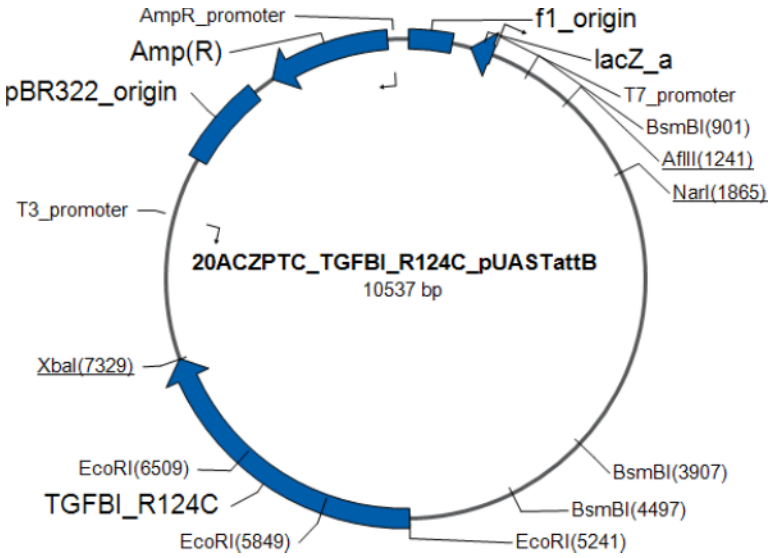

Figure 2.9: *TGFBI-R124C* subcloned from plasmic construct 20ACZPTC into *Drosophila*-specific plasmid pUASTattB for embryo microinjection. *TGFBI-R124C* is equivalent to *TGFBI* wild type except for a single amino acid change. The sequences are shown in **Appendix 9.1.2.**

2.3.8 RESTRICTION DIGESTION TO CONFIRM FINAL IDENTITY

Restriction digestion of pUASTattB plasmids was carried out with EcoRI and XbaI (New England BioLabs®, Ipswich, MA, USA) following the manufacturer's protocol, producing the predicted restriction digestion products. Briefly, 1 µL of restriction enzyme, 1 µg DNA, 5 µL 10X NEBuffer, and distilled water were mixed to make a reaction volume of 50 µL and incubated at 37°C for 15 minutes. The reaction was inactivated at 65°C for 20 minutes, and the products run on a 1 % agarose gel (Merck S. A., Darmstadt, Germany) for 90 minutes at 120V in 1X TAE buffer (Merck S. A., Darmstadt, Germany). Visualization of DNA was facilitated by SYBR Green DNA Gel Stain (Thermo Fisher Scientific, Waltham, MA, USA).

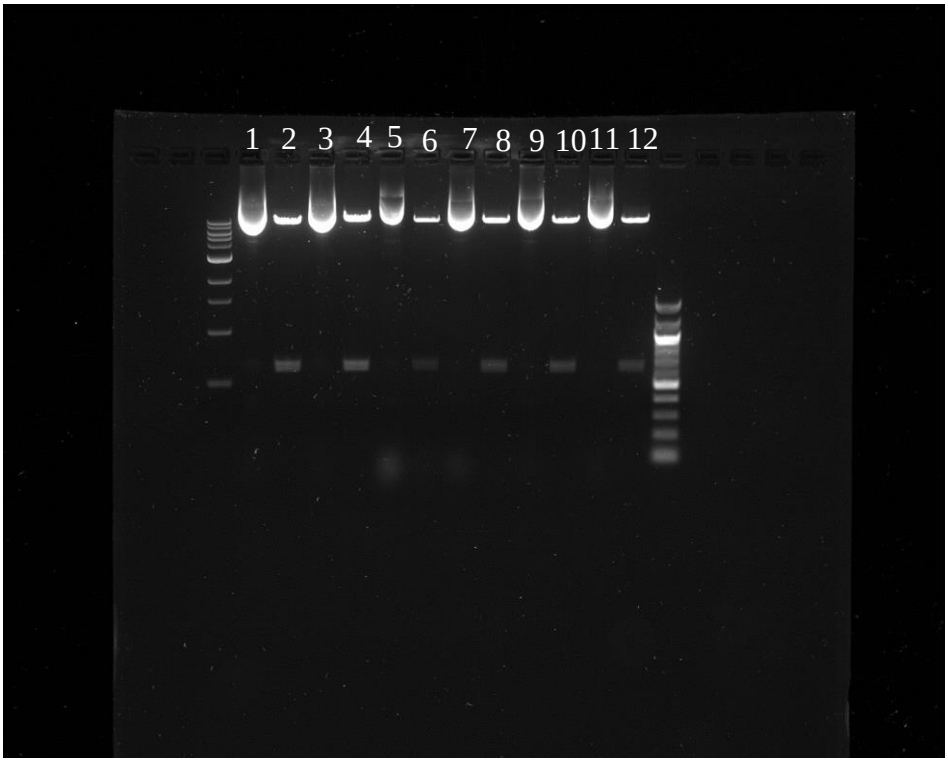

Figure 2.10: Restriction enzyme confirmation (EcoRI and XbaI) of genetic constructs. Lane 1: pUASTattB with *mfas-G623D*. **Lane 2:** pUASTattB with *mfas-G623D* excised with restriction endonucleases. **Lane 3**: pUASTattB with *TGFBI-wild type*. **Lane 4:** pUASTattB with *TGFBI-wild type* excised with restriction endonucleases. **Lane 5:** pUASTattB with *TGFBI-G623D*. **Lane 6:** pUASTattB with *TGFBI-G623D* excised with restriction endonucleases. **Lane 7**: pUASTattB with *TGFBI-H626R*. **Lane 8:** pUASTattB with *TGFBI-H626R* excised with restriction endonucleases. **Lane 9:** pUASTattB with *TGFBI-R555Q*. **Lane 10:** pUASTattB with *TGFBI-R555Q* excised with restriction endonucleases. **Lane 11:** pUASTattB with *TGFBI-R124C*. **Lane 12:** pUASTattB with *TGFBI-R124C* excised with restriction endonucleases. **DNA ladders: Left:** 1 kb ladder (New England Biolabs). **Right:** 500 bp ladder (Thermo Fisher Scientific). The entire plasmid construct is roughly 11 kb, while the excised genes are about 2 kb.

2.3.9 MICROINJECTION OF EMBRYOS TO CREATE TRANSGENIC LINES CARRYING THE DESIRED CONSTRUCTS

This work was done at the Fly Facility, Department of Genetics, Downing Street, University of Cambridge, Cambridge CB3 3EH, UK, with the support of a grant awarded

to Preman Singh from the Balliol Interdisciplinary Institute (BII). An overview of the genome integration scheme is depicted below (**Figure 2.11**).

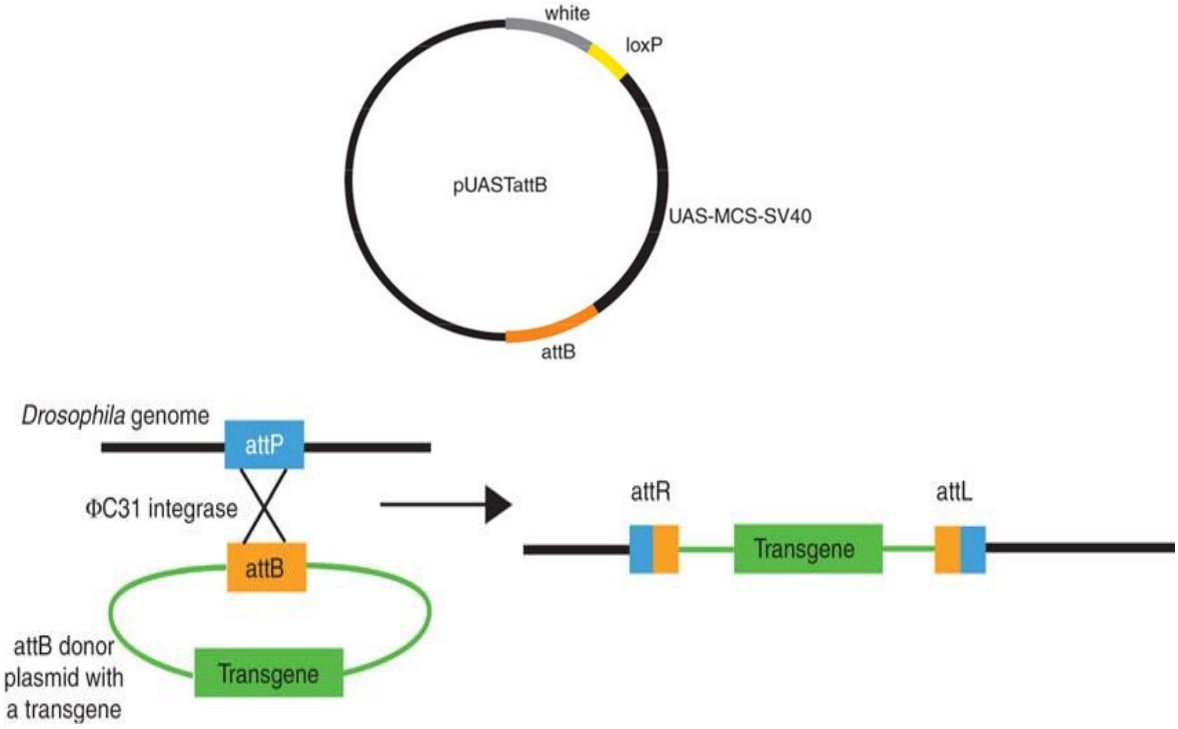

Figure 2.11: Integration of pUASTattB into the Drosophila genome following embryo microinjection.

2.4 *DROSOPHILA* HUSBANDRY

Fruit flies were reared at 18°C on standard cornmeal agar medium with the following composition per litre: 12.5 g agar (F. Gutkind & Co., Ltd.), 75 g cornmeal (B.T.P. Drewitt), 93 g D-(+)-glucose (Sigma-Aldrich®, a subsidiary of Merck), 31.5 g inactivated yeast (Fermipan Red, Lallemand Baking), and 8.6 g potassium sodium tartarte tetrahydrate (Sigma-Aldrich®). Flies were raised in plastic vials (B.T.P. Drewitt) plugged with cotton balls (Fisherbrand®, a subsidiary of Thermo Fisher Scientific), or larger plastic bottles (F-L Plastics Ltd.) plugged with cotton. They were transferred onto fresh medium every 3-4 days.

2.5 CONTROL OF TRANSGENE EXPRESSION IN SECONDARY CELLS

Secondary cell-specific transgene expression was achieved using the yeast *GAL4-UAS* transcriptional regulatory system, previously adapted for use in *Drosophila* (Brand and Perrimon, 1993). This method relies on a powerful transcription activator, *GAL4*, which induces the expression of transgenes (including RNAis, overexpression constructs, and fluorescent-tagged proteins) with a UAS (Upstream Activating Sequence) enhancer sequence. Several different GAL4 lines were used, all of which specifically expressed *GAL4* in secondary cells within the male accessory glands (Leiblich *et al.,* 2012, Corrigan *et al.,* 2014). However, the levels of GAL4 expression, and the other types of cells within the fly that also expressed *GAL4* depend on the enhancer element driving *GAL4.* Temporal regulation of transgene expression was achieved by combining *GAL4-UAS* with *tubulin-GAL80^{ts}*, a ubiquitously expressed, temperature-sensitive transcriptional repressor (McGuire *et al.,* 2003). Flies with this combination of genes were maintained at 25°C during developmental stages, a temperature at which GAL80^{ts} reliably prevents GAL4 from driving transcription of the *UAS-transgene* (a technique known as Temporal and Regional Gene Expression Targeting, or TARGET) (McGuire *et al.,* 2004). Upon eclosion, flies were transferred to 28.5°C, thereby inactivating GAL80^{ts} and terminating its repression of GAL4, which then activates transcription of the *UAS-transgene*. The result is an array of SC-specific phenotypes in male flies which are readily imaged and analyzed.

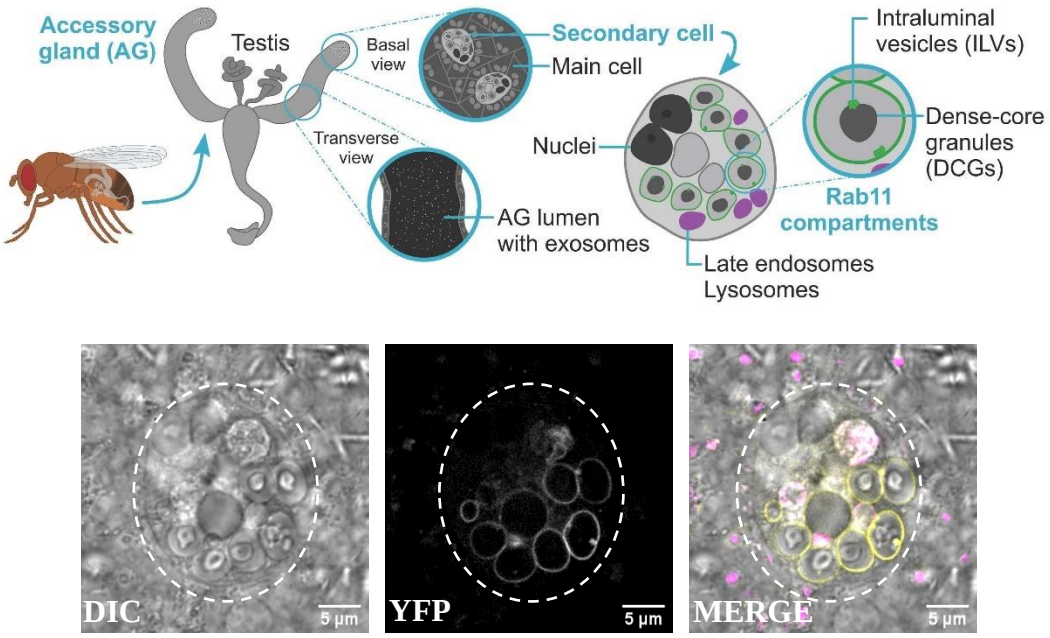

Figure 2.12: Top panel: Following the creation of transgenic flies, accessory glands in males were dissected and imaged. (Adapted from Dar *et al.*, Nat. Commun. 2021, Pg. 6). **Bottom panels:** Live cell imaging shows secondary cells, and the cellular fate of Midline Fasciclin, the amyloid protein which comprises DCGs. **Bottom left:** polarized light channel. **Bottom middle:** YFP channel. **Bottom right:** merged channels showing DCGs within Rab11 compartments. This also confirms that compartment identity is preserved.

The paired male *Drosophila* AGs are the equivalent of the human prostate and seminal vesicles in regard to their seminal fluid-producing function (reviewed in Wilson *et al.*, 2017). The distal third of each gland has 40 large binucleate SCs, each containing 7-11 DCGs. The power and elegance of this system lies in the fact that with simple genetic crosses, designer transgene expression in specific genetic backgrounds can be achieved. The effect then of these various designer proteins and RNAis that they can be precisely measured and quantified through their effects on a DCG marker (GFP-MFAS, an amyloid protein which has turned out to be a reliable and sensitive barometer of a myriad of cellular influences (see **Chapter 3**) and on compartment identity (assessed by specific Rab gene traps; **Figure 2.12** - above). It's reliability is proven by its immutability even in the face of

genetic perturbations severe enough to affect the very viability of the rest of the cell. It's sensitivity is demonstrated in it's overwhelming response to the tiniest alterations in relevant genes.

2.6 MICRO-DISSECTION OF ACCESSORY GLANDS

Adult male flies were anaesthetized using carbon dioxide gas, following which micro-dissection was performed using forceps (5-Dumostar®, B. Dumont, Switzerland) under a dissection microscope (EMZ stereo microscope mounted on a 'P' type pole stand, Meiji Techno, Japan) with an LED light source (LED F1, Photonics). To prevent damage to the forceps, micro-dissection was carried out on a silicone cushion (Sylgard® 184 184 Silicone Elastomer, Dow Corning) in a plastic petri dish (Greiner Bio-One International). During the micro-dissection procedure, anaesthetized flies were submerged in a pool of ice-cold 1X PBS (pH 7.4, Gibco®, Thermo Fisher Scientific) for live samples, or alternatively in 4 % paraformaldehyde (Sigma-Aldrich®) dissolved in 1X PBS at room temperature (around 22°C) for fixed samples. The entire male reproductive tract was carefully pulled out of the abdominal cavity, the testes were removed by scission close to the seminal vesicles to prevent them from obscuring the accessory glands during imaging. Care was taken to prevent damage to the papilla of the anterior ejaculatory duct by keeping the seminal vesicles and vas deferens attached. The accessory gland epithelium can be stressed by damage to this valve-like papilla, through which the spermatozoa and accessory gland contents are transferred during mating (Bairati, 1968). Finally, the remaining reproductive tissues, including the accessory glands, were isolated by separation of the ejaculatory bulb from the external genitalia, fat tissues and gut.

2.7 LYSOTRACKER™ STAINING OF LIVE ACCESSORY GLANDS

The isolated accessory glands were transferred using glass Pasteur pipettes (Fisherbrand®) to clear 1.7 microtubes (Axygen®) containing 1X PBS and kept on ice until sufficient numbers had been obtained. Glands were then incubated with either ice-cold 200 nM LysoTracker™ Red DND-99 (Invitrogen™, Thermo Fisher Scientific) or ice-cold 100 nM LysoTracker™ Deep Red (Invitrogen™, Thermo Fisher Scientific) in 1X PBS for 5 minutes. Finally, the glands were washed in ice-cold 1X PBS for 1 minute before mounting.

2.8 MOUNTING OF LIVE ACCESSSORY GLANDS

Glands were mounted onto High Precision microscope cover glasses thickness No. 1.5H (Marienfeld-Superior). A custom-built holder secured the cover glasses in place during imaging. To avoid dehydration and hypoxia, the glands were carefully maintained in a small drop of 1X PBS, surrounded by 10S Voltalef® (VWR), an oxygen-diffusible hydrocarbon oil (Parton *et al*., 2010), and kept stably in place by the application of a round 13 mm cover glass (VWR).

2.9 FIXATION OF ACCESSORY GLANDS FOR CONFOCAL MICROSCOPY

Following micro-dissection, the isolated accessory glands were transferred using glass Pasteur pipettes to clear 1.7 ml microtubes containing 4 % w/v paraformaldehyde in 1X PBS. They were incubated for 20 minutes in the fixative solution at room temperature (about 22°C) before being processed for immunostaining (see later sections). If they did not require staining, they were washed in 1X PBS for 5 minutes prior to mounting.

2.10 MOUNTING OF FIXED ACCESSORY GLANDS FOR CONFOCAL MICROSCOPY

Accessory glands were mounted onto SuperFrost® microscope slides (VWR). Excess liquid was removed using lint-free tissue and glands were immersed in a drop of Vectashield with or without DAPI (Vector Laboratories). Finally, they were covered with a 22 X 22 mm thickness No. 1 coverslip (Fisherbrand®) and sealed with nail varnish (Natural Collection, Boots, UK). The prepared slides were stored at 4°C, but were brought to room temperature 15 minutes prior to imaging.

2.11 WIDE-FIELD MICROSCOPY

For wide-field imaging, fixed or living accessory glands were imaged using a DeltaVision Elite wide-field fluorescence deconvolution microscope (GE Healthcare Life Sciences equipped with a set of Olympus UPlanSApo objectives including a 100X NA 1.4 oil objective, a 60X NA 1.42 oil objective, a 20X NA 0.75 objective, and a 10X NA 0.4 objective fitted with a CoolSNAP HQ2 CCD camera (Photometrics®) and a 7 colour illuminations system (SPECTRA light engine®), Lumencor). A 1.6X auxiliary magnification lens and objective immersion oil with a refractive index of 1.514 (Cargille Labs) were used throughout. The microscope room was temperature-controlled at 18°C. The images acquired were typically Z-stacks spanning a depth of 8-12 μM with a Z-distance of 0.2 μM. Images were subsequently deconvolved using the Resolve 3D-constrained iterative deconvolution algorithm within the SoftWoRx 5.5 software package (GE Healthcare Life Sciences).

2.12 CONFOCAL MICROSCOPY

Fixed accessory gland samples were imaged on an LSM5 10 Meta Scanning confocal microscope (Axioplan 2, Carl Zeiss) equipped with a 63X NA 1.4Plan APO oil DIC objective (Carl Zeiss) and operated using LSM 510 Meta software. Refractive index 1.518 objective immersion oil (Leica) was employed. Images were acquired at 1.7X zoom, and the microscope was kept at 20°C during experiments. The images were typically Z-stacks spanning a depth of 10 μM with a Z-distance of 5 μM.

2.13 IMAGE ANALYSIS AND FIGURE PRESENTATION

All image analysis was undertaken using ImageJ2 (Schindelin *et al.,* 2015), distributed by Fiji (Schindelin *et al.,* 2012). Detailed accounts of particular analytical methods are provided in other relevant sections. Global image brightness and contrast were regularly adjusted during image production, and figures were prepared using PowerPoint (Microsoft).

2.14 SUBCELLULAR COMPARTMENT ANALYSIS

Secondary cell compartment numbers were manually analysed in ImageJ2 using the Cell Counter plugin. Complete Z-stacks of individual cells were scored for the number of large non-acidic compartments (LysoTracker Red-negative, > 2 μM in diameter) and the number of MVBs (LysoTracker Red-positive, > 2 μM in diameter). The diameter of the largest MVB was measured manually at the Z-plane where the diameter was at its greatest using the line tool (see Corrigan *et al.,* 2014; Redhai *et al.,* 2016). Both fluorescently labelled and non-transgenic w1118 or rosy-RNAi flies were analysed using a combination of fluorescence and DIC microscopy on the Delta-Elite microscope. Three individual

secondary cells per fly (6-10 flies per genotype) were used to calculate the mean compartment number per genotype.

2.15 CHARACTERISATION OF SECONDARY CELLS BY LIGHT MICROSCOPY

Previous work in the Wilson laboratory demonstrated that the unique morphology of *Drosophila* secondary cells makes them ideal for the study of evolutionarily conserved secretory processes (Leiblich *et al.*, 2012, Corrigan *et a*l., 2014, Redhai *et al.*, 2016). The accessory gland epithelium is composed of two binucleate cell types, main cells and secondary cells, which are morphologically distinct and have different gene expression profiles (Bairati, 1968; Bertram *et al.*, 1992; Corrigan *et al.*, 2014; Leiblich *et al.*, 2015). Secondary cells have a rich network of rough endoplasmic reticulum, numerous Golgi complexes and mitochondria, and 1-2 prominent acidic compartments. They also have several large oval compartments which contain dense-core granules surrounded by tubular filaments called filamentous bodies. Main cells, the other cell type, also contain extensive rough endoplasmic reticulum and abundant Golgi complexes, but no dense-core granule compartments. Recent ultrastructural studies of secondary cells in the Wilson lab confirmed and refined all these observations (Corrigan *et al.*, 2014; Redhai *et al.*, 2016).

2.16 EXOSOME SECRETION ASSAY

Exosome secretion was measured according to the method described by Corrigan (Corrigan *et al.*, 2014) and Redhai (Redhai *et al.*, 2016). Briefly, three areas of lumenal fluorescent puncta constituting exosomes or aggregates of exosomes were sampled within the central third of each accessory gland, using identical microscopy equipment and settings. At each location, three different Z-stacks were analyzed, with each Z-stack measuring 10 μm in

thickness, and with the incremental interval in each Z-stack being 2 μm. The raw data from each lumenal area was thresholded in ImageJ using the Kapur-Sahoo-Wong maximum entropy model (Kapur *et al.,* 1985) in order to determine the outlines of GFP-fluorescent particles. The 'Analyze Particles' function was used to determine the total fluorescent area per sample. This method of analysis was found to be preferable to particle counting, which can underrepresent clusters of small vesicles. The mean fluorescent area from the three sample areas was then calculated for each accessory gland (n=10).

2.17 STATISTICAL ANALYSIS

Three SCs were scored per animal, two in one AG lobe, and one in the other. The average of these three values was then used as the data point for the parameter being measured. Six to ten animals were used per experiment, and each experiment was done thrice (hence the three means shown in the graphs). This statistical approach is based on the concept of 'SuperPlots', which allow the depiction of both "cell-to-cell and sample-to-sample variation" (Lord et al, 2020, pg. 1; Altman and Krzywinski, 2015). This analytical approach has been used in assessing all the ensuing data in this thesis. All data were collected using Excel (Microsoft) and subsequently analysed using GraphPad Prism. The Shapiro-Wilk test was then used to assess the normality of the datasets, and Levene's test was used to evaluate the equality of variances. If the datasets were normally distributed and showed equal variance between groups, then a One-Way ANOVA test was employed, with post-hoc Dunnett's Two-Tailed T test used to directly compare control and experimental groups. If datasets were not normally distributed and/or showed unequal variance between groups, then a Kruskal-Wallis test was used, with post-hoc Bonferroni-adjusted pairwise Mann-Whitney-Wilcoxon tests used to compare the control and experimental groups.

CHAPTER 3

THE ESTABLISHMENT OF CONTROLS AND THE BIOLOGY OF MFAS

3. THE ESTABLISHMENT OF CONTROLS AND THE BIOLOGY OF MFAS

3.1 INTRODUCTION

Eukaryotic cells secrete proteins both constitutively and in a regulated manner, examples of the latter being pituitary, pancreatic, adrenal chromaffin, and various neuronal cells, which package their biologically active cargoes into dense-core granules (DCGs) (Gondré-Lewis *et al.*, 2012). Studying the production of DCGs in these diverse cell types has uncovered several common underlying physiological principles governing their formation. These include the requirement of granins for compartment budding and DCG assembly (Day and Gorr, 2003), the interplay of the lipid metabolism regulatory enzymes phospholipase D1 and diacyclglycerol along with cholesterol and raft-like lipid structures for the funnelling of cargoes into nascent DCG compartments in the trans-Golgi network (Tsuchiya *et al.*, 2010; Sidhanta *et al.*, 2000), specific pH and calcium ion concentration requirements (Wu *et al.*, 2001; Yoo and Albanesi, 1990), and the presence of cytosolic adaptor proteins like the AP-1 coatamer complex and the small G-protein Arf1 for the maturation of DCG compartments (Traub *et al.*, 1993; Stamnes and Rothman, 1993). These now-mature DCG compartments then release their cargoes extracellularly by fusing with the plasma membrane in a process which requires vesicle-associated membrane proteins and Ca^{2+}-dependent synaptotagmins (Messenger *et al.*, 2014). The Rab proteins are another set of molecules integral to the process of regulated secretion. Rabs (Ras-related in brain) are small GTPases which control vesicle transport and membrane targeting. Each Rab is localized to a specific subcellular compartment and regulates a membrane trafficking step within both endocytic and exocytic pathways (reviewed in Wandinger-Ness and Zerial, 2014). Rab proteins are evolutionarily conserved and often ubiquitously expressed, with

over 60 being encoded by the human genome and 31 by the *Drosophila* genome (Zhang *et al.,* 2007), of which half are exclusively expressed in *Drosophila* neurons (Chan *et al.,* 2011). Work in the Wilson laboratory has shown that Rab6 to Rab11 transition is required for the formation of DCGs (Corrigan *et al.,* 2014; Redhai *et al.,* 2016; Prince *et al.,* 2019; Fan *et al.,* 2023; Wells *et al.,* 2023), which, taken in conjunction with the Rab6 and Rab11 connections of neurodegeneration, provides a compelling reason to examine whether manipulation af amyloid proteins affects the identity of these compartments.

The unfolding role of Rab proteins in the trafficking of Aβ and Tau has uncovered strong associations between Rab dysfunction, Alzheimer's disease, Parkinson's disease, Huntington's disease, Amyotrophic Lateral Sclerosis, Charcot-Marie-Tooth disease types 2B and 4, and other neurodegenerative conditions (reviewed in Zhang *et al.,* 2019, and in Kiral *et al.,* 2018). Specifically, Rab6 is implicated in Alzheimer's disease (Scheper *et al.,* 2007; Soejima *et al.,* 2013) while Rab11 is associated with Parkinson's disease (Breda *et al*., 2015), Huntington's disease (Li *et al.,* 2009), Amyotrophic Lateral Sclerosis (Deshpande *et al*., 2016; Farg *et al*., 2014) and Charcot-Marie Tooth disease (Roberts *et al.,* 2010).

3.1.1 EXPERIMENTAL APPROACH

In the ensuing experiments, the yeast GAL4 sysytem was used (Kakidane and Ptashne, 1988; Webster *et al.,* 1988; Brand and Perrimon, 1993). In yeast, GAL4 regulates galactose metabolism, and binds to the Upstream Activator Sequence (UAS), thereby transcriptionally activating galactose utilization genes. In *Drosophila*, the system is bipartite, comprised of a transgenic driver line and a transgenic target gene line, with the

progeny of the cross expressing the transgene wherever GAL4 is expressed (see **Figure 3.1**). Using an N-terminally-tagged *GFP-mfas* gene trap line that also contains the *dsx-GAL4* driver, which is specifically expressed in SCs of the AG (w^{1118}*; tub-GAL80*^{ts}*/CyO; dsx-GAL4 mfas-GFP/TM6B*) I show that I can visualise DCGs by fluorescence microscopy. Furthermore, I demonstrate that this gene trap line does not affect DCG morphology. Furthermore, I show that expressing a control RNAi with this driver, rosy-RNAi (*UAS-ry-RNAi*) does not affect DCGs either.

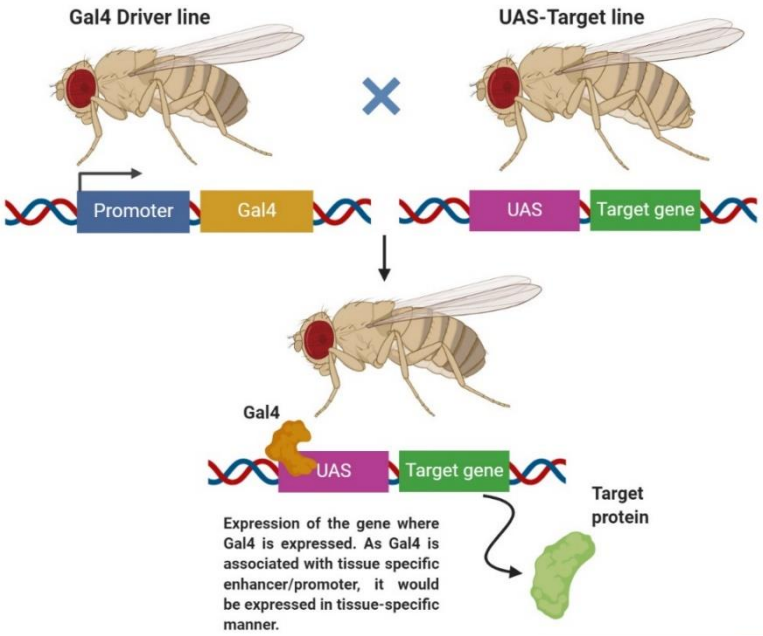

Figure 3.1: The GAL4 transcription system in *Drosophila*. The *dsx*-GAL4 driver is expressed in numerous cells types, but in the adult AG, it is only expressed in SCs. (Adapted from H. Oza, 2021).

3.2 RESULTS

3.2.1 THE N-TERMINALLY TAGGED *GFP-mfas* GENE TRAP LINE DOES NOT AFFECT DCGs

An N-terminally tagged *GFP-mfas* gene trap that had previously been identified in the laboratory was examined to determine whether it affected the morphology of DCGs and SCs in any way. *mfas* had been shown to be expressed at very high levels in the adult male AGs (**Table 3.1**), and preliminary assessment of the *GFP-mfas* gene trap expression indicated that the resultant fusion protein is heavily concentrated in the approximately 40 SCs of each lobe of the AGs (**Figure 3.2C**).

Symbol	Name	Annotation Symbol	FlyBase ID
mfas	midline fasciclin	CG3359	FBgn0260745

Gene FPKMs and Enrichments ☐ SDs ☐ Whole Body ☐ Male v. Female

	Adult Male		Adult Female		Larval	
Tissue	FPKM	Enrichment	FPKM	Enrichment	FPKM	Enrichment
Head	56	0.7	38	3.0		
Eye	31	0.4	19	1.5		
Brain / CNS	63	0.8	51	4.0	9.1	0.6
Thoracicoabdominal ganglion	60	0.7	60	4.7		
Crop	45	0.5	14	1.1		
Midgut	8.0	0.1	1.6	0.1	3.7	0.3
Hindgut	112	1.4	85	6.6	30	2.2
Malpighian Tubules	2.2	0.0	2.1	0.2	0.7	0.0
Rectal pad	73	0.9	56	4.3		
Salivary gland	30	0.4	9.0	0.7	9.1	0.6
Fat body	21	0.2	4.7	0.4	15	1.1
Heart	14	0.2	8.0	0.6		
Trachea					459	33
Ovary			7.7	0.6		
Virgin Spermatheca			86	6.7		
Mated Spermatheca			89	6.9		
Testis	93	1.1				
Accessory glands	888	11				
Carcass	44	0.5	16	1.2	11	0.8
Garland cells					38	2.7

Table 3.1: Expression pattern of *mfas* in various tissues. This shows the extremely high expression of *mfas* in adult male AGs **FPKM:** fragments per kilobase of transcript per million mapped reads. (Taken from flyatlas.gla.ac.uk, accessed on 11/3/2023).

I compared the number and morphology of DCGs in SCs expressing the *GFP-mfas* gene trap in a genetic background (the DTMFAS line) that included the SC-specific *dsx-GAL4* and the temperature-sensitive $GAL80^{ts}$ inhibitor which was inactivated in adults to switch on *GAL4* by increasing the temperature of fly culture from 25°C to 29°C. The number of DCGs and their morphology appeared to be unaffected when compared to SCs in control males, where DCGs can be visualized using differential interference contrast microscopy (DIC) (**Figure 3.2A-C, Figure 3.3**). Co-expression of a control RNAi, *ry-RNAi* under *dsx-GAL4* also had no effect on DCG properties (**Figure 3.2D**, **Figure 3.3**).

By contrast, an alternative *dsx-GAL4* line containing a genomic *mfas* construct tagged with GFP at its C-terminus altered the morphology, but not the number of SCs in DCGs (**Figure 3.4B, Figure 3.5**). In both lines, the fusion protein was incorporated into DCGs. The number of large non-acidic compartments, which includes between two and four DCG proteins which have not been assembled (Wells *et al.*, 2023) as well as DCG compartments, also remain unaltered by the *mfas-GFP* genomic construct (**Figure 3.5**).

Importantly, only about 80 % of males carrying the *GFP-mfas* gene trap had entirely spherical 'normal' DCGs. It was difficult to determine whether the small number of non-uniform DCGs are also present in SCs that do not express the *GFP-mfas* gene trap, because the defects were often not easy to recognize by DIC. In conclusion, the C-terminally-tagged MFAS-GFP protein disrupts DCG morphology in SCs without affecting the basic process of biogenesis. By contrast, the DTMFAS line permits expression of RNAis specifically in

SCs of the AG in combination with a GFP-MFAS fusion protein expressed at endogenous levels from a gene trap without any discernable effects on DCG number or morphology. This line was therefore employed in all subsequent experiments.

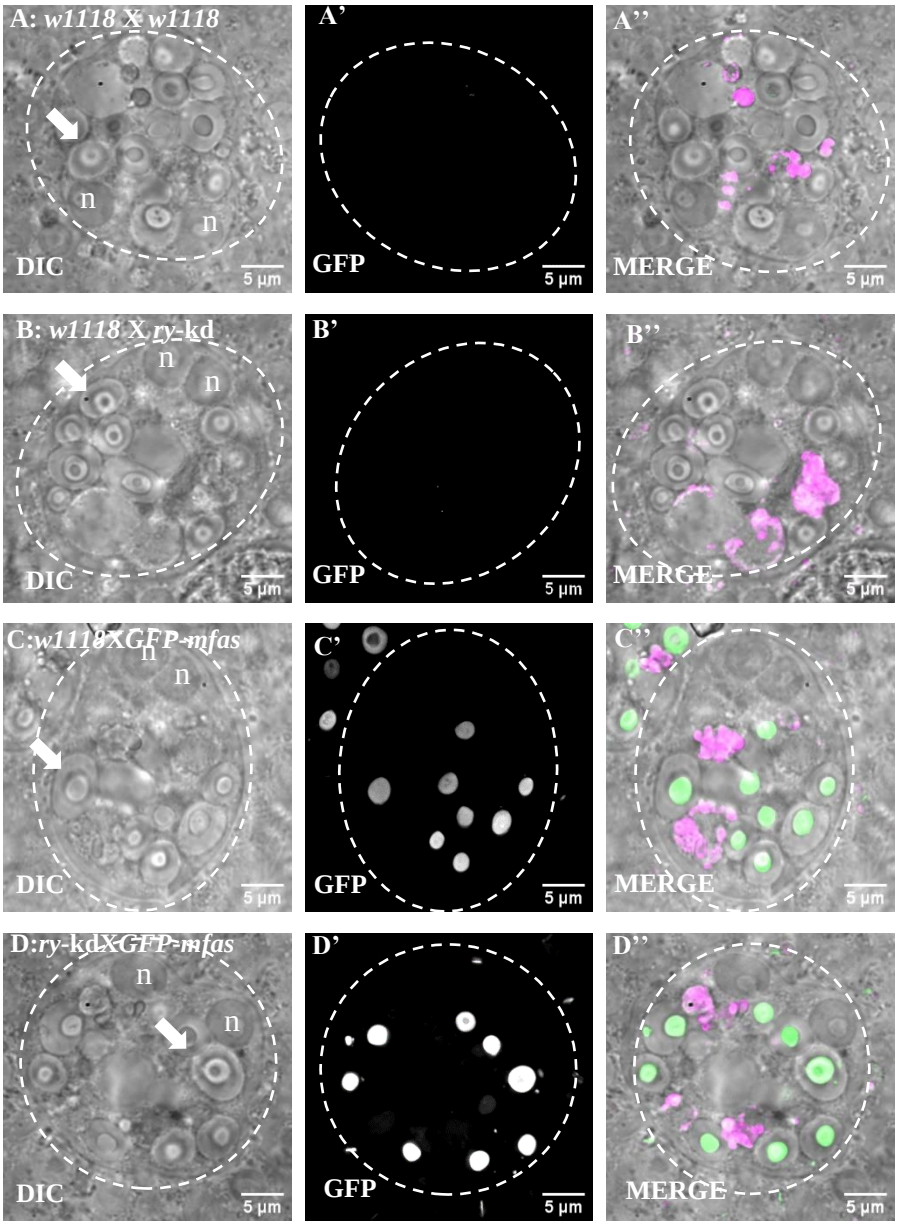

Figure 3.2: The N-terminally tagged *GFP-mfas* gene trap line does not affect DCG number or morphology in SCs. SCs from six-day-old virgin males stained with LysoTracker Red and imaged *ex vivo*, using differential interference contrast (DIC) and fluorescence microscopy for GFP and LysoTracker Red. **A)** w^{1118} X w^{1118}. **B)** w^{1118} X *UAS-ry-RNAi*. **C)** male fly with the genotype w^{1118}*; tub-GAL80*^{ts}*/+; dsx-GAL4 GFP-mfas/+*, progeny from the cross w^{1118} *X* w^{1118}*; tub-GAL80*^{ts}*/CyO; dsx-GAL4 GFP-mfas/TM6B* (DTMFAS with an N-terminal GFP tag) X w^{1118} **D)** male fly with the genotype w^{1118}*; tub-GAL80*^{ts}*/UAS-ry-RNAi; dsx-GAL4 GFP-mfas/+*, progeny from the cross *UAS-ry-RNAi* X DTMFAS with an N-terminal GFP tag X *y,sc,v; UAS-ry-RNAi*. **White arrows**: DCGs; **n:** double nuclei characteristic of SCs. All crosses had the same number of DCGs (**Figure 3.3**). DTMFAS X *UAS-ry-RNAi* was subsequently used as a control cross, since many other crosses involved RNAi constructs. Scale bar = 5µm.

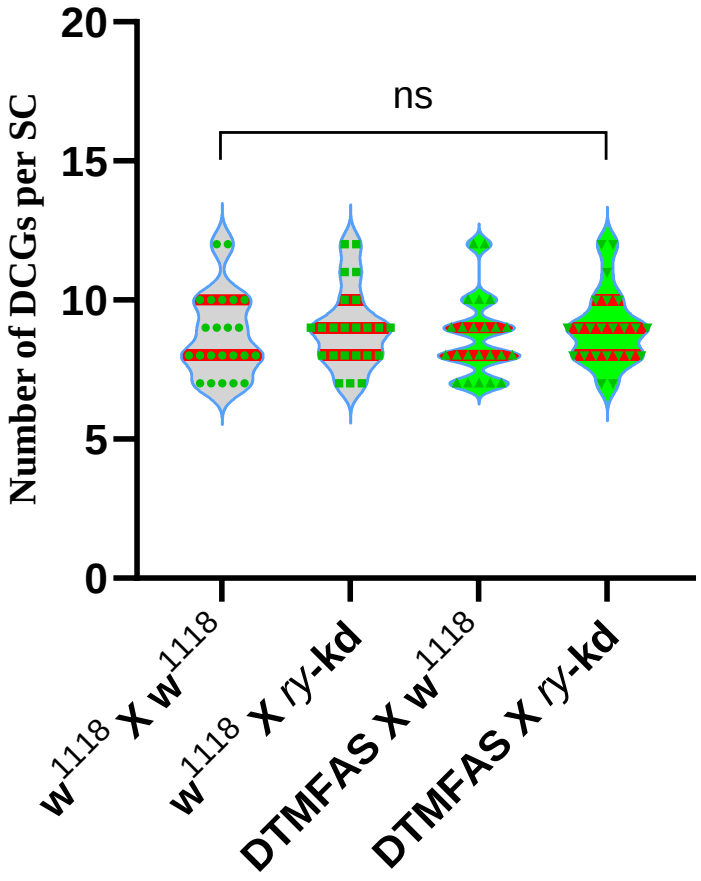

Figure 3.3: All control crosses produce males that have the same number of DCGs per SC (green bars signify crosses made with driver lines containing the *GFP-mfas* gene trap). Plots were produced by the SuperPlot method of Lord (Lord *et al*., 2020), and will be implemented in the the statistical analyses and graphical depictions through the rest of this thesis. This method enables analyses to be carried out on an animal-by-animal rather than a cell-by-cell basis, in order to avoid the overstating of significance. This is accomplished by 'superimposing summary statistics from repeated experiments on a graph of the entire cell-level dataset' (Lord *et al*., 2020, pg. 3). The mean for each set of experiments is shown in red.

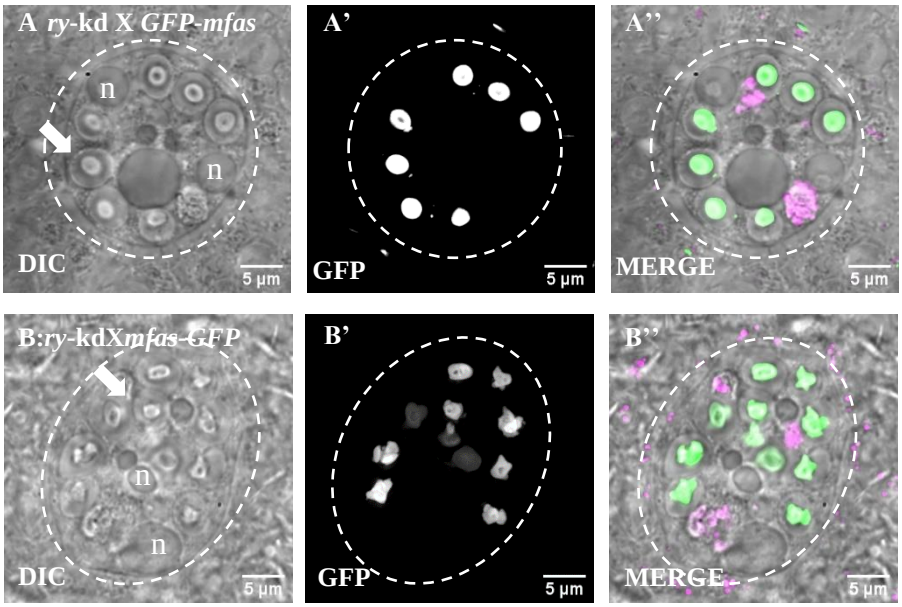

Figure 3.4: *mfas-GFP* (C-terminal attachment) disrupts normal DCG formation. SCs from six-day-old virgin males stained with LysoTracker Red and imaged *ex vivo*, using DIC and fluorescence microscopy for GFP and LysoTracker Red. **A)** Male fly with the genotype w^{1118}*; tub-GAL80*^{ts}*/UAS-ry-RNAi; dsx-GAL4 GFP-mfas/+*, progeny from the cross *UAS-ry-RNAi* X w^{1118}*; tub-GAL80*^{ts}*/CyO; dsx-GAL4 GFP-mfas/TM6B* (DTMFAS with an N-terminal GFP) X *y,sc,v; UAS-ry-RNAi* **B)** Male fly with the genotype w^{1118}*; tub-GAL80*^{ts}*/UAS-ry-RNAi; dsx-GAL4 mfas-GFP/+*, progeny from the cross *UAS-ry-RNAi* X DTMFAS with a C-terminal GFP X *y,sc,v; UAS-ry-RNAi*. **White arrows:** DCGs; **n:** double nuclei characteristic of each SC. Scale bar = 5 µm.

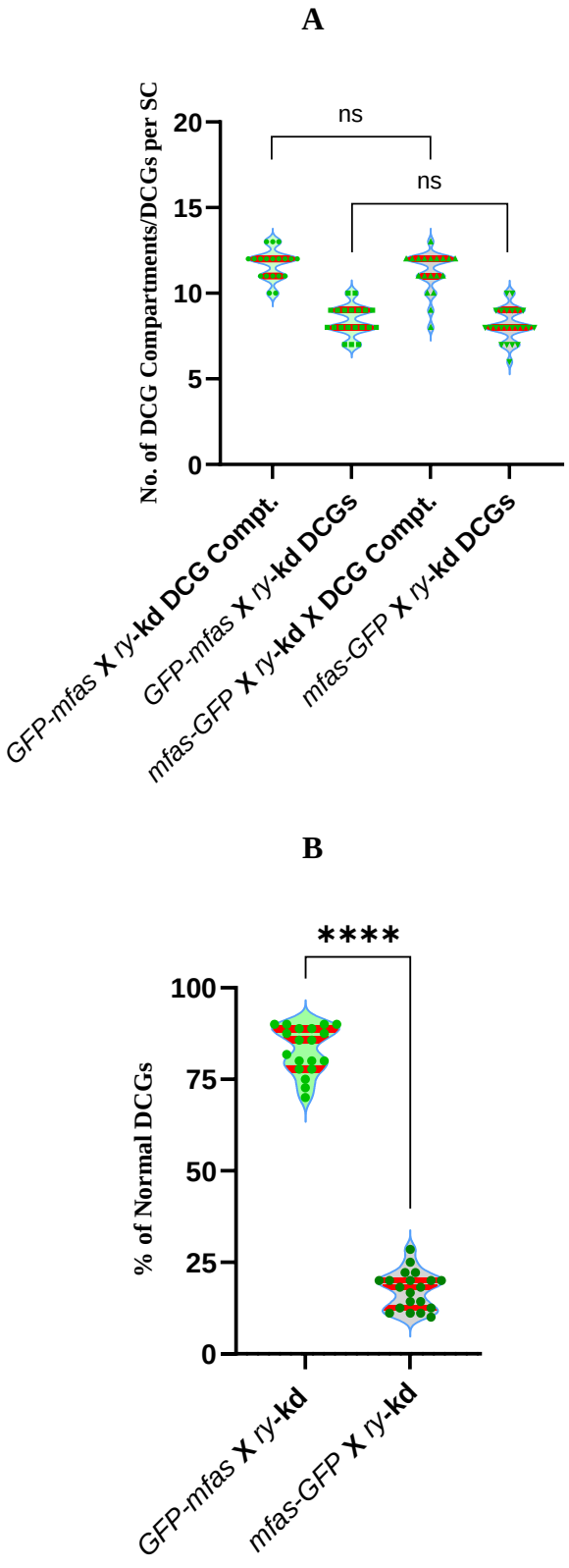

Figure 3.5: **A:** Driver lines with *GFP-mfas* (N-terminal GFP attachment) and *mfas-GFP* (C-terminal GFP attachment). Both show the same number of large non-acidic

compartments (which do not contain DCGs) and DCGs. **B:** The driver line with *GFP-mfas* (N-terminal GFP attachment) produces predominantly single large rounded DCGs (normal), while the driver line with *mfas-GFP* (C-terminal GFP attachment) produces predominantly misshapen DCGs. The mean for each set of experiments is shown in red.

This establishes that neither the presence of an RNAi (UAS-target line) nor the presence of a composite driver line with an N-terminal GFP attachment (GAL4 driver line), both of which were used throughout in subsequent experiments as control crosses, alter the phenotype. The establishment of this integrity of outcome assumes even greater importance in the interpretation of rescue experiments, which are presented later.

3.2.2 C-TERMINALLY GFP-TAGGED *mfas* AND *TGFBI* DISRUPT DCG BIOGENESIS

As part of my ongoing analysis of DCG biogenesis, I generated a series of transgenic lines carrying UAS constructs that permitted the expression of mutant and wild type versions of *mfas* and *TGFBI*, including one *TGFBI-GFP* C-terminal fusion construct. I tested whether this construct affected DCG morphology in a similar way to the *mfas-GFP* genomic construct. Wells *et al*. in 2023 have demonstrated that large DCG precursor compartments in SCs are formed at the face of the trans-Golgi and are all labelled by the small GTPase Rab6, which can be detected using a gene trap in which *CFP-Rab6* is expressed from the endogenous *Rab6* locus. I overexpressed *UAS-TGFBI-GFP* using *dsx-GAL4* or the *mfas-GFP* genomic construct in adult SCs containing the *CFP-Rab6* gene trap. Although the fluorescence of CFP and GFP cannot be fully separated, it was possible to distinguish the membrane-associated CFP-Rab6 from the GFP-labelled DCGs. For both constructs, the number of large Rab-compartments appeared normal (**Figure 3.6**), but most DCGs did not have normal rounded structure when compared to control *GFP-mfas* gene

trap SCs (**Figure 3.7**). Subsequent analysis of SCs overexpressing an untagged *UAS-TGFBI* construct (**Figure 3.6**) suggested that the GFP tag is responsible for DCG disruption, mirroring the finding with *mfas*. This suggests that disrupting the C-terminus of these molecules interferes with their ability to be incorporated into regular DCGs in SCs.

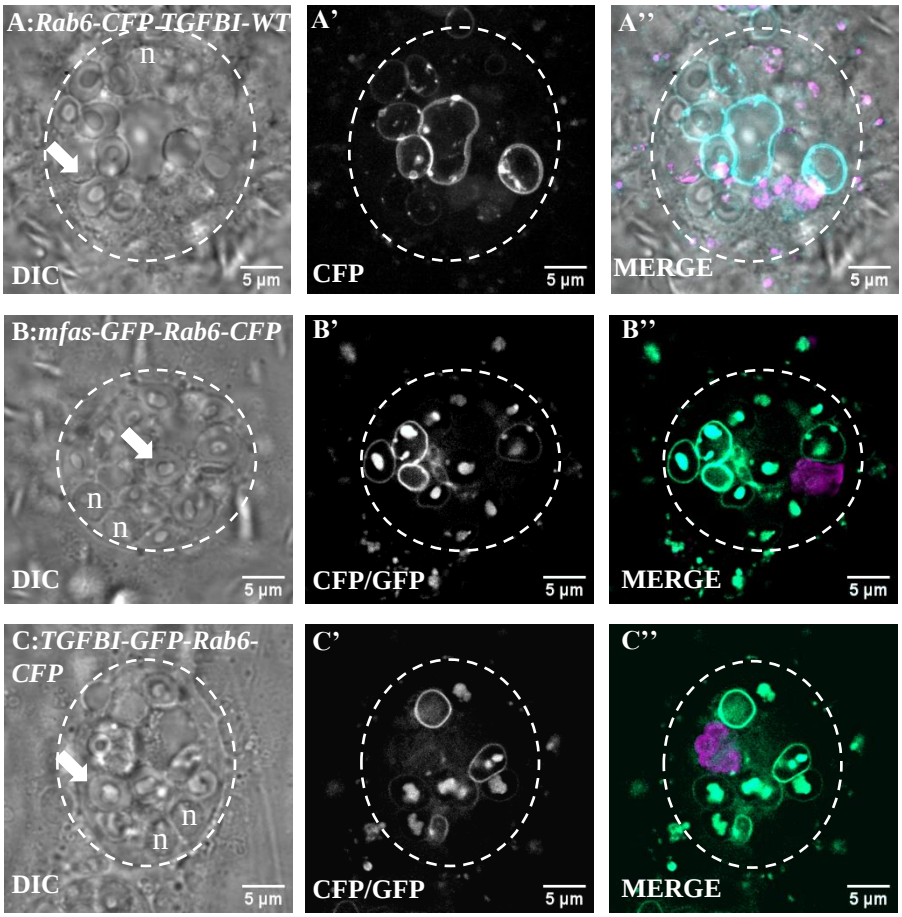

Figure 3.6: C-terminal *GFP* fusion constructs of *mfas* and *TGFBI* disrupt DCG biogenesis when overexpressed in SCs. SCs from six-day-old virgin males stained with LysoTracker Red and imaged ex vivo, using DIC and fluorescence microscopy for GFP, CFP and LysoTracker Red **A)** male fly with the genotype w^{1118}*; Rab6-CFP, tub-GAL80*^{ts}*/ TGFBI-Wild Type; dsx-GAL4/+*, progeny from the cross w^{1118}*; Rab6-CFP, tub-GAL80*^{ts}*/CyO; dsx-GAL4* X w^{1118}*; TGFBI-Wild Type/CyO* **B)** male fly with the genotype w^{1118}*; Rab6-CFP, tub-GAL80ts/mfas-GFP; dsx-GAL4/+*, progeny from the cross w^{1118}*; Rab6-CFP, tub-GAL80ts/CyO; dsx-GAL4 X w; mfas-GFP/CyO* (genomic construct containing *mfas* with a C-terminal *GFP* attachment) **C)** male fly with the genotype w^{1118}*; Rab6-CFP, tub-GAL80ts/UAS-TGFBI-GFP; dsx-GAL4/+*, progeny from the cross w^{1118}*; Rab6-CFP, tub-GAL80ts/CyO; dsx-GAL4 X w; UAS-TGFBI-GFP/CyO* (*TGFBI* with a C-terminal *GFP* attachment). **White arrows**: DCGs. **n:** double nuclei characteristic of each SC. Scale bar = 5 µm.

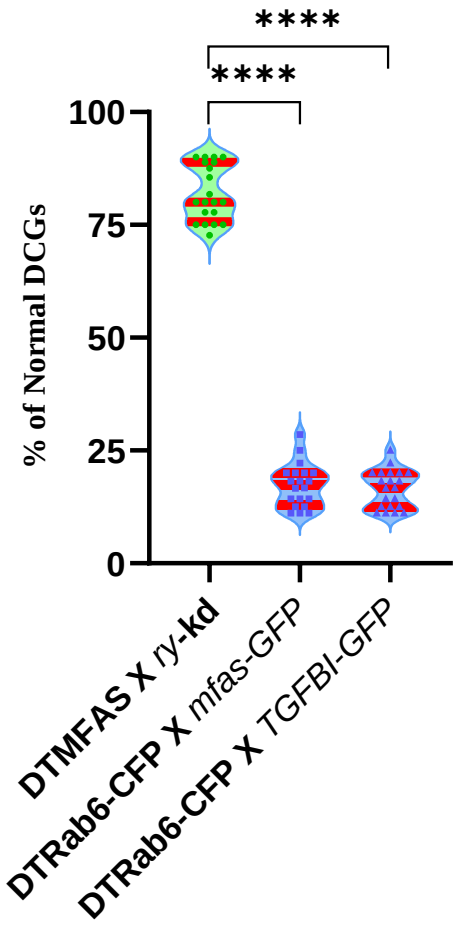

Figure 3.7: The driver line DTMFAS with *GFP-mfas* (*mfas* with *GFP* attached at the N-terminal) produces predominantly normal DCGs. However, crosses between a *Rab6-CFP* driver line and flies with a genomic *mfas-GFP* construct or a *UAS-TGFBI-GFP* transgene (both with *GFP* attached at the C-terminal) produce predominantly abnormal DCGs. The mean for each set of experiments is shown in red. The mean for each set of experiments is shown in red.

3.2.3 RESULTS REGARDING THE BIOLOGY OF MIDLINE FASCICLIN

In light of the very high expression of MFAS in SCs, its strong localisation in DCGs and the role of its homologue TGFBI in extracellular matrix (ECM) organisation and amyloid disease, I reasoned that it might have an important role in DCG biogenesis. SC DCGs themselves have been shown to play crucial roles in *Drosophila*; they store the fly

homologue of angiotensin-I converting enzyme (Rylett *et al.*, 2007), as well as Decapentaplegic, the fly homologue of mammalian bone morphogenetic protein (BMP) ligands BMP2 and BMP4. Decapentaplegic is the main driver of BMP-related processes in SCs, which include the regulation of DCG turnover and the control of *Drosophila* reproductive behaviours (Redhai *et al.*, 2016). For these experiments, *mfas* was knocked down by overexpressing two different *mfas-RNAi*s using the DTMFAS driver line.



Figure 3.8: *mfas-RNAis* act on different areas of *mfas*. *mfas-RNAi* 52905 Bloomington (dsRNA-HMCO3645, exon 4, red oval) and *mfas-RNAi* 58256 Bloomington (dsRNA-HMJ22320, exon 5, orange oval). (Taken from FlyBase, accessed on 12/3/2023).

In both cases, DCGs were completely eliminated from SCs (**Figure 3.9; Figure 3.10B**), even though these cells maintained the normal number of large non-acidic compartments (**Figure 3.9; Figure 3.10A**). Interestingly, the nuclear size in these knockdown cells was significantly reduced (**Fig. 3.10C**). Nuclear size has been used to measure growth in SCs,

which continues after eclosion for at least ten days (Leiblich *et al*., 2012). This growth is regulated in an autocrine fashion by Decapentaplegic (Dpp), which is packaged in DCGs (Redhai *et al.,* 2016), suggesting that disruption of DCGs suppresses the signalling by Dpp in these cells.

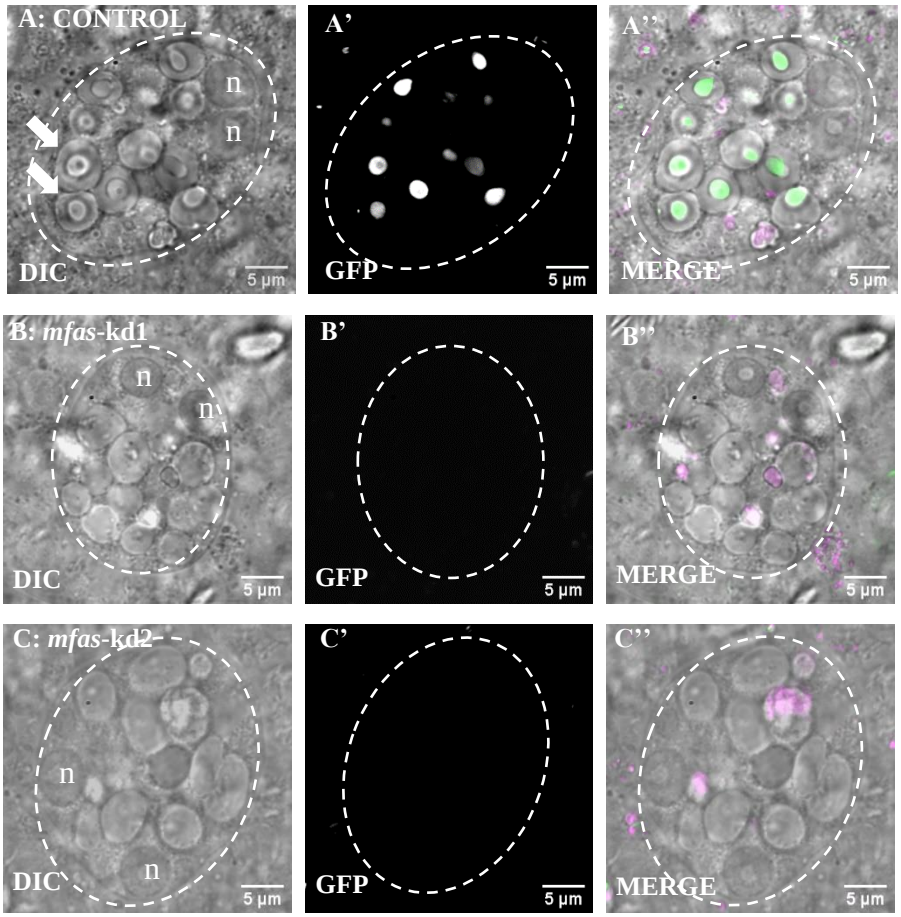

Figure 3.9: *mfas* knockdown prevents DCG formation. SCs from six-day-old virgin males stained with LysoTracker Red and imaged *ex vivo*, using DIC and fluorescence microscopy for GFP and LysoTracker Red. **A)** male fly with the genotype w^{1118}*; tub-GAL80^{ts}/UAS-ry-RNAi; dsx-GAL4 GFP-mfas/+* (control), progeny of w^{1118}*; tub-GAL80^{ts}/CyO; dsx-GAL4 GFP-mfas/TM6B* (DTMFAS) X *UAS-ry-RNAi*. **B)** male fly with the genotype w^{1118}*; tub-GAL80^{ts}/mfas-RNAi-1; dsx-GAL4 GFP-mfas/+*, progeny of DTMFAS X *UAS-mfas-RNAi-1* **C)** male fly with the genotype w^{1118}*; tub-GAL80^{ts}/mfas-RNAi-2; dsx-GAL4 GFP-mfas/+*, progeny of DTMFAS X *UAS-mfas-RNAi-2*. **White arrows** in **A:** DCGs; **n:** double nuclei characteristic of each SC. Scale bar = 5 µm.

A

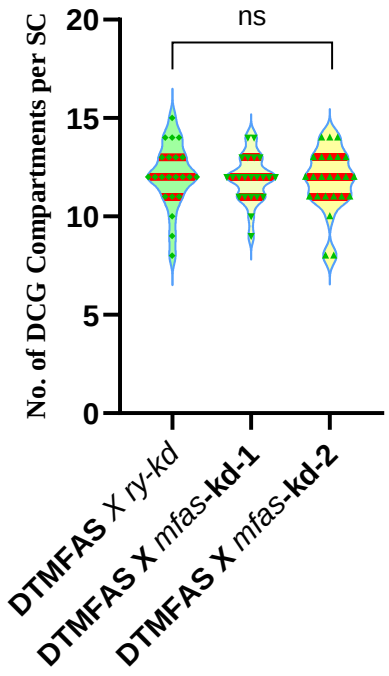
ns
No. of DCG Compartments per SC
20
15
10
5
0
DTMFAS X ry-kd
DTMFAS X mfas-kd-1
DTMFAS X mfas-kd-2

B

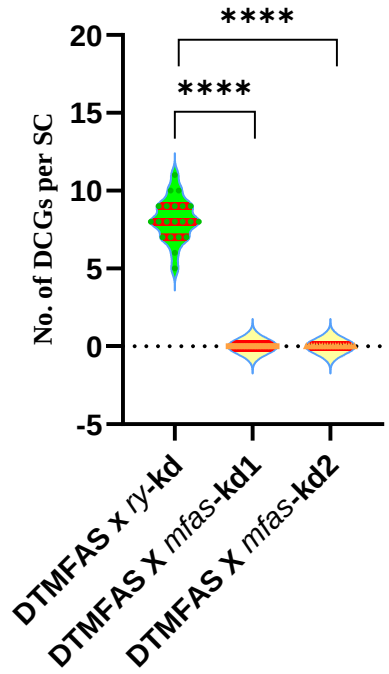
****
****
No. of DCGs per SC
20
15
10
5
0
-5
DTMFAS x ry-kd
DTMFAS X mfas-kd1
DTMFAS X mfas-kd2

C

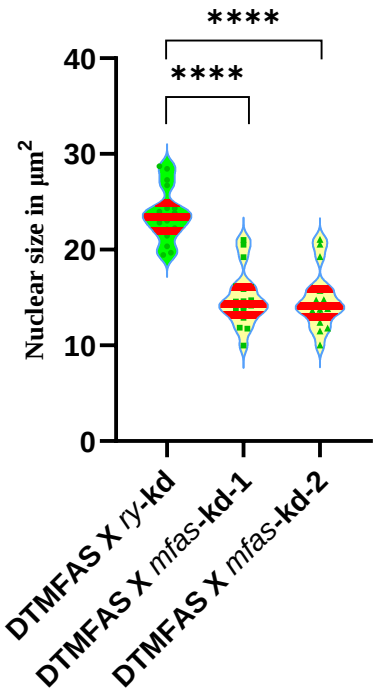

Figure 3.10: The effects of *mfas*-knockdown on DCG compartments, DCGs, and nuclear size of SCs. A: *mfas*-knockdowns have the same number of DCG compartments as controls. **B:** *mfas*-knockdowns block all DCG formation in SCs. **C:** *mfas*-knockdowns decrease nuclear size as compared to controls, suggesting autocrine activity. The mean for each set of experiments is shown in red.

3.2.4 THE RAB6 AND RAB11 IDENTITIES OF LARGE NON-ACIDIC COMPARTMENTS ARE UNAFFECTED BY *mfas* KNOCKDOWN

Rab (Ras-related in brain) proteins are small GTPases which control vesicle transport and membrane targeting. Each Rab is localized to a specific subcellular compartment and regulates a membrane trafficking step within both endocytic and exocytic pathways (reviewed in Wandinger-Ness and Zerial, 2014). Rab proteins are evolutionarily conserved and often ubiquitously expressed, with over 60 being encoded by the human genome and 31 by the *Drosophila* genome (Zhang *et al.*, 2007), of which half are exclusively expressed

in *Drosophila* neurons (Chan *et al.,* 2011). The emerging role of Rab proteins in the trafficking of Aβ and Tau has uncovered strong associations between Rab dysfunction, Alzheimer's disease, Parkinson's disease, Huntington's disease, Amyotrophic Lateral Sclerosis, Charcot-Marie-Tooth disease types 2B and 4, and other neurodegenerative conditions (reviewed in Zhang *et al.,* 2019, and in Kiral *et al.,* 2018). Specifically, Rab6 is implicated in Alzheimer's disease (Scheper *et al.,* 2007; Soejima *et al.,* 2013) while Rab11 is associated with Parkinson's disease (Breda *et al.*, 2015), Alzheimer's disease in terms of the secretion of cleaved forms of APP, Huntington's disease (Li *et al.,* 2009), amyotrophic Lateral Sclerosis (Deshpande *et al.,* 2016; Farg *et al.,* 2014) and Charcot-Marie Tooth disease (Roberts *et al.,* 2010). While I showed that *mfas* is central to the formation of DCGs in SCs, its wider influence on other cellular processes in these cells remained unknown. Experiments were therefore designed to explore whether *mfas*-knockdown influenced the identity of DCG compartments and their precursors. To do this, I tested whether *mfas*-knockdown altered the Rab identity of large non-acidic compartments in SCs, which might provide an alternative explanation for the loss of DCGs in these cells. The Rab identity of these specific compartments is particularly important, since work in the Wilson laboratory has shown that the transition from Rab6 to Rab11 is required for the formation of DCGs (Wells *et al.,* 2023) which, taken in conjunction with the Rab6 and Rab11 connections of neurodegeneration, provides a compelling reason to examine whether manipulation af amyloid proteins affects the identity of these compartments. Knockdown of *mfas* in SCs expressing a *CFP-Rab6* gene trap produced SCs that lacked DCGs (**Figure 3.11B, C**), unlike controls (**Figure 3.11A**), but the same number of large non-acidic compartments were labelled with Rab6 as were labelled in controls (**Figures 3.11** and **3.12A**). Following

the Rab6 to Rab11 transition, exosome biogenesis begins in the new Rab11-compartments, which can be visualised by the presence of Rab6-labelled puncta inside the lumen of Rab6-compartments (Wells *et al.*, 2023). The proportion of Rab6-compartments containing these puncta was unaltered by *mfas* knockdown (**Figure 3.11** and **3.12B**), suggesting that *mfas* does not affect exosome biogenesis or the Rab6 to Rab11 transition.

Indeed, knockdown of *mfas* in SCs expressing the *YFP-Rab11* gene trap led to the inhibition of formation of all DCGs (**Figure 3.13B, C**), but the number of Rab11-positive large non-acidic compartments also remained unaltered (**Figures 3.13** and **3.14A**). Exosome biogenesis can also be assessed by scoring the proportion of Rab11-compartments containing Rab11-positive puncta. Again, this was unaffected by *mfas* knockdown (**Figures 3.13** and **3.14B**). Thus, the unique size of DCG compartments in SCs permitted me to test whether the identity of large DCG precursor compartments and DCG compartments themselves, as well as their function in exosome biogenesis, was altered by *mfas* knockdown and allowed me to conclude that the Rab6 to Rab11 transition that drives DCG biogenesis and exosome formation had occurred normally. However, the process of protein aggregation is specifically blocked by this knockdown, suggesting that the assembly properties of the MFAS protein are required for this process.

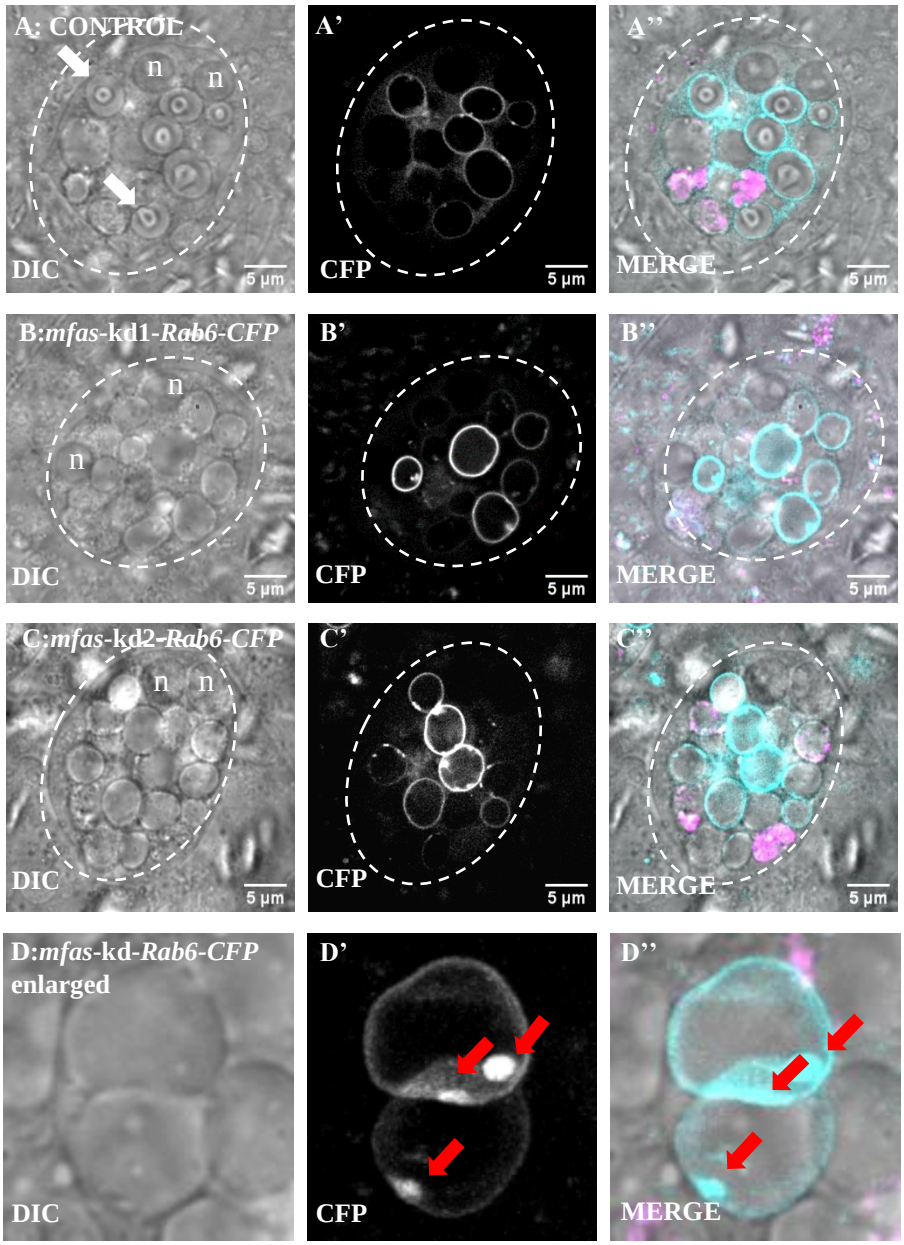

Figure 3.11: The Rab6 identity of large non-acidic compartments in SCs is not affected by *mfas*-knockdown. SCs from six day-old virgin males stained with LysoTracker Red and imaged *ex vivo*, using DIC and fluorescence microscopy for GFP and LysoTracker Red. **A)** w^{1118}*; Rab6-CFP, tub-GAL80*^{ts}*/UAS-ry-RNAi; dsx-GAL4* (control) **B)** w^{1118}*; Rab6-CFP, tub-GAL80*^{ts}*/UAS-mfas-RNAi-1; dsx-GAL4* **C)** w^{1118}*; Rab6-CFP, tub-GAL80*^{ts}*/UAS-mfas-RNAi-2; dsx-GAL4* **D)** Magnified view of w^{1118}*; Rab6-CFP, tub-GAL80*^{ts}*/UAS-mfas-RNAi-2; dsx-GAL4* showing Rab6-labelled exosomes (arrows) within empty DCG compartments (due to the *mfas*-knockdown effect resulting in non-formation of dense-cores). **White arrows in A:** DCGs; **Red arrows** in D' and D'': Rab6-labelled exosomes; **n:** double nuclei characteristic of SCs. Scale bar = 5 µm.

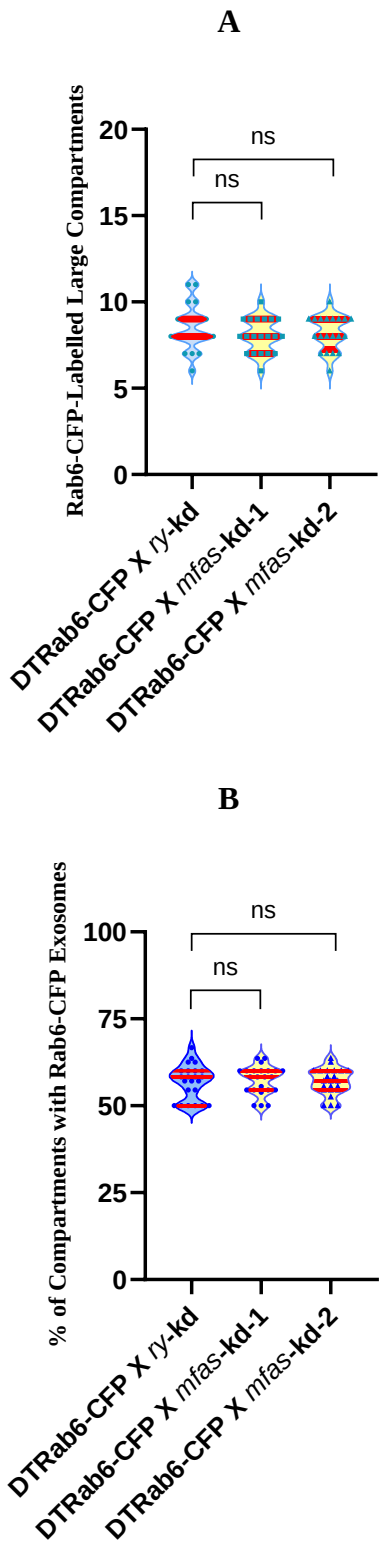

Figure 3.12: The Rab6 identity of large non-acidic compartments is not affected by *mfas*- knockdown. A: *mfas*-knockdown SCs have the same number of Rab6-labelled large non-acidic compartments as controls (DTRab6-CFP driver line: w^{1118}; *Rab6-CFP*,

tubGAL80ts/CyO; dsxGAL4). **B:** *mfas*-knockdown SCs have the same percentage of large compartments with Rab6-CFP labelled exosomes as controls. The mean for each set of experiments is shown in red.

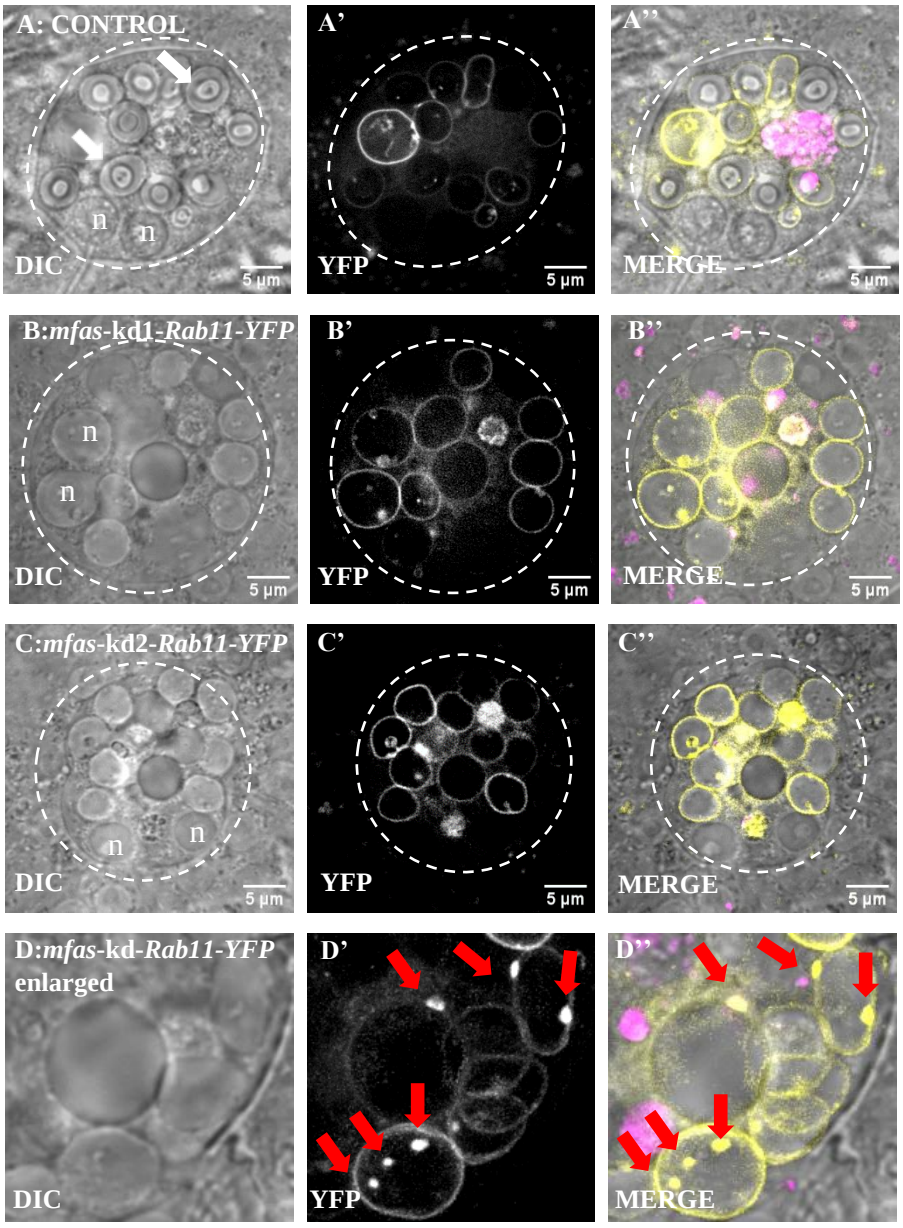

Figure 3.13: The Rab11 identity of large non-acidic compartments is not affected by *mfas*-knockdown. SCs from six-day-old virgin males stained with LysoTracker Red and imaged *ex vivo*, using DIC and fluorescence microscopy for GFP and LysoTracker Red. **A)** w^{1118}*; tub-GAL80*^{ts}*/UAS-ry-RNAi; YFP-Rab11, dsx-GAL4/+* (control) **B)** w^{1118}*; tub-GAL80*^{ts}*/UAS-mfas-RNAi-1; YFP-Rab11, dsx-GAL4/+* **C)** w^{1118}*; tub-GAL80*^{ts}*/UAS-mfas-RNAi-2; YFP-Rab11, dsx-GAL4/+* **D)** Magnified view of w^{1118}*; tub-GAL80*^{ts}*/UAS-mfas-RNAi-2; YFP-Rab11, dsx-GAL4/+* showing Rab11-labelled exosomes (arrows) within empty DCG compartments (due to the *mfas*-knockdown). **White arrows** in **A:** DCGs; **Red**

arrows in **D'** and **D''**: exosomes; **n:** double nuclei characteristic of each SC. Scale bar = 5 μm.

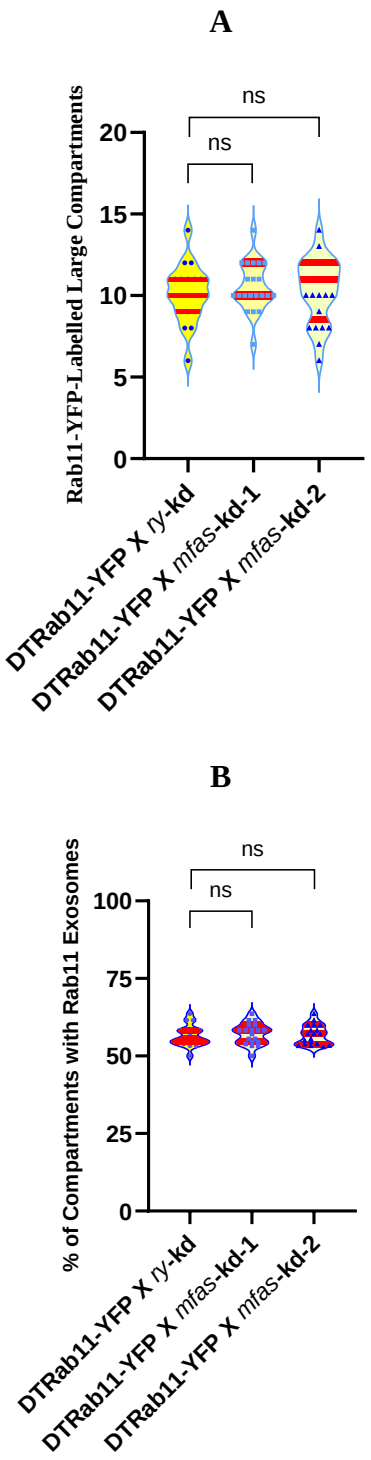

Figure 3.14: The Rab11 identity of large non-acidic compartments is not affected by *mfas*-knockdown. A: *mfas*-knockdowns have the same number of YFP-Rab11

compartments as controls. **B:** *mfas*-knockdowns have the same proportion of YFP-Rab11-containing-exosomes as controls. The mean for each set of experiments is shown in red.

The lack of impact of *mfas*-knockdown on the identity of Rab6- and Rab11- compartments, as well as on the production of Rab6 and Rab11 exosomes underlines the insularity of MFAS' role in the biogenesis of DCGs.

3.3 DISCUSSION

3.3.1 THE DIFFERENCE BETWEEN N-TERMINAL-TAGGED VERSUS C-TERMINAL TAGGED MFAS IN INFLUENCING DCG BIOGENESIS

These experiments in which differently tagged MFAS and TGFBI proteins were expressed in SCs demonstrate suggest that the C-terminals of MFAS (and TGFBI) are important in the production of normal DCGs, since the fusion causes a change in the resultant phenotype. MFAS is the *Drosophila* homologue of TGFBI, a human corneal structural protein which has an RGD binding motif at it's C-terminal. The integrin-binding RGD motif underscores the crucial adhesive function of TGFBI, since the ordered lamellar alignment of keratocytes, which it binds together, is imperative to the cornea's transparency (Munier *et al.,* 1997, Andersen *et al.*, 2004). While the exact mechanism of DCG disruption by a GFP tag at the C-terminal of MFAS is unknown, the structural role of TGFBI's C-terminal suggests a similar role for MFAS in maintaining the structural integrity of DCGs. This is further supported by sequence alignment of the human and *Drosophila* homologues, showing some conservation at the C-terminal. Intriguingly, though, unlike TGFBI, MFAS does not have an RGD sequence at it's C-terminal, suggesting that motifs other than the RGD sequence are likely to be involved (the sequence alignment of TGFBI and MFAS is shown in **Appendix 9.2**).

3.3.2 THE SIGNIFICANCE OF THE PIVOTAL ROLE OF MFAS IN DCG FORMATION

MFAS, the *Drosophila* homologue of the human amyloidogenic protein TGFBI, is highly expressed in SCs, and, as shown by these results, is essential for the formation of physiologically important DCGs. DCG generation is a continuous process, occurring in approximately 30 minutes, as seen in time-lapse videos (Singh *et al.,* manuscript in preparation). *mfas*-knockdown blocks DCG biogenesis, suggesting that this protein's aggregation under physiological conditions is critical for the process of DCG biogenesis in SCs. It also reduces nuclear size suggesting that it disrupts autocrine growth-promoting Decapentaplegic (Dpp) activity, corroborating earlier findings from the Wilson lab that Dpp, the *Drosophila* homologue of mammalian Bone Morphogenetic Protein (BMP) ligands BMP2 and BMP4, is packaged in DCGs and controls nuclear size (Redhai *et al.*, 2016). The study of MFAS as a model amyloid thus has larger implications, given the increasing recognition of autocrine BMP signalling in numerous physiological processes like synaptic secretion (Goold and Davis, 2007), and it's mis-regulation in diabetes (Goulley *et al.,* 2007).

It is now well accepted that numerous peptide hormones are stored and released as functional amyloids. In addition to insulin in the β-cells of the islets of Langerhans in the pancreas, these include ACTH, β-endorphin, prolactin, and growth hormone in the anterior pituitary, and oxytocin and vasopressin in the posterior lobe (Maji *et al.,* 2009). During their aggregation and maturation into secretory granule cores, these hormone amyloids are surrounded by membranes, and separate in vesicles from the Golgi. Amyloids have been

shown to have an affinity for membranes (Gellermann *et al.,* 2005), but whether this is involved in the formation of DCG compartments remains unclear in most cases. In this regard, a potential hypothesis explaining the protein aggregation phenomenon is that since all amyloids have a cross-β-sheet as their single common structural epitope, this might act as a recognition motif for a yet undiscovered granule-recruiting membrane protein. Once encased in membrane-bound vesicles, these storage granules are extremely stable for long periods, and are released only upon receiving the appropriate signalling. When this happens, the cross-β-sheet brings about the controlled release of monomeric hormone, a process which is quite likely supported by chaperones (Maji *et al.,* 2008). Another potentially instructive characteristic is that DCGs are separated from the surrounding compartment membranes, as is observed in the mature DCGs of SCs (refer to **Figure 3.15** below).

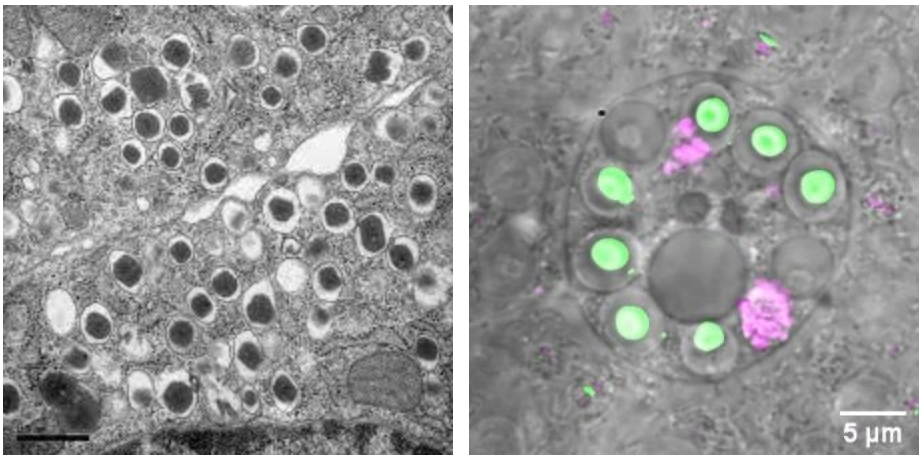

Figure 3.15: The amyloid-comprised components of DCGs are separated from the surrounding compartment membranes. Left: Mouse islet cell showing amyloid-comprised insulin granules. Scale bar = 20 µm. (Rorsman and Ashcroft, Phys. Rev. 2018, p. 119). **Right:** *Drosophila* SC showing putative amyloid-comprised DCGs. Both of these granule forms contain or store bioactive molecules, and when mature are separated from the limiting membrane of the compartment. Scale bar = 5 µm.

The inherent complexity of normal peptide hormone storage as amyloid is compounded by the fact that several hormones are also stored as amyloids in disease states. These include calcitonin in medullary carcinoma of the thyroid, amylin (also known as human Islet Amyloid Polypeptide or hIAPP) in type 2 diabetes, and atrial natriuretic factor in atrial amyloidosis (Chiti and Dobson, 2006). This normal-to-abnormal continuum of amyloid functionality will be explored further in my thesis.

The situation as we currently know it, therefore, is as follows: a fly amyloid protein (MFAS) whose human homologue (TGFBI) leads to amyloid disease, is itself indispensable for the formation of MFAS-comprised granules in the fly. These amyloid granules of MFAS store signalling molecules which in turn are crucial for reproduction in the fly. Similar signalling molecules (hormones) in higher animals are also composed of amyloid, and are vitally important for all aspects of life. Taken together, these facts suggest powerful connections between MFAS, TGFBI, and elementally important amyloid biology, all of which beg further investigation.

3.3.3 SIGNIFICANCE OF THE PRESERVATION OF RAB6 AND RAB11 COMPARTMENT IDENTITIES DESPITE THE KNOCKDOWN OF *mfas*

The choice of Rab6 and Rab11 compartments was an informed one; The Wilson laboratory has shown that the fusion of these two compartments is required for the formation of DCGs. Thus despite the crucial physiological roles that Rab6 and Rab11 play in MFAS' coalescence, their compartments remain unaffected by the loss of *mfas*, suggesting that the Rab6 to Rab11 transition is unaffected. Rab11 in particular, first identified as a marker for recycling endosomes, and in regulating vesicular transport from recycling and early

endosomes to the trans-Golgi network and the cell membrane (Ullrich *et al*., 1996), has numerous links to neurodegenerative diseases, which will be relevant to my subsequent studies of the role of *APP* in normal DCG biogenesis.

The likely explanation for this is that Rab6- and Rab11-mediated trafficking is critical in specific amyloidogenic or protein aggregation processes, but that these processes are events that lie downstream of trafficking. Therefore, blocking DCG biogenesis by inhibiting protein aggregation does not affect the identity of DCG compartments or their other cell biological roles associated with these compartments, like exosome formation.

3.3.4 SUMMARY OF SIGNIFICANT POINTS

I have shown that the use of an *mfas* gene trap line with an N-terminal, but not a C-terminal GFP attachment results in the production of normal DCGs. The use of *UAS-rosy-RNAi* (*UAS-ry-RNAi*) as a control RNAi cross for knockdown experiments also results in the formation of normal DCGs, demonstrating it's suitability for further experiments. This was a crucial fact to establish, since several genotypes used in the ensuing experiments employed *UAS-RNAi* transgenes. The structural uniformity of DCGs and their unambiguity in relating to specific genotypes assumes even greater importance in the interpretation of rescue experiments as will be presented in later chapters, since these results hinge upon an accurate characterization of DCG morphology. I also showed that *mfas* is essential for the formation of DCGs, since its knockdown results in the complete non-formation of DCGs. Finally, the knockdown of *mfas* does not affect the identity of Rab6 or Rab11 large non-acidic compartments, nor the production of Rab6 and Rab11 exosomes. Taken together,

these results demonstrate the insularity of MFAS′ function, as well as its sensitivity and specificity as an indicator of the genetic forces which inform its fate.

CHAPTER 4

OTHER FACTORS INFLUENCING DCG FORMATION

4. OTHER FACTORS INFLUENCING DCG FORMATION

4.1 INTRODUCTION

In **Chapter 3**, I identified GFP-MFAS as an excellent marker for DCGs (**Figure 3.4A**). Furthermore, I showed that *mfas* is a key regulator of DCG formation, since it's knockdown results in the complete absence of DCG biogenesis (**Figure 3.9B, C**). Based on these discoveries, I used *GFP-mfas* as a tool to look at other candidate molecules that have connections to Alzheimer's disease, and might therefore plausibly affect DCG biogenesis.

4.1.1 GAPDH AND NEURODEGENERATION

Glyceraldehyde-3-phosphate dehydrogenase (GAPDH) is a ubiquitous glycolytic enzyme, which catalyzes the conversion of glyceraldehyde-3-phosphate to 1,3-biphosphoglycerate.

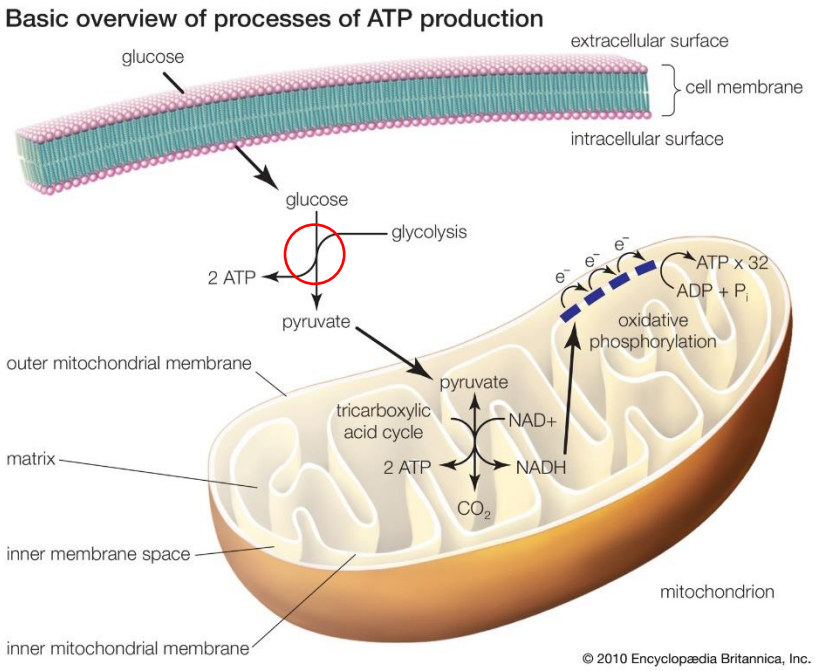

Figure 4.1: An overview of cellular energy production. GAPDH acts in the cytosol (red circle). (Source: Encyclopedia Brittanica 2010).

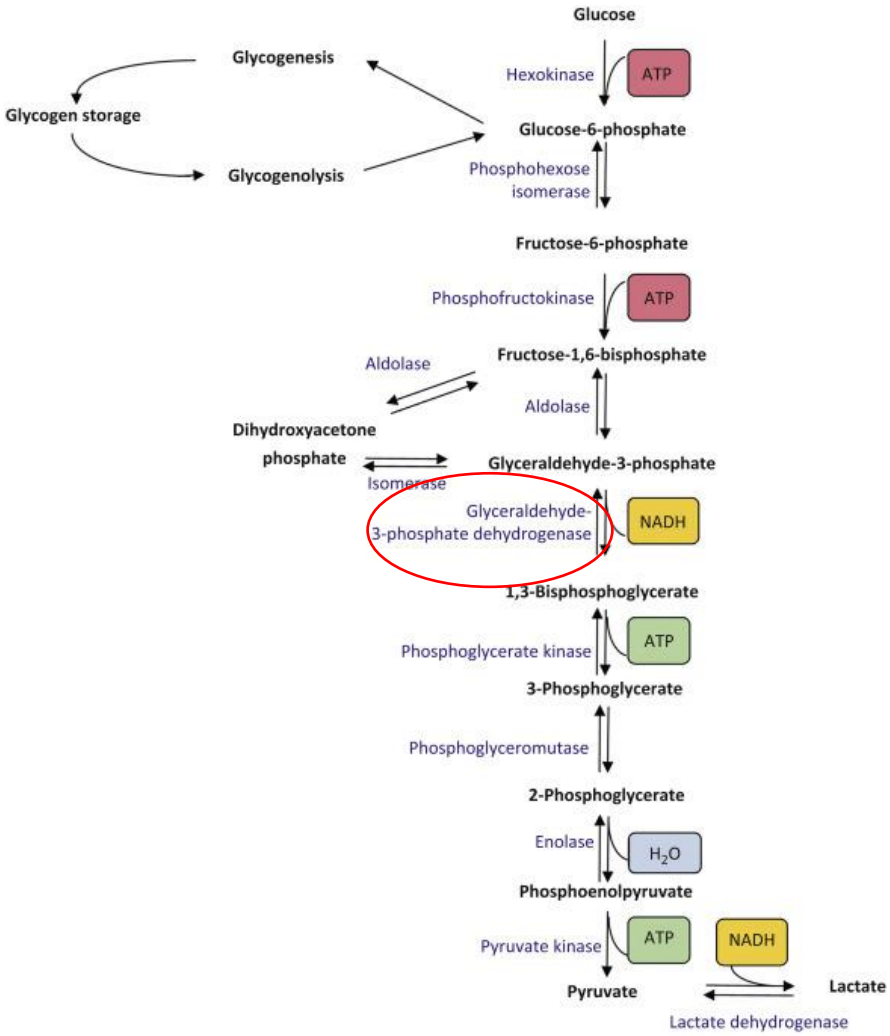

Figure 4.2: GAPDH's central role in glycolysis. GAPDH is highlighted by the red oval. (Source: Encyclopedia Brittanica 2010).

It is now also recognized as having other pleotropic roles, seemingly independent of it's role in energy metabolism. These include microtubule binding, membrane fusion, endocytosis, mRNA regulation, and nuclear translocation in apoptosis, all of which suggest involvement in neurodegeneration (Sirover, 1999; Lazarev *et al.*, 2021). Additionally, GAPDH rises in direct correlation with the Aβ plaque burden in Alzheimer's (Tsai *et al.*, 2020), *GAPDH* gene variants are associated with late-onset Alzheimer's disease (Li *et al.*, 2004) and GAPDH's surface lysines form transglutaminase-mediated covalent bonds with

Q15 in Aβ42, decreasing the clearance of these AB_{42}-GAPDH complexes from cerebrospinal fluid (Lazarev *et al.,* 2021). GAPDH also has a propensity to complex with Tau in neurofibrillary tangles (Wang *et al.,* 2005), with α-synuclein in Lewy bodies in Parkinson's disease, and with Huntingtin in Huntington's disease (Mazzola and Sirover, 2002).

Recently, the Wilson laboratory has shown that one of the *Drosophila* GAPDH isoforms, GAPDH2, is required for normal DCG biogenesis and for clustering of ILVs in Rab11 compartments of SCs (Dar *et al.,* 2021), and so in this chapter, I investigated its role in more detail, using the *GFP-mfas* line.

4.1.2 THE LINK BETWEEN RAB11, RAB6, APP AND NEURODEGENERATION

In **Figures 3.11** and **3.13** of **§ 3.2.5** of the previous Chapter, I showed that *mfas*-knockdown does not affect the identity of Rab6 and Rab11 compartments. Rab6 and Rab11 were specifically chosen pursuant to the discovery that fusion of Rab6 and Rab11 compartments was necessary for the formation of DCGs, and because of their extensive links to neurodegeneration.

In Alzheimer's disease, Rab11 impacts the secretory pathway through interaction with lemur tail kinase 1 (LMTK1), which in turn regulates the endosomal location of BACE-1, APP's β-secretase (Komaki *et al.,* 2022). Rab11 silencing also significantly decreases the BACE-1 processing of APP (Udayar *et al*., 2013), while retromer dysfunction, a known cause of Alzheimer's, also unbalances the Rab11-mediated cycling of protein cargoes and

leads to APP accumulation in presynaptic terminals in *Drosophila* (Walsh *et al.,* 2021). In Parkinson's disease, mutations in leucine-rich repeat kinase 2 (LRRK2) are the principal genetic drivers of the familial disease (Paisan-Ruiz *et al*., 2004; Zimprich *et al.,* 2004), which results in neuronal death in the basal ganglia and the intraneuronal presence of Lewy bodies, comprised of misfolded α-syncuclein. LRRK2, along with Rab11 and Vps35 regulates synaptic endocytosis, and mutated LRRK2 is less efficient in clearing α-synuclein through this pathway (Maekawa *et al.,* 2016; Inoshita *et al.,* 2017). Rab11 silencing resulted in increased secretion of α-synuclein (Chutna *et al.,* 2014), while overexpression of Rab11 in *Drosophila* corrected the abnormalities in synaptic vesicle size and function brought about by α-synuclein (Breda *et al.,* 2015). In Huntington's disease, mutant Huntingtin impairs Rab11 function, inhibits endocytic recycling from the endoplasmic reticulum to the cell membrane, and by disrupting the traffic of membrane materials to dendritic spines, ultimately leads to the loss of spines (Li *et al.,* 2008; Richard *et al.,* 2011). Mutant Huntingtin also enhances Bone Morphogenetic Protein (BMP) signalling, thus causing excessive synaptic growth and synaptic deformities, and contributing to the pathology seen in Huntington's disease (Akbergenova and Littleton, 2017). In addition, disrupted Rab11 endosomal recycling has also been linked to the neurodegeneration of amyotrophic lateral sclerosis (Mitra *et al.,* 2019). Rab6, on the other hand, while not as encompassing in it's association with neurodegenerative diseases, is strongly implicated in Alzheimer's disease (Scheper *et al.,* 2007; Soejima *et al.,* 2013). The overall role of Rab GTPases in neurons is depicted in **Figure 4.3**, while Rab11's role in the endocytic pathway and vesicle transport is shown in **Figure 4.4**.

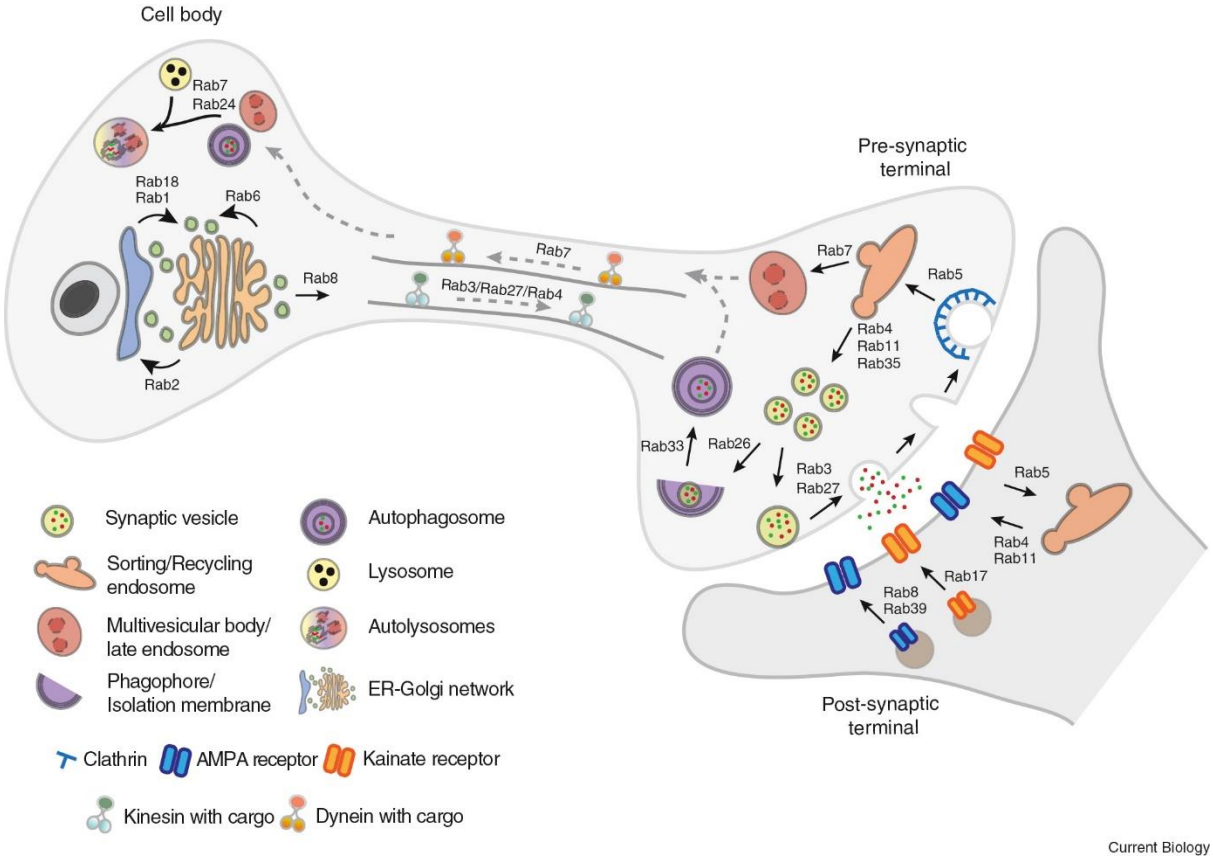

Figure 4.3: The roles of Rab GTPases in neurons. (From Kiral et al., Curr. Biol. 2018, p. R472).

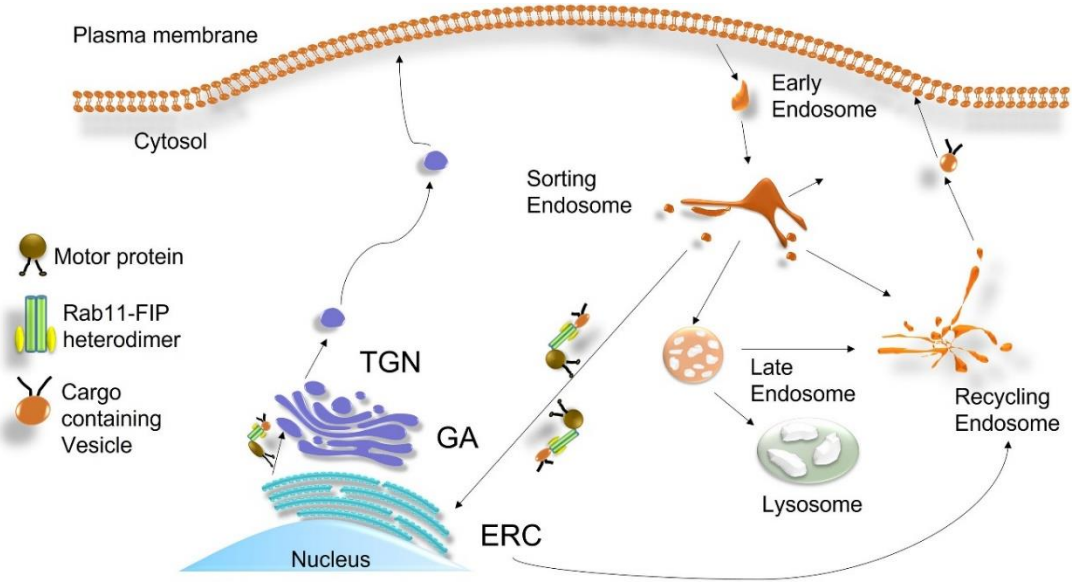

Figure 4.4: The endocytic pathway and Rab11's role in vesicle transport. ERC: endoplasmic reticulum compartment; **GA:** Golgi apparatus; **Rab11-FIP:** Rab11-family interacting proteins; **TGN:** trans-Goldi network. (From Sultana and Novotny, Am. Soc. Neurochem. Neuro. 2022, p. 5).

It was these associations between Rab proteins and neurodegenerative pathways, particularly the links between Rab11, APP, and Alzheimer's disease that prompted me to speculate about possible interactions between Rab11 and APPL, the *Drosophila* homologue of APP.

4.1.3 *APPL*, THE *DROSOPHILA* HOMOLOGUE OF *APP*, IS REQUIRED FOR DCG BIOGENESIS, SUGGESTING LINKS TO NEURODEGENERATION

Human APP is a type I transmembrane glycoprotein upto 770 amino acids in it's longest isoform, composed of a large extracellular domain, a relatively short cytoplasmic domain, and a single transmembrane segment (Kang *et al.,* 1987). It's mammalian homologues are APP-like proteins APLP1 and APLP2 (Wasco *et al.,* 1992; Wasco *et al.,* 1993). The *Drosophila* homologue of APP is APP-like (APPL) which has an overall 37-47 % homology to human APP_{695}, the major isoform found in the nervous sytem (Rosen *et al.,* 1989; Martin-Morris and White, 1990).

APP is the parent molecule of several physiologically active cleavage fragments, however its most recognisable by-product is Aβ. APP is processed through proteolysis by α-, β- and γ-secretases, and depending on these cleavages, is steered down either non-amyloidogenic or amyloidogenic pathways. Thus, if APP's initial processing scission is the α-cleavage, the Aβ sequence is disrupted, precluding the formation of Aβ oligomers. If, however, APP escapes α-cleavage, it then undergoes β- and γ-cleavages, which release the membrane-tethered Aβ segment (summarised in **Figure 4.5**). These physiological pathways can be affected by mutations either in APP (the substrate) or in the α-, β- and γ-secretases (the processing enzymes). Amongst the secretases, clinically relevant mutations are by far the

commonest in the γ-secretase (also called Presenilin). These APP and γ-secretase-mutation-driven alterations in the processing of APP skew the process of Aβ generation by altering the amount and relative ratios of fibrillogenic Aβ species produced. Collectively, these autosomal dominant mutations are the underlying causes of Familial Alzheimer's Disease (FAD).

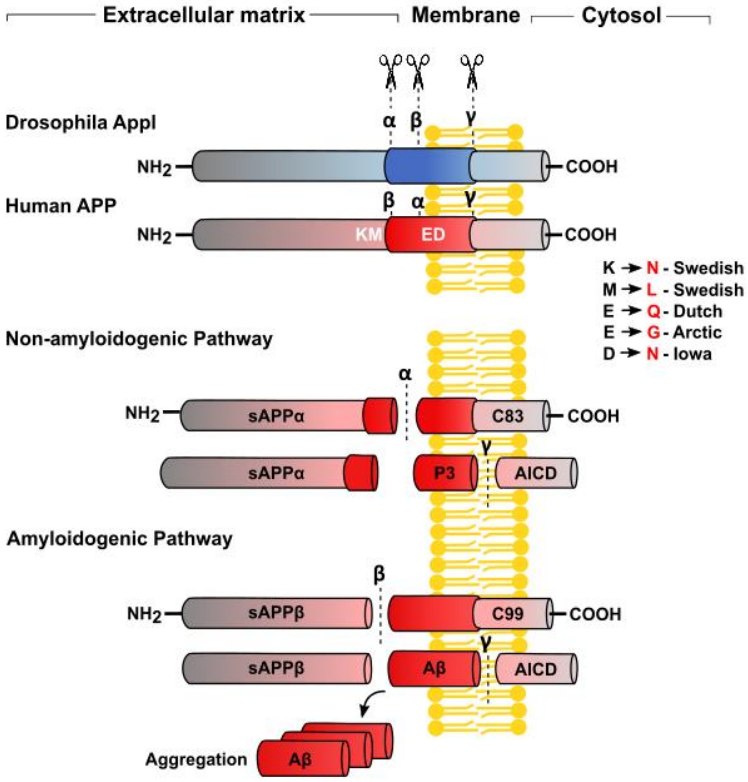

Figure 4.5: Alpha, β- and γ-secretase cleavages drive APPL and APP down either amyloidogenic or non-amyloidogenic pathways. Alpha-cleavage disrupts the Aβ sequence and leads to non-amyloidogenic processing of APP, while the avoidance of α-cleavage allows β- and γ-cleavages to release fibrillogenic Aβ species from APP. The four APP/Aβ FAD mutations I studied in this work are also shown (Swedish, Dutch, Arctic and Iowa). (From Singh, P. J., Verma, B., *et al.*, manuscript in preparation. Figure by B. Verma).

In **Figure 4.5** (above), the amino acid changes in the four mutations I studied (*APP-Swedish, Arctic, Iowa,* and *Dutch*) are shown. While the overwhelming preponderance of APP mutations are pathological, some, like *APP-Seoul, APP-Leuven* and *APP-English* are of uncertain significance, while another, *APP-Icelandic,* is protective against AD (**Figure 1.7**) (www.Alzforum.org).

The five *Drosophila* APPL isoforms range from 830 to 890 amino acids (Attrill *et al.*, 2016), and bear an overall organizational similarity to human APP (**Figure 1.9** and **Figure 4.6**) with the exception that the α- and β-secretase cleavage sites are reversed, with the β-site located closer to the transmembrane region and the α-site being more distal (Carmine-Simmen *et al*., 2009; Stempfle *et al.,* 2010). The *Drosophila* counterparts of these human and other mammalian secretases are kuzbanian (the homologue of α-secretase), dBACE (the homologue of β-secretase), and dPS (the homologue of Presenilin or γ-secretase). The similarities between human APP and *Drosophila* APPL are unsurprising, since both are members of the large, evolutionarily ancient APP family, which, due to its congruency in multiple organisms, has lent itself to species-spanning studies of developing and mature nervous sytems (Ramaker and Copenhaver, 2017). The similarities between APP family members in humans, other mammals, nematodes, and *Drosophila* are illustrated in **Figure 4.6**.

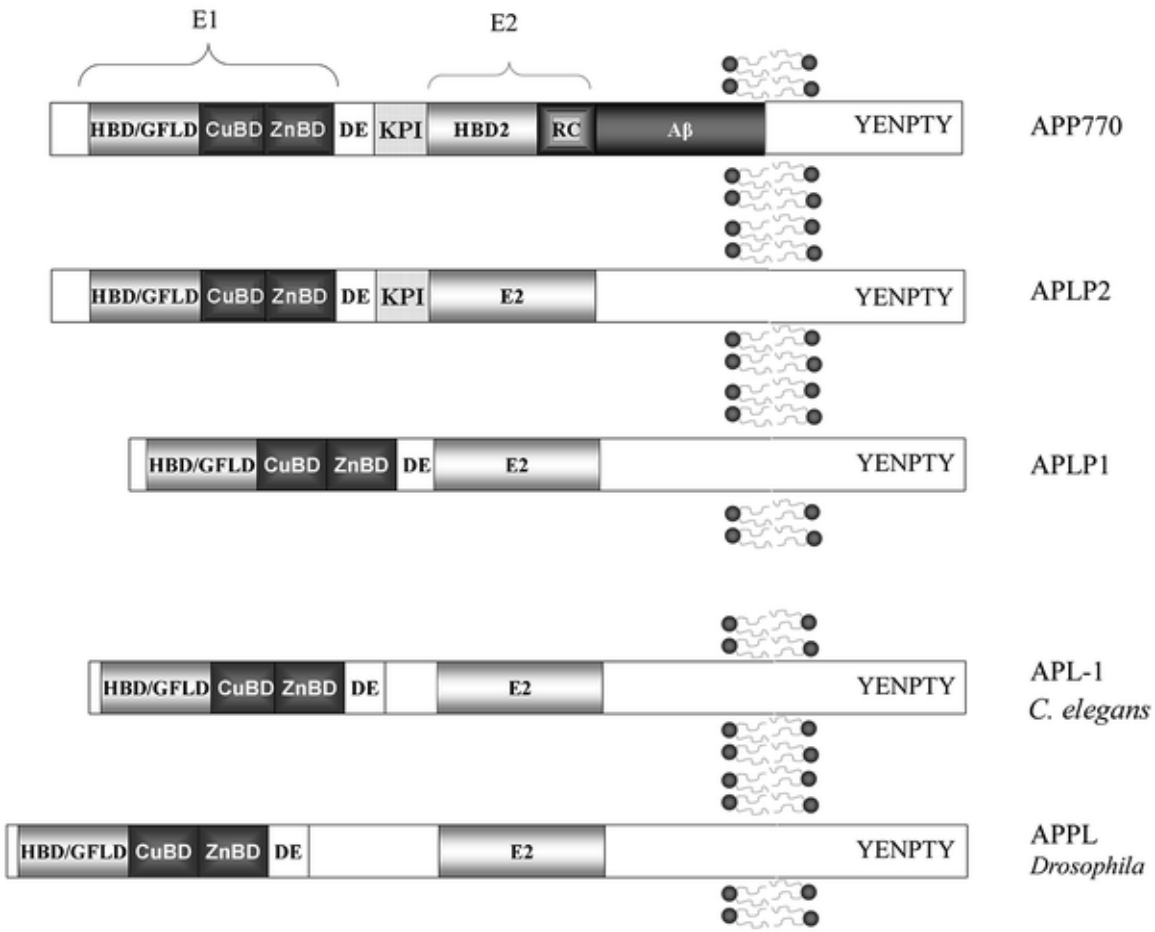

Figure 4.6: Comparison of APP in various species. Top to bottom: **APP70:** human APP isoform 770; **APLP1** and **2:** APP-like-protein-1 and -2, the mammalian homologues; **APL-1:** amyloid precursor-like, the *C. elegans* homologue; **APPL:** APP-like, the *Drosophila* homologue; **CuBD:** copper-binding domain; **DE:** aspartic acid (D) and glutamic acid (E)-rich acidic domain; **E1** and **E2**: ectoplasmic E1 and E2 domains; **HBD/GFLD:** heparin-binding/growth factor-like domains; **KPI:** Kunitz Protease Inhibitor domain; **RC:** random coil region; **YENPTY:** protein interaction motif; **ZnBD:** zinc-binding domain. (Jacobsen and Iverfeldt, Cell. Mol. Life Sci. 2009, p. 2300).

Like other members of the APP family, human APP has numerous functional areas, including extracellular and transmembrane binding sites for metal ions like copper, zinc and iron, heparin, ligands, and lipids, and intracellular areas specifically associated with trafficking, gene regulation and signal transduction **(Figure 4.7).**

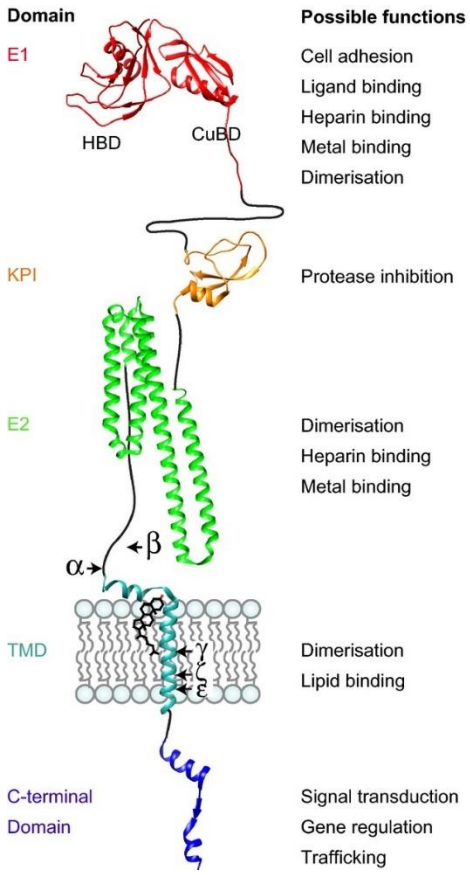

Figure 4.7: Human APP's functional sites. The extracellular and transmembrane domains include several binding sites. (Dawkins and Small, Journal of Neurochemistry 2014, p. 759).

The cytoplasmic segment of all APP family members has a conserved YENPTY protein interaction motif (**Figure 4.6**) which also includes the NPXY internalization signal. This, and the presence of several other similarly purposed domain structures in APP homologues (reviewed in Gralle and Ferreira, 2007) has led to suggestions that the known functions of

human APP summarized in **Figure 4.7** might hold true in other species (Jacobsen and Iverfeldt, 2009; Ramaker and Copenhaver, 2017). Thus, taking into consideration the similarities between members of the APP family - with human APP being the most studied point of reference - I conducted experiments to study the effects of deletion of *Drosophila* APPL's extra- and intracellular portions on DCG formation. I reasoned that just as various segments of APP influence amyloid formation in FAD, so too might various segments of APPL.

4.1.4 AIMS

In this chapter, I first analysed the effects of modulating GAPDH expression in SCs to further study its roles in DCG biogenesis, then tested the hypothesis that APPL might also be involved in this process. Having shown that the latter does have an important role, I then investigated what parts of the molecule might be crucial for this function.

4.2 RESULTS

4.2.1 DROSOPHILA *GAPDH2* IS REQUIRED FOR NORMAL DCG ASSEMBLY IN SCs

As mentioned in the introduction, multiple reports going back several decades link GAPDH with neurodegeneration in general and Alzheimer's disease in particular. Given these historical correlations, I investigated the effects of the knockdown of its *Drosophila* homologue, GAPDH2, as well as the effects of overexpression of human GAPDH on MFAS. To do this, I overexpressed *Drosophila GAPDH2*-kd and human *GAPDH* in adult SCs under dsx-GAL4 control, and compared the resultant DCG phenotypes from both of these manipulations to control cells expressing a *UAS-ry-RNAi* construct. *GAPDH2*-knockdown prevented the normal coalescence of MFAS in forming DCGs; rather than

coalescing into a single large core located centrally within the compartment, the particles of MFAS instead formed a ring of peripheral ‘mini-cores’. I describe this appearance as ‘pearls on a string’, since the individual MFAS moeities appear to adhere to the compartment membrane in a circumferential pattern (**Figure 4.8B**). This is consistent with previous observations (Dar *et al.*, 2021), and suggests an additional link between GAPDH2 and amyloid formation. The overexpression of human GAPDH, however, resulted in a significant increase in the number of DCGs, as is shown in **Figure 4.8C** and **Figure 4.9**.

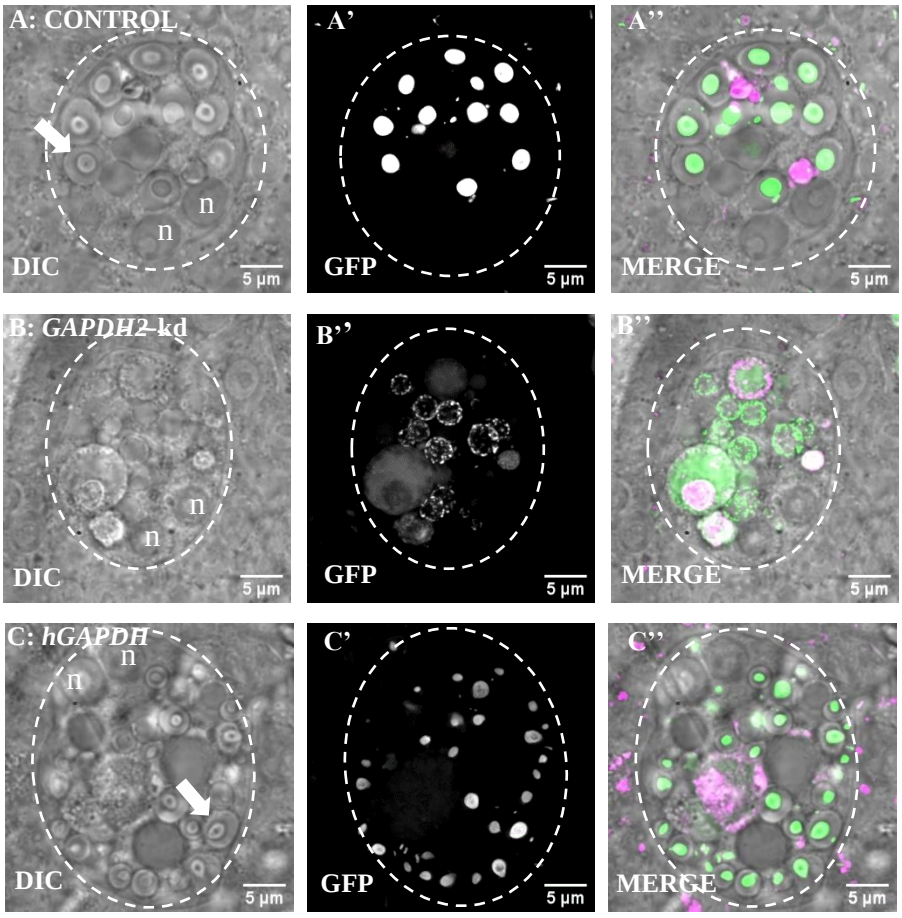

Figure 4.8: *GAPDH₂* is required for the normal biogenesis of DCGs. SCs from six day-old virgin males stained with LysoTracker Red and imaged *ex vivo*, using DIC and fluorescence microscopy for GFP and LysoTracker Red. **A)** male fly with the genotype *w*^{1118}*; tub-GAL80*^{ts}*/ UAS-ry-RNAi; dsx-GAL4 GFP-mfas/+* (control) **B)** *w*^{1118}*; tub-GAL80*^{ts}*/+; dsx-GAL4 GFP-mfas/UAS-GAPDH2-RNAi* showing the non-formation of DCGs in a string-of-pearls pattern which is characteristic of *GAPDH2*-knockdown **C)** *w*^{1118}*; tub-GAL80*^{ts}*/+; dsx-GAL4 GFP-mfas/UAS-human-GAPDH* showing an increased number of DCGs. **White arrows** in **A** and **C:** DCGs; **n:** double nuclei characteristic of each SC. Scale bar = 5 µm.

To summarise, in the *GAPDH2*-kd phenotype, rather than coalesce into a single large core located centrally within the compartment, the particles of MFAS instead formed a ring of 'mini-cores' in nearly 100 % of compartments. This 'pearls on a string'appearance becomes important in differentiating it from knockdown of *APPL*, which also produces mini-cores, and which will be presented in the next section. I also confirmed that

overexpression of human GAPDH, which appears to cluster in SC Rab11-compartments, increased the number of DCG compartments as had previously been reported by Dar *et al.* (2021), a phenotype that we do not yet fully understand. Overall, the results of these two experiments allow me to conclude that *GAPDH2* plays a critical role in permitting MFAS aggregation into a single large DCG in SCs, and that the human GAPDH-amyloid link is further strengthened.

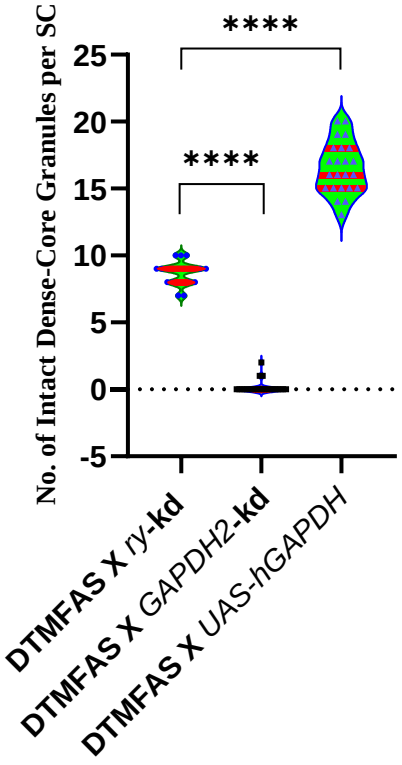

Figure 4.9: Knockdown of *Drosphila GAPDH2* results in the non-formation of normal DCGs. Overexpression of *human-GAPDH*, however, significantly increases the number of DCGs. The mean for each set of experiments is shown in red.

4.2.2 *APPL*, THE *DROSOPHILA* HOMOLOGUE OF *APP*, IS REQUIRED FOR NORMAL DCG ASSEMBLY IN SCs

As mentioned in the introductory section (**§ 4.1.3**) of this chapter, human *APP* and *Drosophila APPL* are similarly organised homologues. Amyloid Precursor Protein (APP) is the human parent protein of β-amyloid (Aβ) which under specific circumstances fibrillates and aggregates into the amyloid plaques which characterize Alzheimer's disease. The similarities between APP and APPL (**Figure 1.9, Figure 4.6**) are unsurprising, since both are members of the large, species-spanning family of amyloid precursor proteins which often share similarities in their processing, and, once the final amyloids are generated, the final protein products are found to be virtually identical in their biophysical properties and ultrastructural characteristics (reviewed in Sawaya *et al.*, 2021). Furthermore, there are multiple associations between Rab11, Rab6, APP and neurodegeneration as outlined in **§ 4.1.2**. Given this background, my experimental plan was to knock down *Drosophila APPL* using three different RNAis (**Figure 4.10**) and to observe their effects on MFAS and DCG biogenesis.

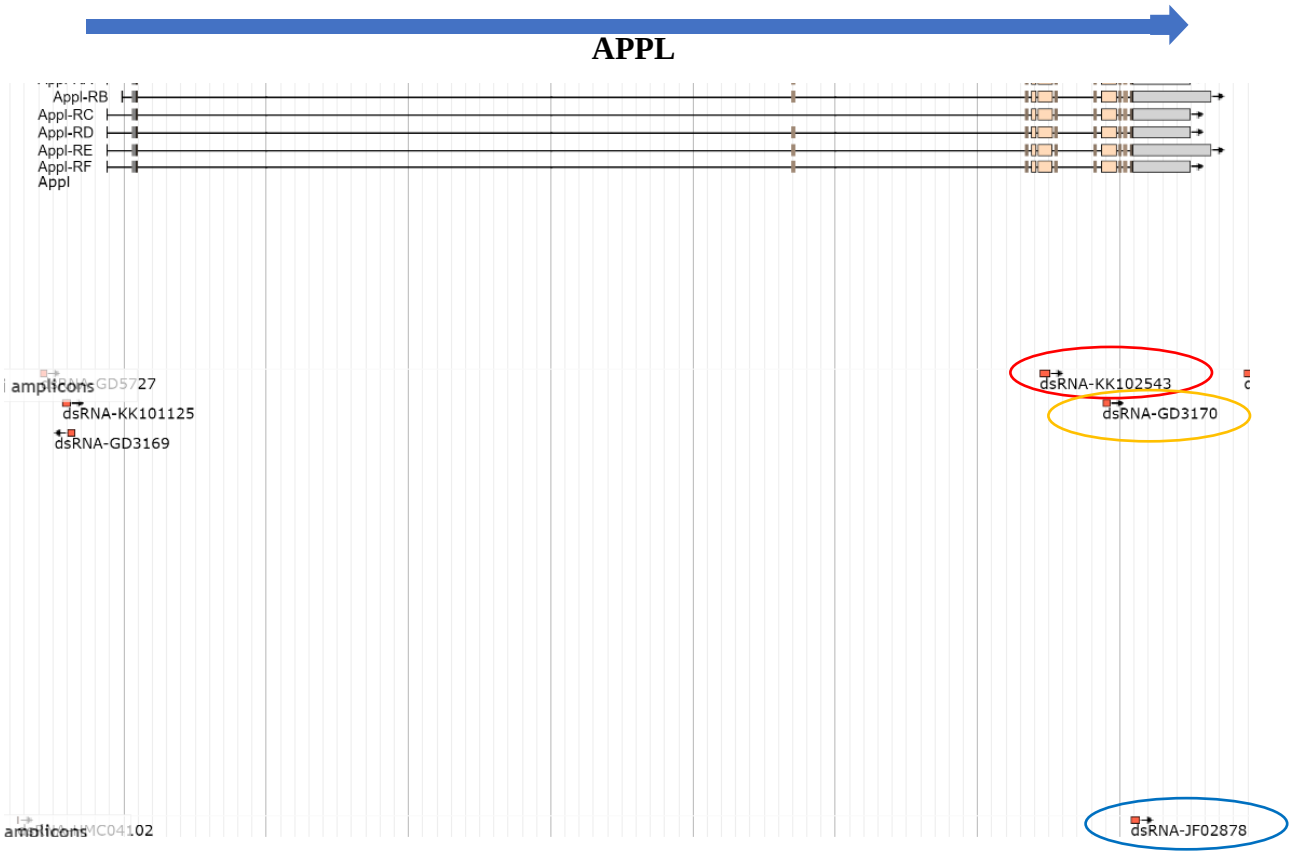

Figure 4.10: The 3 *APPL*-RNAis (red, orange, and blue ovals) used in the knockdown experiments act at different locations. GD3170: exon 7; **JF02878:** exon 10; **KK102543**: exon 4. (Adapted from FlyBase, accessed on 10/3/2023).

An additional benefit of this experiment would be to test the larger question of whether the knockdown of one amyloid (APPL) had any effect on the behaviour of another (MFAS). My motive behind looking into this question of amyloid behaviour was knowledge of the clinical fact that brain amyloids march forward in a prion-like fashion, suggesting that they somehow influence each other into misfolding through a mysterious and as yet undeciphered 'crosstalk' (**Sections 1.41**, **1.42**, and **Figure 1.15**). To test the three *APPL-RNAis*, I overexpressed all three in adult SCs under dsx-GAL4 control in three separate fly lines, and compared the resultant DCG phenotypes from each of these three manipulations

to control cells expressing a *UAS-ry-RNAi* construct. With each of the knockdowns, the MFAS moeities failed to fuse into a physiological central core, as shown in **Figure 4.11**.

This non-fusion of MFAS with the knockdown of *APPL* was similar to the outcome seen with the knockdown of *GAPDH2*, but with important differences. Like with *GAPDH2*-kd, the knockdown of *APPL* also resulted in the non-coalescence of MFAS, with individual MFAS moeities unable to fuse into a single, centrally-located DCG, and instead forming multiple 'mini-cores'. Unlike the mini-cores formed by *GAPDH2*-kd, however, the mini-cores formed by *APPL*-kds had a different distribution within the DCG compartment. Specifically, while *GAPDH2*-kd resulted in a phenotype where mini-cores appeared to adhere circumferentially to the DCG compartment membrane (**Figure 4.8B**), *APPL*-kd mini-cores were more evenly distributed throughout the compartment space (**Figure 4.11B, C** and **D**). The second difference was seen in the kinetics of *GAPDH2*-kd and *APPL*-kd mini-cores as observed on time-lapse videos. On discovering the difference between mini-cores seen with *GAPDH2*- and *APPL*-knockdowns, I made time-lapse videos of DCG biogenesis, in which I compared these knockdowns to controls. I found that with controls, the individual MFAS moeities came together in about 15-30 minutes, while with the knockdowns they did not and remained dispersed (Singh *et al.*, manuscript in preparation; videos not shown in this thesis). My colleague in the Wilson laboratory, Adam Wells, made several time-lapse videos of *GAPDH2*-kd and found that the movement of mini-cores with this genotype differed from the movement of mini-cores as seen with *APPL*-kds (Adam Wells, personal communication). The *GAPDH2*-kd mini-cores displayed more latitude of movement, even touching each other, but having done so, failed to adhere.

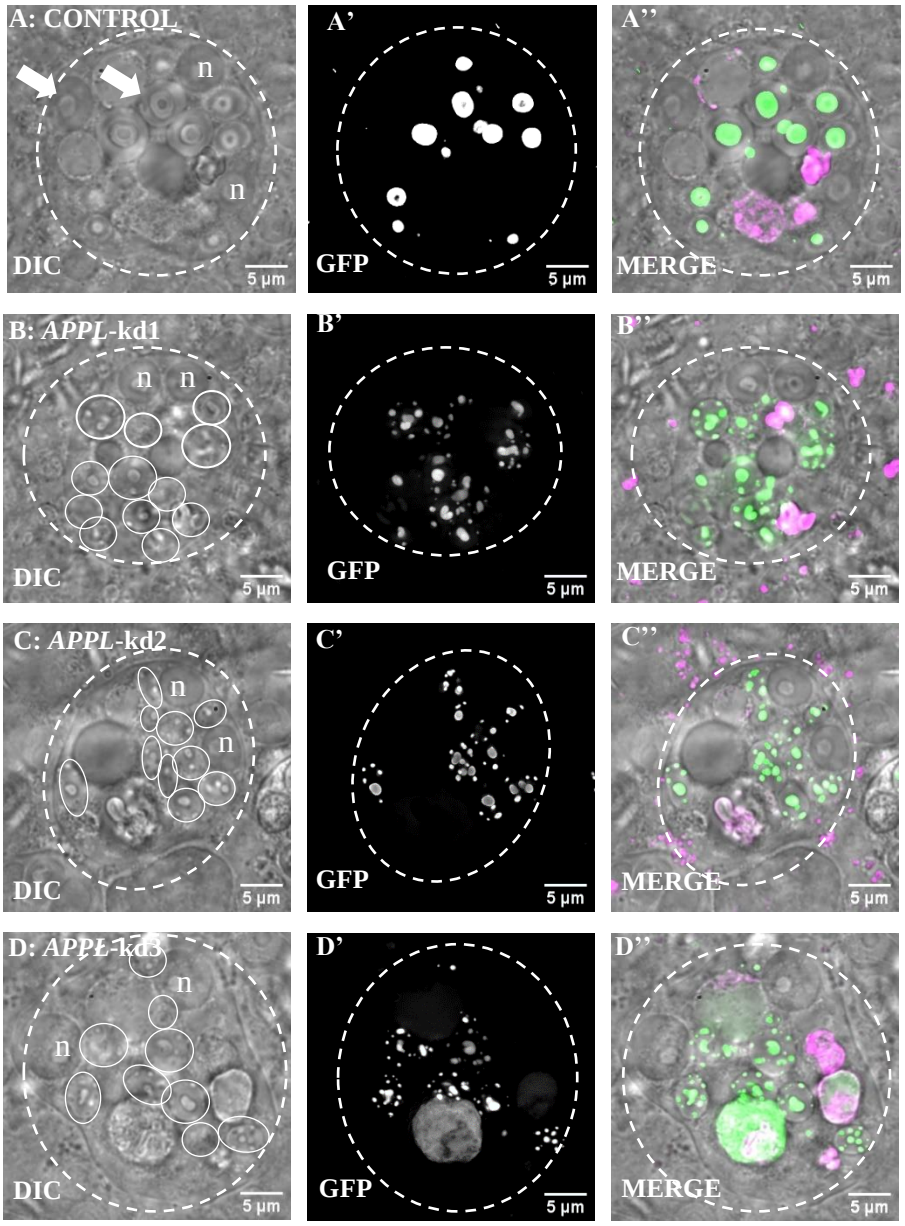

Figure 4.11: The *Drosophila APP* homologue, *APPL*, is required for normal DCG assembly in SCs. *APPL*-knockdown results in non-coalescence of MFAS, giving a 'mini-core' or 'fragmented' appearance to DCGs. SCs from six day-old virgin males stained with LysoTracker Red and imaged *ex vivo*, using DIC and fluorescence microscopy for GFP and LysoTracker Red. **A)** w^{1118}*; tub-GAL80*^{ts}*/UAS-ry-RNAi; dsx-GAL4 GFP-mfas/+* (control) **B)** w^{1118}*; tub-GAL80*^{ts}*/UAS-APPL-RNAi-1; dsx-GAL4 GFP-mfas/+* **C)** w^{1118}*; tub-GAL80*^{ts}*/+; dsx-GAL4 GFP-mfas/UAS-APPL-RNAi-2* **D)** w^{1118}*; tub-GAL80*^{ts}*/+; dsx-GAL4 GFP-mfas/UAS-APPL-RNAi-3*. **White arrows** in **A**: DCGs; **solid white circles/ovals** in **B, C** and **D:** dense-core compartments with the *APPL*-knockdown mini-core phenotype; **n:** double nuclei characteristic of each SC. Scale bar = 5 µm.

A

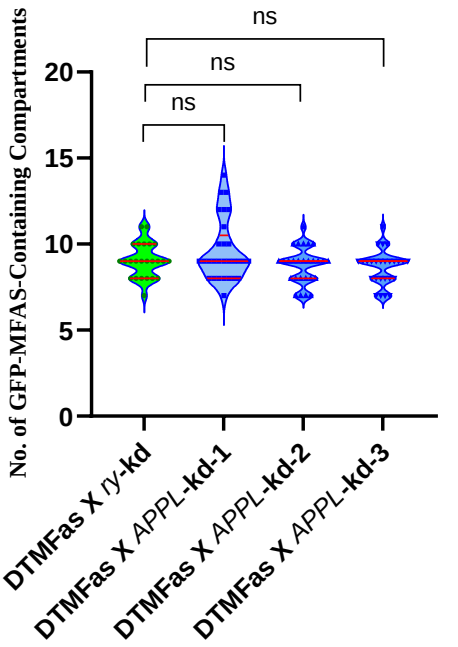

B

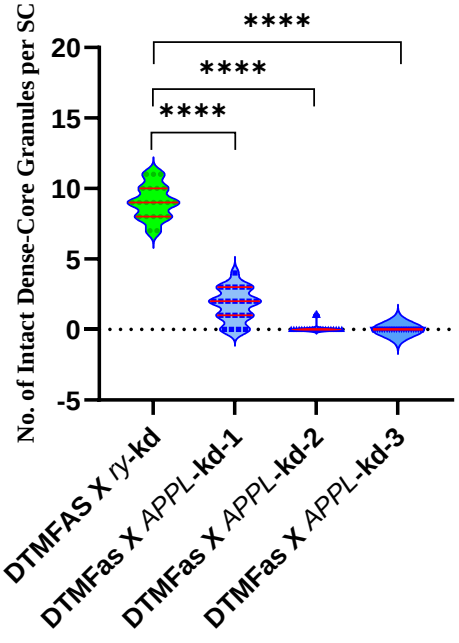

Figure 4.12: The effect of *APPL*-kd on MFAS-containing-compartments and DCGs. **A:** All three *APPL*-kd lines have the same number of large, potentially dense-core-forming

compartments as controls. **B:** All three tested *APPL*-kd lines have significantly less DCGs than controls. In subsequent experiments, the more effective *APPL*-knockdown lines (2 and 3) were used. The mean for each set of experiments is shown in red.

4.2.3 THE RAB6 AND RAB11 IDENTITIES OF LARGE NON-ACIDIC COMPARTMENTS ARE NOT AFFECTED BY *APPL*-KNOCKDOWN

As mentioned in **§ 4.1.2**, Rab6 and Rab11 have strong associations with the amyloid precursor APP and human neurodegenerative diseases, particularly AD. Furthermore, the fusion of Rab6 and Rab11 is required for the formation of DCGs, which are comprised of the fly amyloid MFAS. It was also previously established that while the knockdown of the neurodegeneration-associated genes *GAPDH$_2$* and *APPL* profoundly affect MFAS and the biogenesis of DCGs, the knockdown of *mfas* does not affect the idenity of Rab6 or Rab11 compartments. Given these emerging links between various amyloid- and neurodegeneration-associated genes in both humans and flies, I examined the effects of *APPL*-knockdowns on Ra6 and Rab11 compartment identities. To do this, I overexpressed the two most effective *APPL*-kd lines (lines 2 and 3, **Figure 4.11C** and **D**) in adult SCs under dsx-GAL4 control in CFP-Rab6 and YFP-Rab11 backgrounds, and compared the resultant DCG phenotypes from each of these manipulations to control cells expressing a *UAS-ry-RNAi* construct in the same backgrounds.

For both Rab6 and Rab11, as shown in results from these experiments below, the numbers of marked non-acidic compartments and the proportions of these compartments containing Rab-labelled puncta were unchanged when *APPL* was knocked down with the two strongest RNAi lines (**Figures 4.13-4.16**). This suggests that *APPL* knockdown does not

affect compartment identity and maturation in SCs, and that the DCG phenotype is associated with a defect in protein aggregation inside each compartment.

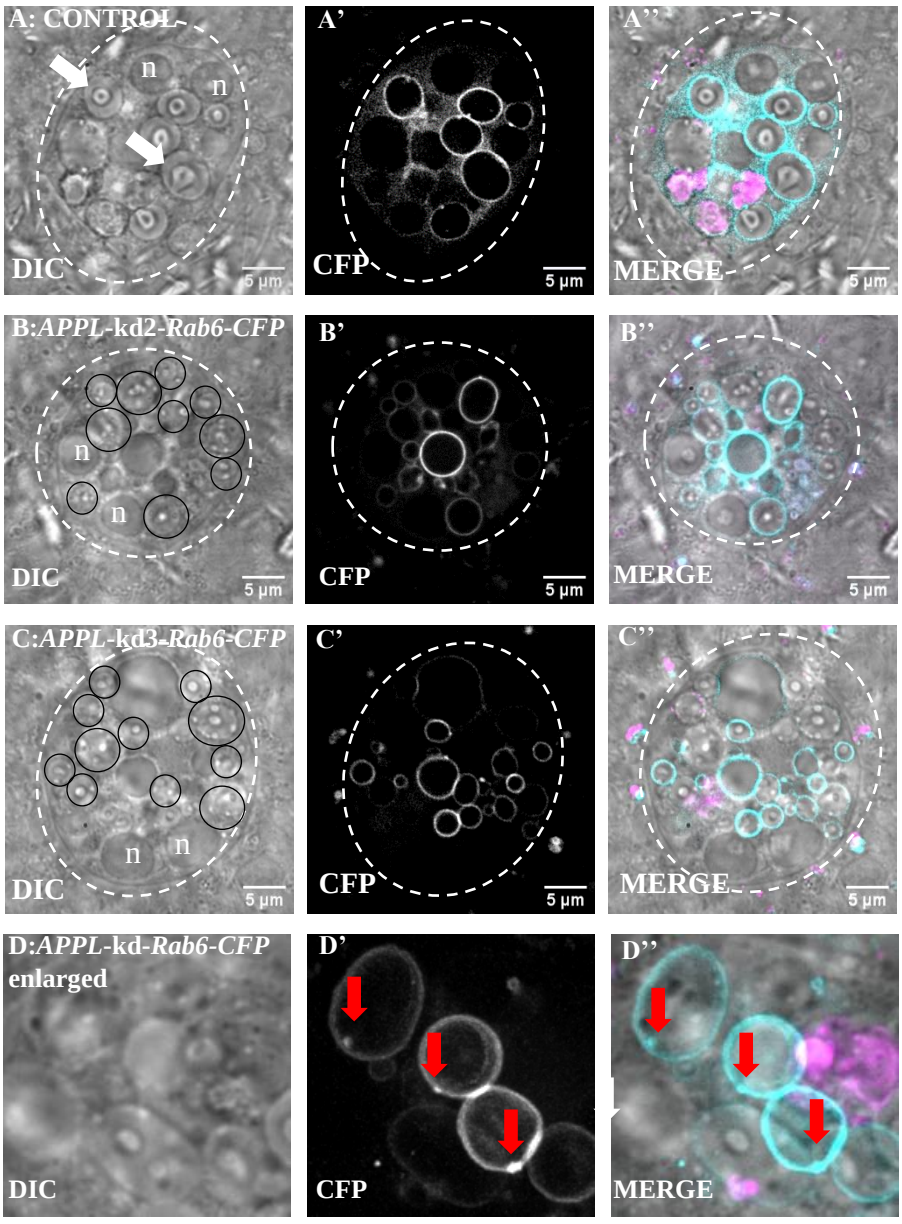

Figure 4.13: The Rab6 identity of large non-acidic compartments is not affected by *APPL*-knockdown. SCs from six day-old virgin males stained with LysoTracker Red and imaged *ex vivo*, using DIC and fluorescence microscopy for GFP and LysoTracker Red. **A)** w^{1118}*; CFP-Rab6 tub-GAL80*^{ts}*/UAS-ry-RNAi; dsx-GAL4/+* (control) **B)** w^{1118}*; CFP-Rab6 tub-GAL80*^{ts}*/+; dsx-GAL4/UAS-APPL-RNAi-2* **C)** w^{1118}*; CFP-Rab6 tub-GAL80*^{ts}*/+; dsx-GAL4/UAS-APPL-RNAi-3* **D)** Magnified view, showing CFP-labelled Rab6 exosomes (arrows) within DCG compartments with mini-cores (due to the *APPL*-knockdown effect of non-coalescence of MFAS in dense-cores) **White arrows** in **A:** DCGs; **Red arrows** in

D' and **D'':** Rab6-labelled exosomes; **black circles** in **B** and **C:** dense-core compartments with the *APPL*-knockdown mini-core phenotype; **n:** double nuclei characteristic of each SC. Scale bar = 5 μm.

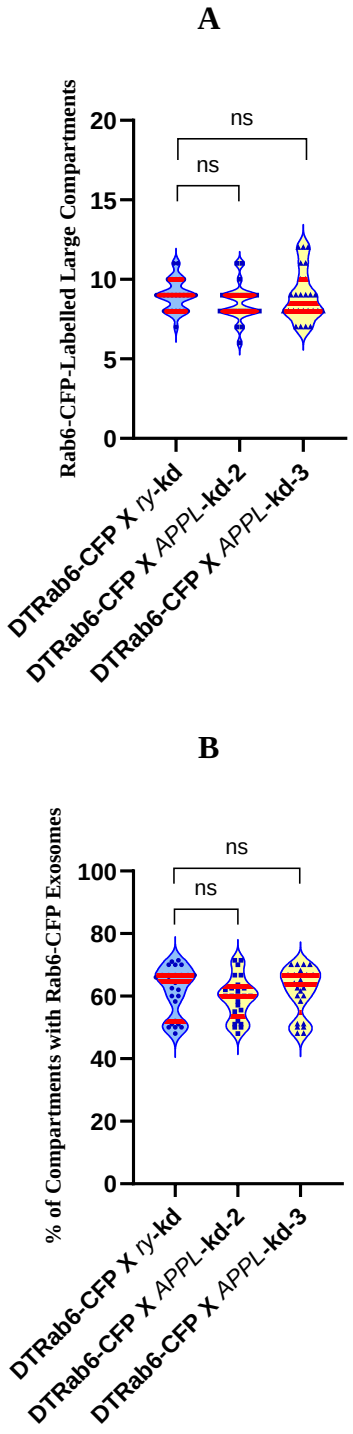

Figure 4.14: The effect of *APPL*-kd on Rab6-CFP-labelled compartments and exosomes. A: both *APPL*-kd lines have the same number of Rab6-CFP-labelled large compartments as controls. **B:** both *APPL*-kd lines have the same percentage of Rab6-CFP

exosomes within large non-acidic compartments as controls. The mean for each set of experiments is shown in red.

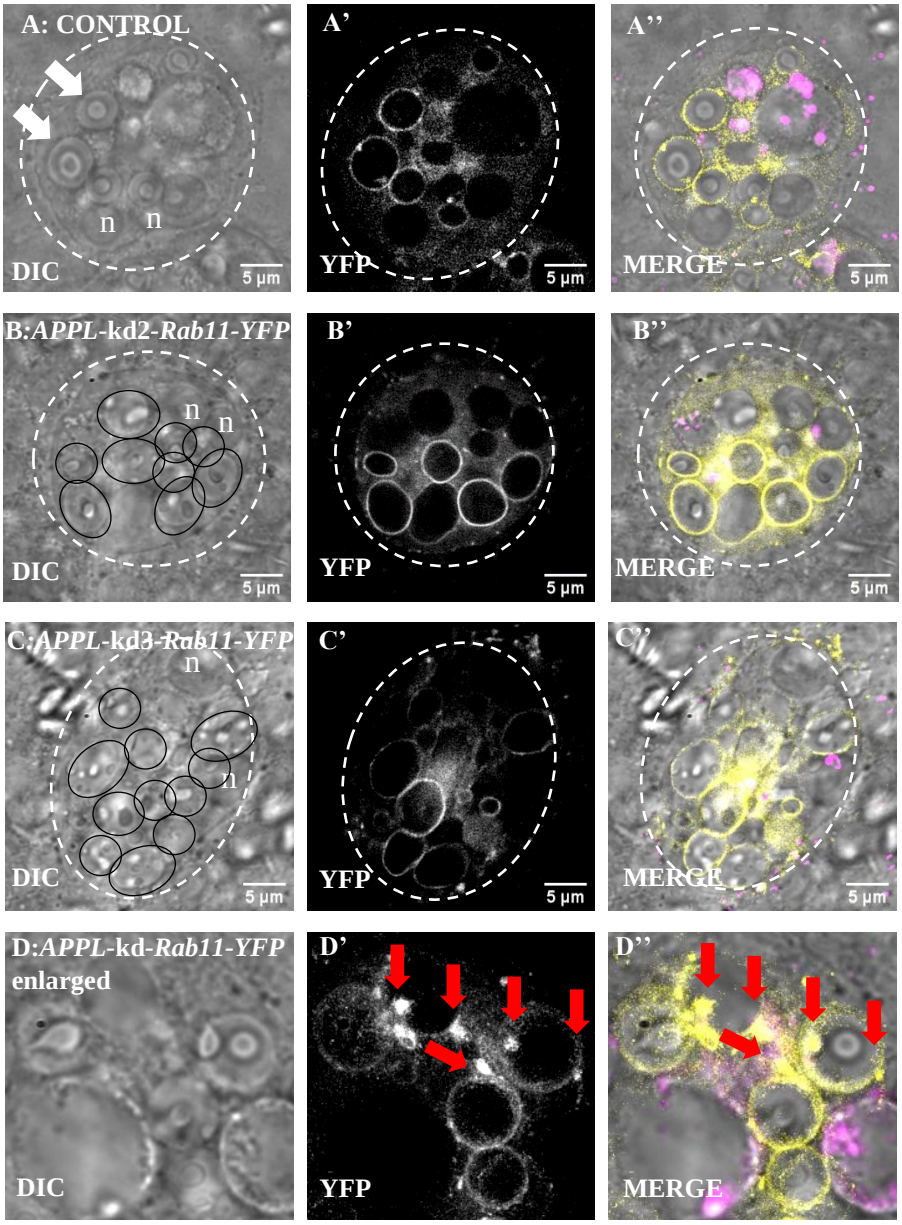

Figure 4.15: The Rab11 identity of large non-acidic compartments is not affected by *APPL*-knockdown. SCs from six day-old virgin males stained with LysoTracker Red and imaged *ex vivo*, using DIC and fluorescence microscopy for GFP and LysoTracker Red. **A)** w^{1118}*; tub-GAL80*^{ts}*/UAS-ry-RNAi; Rab11-YFP dsx-GAL4/+* (control) **B)** w^{1118}*; tub-GAL80*^{ts}*/UAS-ry-RNAi; Rab11-YFP dsx-GAL4/UAS-APPL-RNAi-2* **C)** w^{1118}*; tub-GAL80*^{ts}*/UAS-ry-RNAi; Rab11-YFP dsx-GAL4/UAS-APPL-RNAi-3* **D)** Magnified view showing Rab11-YFP-labelled exosomes (arrows) within DCG compartments with mini-cores (due to the *APPL*-knockdown effect of non-coalescence of MFAS in dense-cores). **White arrows** in **A:** DCGs; **Red arrows** in **D'** and **D'':** Rab11-labelled exosomes; **black**

circles in **B** and **C:** compartments with mini-cores; **n:** double nuclei characteristic of each SC. Scale bar = 5 μm.

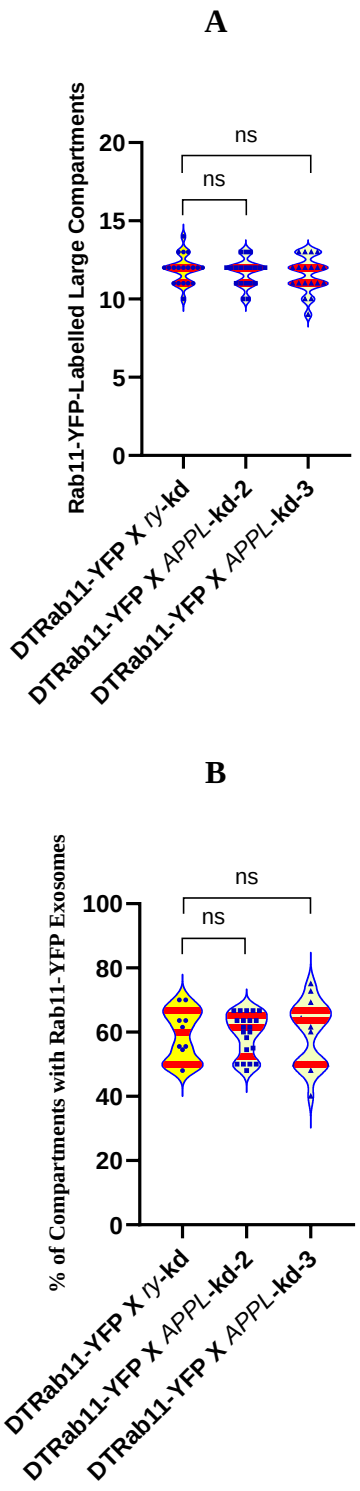

Figure 4.16: The effect of *APPL*-kd on Rab11-YFP-labelled compartments and exosomes. A: Both *APPL*-kd lines have the same number of Rab11-YFP-labelled

compartments as controls. **B:** Both *APPL*-kd lines have the same percentage of Rab11-YFP exosomes as controls. The mean for each set of experiments is shown in red.

4.2.4 NEITHER *mfas* OR *APPL*-KNOCKDOWNS AFFECT ILVs OR EXOSOMES

Intraluminal vesicles (ILVs) are contained within multivesicular bodies (MVBs); when MVBs fuse with the cell membrane, ILVs are released as exosomes (**Figure 4.17**).

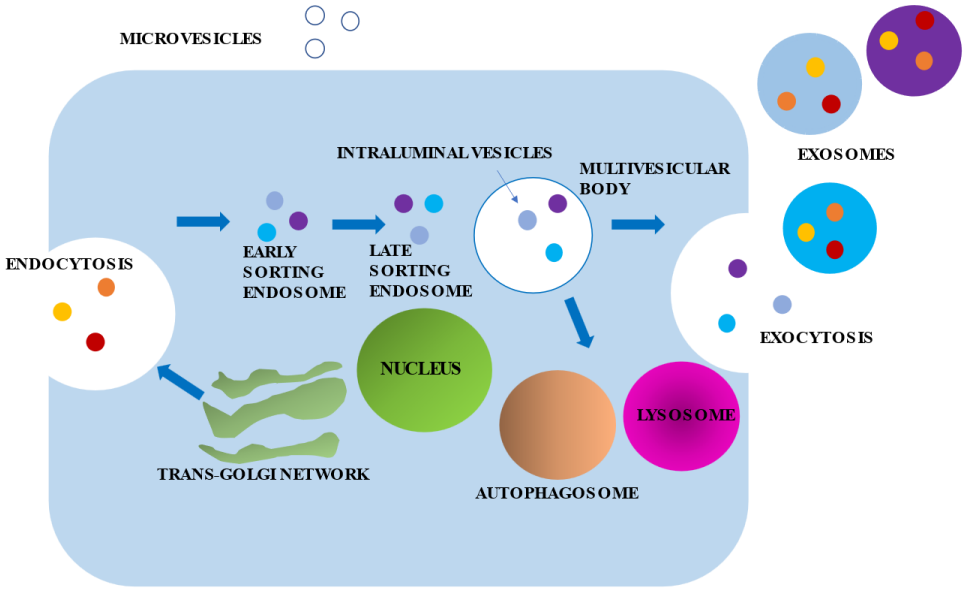

Figure 4.17: Intraluminal vesicles (ILVs) form within multivesicular bodies (MVBs), and are then released extracellularly as exosomes.

Previous work from the Wilson laboratory established that proteins which are important in *Drosophila* mating behaviour are packaged into ILVs, which are then secreted extracellularly as exosomes (Corrigan *et al.*, 2014). However, Rab6 and Rab11 only mark a subset of Intraluminal vesicles (ILVs) formed in Rab11 secretory compartments of SCs (Fan *et al.*, 2020; Wells *et al.*, 2023). Recognizing the many parallels between amyloid-structured DCGs and amyloid-storing granules in CNS-located pituitary and various other

neuroendocrine cells, I therefore extended my analysis with Rab6 and Rab11 and examined ILV production in response to the knockdowns of *mfas* and *APPL*, this time using Breathless-GFP (Btl-GFP), a more generic exosome marker in SCs. Breathless is a *Drosophila* fibroblast growth factor receptor which traffics at high levels onto the surface of numerous ILVs, but not acidic compartments (Sato and Kornberg, 2002). The utility of using Btl and similarly GFP-tagged fusion proteins in studying the cellular mechanics within SCs was previously demonstrated in the Wilson laboratory (Corrigan *et al.*, 2014; Kroeger, B. R., D.Phil Thesis, 2017, pg. 235). I therefore utilised *Breathless-GFP* for this experiment, in which I overexpressed *UAS-ry-RNAi* constructs in adult SCs under dsx-GAL4 control, driving one line with *w^{1118}; tub-GAL80^{ts}/CyO; dsx-GAL4 GFP-mfas/TM6B* (DTMFAS), and the other with *w; tub-GAL80^{ts}/CyO; dsx-GAL4-Btl-GFP*. The results below show that Btl significantly increased the number of large non-acidic compartments in SCs (**Figures 4.18** and **4. 19**).

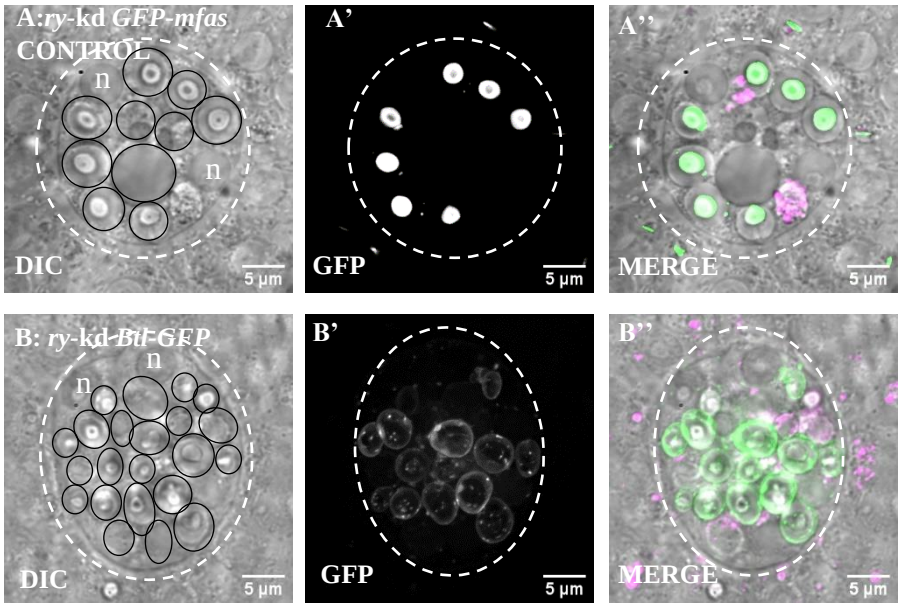

Figure 4.18: *Btl-GFP* increases the number of large non-acidic compartments. SCs from six day-old virgin males stained with LysoTracker Red and imaged *ex vivo*, using DIC and fluorescence microscopy for GFP and LysoTracker Red. **A)** w^{1118}*; tub-GAL80*^{ts}*/UAS-ry-RNAi ; dsx-GAL4 GFP-mfas/+* (control) **B)** *y, w; tub-GAL80*$^{t/s}$*/UAS-ry-RNAi; dsx-GAL4 UAS-Btl-GFP/+* .**Black circles:** large non-acidic compartments; **n:** double nuclei characteristic of each SC. Scale bar = 5 µm.

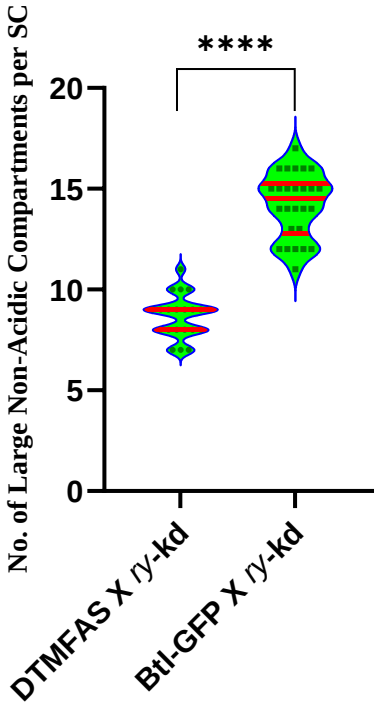

Figure 4.19: *Btl-GFP* increases the number of large non-acidic compartments as compared to controls. The mean for each set of experiments is shown in red.

In the next series of experiments, I overexpressed two *mfas*-kd lines and the two strongest *APPL*-kd lines in adult SCs under dsx-GAL4 control. I used flies overexpressing *Btl-GFP* as the driver line, and compared the resultant phenotypes from each of these manipulations to control cells expressing a *UAS-ry-RNAi* construct in the same background. The number of Btl-GFP-labelled compartments and exosomes were then visualised. As shown in **Figures 4.20** and **4.21**, the number of Btl-GFP-labelled large non-acidic compartments (**Figure 4.20A-E** and **4.21A**) and Btl-GFP-labelled exosomes (**Figure 4.21B**) in each of the four knockdown lines tested were the same as in controls. This experiment also showed that using *UAS-Btl-GFP* as the driver line increases the number of large non-acidic compartments (**Figures 4.18** and **4.19**). Taken together, these results show that the knockdown of *mfas* and *APPL* do not affect compartments which themselves are labelled and affected by Breathless.

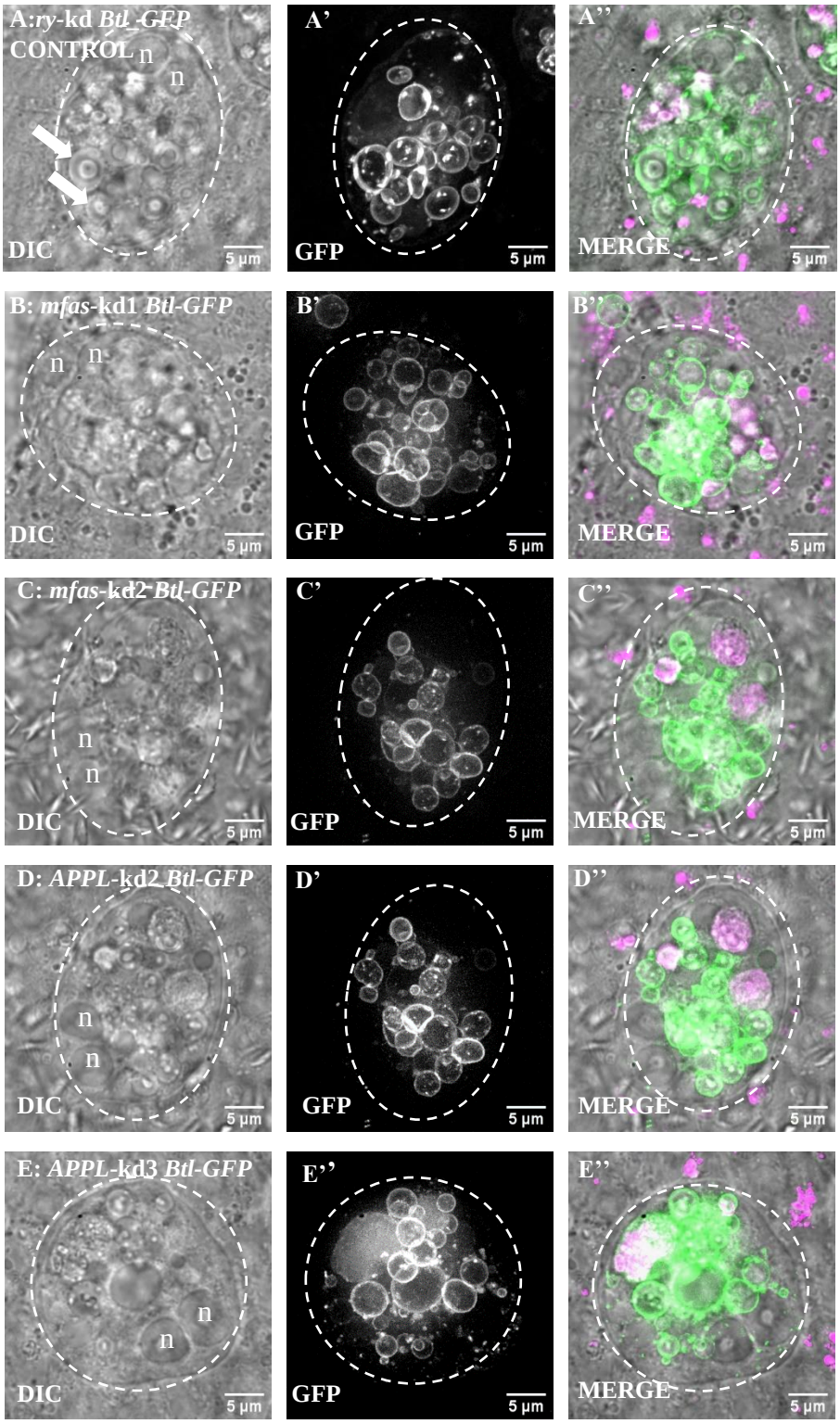

Figure 4.20: Neither *mfas*- nor *APPL*-knockdowns alter the number of large non-acidic compartments containing intraluminal vesicles (ILVs). SCs from six day-old virgin males stained with LysoTracker Red and imaged *ex vivo*, using DIC and fluorescence microscopy for GFP and LysoTracker Red. **A)** *y, w; tub-GAL80^{ts}/UAS-ry-*

RNAi; dsx-GAL4 UAS-Btl-GFP/+ (control) **B)** *y, w; tub-GAL80^{ts}/UAS-mfas-RNAi-1; dsx-GAL4 UAS-Btl-GFP/+* **C)** *y, w; tub-GAL80^{ts}/UAS-mfas-RNAi-2; dsx-GAL4 UAS-Btl-GFP/+* **D)** *y, w; tub-GAL80^{ts}/UAS-APPL-RNAi-2; dsx-GAL4 UAS-Btl-GFP/+* **E)** *y, w; tub-GAL80^{ts}/UAS-APPL-RNAi-3; dsx-GAL4 UAS-Btl-GFP/+*. **White arrows** in **A:** DCGs; **n:** double nuclei characteristic of each SC. Scale bar = 5 µm.

A

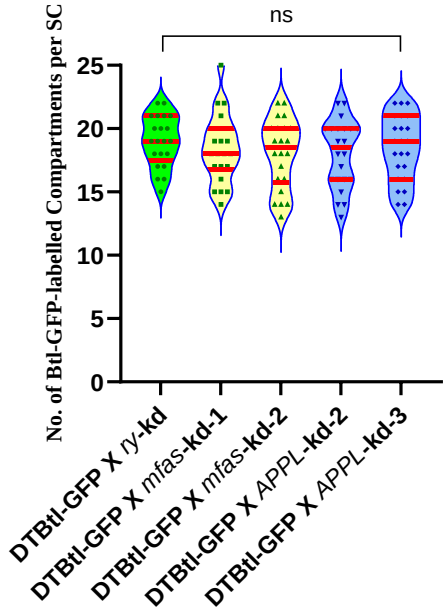

B

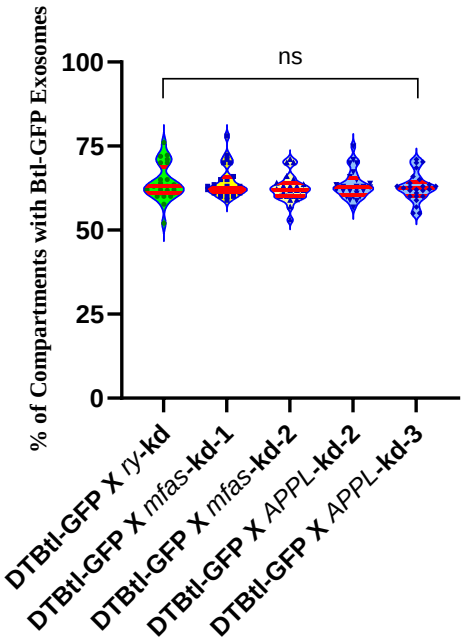

Figure 4.21: A: *mfas*-kds and *APPL*-kds have the same number of Btl-GFP-labelled compartments as controls. B: Both of the *mfas*-kds and the *APPL*-kds have the same percentage of Btl-GFP compartments which contain exosomes as controls. The mean for each set of experiments is shown in red.

4.2.5 THE RELATIONSHIP BETWEEN VARIOUS SEGMENTS OF APP/APPL AND DCG BIOGENESIS

In this chapter, having demonstrated a role for *APPL* in DCG biogenesis, I explored the effects of various manipulations of APPL on DCG biogenesis. Like human APP, Drosophila APPL undergoes processing by proteolytic cleavages at its α-, β- and γ-sites (Rooke *et al.,* 1996; Carmine-Simmen *et al.,* 2009; Hong and Koo, 1997; Boulianne *et al.,* 1997). The α- and γ-cleavages are considered critical in the pathogenesis of AD, since the former disrupts the Aβ sequence and determines whether the amyloidogenic or non-amyloidogenic pathway is followed. Gamma-cleavage, the crucial final step, releases Aβ (that has escaped α-cleavage) from the membrane. I therefore studied the effects of knockdowns of *Drosophila α-* and *γ-secretases* on DCG formation (the *β-secretase*-knockdown line was not available at the time).

As a reference for the experiments to be described below which manipulate various segments of APP and APPL, an overview of the cleavage process of this parent molecule of Aβ is shown in **Figure 4.22A** and **B.** (For greater detail on the location of APP cleavages in relation to the FAD mutations studied in this work, please see **Figure 4.5).**

A

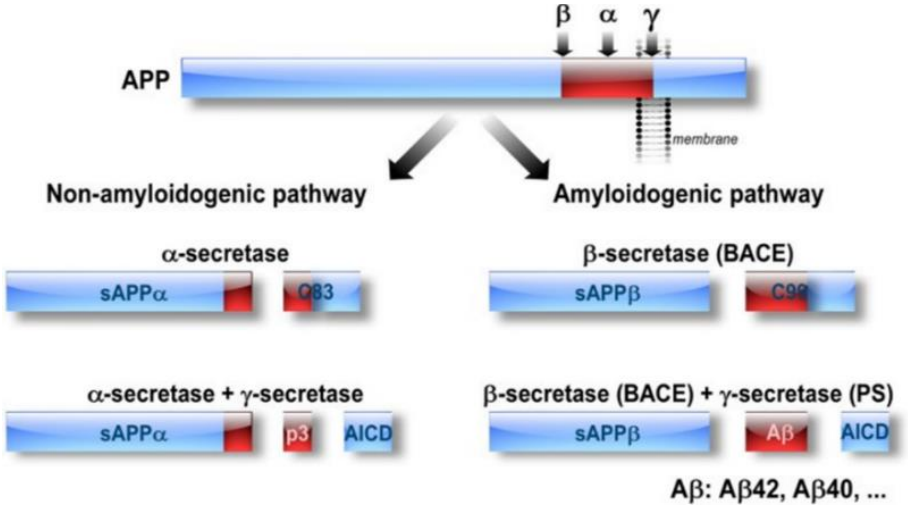

B

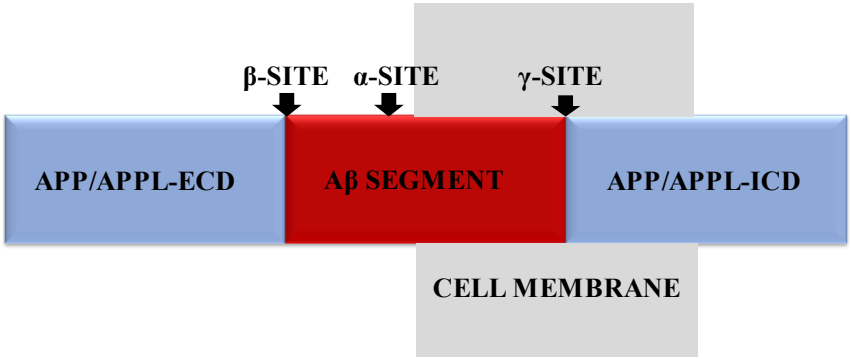

Figure 4.22: Alpha, β- and γ-secretase cleavages drive APPL and APP down either amyloidogenic or non-amyloidogenic pathways. A: Alpha-cleavage disrupts the Aβ sequence and leads to non-amyloidogenic processing of APP. **B:** Enlarged view of the location of secretase cleavages of APP. *Drosophila* APPL is cleaved in a similar fashion, with the exception that the α- and β-cleavage sites are reversed.

As mentioned earlier, these human APP secretases all have *Drosophila* homologues; for the α-secretase experiment a *kuzbanian*-knockdown line was used, while for γ-secretase, the line used was a knockdown of the *Drosophila* homologue of *Nicastrin*, a crucial component of the tetrameric enzyme which holds APPL in position between dPS's intramembranous catalytic aspartates (shown below in **Figure 4.23).** In an example of eponymous whimsy, *Nicastrin* was named after the small Italian town of Nicastro, where Yale researchers found several members of an extended family who suffered from FAD, later found to be due to *Nicastrin* mutations (Feldman *et al.*, 1963).

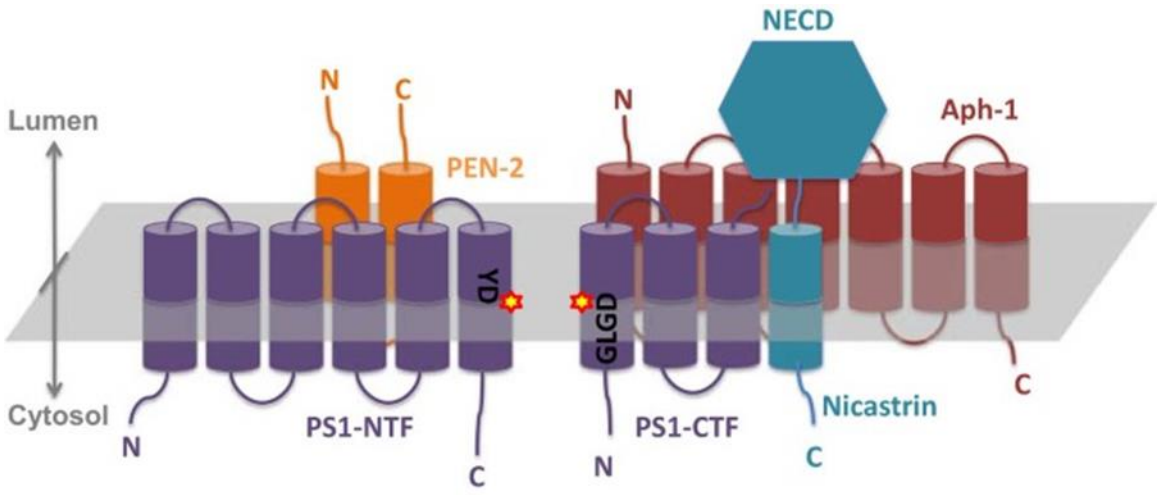

Figure 4.23: The overall structure of Presenilin, APP's γ-secretase. CTF: C-terminal fragment; **D:** catalytic aspartates on the adjacent transmembrane domains 6 and 7; **NECD:** nicastrin extracellular domain; **NTF:** N-terminal fragment; **PS1:** presenilin-1. (Yi *et al.*, Mol. Neurodegeneration 2014, p. 3).

The γ-secretase is an aspartyl protease with the following four components: Aph-1 (anterior pharynx defective-1), Nicastrin, Presenilin-1 or -2, and Pen-2 (presenilin enhancer-2). Presenilin has highly conserved catalytic aspartates (Asp^{257} and Asp^{385}) on adjoining transmembrane domains 6 and 7 respectively (Wolfe *et al.*, 1999). Nicastrin has a prominent cap-like ectodomain which aids it in it's roles of substrate receptivity, locking

the substrate in place, gatekeeping the catalytic site, and assembly of the γ-secretase complex (Shah *et al.,* 2005). Aph-1 stabilizes Presenilin (Verdile *et al*., 2006), while Pen-2 stabilizes the γ-secretase complex (Wolfe, 2006). *Drosophila* PS has the same four components as human Presenilin (Hong and Koo, 1997; Boulianne *et al.,* 1997).

The human α-secretase is a zinc metalloproteinase which cleaves APP between Lys^{613} and Leu^{614} (Roberts *et al.,* 1994). While several members of the ADAM (a disintegrase and metalloproteinase) family were initially considered α-secretase candidates, the field was narrowed down to ADAM10, ADAM17 and ADAM9 (Howard *et al*., 1996). Kuzbanian is the *Drosophila* homologue of ADAM10, the human α-secretase with the highest activity (Rooke *et al*., 1996). Intriguingly, although APP's Aβ sequence is not conserved in APPL, APPL is cleaved by kuzbanian, dBACE, human BACE, and *Drosophila* Presenilin. Additionally, when dBACE and APPL were overexpressed together, *Drosophila* Aβ (dAβ) aggregates were formed, which caused behavioural abnormalities, spongiform lesions, and the death of neurons (Jacobsen and Iverfeldt, 2009; Carmine-Simmen *et al.,* 2008).

4.2.5.1 THE EFFECTS OF *DROSOPHILA α-* AND *γ-SECRETASE* KNOCKDOWNS ON DCGs

To test the possible roles for the secretases involved in APPL processing in SC biogenesis, I expressed one *RNAi* targeting Drosophila *α-secretase (kuzbanian)* and two targeting its *γ-secretase (Nicastrin*) in SCs under dsx-GAL4 control, and compared them to control cells expressing a *UAS-ry-RNAi* construct. Perhaps surprisingly, I found no morphological defects in DCGs (**Figure 4. 24**), but in all knockdowns, the number of DCG compartments

was slightly, but significantly increased (**Figure 4. 25**), suggesting that these proteases do play a role in the overall DCG biogenesis process.

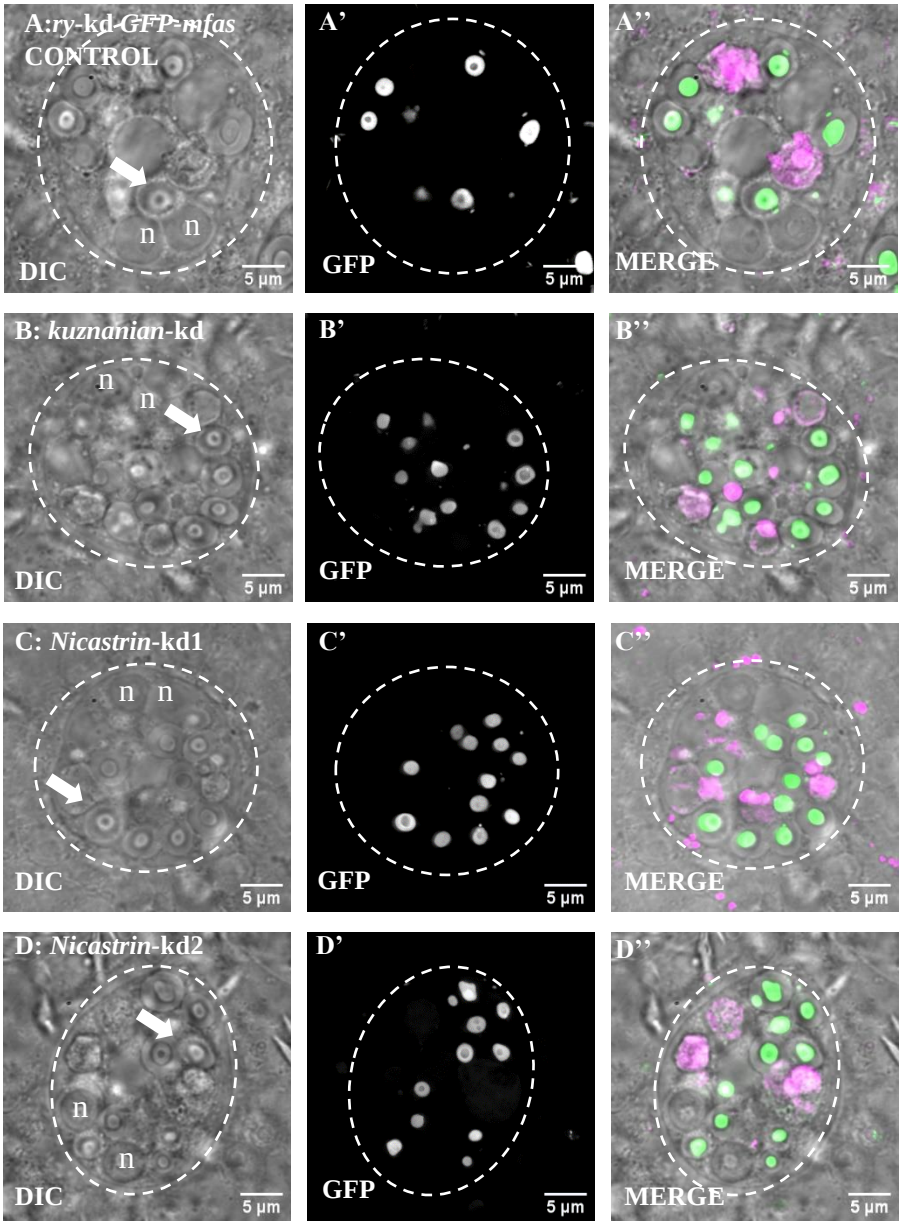

Figure 4.24: The effect of *α*- and *γ-secretase*-knockdowns on DCG formation. SCs from six day-old virgin males stained with LysoTracker Red and imaged *ex vivo*, using DIC and fluorescence microscopy for GFP and LysoTracker Red. **A)** w^{1118}*; tub-GAL80*^{ts}*/UAS-ry-RNAi; dsx-GAL4 GFP-mfas/+* (control) **B)** w^{1118}*; tub-GAL80*^{ts}*/UAS-kuz-RNAi; dsx-GAL4 GFP-mfas/+* **C)** w^{1118}*; tub-GAL80*^{ts}*/UAS-Nicastrin-RNAi-1; dsx-GAL4 GFP-mfas/+* **D)** w^{1118}*; tub-GAL80*^{ts}*/+; dsx-GAL4 GFP-mfas/UAS-Nicastrin-RNAi-2.* **White arrows** in **A** through **D:** DCGs; **n:** double nuclei characteristic of each SC. Scale bar = 5 µm.

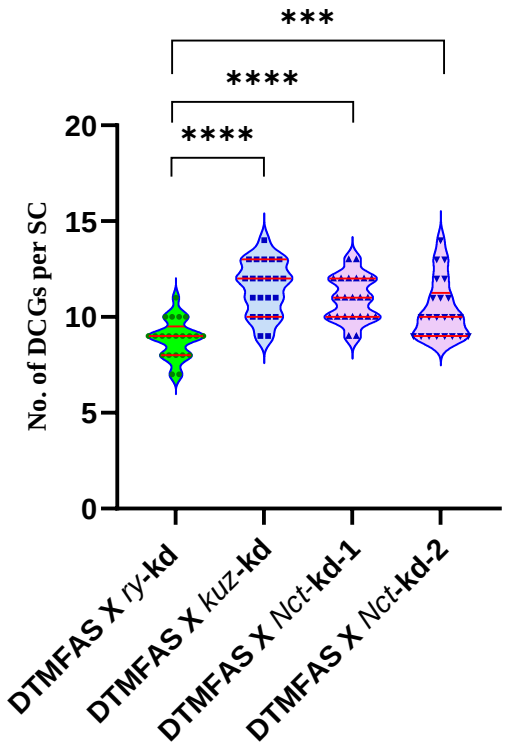

Figure 4.25: The effect of *Drosophila α-* and *γ-secretase*-knockdowns on DCGs. *Drosophila α-secretase (Kuzbanian)* and *γ-secretase (Nicastrin)* knockdowns produce a higher number of DCGs as compared to controls. All listed genotypes were driven by w^{1118}; *tub-GAL80^{ts}/CyO; dsx-GAL4 GFP-mfas/TM6B* (DTMFAS). The mean for each set of experiments is shown in red.

4.2.5.2 EFFECTS OF *DROSOPHILA* APPL EXTRA- AND INTRACELLULAR DOMAIN DELETIONS ON DCGs

Taking into consideration the similarities between members of the APP family - with human APP being the most studied point of reference - I conducted experiments to study the effects of deletion of *Drosophila* APPL's extra- and intracellular portions on DCG formation. These experiments were suggested by Dr. Bhavna Verma, post-doctoral scientist in the Wilson laboratory, who I gratefully acknowledge. I undertook two experiments to perform an initial test of the importance of different domains within the APPL molecule. In the first experiment I overexpressed APPL with the deletion of part of

the extracellular domain 1 (domain E1, amino acids 85-321) and also the α- and β-cleavage sites near to the transmembrane domain (Torroja *et al*., 1999). As a result, the remainder of the protein stays tethered to the membrane. The second experiment looked at the overexpression of *APPL* with deletion of the short intracellular domain. The remaining portion of APPL is also membrane-bound, since the deletion includes the cleavage site, the G_0 binding domain, and the internalization signal of the APPL coding region (amino acids 836-886). The intracellular portion has an YENPTY motif (**Figure 4.6**) which mediates interaction with clathrin, but is otherwise known primarily to be involved in gene regulation through protein-protein interactions.

For these experiments, I overexpressed in SCs under the control of dsx-GAL4 both the above mentioned *APPL* constructs – one with the deletion of part of the extracellular domain, and the other with the deletion of the short APPL intracellular domain. I then compared them to control cells expressing a *UAS-ry-RNAi* construct which was used as a control.

As shown in the results below, deletion of the extracellular domain of APPL resulted in fewer DCGs, with the majority of them being normal (**Figure 4.26B**). Some APPL-ECD-deletion DCGs, however, were mis-shapen and contacted the limiting membrane of the compartment (similarly mis-shapen DCGs contacting the limiting membrane were also subsequently found by Dr. Bhavna Verma in the Wilson laboratory in experiments on APPL lacking the cleavage domains). However, deletion of APPL's short intracellular

domain resulted in the complete non-formation of DCGs, and the frequent presence of enlarged lysosomes (**Figure 4.26C** and **D**). This result is consistent with published data on APP-ICD's multiplicity of functions, which makes it's involvement in DCG biogenesis all the more likely. The ICD is also a highly conserved segment of APP/APPL, of note being it's YENPTY sorting motif which facilitates clathrin-mediated endocytosis, and which is involved in APP's trafficking (Leysson *et al.,* 2005; Lai *et al.,* 1995; Perez *et al.,* 1999; Ring *et al.,* 2007).

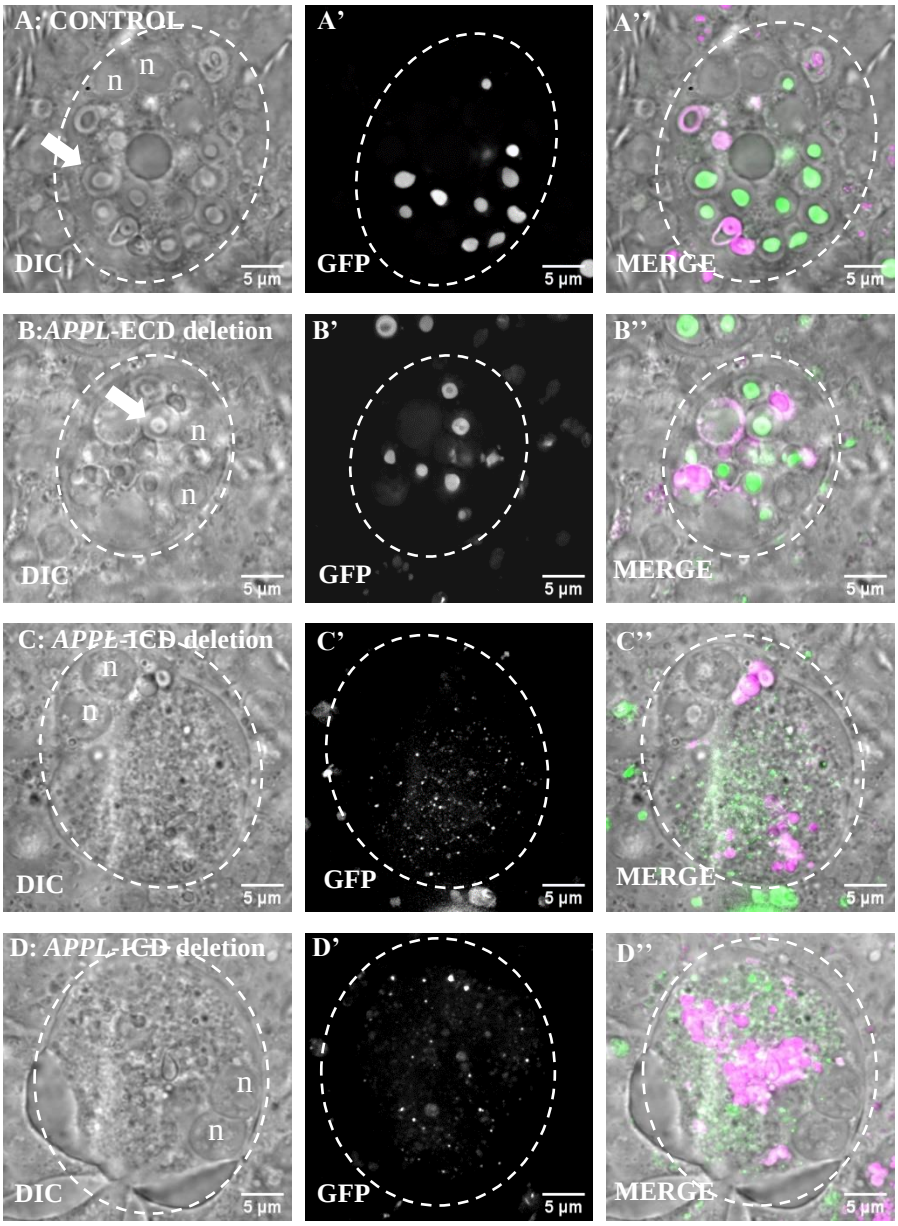

Figure 4.26: The extra and intracellular domains of APPL play distinct roles in the formation of DCGs, as shown by experiments involving their deletion. SCs from six day-old virgin males stained with LysoTracker Red and imaged *ex vivo*, using DIC and fluorescence microscopy for GFP and LysoTracker Red. **A)** *w^{1118}; tub-GAL80^{ts}/UAS-ry-RNAi; dsx-GAL4 GFP-mfas/+* (control) **B)** *w^{1118}; tub-GAL80^{ts}/+; dsx-GAL4 GFP-mfas/ P{w[+mC}=UAS-sdDeltaE1}3* (APPL with extracellular deletion from amino acids 85-231 including part of the E1 domain) showing fewer DCGs **C)** *w^{1118}; tub-GAL80^{ts}/P{w[+mC}=UAS-sdDeltaC}2; dsx-GAL4 GFP-mfas/+* (APPL with intracellular deletion) showing non-formation of DCGs **D)** a second example of *w^{1118}; tub-GAL80^{ts}/P{w[+mC}=UAS-sdDeltaC}2; dsx-GAL4 GFP-mfas/+* (APPL with intracellular deletion) showing the non-formation of DCGs, in addition to large lysosomes, indicative of degradation of abnormal dense-cores. **White arrows** in **A** and **B:** DCGs; **n:** double nuclei characteristic of each SC. Scale bar = 5 µm.

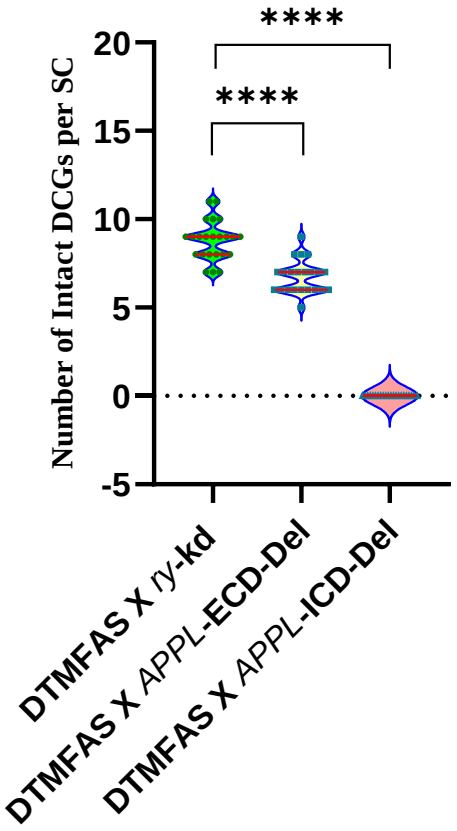

Figure 4.27: APPL-extracellular domain deletion lines (*APPL-ECD-Del*) have fewer intact DCGs, whereas APPL-intracellular domain deletion lines (*APPL-ICD-Del*) have no intact DCGs. All listed genotypes were driven by *w*^{1118}*; tub-GAL80*^{ts}*/CyO; dsx-GAL4 GFP-mfas/TM6B* (DTMFAS). The mean for each set of experiments is shown in red.

4.2.5.3 EFFECTS OF FULL-LENGTH AND β-SECRETASE CLEAVED HUMAN APP ON DCGs

Having established that the complete or partial absence of *Drosophila* APPL influences MFAS, and that the absence of *Drosophila* APPL α- and γ-secretases do not, I then examined the effects of human APP on MFAS. To this end, I studied flies transgenic for both full-length *APP*, as well as *APP* co-expressed with it's human β-secretase (*APP-BACE-1*). The precise site of it's β-cleavage is shown in **Figure 4.28**.

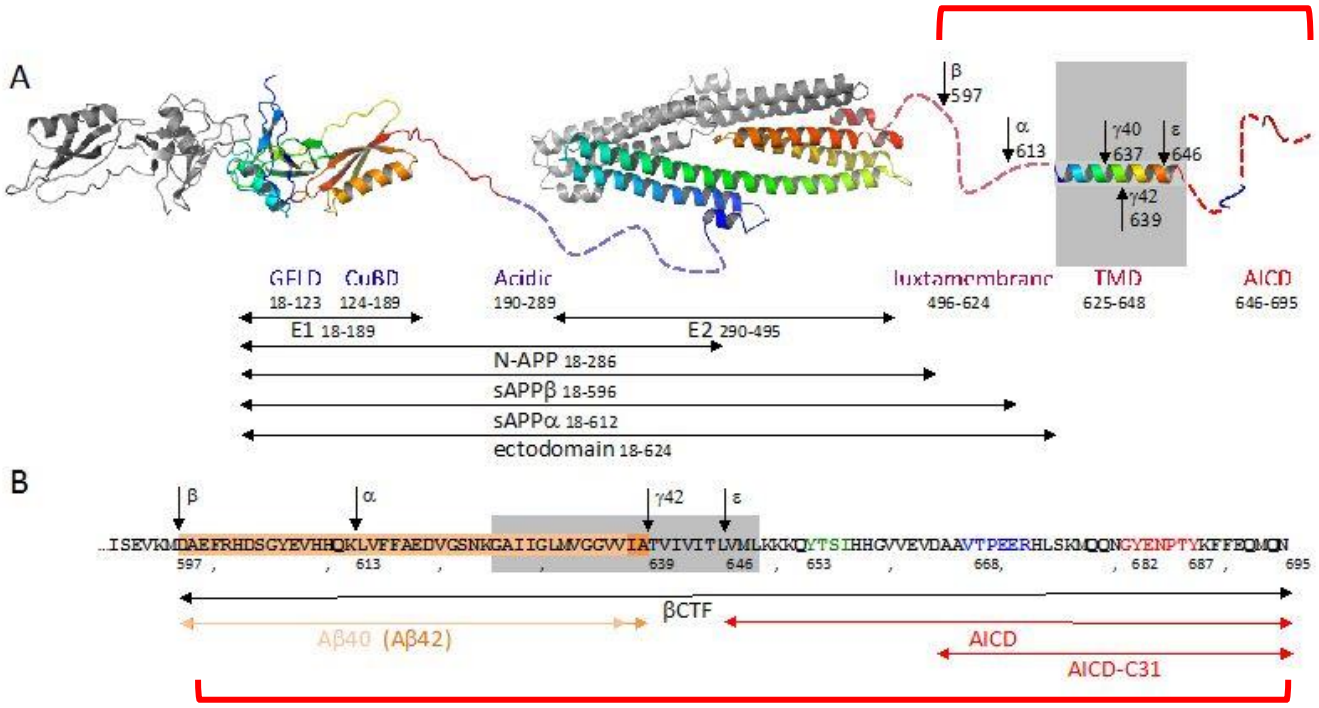

Figure 4.28: Human APP, it's architecture and cleavage sites. A: Domain architecture of the 695 amino acid neuronal splice variant, which is the splice variant used in the Bloomington fly line employed for this experiment. Dashed lines are structurally unknown regions in three dimensions. The juxta-membrane region between ectodomain E2 and the transmembrane domain, which consists of amino acids 496 to 624, is intrinsically disordered based on predictions of it's secondary structure. However, it contains the α- and β-cleavage sites. **B:** Amino acid sequence and proteolytic fragments. **AICD:** APP intracellular domain; **CTF:** C-terminal fragment; **CuBD:** copper-binding domain; **GFLD:** growth factor like domain; **TMD:** transmembrane domain. The red bracketed areas in **A** and **B** show the remaining membrane-tethered 98 amino acid APP fragment following β-secretase cleavage. (Adapted from Müller and Wild, Understanding Alzheimer's Disease 2013, p. 2).

To perform this experiment, I overexpressed both full-length human APP as well as APP co-expressed with its β-site-cleaving protease in SCs under dsx-GAL4 control. I compared these experimental lines to control cells expressing a *UAS-ry-RNAi* construct. In the results shown below, I found that neither the overexpression of full-length human APP nor the overexpression of it's human β-secretase-cleaved version affects the coalescence of MFAS in the formation of DCGs. Thus, both the number and morphology of DCGs seen with

these lines were normal (Figure **4.29B** and **C**). This is consistent with results showing that the absence of the ECD does not affect DCG morphology (**Figure 4.26B**).

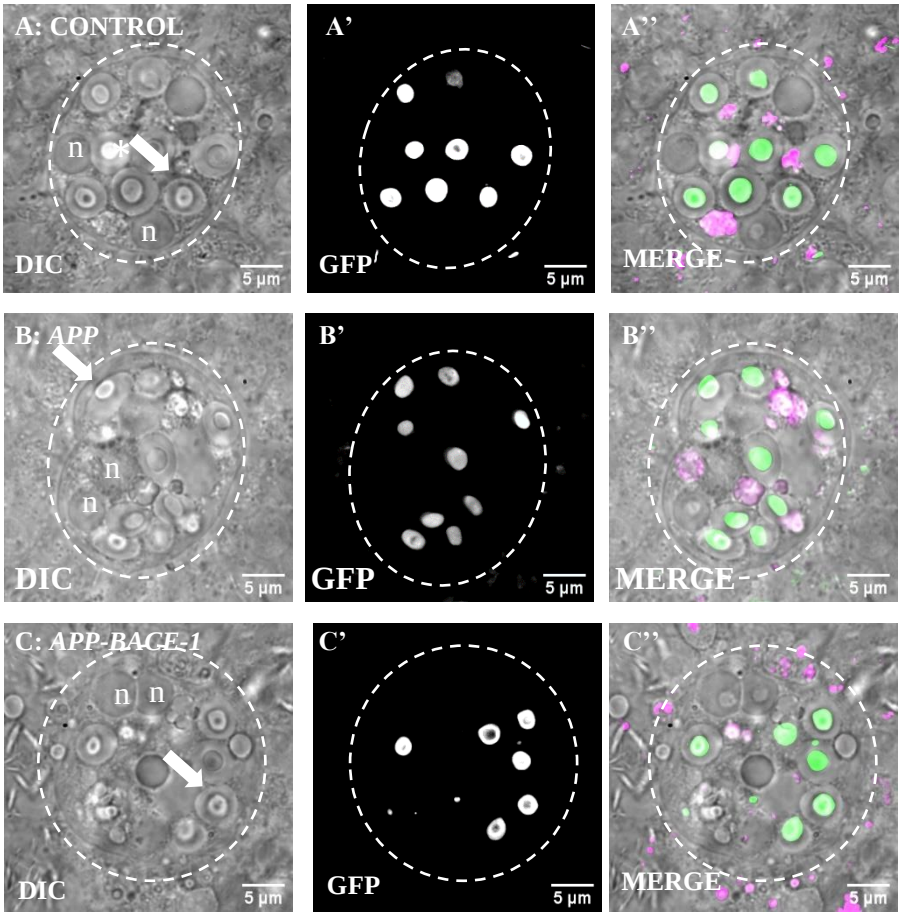

Figure 4.29: The presence of human APP, either full-length or cleaved by it's β-secretase BACE-1, does not affect DCG formation. SCs from six-day-old virgin males stained with LysoTracker Red and imaged *ex vivo*, using DIC and fluorescence microscopy for GFP and LysoTracker Red. **A)** *w^{1118}; tub-GAL80^{ts}/UAS-ry-RNAi; dsx-GAL4 GFP-mfas/+* (control) **B)** *w^{1118}; tub-GAL80^{ts}/UAS-APP-YFP; dsx-GAL4 GFP-mfas/+* **C)** *w^{1118}; tub-GAL80^{ts}/+; dsx-GAL4 GFP-mfas/UAS-BACE-1-APP-isoform 695*. **White arrows** in **A** to **C:** DCGs; **n:** double nuclei characteristic of each SC. Scale bar = 5 µm.

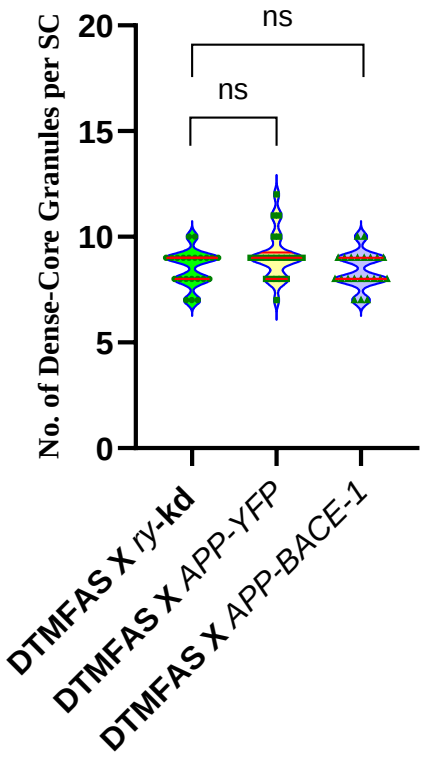

Figure 4.30: The overexpression of both full-length human *APP* and human *APP-BACE-1* produce the same number of DCGs as controls. These DCGs also appear morphologically normal. All listed genotypes were driven by *w^{1118}; tub-GAL80^{ts}/CyO; dsx-GAL4 GFP-mfas/TM6B* (DTMFAS). The mean for each set of experiments is shown in red.

4.3 DISCUSSION

4.3.1 *GAPDH2* IS REQUIRED FOR DCG FORMATION

GAPDH is a ubiquitous glycolytic enzyme now recognized as having multiple roles, earning it the moniker of the 'moonlighting molecule'. The knockdown of it's *Drosophila* homologue *GAPDH2* results in the dysgenesis of DCGs in a signature pattern, a result also shown by Dar et al. (Dar *et al.*, 2021) and adds yet another role to the multiplicity of it's known cellular functions.

Human GAPDH has numerous historical associations with neurodegenerative diseases, and these results underscore the emerging relationship between MFAS and protein aggregation, now observed for MFAS in SCs. GAPDH's several 'extra-glycolytic' roles include it's role as an initiator of apoptosis (Berry and Boulton, 2000; Berry, 2004; Butera *et al.,* 2019). Some of the most compelling bodies of evidence for this have come from the polyglutamine-repeat diseases, wherein polyglutamine repeats were found to bind to GAPDH, translocate to the nucleus, and initiate apoptosis. These GAPDH-poly-Q-complexes are found in the polyglutamine repeat conditions Machado-Joseph disease, Dentatorubral Pallidoluysian Atrophy (DRPLA) and Huntington's disease (Ishitani *et al.,* 2003; Mazzola and Sirover, 2002). In Alzheimer's disease, antibodies raised against Aβ plaques reacted strongly with nuclear GAPDH in cells undergoing apoptosis in culture (Sunaga *et al.,* 1995). Furthermore, GAPDH binds to the C-terminal region of APP (Schulze *et al.,* 1993), rises in correlation with Aβ plaque volume (Tsai *et al.,* 2020), and $A\beta_{42}$-GAPDH complexes in cerebrospinal fluid are cleared more slowly than non-complexed $A\beta_{42}$ (Lazarev *et al.,* 2021). GAPDH also has a propensity to complex with Tau in neurofibrillary tangles (Wang *et al.,* 2005), and has a long association with Parkinson's disease, having been found by immunostaining to be located in the nuclei of diseased substantia nigra neurons from Parkinson's patients (Tatton, 2000). More recent studies have started to unravel the mechanisms whereby nuclear GAPDH triggers autophagy, a phenomenon perhaps in keeping with it's role as a glycolytic enzyme. During glucose starvation, cytoplasmic GAPDH is phosphorylated by activated AMPK, prompting it's migration into the nucleus. In the nucleus, it directly interacts with SIRT1, displacing it's repressor and enhancing SIRT1 deacetylase activity (Chang *et al.,* 2015). Finally, as I show

(albeit without a mechanistic explanation) overexpressing human *GAPDH* in *Drosophila* increases the number of DCGs (**Figure 4.8C**). Taken together, these results strengthen the asssociation between *GAPDH/GAPDH2* and protein aggregation, whch can lead to amyloidogenesis. They also show the the ease and efficiency of using the MFAS-GFP marker to track the fate of MFAS in DCGs, as DCG formation is tested by genetic influences with links to human amyloid neurodegeneration.

4.3.2 *APPL* IS REQUIRED FOR DCG FORMATION

The knockdown of *APPL* results in the non-coalsecence of MFAS in a pattern distinct from that seen with the knockdown of $GAPDH_2$. Specifically, while $GAPDH_2$-kd results in MFAS moeities adherent to the circumference of the DCG membrane, *APPL*-kd results in a more uniform distribution of MFAS throughout the compartment. The movement of these flecks of MFAS are also different for these two knockdowns. This suggests that the molecular influences governing the effects of $GAPDH_2$ and APPL are distinct from each other, and are the subject of ongoing investigation in the Wilson laboratory.

The other, more overarching inference from these results is that amyloids influence each other. Given parallel evidence emerging from the burgeoning field of amyloid biology, this is unsurprising, since amyloids belong to a common family, and have developed evolutionarily to retain common properties (Sawaya *et al.,* 2021). These common ancestral origins might explain the shared rules of structure which all amyloid proteins obey once in their final forms, no matter how far-removed they are from each other in function or organismic origin. Historically they have been classified into three classes based on order of discovery and pathogenicity. The first discovered group were the pathological amyloids

– β-amyloid, Tau, α-synuclein, and human islet amyloid polypeptide (hIAPP). The 35 members of this group showed little sequence similarity, but in their mature and processed forms all assumed the identical and unmistakeable biophysical signatures of amyloid. The second group to be discovered in the 1990s were the artificial amyloids, created when globular proteins were subjected to denaturing conditions (Gustavsson *et al.*, 1991; Colon and Kelly, 1992). The ease and ubiquity of their formation even led to speculation that amyloids might have been pre-RNA prehistoric enzymes, a theory known as the 'amyloid-world hypothesis' (Greenwald *et al.*, 2018; Rufo *et a*l., 2014). The final group to be discovered were the functional amyloids, found everywhere from microbes to humans, examples of these being curli fibres in bacterial biofilms and PMEL protein scaffolds for melanin in melanocytes (Fowler *et al*., 2007).

Further emphasizing both the diversity as well as the linked nature of these functional amyloids were discoveries illuminating their functions. These functions are: a) structural (for example, bacterial curli fibres), b) acting as reservoirs (for example, the amyloid storage form of hormones), c) the carriage of information (for example, HET-s fibrils in yeast transfer information to daughter cells regarding compatibility of fusion to other yeast cells), d) function suppression (for example, hypoglycemia induces Cdc19 fibrillization and reduces it's pyruvate kinase activity), and e) signalling (for example, RIPK1/RIPK3 fibrillizes to signal that necroptosis has occurred) (the functional roles of amyloids are reviewed in Otzen and Riek, 2019). In keeping with the functional utility of amyloids, *Drosophila* APPL is known to be required for associative olfactory memory and middle-term memory formation, as well as for the development of visual working memory (Preat

and Goguel, 2016; Rieche *et al.,* 2018). Furthermore, these and several other studies have demonstrated that the interplay between memory development and APPL is complex, with different aspects of *Drosophila* memory requiring different segments of APPL. APPL therefore is sophisticated in it's functionality, and like APP, it's still-enigmatic human counterpart, probably guards just as many undiscovered secrets. Taken together, all these facts paint the emerging picture that amyloids share a common ancestral provenance, possess functionality, and that therefore coming to terms with their influence on each other might not be such a stretch.

My experimental results regarding MFAS show that it too, like all other amyloids, is functionally important, since at the very least it is required for the formation of DCGs, which therefore also links it to DCG's signalling functions. However, as **Table 3.1** suggests, MFAS likely has a role in other organs like the trachea. My overall conclusion, therefore, is that MFAS is functionally nuanced and sophisticated, much like other amyloids. This inference is lent further credence by the finding that MFAS' behaviour is influenced by the knockdown of another functional amyloid (APPL), as well as by the knockdown of a highly active, amyloid-associated enzyme (GAPDH2), in patterns which are quite different from each other. As the various interconnected functions of APPL, GAPDH2 and MFAS (and their human counterparts APP, GAPDH and TGFBI) emerge, as I believe they will, I hope that these results, as the first glimpse of these connections, lead to discoveries which improve human health and well-being.

4.3.3 THE RAB6 AND RAB11 IDENTITIES OF LARGE NON-ACIDIC COMPARTMENTS ARE UNAFFECTED BY *APPL*-KNOCKDOWN

As mentioned in **§ 4.12**, Rab6 and Rab11 have strong associations with the amyloid precursor APP and human neurodegeneration. Furthermore, the fusion of Rab6 and Rab11 compartments is required for the formation of DCGs which are comprised of the fly amyloid MFAS. It was also previously established that while the knockdown of the neurodegeneration-associated genes *GAPDH2* and *APPL* profoundly affect MFAS and the biogenesis of DCGs, the knockdown of *mfas* does not affect the identity of Rab6 or Rab11 compartments. Given these emerging links between various amyloid- and neurodegeneration-associated genes in both humans and flies, the effect of APPL-knockdown on Rab6 and Rab11 compartment identity was examined.

For both Rab6 and Rab11, the numbers of marked non-acidic compartments and the proportion of these compartments containing Rab-labelled puncta was unchanged when *APPL* was knocked down with the two strongest RNAi lines (**Figures 4.13-4.16**).This suggests that *APPL*-knockdown does not affect compartment identity and maturation in SCs, and that the DCG phenotype is associated with a defect in protein aggregation inside each compartment. Thus, to summarise the influences of amyloid-knockdowns on Rab compartment identity, knockdowns of the genes encoding the *Drosophila* amyloid proteins MFAS and APPL, while having profound effects on DCG formation, do not affect the identity of Rab6 or Rab11 compartments. Dysfunction of the evolutionarily conserved Rab6 and Rab11 GTPases is strongly associated with several amyloid-driven neurodegenerative diseases in humans, while in *Drosophila* both Rab6 and Rab11 are

expressed in neurons, and the fusion of Rab6 and Rab11 compartments is a prerequisite for the formation of MFAS-comprised DCGs. Given the experimental results I obtained thus far which interconnect various amyloid- and neurodegeneration-associated molecules, I felt it reasonable to surmise that the knockdown of either *mfas, APPL*, or both, might influence Rab6 and Rab11 compartments, which play key roles in their trafficking and cellular fates. However, I found that this was not the case with either gene, suggesting that both MFAS and APPL enjoy a certain insularity regarding their respective roles in the formation of DCGs.

This is a surprising result, taking a closer look at the extensive links between these particular Rab proteins, the *Drosophila* nervous system, and the human nervous system, both in health and disease. In *Drosophila*, Rab6 influences synaptic specificity through the Ric1 homologue-Rab6-N-cadherin pathway (Tong *et al*., 2011), and is important in the ELKS1-dependent delivery of cargoes to synapses (Nyitrai *et al.*, 2020). In human neurodegeneration, high Rab6 expressions have been reported in Alzheimer's brains (Scheper *et al*., 2004) as well as in cultured cells with *Presenilin-1* mutations (Scheper *et al*., 2007). Rab6 also influences whether APP is sorted into the amyloidogenic (β-secretase) or non-amyloidogenic (α-secretase) pathways (McConlogue *et a*l., 1996), and plays a role in controlling retrograde vesicle transport from the Golgi towards the ER (Opdam *et al.*, 2000). Rab11, on the other hand, regulates trafficking of recycling endosomes and early endosomes to the TGN, demonstrates neuroprotection in *Drosophila* models of Parkinson's disease by rescuing α-synuclein-induced locomotor defects (Breda *et al.*,

2015) and protects against mitochondrial dysfunction caused by *parkin* mutations (Rai and Roy, 2022).

4.3.4 THE EFFECTS OF *mfas*- AND *APPL*-KDS ON LARGE NON-ACIDIC COMPARTMENTS

It was established in the previous chapter **(§ 3.2.4.2)** that knockdown of the *Drosophila* amyloid MFAS and in this chapter **(§ 4.2.2)** that knockdown of the *Drosophila* amyloid APPL have profound effects on the biogenesis of DCGs. Additionally, it was shown that knockdown of GAPDH2, the fly homologue of the human amyloid-associated enzyme GAPDH also prevents the normal formation of DCGs **(§ 4.2.1).** Thus, like *GAPDH2, mfas* and *APPL,* which are both amyloid proteins and therefore have more direct connections with amyloidogenesis, are both also indispensable for the biogenesis of normal DCGs.

In light of these findings, I next made crosses between *mfas*- and *APPL*-knockdowns and a driver line which included the exosome marker Breathless-GFP (Btl-GFP). The progeny from these crosses showed an increase in the number of non-acidic compartments in SCs, similar to the increase in compartment number seen when the *Btl-GFP* driver line was crossed with a control (*Btl-GFP* X *ry*-kd). Furthermore, knockdowns of *mfas* and *APPL* were not found to affect the number of Btl-GFP exosomes relative to controls. These results showed me that *APPL,* like *mfas,* while necessary for the formation of normal DCGs, does not influence the other essential cellular functions studied.

4.3.5 EFFECTS OF MANIPULATING VARIOUS SEGMENTS OF APP/APPL ON DCG FORMATION

Like it's human homologue, *Drosophila* APPL undergoes cleavage by α-, β- and γ-secretases **(Figure 4.22A** and **B).** Knockdowns of *Drosophila α-secretase* (*kuzbanian*) and *γ-secretase* (*Nicastrin*) alter the DCG phenotype only minimally, in the form of a slight increase in DCG numbers (**Figure 4.24B**, **C** and **D**). Thus, non-cleavage of APPL at either the α- or γ-secretase sites does not disrupt DCG biogenesis. However, the modest increase in DCG numbers produced by these knockdowns suggests that physiological APPL cleavage confers some form of regulation over MFAS behaviour. To further examine the APPL-MFAS connection, I conducted experiments on flies overexpressing *APPL* with the deletion of the Extra-Cellular Domain (*UAS-APPL-ECD-deletion*), and also with the deletion of the Intra-Cellular Domain (*UAS-APPL-ICD-deletion*). These experiments showed that the *APPL-ECD* deletion line resulted in a minimally altered phenotype consisting of fewer, but morphologically mostly normal DGCs, while the *APPL-ICD* deletion line produced a severe phenotype with miniscule, fragmented DCGs **(Figure 4.26C** and **D).** This is an intriguing result, since human APP's extracellular and intramembranous domains have binding sites for copper, zinc, iron, heparin, and cholesterol (Dawkins and Small, 2014). Some of these ions are implicated in DCG biogenesis, raising the possibility that without the extracellular domain's metal binding sites, more cores assemble abnormally and are targeted for destruction. This might also explain the fewer DCGs seen with the *APPL-ECD deletion* line, their modest deformities (**Figure 4.26B**), and the finding that these mis-shapen DCGs touch the limiting membrane of their compartments (this last finding was made by Dr. Bhavna Verma of the Wilson

laboratory). Furthermore, APP's highly conserved intracellular domain contains a YENPTY sorting motif conserved in APPL (Leysson *et al*, 2005) which facilitates clathrin-mediated endocytosis and is involved in APP's trafficking (Lai *et al*., 1995; Perez *et al.*, 1999; Ring *et al.*, 2007). This observation is also experimentally supported by work from the Wilson laboratory which suggested that clathrin plays a role in DCG loading in SCs (Kroeger, Benjamin R., 2017, DPhil thesis, pp. 355-356).

Since human APP has been studied in much greater detail than its other family members, and since there is conservation of the protein binding YENPTY motif as well as several other sequences at the C-terminal across species (**Figure 4.6**), this ensuing discussion is based on what is known about the C-terminal of APP, or the APP intracellular domain (AICD). Interacting motifs in the C-terminal include YTSI, GYENPTY, and VTPEER, and their interacting proteins include PAT1, Fe65, 14-3-3, X11/Mint, JIP1, Dab1, ShcA/Grb2, and Numb. Their interactions variously influence basolateral sorting, endocytosis, exocytosis, AICD/Fe65 stabilization, synapse formation, transcriptional activation, and Notch crosstalk. Finally, depending on the individual APP-protein interactions, it has been found that either amyloidogenic or non-amyloidogenic processing of APP is favoured (Cao and Südhof, 2001; Sumioka *et al.*, 2005; Mueller *et al.*, 2000; Wang *et al.*, 2009; Szodorai *et al.*, 2009; Roncarati *et al.*, 2002; Müller and Wild, 2013). While the subcellular sorting and trafficking of APP remain incompletely understood, much of the emerging evidence continues to point to an important role played by it's C-terminal (Brunholz *et al.*, 2012).

As an example of this, the C-terminal ^{651}YTSI sequence is involved in the basolateral sorting of APP in Madin-Darby Canine Kidney (MDCK) cells (Lai *et al.,* 1998). This sequence has been found to be similar to the YXXΦ consensus motif (Φ being an aromatic or large hydrophobic residue, and X being any residue), which is a tyrosine- and clathrin-based endocytic-sorting signal (Bonifacino *et al.,* 2003). The second fingerprint, ^{667}VTPEER, is the major site of APP phosphorylation, which is brought about by glycogen synthase kinase-3β and cyclin-dependent kinase 5 in neurons. Phosphorylation of Thr^{668} is in turn dependent on the presence of Pro^{669}, in which case the prolyl isomerase Pin1 catalyzes the *cis-trans* isomerization of the Thr-Pro bond, which increases amyloidogenic processing and selectively promotes $A\beta_{42}$ production (Pastorino *et al.,* 2006). Thr^{668} phosphorylation also increases APP cleavage by caspases between Asp^{664} and Ala^{665}, which produces the cytotoxic AICD-C31 fragment (Lu *et al*., 2003). This phosphorylation of Thr^{668} as a driver for $A\beta_{42}$ production, and the overall enhancement of APP processing is reminsiscent of the phosphorylation of Tau as a prerequiste to Tau tangle formation. Additionally, the ^{681}GYENPTY motif contains the NPXY sequence, which is an internalization signal for membrane proteins via clathrin-coated pits (Chen et al., 1990), as well as a tyrosine-based sorting signal for internalized transmembrane proteins, directing them to endosomes and lysosomes (Bonifacino *et al.*, 2003). Furthermore, the NPXY motif in APP has a GYE motif on it's N-terminal side, which is found in many lysosomal glycoproteins which are endocytosed and directed to lysosomes (Kornfeld and Mellman, 1989). The Tyr^{682} within this GYE motif is crucial, since it's phosphorylation by the nerve growth factor receptor TrkA and the tyrosine kinases Abl and Src also influences APP's cleavage patterns. Thus, non-phosphorylated Tyr^{682} keeps APP at the plasma membrane

and favours α-secretase (non-amyloidogenic) cleavage, while phosphorylation-dependent relocalization favours amyloidogenic β-cleavage (Barbagallo *et al.,* 2010).

In addition to it's activity based on it's protein-binding motifs, a substantial body of research shows that APP's AICD enters the nucleus and acts as a transcription factor, regulating a large number of genes (reviewed in Pardossi-Picard and Checler, 2012). Among APP-AICD's numerous nuclear actions is it's upregulation of the Aβ-degrading metallopeptidase neprilysin (Pardossi-Picard *et al.,* 2005), which has the effect of increasing the ratio of $A\beta_{42}/A\beta_{40}$, since neprilysin degrades $A\beta_{40}$ more efficiently. This significantly enhances neuronal toxicity, and is considered one of the few unambiguous pathways by which AICD affects the severity of Alzheimer's disease (Kupperstein *et al.*, 2010).

This plethora of evidence makes it abundantly clear that AICD is remarkably active biologically, and thus a worthy target to focus on (the large volume of work done on AICD reflects the widespread acknowledgement of this fact). However AICD's multiple and protean effects remain poorly understood, the great impediment to it's study being it's extreme instability and susceptibility to rapid proteolysis by insulysin, with insulysin cleavages occurring in multiple areas and without apparent prediliction for any particular site (Edbauer *et al*., 2002; Venugopal *et al.,* 2007). In my experimental results, the deletion of the intracellular portion of *Drosophila* APPL prevented the formation of large DCGs and led to the formation of large numbers of compartments with very small DCG structures,

roughly equivalent in size to the mini-cores observed in the *GAPDH2*- and *APPL*-knockdown genotypes. This defect is linked to the loss of the ICD and not overexpression of APPL, because overexpression of APPL that only lacked regions in the extracellular domain or full-length APP, either in the absence or presence of BACE-1, did not affect DCGs in the same way. Thus, the non-formation of DCGs by the overexpression of *APPL-ICD-deletion* is a good entry point from which to pursue the technically difficult subject of AICD function in this highly tractable and convenient *Drosophila* model.

As alluded to above, my results also showed that the overexpression of human APP, whether full-length or cleaved by it's β-secretase BACE-1, does not affect the coalescence of MFAS and does not interfere with the production of normal DCGs. The β-secretase, like the γ-secretase, is also an aspartyl protease which cleaves APP between Met^{597}-Asp^{598} (**Figure 4.28**). As is deducible from APP's extracellular β-cleavage site, BACE-1 is an enzyme with it's active site on the ectoplasmic side of the cell membrane. It has an optimal pH of 4.5 for activity, suggesting that β-cleavage of APP occurs within more acidic compartments (Vassar *et al*., 1999). Other evidence, however suggests it takes place within lipid rafts (Enehalt *et al*., 2003). BACE has two isoforms, BACE-1 and -2, with BACE-1 being the form widely expressed in the brain (and the form used in this experiment). BACE-1 knockout mice do not produce any detectable Aβ, and are initially healthy (Luo *et al*., 2001; Roberds *et al*., 2001), until they begin to show myelination defects and abnormalities in synaptic activity later in life, in some studies as early as at the age of 4 months (Kim *et al.,* 2011). In *Drosophila*, on the other hand, the absence of *dBACE* results in late larval or

early pupal lethality, showing that the β-secretase is essential in flies (Bolkan *et a*l., 2012), and plays a somewhat unclear role in mammals.

Further alignment of results are also seen with my *Drosophila APPL-ECD-deletion* and human *APP-BACE-1* overexpression experiments, which are in agreement with each other. In both, the preservation of the intracellular portions of APPL or APP result in the formation of mostly normal DCGs. The slight distinction between them was that *APPL-ECD-deletion* decreased the number of DCGs and produced the occasional mis-shapen DCG (**Figure 4.26B** and **Figure 4.27)** whereas the *APP-BACE-1* line resulted in a normal number of DCGs (**Figure 4.29C** and **Figure 4.30**). Since both these lines resulted in the removal of approximately the same extracellular stretch of APPL/APP, I surmise that the slight drop in the number of DCGs seen with the APPL deletion might reflect the fact that APPL, which is a *Drosophila* amyloid precursor, affects *Drosophila* MFAS to a greater extent than does APP, which is a human amyloid precursor. Finally, recent work in the Wilson laboratory done by Dr. Bhavna Verma showed that double-tagged APPL is trafficked to DCG compartments and is ultimately cleaved, so the ECD is in the DCG and the ICD is at the surface of the compartment. Additionally, time-lapse videos made by Adam Wells also in the Wilson laboratory showed that the formation of DCGs occurs by the fusion of mini-cores, which prior to that, in their nascent form, first make their appearance at the periphery of DCG compartments. The detailed consideration and synthesis of all these emerging facts will undoubtedly contribute to our understanding of these just-discovered biological entities of mini-core phenotypes.

CHAPTER 5

MUTATIONS IN *DROSOPHILA mfas* AND IT'S HUMAN HOMOLOGUE *TGFBI* AFFECT DCG FORMATION

5. MUTATIONS IN *DROSOPHILA mfas* AND ITS HUMAN HOMOLOGUE *TGFBI* AFFECT DCG FORMATION

5.1 INTRODUCTION

Drosophila mfas and human *TGFBI* are homologues, and their protein products are organizationally identical (**Figure 1.13, Chapter 1**). As shown earlier, MFAS is essential for the formation of DCGs. In a similar vein, TGFBI is a structural protein complete with an RGD adhesion motif, and plays the crucial role of maintaining the tightly ordered lattice of keratocytes, thereby keeping the cornea transparent.

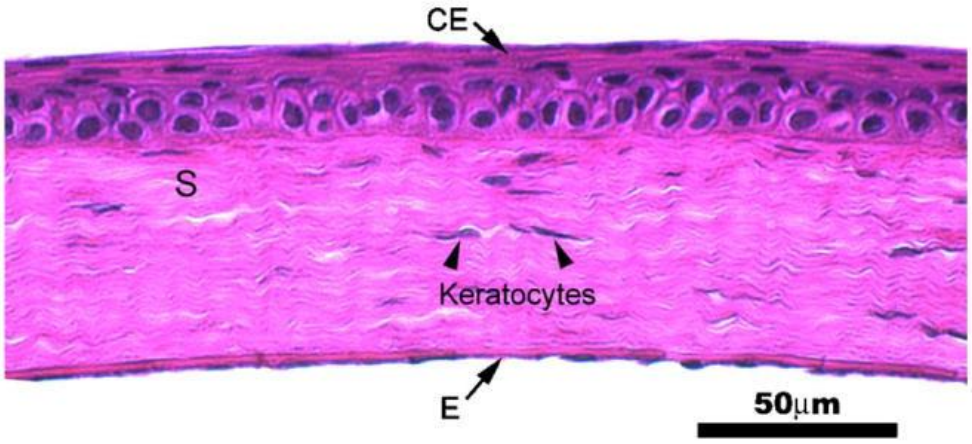

Figure 5.1: Cross-section of the cornea of an adult mouse stained with haematoxylin and eosin. CE: corneal epithelium; **E:** endothelium; **S:** stroma. (West-Mays and Dwivedi, Int. J. Biochem. Cell Biol. 2006, p. 7).

Amyloid corneal dystrophies, characterized by the disruption of the ordered corneal layers by the deposition of TGFBI-derived amyloid, are caused by mutations in *TGFBI*. First isolated from an adenocarcinoma cell line, *TGFBI* was subsequently found to be expressed in a wide variety of tissues including the cornea, heart, liver, pancreas, skin, bone, endometrium, kidney, and blood plasma (Skonier *et al.*, 1992; Kitahama *et al.*, 2000;

Carson *et al.*, 2002; Lee *et al*., 2003; Klintworth *et al.*, 1998). It was subsequently found to be associated with an equally wide array of cancers, including brain, breast, bone, liver, lung, ovary, and pancreas. In the cornea, it is expressed in the corneal epithelium (Escribano *et al.,* 1994), in the stroma in association with collagen type VI and XII (Runager *et al.,* 2013), and at the stromal/Descemet membrane interface (Hirano *et al.,* 1996). Additionally, it was also found to be significantly up-regulated during wound healing of the rabbit cornea (Rawe *et al.,* 1997).

TGFBI is a 68-kDa extracellular matrix protein with 683 amino acid residues, and has variously been referred to as keratoepithelin, BIGH3, or βig-h3 depending on where it was isolated from. It is a 34,924-nucleotide transcript with 17 exons which, after processing, results in a 2052-nucleotide protein coding sequence (Skonier *et al.,* 1992, GenBank accession number M77349). It has four fasciclin 1 (FAS1) domains, each composed of 140 amino acids, and an arginine-glycine-aspartate (RGD) motif at the C-terminal which binds to integrin. It plays physiological roles in cell adhesion and in spreading through integrins α1β1, α3β1, αvβ3, αvβ5, α6β4, and αmβ2 (Nam *et al.,* 2006; Kim *et al.,* 2002; Kim *et al.,* 2003), in cell proliferation and differentiation (Park *et al*., 2009) and in the dissemination of glioblastoma multiforme *in vitro* (Fan *et al*., 2014). These discoveries regarding TGFBI turned out to be extremely important in the design of chemotherapy protocols for patients with glioblastoma multiforme (Yin *et al.,* 2020) and lung cancer (Hung *et al.,* 2015).

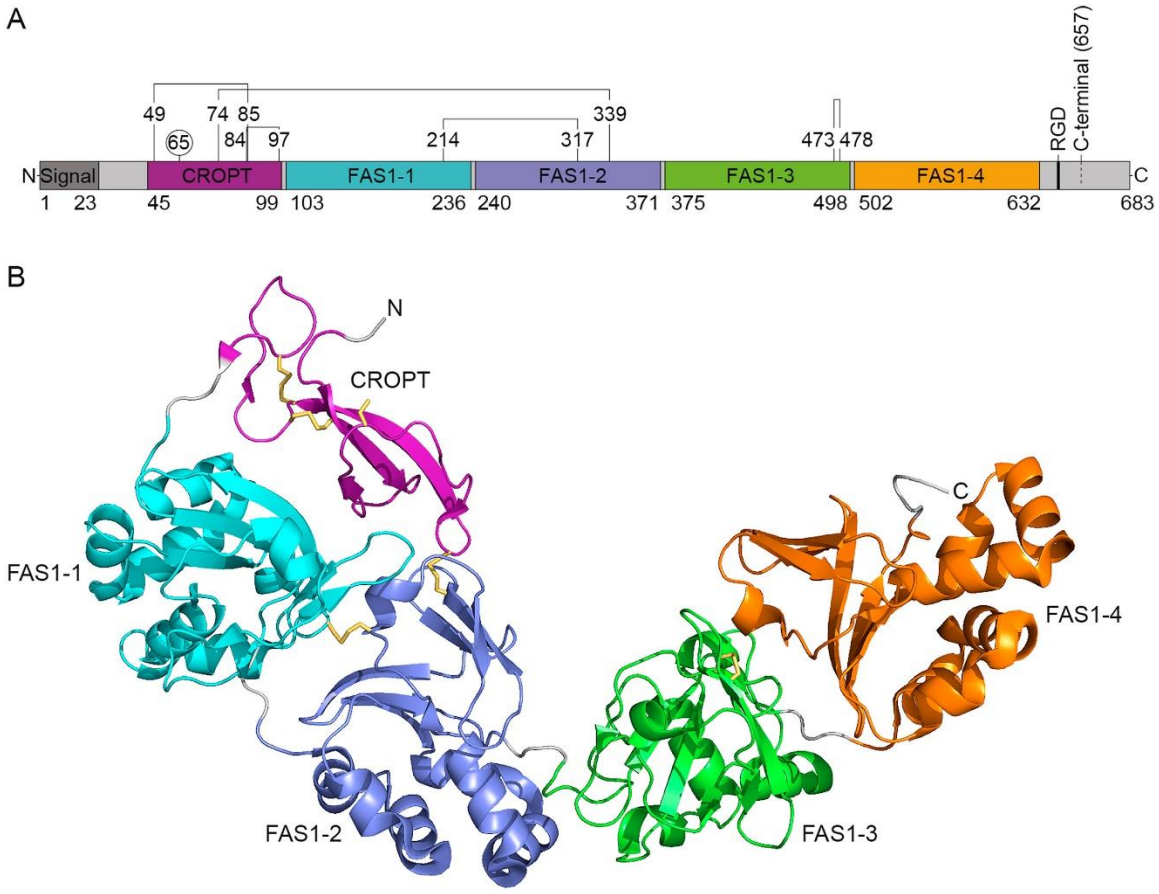

Figure 5.2: A: The secreted form of TGFBI has an N-terminal CROPT domain (previously called the emilin or EMI domain), followed by four FAS1 domains. The bracketed sections represent disulfide bridges. There is an RGD binding motif at the C-terminal as well as a truncation site at residue A657. **B:** Ribbon model of TGFBI with CROPT in magenta, FAS1-1 in cyan, FAS1-2 in blue, FAS1-3 in green, FAS1-4 in orange, and the disulfide bridges in yellow. (Nielsen et al., Prog. Ret. Eye Res. 2020, p. 2).

Corneal dystrophies are the result of pathological amyloidogenesis of mutated TGFBI, which then infiltrates various corneal layers as opaque amyloid deposits. Its processing takes place through the serine protease HTRA1, which is found to be enriched seven-fold in corneal amyloid deposits of patients as compared to controls, and is known to preferentially mediate the proteolytic processing of TGFBIp amyloid mutants, particularly those found in domain-4 (Karring *et al.*, 2012; Karring *et al.*, 2013; Pouslen *et al.*, 2019). These conditions are autosomal dominant, bilateral, progressive, and left untreated, can

cause blindness. Historically, the following associations were identified between *TGFBI* mutations and the major types of CDs: *R124C* for Lattice CD (the commonest form of CD); *R555Q* for Thiel-Behnke CD; *R555W* and *G623D* for Granular CD Type I; *R555Q* and *M619K* for Granular CD Type II, *G623D* for Lattice, Thiel-Behnke, Reis-Bückler, and Epithelial Basement Membrane CDs; and *H626R* again for Lattice CD (Munier *et al.*, 1997). So far, 74 *TGFBI* mutations are known to cause amyloid CDs (reviewed in Nielsen *et al*., 2020). This is, however, a protean group of diseases, and genotype-phenotype correlations are heavily influenced by ethnicities and geographic locations (Han *et al.*, 2016). Furthermore, until the relatively recent recognition of their genetic underpinnings, amyloid corneal dystrophies were often erroneously treated as outbreaks of recurrent bilateral herpes simplex keratitis (Evans *et al.*, 2016). Due to these limitations, along with their relatively recent syndromic recognition and the ongoing discovery of new disease-causing mutations, their clinical classification is still considered a work in progress (Weiss *et al.*, 2015; Kheir *et al*., 2019).

5.1.1 TYPES OF *TGFBI*-ASSOCIATED CORNEAL DSYTROPHIES

5.1.1.1 LATTICE CD (LCD)

This is characterized by branching refractile lines and opaque white dots in the corneal stroma which appear from the first to the third decades of life. The amyloid fibrils which comprise these deposits are highly aligned and have a diameter of 8-10 nm, similar to the Meretoja syndrome of primary systemic amyloidosis, which is an ocular mimic and primary differential diagnosis of LCD. There are several clinical subvariants of LCD, but patients as a rule suffer from painful and recurrent corneal erosions.

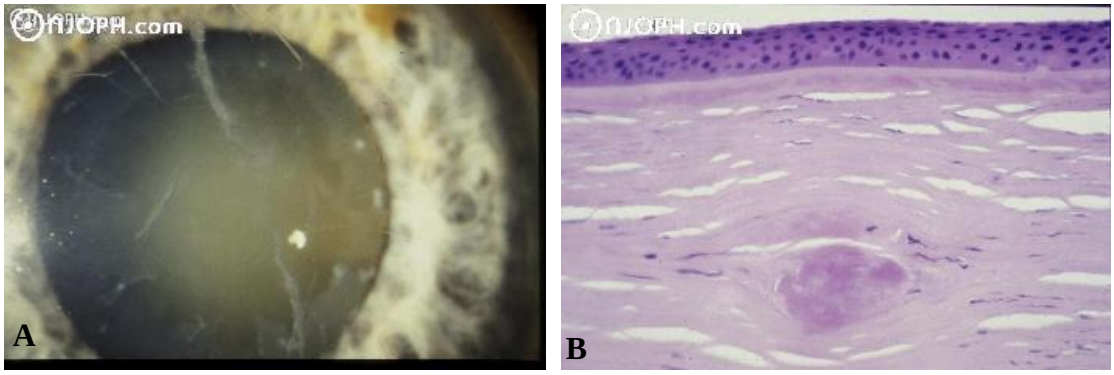

Figure 5.3: Lattice Corneal Dystrophy. A: clinical phenotype. **B:** Histology showing disruption of the corneal stroma by amyloid. (Reproduced with permission from the Atlas of Ophthalmology).

5.1.1.2 THIEL-BEHNKE CD

TBCD is characterized by reticulate honeycomb-shaped subepithelial amyloid deposits in Bowman's layer, initially appearing during the first or second decades of life. Unlike the highly aligned fibrils of LCD, TBCD has irregular aggregates of larger curly fibrils, 9-15 nm in diameter. Starting as a mild vision impediment, as the amyloid deposits coalesce, severe visual impairment ensues (Thiel and Behnke, 1967).

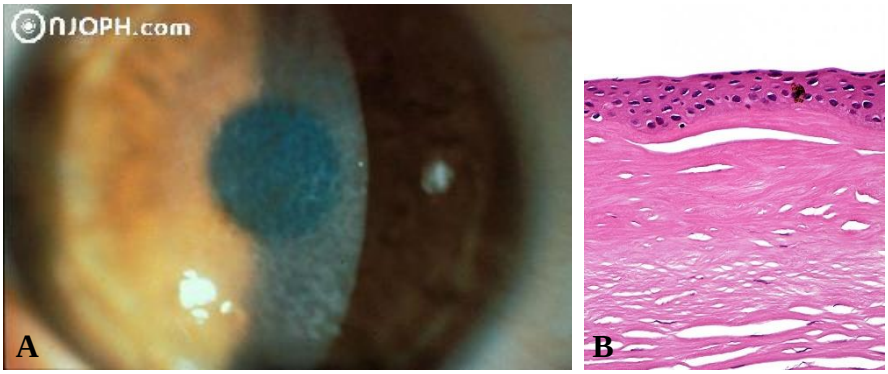

Figure 5.4: Thiel-Behnke Corneal Dystrophy. **A:** Clinical phenotype. **B:** Histology showing amyloid disruption of the subepithelial Bowman's layer, along with deposits in the underlying anterior corneal stroma. (Reproduced with permission from the Atlas of Ophthalmology).

5.1.1.3 REIS-BÜCKLER CD

Like TBCD, RBCD also primarily affects Bowman's layer, presents in the first and second decades of life, but unlike the former, due to an aggressive clinical course leads to the early impairment of vision. RBCD opacities appear as irregular gray-white deposits which spread both centrally and peripherally, ultimately assuming a fishnet or honeycomb pattern. On electron microscopy, the amyloid deposits are electron-dense, rod-shaped or trapezoidal, and are surrounded by large proteoglycan filaments (Weiss *et al.*, 2015).

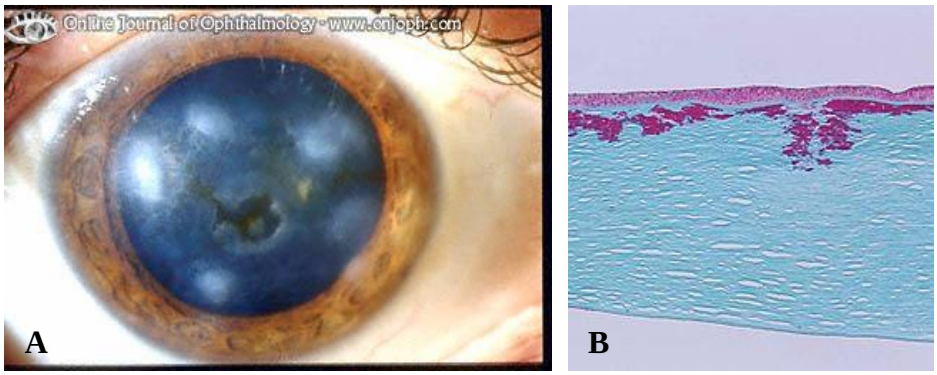

Figure 5.5: Reis-Bückler Corneal Dystrophy. A: Clinical phenotype showing a large corneal erosion. **B:** Histology with Masson's trichrome stain, showing large sub-epithelial amyloid deposits. (Reproduced with permission from the Atlas of Ophthalmology).

5.1.1.4 GRANULAR CD

GCD is characterized by the appearance of multiple well-defined granular deposits in the anterior stroma in the first or second decades of life, with some variants of the disease (the Avellino type) appearing as early as 3 years of age. The clinical classification of GCD is based on the morphology of these deposits (drop, crumb or ring-shaped) (Weidle and Lisch, 1984), which progressively enlarge, then become confluent to produce recurrent painful corneal erosions. With the onset of erosions, vision decreases precipitously, requiring

prompt corneal transplantation. On electron microscopy, the amyloid deposits are large, eosinophilic rod-shaped or trapezoidal bodies measuring 50-100 nm in diameter with a moth-eaten appearance (Akiya and Brown, 1970). Due to the aggressive nature of the disease in all it's variations and subtypes, early corneal transplantation is the only therapeutic recourse (Han *et al.*, 2016).



Figure 5.6: Granular Corneal Dystrophy. A: Clinical phenotype. **B:** Histology with Masson's trichrome stain, showing large stromal amyloid deposits. (Reproduced with permission from the Atlas of Ophthalmology).

With the development of increasingly sophisticated clinical and research tools, the variants and subtypes of *TGFBI*-related CDs have expanded, along with the details of their molecular characterizations. This expanding compendium has led to the realization that occasionally multiple phenotypes might arise from the same mutation, and conversely, that different mutations might produce similar phenotypes. These nuances, found just within a highly circumscribed, cornea-specific amyloid syndrome underline the fact that the universe of amyloid diseases is a complex one. The clinical manifestations of amyloidoses, unlike other diseases, rely on details pertaining both to the amyloidogenic precursor molecules, as well as on details pertaining to the multiple enzymes processing those specific molecules. The story of Aβ and Alzheimer's disease is 120 years old and is still

very much being written. With regards to TGFBI, it's story has only just begun. The following results provide a glimpse into the unplumbed depths that research into TGFBI promises. The uniqueness of this approach to TGFBI-linked corneal dystrophies also rests with the novelty of the *Drosophila* system presented here.

5.1.2 AIMS

Having shown that the *Drosophila* homologue of TGFBI, MFAS, is absolutely required for the protein aggregation to make DCGs in SCs, I set out to test the following questions:

1. Does overexpression of mutant MFAS containing a corneal dystrophy-inducing mutation in a conserved amino acid lead to changes in DCG biogenesis in SCs?
2. Does overexpression of wild type or mutant TGFBI affect DCG biogenesis in SCs?
3. Can mutational changes in TGFBI affect the DCG mini-core phenotype brought about by APPL-knockdown? In other words, can this human homologue of MFAS influence the fusion defects effects engendered by the loss of APPL, another *Drosophila* amyloid?

5.2 RESULTS

5.2.1 THE EFFECTS OF *mfas-WT* AND *TGFBI-WT* ON DCG FORMATION

I initially tested the effects of overexpressing an extra copy of wild type *mfas,* or wild type *TGFBI,* each under the control of the GAL4/UAS system, on DCG formation. The creation of the fly lines used in these experiments is described in **§ 2.3** through **§ 2.3.9**. I compared these phenotypes to a control line produced by expressing a *UAS-ry-RNAi* construct in SCs, also under dsx-GAL4 control.

As shown in **Figure 5.7** below, both wild type *mfas* and wild type *TGFBI*, when overexpressed, produced DCGs indistinguishable from controls. Thus, the number of DCGs produced per SC, as well as their morphology, were completely normal in each of these lines. These experiments show that the overexpression of wild-type *mfas* and wild-type *TGFBI* does not affect the physiological formation of DCGs. These results are not surprising, since the introduction of a normal third copy of *mfas* would in all likelihood not be expected to disrupt DCG formation, because it is already in the top ten genes expressed in SCs (Immarigeon *et al.*, 2020) (**Figure 7.7**). The same reasoning predicted that the introduction of wild-type *TGFBI*, the identically organized homologue of *mfas*, would not perturb physiological DCG biogenesis. In the context of human physiology, wild-type *TGFBI* is responsible for the unblemished development of that apotheosis of ordered architecture, the crucially transparent cornea, where any misstep would quickly and surely be manifest. Thus, wild-type *TGFBI*'s non-interference with the production of pristine DCGs came as no great surprise.

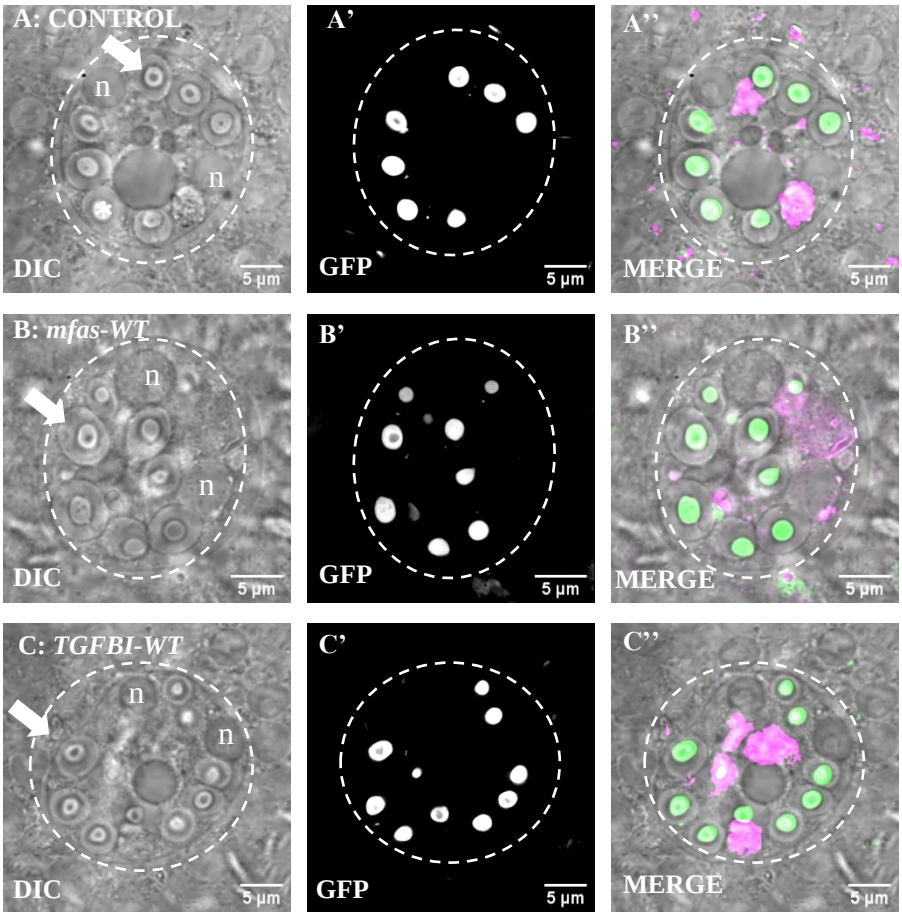

Figure 5.7: Neither the introduction of an extra copy of wild-type *mfas* nor the presence of wild-type *TGFBI* affects the normal formation of DCGs. SCs from six day-old virgin males stained with LysoTracker Red and imaged *ex vivo*, using DIC and fluorescence microscopy for GFP and LysoTracker Red. **A)** w^{1118}*; tub-GAL80*^{ts}*/UAS-ry-RNAi; dsx-GAL4 GFP-mfas/+* (control) **B)** w^{1118}*; tub-GAL80*^{ts}*/UAS-mfas-wild type; dsx-GAL4 GFP-mfas/+* **C)** w^{1118}*; tub-GAL80*^{ts}*/UAS-TGFBI-wild type; dsx-GAL4 GFP-mfas/+*. **White arrows** in **A, B** and **C:** DCGs; **n:** double nuclei characteristic of each SC. Scale bar = 5 µm.

The next experimental step, then, was to introduce *mfas* and *TGFBI* bearing corneal dystrophy mutations into the *Drosophila* genome, in order to test their effects on DCG formation. These results are presented in two sections: the effects of the two conserved mutations (*TGFBI-G623D* and *TGFBI-H626R*, **§ 5.2.2**), and the effects of the two non-conserved mutations (*TGFBI-R555Q* and *TGFBI-R124C,* **§ 5.2.3**). Having established the

benignity of the effects of wild type *mfas* and *TGFBI* on DCG biogenesis, these experiments would directly address the question of whether a single nucleotide change in *mfas* or *TGFBI* would be sufficient to produce abnormal DCGs.

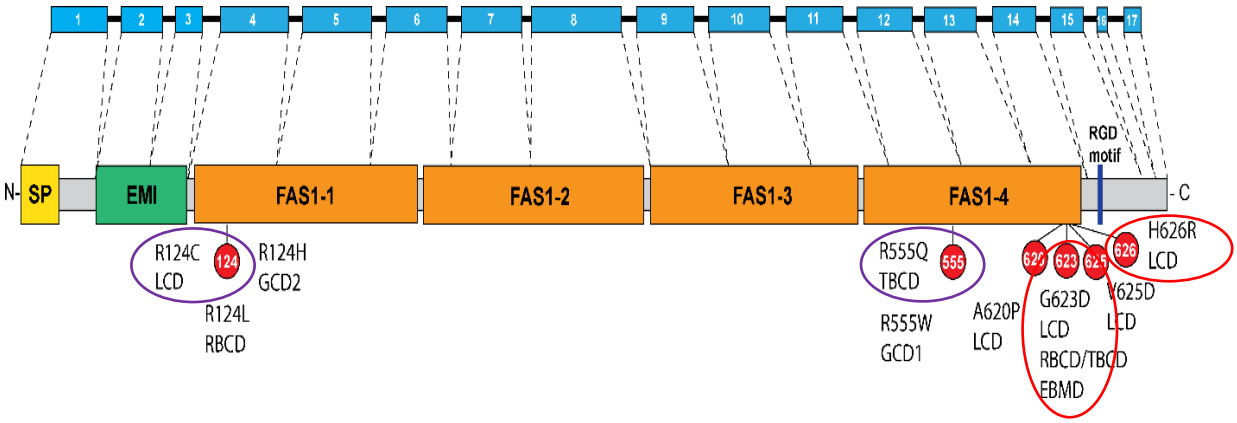

Figure 5.8: Human *TGFBI*-CD mutations cluster in two hotspots located in FAS1 domains-1 and -4. Red ovals: mutations conserved between *TGFBI* and *mfas*. **Purple ovals:** non-conserved mutations. **EBMD:** Epithelial Basement Membrane CD; **GCD:** Granular CD; **LCD:** Lattice CD; **RBCD:** Reis-Bückler CD; **TBCD:** Thiel-Behnke CD. (Adapted from Evans *et al.*, Invest. Ophthalmol. Vis. Sci. 2016, p. 5413).

5.2.2 THE EFFECTS OF CONSERVED *TGFBI* MUTATIONS *G623D* AND *H626R* ON DCG FORMATION

Following experiments testing wild type *mfas* and *TGFBI*, the effects of conserved *TGFBI* mutations *G623D* and *H626R* on DCGs were tested next (preparation of these transgenic lines is described from **§ 2.3 to § 2.3.9**). As described earlier, I overexpressed *TGFBI-G623D* and *TGFBI-H626R* in adult SCs under dsx-GAL4 control, and compared the DCG and SC phenotypes of both of these manipulations to control cells expressing a *UAS-ry-RNAi* construct. As seen below, these conserved mutations produced dysmorphic DCGs

(**Figure 5.9C** and **D**). The introduction of the same conserved *TGFBI* mutation (*G623D*) into a third copy of *mfas* similarly overexpressed in SCs was also sufficient to produce dsymorphic DCGs (Figure **5.9B**). These single nucleotide changes led to the disrupted shape of DCGs and multiple cores in some compartments, so that most compartments were abnormal. Thus, mutations in these conserved residues prevents normal aggregation of MFAS to form DCGs.

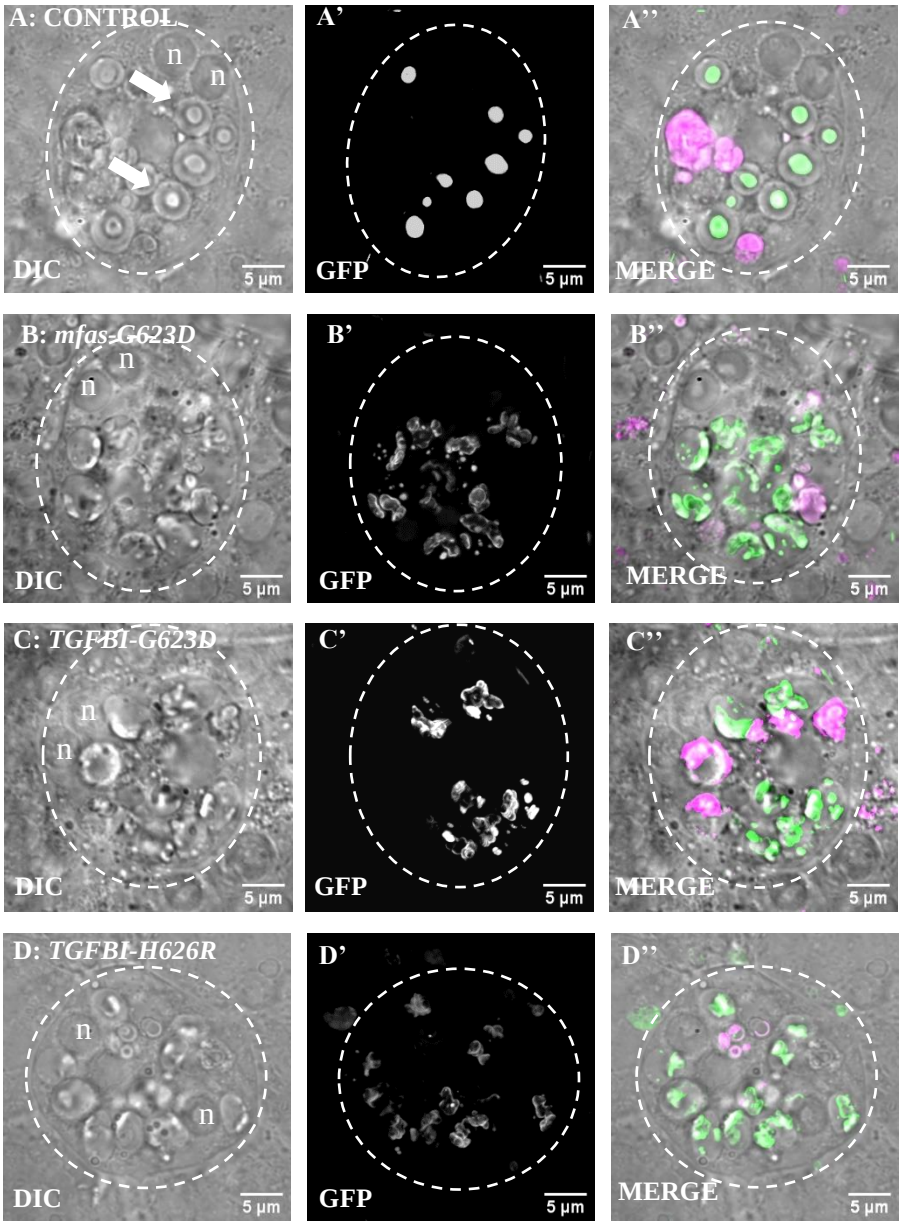

Figure 5.9: The introduction of conserved *mfas* and *TGFBI*-CD mutations (*G623D* and *H626R*) into the *Drosophila* genome results in the formation of abnormal DCGs. SCs from six-day-old virgin males stained with LysoTracker Red and imaged *ex vivo*, using DIC and fluorescence microscopy for GFP and LysoTracker Red. **A)** w^{1118}*; tub-GAL80*^{ts}*/UAS-ry-RNAi; dsx-GAL4 GFP-mfas/+* (control) **B))** w^{1118}*; tub-GAL80*^{ts}*/UAS-mfas-G623D; dsx-GAL4 GFP-mfas/+* **C)** w^{1118}*; tub-GAL80*^{ts}*/UAS-TGFBI-G623D; dsx-GAL4 GFP-mfas/+* **D)** w^{1118}*; tub-GAL80*^{ts}*/UAS-TGFBI-H626R; dsx-GAL4 GFP-mfas/+*. **White arrows** in **A:** DCGs; **n:** double nuclei characteristic of each SC. Scale bar = 5 µm.

5.2.3 THE EFFECTS OF NON-CONSERVED *TGFBI* MUTATIONS *R555Q* AND *R124C* ON DCG FORMATION

Along with two mutations conserved between *TGFBI* and *mfas* (*G623D* and *H626R*), two non-conserved TGFBI mutations (*R555Q* and *R124C*) (**Figure 5.8**) were also introduced into the *Drosophila* genome. In clinical practice, CD's wide ethnic and geographic variations, compounded by the fact that there is little consensus about classification systems, make generalizations about conserved versus non-conserved mutations difficult. Thus, one of the secondary aims behind these experiments was to determine whether there were any phenotypic differences between DCGs produced by conserved and non-conserved mutations, in the hope of providing some clarity and insight to clinical practitioners.

Following the experimental procedure described with the conserved *TGFBI* mutations, I overexpressed *TGFBI-R555Q* and *TGFBI-R124C* in adult SCs under dsx-GAL4 control, and compared the DCG and SC phenotypes of both of these manipulations to control cells expressing a *UAS-ry-RNAi* construct. As shown below, both tested non-conserved mutations produced dysmorphic DCGs (**Figure 5.10B** and **C**). However, I found that non-conserved mutations produced milder phenotypes. Since the residues affected by these mutations are not present in *mfas*, the effects observed are presumably explained by a model in which the conformational changes introduced in these mutant molecules disrupt the organisation of MFAS molecules, because of aberrant contacts between broadly conserved domains within these homologous proteins. Additionally, in comparing all four tested *TGFBI* mutations (*G623D, H626R, R555Q* and *R124C*), it emerges that mutations

within TGFBI domain 4 (*G623D, H626R* and *R555Q*) produce more consistently dysmorphic DCGs than the sole mutation in TGFBI domain 1 (*R124C*). This aligns with the fact that most of TGFBI's mutational hotspsots cluster in domain 4 (**Figure 5.8**).

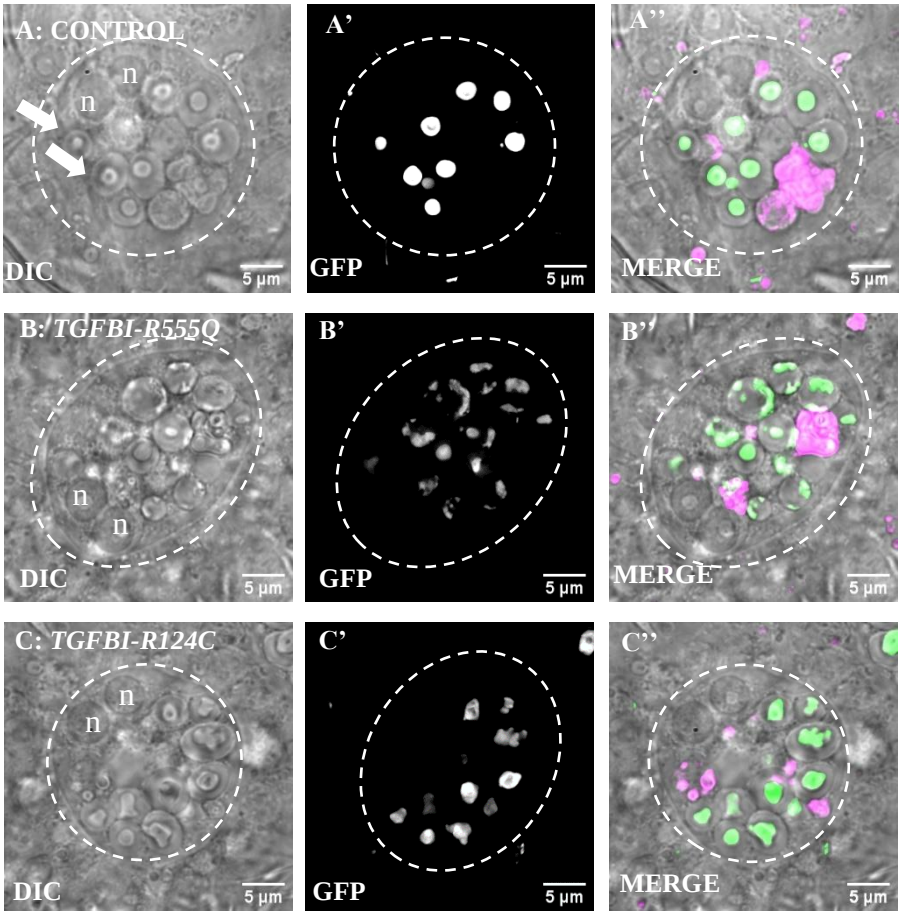

Figure 5.10: The introduction of non-conserved *TGFBI*-CD mutations (*R555Q* and *R124C*) into the *Drosophila* genome also results in the formation of abnormal DCGs. SCs from six-day-old virgin males stained with LysoTracker Red and imaged *ex vivo*, using DIC and fluorescence microscopy for GFP and LysoTracker Red. **A)** w^{1118}*; tub-GAL80*^{ts}*/UAS-ry-RNAi; dsx-GAL4 GFP-mfas/+* (control) **B)** w^{1118}*; tub-GAL80*^{ts}*/UAS-TGFBI-R555Q; dsx-GAL4 GFP-mfas/+* **C)** w^{1118}*; tub-GAL80*^{ts}*/UAS-TGFBI-R124C; dsx-GAL4 GFP-mfas/+*. **White arrows** in **A:** DCGs; **n:** double nuclei characteristic of each SC. Scale bar = 5 µm.

As presented in Sections **5.2.1, 5.2.2** and **5.2.3**, DCG morphologies varied in accordance with the normality or abnormality of the underlying genetic construct. Thus, in response to the genomic insertion of wild type *mfas* and wild type *TGFBI*, the resultant DCGs were

physiological, or normal-appearing. In contrast, with the genomic insertion of *TGFBI* amyloidogenic mutations, the resultant DCGs were abnormal. The degree of abnormality appeared to follow domain clustering of hotspots. Thus domain 4 mutations, where most clinically relevant mutations are found, produced greater DCG abnormalities. They also appeared to follow conservation: conserved mutations also produced greater DCG deformities.

5.2.4 INTERACTIONS BETWEEN HUMAN *TGFBI* MUTANTS AND *DROSOPHILA APPL*-RNAi

TGFBI amyloidogenic mutations generate typically tenacious, but deformed amyloid protein deposits in the cornea (Han *et al*, 2016). In *Drosophila* SCs, the DCGs they produce are correspondingly deformed, but for the most part unfragmented (**Figures 5.9** and **5.10**). *APPL-RNAi* on the other hand consistently produces a preponderance of fragmented-appearing mini-cores (**Figure 4.11**). The effect of combining amyloidogenic *TGFBI* mutations with *APPL*-RNAi was therefore tested to determine whether these mutant molecules could partially induce aggregation of MFAS mini-cores formed following *APPL* knockdown. Additionally, the effect of the insertion into the fly genome of an extra copy of *mfas* bearing the conserved *G623D* mutation was also studied. It has earlier been shown that flies expressing an extra copy of *mfas-wild type* or *TGFBI-wild type* (**Figure 5.7**) both produced normal DCGs.

5.2.4.1 INTERACTION BETWEEN *mfas-G623D* AND *APPL-RNAi*

Through a series of genetic crosses, I generated a fly line bearing both *mfas-G623D* and *APPL-RNAi* constructs, in order to test whether the amyloidogenic effect of the former exerted any rescue influence on the mini-core phenotype of the latter. I then overexpressed

these *mfas-G623D* and *APPL-RNAi* constructs in adult SCs under dsx-GAL4 control, and compared the resultant DCG phenotype to that of control cells expressing a *UAS-ry-RNAi* construct. The results shown below demonstrate that these rescue lines have a greater number of intact DCGs (**Figures 5.11** and **12**). Most DCG compartments have an abnormally shaped large DCG, similar to that seen with mutant MFAS alone, which suggests that the mutant MFAS molecule may be able to partially overcome the defects in mini-core fusion induced by *APPL*-kd. This would provide some evidence for this mutant protein behaving in a fashion that induces abnormal aggregation, i.e., a partial rescue. However, as with all the experiments presented below, an alternative hypothesis is that the addition of the additional UAS transgene reduces expression of *APPL-RNAi*, and therefore leads to a weaker mini-core phenotype.

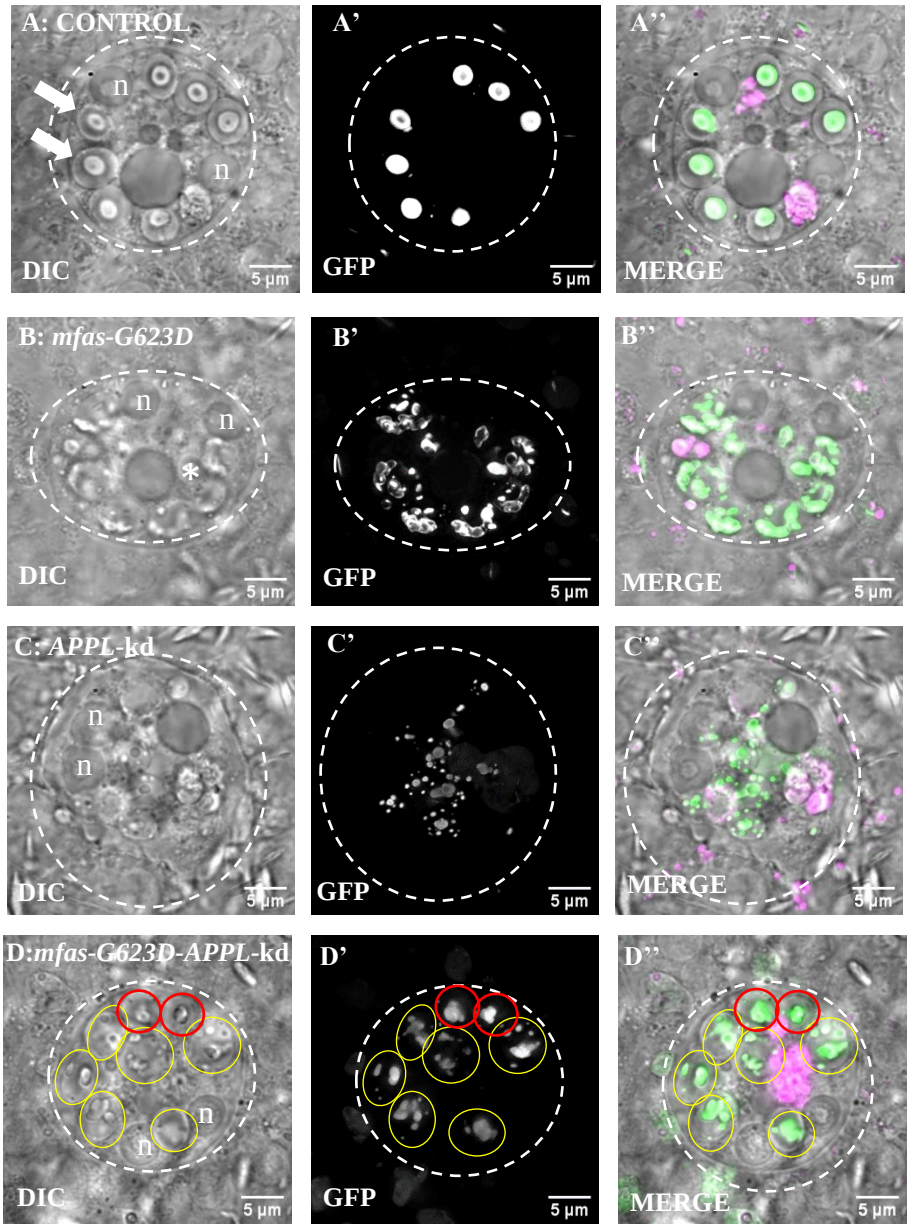

Figure 5.11: The interaction between *mfas-G623D* and *APPL-RNAi* produces a combination of deformed DCGs and mini-cores. SCs from six day-old virgin males stained with LysoTracker Red and imaged *ex vivo*, using DIC and fluorescence microscopy for GFP and LysoTracker Red. **A)** *w^{1118}; tub-GAL80^{ts}/UAS-ry-RNAi; dsx-GAL4 GFP-mfas/+* (control) **B)** *w^{1118}; tub-GAL80^{ts}/UAS-mfas-G623D; dsx-GAL4 GFP-mfas/+* **C)** *w^{1118}; tub-GAL80^{ts}/+; dsx-GAL4 GFP-mfas/UAS-APPL-RNAi* **D)** *w^{1118}; tub-GAL80^{ts}/UAS-mfas-G623D; dsx-GAL4 GFP-mfas/UAS-APPL-RNAi*. **White arrows** in **A:** DCGs. **Yellow ovals/circles:** compartments with both large cores and mini-cores; **red circles:** compartments with large or solitary cores; **n:** double nuclei characteristic of each SC. Scale bar = 5 µm.

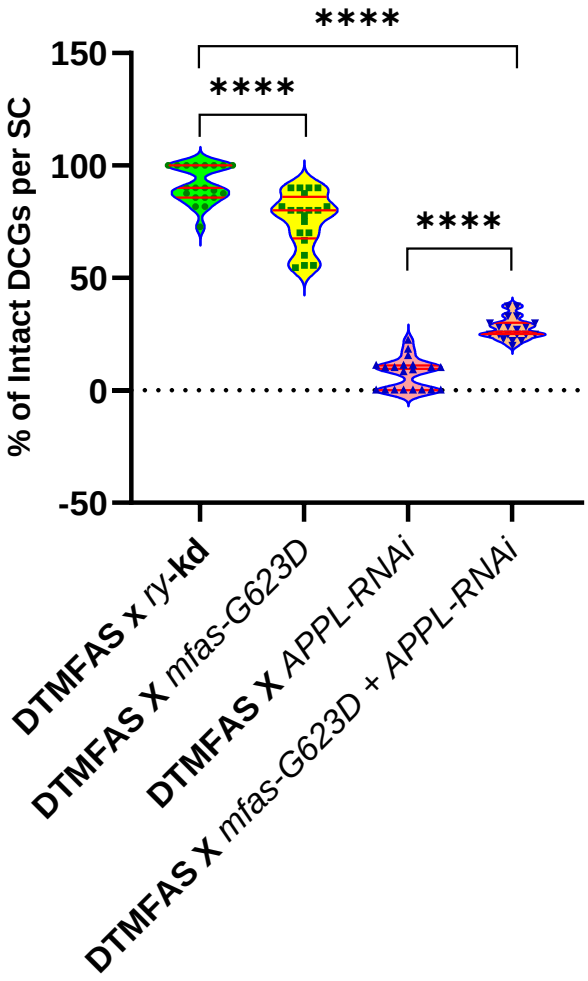

Figure 5.12: Interaction between *mfas-G623D* and *APPL*-RNAi. *mfas-G623D* produces less intact DCGs than *ry*-kd controls, and all of the former are severely deformed. *APPL-RNAi* produces significantly less intact DCGs, producing fragmented-appearing mini-cores instead. However, the combination of *mfas-G623D* and *APPL-RNAi* results in a partial rescue of the mini-core phenotype by producing the occasional intact, albeit deformed core. Mini-cores are still produced, but often at a reduced frequency in most compartments, which also typically contain a larger, although abnormally shaped major core than in *APPL*-knockdown SCs. As also indicated in the microscopy images (**Figure 5.11)** which correspond to this bar chart, all genotypes listed here were driven by w^{1118}*; tub-GAL80^{ts}/CyO; dsx-GAL4 GFP-mfas/TM6B* (DTMFAS). The mean for each set of experiments is shown in red.

5.2.4.2 INTERACTION BETWEEN *TGFBI-G623D* AND *APPL-RNAi*

Through a series of genetic crosses, I generated another fly line bearing both *TGFBI-G623D* and *APPL-RNAi* constructs, in order to test whether the amyloidogenic effect of the former exerted any rescue influence on the mini-core phenotype of the latter. I then overexpressed these combined *TGFBI-G623D* and *APPL-RNAi* constructs in adult SCs under dsx-GAL4 control, and compared the resultant DCG phenotype to that of control cells expressing a *UAS-ry-RNAi* construct. *G623D* is the same conserved mutation which I had earlier introduced into *mfas* (**§ 5.2.4.1**), and used in its attempted rescue of *APPL-RNAi*, as shown in the **Figure 5.11**. There, as also seen here in the effects of *TGFBI-G623D* on DCGs, I demonstrated that the *G623D* mutation produces intact, but severely deformed DCGs. *APPL-RNAi*, on the other hand, consistently produces fragmented-appearing mini-cores, the result of the failure of MFAS to coalesce. When *TGFBI-G623D* and *APPL-RNAi* were combined in the same fly, the result was a combination of malformed DCGs, along with malformed DCGs accompanied by mini-cores, often sharing the same DCG-forming compartment. This also suggests the production of a phenotype intermediate between *TGFBI-G623D* and *APPL-RNAi*, since many of the compartments in rescue cells do not contain a distorted large central core (*cf.* **Figure 5.11D** and **Figure 5.13D**).

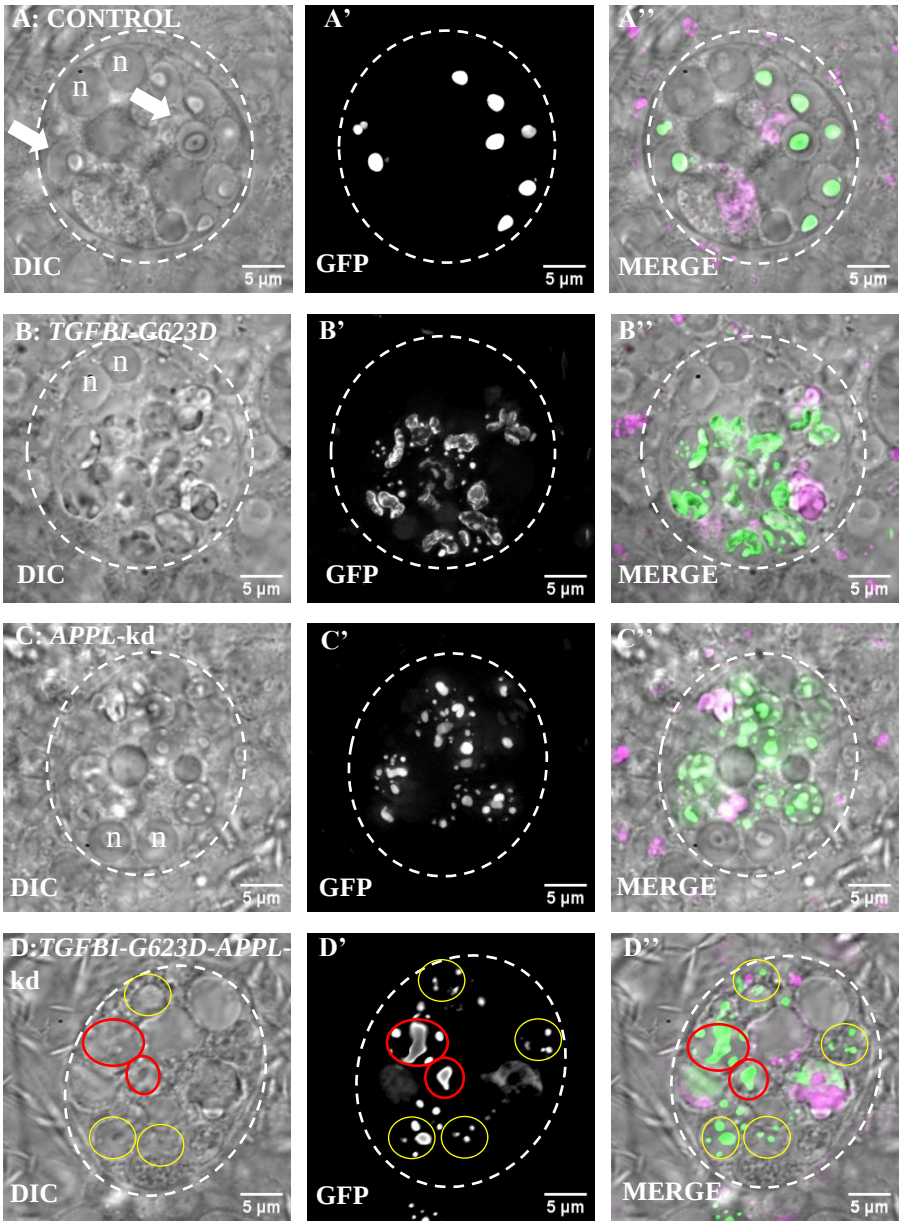

Figure 5.13: Interaction between *TGFBI-G623D* and *APPL-RNAi.* SCs from six-day-old virgin males stained with LysoTracker Red and imaged *ex vivo*, using DIC and fluorescence microscopy for GFP and LysoTracker Red. **A)** w^{1118}*; tub-GAL80*^{ts}*/UAS-ry-RNAi; dsx-GAL4 GFP-mfas/+* (control) **B)** w^{1118}*; tub-GAL80*^{ts}*/UAS-TGFBI-G623D; dsx-GAL4 GFP-mfas/+* **C)** w^{1118}*; tub-GAL80*^{ts}*/+; dsx-GAL4 GFP-mfas/UAS-APPL-RNAi* **D)** w^{1118}*; tub-GAL80*^{ts}*/UAS-TGFBI-G623D; dsx-GAL4 GFP-mfas/UAS-APPL-RNAi*. **White arrows** in **A:** DCGs; **yellow circles/ovals:** compartments with large cores and mini-cores; **red circles:** compartments with large or solitary cores; **n:** double nuclei characteristic of each SC. Scale bar = 5 µm.

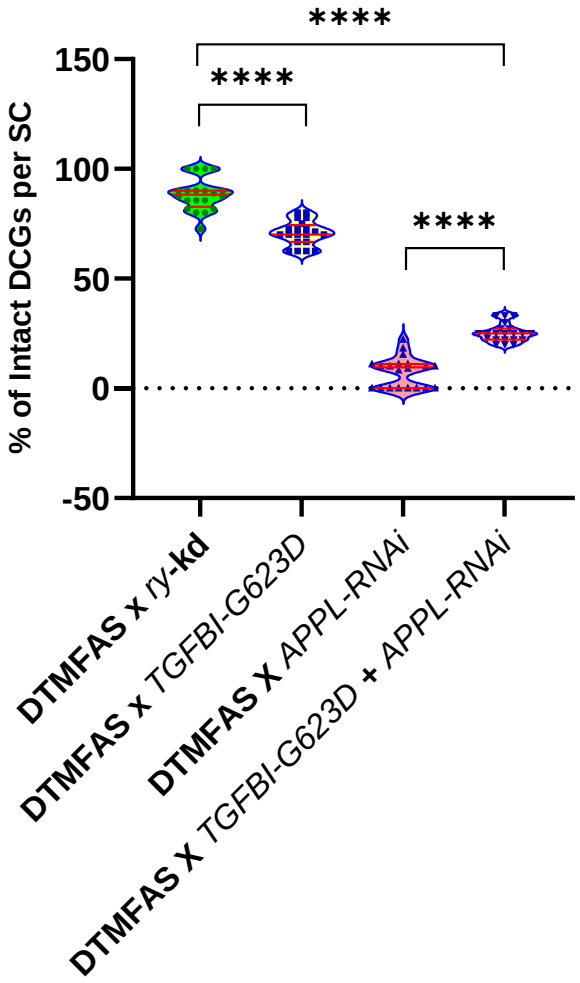

Figure 5.14: Interaction between *TGFBI-G623D* and *APPL-RNAi.* *TGFBI-G623D* produces less intact DCGs as compared to *ry*-kd controls, and all the *TGFBI-G623D* DCGs are severely deformed. *APPL-RNAi* produces significantly less intact DCGs, producing fragmented-appearing mini-cores instead. However, the combination of *TGFBI-G623D* and *APPL-RNAi* results in a phenotype intermediate between the deformed DCGs of *TGFBI-G623D* and the mini-cores of *APPL-RNAi*. As also indicated in the microscopy images (**Figure 5.13)** which correspond to this bar chart, all genotypes listed here were driven by w^{1118}*; tub-GAL80*^{ts}*/CyO; dsx-GAL4 GFP-mfas/TM6B* (DTMFAS). The mean for each set of experiments is shown in red.

TGFBI-G623D is a prolific disease-causing mutation, resulting in several corneal dystrophies. When introduced into the *Drosophila* genome, it produces severely malformed DCGs (**Figure 5.9C**). When combined, however, with the mini-core-producing

APPL-RNAi, it generates a combination of malformed DCGs occupying the same dense-core compartment space as mini-cores, but no normal DCGs. This suggests the creation of a phenotype intermediate between human *TGFBI-G623D* and *APPL-RNAi.*

5.2.4.3 INTERACTION BETWEEN *TGFBI-H626R* AND *APPL-RNAi*

Through another series of the appropriate genetic crosses, I generated another fly line bearing both *TGFBI-G623D* and *APPL-RNAi* constructs, again to test whether the amyloidogenic effect of the former exerted any rescue influence on the mini-core phenotype of the latter. I then overexpressed these combined *TGFBI-H626R* and *APPL-RNAi* constructs in adult SCs under dsx-GAL4 control, and compared the resultant DCG phenotype to that of control cells expressing a *UAS-ry-RNAi* construct. By itself, *TGFBI-H626R* produces severely deformed DCGs (**Figure 5.9D** and **Figure 5.15B**, below). When combined with *APPL-RNAi*, the individual DCG compartments had a large, distorted central core, with some of these compartment spaces also containing mini-cores (**Figure 5.15D**).

Like *G623D, H626R* is a *TGFBI* mutation conserved between *TGFBI* and *mfas*, and like *G623D*, it causes Lattice CD (among others). When introduced into the *Drosophila* genome, *TGFBI-H626R* produces severely malformed DCGs. When combined with the mini-core-forming *APPL-RNAi*, however, it produces a combination of solitary malformed DCGs, and malformed DCGs sharing compartment space with the mini-cores. This suggests a partial rescue by *TGFBI-H626R* of the mini-core phenotype of *APPL-RNAi.* Additionally, these attempted rescues appear closer to the *mfas-G623D-APPL-RNAi* rescue

in terms of having a large distorted central core (*cf.* **Figure 5.11D** and **Figure 5.15D**), rather than the TGFBI-G623D-APPL-RNAi rescue (*cf.* **Figure 5.13D** and **Figure 5.15D**).

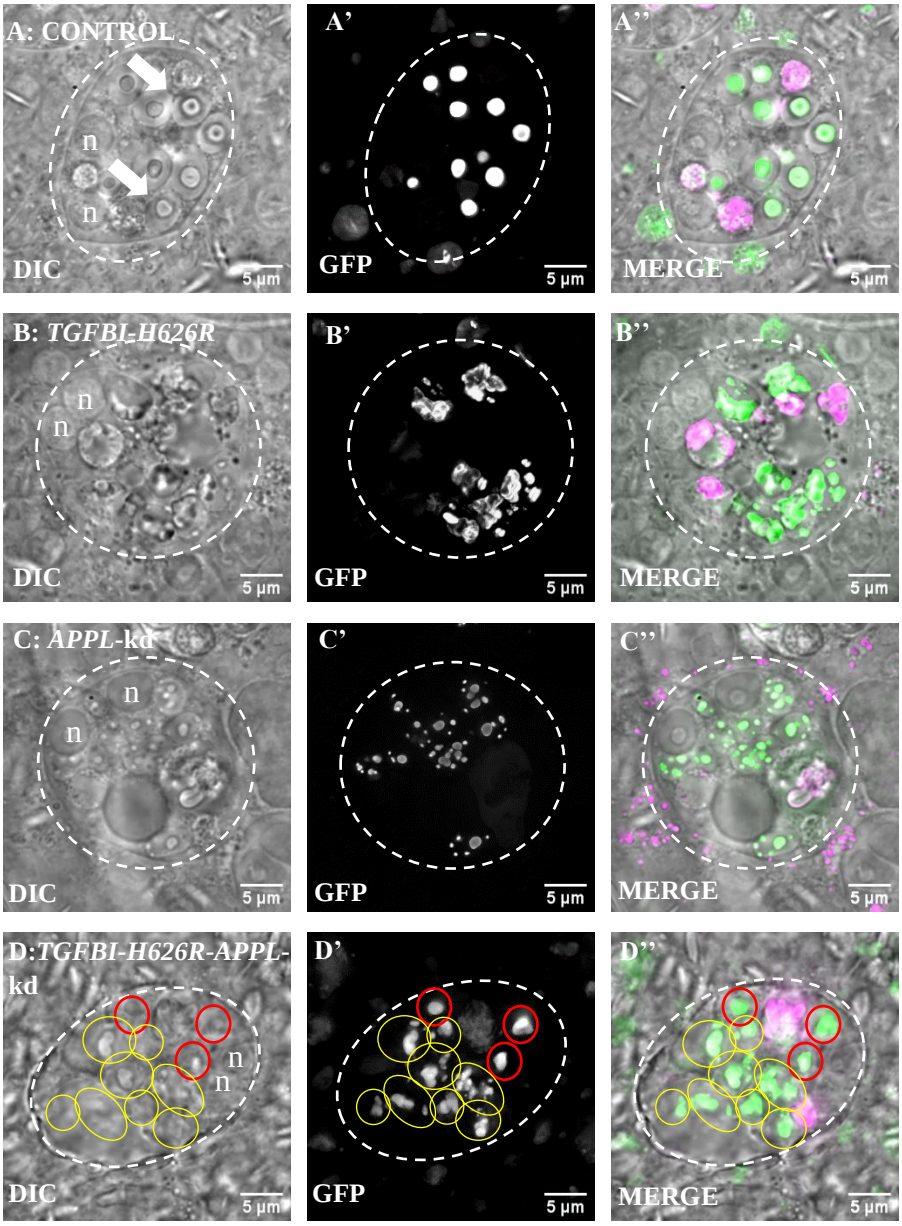

Figure 5.15: Interaction between *TGFBI-H626R* and *APPL-RNAi.* SCs from six day-old virgin males stained with LysoTracker Red and imaged *ex vivo*, using DIC and fluorescence microscopy for GFP and LysoTracker Red. **A)** w^{1118}*; tub-GAL80*^{ts}*/UAS-ry-RNAi; dsx-GAL4 GFP-mfas/+* (control) **B)** w^{1118}*; tub-GAL80*^{ts}*/UAS-TGFBI-H626R; dsx-GAL4 GFP-mfas/+* **C)** w^{1118}*; tub-GAL80*^{ts}*/+; dsx-GAL4 GFP-mfas/UAS-APPL-RNAi* **D)** w^{1118}*; tub-GAL80*^{ts}*/UAS-TGFBI-H626R; dsx-GAL4 GFP-mfas/UAS-APPL-RNAi*. **White arrows in A:** DCGs; **yellow circles/ovals:** compartments with both large cores and mini-

cores; **red circles:** compartments with large or solitary cores; **n:** double nuclei characteristic of each SC. Scale bar = 5 μm.

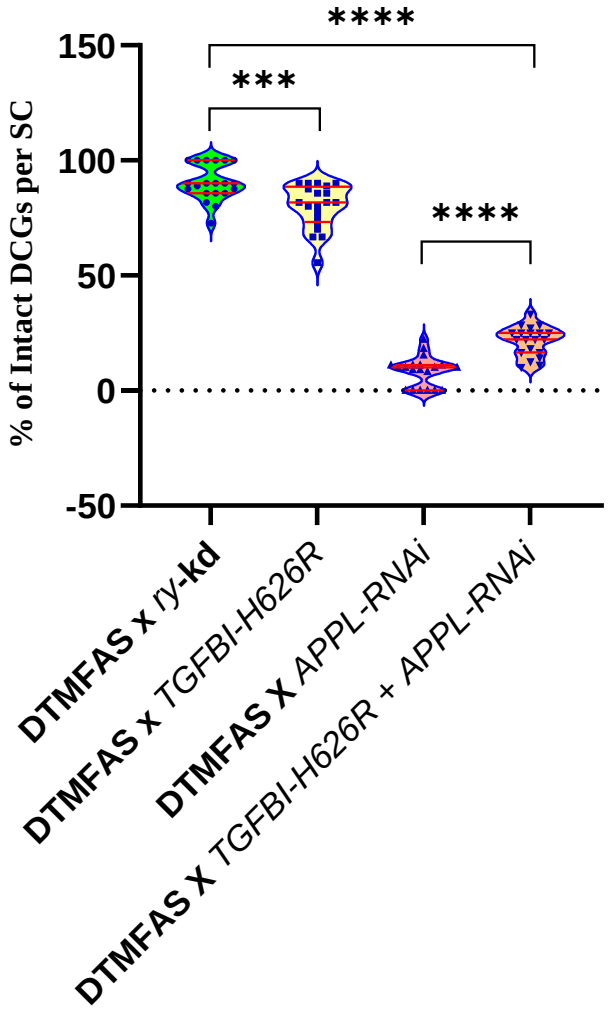

Figure 5.16: Interaction between *TGFBI-H626R* and *APPL-RNAi*. *TGFBI-H626R* produces less intact DCGs as compared to *ry*-kd controls, and all the *TGFBI-H626R* DCGs are severely deformed. *APPL-RNAi* produces significantly less intact DCGs, producing fragmented-appearing mini-cores instead. However, the combination of *TGFBI-H626R* and *APPL-RNAi* in the *Drosophila* genome results in an intermediate phenotype, with a combination of deformed DCGs and mini-cores. As also indicated in the microscopy images (**Figure 5.15)** which correspond to this bar chart, all genotypes listed here were driven by w^{1118}*; tub-GAL80*^{ts}*/CyO; dsx-GAL4 GFP-mfas/TM6B* (DTMFAS). The mean for each set of experiments is shown in red.

5.2.4.4 INTERACTION BETWEEN *TGFBI-R555Q* AND *APPL-RNAi*

Through another series of the appropriate genetic crosses, I generated another fly line bearing both *TGFBI-R555Q* and *APPL-RNAi* constructs, again to test whether the amyloidogenic effect of the former exerted any rescue influence on the mini-core phenotype of the latter. I then overexpressed these combined *TGFBI-R555Q* and *APPL-RNAi* constructs in adult SCs under dsx-GAL4 control, and compared the resultant DCG phenotype to that of control cells expressing a *UAS-ry-RNAi* construct.

The experiment below was different from the previous rescues in that it examined the interaction between the non-conserved mutation *TGFBI-R555Q* and *APPL-RNAi* in an attempt to ascertain whether differences exist between conserved and non-conserved mutations with regards to their rescue potential. As demonstrated earlier, *TGFBI-R555Q* produces deformed DCGs (**Figure 5.10B**). However, when combined with *APPL-RNAi*, the result was an often smaller main core, which frequently shared compartment space with mini-cores (**Figure 5.17D**).

TGFBI-R555Q, unlike the conserved mutations *TGFBI-G623D* and *TGFBI-H626R*), is not associated with a wide range of corneal dystrophies. Rather, it is known to cause Thiel-Behnke CD, which presents in early childhood and is distressingly recurrent, even after corneal transplantation, and in corneal grafts (Gear *et al.*, 2005). As is shown later, *TGFBI-R555Q* imparts a distinctive appearance to MFAS within the gland lumen (**Figure 6.37D** and **Figure 6.39C**), consistent with studies showing that mutations at the arginine 555

position confers greater stability to the resultant amyloid (Runager *et al*., 2011). Like other *TGFBI* mutations, it also produces malformed DCGs, and when combined with *APPL-RNAi,* it created a phenotype producing compartments with a combination of abnormal main cores as well as mini-cores. Given the relative paucity of large abnormal cores in favour of smaller ones, this too, was deemed to be an example of an intermediate phenotype.

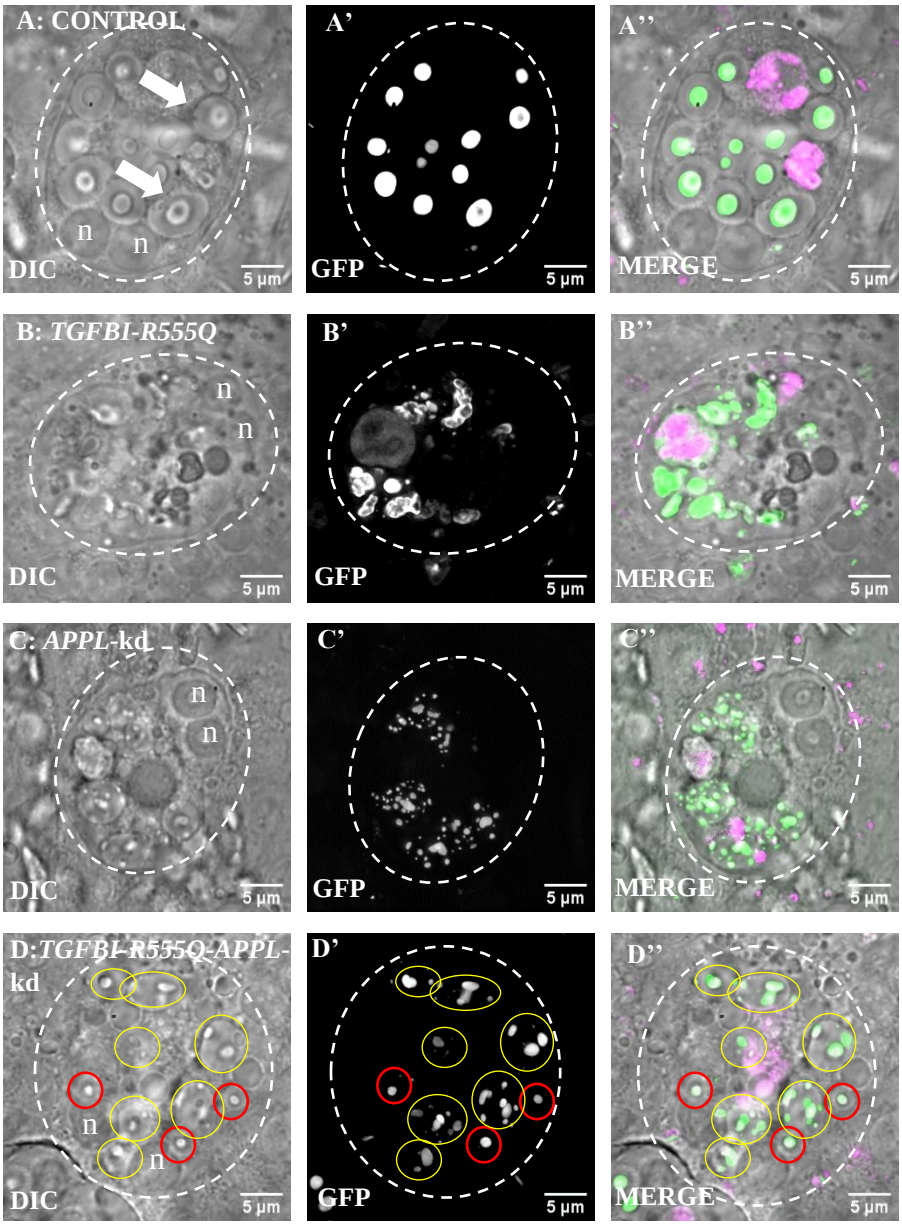

Figure 5.17: Interaction between *TGFBI-R555Q* and *APPL-RNAi*. SCs from six day-old virgin males stained with LysoTracker Red and imaged *ex vivo*, using DIC and fluorescence microscopy for GFP and LysoTracker Red. **A)** *w^{1118}; tub-GAL80^{ts}/UAS-ry-RNAi; dsx-GAL4 GFP-mfas/+* (control) **B)** *w^{1118}; tub-GAL80^{ts}/UAS-TGFBI-R555Q; dsx-GAL4 GFP-mfas/+* **C)** *w^{1118}; tub-GAL80^{ts}/+; dsx-GAL4 GFP-mfas/UAS-APPL-RNAi* **D)** *w^{1118}; tub-GAL80^{ts}/UAS-TGFBI-R555Q; dsx-GAL4 GFP-mfas/UAS-APPL-RNAis*. **White arrows** in **A:** DCGs; **yellow circles/ovals:** compartments with larger cores and mini-cores; **red circles:** compartments with single cores; **n:** double nuclei characteristic of each SC. Scale bar = 5 µm.

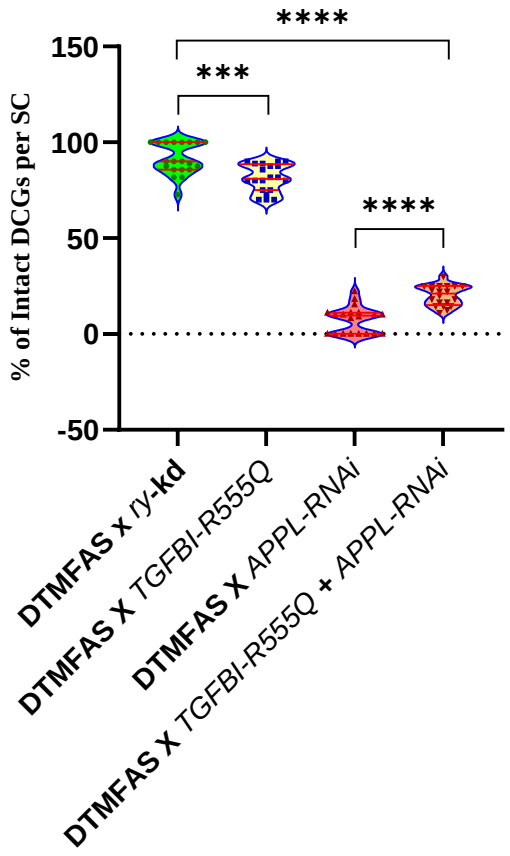

Figure 5.18: Interaction between *TGFBI-R555Q* and *APPL-RNAi.* *TGFBI-R555Q* produces less intact DCGs than *ry*-kd controls. *APPL-RNAi* produces significantly less intact DCGs, forming fragmented-appearing mini-cores instead. However, the combination of *TGFBI-R555Q* and *APPL-RNAi* results in the production of an intermediate phenotype with both the deformed DCGs characteristic of *TGFBI-R555Q* and mini-cores characteristic of *APPL-RNAi.* As also indicated in the microscopy images (**Figure 5.17)** which correspond to this bar chart, all genotypes listed here were driven by w^{1118}*; tub-GAL80*^{ts}*/CyO; dsx-GAL4 GFP-mfas/TM6B* (DTMFAS). The mean for each set of experiments is shown in red.

5.2.4.5 INTERACTION BETWEEN *TGFBI-R124C* AND *APPL-RNAi*

The final *TGFBI* mutation studied was the non-conserved, domain-1 *R124C* mutation (**Figure 5.8**). By itself, it has already been established that *TGFBI-R124C* produces somewhat milder phenotypic abnormalities in DCGs (**Figure 5.10C** and **Figure 5.19B**). Through the appropriate genetic crosses, I generated another fly line bearing both the

TGFBI-R124C and *APPL-RNAi* constructs, again to test whether the amyloidogenic effect of the former exerted any rescue influence on the mini-core phenotype of the latter. I then overexpressed these combined *TGFBI-R124C* and *APPL-RNAi* constructs in adult SCs under dsx-GAL4 control, and compared the resultant DCG phenotype to that of control cells expressing a *UAS-ry-RNAi* construct.

In keeping with its previously seen phenotype of producing somewhat less abnormal-appearing DCGs as compared to other *TGFBI* mutants (**Figure 5.10C**), when combined with the mini-core-producing phenotype of *APPL-RNAi*, *TGFBI-R124C* results in an intermediate phenotype. This was evidenced by the production of smaller than normal but not greatly deformed main cores (similar to, but smaller than those seen when *TGFBI-R124C* is overexpressed on its own) along with *APPL-RNAi*-type mini-cores in the same compartment space.

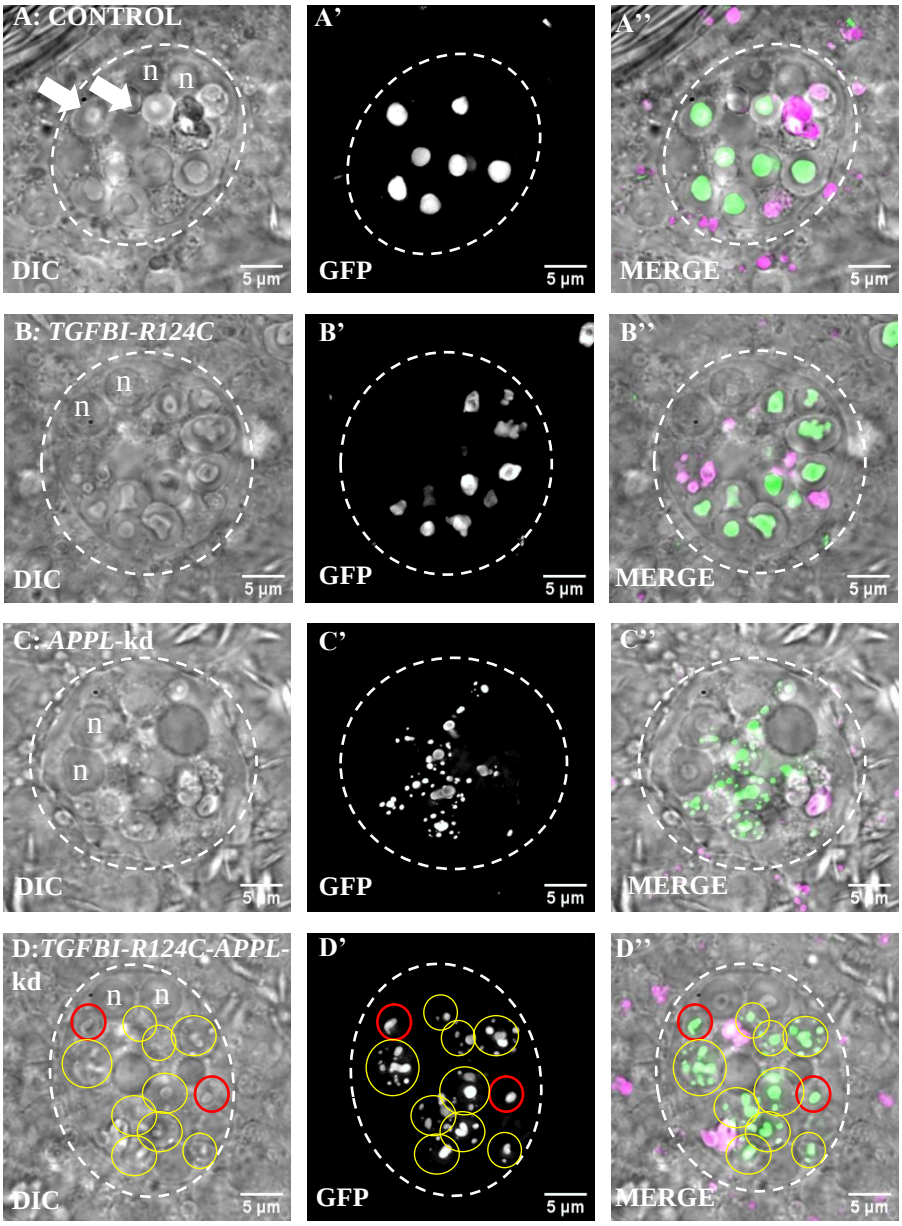

Figure 5.19: Interaction between *TGFBI-R124C* and *APPL-RNAi.* SCs from six day-old virgin males stained with LysoTracker Red and imaged *ex vivo*, using DIC and fluorescence microscopy for GFP and LysoTracker Red. **A)** *w^{1118}; tub-GAL80^{ts}/UAS-ry-RNAi; dsx-GAL4 GFP-mfas/+* (control) **B)** *w^{1118}; tub-GAL80^{ts}/UAS-TGFBI-R124C; dsx-GAL4 GFP-mfas/+* **C)** *w^{1118}; tub-GAL80^{ts}/+; dsx-GAL4 GFP-mfas/UAS-APPL-RNAi* **D)** *w^{1118}; tub-GAL80^{ts}/UAS-TGFBI-R124C; dsx-GAL4 GFP-mfas/UAS-APPL-RNAi*. **White arrows** in **A:** DCGs; **yellow circles/ovals:** compartments with larger cores and mini-cores; **red circles:** compartments with larger solitary cores; **n:** double nuclei characteristic of each SC. Scale bar = 5 µm.

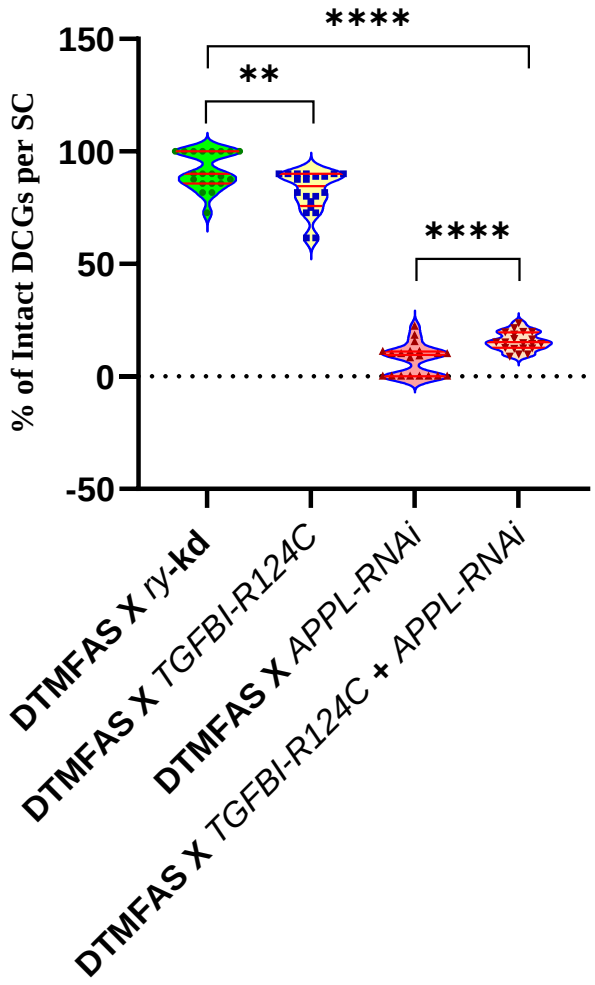

Figure 5.20: Interaction between *TGFBI-R124C* and *APPL-RNAi.* *TGFBI-R124C* produce less intact DCGs than *ry*-kd controls. Unlike *TGFBI* domain-4 mutations (*G623D*, *H626R* and *R555Q*) *TGFBI-R124C* does not produce severely deformed DCGs. *APPL-RNAi* produces significantly less intact DCGs, predominantly producing fragmented-appearing mini-cores. The combination of *TGFBI-R124C* and *APPL-RNAi* results in an intermediate phenotype. As also indicated in the microscopy images (**Figure 5.19)** which correspond to this bar chart, all genotypes listed here were driven by w^{1118}*; tub-GAL80*^{ts}*/CyO; dsx-GAL4 GFP-mfas/TM6B* (DTMFAS). The mean for each set of experiments is shown in red.

5.3 DISCUSSION

5.3.1 AN OVERVIEW OF THE EFFECTS OF *TGFBI* AMYLOIDOGENIC MUTATIONS ON DCGs

As shown earlier in Sections **5.2.1, 5.2.2** and **5.2.3**, DCG morphology varies in accordance with the normality or abnormality of the underlying genetic construct. Thus, in response to the genomic insertion of *wild type-mfas* and *wild type-TGFBI*, the resultant DCGs were physiological, or normal-appearing. In contrast, pursuant to the genomic insertion of *TGFBI* amyloidogenic mutations, the resultant DCGs were abnormal. The degree of abnormality appears to follow domain clustering of hotspots: domain 4 mutations, where most clinically relevant mutations are found, produced greater DCG abnormalities. Thus DCG abnormalities are most prevalent with constructs bearing the domain-4 mutations *G623D, H626R* and *R555Q*, while the sole construct with a domain-1 mutation, *R124C* produced fewer abnormal DCGs. (**Figure 5.21**).

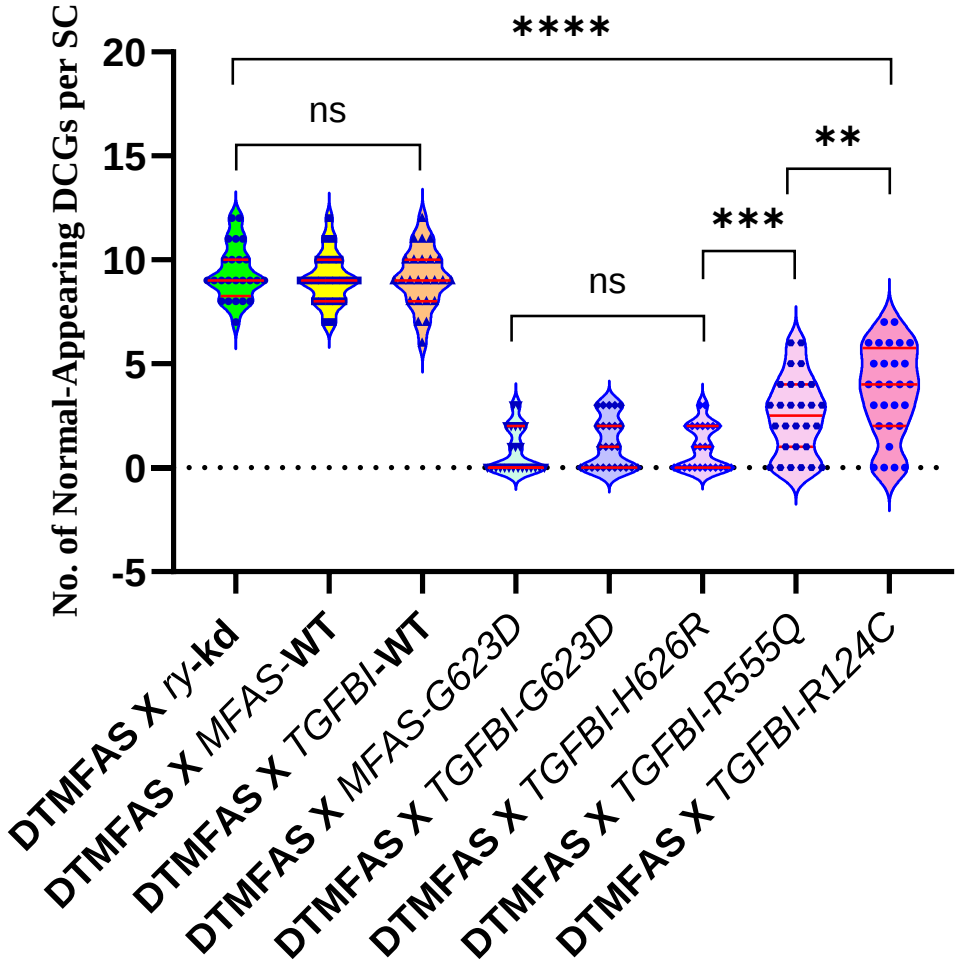

Figure 5.21: Flies with *mfas-wild type* and *TGFBI-wild type* have normal-appearing DCGs, while those with CD mutations do not. Flies with *mfas-G623D* and *TGFBI* with corneal dystrophy mutations have predominantly abnormal DCGs. These abnormalities are most pronounced with the *mfas-G623D*, *TGFBI-G623D* and *TGFBI-H626R* mutations (conserved), and are less so with *TGFBI-R555Q*, and particularly with *TGFBI-R124C* mutations (both non-conserved). All listed genotypes were driven by w^{1118}*; tub-GAL80^{ts}/CyO; dsx-GAL4 GFP-mfas/TM6B* (DTMFAS). The mean for each set of experiments is shown in red.

My data have revealed that expressing mutant forms of MFAS and TGFBI that are associated with corneal dystrophies interfere with the normal aggregation of MFAS protein in SC DCGs. This interference with the aggregation of MFAS is more pronounced with constructs bearing domain-4 mutations (*G623D*, *H626R* and *R555Q*) than with the

construct bearing a domain-1 mutation (*R124C*), which shows fewer abnormal DCGs. This correlates well with the clinical severity of human disease, as well as with structural studies of TGFBI. The crystal structure of the *Drosophila* FAS1 domains reveals that each domain consists of a seven-stranded β-structure surrounded by α-helices (Clout and Hohenester, 2003). The domain-1 mutation, *R124C*, located in a solvent-exposed α-helix, is predicted to cause changes only in the solubility of the protein, and accordingly presents as milder, later-onset disease. Interestingly though, it causes Lattice CD, which based on numbers alone, is the commonest CD worldwide. Based on extensive modelling studies, this fact has been cited as evidence that *R124C*'s relative benignity has saved it from evolutionary extinction. In contrast, the conserved domain-4 mutations *G623D* and *H626R* are located on the β-structures, as is the non-conserved domain-4 mutation *R555Q.* These mutations are predicted to alter the structure of the protein (Clout *et al.,* 2003), and are accordingly characterized by earlier disease onsets and a more aggressive clinical progression (Kannabiran and Klintworth, 2006).

As with *R124C*, the *R555Q* hotspot was also found to be highly mutable. Extensive analyses of mutations across *TGFBI* showed that the survivorship of these two mutations is the result of survivor bias, despite the opposing force of purifying selection on *TGFBI* mutations (Leiden Open Variation Database: databases.lovd.nl/shared/genes/TGFBI). This is because in general, perniciously harmful disease mutations will have detrimental and pleiotropic effects. Other *TGFBI* mutations were not found to be 'mild' enough to survive the processes of germ cell differentiation, fertlization, maturation and embryogenesis, all processes in which *TGFBI* is shown to be involved. Furthermore, *R124C* and *R555Q* also

reflect the mutability of CpG arginine codons – CpG dinucleotides are noted mutation hotspots in vertebrate genomes, with over ten-fold mutability occurring in these spots over that predicted by chance alone (Cooper *et al.,* 2010). These facts assume greater significance when considered in the light that *TGFBI* sequences are highly conserved across all vertebrate genomes (Song *et al*., 2014), and that *TGFBI* plays dual roles as both a cancer promoter and suppressor (Ween *et al*., 2012), with links to prostate, ovarian, colon, bone, breast, lung, hepatocellular, and brain cancer, as well as to their invasion and metastasis (Ween *et al*., 2012; Guo *et al.,* 2011).

5.3.2 CONCLUDING REMARKS AND PERSPECTIVES ON TGFBI AS A BIOLOGICALLY IMPORTANT AMYLOID RESEARCH MODEL

The introduction of mutated *TGFBI* into the *Drosophila* genome induces the pathological reorganization of MFAS in degrees corresponding to *TGFBI's* human pathogenicity. *TGFBI* and *mfas* are homologues, and are traceable by Cambrian fossil records to ancient chordate lineages going back to the basal chordate, Amphioxus (*Branchiostoma belcheri*). *TGFBI* and *mfas* share 39.1 % and 16.5 % homology with Amphioxus *TGFBI* respectively (Song *et al.,* 2014). It is therefore revelatory, yet unsurprising, that highly penetrant corneal dystrophy-inducing mutations in *TGFBI* (reviewed in Klintworth, 2003) direct MFAS to produce abnormal DCGs commensurate with their human pathological potential.

As alluded to earlier, the welter of clinical and molecular information exploding onto the field of *TGFBI* research makes it clear that this is a complex and protean group of amyloid diseases, and that earlier genotype-phenotype classifications (Munier *et al.,* 1997) require constant updating. Historically, this has certainly been true for Alzheimer's disease, which

grew from one neglected case to becoming the high-powered focus of institutions and funding agencies around the world (Querfurth and LaFerla, 2010). Indeed, when Alois Alzheimer presented his single case study at the meeting of Southwest German Psychiatrists in 1906, it was met with disinterest, quite likely because the other speakers presented more salacious case studies like paraphilias. Furthermore, the chairman of the seesion, the influential academic psychiatrist and eugenicist Alfred Hoche was a scientific enemy of Emil Kraepelin, Alzheimer's colleague and collaborator, and quickly ushered Alzheimer off the podium without the courtesy of the customary chairman's summary, while also stating there was no need for questions or discussion (Hippius and Neundorfer, 2003; Zilka and Novak, 2006). This was in marked contrast to the long, lively and friendly discussions he elicited for the other speakers, particularly for the talk that followed, dealing with an unusual paraphilia (Cipriani et al., 2011). Adding insult to injury, the organisers deemed Alzheimer's presentation unsuitable for publication in the meeting's proceedings, so it was only covered by a single sentence in the local Tübingen newspaper (Dahm, 2006).

To draw an analogy, CD research today, though on a much smaller scale, might be what AD research was a century ago. Still very much in it's infancy, research in TGFBI and APP will hopefully benefit from the relatively unambiguous nature of the *Drosophila* results presented here, which point to the fly as a potentially overarching paradigm for human amyloid research in multiple organ systems. Already, TGFBI and APP have been reported to be found in high quantities in supermeres (supernatant of exomeres), which are extracellular nanoparticles distinct from exomeres (Zhang *et al.*, 2021). Indeed, TGFBI is the most abundant protein in supermeres. Considered in light of the fact that supermere's

cargoes are linked to multiple cancers, Alzheimer's disease, cardiovascular disease, and COVID-19 infection, these linked discoveries hold out great promise in multiple areas of biomedical research.

5.3.3 OVERVIEW OF INTERACTIONS BETWEEN *TGFBI* MUTANTS AND *APPL-RNAi*

The results obtained when combining DCG-deforming TGFBI mutations and minicore-producing APPL-RNAi suggested some level of rescue of the APPL-RNAi phenotype (**Figure 5.22**). However, the relatively 'weak' rescues might alternatively be explained as an intermediate phenotype induced by reduced expression of both transgenes, when compared to expression of the transgenes alone. Indeed, in all combinations, most SC DCG compartments continued to display mini-core phenotypes, suggesting that this fundamental defect was poorly rescued.

In this regard, overexpression of *mfas-G623D* and *TGFBI-H626R*, representing the most pernicious corneal dystrophy mutants, appeared to produce the most dramatic 'rescues', since even if mini-cores were still present, most compartments produced in these cells contained a central large distorted core, which was characteristic of expressing the mutant protein alone. This suggests that these mutant proteins have more protein aggregation activity than wild type-MFAS, which is expressed at high levels in all these genetic backgrounds. It therefore supports the idea that these proteins are not only able to disrupt normal DCG formation, but that they may partly do this by driving protein aggregation events. As we will see in Chapter 6, other amyloidogenic versions of APP are much better

at rescuing at rescuing the *APPL*-knockdown phenotype, strongly suggesting that the protein aggregation roles of APPL and MFAS in SCs are distinct.

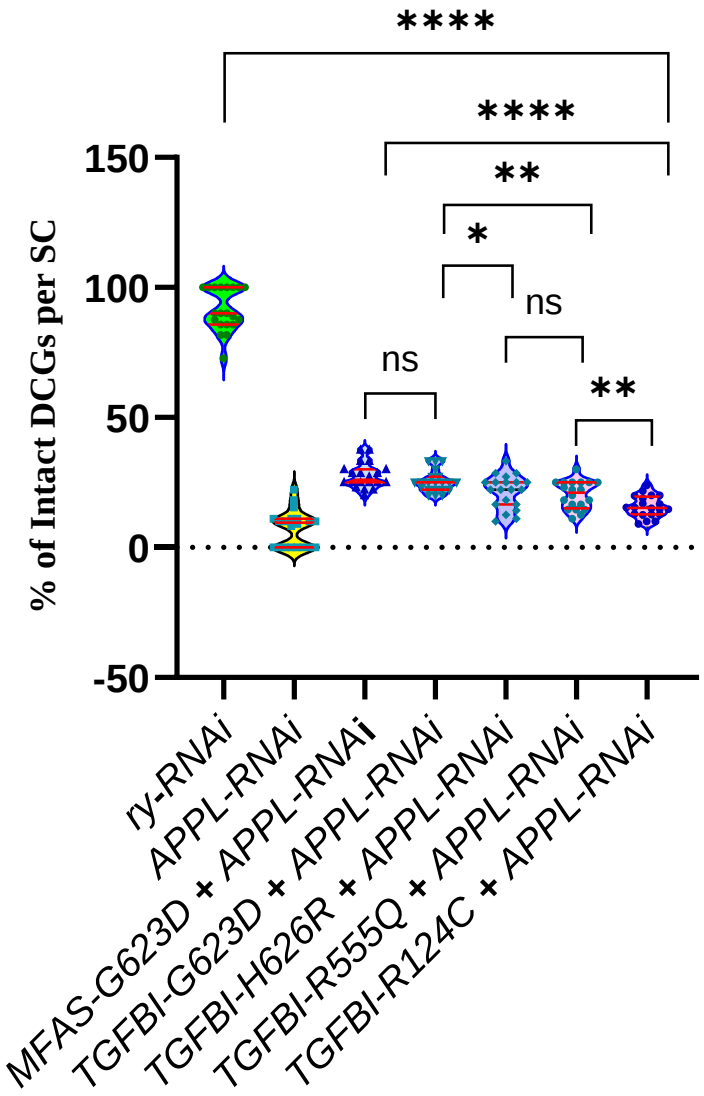

Figure 5.22: *TGFBI* domain-4 mutations (*G623D*, *H626R* and *R555Q*) were incrementally more effective than the domain-1 mutation (*R124C*) in producing an intermediate phenotype when combined with the *APPL-RNAi* mini-core phenotype. This intermediate phenotype production effect correlates well with the severity of amyloid CDs these mutations cause, and underscores the well-accepted maxim that amyloid proteins are tenacious and stable. All genotypes shown were driven by w^{1118}*; tub-GAL80*^{ts}*/CyO; dsx-GAL4 GFP-mfas/TM6B* (DTMFAS). The mean for each set of experiments is shown in red.

In summary, when the *mfas* and *TGFBI* amyloidogenic mutant constructs were individually combined with *APPL-RNAi* in the same fly in an attempted rescue, the results were a combination of the mini-core phenotype of *APPL-RNAi* and the deformed DCGs of the *TGFBI* mutants. *TGFBI* mutations which cause more clinically severe amyloid CDs are more effective in increasing the proportion of intact, albeit deformed DCGs over the proportion of mini-cores produced by *APPL-RNAi*. This is likely a reflection of the tenacity (and therefore stability) of amyloid proteins. Transverse Urea Gel (TUG) Electrophoresis studies have shown that domain-4 mutations vastly increased the stability of TGFBI, while various mutations in the 124 position of domain-1 did not (Runager *et al.,* 2011). These experimental findings showing that the stability of *TGFBI* mutants correlates well with the severity of disease they produce is therefore not an unexpected result. These results also align with work which showed that domain-4 mutations directly affect the protein structure, while domain-1 muations only affect it's solubility (Clout *et al.,* 2003; Clout, 2003; Kannabiran and Klintworth, 2006).

Overall, my work has led to the development of a new cellular model in which the aberrant activity of *TGFBI* mutants can be detected through simple expression in SCs. At least in some cases, this probably involves a mechanism whereby the mutants induce inappropriate protein aggregation, as they do in human corneal dystrophies. This model may therefore pave the way for genetic experiments in which suppressors of these aberrant phenotypes are identified, which might suggest new treatment strategies to alleviate the pathology of this amyloidogenic disease.

CHAPTER 6

THE EFFECTS OF FAD MUTATIONS ON DCGs, AND DCG AGEING CHARACTERISTICS IN AMYLOIDOGENIC GENETIC BACKGROUNDS

6. THE EFFECTS OF FAD MUTATIONS ON DCGs, AND DCG AGEING CHARACTERISTICS IN AMYLOIDOGENIC GENETIC BACKGROUNDS

6.1 INTRODUCTION

As discussed earlier, APP has numerous structural and functional segments. Broadly, these include it's extracellular and intracellular domains, and an internal, partially intramembranous Aβ segment. Mutations along APP's length, along with mutations in it's processing enzymes, form the basis for Familial Alzheimer's Disease (FAD).

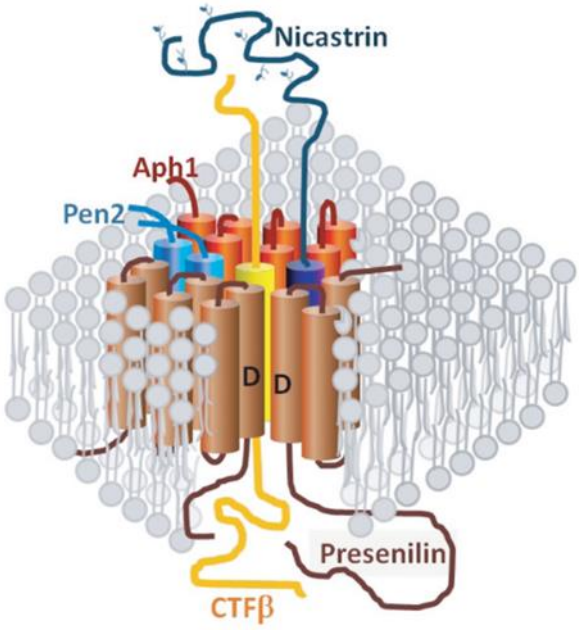

Figure 6.1: APP and its relation to its γ-secretase. This is comprised of Presenilin, Aph-1, Pen-2, and Nicastrin, the latter acting as a stabilizing cap which holds APP (yellow) firmly in place as it is cleaved by the intramembranous catalytic aspartates (D) of Presenilin. (Xu, J. Alz. Dis. 2009, pg. 216).

Figure 6.1 shows the four components of γ-secretase with it's substrate, APP (shown in yellow), locked into place and ready for intramembranous cleavage. The initial skepticism surrounding this process was dispelled with the discovery of regulated intramembrane

proteolysis (RIP), a biological phenomenon which APP, Notch and their γ-secretases led the way in illuminating (Lichtenthaler *et al.,* 2011; Kopan and Ilagan, 2009). The understandable objections to RIP were to the improbability of proteolysis occurring within the hydrophobic lipid milieu of the cell membrane. However, the discovery of a hydrophilic water-filled core between Presenilin's transmembrane domains 6 and 7 into which the catalytic aspartates abutted, explained the enzyme's function (Sato *et al.,* 2006; Tolia *et al.,* 2006).

Analysis of APP's C-terminal fragments after γ-secretase cleavage found that some of these were longer than expected. This led to the finding that although the final γ-secretase cleavage produces Aβ fragments largely 40 or 42 amino acids in length, this is actually preceded by a cut at an ε-site between Leu^{646} and Val^{647}, generating $A\beta_{49}$, followed by a cut at a ζ-site between Val^{643} and Ile^{644}, generating $A\beta_{46}$ (Yu *et al.,* 2001; Weidemann *et al.,* 2002; Zhao *et al.,* 2004) **(Figure 1.5** and **Figure 6.2).** These insights grew alongside an ever-expanding list of FAD mutations (**Figure 1.7** and **Figure 1.8**), making RIP dysregulation with respect to APP and Notch important in the fields of AD and cancer respectively.

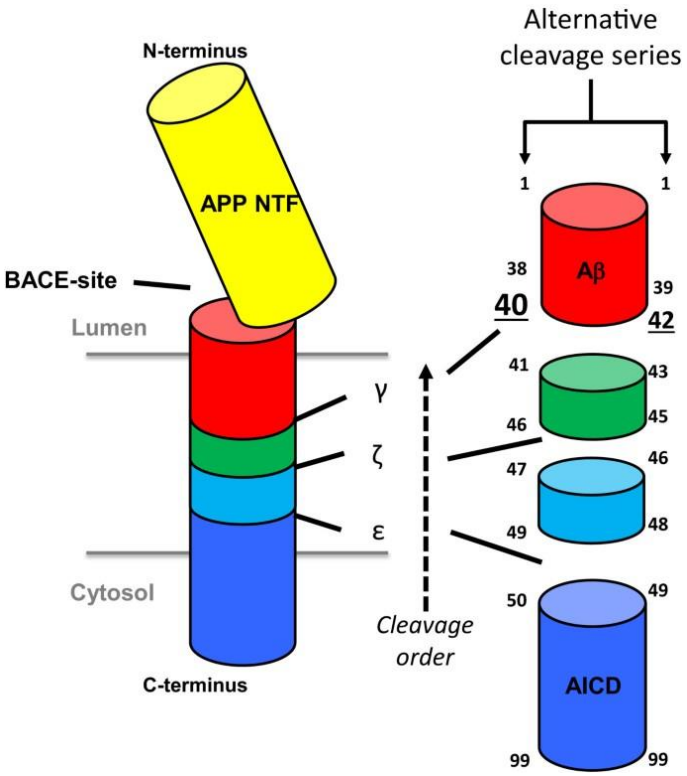

Figure 6.2: Detail of APP's primary (γ) and ancillary (ζ, ε) cleavage sites by Presenilin, generating Aβ species from 40 to 49 amino acids in length. In addition to those shown, there are even more minor cleavage sites which produce yet more fragments (see **Figure 1.5**). Each of these Aβ species have varying propensities to fibrillate and aggregate, a phenomenon which also varies depending upon the relative ratios of the Aβ species to one another. (Li *et al*., Mol. Neurodegeneration 2014, p. 2).

6.1.1 FAD MUTATIONS IN AND AROUND APP'S Aβ SEQUENCE

While FAD mutations occur through the length of *APP*, intra-$A\beta_{42}$ mutations are unique (**Figure 6.3**). This is because in addition to FAD they also cause Cerebral Amyloid Angiopathy (CAA), a syndrome characterized by the replacement of cerebral arterial and arteriolar walls with amyloid, which leads to intra-cerebral hemorrhages and premature death (**Figure 6.4A**). The brain amyloid plaques produced by the intra-$A\beta_{42}$ mutations also have distinctive morphologies: $A\beta_{42}$-*E693G-Arctic* plaques are described as 'targetoid', while $A\beta_{42}$-*E693Q-Dutch* and $A\beta_{42}$-*D694N-Iowa* plaques are characterized as 'cloud-like'

(**Figure 6.4B** and **C**). The *APP-K595N/M596L-Swedish* double mutation, lying just outside the Aβ sequence towards its N-terminal end (**Figure 6.3**), increases the production of $A\beta_{40}$ and $A\beta_{42}$ nine to tenfold by increasing cleavage at the primary β-site rather than the secondary (β') site, and produces the traditional 'cotton wool' plaques of AD. It causes an aggressive, premature, relentlessly progressive form of the disease in which 65 % of patients also suffer from myoclonus or seizures. This unique and somewhat enigmatic mutation also appears to have other unclear effects beyond just enhancing β-cleavage; some groups have reported that it increased synapse numbers and enhanced synaptic transmission (Zhou *et al*., 2022), while other groups reported the opposite (Schmid *et al.*, 2016). The three intra-*Aβ* mutations (*Arctic, Dutch* and *Iowa*) as well as the *Aβ*-adjacent *Swedish* double mutation are shown in **Figure 6.3** below.

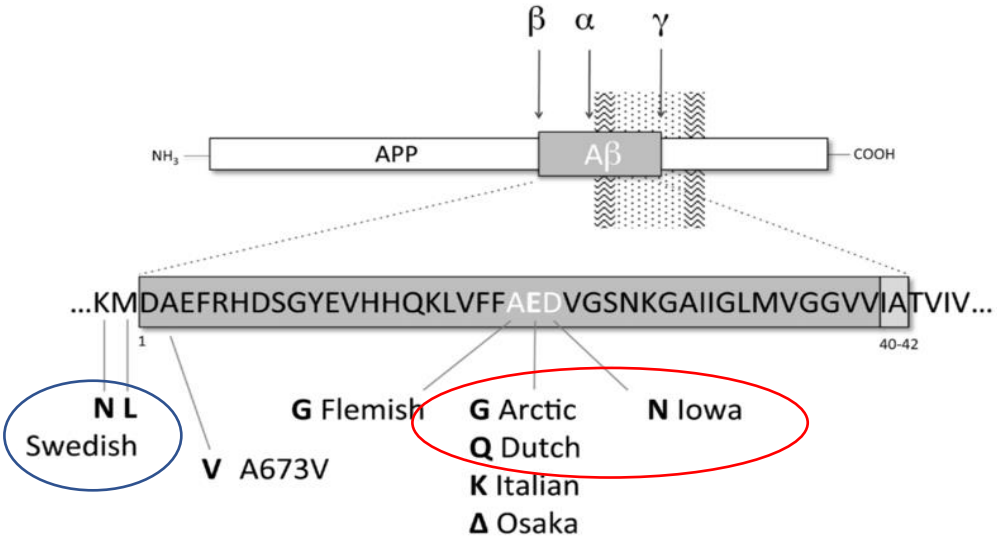

Figure 6.3: Human APP, showing it's principal secretase cleavage sites, and the location of the *Arctic, Dutch* and *Iowa* mutations within the $A\beta_{42}$ sequence (red oval). The Swedish double mutation is located just outside the Aβ sequence, towards the N-terminal end of APP (blue oval). (Adapted from Nilsberth *et al*., Nature Neuroscience 2001, pg. 888).

The clinical and neuropathological effects of the intra-Aβ mutations (cerebral amyloid angiopathy, and distinctively-shaped Aβ plaques respectively) are shown in **Figure 6.4** below.

A

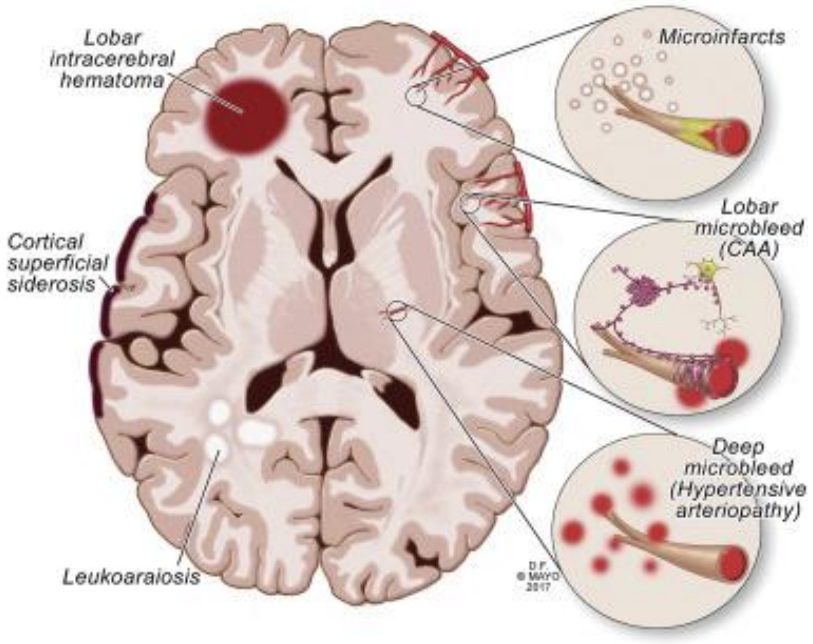

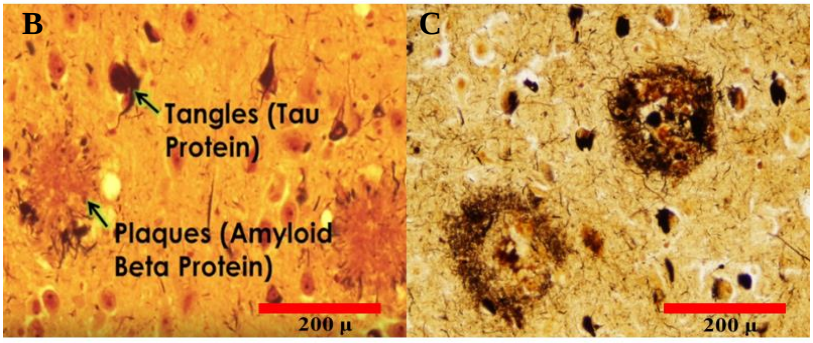

Figure 6.4: A: Intra-*Aβ* mutations cause Cerebral Amyloid Angiopathy (CAA) characterised by cerebral vessel wall infiltration with amyloid, and recurrent intracerebral hemorrhages which are ultimately fatal. (Adapted from DeSimone *et al*., J. Amer. Coll. Cardiol. 2017, p. 1175). **B:** Fluffy plaques, representative of those seen with the *Dutch* and *Iowa* mutations. **C:** Targetoid plaques seen with the *Arctic* mutation. (**B** and **C** are adapted from Neuropathologyweb.org).

Having established the benignity of the effects on MFAS of both full-length human APP, as well as that of human APP cleaved by human BACE-1 (**§ 4.2.5.3**, **Figure 4.29B** and **C**), my next experimental step was to investigate the effects of FAD-causing APP mutations on MFAS behaviour. For this study, I examined *$A\beta_{42}$-E693G-Arctic, $A\beta_{42}$-E693Q-Dutch*, *$A\beta_{42}$-D694N-Iowa*, and *APP-K595N/M596L-Swedish.*

6.1.2 RETROMER DYSFUNCTION AND NEURODEGENERATIVE DISEASES

The retromer is a protein complex initially identified in yeast, and which was found to be crucial for transporting protein cargoes from yeast endosomes to the TGN (Seaman et al., 1998). The discovery of retromer's mammalian homologues quickly revealed the mammalian system's complexities as compared to the yeast system, showing that the retromer was indeed a master orchestrator of the endosomal sorting and trafficking of proteins (Burd and Cullen, 2014). Since the endosomal trafficking of receptors determines their density on post-synaptic membranes, while the endosomal trafficking of neurotransmitters influences their release from pre-synaptic membranes, the retromer's role in neurological conditions was quick to emerge (Choy *et al*., 2014; Zhang *et al.*, 2012; Hussain *et al.*, 2014). As the archetype of neurodegenerative diseases caused by disordered protein processing and trafficking, AD was in fact the first human disorder linked to retromer dysfunction (Small *et al*., 2005). Since then, retromer abnormalities have been associated with a rapidly expanding cohort of neurodegenerative diseases (reviewed in Reitz, 2018).

Thus, in addition to AD (reviewed in Small and Petsko, 2015), mutations or deficiencies in retromer components result in the accumulation of a variety of protein aggregates and are therefore linked to numerous other neurodegenerative diseases like Parkinson's (Munsie *et al.,* 2015), Tauopathies (Wang and Mandelkow, 2016), Down's syndrome (Wang *et al*., 2013), Hereditary Spastic Paraplegia (an associated gene of which encodes strumpellin, a member of retromer's WASH complex) (Valdmanis *et al.,* 2007), and Lysosomal Storage Disorders (Khurana *et al.,* 2010). The last mentioned category of endolysosomal storage disorders with retromer connections includes Batten disease (ceroid lipofuscinosis neuronal-3 deficiency), Gaucher disease (glucocerebroside deficiency), Danon disease (lysosome associated membrane protein-2 deficiency), and Cystinosis (chaperone-mediated autophagy mislocalization (Myerowitz *et al.,* 2021; Ysselstein *et al*., 2019).

The retromer's cargo recognition core (**Figure 6.5B, Figure 6.6**) includes Vacuolar Sorting Protein-Associated Proteins 26, 29, and 35 (VPS26, 29 and 35). VPS26 and VPS35 reductions in the entorhinal cortex are the very earliest indicators of preclinical Alzheimer's disease (Andersen *et al.,* 2005), and VPS35 dysfunction in a *Drosophila* model of Parkinson's disease impairs lysosomal degradation of alpha-synuclein, exacerbating it's neurotoxicity (Miura *et al.,* 2014). **Figure 6.6** shows a more detailed structure of the retromer complex, while **Figure 6.7** summarizes the three primary pathways through which it's dysfunction brings about neurological disease.

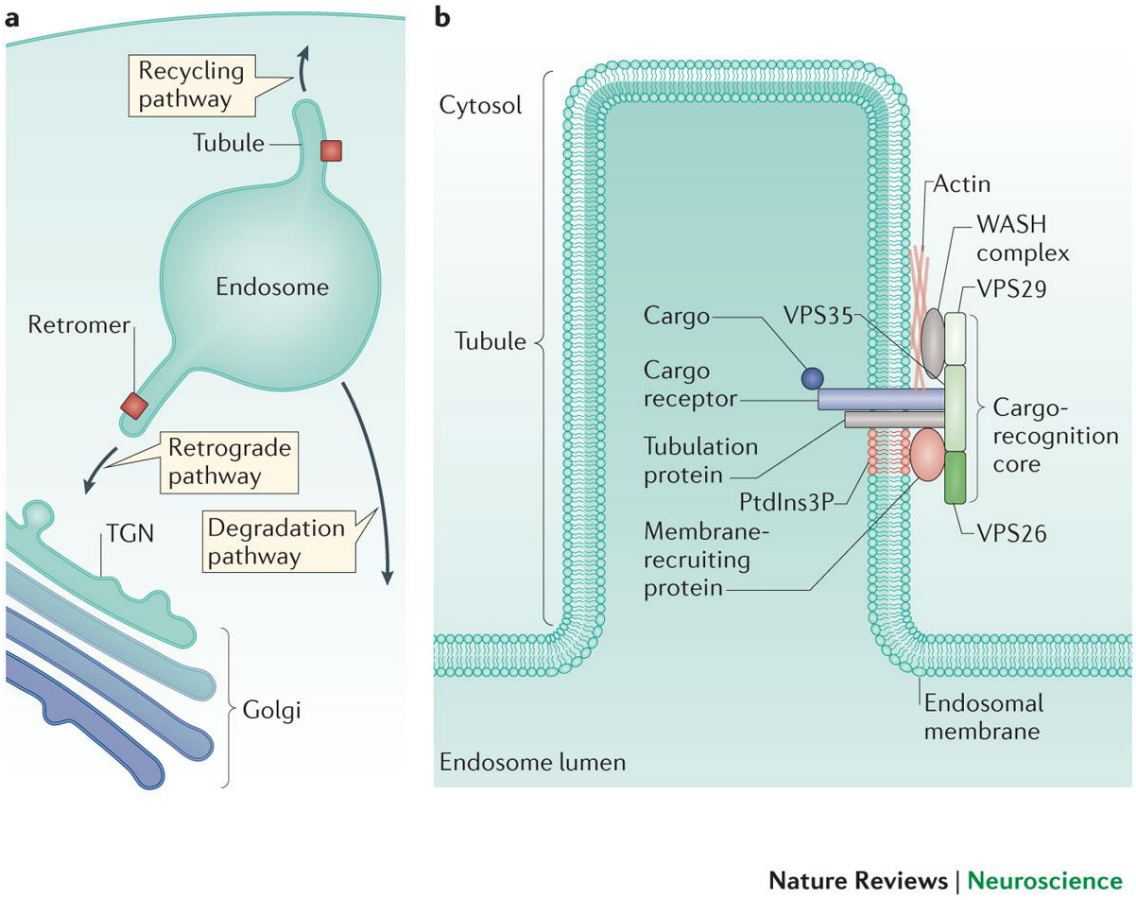

Figure 6.5: Retromer mediates two routes out of the endosome via tubules emanating from it. A: The retrograde pathway traffics cargoes to the *trans*-Golgi network (TGN) while the recycling pathway transports them to the cell surface. The non-retromer-mediated degradation pathway carries cargoes to lysosomes for degration. **B:** Retromer's cargo recognition core is comprised of a trio of proteins – vacuolar sorting protein-associated proteins (VPS) 26, 29 and 35.The WAS protein family homologue (WASH) complex also binds the cargo-recognition core and forms actin 'patches' which direct cargoes to their destinations via the tubules. (Small and Petsko, Nature Rev. Neurosci. 2015, p. 127).

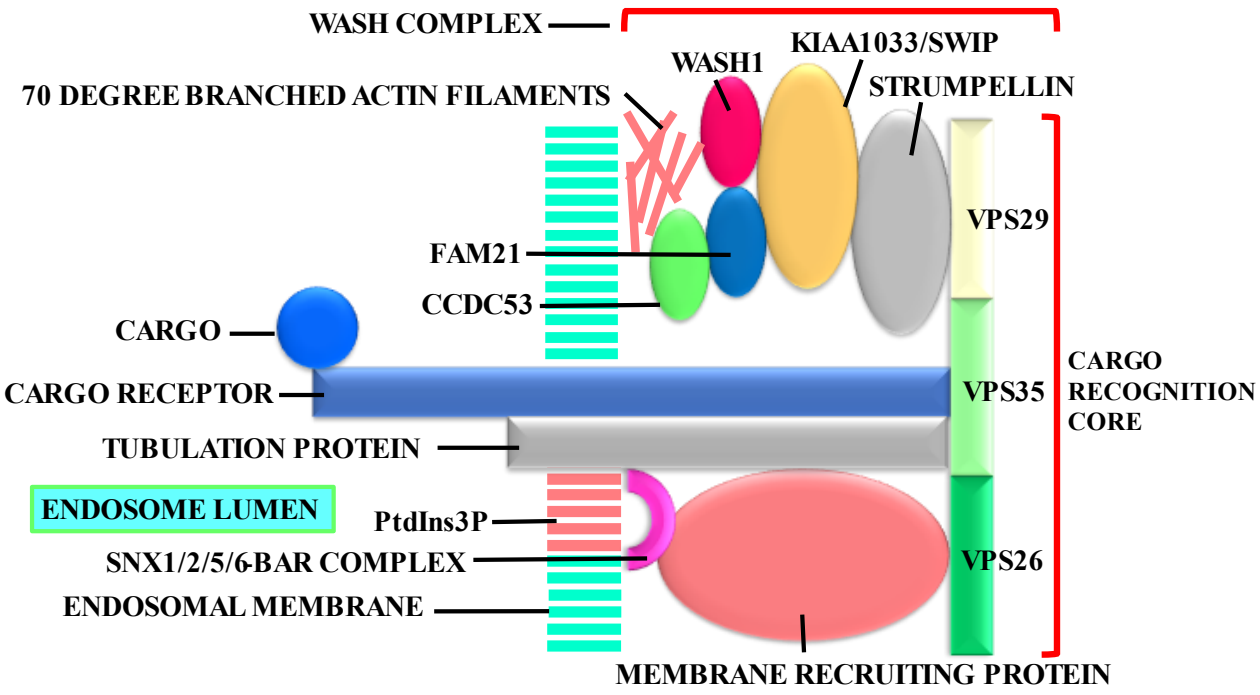

Figure 6.6: Detailed structure of the retromer shown in Figure 6.5B. The cargo recognition core consists of the VPS26, VPS29, and VPS35 proteins. A dimer of sorting nexin proteins (SNX) and the Bin/Amphyphysin/Rvs (BAR) domains make up the SNX-BAR complex which leads to tubulation of the endosomal membrane. Accessory proteins which regulate membrane tubule dynamics include the WASH complex which is formed by strumpellin, KIAA1033 (SWIP), FAM1, and CCDC53. The WASH complex also plays a role in the formation of endosomal sub-compartments through the organisation of existing and new actin filaments in the endosomal membrane into mother and daughter filaments, at a characetristic 70° branching angle.

Retromer dysfunction has three main pathophysiological outcomes. In the first instance, it causes a larger than normal amount of cargo to accumulate in endosomes, the best known example of this being APP. The backed-up APP then undergoes accelerated processing in the endosome, resulting in an accumulation of it's neurotoxic cleavage products, most notably Aβ, and it's β-carboxy terminal fragment (β-CTF). The second pathological pathway is the result of decreased cargoes being transported to the cell surface. For

example, the decreased transport of phagocytic receptors to the plasma membranes of microglial cells causes accelerated Alzheimer's disease in this cellular phenotype. Finally, retromer pathology leads to decreased protease delivery to the endosome. An example of this is the retromer-mediated delivery of the cation-independent mannose-6-phosphate receptor (CIMP6R) from the endosome to the TGN. Once in the TGN, CIMP6R binds cathepsin D and transports it back to the endosome, where along with other proteases it is part of the machinery of the endolysosomal system. Cathepsin D deficiency in the endolysosomal system triggers Tau pathology both within the endosome and, as a consequence, in the cytosol as well (**Figure 6.7**) (Tau, which is in the cytosol, in it's aggregated form is ultimately taken up by the endosomal system).

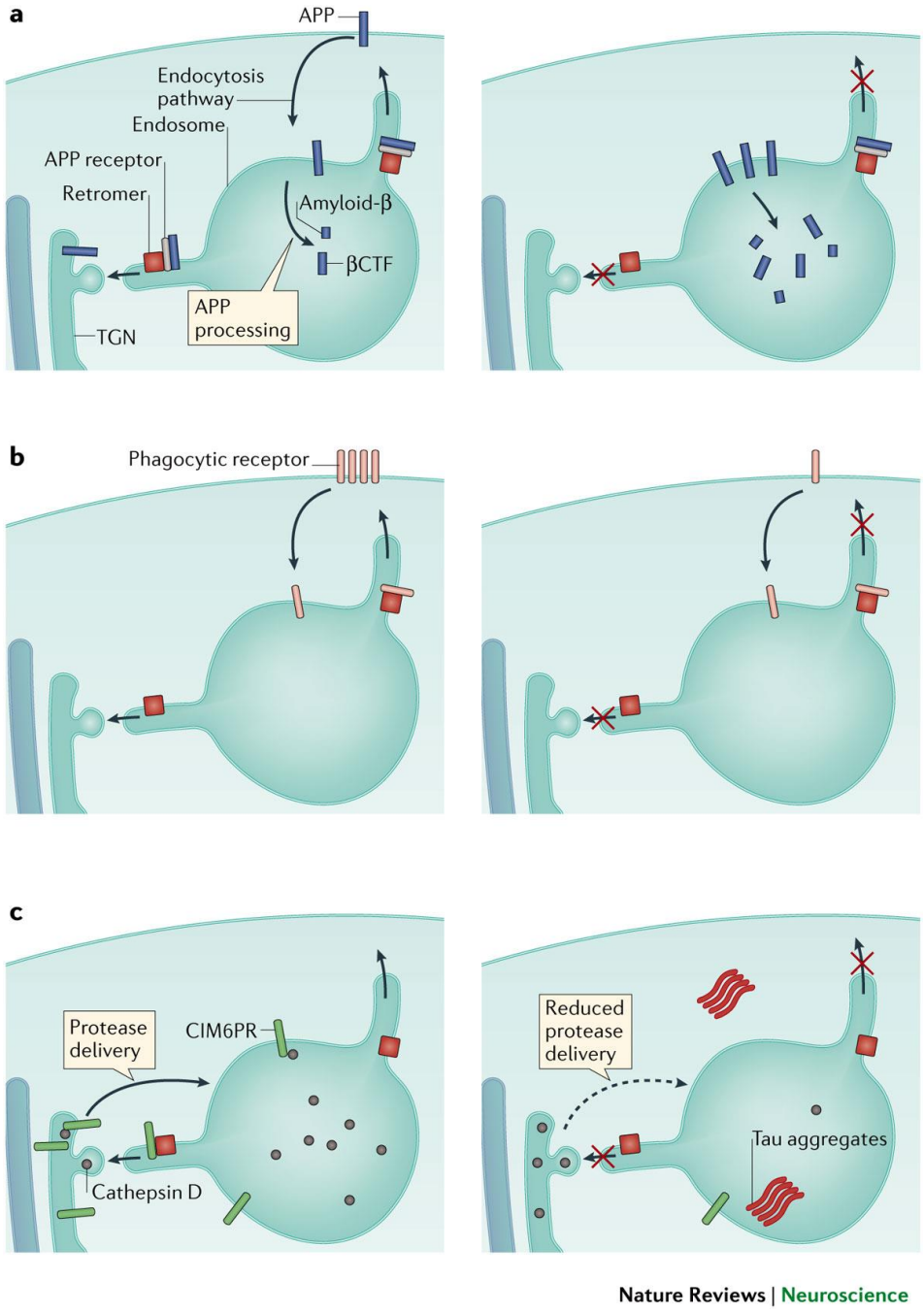

Figure 6.7: The three principal pathophysiological mechanisms of retromer dysfunction. A: The trapping of proteins like APP in endosomes, and the resultant accumulation of toxic cleavage products like Aβ and APP's β-C-terminal fragment (β-CTF). **B:** The impairment of cell surface transport of receptors, for example phagocytic receptors in microglial cells, a phenotype which is linked to AD. **C:** Impaired protease delivery to the endosome, for example, impeding the endosomal movement of cathepsin D, which leads to the accumulation of endosomal and cytosolic Tau aggregates. (Small and Petsko, Nature Rev. Neurosci. 2015, p. 128).

Retromer research is therefore opening up fruitful avenues of investigation, particularly in the areas of early diagnosis of neurodegeneration, and in understanding the cellular trafficking of neurodegenerative amyloids. In experiments conducted as part of this work, I examined the effects of the knockdown of VPS26 and VPS35, components of it's crucial cargo recognition core, on the formation of DCGs.

6.1.3 AIMS

In this chapter, I addressed the following research questions:

1. Do amyloidogenic mutants of *APP* ansd $A\beta_{42}$ affect DCGs when overexpressed in SCs?
2. Does knockdown of retromer components affect DCG biogenesis? Given the extensive links between retromer dysfunction and neurodegeneration, such an effect is plausible.
3. Can these mutants interact with other regulators of DCG biogenesis, and can they rescue loss of APP/APPL function?
4. Does overexpression of these mutants in SCs have any effects in the ageing accessory gland?

6.2 RESULTS

6.2.1 THE EFFECTS OF $A\beta_{42}$-*WT* AND $A\beta_{42}$-*ARCTIC* ON DCG MORPHOLOGY

I first tested the effect of overexpressing $A\beta_{42}$-*wild type* and $A\beta_{42}$-*E693G-Arctic* in adult SCs under dsx-GAL4 control. Both of these manipulations had no effect on the number of DCGs in SCs, when compared to control cells similarly overexpressing a *UAS-ry-RNAi* construct (**Figure 6.8A-C**; **Figure 6.9A**). However, in approximately 35 % of DCGs in SCs expressing $A\beta_{42}$-*wild type*, the central part of the core did not appear to contain any GFP-MFAS (**Figure 6.8D; Figure 6.9B**), while for $A\beta_{42}$-*E693G-Arctic*, this was the case

for more than 90 % of cores (**Figure 6.8E**; **Figure 6.9B**). This surprising result suggests that these peptides can play a role in organising the DCGs within SCs, perhaps providing a central assembly point around which MFAS mini-cores cluster. For the *$A\beta_{42}$-E693G-Arctic* mutant, the DCGs were often 'targetoid' in appearance, with concentric circles of MFAS. As discussed in the introductory section of this chapter, the Arctic mutation is uniquely associated with targetoid plaques in human brains, where immunostaining revealed full-length $A\beta_{42}$ species constituting the outer corona, intermediate length $A\beta_{17-24}$ peptides making up the intermediate portion, and the shortest $A\beta_{1-5}$ monomers and oligomers populating the centre (Kalimo et al., 2013).

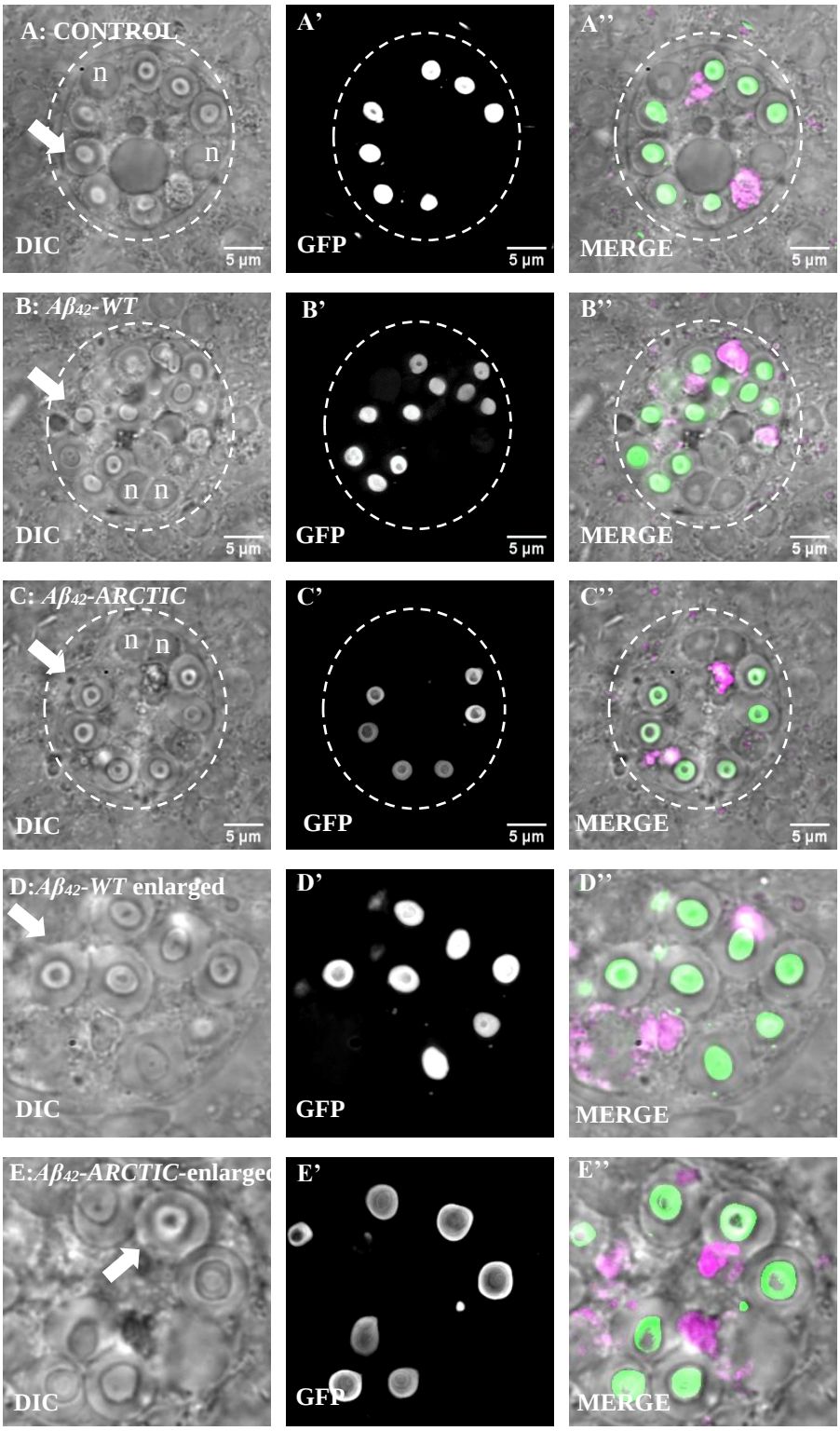

Figure 6.8: The effects of *Aβ42-wild type* and *Aβ42-E693G-Arctic* on DCG morphology. SCs from six day-old virgin males stained with LysoTracker Red and imaged *ex vivo*, using DIC and fluorescence microscopy for GFP and LysoTracker Red. **A)** w^{1118}*; tub-GAL80*^{ts}*/UAS-ry-RNAi; dsx-GAL4 GFP-mfas/+* (control) **B)** w^{1118}*; tub-GAL80*^{ts}*/UAS-*

Aβ42-wild type; dsx-GAL4 GFP-mfas/+ **C)** *w1118; tub-GAL80ts/UAS-Aβ42-E693G-Arctic; dsx-GAL4 GFP-mfas/+* **D)** Magnified view of *w1118; tub-GAL80ts/UAS- Aβ42-wild type; dsx-GAL4 GFP-mfas/+* **E)** Magnified view of *w1118; tub-GAL80ts/UAS-Aβ42-E693G-Arctic; dsx-GAL4 GFP-mfas/+*. **White arrows** in **A, B, C, D** and **E:** DCGs; **n:** double nuclei characteristic of each SC. Scale bar = 5 μm.

A

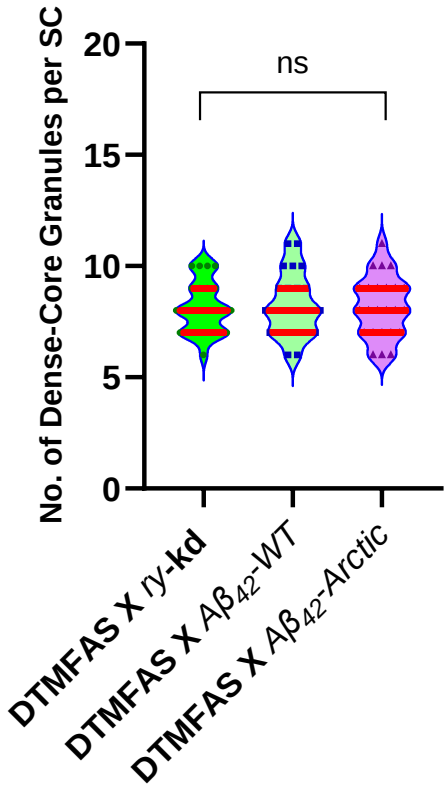

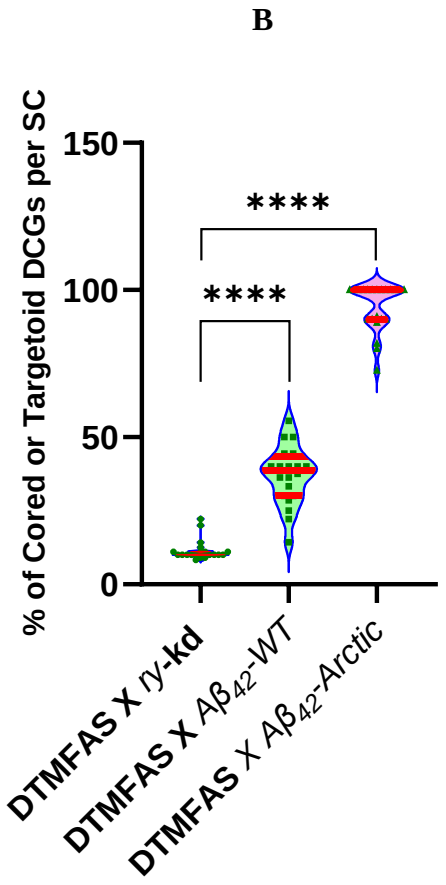

Figure 6.9: **A:** *Aβ42-wild type* and *Aβ42-E693G-Arctic* mutants have the same number of DCGs as controls. **B:** *Aβ42-wild type* and *Aβ42-E693G-Arctic* lines with 'cored' or 'targetoid' dense-cores are 37 % and 94 % respectively, as compared to 12 % of controls. The appearance of concentric rings or a 'targetoid' appearance of MFAS deposition in DCGs is a distinctive feature of flies transgenic for the human *Aβ42-E693G-Arctic* mutation. As also indicated in the microscopy images (**Figure 6.8)** which correspond to this bar chart, all genotypes listed here were driven by w^{1118}*; tub-GAL80*^{ts}*/CyO; dsx-GAL4 GFP-mfas/TM6B* (DTMFA). The mean for each set of experiments is shown in red.

6.2.2 THE EFFECTS OF *Aβ42-DUTCH* AND *Aβ42-IOWA* ON DCG MORPHOLOGY

Next, I tested the effect of overexpressing the *Aβ42-E693Q-Dutch* and *Aβ42-D694N-Iowa* FAD mutations in adult SCs under dsx-GAL4 control, comparing them to controls which in the same manner overexpressed the construct *UAS-ry-RNAi*. Both of these manipulations had no effect on the total number of compartments. However, about three-quarters of these

compartments contained mini-cores, with only 27 % (with the Dutch mutation) and 29 % (with the Iowa mutation) of compartments appearing relatively normal.

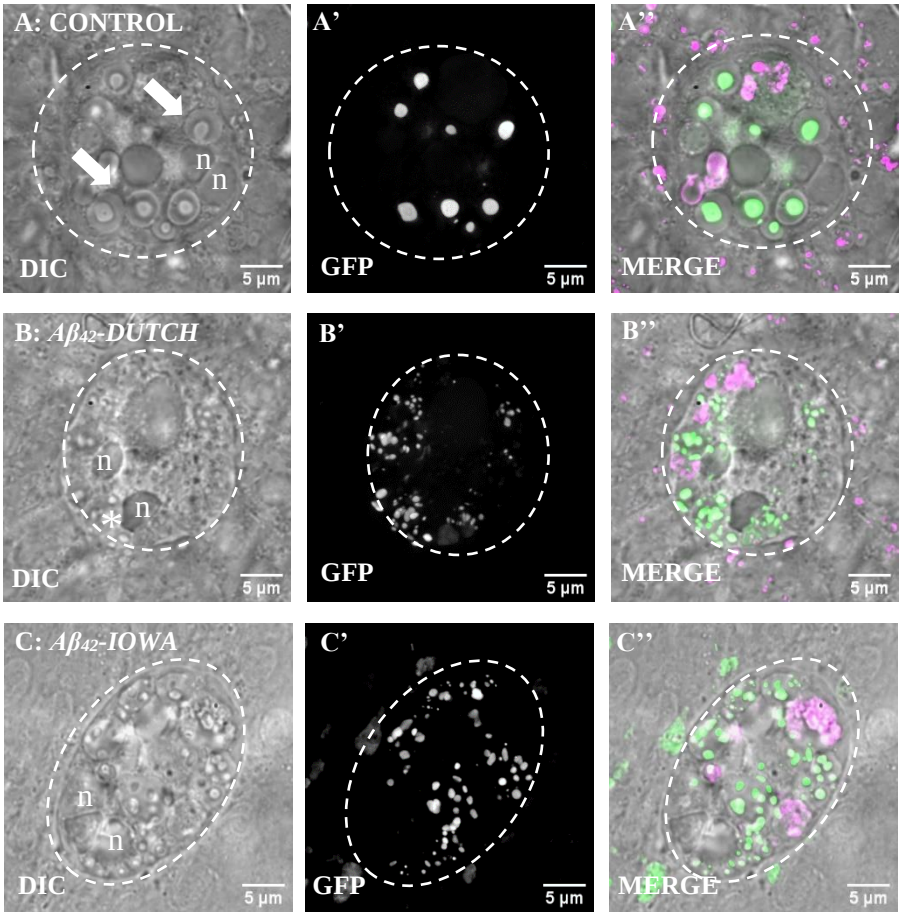

Figure 6.10: The effects of *Aβ42-E693Q-Dutch* and *Aβ42-D694N-Iowa* on DCG morphology. SCs from six day-old virgin males stained with LysoTracker Red and imaged *ex vivo*, using DIC and fluorescence microscopy for GFP and LysoTracker Red **A)** w^{1118}*; tub-GAL80*^{ts}*/UAS-ry-RNAi; dsx-GAL4 GFP-mfas/+* (control) **B)** w^{1118}*; tub-GAL80*^{ts}*/UAS-Aβ42-E693Q-Dutch; dsx-GAL4 GFP-mfas/+* **C)** w^{1118}*; tub-GAL80*^{ts}*/+; dsx-GAL4 GFP-mfas/UAS-Aβ42-D694N-Iowa.* **White arrows** in **A:** DCGs; **n:** double nuclei characteristic of each SC. Scale bar = 5 µm.

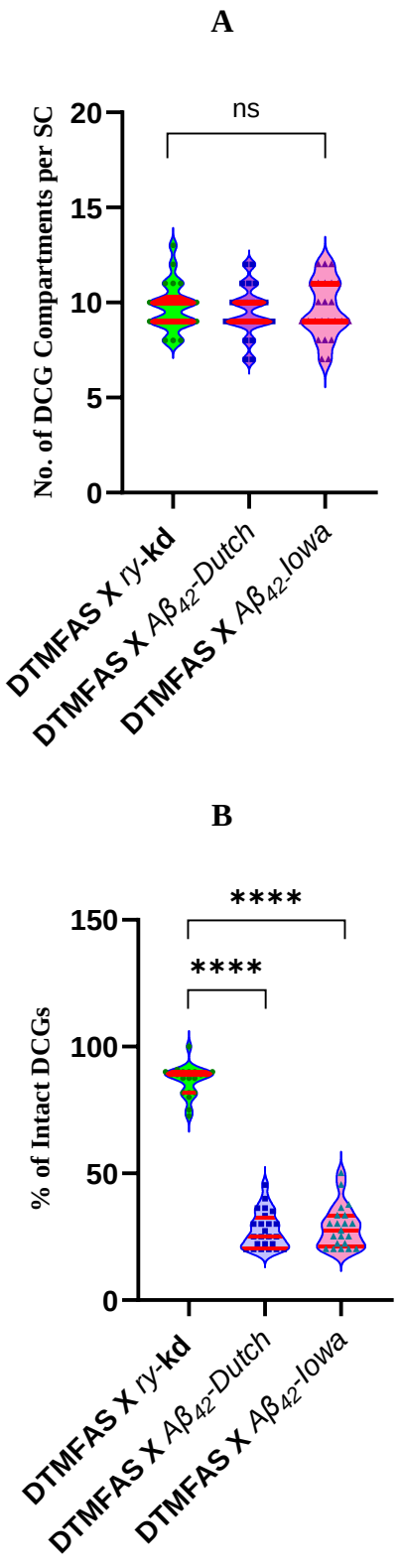

Figure 6.11: A: ***Aβ42-E693Q-Dutch*** **and** ***Aβ42-D694N-Iowa*** **have the same number of DCG-forming compartments. B:** *Aβ42-E693Q-Dutch* and *Aβ42-D694N-Iowa* have 27 % and 29 % intact DCGs within dense-core compartments respectively, as compared to 87 %

for controls. As also indicated in the microscopy images (**Figure 6.10)** which correspond to this bar chart, all genotypes listed here were driven by *w^{1118}; tub-GAL80^{ts}/CyO; dsx-GAL4 GFP-mfas/TM6B* (DTMFAS). The mean for each set of experiments is shown in red.

6.2.3 THE EFFECT OF *APP-K595N/M596L-SWEDISH* ON DCG MORPHOLOGY

Finally, I tested the effect of overexpressing the *APP-K595N/M596L-Swedish* double mutation in adult SCs under dsx-GAL4 control, comparing them to controls which overexpressed the construct *UAS-ry-RNAi*. The APP tested here was the full-length molecule, with the Swedish double mutation lying just outside the Aβ sequence, towards the N-terminal end (**Figure 6.3**). As alluded to in the introductory passages, this particular mutation enhances β-secretase cleavage of APP but also has other, somewhat unclear influences on the number of synapses and on synaptic transmission (Zhou *et al.*, 2022; Schmid *et al.,* 2016).

I had earlier examined the effect of overexpressing full-length, *wild type APP* on DCGs (**§ 4.2.5.3**, **Figure 4.29B**), a manipulation which essentially showed no variation when compared to controls (**Figure 4.29A**) or to the overexpression of wild type APP cleaved by BACE-1 (**Figure 4.29C**). When compared to wild type APP, the presence of the Swedish mutation resulted in the following distinctions, all of which are seen below: **a)** a variability in the number of DCGs, with on average, the production of about half the number of DCGs, **b)** the fact that almost half of these DCGs have a 'cored' appearance, with a central clearing (highlighted below with yellow ovals in **Figure 6.12B**), and **c)** the presence of large lysosomes (**Figure 6.12B** and **C**), which occasionally contain GFP-

MFAS. This suggests that the GFP-MFAS fails to be broken down, indicating an overloading of the degradation system in these cells.

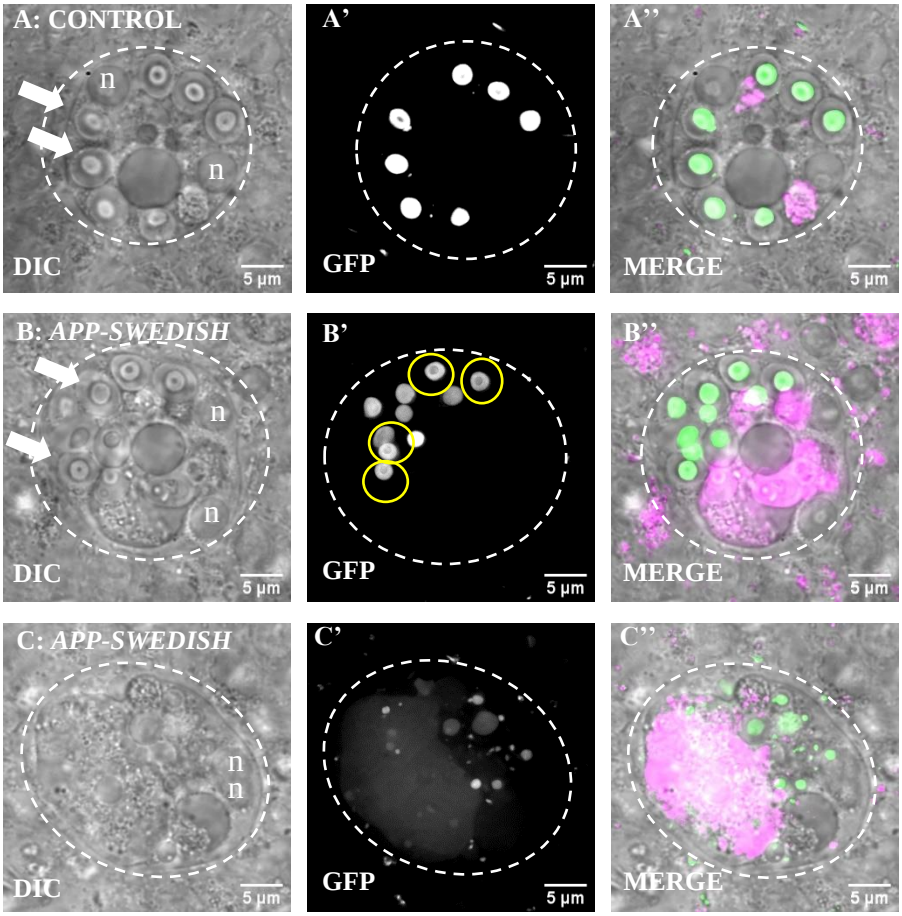

Figure 6.12: *APP-K595N/M596L-Swedish* has on average fewer intact DCGs and more cored DCGs than controls. SCs from six-day-old virgin males stained with LysoTracker Red and imaged *ex vivo*, using DIC and fluorescence microscopy for GFP and LysoTracker Red. **A)** *w^{1118}; tub-GAL80^{ts}/UAS-ry-RNAi; dsx-GAL4 GFP-mfas/+* (control) **B)** *w^{1118}; tub-GAL80^{ts}/+; dsx-GAL4 GFP-mfas/UAS-APP-K595N/M596L-Swedish* showing cored DCGs (yellow circles) **C)** Another example of *w^{1118}; tub-GAL80^{ts}/+; dsx-GAL4 GFP-mfas/UAS-APP-K595N/M596L-Swedish* showing variability in the number of intact DCGs. The *APP-Swedish* mutation is also characterized by consistently large lysosomes, seen in both **B** and **C** in magenta. **White arrows** in **A** and **B:** DCGs; **n:** double nuclei characteristic of each SC. Scale bar = 5 µm.

A

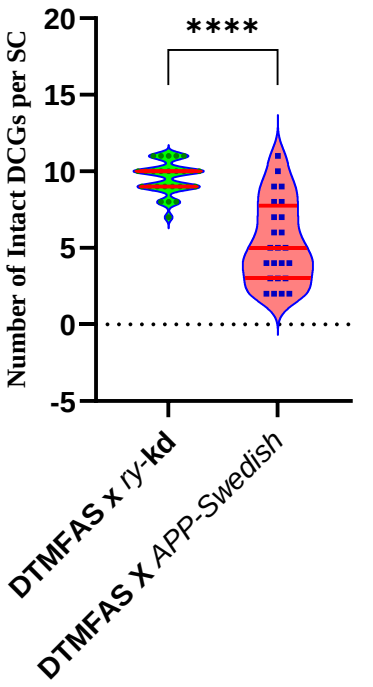
****
Number of Intact DCGs per SC
20
15
10
5
0
-5
DTMFAS x ry-kd
DTMFAS X APP-Swedish

B

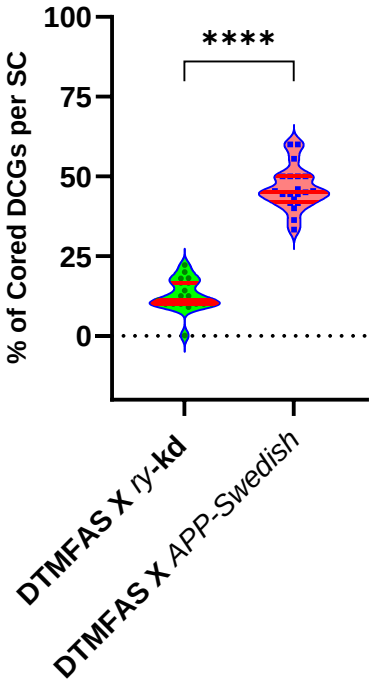
****
% of Cored DCGs per SC
100
75
50
25
0
DTMFAS X ry-kd
DTMFAS X APP-Swedish

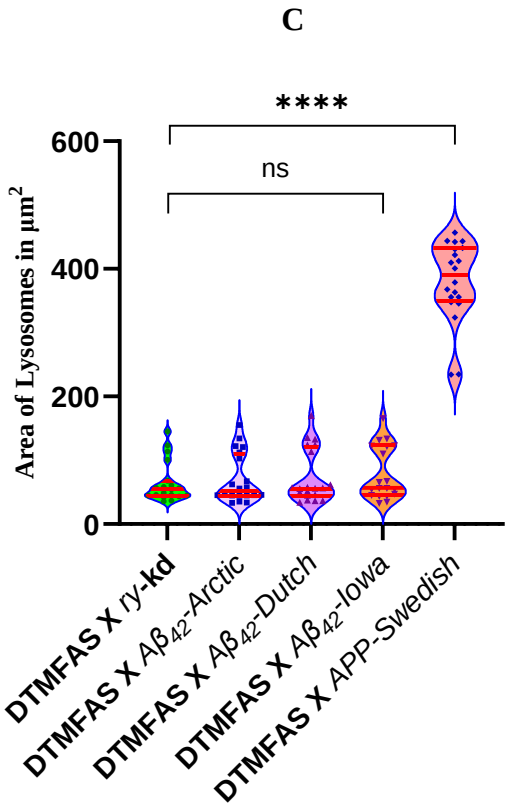

Figure 6.13: A: *APP-Swedish* transgenic flies on average produce fewer intact DCGs. B: *APP-Swedish* produces more 'cored' DCGs, with a relative paucity of GFP-MFAS in the centre. **C:** The size of control and *Aβ42*-mutant (*Arctic, Dutch* and *Iowa*) lysosomes vary from about 40-60 µm^2, whereas *APP-Swedish* double mutants have an average lysosomal size of approximately 380 µm^2. As also indicated in the microscopy images (**Figure 6.12)** which correspond to this bar chart, all genotypes listed here were driven by *w^{1118}; tub-GAL80^{ts}/CyO; dsx-GAL4 GFP-mfas/TM6B* (DTMFAS). The mean for each set of experiments is shown in red.

6.2.4 THE EFFECTS OF *GAPDH2-RNAi, APPL-RNAi, Aβ42-WT, Aβ42-ARCTIC* AND *APP-SWEDISH* ON EXOSOME SECRETION

One other key function of DCG compartments is that they also make ILVs, which are then released as Rab11 exosomes (Fan *et al.*, 2020). In some knockdowns that affect ILV biogenesis, the formation of DCGs is also disrupted (Marie *et al.*, 2023). In **Chapter 4**, I demonstrated that knockdowns of *mfas* or *APPL*, which induce DCG loss or mini-core

production in SCs respectively, do not affect the proportion of Rab6- and Rab11-labelled compartments that contain ILVs marked by these Rabs, suggesting that these knockdowns do not affect Rab11-exosome biogenesis (**§ 4.2.4**). This finding was further supported by using a more generic marker for Rab11-exosomes in SCs, Breathless-GFP, a GFP fusion to a *Drosophila* FGF receptor (Fan *et al.,* 2020). This latter fusion protein labels SC exosomes sufficiently that they can be detected in the AG lumen and quantified as number of puncta within several projected images from a z-stack, an approach that has been used to confirm that some genetic manipulations in SCs block Rab11-exosome biogenesis (Marie *et al.,* 2023).

I therefore set out to test whether knockdown of *GAPDH2* or *APPL*, or overexpression of *$A\beta_{42}$-wild type* or mutant *$A\beta_{42}$* peptide or the *APP-Swedish* mutant could affect Rab11-exosome secretion, which might be relevant to their effects on DCGs. As a control I overexpressed a *Chmp2-RNAi*, which knocks down an ESCRT-III molecule with a key role in Rab11-exosome biogenesis (Marie *et al.,* 2023). In the results shown below, only *Chmp2b-RNAi*, the positive control, had the expected effect of decreasing the number of exosomes in the lumen of AGs. Furthermore, as an incidental finding, a multicore phenotype, first reported by the Wilson laboratory (Marie *et al.,* 2023) was also seen with this particular genotype (data not shown). All other genotypes – *GAPDH2*- and *APPL*-knockdowns, as well as overexpressions of *$A\beta_{42}$-wild type*, *$A\beta_{42}$-Arctic*, and the *APP-Swedish* mutant showed no reduction in exosome counts. This result is particularly surprising for the *APP-Swedish* mutant, if indeed it's DCG compartments are being

trafficked to lysosomes and not secreted (the large lysosomes characteristic of this particular mutation are seen as an incidental finding in **Figure 6.15D**).

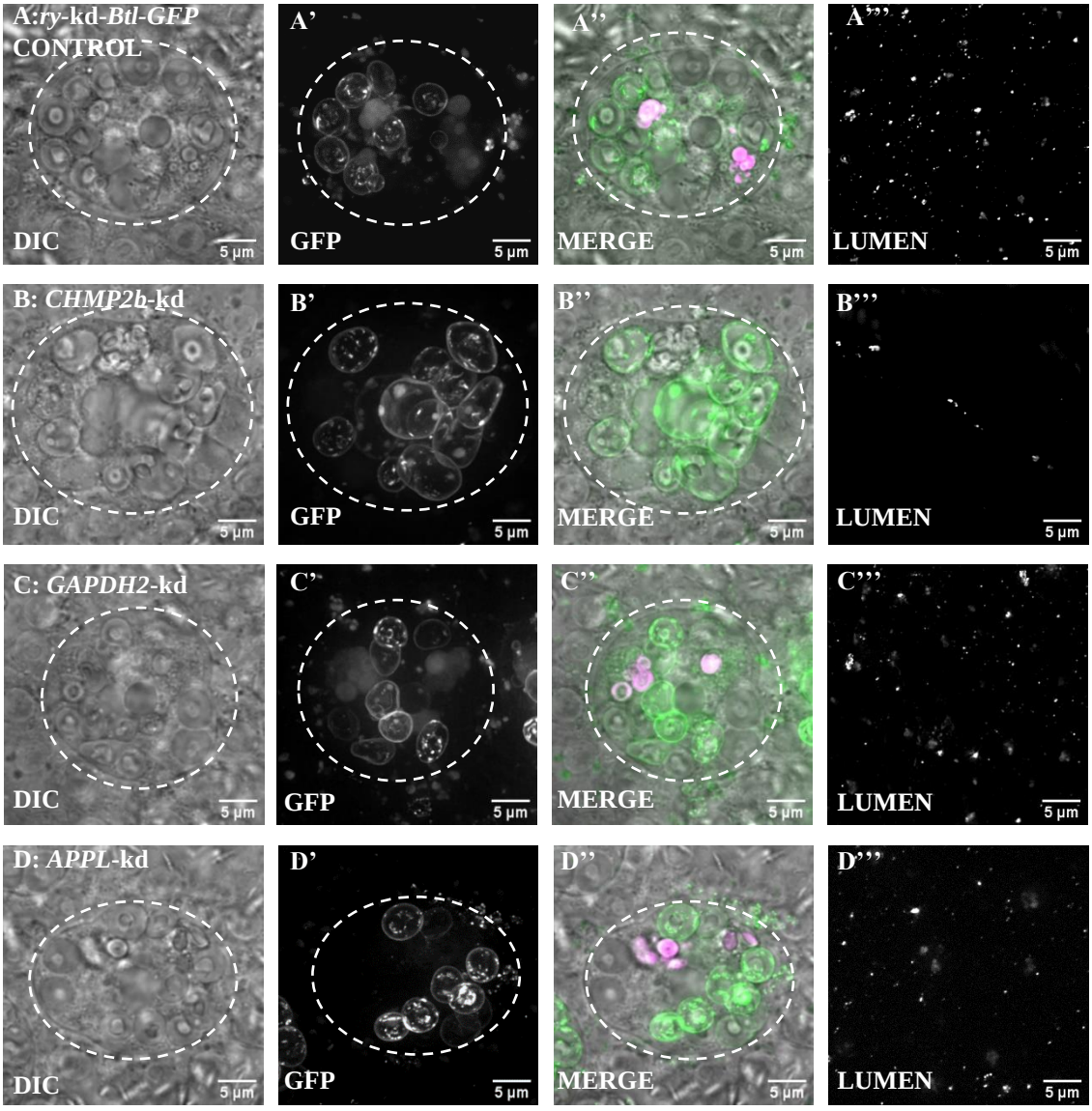

Figure 6.14: The effect of *GAPDH2* and *APPL*-knockdowns on exosome secretion. SCs from six day-old virgin males stained with LysoTracker Red and imaged *ex vivo*, using DIC and fluorescence microscopy for GFP and LysoTracker Red. **A)** *w; tub-GAL80^{ts}/ UAS-ry-RNAi; dsx-GAL4 Btl-GFP/+* (control) **B)** *w; tub-GAL80^{ts}/UAS-chmp2b-RNAi; dsx-GAL4 Btl-GFP/+* (positive control) **C)** *w; tub-GAL80^{ts}/+; dsx-GAL4 Btl-GFP/UAS-GAPDH2-RNAi* **D)** *w; tub-GAL80^{ts}/+; dsx-GAL4 Btl-GFP/UAS-APPL-RNAi.* The first three images in each row show SCs imaged by DIC, Btl-GFP fluorescence and a merge. The right-hand image in each row shows a fluorescence image obtained with the same wide-field live microscope taken from the central part of the AG lumen. Scale bar = 5 µm.

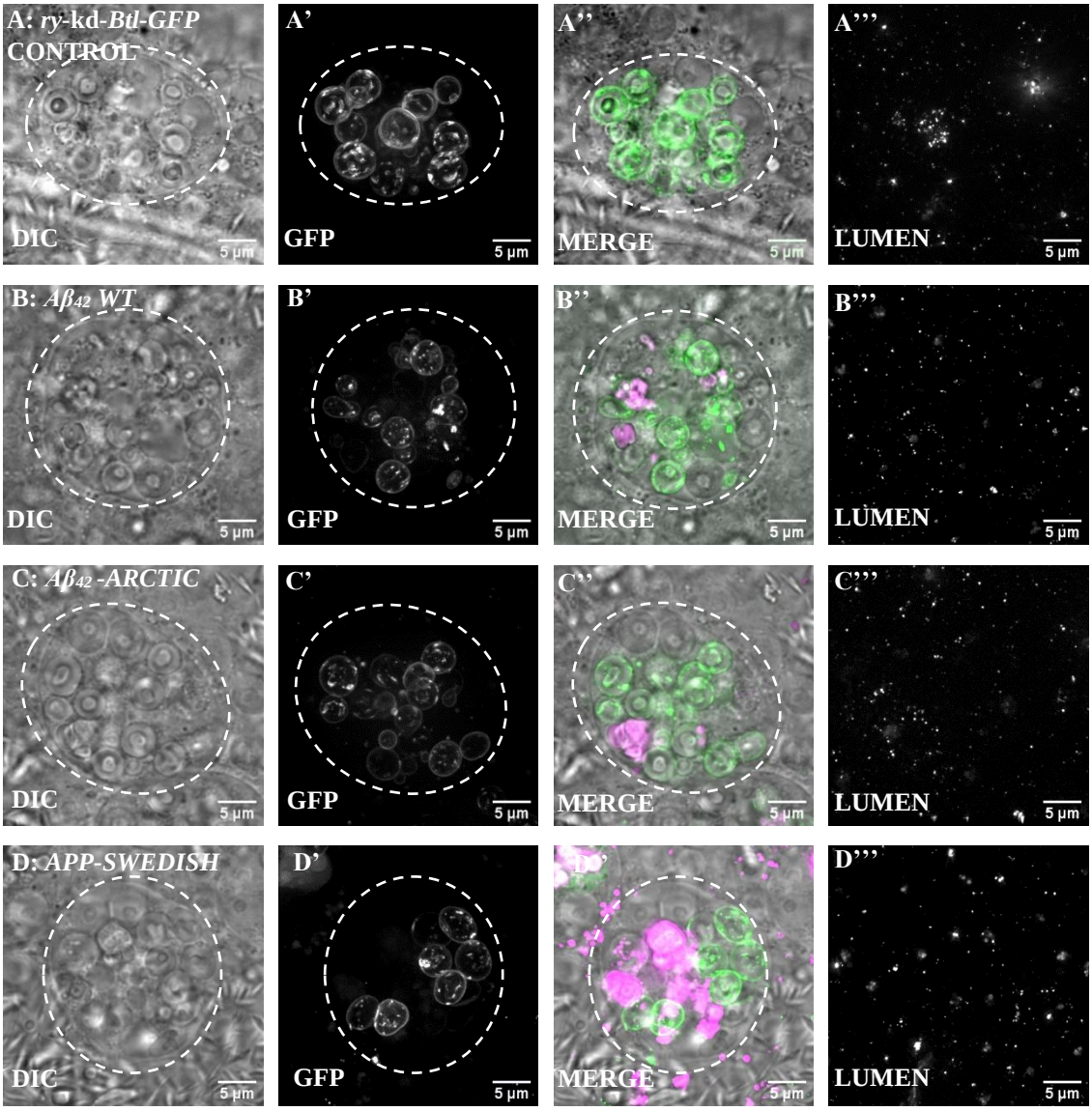

Figure 6.15: The effect of overexpression of *Aβ42-wild type, Aβ42-E693G-Arctic* and *APP- K595N/M596L-Swedish* on exosome secretion. SCs from six day-old virgin males stained with LysoTracker Red and imaged *ex vivo*, using DIC and fluorescence microscopy for GFP and LysoTracker Red. **A)** *w; tub-GAL80^{ts}/UAS-ry-RNAi; dsx-GAL4 Btl-GFP* (control) **B)** *w; tub-GAL80^{ts}/UAS-Aβ42-wild-type; dsx-GAL4 Btl-GFP* **C)** *w; tub-GAL80^{ts}/UAS-Aβ42-E693G-Arctic; dsx-GAL4 Btl-GFP* **D)** *w; tub-GAL80^{ts}/+; dsx-GAL4 Btl-GFP/UAS-APP-K595N/M596L-Swedish (*showing as an incidental finding the large lysosomes characteristically seen with the *APP-Swedish* mutation). The first three images in each row show SCs imaged by DIC, Btl-GFP fluorescence and a merge. The right-hand image in each row shows a fluorescence image obtained with the same wide-field live microscope taken from the central part of the AG lumen. Scale bar = 5 µm.

As shown in **Figure 6.16** below, none of the tested knockdowns had any effect on exosome secretion. The only exception was the knockdown of the ESCRT-III component *Chmp2b*, which, having previously been shown in the Wilson laboratory to decrease exosome counts, was used as a positive control.

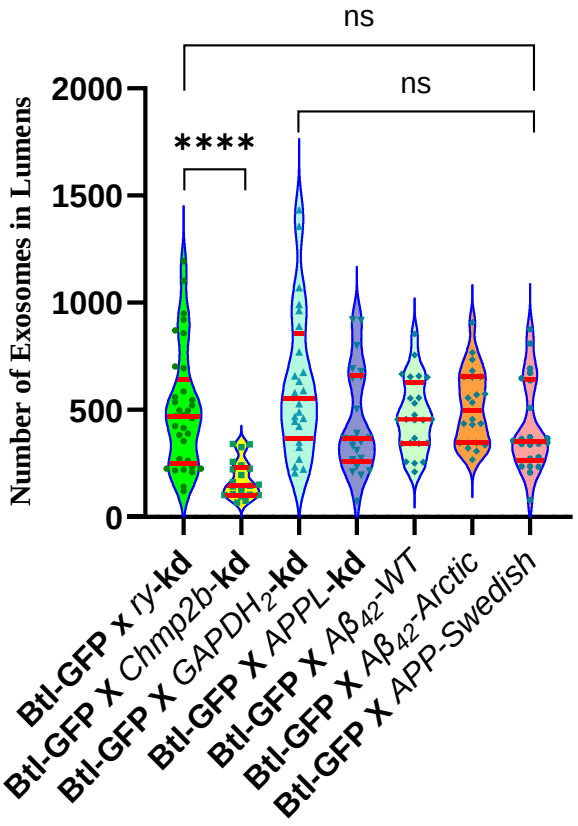

Figure 6.16: *GAPDH2*- and *APPL*-kds, as well as the overexpression of *Aβ$_{42}$-wild type*, *Aβ$_{42}$-E693G-Arctic*, and *APP-K595N/M596L-Swedish* do not affect exosome secretion as compared to controls. The knockdown of *Chmp2b*, an ESCRT component, was used as a positive control. The mean for each set of experiments is shown in red.

6.2.5 THE EFFECTS OF KNOCKDOWNS OF RETROMER COMPONENTS VPS26 AND VPS39 ON DCGs

As discussed in the introductory section (**§ 6.1.2**), the retromer is a multimeric protein essential for recycling and retrieving protein cargoes from the endosome to the *trans*-Golgi network or the cell surface. Mutations or deficiencies in it's components result in accumulation of abnormal protein aggregates, and unsurprisingly have been linked to various amyloid neurodegenerative diseases, since a hallmark of these conditions is the accumulation of abnormally folded protein aggregates. Since the results I presented earlier have shown a clear link between neurodegeneration-associated genes and DCGs, I decided to examine the connection between retromer and DCGs by knocking down *VPS26* and *VPS39*, which encode for two essential components of it's cargo-recognition core. Indeed, low levels of VPS26 and VPS39 in the entorhinal cortex **(Figure 6.17)** are the earliest known findings of AD, far predating any clinical manifestations of the disease itself (Small *et al.*, 2005; Lucin *et al.*, 2013: reviewed in Li *et al.*, 2016).

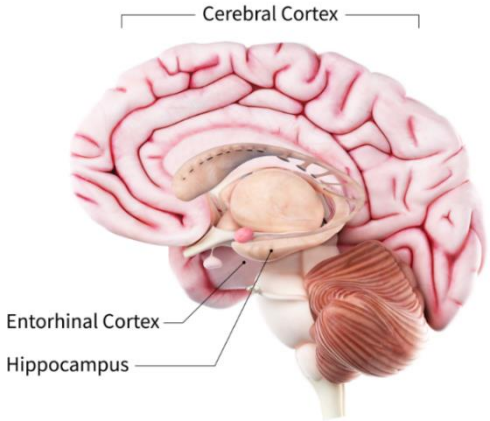

Figure 6.17: The location of the entorhinal cortex. (Taken from National Institute of Aging, National Institute of Health, https://www.nia.nih.gov/health/what-happens-brain-alzheimers-disease; accessed on 12/3/2023).

I tested the effect of overexpressing *VPS26-RNAi* and *VPS35-RNAi* in adult SCs under dsx-GAL4 control, and the resultant SCs and DCGs were compared to control cells expressing a *UAS-ry-RNAi* construct.As shown in the experimental results below (**Figure 6.18B** and **C**), knockdowns of *VPS26* and *VPS35* result in normal-appearing DCGs, although their numbers are increased. The mechanism underlying the increase in number of DCGs pursuant to the knockdown of *VPS26* and *VPS35* is unclear; however one potential explanation is that DCG compartments are not fusing to the plasma membrane at their normal efficiency, perhaps because they are not maturing properly, leading to accumulation of these compartments in SCs. The results shown here establish a link between key retromer components and *Drosophila* MFAS, which in preceding sections has been demonstrated to be a high-fidelity model for the study of amyloid-related degenerative diseases. In addition, the ever-expanding ties between retromer dysfunction and endolysosomal neurodegenerative disorders hold out enormous promise in studying this vast swathe of diseases. With the demonstration of this connection, hopefully the richly promising field of retromer-related neurodegeneration will be taken forward in this fly model.

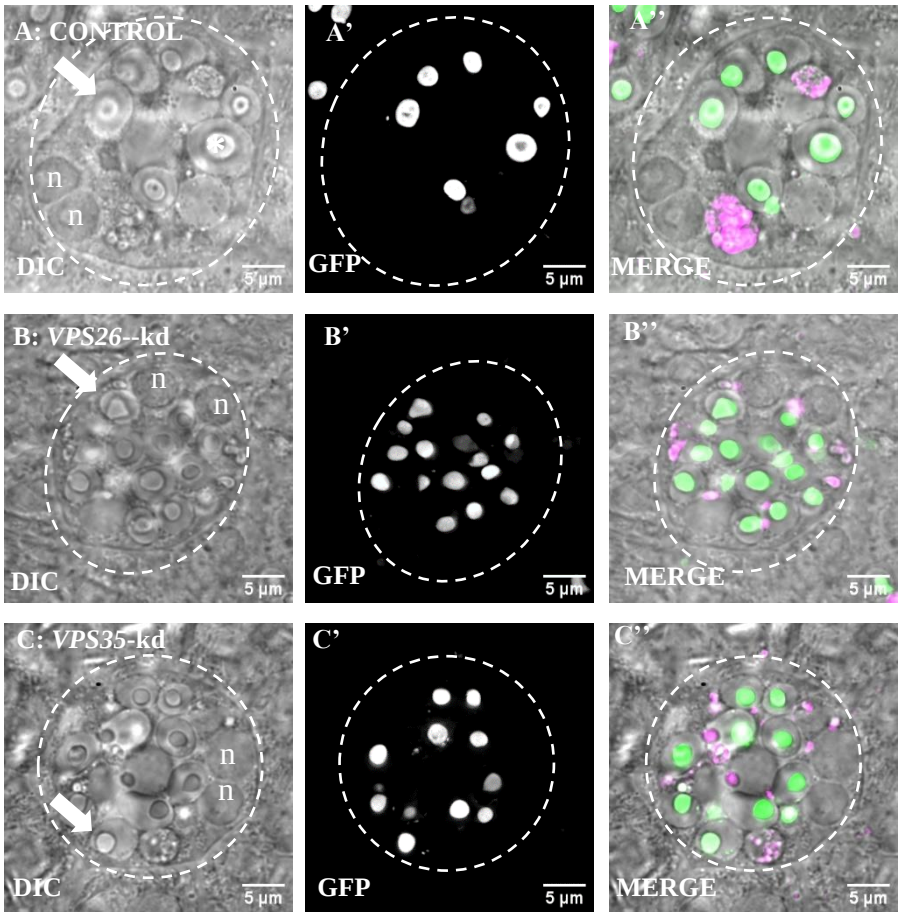

Figure 6.18: A) *w^{1118}; tub-GAL80^{ts}/UAS-ry-RNAi; dsx-GAL4 GFP-mfas/+* (control). **B)** *w^{1118}; tub-GAL80^{ts}/UAS-vps26-RNAi; dsx-GAL4 GFP-mfas/+* **C)** *w^{1118}; tub-GAL80^{ts}/UAS-vps35-RNAi; dsx-GAL4 GFP-mfas/+* . **White arrows in A, B** and **C:** DCGs; **n:** double nuclei characteristic of each SC. Scale bar = 5 µm.

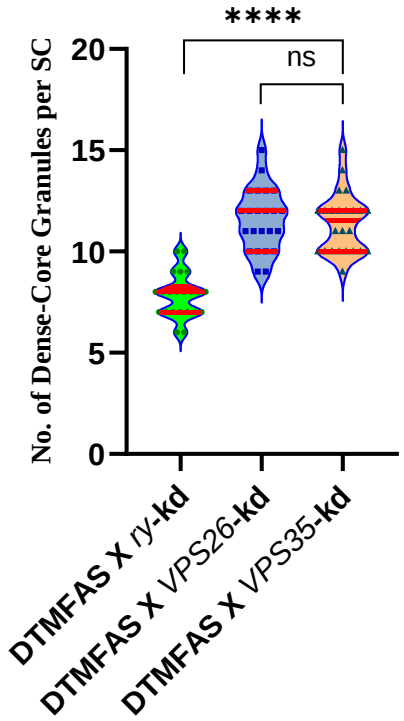

Figure 6.19: *VPS*-kds have significantly more DCGs than controls. As also indicated in the microscopy images (**Figure 6.18)** which correspond to this bar chart, all genotypes listed here were driven by *w^{1118}; tub-GAL80^{ts}/CyO; dsx-GAL4 GFP-mfas/TM6B* (DTMFAS). The mean for each set of experiments is shown in red.

6.2.6 RESULTS REGARDING INTERACTIONS BETWEEN ALZHEIMER'S GENES AND 'MINI-CORE' PRODUCING GENOTYPES

As discussed in the introduction (**§ 1.4.3**) despite the vast volume of data on the general effects of Aβ on neurons, there are no studies specifically examining their individual toxicities when broken down by genotype. As a launching point to preliminarily explore this deficiency, I took the opposite approach: rather than examining their damaging powers, I decided instead to examine the 'rescue' powers of selected *APP* and *$A\beta_{42}$* lines. The 'targets' of these rescue efforts were the MFAS-dispersive, mini-core-producing genotypes *APPL-RNAi* and *GAPDH2-RNAi*. The reasoning behind this was that amyloid, a highly ordered structure, might possibly rescue the reliably dissipative effects of DCG-disrupting

genotypes. The answers to these questions are presented in the following experimental results.

6.2.6.1 INTERACTION BETWEEN HUMAN *APP* AND FLY *APPL-RNAi*

In this experiment, I first overexpressed human *APP* and *Drosophila APPL-RNAi* separately, and then together in the same fly, in each instance in adult SCs under dsx-GAL4 control. I then compared these results to control cells expressing a *UAS-ry-RNAi* construct. As seen in **Figure 6.20B**, overexpression of full-length wild type APP resulted in normal DCGs, a result which had earlier been established in **Section 4,** and shown in **Figure 4.29B**. **Figure 6.20C** shows the well-established mini-core appearance of *APPL*-knockdown. When both these genetic influences are combined in the same fly as shown in **Figure 6.20D**, the resultant phenotype shows a combination of intact cores and mini-cores within the same compartment space, suggesting a partial rescue. This primarily argues that human APP can undertake the function of, or substitute for *Drosophila* APPL. Secondarily, this seems to provide yet more evidence that amyloids across species are related, and, as has been suggested, can influence each other. Finally, this confirms that the *APPL*-kd mini-core phenotype is indeed due to loss of APPL function, and not just an off-target effect.

A more nuanced view of this result is that APP, the parent molecule of Aβ species, might possess amyloid-like properties of it's own, similar to its cleavage fragments, even prior to being processed into its derivative amyloid. It is now recognized that cleavage products of APP guide physiological neural development, while intact APP itself is emerging as a developmental adhesion molecule (reviewed in Sosa *et al.*, 2017). This result would

therefore argue in favour of amyloid precursor molecules playing physiological roles in their own right. This idea will be explored further in subseqeunt rescue attempts on *APPL*-knockdowns by the wild type and mutated internal segments of APP ($A\beta_{42}$ and $A\beta_{42}$-Arctic respectively). This parsed-out perspective does not, however detract from the larger conclusion that some version or attribute of APP is indeed substituting or filling in for APPL.

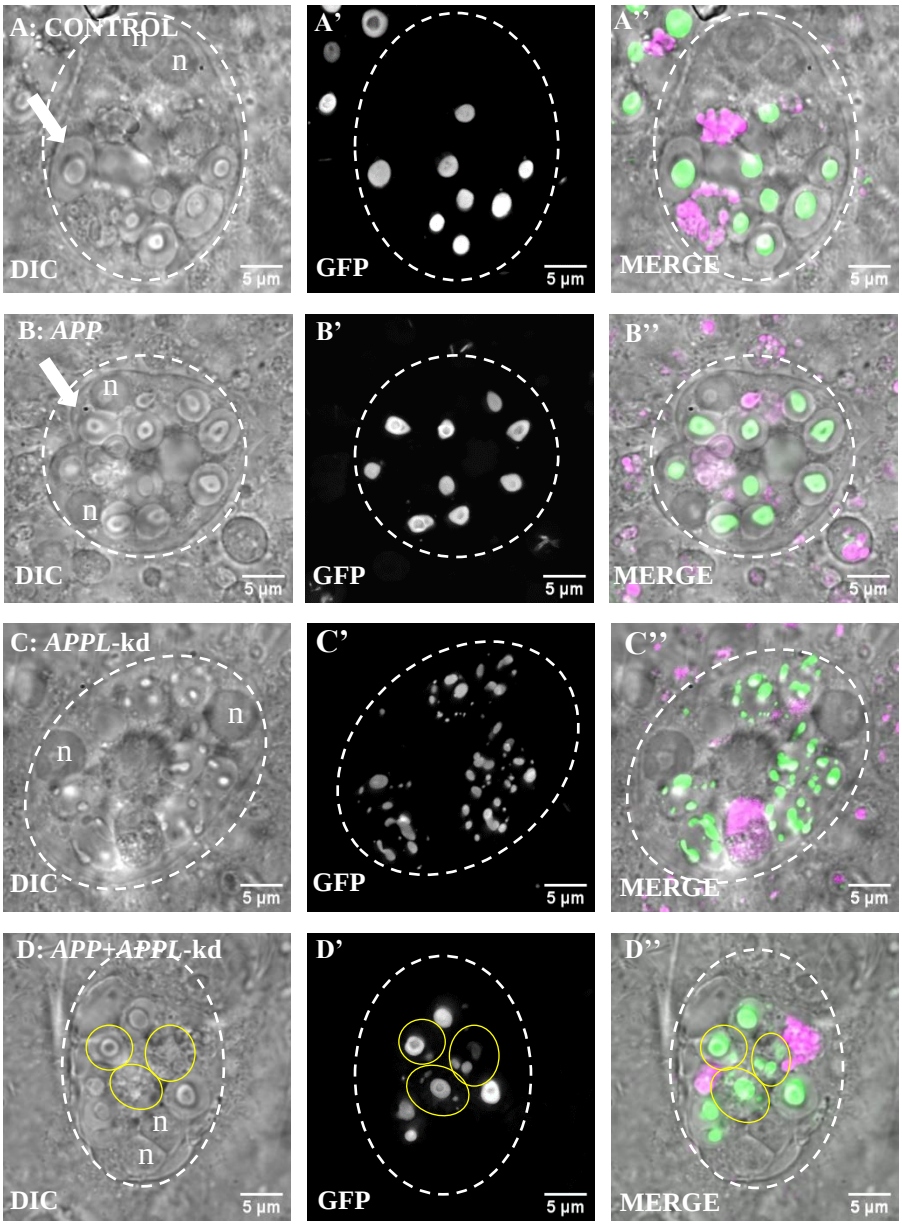

Figure 6.20: Interaction between human *APP* and *Drosophila APPL-RNAi.* SCs from six-day-old virgin males stained with LysoTracker Red and imaged *ex vivo*, using DIC and fluorescence microscopy for GFP and LysoTracker Red. **A)** *w^{1118}; tub-GAL80^{ts}/UAS-ry-RNAi; dsx-GAL4 GFP-mfas/+* (control) **B)** *w^{1118}; tub-GAL80^{ts}/UAS-APP-YFP; dsx-GAL4 GFP-mfas/+* **C)** *w^{1118}; tub-GAL80^{ts}/+; dsx-GAL4 GFP-mfas/UAS-APPL-RNAi* **D)** *w^{1118}; tub-GAL80^{ts}/UAS-APP-YFP; dsx-GAL4 GFP-mfas/UAS-APPL-RNAi*. **White arrows** in **A** and **B:** DCGs; **yellow circles/ovals:** outline of compartments which contain cores and mini-cores; **n:** double nuclei characteristic of each SC. Scale bar = 5 µm.

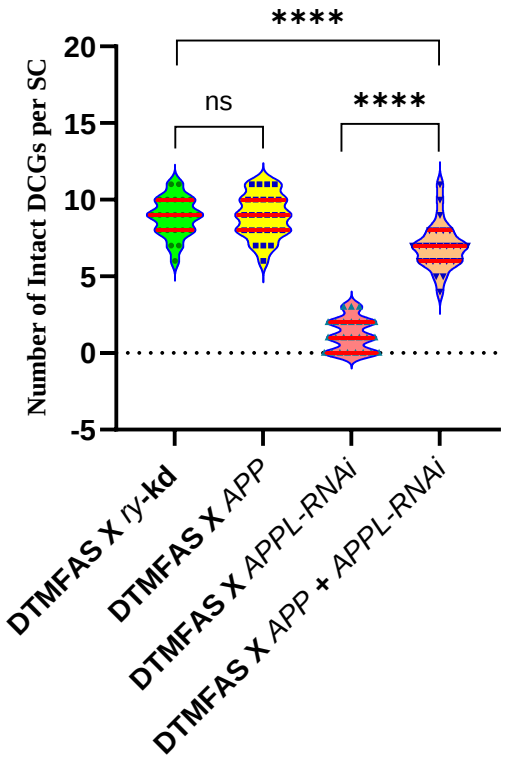

Figure 6.21: Results of the interaction between human *APP* and *Drosophila APPL-RNAi*. Flies with wild type human *APP* produced the same number of DCGs as controls, while *APPL-RNAi*, as seen earlier, resulted in a significant reduction in intact DCGs. However, the *APP-APPL-RNAi* combination increased the number of intact DCGs, demonstrating a partial rescue of *APPL-RNAi*'s mini-core phenotype by human *APP*. As also indicated in the microscopy images (**Figure 6.20)** which correspond to this bar chart, all genotypes listed here were driven by *w^{1118}; tub-GAL80^{ts}/CyO; dsx-GAL4 GFP-mfas/TM6B* (DTMFAS). The mean for each set of experiments is shown in red.

6.2.6.2 INTERACTION BETWEEN HUMAN *$A\beta_{42}$-WILD TYPE* AND FLY *APPL-RNAi*

Having established that APP, the parent molecule of $A\beta_{42}$, can rescue the mini-core phenotype of *APPL-RNAi*, I next investigated the rescue powers of $A\beta_{42}$ itself. If *$A\beta_{42}$-wild type* also rescued *APPL-RNAi*'s mini-core phenotype, this would be a significant result, since it would demonstrate that APP's rescue powers were shared by it's internal $A\beta_{42}$ segment, and therefore that $A\beta_{42}$-wild type could also substitute for APPL. In this

experiment, therefore, I first overexpressed *$A\beta_{42}$-wild type* and *Drosophila APPL-RNAi* separately, and then together in the same fly, in each instance in adult SCs under dsx-GAL4 control. As always, I compared these results to control cells expressing a *UAS-ry-RNAi* construct. The resultant phenotype shows a combination of intact cores and mini-cores within the same compartment space, suggesting a partial rescue. This primarily argues that human $A\beta_{42}$-wild type can undertake the function of, or substitute for *Drosophila* APPL. The potential problems I considered in the interpretation of these results, however, are that GAL4 might be titered out, or that the amyloid properties of $A\beta_{42}$-wild type are in fact substituting for the inability of the MFAS particles to come together in forming a single core (the established effect of *APPL*-kd). Thus, instead of effecting a true rescue, $A\beta_{42}$-wild type might merely be exerting its influence in helping to stick the core together.

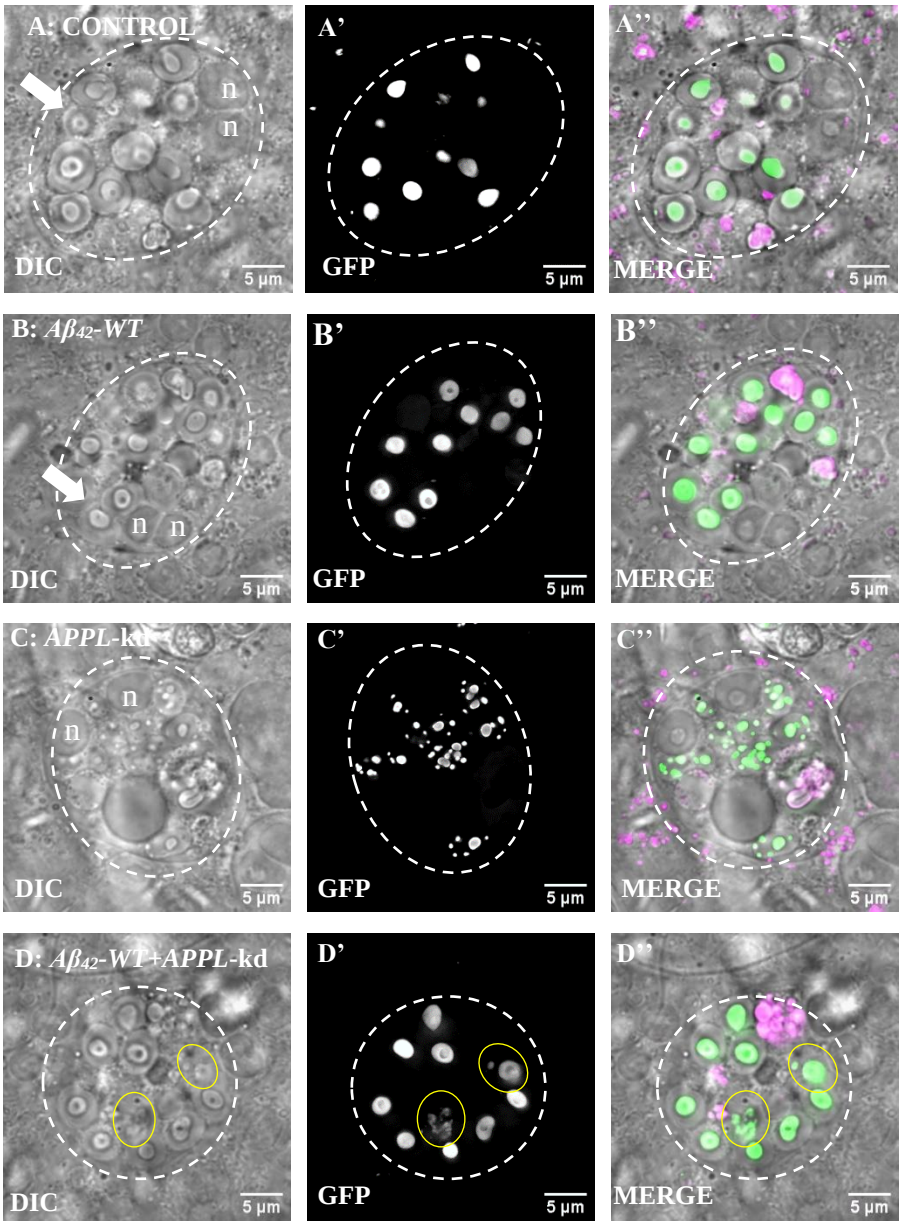

Figure 6.22: Interaction between *Aβ42-wild type* and *Drosophila APPL-RNAi.* SCs from six- day-old virgin males stained with LysoTracker Red and imaged *ex vivo*, using DIC and fluorescence microscopy for GFP and LysoTracker Red. **A)** *w^{1118}; $GAL80^{ts}$/UAS-ry-RNAi; dsx-GAL4 GFP-mfas/+* (control) **B)** *w^{1118}; $GAL80^{ts}$/UAS-Aβ42-wild type; dsx-GAL4 GFP-mfas/+* **C)** *w^{1118}; $GAL80^{ts}$/+; dsx-GAL4 GFP-mfas/UAS-APPL-RNAi* **D)** *w^{1118}; $GAL80^{ts}$/UAS-Aβ42-wild type; dsx-GAL4 GFP-mfas/UAS-APPL-RNAi*. **White arrows** in **A** and **B:** DCGs; **yellow ovals:** outlines of compartments which includes a core and mini-cores; **n:** double nuclei characteristic of each SC. Scale bar = 5 µm.

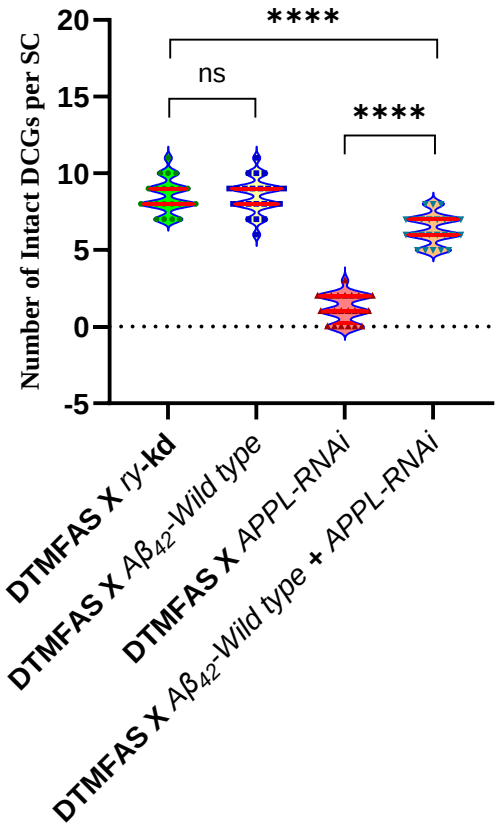

Figure 6.23: The combination of human *Aβ42-wild type* and *Drosophila APPL-RNAi* increases the number of intact DCGs. This demonstrates a partial rescue of *APPL-RNAi*'s mini-core phenotype by *Aβ42-wild type*, which produces normal DCGs. As also indicated in the microscopy images (**Figure 6.22)** which correspond to this bar chart, all genotypes listed here were driven by w^{1118}*; tub-GAL80*^{ts}*/CyO; dsx-GAL4 GFP-mfas/TM6B* (DTMFAS. The mean for each set of experiments is shown in red.

6.2.6.3 INTERACTION BETWEEN *Aβ42-E693G-ARCTIC* AND *APPL-RNAi*

In this experiment, I first overexpressed *Aβ42-E693G-Arctic* and *Drosophila APPL-RNAi* separately and then together in the same fly, in each instance in adult SCs under dsx-GAL4 control. I compared these results to control cells expressing a *UAS-ry-RNAi* construct. *Aβ42-E693G-Arctic* was chosen since it is a particularly pernicious amyloidogenic mutation, occurring within the internally-located *Aβ42* segment of *APP*. Furthermore, as part of the family of *APP*'s intra-*Aβ42* mutations, it also produces CAA, the unique subvariant of FAD

characterised by intracerebral haemorrhages. Finally, it is the only intra-*Aβ42* mutation known to cause 'targetoid' Aβ plaques in the brain. As was seen in the previous experiment, APP is able to substitute for *Drosophila* APPL in rescuing *APPL*-kd's mini-core phenotype. Furthermore, a derivative of human APP in its physiological form – its cleavage fragment $A\beta_{42}$-wild type – was also able to partially rescue *Drosophila APPL*-kd's mini-core phenotype. Thus, the reasoning behind this experiment was that a pathogenic mutant derivative of APP - $A\beta_{42}$-E693G-Arctic – might also possess sufficient if not even greater amyloidogenic organisational abilities in overcoming *APPL-RNAi*'s MFAS-dispersive effects. It has been previously established that *Aβ42-E693G-Arctic* when overexpressed by itself in SCs displays highly distinctive 'MFAS-organising' activity, producing tightly arranged MFAS in DCGs in the form of targetoid concentric circles **(§ 6.2.1**, **Figure 6.8C** and **E**; and below, **Figure 6.24B**).

Answering the question posed above, when overexpressed here in combination with *APPL-RNAi*, a genotype known consistently to produce 'mini-cores', the organising activity of *Aβ42-E693G-Arctic* was indeed able to 'glue' together MFAS in a way that overcomes the loss of *APPL* and the manifestation of mini-cores (**Figure 6.24D** and **E**). Thus, many compartments which would otherwise form mini-cores now form intact DCGs. It is likely that the amyloid properties of *Aβ42-E693G-Arctic* are substituting for MFAS' inability to come together into a single core, and are actually helping the core to stick together. This is suggested by the presence of the characteristic *Aβ42-E693G-Arctic* 'targetoid' DCGs, accompanied by *APPL-RNAi'*s characteristic mini-cores in their immediate vicinity (**Figure 6.24D** and **E)**. This could further be interpreted as *Aβ42-E693G-Arctic* prompting

the formation of the centre, or nidus of the core, while the flecks of MFAS which escaped *$A\beta_{42}$-E693G-Arctic's* organising power remained as mini-cores on the sidelines.

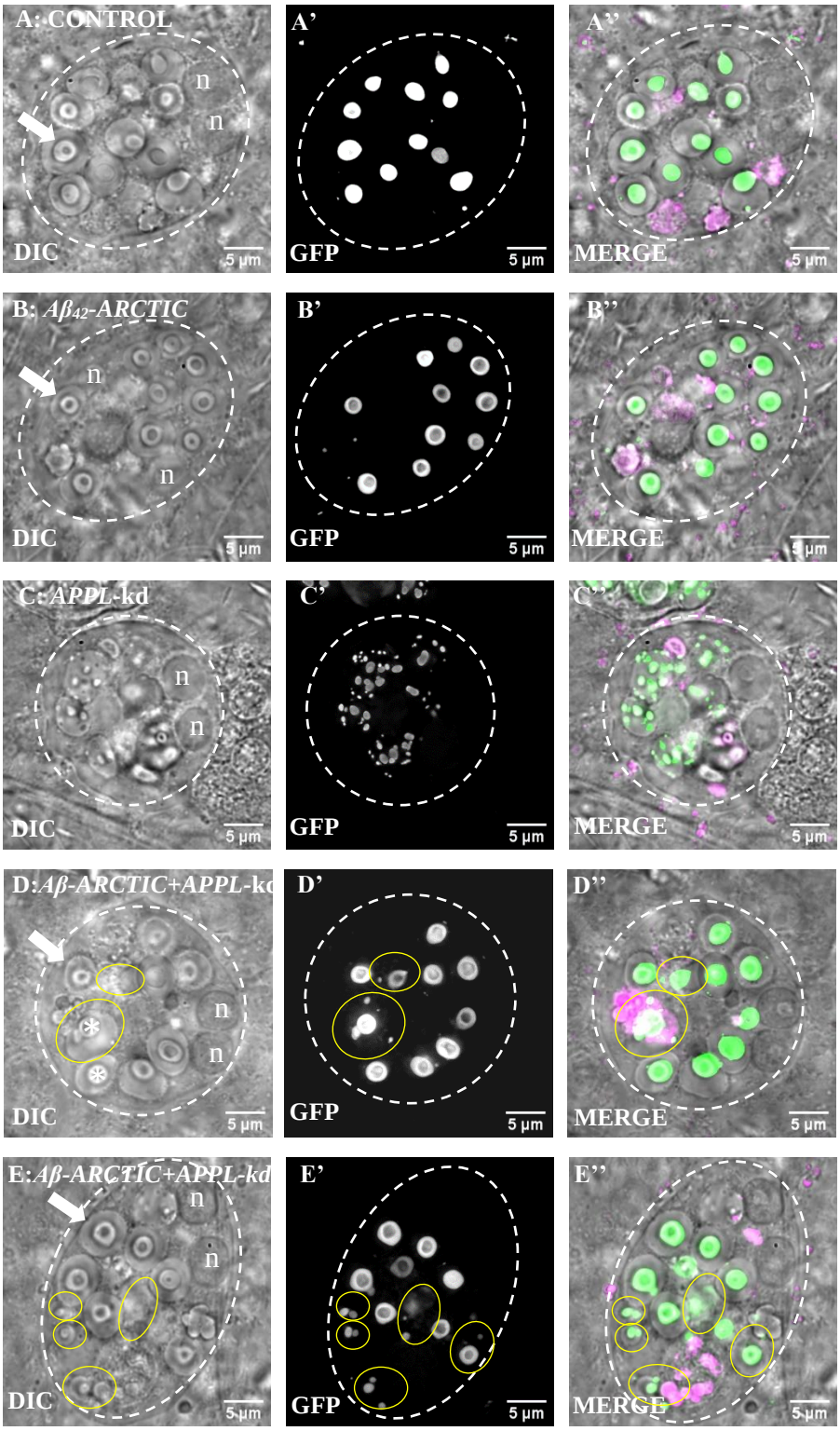

Figure 6.24: Interaction between *Aβ42-E693G-Arctic* and *APPL-RNAi*. SCs from six-day-old virgin males stained with LysoTracker Red and imaged *ex vivo*, using DIC and fluorescence microscopy for GFP and LysoTracker Red. **A)** w^{1118}*; GAL80*^{ts}*/UAS-ry-RNAi; dsx-GAL4 GFP-mfas/+* (control) **B)** w^{1118}*; GAL80*^{ts}*/UAS-Aβ42-E693G-Arctic; dsx-GAL4*

GFP-mfas/+ **C)** *w^{1118}; $GAL80^{ts}$/+; dsx-GAL4 GFP-mfas/UAS-APPL-RNAi* **D)** and **E)** *w^{1118}; $GAL80^{ts}$/UAS-$A\beta_{42}$-E693G-Arctic; dsx-GAL4 GFP-mfas/UAS-APPL-RNAi* showing the variation in intact and non-intact DCGs between the two representative images. **White arrows:** DCGs; **yellow circles/ovals:** outlines of compartments which include a core and mini-cores; **n:** double nuclei characteristic of each SC. Scale bar = 5 μm.

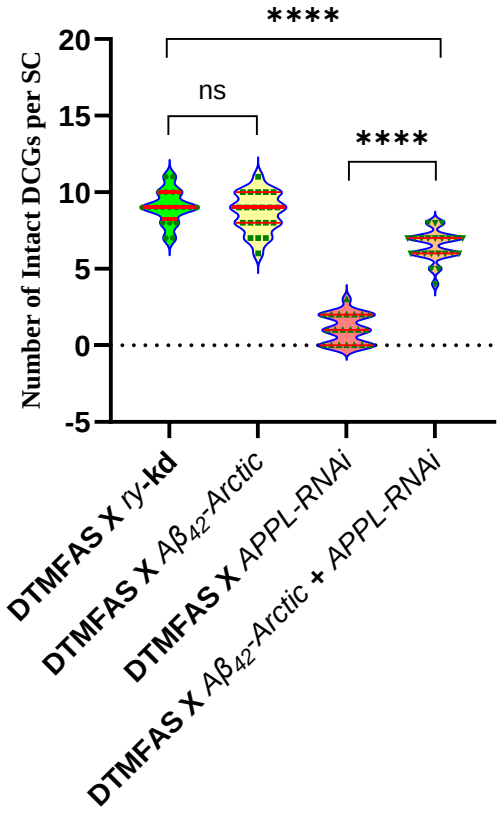

Figure 6.25: The combination of *$A\beta_{42}$-E693G-Arctic* and *APPL-RNAi* in the same fly increases the number of intact DCGs as compared to flies overexpressing *APPL-RNAi* alone, a genotype which produces mini-cores. This demonstrates that the MFAS-organizing influence of *$A\beta_{42}$-E693G-Arctic* exerts a rescue effect over the minicore-producing effect of *APPL-RNAi.* As also indicated in the microscopy images (**Figure 6.24)** which correspond to this bar chart, all genotypes listed here were driven by *w^{1118}; tub-$GAL80^{ts}$/CyO; dsx-GAL4 GFP-mfas/TM6B* (DTMFAS). The mean for each set of experiments is shown in red.

6.2.6.4 INTERACTION BETWEEN *$A\beta_{42}$-WILD TYPE* AND FLY *GAPDH2-RNAi*

Here, following the experimental format I previously employed with other attempted rescues, I overexpressed human *$A\beta_{42}$-wild type* and *Drosophila GAPDH2-RNAi* separately,

and then together in the same fly, in each instance in adult SCs under dsx-GAL4 control. I then compared these results to control SCs expressing a *UAS-ry-RNAi* construct.

As shown earlier, *$A\beta_{42}$-wild type* is able to rescue the mini-core phenotype of *APPL-RNAi* (**Figure 6.22D** and **Figure 6.23**). Therefore, *$A\beta_{42}$-wild type* was tested for its rescue effects on *GAPDH2-RNAi*, another genotype that produces mini-cores is. However unlike the uniformly distributed mini-cores of the *APPL*-knockdowns, *GAPDH2*-kd produces mini-cores in a 'pearls-on-a-string' appearance **(§ 4.2.1, Figure 4.8B**). Furthermore, time-lapse videos of *APPL-RNAi* and *GAPDH2-RNAi* showed very different motility behaviours of the mini-cores. My time-lapse videos of *APPL-kd* mini-cores showed that they did not move, while in comparison videos of *GAPDH2-kd* made by a colleague showed that these mini-cores did move, but then did not fuse when they met or collided (Adam Wells, personal communication). Having concluded that there appears to be a fundamental mechanistic difference between how *APPL*-kd and *GAPDH2*-kd mini-cores are produced, I decided to attempt rescues of *GAPDH2*-kd first with *$A\beta_{42}$-wild type*, and then with *$A\beta_{42}$-E693G-Arctic* (shown in **§ 6.2.6.5**, the next section).

As seen in the results below, overexpression of *$A\beta_{42}$-wild type* does not affect normal DCG formation, other than producing a slight increase in the numbers of DCGs with a doughnut phenotype (**Figure 6.26B**). *GAPDH2-RNAi* produces mini-cores with its distinctive 'string of pearls' appearance **Figure 6.26C**. However, the combination of *$A\beta_{42}$-wild type* and *GAPDH2-RNAi* in the same fly produced compartments which included mini-cores from

the *GAPDH2-RNAi* influence, as well as a larger core from the *$A\beta_{42}$-wild type* influence (**Figure 6.26D** and **E**). It was noticeable, however, that the shapes of the *$A\beta_{42}$-wild type* DCGs in the rescue attempts were more irregular and abnormal-appearing than DCGs produced by rescue attempts driven by *$A\beta_{42}$-E693G-Arctic* (see next Section, **§ 6.2.6.5**). This is consistent with the greater organising power of the *$A\beta_{42}$-E693G-Arctic* mutation as compared to its non-mutated version, *$A\beta_{42}$-wild type*, as was demonstrated in **Section 6.2.1**, **Figure 6.8B, C, D** and **E**. The apparent explanation, then, for the somewhat irrgeular shapes of the *$A\beta_{42}$-wild type* DCGs seen here would be the greater 'glueing' power that pathological amyloidogenic transformation confers upon *$A\beta_{42}$-E693G-Arctic,* which I previously alluded to in *$A\beta_{42}$-E693G-Arctic's* rescue of *APPL*-kd (**§ 6.2.6.3**). Without the glueing power of a powerful amyloidogenic mutation like *$A\beta_{42}$-E693G-Arctic*, *$A\beta_{42}$-wild type* DCGs would be less likely to hold their shape when confronted with the DCG-dispersive influence of *GAPDH2*-kd. This would account for *$A\beta_{42}$-wild type'*s seemingly 'weaker' rescue of *GAPDH2-RNAi* when compared to the more robust rescue effected by *$A\beta_{42}$-E693G-Arctic*, as will be seen in the section following this one.

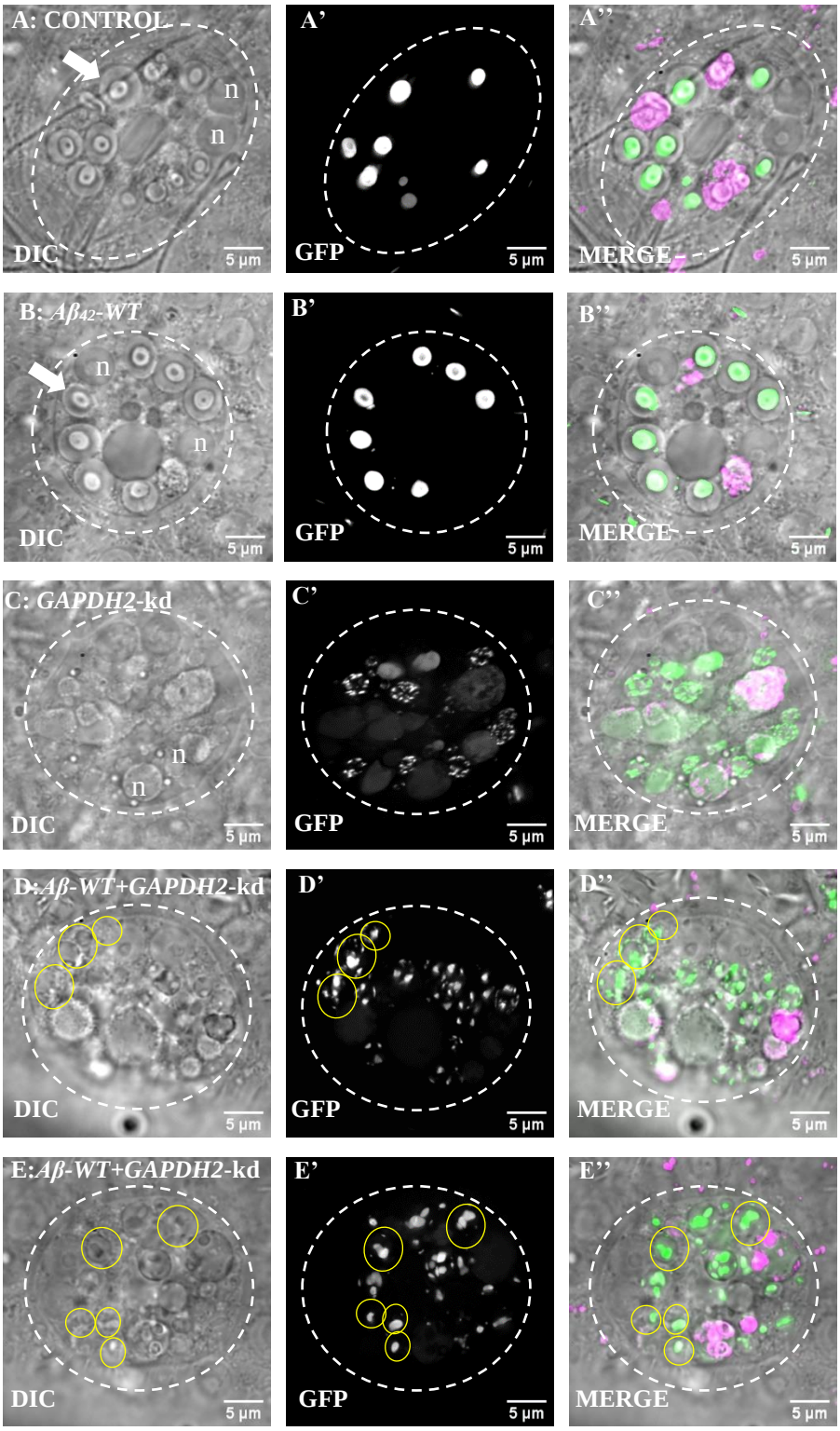

Figure 6.26: Interaction between *Aβ42-wild type* and *GAPDH2-RNAi*. SCs from six-day-old virgin males stained with LysoTracker Red and imaged *ex vivo*, using DIC and fluorescence microscopy for GFP and LysoTracker Red. **A)** *w^{1118}; $GAL80^{ts}$/UAS-ry-RNAi; dsx-GAL4 GFP-mfas/+* (control) **B)** *w^{1118}; $GAL80^{ts}$/UAS-Aβ42-wild type; dsx-GAL4 GFP-*

mfas/+ **C)** *w*^{1118}*; GAL80*^{ts}*/+; dsx-GAL4 GFP-mfas/UAS-GAPDH2-RNAi* **D** and **E)** *w*^{1118}*; GAL80*^{ts}*/UAS-Aβ*$_{42}$*-wild type; dsx-GAL4 GFP-mfas/UAS-GAPDH2-RNAi*, showing phenotypic variations of the same genotype. **White arrows** in **A** and**d B:** DCGs; **yellow circles/ovals:** outlines of compartments which have an intact larger core; **n:** double nuclei characteristic of each SC. Scale bar = 5 μm.

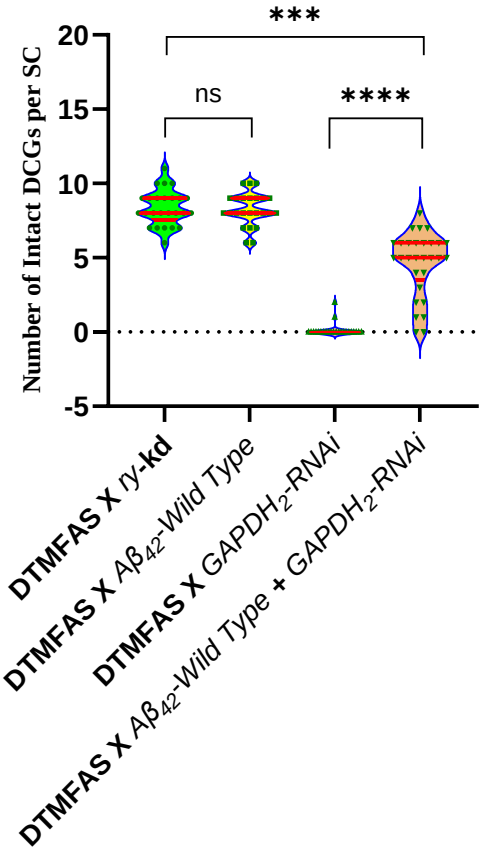

Figure 6.27: The combination of *Aβ*$_{42}$*-wild type* and *GAPDH2-RNAi* increases the number of intact DCGs, but not to the same extent that the *Aβ*$_{42}$*-E693G-Arctic* does (*cf.* Figure 6.29). This demonstrates that *Aβ*$_{42}$*-wild type* also rescues the mini-core phenotype of *GAPDH2-RNAi*, but with less 'glueing' power than *Aβ*$_{42}$*-E693G-Arctic* has. As also indicated in the microscopy images (**Figure 6.26)** which correspond to this bar chart, all genotypes listed here were driven by *w*^{1118}*; tub-GAL80*^{ts}*/CyO; dsx-GAL4 GFP-mfas/TM6B* (DTMFAS). The mean for each set of experiments is shown in red.

6.2.6.5 INTERACTION BETWEEN *Aβ*$_{42}$*-E693-ARCTIC* AND *GAPDH2-RNAi*

Here, following the same format I outlined with other rescue experiments, I overexpressed

Aβ$_{42}$*-E693G-Arctic* and *Drosophila GAPDH2-RNAi* separately in different flies, and then

together in the same fly, in each instance in adult SCs under dsx-GAL4 control. I then compared these results to control cells in flies expressing a *UAS-ry-RNAi* construct.

As seen in the results below and in keeping with earlier results, overexpression of *$A\beta_{42}$-E693G-Arctic* produces targetoid DCGs (**Figure 6.28B**), while overexpression of *GAPDH2-RNAi* again results in micro-cores with a distinctive 'string of pearls' appearance (**Figure 6.28C**). The combination of these two genetic constructs in the *Drosophila* genome increases the number of intact DCGs as compared to the number produced by *GAPDH2-RNAi* alone, suggesting an interaction between these opposing forces. Given the fact that the typical 'string of pearls' appearance of *GAPDH2*-RNAi is superceded by the intact DCG phenotype of *$A\beta_{42}$-E693G-Arctic*, this appears to be a rescue of *GAPDH2-RNAi* by *$A\beta_{42}$-E693G-Arctic.* This rescue by *$A\beta_{42}$-E693G-Arctic* (**Figure 6.28D**) appears much more pronounced than that brought about by *$A\beta_{42}$-wild type* (**Figure 6.26D** and **E**), making a case for *$A\beta_{42}$-E693G-Arctic*'s more powerful intrinsic aggregating activity that can assemble DCGs and overcome the fusion defects engendered by *GAPDH2*-kd.

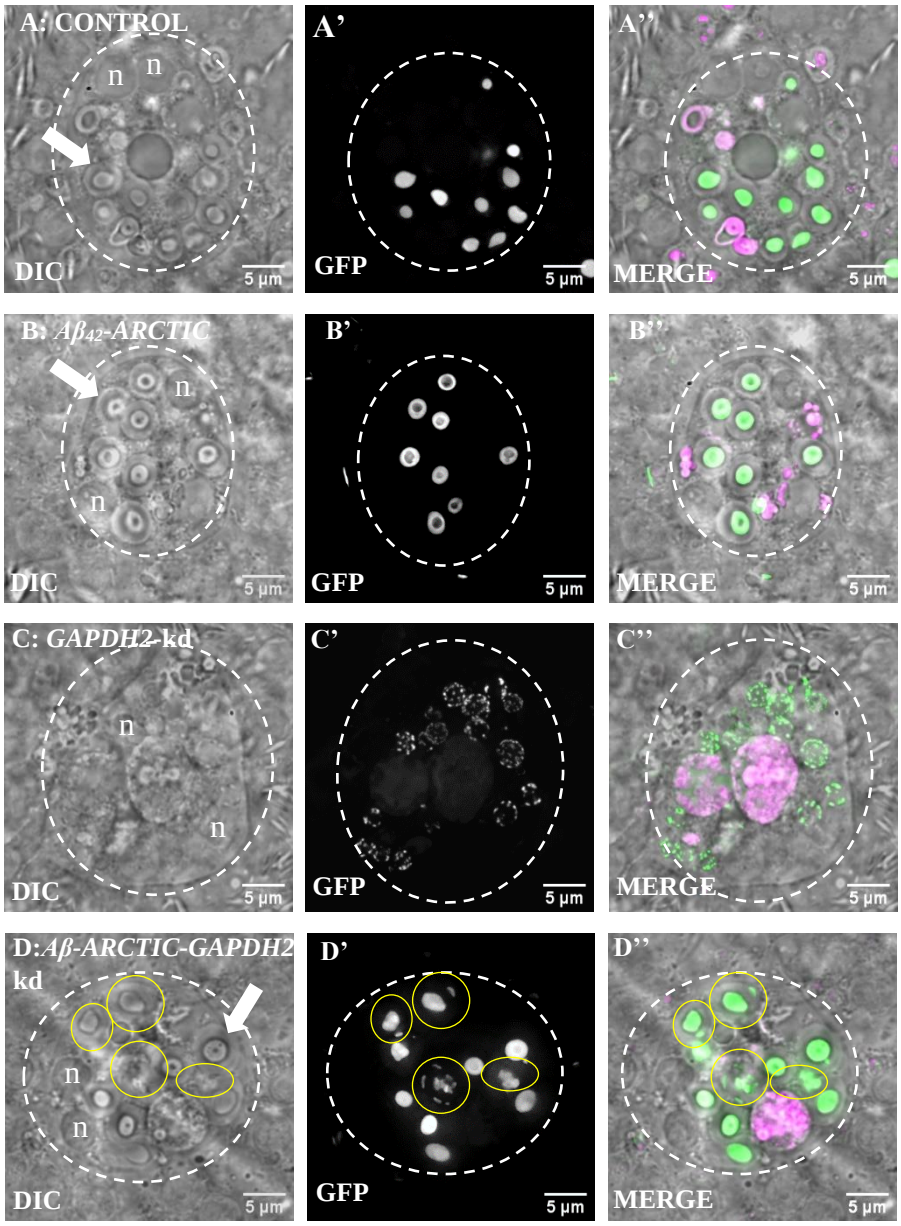

Figure 6.28: Interaction between *Aβ$_{42}$-E693G-Arctic* and *GAPDH2-RNAi*. SCs from six-day-old virgin males stained with LysoTracker Red and imaged *ex vivo*, using DIC and fluorescence microscopy for GFP and LysoTracker Red. **A)** *w^{1118}; GAL80^{ts}/UAS-ry-RNAi; dsx-GAL4 GFP-mfas/+* (control) **B)** *w^{1118}; GAL80^{ts}/UAS-Aβ$_{42}$-E693G-Arctic; dsx-GAL4 GFP-mfas/+* **C)** *w^{1118}; GAL80^{ts}/+; dsx-GAL4 GFP-mfas/UAS-GAPDH2-RNAi* **D)** *w^{1118}; GAL80^{ts}/UAS-Aβ$_{42}$-E693G-Arctic; dsx-GAL4 GFP-mfas/UAS-GAPDH$_2$-RNAi*. **White arrows** in **A, B** and **D:** DCGs; **yellow circles/ovals:** outlines of compartments which includes a core and mini-cores; **n:** double nuclei characteristic of each SC. Scale bar = 5 µm.

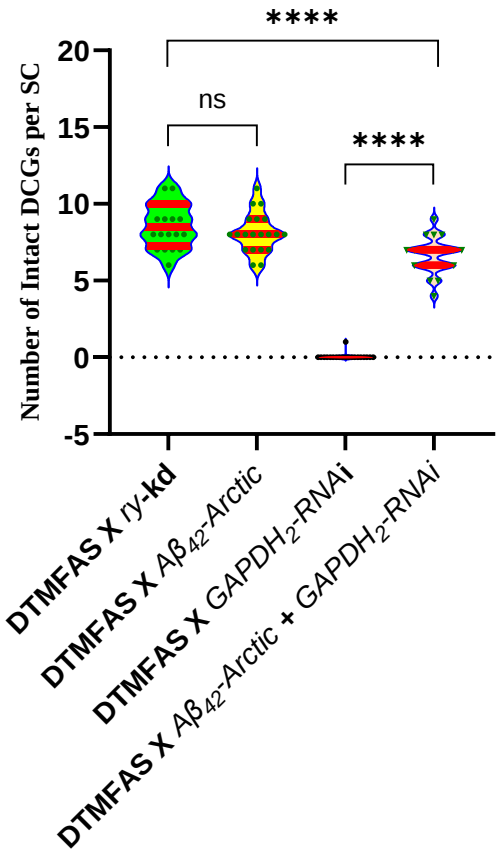

Figure 6.29: The combination of *Aβ$_{42}$-E693G-Arctic* and *GAPDH$_2$-RNAi* increases the number of intact DCGs. This demonstrates a rescue of *GAPDH$_2$-RNAi's* mini-core phenotype by *Aβ$_{42}$-E693G-Arctic*. As also indicated in the microscopy images (**Figure 6.28)** which correspond to this bar chart, all genotypes listed here were driven by *w^{1118}; tub-GAL80^{ts}/CyO; dsx-GAL4 GFP-mfas/TM6B* (DTMFAS). The mean for each set of experiments is shown in red.

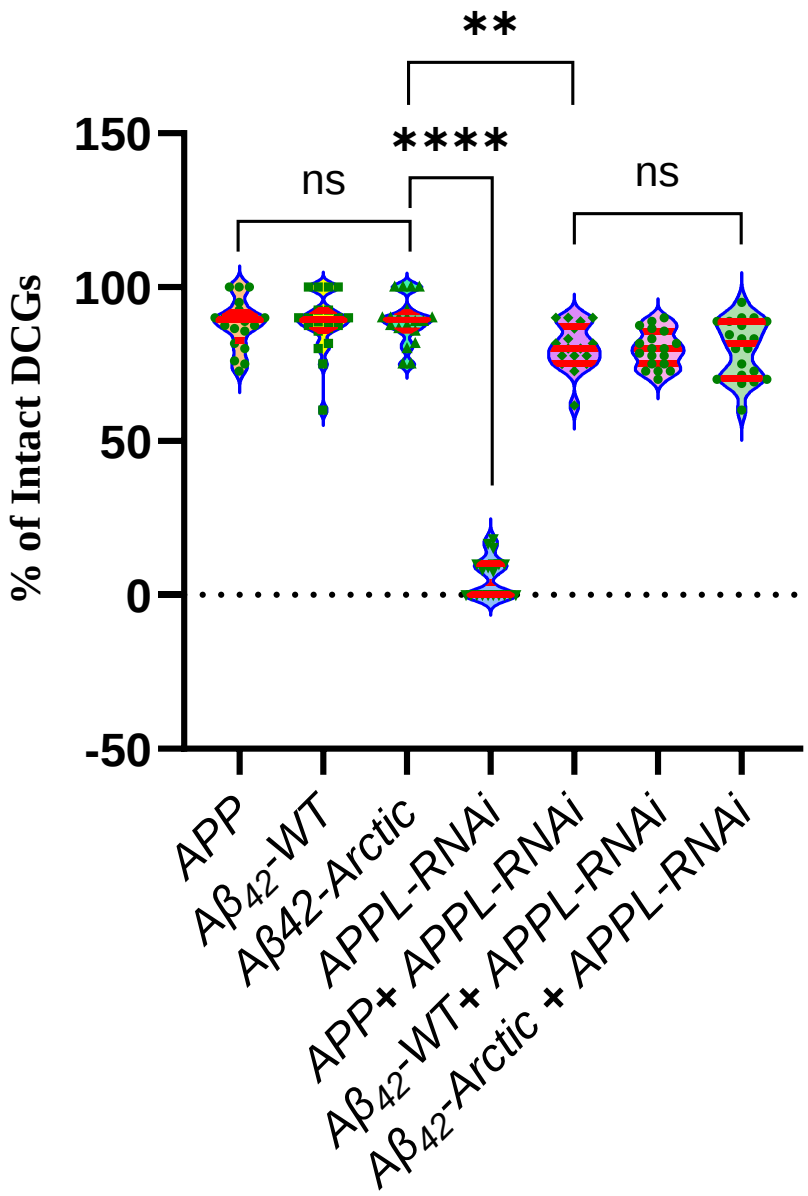

Figure 6.30: Effectiveness of rescues of *APPL-RNAi* by *APP* and its internal fragment, *$A\beta_{42}$*, both wild type and mutated (*$A\beta_{42}$-E693G-Arctic*). as measured by the production of intact DCGs. Lines overexpressing *APP, $A\beta_{42}$-wild type*, and *$A\beta_{42}$-E693G-Arctic* all produced approximately 90 % intact DCGs. The line overexpressing APPL-RNAi produced 6 % intact DCGs. All these percentages were consistent with numbers obtained with previous experiments. However, when *APPL-RNAi* was overexpressed together with *APP, $A\beta_{42}$-wild type*, and *$A\beta_{42}$-E693G-Arctic*, each of these combination lines produced approximately 80 % intact DCGs, demonstrating a rescue of *APPL-RNAi* by each of these genotypes. As also indicated in the microscopy images which correspond to this bar chart, all genotypes listed here were driven by *w^{1118}; tub-GAL80^{ts}/CyO; dsx-GAL4 GFP-mfas/TM6B* (DTMFAS). The mean for each set of experiments is shown in red.

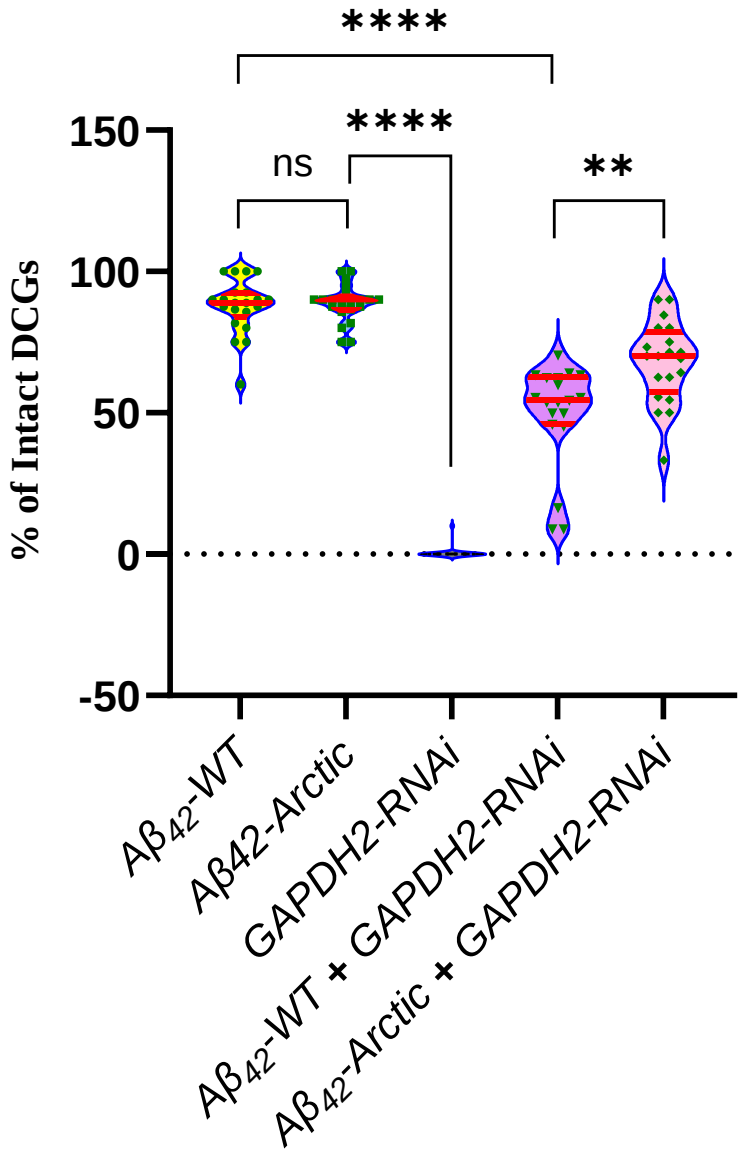

Figure 6.31: Effectiveness of rescues of *GAPDH2-RNAi* by *Aβ42-wild type* and *Aβ42-E693G-Arctic*, as measured by the production of intact DCGs. Lines overexpressing *Aβ42-wild type* and *Aβ42-E693G-Arctic* both produced close to 90 % intact DCGs. The line overexpressing *GAPDH2-RNAi* produced essentially no intact DCGs. All these percentages were consistent with numbers obtained with previous experiments. However, when *GAPDH2-RNAi* was overexpressed together with *Aβ42-wild type* and then with *Aβ42-E693G-Arctic*, the combination lines produced 50 % and approximately 68 % intact DCGs respectively, demonstrating a rescue of *GAPDH2-RNAi* by each of these genotypes. As also indicated in the microscopy images which correspond to this bar chart, all genotypes listed here were driven by *w^{1118}; tub-GAL80^{ts}/CyO; dsx-GAL4 GFP-mfas/TM6B* (DTMFAS). The mean for each set of experiments is shown in red.

In summary, both *APP* and it's derivatives, *$A\beta_{42}$-wild type* and *$A\beta_{42}$-E693G-Arctic* have the same efficacy in rescuing *APPL-RNAi,* as judged by the shift from non-intact to intact DCGs when these genotypes were combined with *APPL-RNAi.* Thus, this percentage went from 7 % intact DCGs with *APPL-RNAi* alone, to 80 % when *APPL-RNAi* is combined with *APP*, *$A\beta_{42}$-wild type*, or *$A\beta_{42}$-E693G-Arctic.* These experiments also show that *$A\beta_{42}$-E693G-Arctic* is more effective than *$A\beta_{42}$-wild type* in rescuing *GAPDH2-RNAi* (these combinations produced 68 % versus 50 % intact DCGs respectively). Taken together, these data show the following: **a)** the *$A\beta_{42}$* segment confers some degree of amyloidogenic adhesivity. **b)** *$A\beta_{42}$-E693G-Arctic*, shown to cause greater organization of dense-cores, is nonetheless no more effective than *$A\beta_{42}$-wild type* in rescuing mini-cores when combined with *APPL-RNAi*. (This observation comes with the caveat that on visual inspection, DCGs produced by *$A\beta_{42}$-E693G-Arctic* rescuing *APPL-RNAi* appear more well-knit than those produced by *$A\beta_{42}$-wild type* rescues). **c)** *$A\beta_{42}$-E693G-Arctic* exerts a greater rescue effect over *GAPDH2-RNAi* (68 %) than *$A\beta_{42}$-wild type* does over *GAPDH2-RNAi* (50 %). **d**) *$A\beta_{42}$-wild type's* rescue efficiency of 80 % over *APPL-RNAi* drops to 50 % when a rescue of *GAPDH2-RNAi* is attempted. **e**) *$A\beta_{42}$-E693G-Arctic's* rescue efficiency of 80 % over *APPL-RNAi* drops to 68 % when a rescue of *GAPDH2-RNAi* is attempted. The last three points (**c**, **d** and **e**) allow for the further conclusion that the *GAPDH2*-knockdown is in some way fundamentally different from the *APPL*-knockdown.

This is because with the *APPL*-kd, a rescue is effected by *APPL*-related molecules (its human homologue *APP* and its cleavage derivates *$A\beta_{42}$-wild type* and *$A\beta_{42}$-E693G-Arctic*). With the *GAPDH2*-kd, there is already *APPL* in the flies, but that fails to rescue the mini-

core phenotype of *GAPDH2*-kd. This is also reflected in the patterns of mini-cores produced by *GAPDH2* and *APPL* knockdowns, with the former producing a 'string of pearls' appearance in which MFAS adheres to the compartment membrane, while the latter produces larger mini-cores which appear to be distributed throughout the volume of the compartment, with the frequent presence of a centrally-appearing 'nidus'. These differences in mini-core biogenesis patterns, along with differences in motility patterns of these two sets of non-fusing mini-cores, have been captured in time-lapse videos (Singh *et al*., manuscript in preparation, and Adam Wells, personal communication), and have already paved the way in the Wilson laboratory for exploring the differences between these two distinct 'failures of MFAS fusion'. Finally, this allows me to conclude that the overtly amyloid *$A\beta_{42}$-E693G-Arctic* mutant exerts a greater 'glueing' or organising power over MFAS' non-fusion caused by *GAPDH2*-knockdown than does *$A\beta_{42}$-wild type.* This stands to reason, since while being potentially amyloidogenic, *$A\beta_{42}$-wild type* still remains a single amino acid away from crossing that threshold.

The other theme emerging through these experiments is that amyloid proteins influence each other. This is seen firstly with the rescue of *APPL*-kd's mini-core phenotype by human APP. This tells us that conserved amyloid molecules can substitute for each other's functions in SCs in the fly. It also tells us that in the rescue of an APPL loss-of-function phenotype, $A\beta_{42}$-E693G-Arctic's amyloidogenic activity is not required for DCG aggregation in the same way it is for the *GAPDH2*-kd, where its organising power is substituting for the loss of a completely different gene. In the case of a conserved gene, $A\beta_{42}$-wild type and $A\beta_{42}$-E693G-Arctic proteins, both internally located segments of APP,

the first physiological and the second amyloidogenic, are equally successful as their parent APP in rescuing *APPL*-kd's mini-core phenotype. This suggests that here, the rescue is not a function of mutation-driven amyloidogenic pathogenicity, but rather a reflection of a common ancestral amyloidogenic provenance. While my results are to the best of my knowledge the first to demonstrate a structural rescue between APP family members in a living system, a functional rescue was shown years ago by Luo, who found that transgenes encoding APPL or APP both rescue behavioural defects of *APPL* null flies (Luo 1992). This further underscores the beauty of this *Drosophila* DCG model, which I believe going forward will corroborate previously done functional studies by providing the corresponding visible, structurally-based underpinnings.

6.2.7 RESULTS REGARDING THE DURABILITY OF $A\beta_{42}$-WT, $A\beta_{42}$-ARCTIC AND *TGFBI* MUTANT DCGS AS MEASURED BY AGEING EXPERIMENTS

Amyloids are known to be durable and tenacious (Rambaran and Serpell, 2008). To test this staying power, control flies and those bearing amyloidogenic $A\beta_{42}$ and *TGFBI* mutations were aged and analyzed using confocal microscopy. Specifically, mutants were compared with controls to assess the durability of the MFAS-comprised DCGs in each line. As shown in earlier results, DCGs undergo morphological alterations when subjected to the influence of amyloidogenic mutations in either $A\beta_{42}$ or *TGFBI*, both of which were tested here. Measurements of DCG durability were made at 6 and 18 days, and these results are shown in the following confocal images.

6.2.7.1 THE NORMAL AGEING OF DCGs IN CONTROL FLIES

In the following series of experiments, similar to the experimental approach I described in **§ 3.2.1**, the bipartite GAL4 sysytem comprised of a transgenic driver line and a transgenic

target gene line was used, with the progeny of the cross expressing the transgene wherever GAL4 is expressed. I examined the morphology of DCGs in SCs expressing a *GFP-mfas* gene trap in a genetic background (the DTMFAS driver line) that included the SC-specific dsx-GAL4 and the temperature-sensitive $GAL80^{ts}$ inhibitor, which was inactivated in adults to switch on GAL4 by increasing the temperature of fly culture from 25°C to 29°C. Co-expression of *UAS-ry-RNAi* under *dsx-GAL4* control, consistent with earlier results, was confirmed to have no effect on DCG properties (**Figure 3.2D**, **Figure 3.3**), and therefore was used as a control in this series of experiments as well. In all these experiments, six-day-old virgin males were aged to 6 and 18 days, at which time their AGs were dissected, fixed, and mounted as described in **Sections 2.9** and **2.10**, followed by imaging by confocal microscopy using GFP and DAPI channels.

The confocal microscopy images below depict control flies (w^{1118}*; GAL80*^{ts}*/UAS-ry-RNAi; dsx-GAL4 GFP-mfas/+*) imaged at 6 and 18 days. At day 6, the standard age at which all imaging in this thesis was done, DCG morphology was considered representative of normal young animals, and imaging at both 10X and 40X showed normal DCGs, in which MFAS-GFP was concentrated. Furthermore, the AG lumens appeared clear, without the dispersion of GFP-MFAS. When aged to 18 days, however, the GFP-MFAS in DCGs appeared to be disintegrating, being dispersed instead at high levels throughout the AG lumen in a non-homogeneous pattern (**Figure 6.32**).

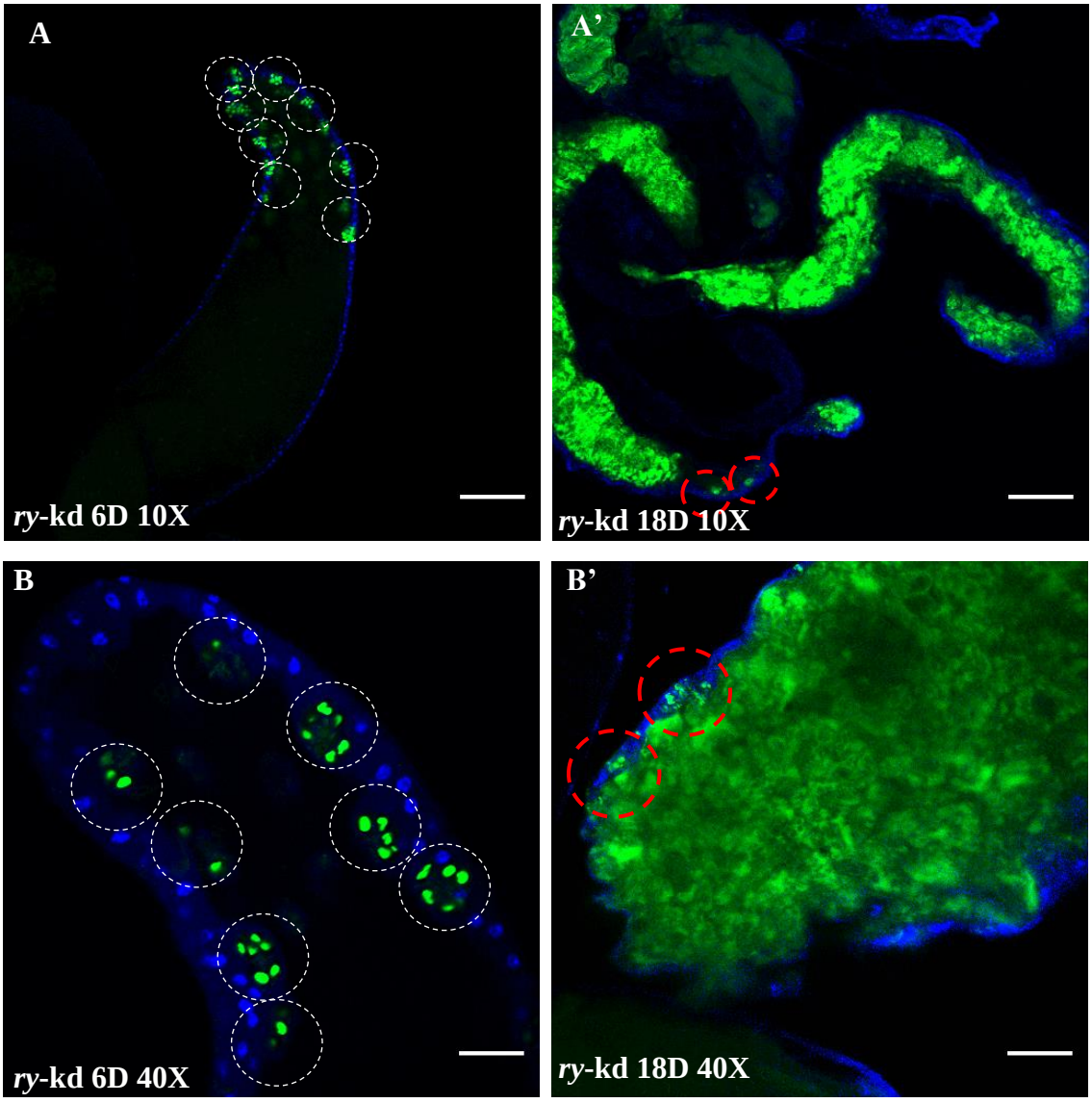

Figure 6.32: Comparison of SCs and AGs expressing GFP-MFAS at 6 and 18 days. AGs were imaged by confocal microscopy using GFP and DAPI channels. **A)** *w^{1118}; $GAL80^{ts}$/UAS-ry-RNAi; dsx-GAL4 GFP-mfas/+* (control) at 6 days, 10 X magnification. **A')** *w^{1118}; $GAL80^{ts}$/UAS-ry-RNAi; dsx-GAL4 GFP-mfas/+* (control) at 18 days, 10 X magnification. **B)** *w^{1118}; $GAL80^{ts}$/UAS-ry-RNAi; dsx-GAL4 GFP-mfas/+* (control) at 6 days, 40 X magnification. **B')** *w^{1118}; $GAL80^{ts}$/UAS-ry-RNAi; dsx-GAL4 GFP-mfas/+* (control) at 18 days, 40 X magnification. **Dashed white circles:** DCGs within SCs, showing intact DCGs at 6 days. **Dashed red circles:** disintegrating DCGs at 18 days. **A'** and **B'** show accumulated secreted MFAS dispersed at high levels throughout the AG lumen in a non-homogeneous pattern. In addition, **A'** and **B'** demonstrate the age-related dissolution of DCGs. Scale bar in **A** and **A'**:100 μm. Scale bar in **B** and **B**': 20 μm

6.2.7.2 THE AGEING OF DCGs IN *Aβ42-WT* AND *Aβ42-E693G-ARCTIC* FLIES

In the experiments below, DCGs from flies overexpressing *Aβ42-wild type* were compared to DCGs from flies overexpressing the amyloidogenic mutation *Aβ42-E693G-Arctic* at 6 and 18 days. A key rationale prompting this experiment was the finding that *Aβ42-E693G-Arctic* was more effective than *Aβ42-wild type* in rescuing the mini-core phenotype of *GAPDH2*-kd (**§ 6.2.6.4** and **§ 6.2.6.5**). This suggests that the point mutation-driven amyloidogenic transformation of *Aβ42-wild type* to *Aβ42-E693G-Arctic* confers greater DCG-organising, or 'glueing' powers. Taken in conjunction with the greater tenacity known to be possessed by amyloid, I decided to compare the resilience of *Aβ42-wild type* and *Aβ42-E693G-Arctic* DCGs to age-related degradation.

To do this, I overexpressed *Aβ42-wild type* and *Aβ42-E693G-Arctic* in separate fly lines, then compared the morphologies of their DCGs to each other and to those of control flies at 6 and 18 days. The confocal microscopy images below (**Figure 6.33**) show that while the DCGs of control flies and those of flies overexpressing *Aβ42-wild type* undergo normal senescence-related dissolution, flies overexpressing *Aβ42-E693G-Arctic* had DCGs which persisted at 18 days. The other difference was that in the AG lumens of the *Aβ42-E693G-Arctic* flies, the MFAS was not uniformly distributed throughout the lumen. This raised the possibility that the persistence of GFP-MFAS within *Aβ42-E693G-Arctic* DCGs was a reflection of the durability conferred by an amyloidogenic transformation (which, as was seen earlier, could then be communicated to another amyloid, MFAS). The other difference between *Aβ42-E693G-Arctic* and control aged flies is that in the *Arctic* mutant flies, the

MFAS is not uniformly distributed throughout the lumen, not being present in the tip (**Figure 6.33C'**).

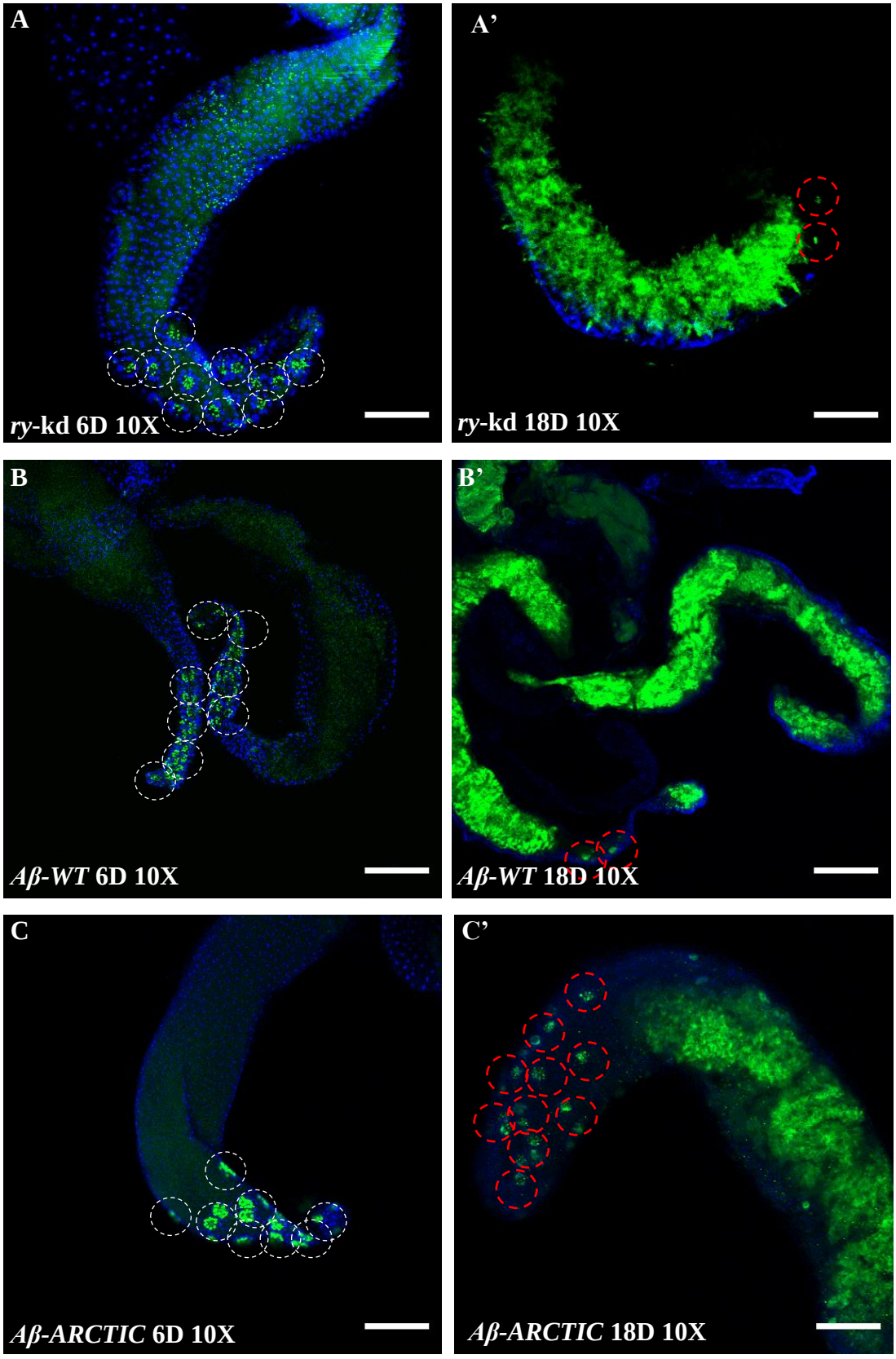
A
ry-kd 6D 10X
A'
ry-kd 18D 10X
B
Aβ-WT 6D 10X
B'
Aβ-WT 18D 10X
C
Aβ-ARCTIC 6D 10X
C'
Aβ-ARCTIC 18D 10X

Figure 6.33: Comparison of SCs and AGs expressing GFP-MFAS at 6 and 18 days. AGs were imaged by confocal microscopy using GFP and DAPI channels. **A)** *w^{1118}; $GAL80^{ts}$/UAS-ry-RNAi; dsx-GAL4 GFP-mfas/+* (control) at 6 days, 10 X magnification. **A')** *w^{1118}; $GAL80^{ts}$/UAS-ry-RNAi; dsx-GAL4 GFP-mfas/+* (control) at 18 days, 10 X magnification. **B)** *w^{1118}; $GAL80^{ts}$/UAS- $A\beta_{42}$-wild-type; dsx-GAL4 GFP-mfas/+* at 6 days, 10X magnification. **B')** *w^{1118}; $GAL80^{ts}$/UAS-$A\beta_{42}$-wild-type; dsx-GAL4 GFP-mfas/+* at 18 days, 10X magnification. **C)** *w^{1118}; $GAL80^{ts}$/UAS-$A\beta_{42}$-E693G-Arctic; dsx-GAL4 GFP-mfas/+* at 6 days, 10X magnification. **C')** *w^{1118}; $GAL80^{ts}$/UAS-$A\beta_{42}$-E693G-Arctic; dsx-GAL4 GFP-mfas/+* at 18 days, 10X magnification. **Dashed white circles:** DCGs at 6 days. **Dashed red circles:** DCGs at 18 days. **A'** and **B'** show the age-related dissolution of DCGs and the dissipation of MFAS in non-amyloidogenic situations. In **C'** the amyloidogenic *$A\beta_{42}$-E693G-Arctic* mutation, however, confers greater stability to DCGs, as evidenced by the relative persistence of DCGs. Scale bar: 100 μm.

In **Figure 6.34** below, the persistence of *$A\beta_{42}$-E693G-Arctic* DCGs at 18 days is shown at a higher magnification to highlight the features of SCs and DCGs at 6 and 18 days. At 6 days, as seen in **Figure 6.34A** and **B**, the anatomy of the AGs, SCs, and DCGs appear undistorted and well-defined in both controls and *$A\beta_{42}$-E693G-Arctic* flies. However, at 18 days, as seen in **Figure 6.34A'** and **B'**, these same structures appear distorted, particularly in controls. Furthermore, MFAS has now dissipated and/or been secreted into the gland lumen and appears as amorphous-appearing GFP-tagged proteinaceous flocculations. This is consistent with earlier work in the Wilson laboratory which showed that DCGs dissipate when MFAS secretion takes place into the lumen.

Drosophila MFAS in control flies undergoes normal age-related attrition, as evidenced by a decline in the number of DCGs and the accumulation of amorphous-appearing MFAS in the AG lumen (**Figure 6.34A** and **A'**; **Figure 6.35A** and **A'**). This attritional process remains unchanged with the introduction of human *$A\beta_{42}$-wild type* to the fly genome (**Figure 6.33B** and **B'**). However, with the introduction of human *$A\beta_{42}$* bearing the

amyloidogenic *Arctic* mutation, the resultant DCGs become more stable, as evidenced by their relative persistence in aged flies (**Figure 6.33C** and **C'**). This is consistent with the known stability of amyloid proteins. Figure **6.34B'** is also demonstrates MFAS in the lumen extending to the distal tip of the AG, an inconsistent feature found in both control flies and mutants.

In summary, combining the results of all the *$A\beta_{42}$-E693G-Arctic* experiments with previous work on MFAS secretion done in the laboratory, the model of the fate of DCGs/MFAS in flies with the *$A\beta_{42}$-E693G-Arctic* mutation is that these more stable DCGs remain for longer periods in SCs, decreasing the need of SCs to secrete MFAS. Once MFAS is secreted into the lumen however, there is no obvious phenotype differentiating the *$A\beta_{42}$-E693G-Arctic* mutants from control flies. This observation must be tempered, however, by the fact that once in the luminal space, MFAS is diluted, since it is in aqueous solution rather than in an extracellular matrix.

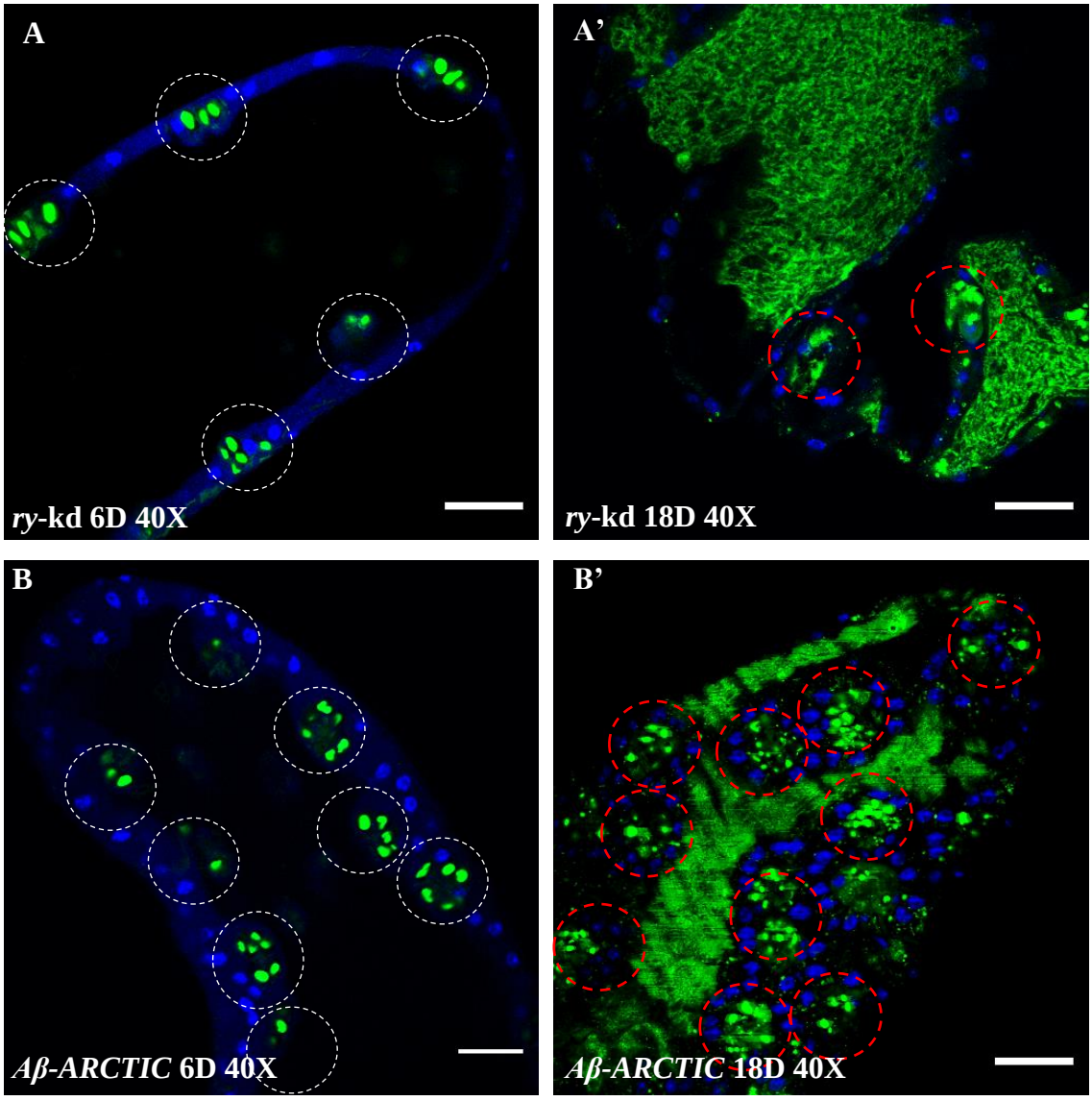

Figure 6.34: Comparison of SCs and AGs expressing GFP-MFAS at 6 and 18 days. AGs were imaged by confocal microscopy using GFP and DAPI channels. **A)** *w^{1118}; tub-GAL80^{ts}/UAS-ry-RNAi; dsx-GAL4 GFP-mfas/+* (control) at 6 days, 40 X magnification. **A')** *w^{1118}; tub-GAL80^{ts}/UAS-ry-RNAi; dsx-GAL4 GFP-mfas/+* (control) at 18 days, 40 X magnification. **B)** *w^{1118}; tub-GAL80^{ts}/UAS-Aβ$_{42}$-E693G-Arctic; dsx-GAL4 GFP-mfas/+* at 6 days, 40X magnification. **B')** *w^{1118}; tub-GAL80^{ts}/UAS-Aβ$_{42}$-E693G-Arctic; dsx-GAL4 GFP-mfas/+* at 18 days, 40X magnification. The amyloidogenic *Aβ$_{42}$-E693G-Arctic* mutation confers greater stability to DCGs as compared to controls, as evidenced by the persistence of DCGs. In this experimental example, MFAS is in the distal tip of the AG lumen for the *Arctic* genotype, *cf.* the last image. **Dashed white circles:** DCG at 6 days. **Dashed red circles:** DCGs at 18 days. Scale bar: 20 μm.

6.2.7.3 THE AGEING OF DCGs IN *mfas-WT* AND *TGFBI-WT* FLIES

In the experiments below, DCGs from flies overexpressing MFAS wild type and its homologue, the potentially amyloidogenic human protein TGFBI, were compared to controls. Here, TGFBI was in its wild type, devoid of any of the amyloidogenic point mutations studied in **Section 5**. The rationale behind these experiments was to investigate whether the presence of amyloidogenic proteins in their non-mutated form had an effect on the durability of DCGs.

In these experiments, similar to the previously described experimental approach, the bipartite GAL4 sysytem comprised of a transgenic driver line and a transgenic target gene line was used, with the progeny of the cross expressing the transgene wherever GAL4 is expressed. I examined the morphology of DCGs in SCs expressing a *GFP-mfas* gene trap in a genetic background (the DTMFAS driver line) that included the SC-specific dsx-GAL4 and the temperature-sensitive $GAL80^{ts}$ inhibitor, which was inactivated in adults to switch on GAL4 by increasing the temperature of fly culture from 25°C to 29°C. Co-expression of *UAS-ry-RNAi* under *dsx-GAL4* control, consistent with earlier results was confirmed to have no effect on DCG properties (**Figure 3.2D** and **Figure 3.3**), and therefore was used as a control in this series of experiments as well. In all these experiments, the AGs of six-day-old virgin males were were dissected, fixed, and mounted as described in **Sections 2.9** and **2.10**. They were then imaged by confocal microscopy using GFP and DAPI channels at days 6 and 18, and controls were compared to flies overexpressing *mfas-wild type* and *TGFBI-wild type*.

As shown below, both wild type *mfas* and wild type *TGFBI* produced DCGs which underwent the same age-related attrition as controls, as evidenced by the fact that DCGs were lost in equal measure in all lines tested. This shows that in the absence of a mutation-driven amyloidogenic influence, *Drosophila* DCGs display no more longevity than controls.

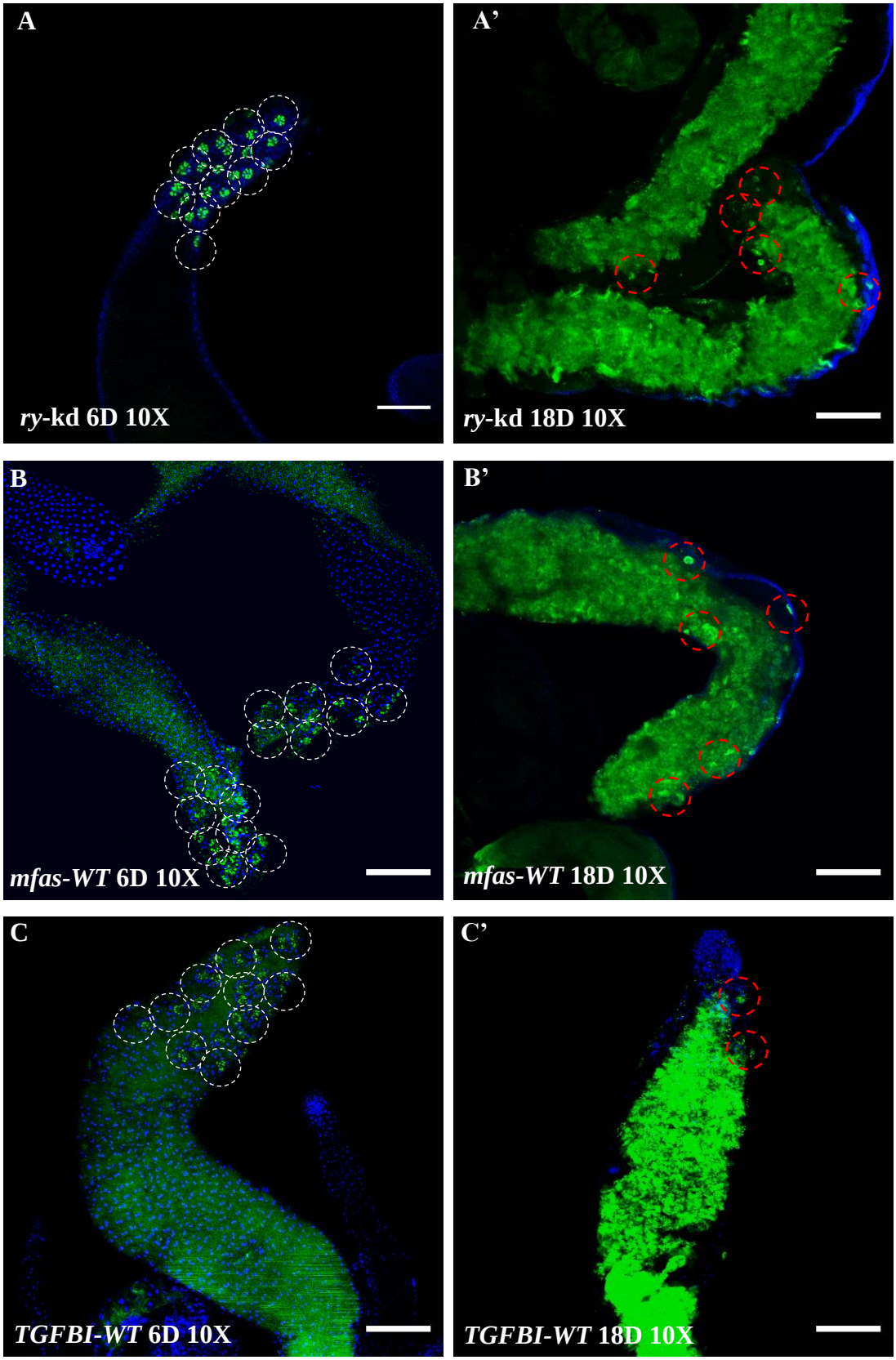
A
ry-kd 6D 10X
A'
ry-kd 18D 10X
B
mfas-WT 6D 10X
B'
mfas-WT 18D 10X
C
TGFBI-WT 6D 10X
C'
TGFBI-WT 18D 10X

Figure 6.35: Comparison of SCs and AGs expressing GFP-MFAS at 6 and 18 days. AGs were imaged by confocal microscopy using GFP and DAPI channels. **A)** *w^{1118}; $GAL80^{ts}$/UAS-ry-RNAi; dsx-GAL4 GFP-mfas/+* (control) at 6 days, 10 X magnification. **A')** *w^{1118}; tub-$GAL80^{ts}$/UAS-ry-RNAi; dsx-GAL4 GFP-mfas/+* (control) at 18 days, 10 X magnification. **B)** *w^{1118}; tub-$GAL80^{ts}$/mfas-wild type; dsx-GAL4 GFP-mfas/+* at 6 days, 10X magnification. **B')** *w^{1118}; tub-$GAL80^{ts}$/mfas-wild type; dsx-GAL4 GFP-mfas/+* at 18 days, 10X magnification. **C)** *w^{1118}; tub-$GAL80^{ts}$/TGFBI-wild type; dsx-GAL4 GFP-mfas/+* at 6 days, 10X magnification. **C')** *w^{1118}; tub-$GAL80^{ts}$/TGFBI-wild type; dsx-GAL4 GFP-mfas/+* at 18 days, 10X magnification. **Dashed white circles:** DCGs at 6 days. **Dashed red circles:** DCGs at 18 days. Flies with the genomic insertion of an extra copy of wild type *mfas* or wild type *TGFBI* showed no difference as compared to controls with regards to age-related dissolution of DCGs. Scale bar: 100 μm.

DCGs were previously shown to be reliable barometers of the enhanced stability conferred upon them by the genomic insertion of a construct with an amyloidogenic mutation (*$A\beta_{42}$-E693G-Arctic*) (**§ 6.2.7.2**). Conversely, DCGs degenerate normally with the genomic insertion of non-amyloidogenic constructs (*$A\beta_{42}$-wild type*, *TGFBI-wild type*, and an extra copy of *mfas-wild type*) (**§ 6.2.7.2** and **§ 6.2.7.3**).

The reasoning behind this was that since amyloid is a durable, tenacious form of protein, then if amyloidogenic mutations like *$A\beta_{42}$-E693G-Arctic* when genomically inserted are indeed influencing MFAS, the structures MFAS forms (DCGs), might also be more durable. With flies overexpressing the *$A\beta_{42}$-E693G-Arctic* mutation, DCGs persisted at 18 days, and in the small number of flies that lived to the age of 21-28 days, DCGs persisted even until those time points (data not shown). The ageing experiments performed on flies transgenic for *TGFBI-wild type* and on flies with an extra copy of *mfas* confirm the fidelity of DCGs as an accurate sensor in the opposite sense: with no underlying amyloidogenic mutations in the fly genome, DCGs showed their normal vulnerability to physiological dissolution. The next section will examine the effects of amyloid mutation-bearing human

TGFBI constructs on DCG stability. These experiments tested whether the durability conferred on DCGs by *Aβ42-E693G-Arctic* is similarly seen with amyloidogenic mutations in *TGFBI,* which encodes an entirely different protein, in an entirely different organ (the cornea), and, like *Aβ42-Arctic's* parent APP, in an entirely different species.

6.2.7.4 DCG AGEING IN CONSERVED *TGFBI-G623D* AND -*H626R* MUTANTS

In the experiments below, DCGs from flies overexpressing the conserved *TGFBI* mutations *G623D* and *H626R* were compared to controls, the rationale behind these experiments being to investigate whether the presence of amyloidogenic proteins had an effect on the durability and stability of DCGs. To do this, I overexpressed *TGFBI-G623D* and *TGFBI-H626R* in adult SCs under dsx-GAL4 control, and compared each phenotype to that of control SCs in flies expressing a *UAS-ry-RNAi* construct. For each of these lines, DCGs and lumenal MFAS were studied at 6 and 18 days by confocal microscopy using GFP and DAPI channels.

As shown below, DCGs from control flies underwent physiological dissolution (**Figure 6.36A** and **A'**). However, flies overexpressing the CD-causing conserved mutation *TGFBI-G623D* displayed greater age-related stability, as demonstrated by the preservation of more DCGs at 18 days (**Figure 6.36B** and **B'**). Similarly, flies overexpressing the other CD-causing conserved mutation, *TGFBI-H626R,* also showed persistent DCGs at 18 days (**Figure 6.36C** and **C'**). When viewed at higher magnification, both these mutations were found to result in SCs and DCGs with relatively preserved organisation and archictecture (**Figure 6.36D** and **D'**).

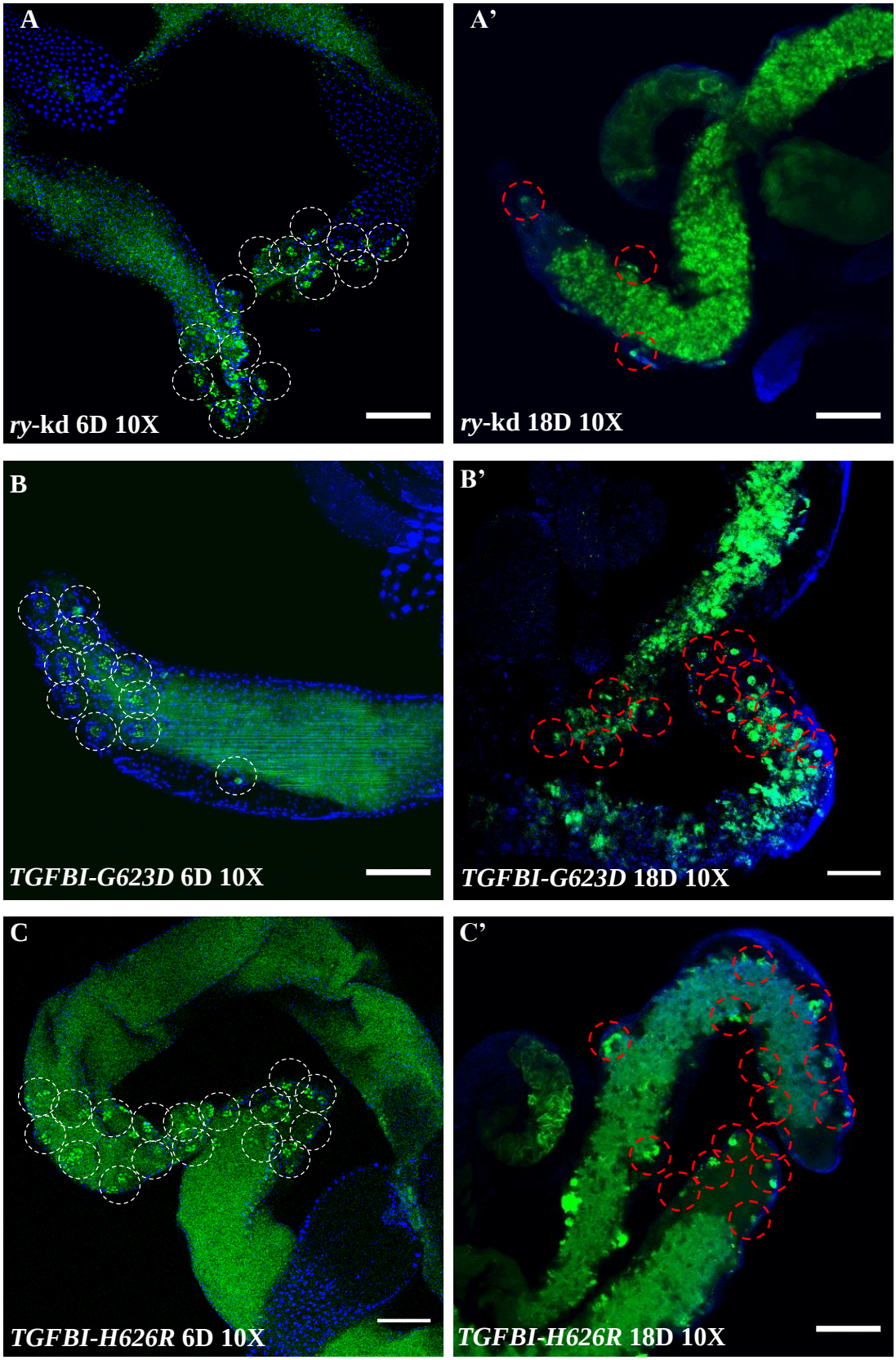
A
ry-kd 6D 10X
A'
ry-kd 18D 10X
B
TGFBI-G623D 6D 10X
B'
TGFBI-G623D 18D 10X
C
TGFBI-H626R 6D 10X
C'
TGFBI-H626R 18D 10X

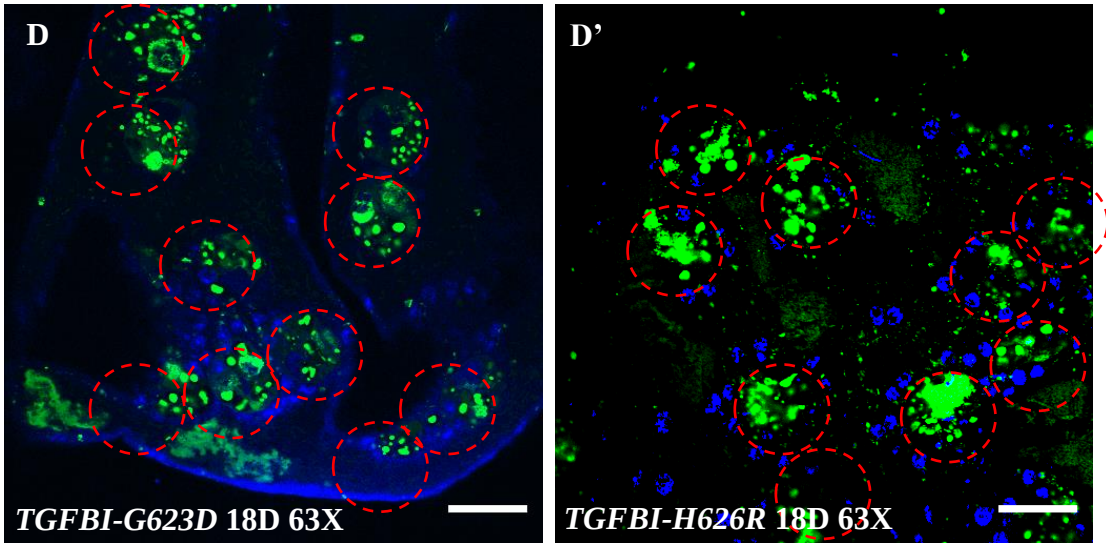

Figure 6.36: Comparison of SCs and AGs expressing GFP-MFAS at 6 and 18 days. AGs were imaged by confocal microscopy using GFP and DAPI channels. **A)** *w^{1118}; $GAL80^{ts}$/ UAS-ry-RNAi; dsx-GAL4 GFP-mfas/+* (control) at 6 days, 10 X magnification. **A')** *w^{1118}; tub-$GAL80^{ts}$/ UAS-ry-RNAi; dsx-GAL4 GFP-mfas/+* (control) at 18 days, 10 X magnification. **B)** *w^{1118}; tub-$GAL80^{ts}$/TGFBI-G623D; dsx-GAL4 GFP-mfas/+* at 6 days, 10X magnification. **B')** *w^{1118}; tub-$GAL80^{ts}$/TGFBI-G623D; dsx-GAL4 GFP-mfas/+* at 18 days, 10X magnification **C)** *w^{1118}; tub-$GAL80^{ts}$/TGFBI-H626R; dsx-GAL4 GFP-mfas/+* at 6 days, 10X magnification. **C')** *w^{1118}; tub-$GAL80^{ts}$/TGFBI-H626R; dsx-GAL4 GFP-mfas/+* at 18 days, 10X magnification. **D)** *w^{1118}; tub-$GAL80^{ts}$/TGFBI-G623D; dsx-GAL4 GFP-mfas/+* at 18 days, 63X magnification. **D')** *w^{1118}; tub-$GAL80^{ts}$/TGFBI-H626R; dsx-GAL4 GFP-mfas/+* at 18 days, 63X magnification. **Dashed white circles:** DCGs at 6 days. **Dashed red circles:** DCGs at 18 days. Flies with *TGFBI*-bearing conserved CD-causing mutations showed greater age-related durability of DCGs compared to controls. Scale bar in **A** to **C**: 100 μm. Scale bar in **D**: 10 μm.

In summary, the prolific CD-causing amyloidogenic mutations *G623D* and *H626R* in *TGFBI* are conserved in *mfas*, it's homologue. When *TGFBI* constructs with these conserved mutations were introduced into the fly genome, they imparted tenacity to DCGs as measured by their relative durability with age as compared to controls. This is in contrast to flies overexpressing wild type *mfas* and wild type TGFBI, which produced normal DCGs, susceptible to the normal dissipation of ageing (**§ 6.2.7.3**). Subsequent experiments address the question of whether the non-conserved *TGFBI* mutations *R555Q* and *R124C* also confer a similar ageing-resistant effect on DCGs as do their conserved counterparts.

6.2.7.5 DCG AGEING IN NON-CONSERVED *TGFBI-R555Q* AND *-R124C* MUTANTS

The next experimental step was to investigate whether the non-conserved CD-causing *TGFBI* mutations *R555Q* and *R124C* were as effective as their conserved counterparts in imparting tenacity and longevity to DCGs. To do this, I overexpressed *TGFBI-R555Q* and *TGFBI-R124C* in adult SCs under dsx-GAL4 control, and compared each phenotype to that of control SCs in flies expressing a *UAS-ry-RNAi* construct. For each of these lines, DCGs and lumenal MFAS were studied at 6 and 18 days by confocal microscopy using GFP and DAPI channels.

As shown in the results below, control flies displayed the normal dissolution of DCGs at 18 days (**Figure 6.37A** and **A'**). Both *TGFBI-R555Q* (**Figure 6.37B** and **B'**) and *TGFBI-R124C* (**Figure 6.37C** and **C'**) produced DCGs with enhanced structural stability as compared to controls, confirmed by views at higher magnification (**Figure 6.37D** and **D'**). In addition to conferring a relative age-impervious stability to DCGs, *R555Q* produced MFAS flocculations with a distinctive appearance (**Figure 6.37B'** and **Figure 6.37D**). This is consistent with the known stability R555Q and the other arginine mutation at this location, R555W, confer on their resultant proteins (Runager *et al.*, 2011). In producing amyloid with distinctive physicochemical properties, *TGFBI-R555Q* is responsible for Thiel-Behnke corneal dystrophy (**Figure 5.8**), which is characterised by an early age of onset and the distressing recurrence of amyloid infiltration of the cornea, surprsingly even after corneal transplantation (Gear *et al.*, 2005).

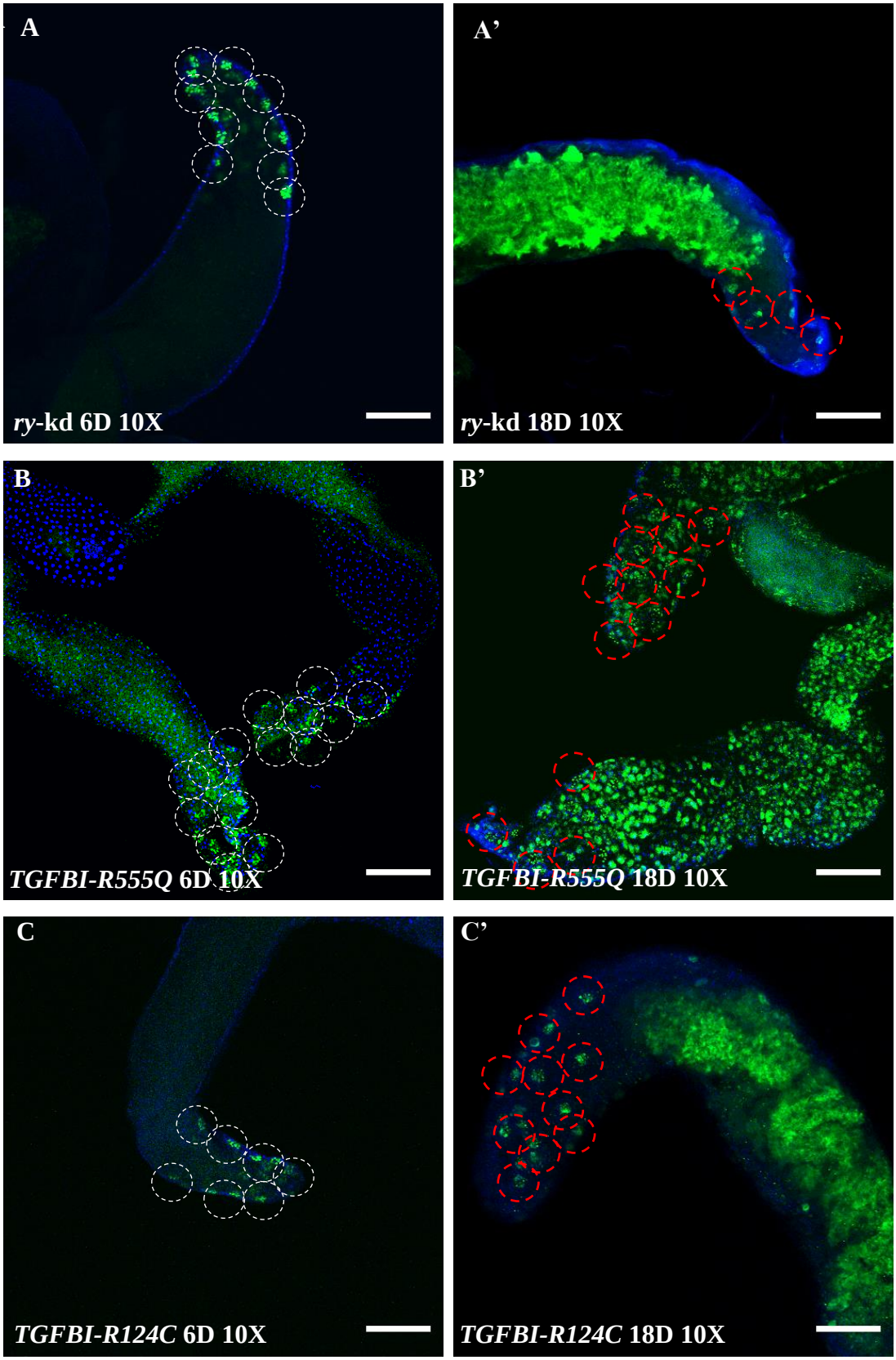
A
ry-kd 6D 10X
A'
ry-kd 18D 10X
B
TGFBI-R555Q 6D 10X
B'
TGFBI-R555Q 18D 10X
C
TGFBI-R124C 6D 10X
C'
TGFBI-R124C 18D 10X

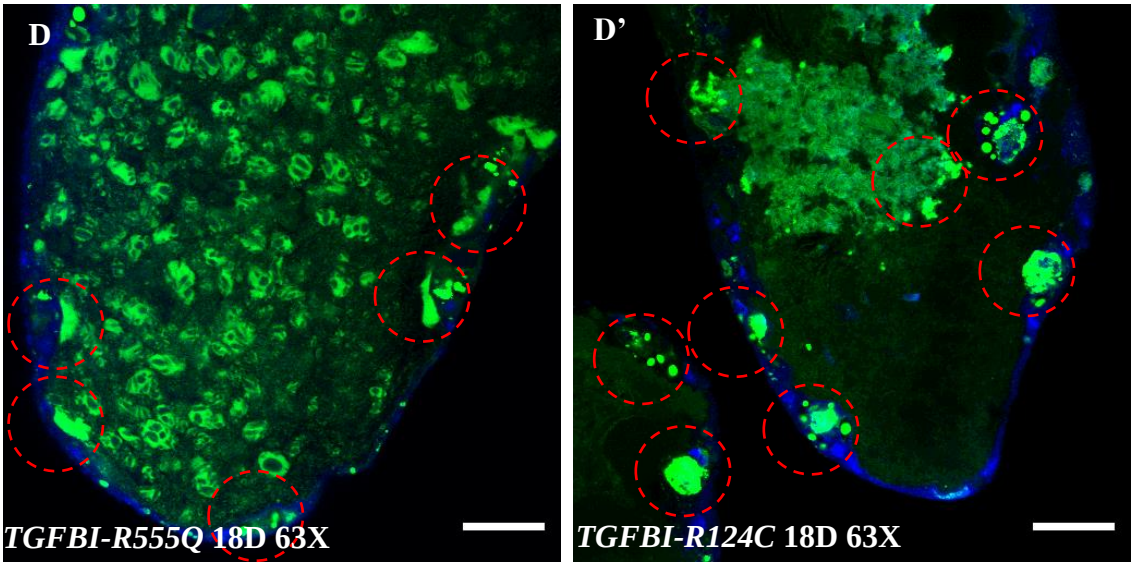

Figure 6.37: **Comparison of SCs and AGs expressing GFP-MFAS at 6 and 18 days.** AGs were imaged by confocal microscopy using GFP and DAPI channels. **A)** *w^{1118}; tub-GAL80^{ts}/UAS-ry-RNAi; dsx-GAL4 GFP-mfas/+* (control) at 6 days, 10 X magnification. **A')** *w^{1118}; tub-GAL80^{ts}/UAS-ry-RNAi; dsx-GAL4 GFP-mfas/+* (control) at 18 days, 10 X magnification. **B)** *w^{1118}; tub-GAL80^{ts}/TGFBI-R555Q; dsx-GAL4 GFP-mfas/+* at 6 days, 10X magnification. **B')** *w^{1118}; tub-GAL80^{ts}/TGFBI-R555Q; dsx-GAL4 GFP-mfas/+* at 18 days, 10X magnification. **C)** *w^{1118}; tub-GAL80^{ts}/TGFBI-R124C; dsx-GAL4 GFP-mfas/+* at 6 days, 10X magnification. **C')** *w^{1118}; tub-GAL80^{ts}/TGFBI-R124C; dsx-GAL4 GFP-mfas/+* at 18 days, 10X magnification. **D)** *w^{1118}; tub-GAL80^{ts}/TGFBI-R555Q; dsx-GAL4 GFP-mfas/+* at 18 days, 63X magnification **D')** *w^{1118}; tub-GAL80^{ts}/TGFBI-R124C; dsx-GAL4 GFP-mfas/+* at 18 days, 63X magnification **Dashed white circles:** DCGs at 6 days. **Dashed red circles:** DCGs at 18 days. Flies transgenic for *TGFBI* with non-conserved CD-causing mutations also showed greater age-related durability of their DCGs. Scale bar from **A** to **C:** 100 μm. Scale bar in **D:** 10 μm.

6.2.7.6 THE AGE-RELATED FATE OF MFAS IN THE AG LUMEN

In the next series of experiments, in flies overexpressing *TGFBI-wild type* as well as all its CD-causing amyloidogenic mutations (*G623D, H626R, R555Q* and *R124C*), the corresponding lumenal phenotypes of MFAS were examined at 6 and 18 days of age. To do this, I overexpressed *TGFBI-wild type*, *TGFBI-G623D*, *TGFBI-H626R*, *TGFBI-R555Q* and *TGFBI-R124C* in adult SCs under dsx-GAL4 control, and compared each phenotype to that of control SCs in flies expressing a *UAS-ry-RNAi* construct. For each of these lines,

lumenal MFAS was studied at 6 and 18 days by confocal microscopy using GFP and DAPI channels. The lumenal MFAS of control flies at 6 and 18 days is shown in **Figure 6.38A** and **C**, while the lumenal MFAS in flies overexpressing *TGFBI-wild type*, also visualised at 6 and 18 days is shown in **Figure 6.38B** and **D**. Flies overexpressing the *TGFBI*-CD mutations were then examined at day 18 (**Figure 6.39A** – **D**). For greater resolution, all confocal imagery in these experiments was performed at 63X magnification.

As seen in representative images below, the appearance of lumenal MFAS at days 6 and 18 in control flies and in flies overexpressing *TGFBI-wild type* was identical. This is in agreement with the findings presented in **§ 6.2.7.3** which showed that in *TGFBI*-wild type, the AG and its contained structures underwent senescence in a physiological fashion, which was in no way different from the process seen in control flies.

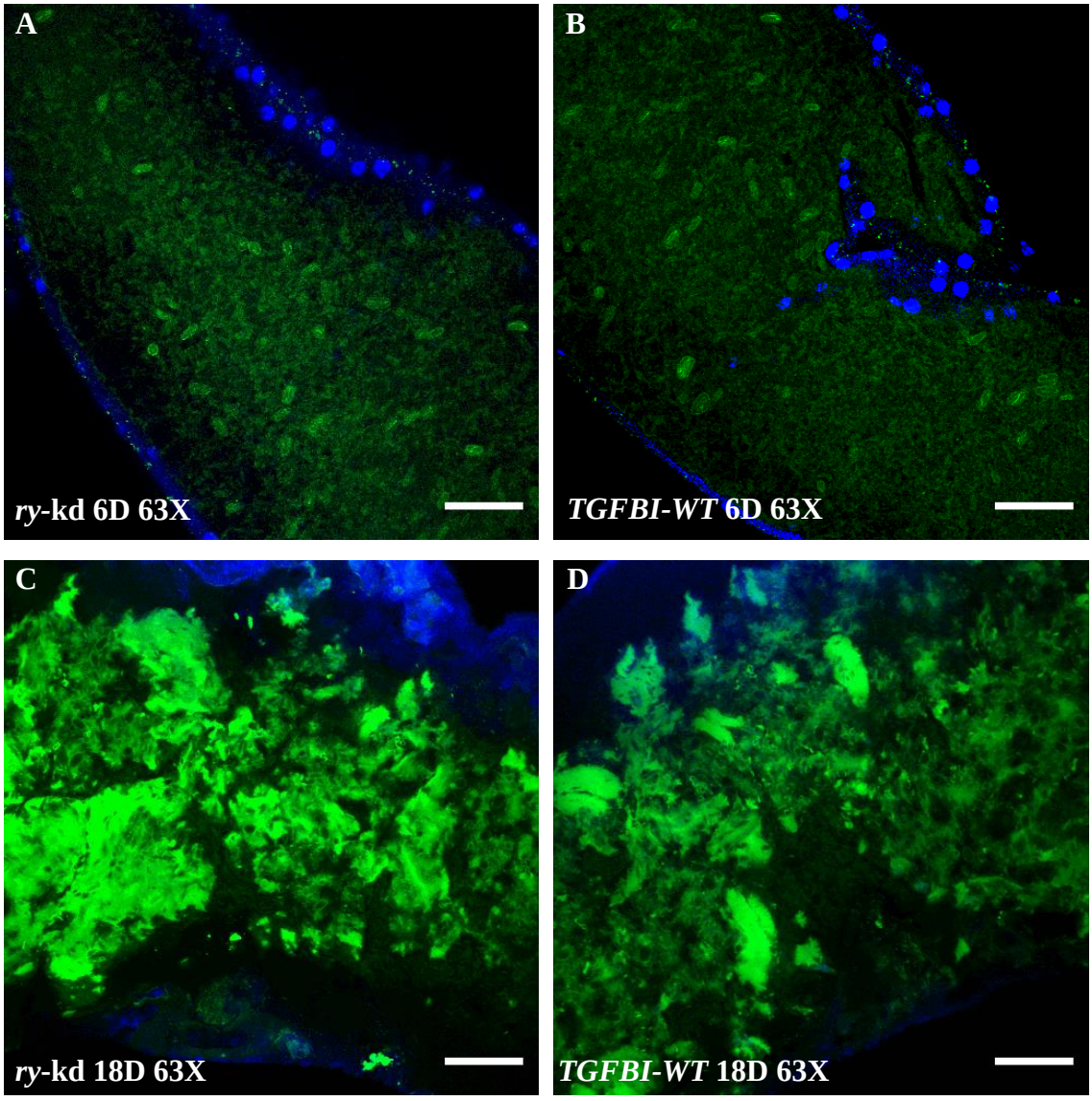

Figure 6.38: Comparison of MFAS in AG lumens at 6 and 18 days. AGs from virgin males were imaged by confocal microscopy using GFP and DAPI channels, which showed the age-related fate of MFAS in the AG lumen in flies transgenic for wild type *TGFBI*. **A)** *w^{1118}; tub-GAL80^{ts}/UAS-ry-RNAi; dsx-GAL4 GFP-mfas/+* (control) at 6 days, 63X magnification. **B)** *w^{1118}; tub-GAL80^{ts}/TGFBI-wild type; dsx-GAL4 GFP-mfas/+* at 6 days, 63X magnification. **C)** *w^{1118}; tub-GAL80^{ts}/UAS-ry-RNAi; dsx-GAL4 GFP-mfas/+* (control) at 18 days, 63X magnification. **D)** *w^{1118}; tub-GAL80^{ts}/TGFBI-wild type; dsx-GAL4 GFP-mfas/+* at 18 days, 63X magnification. **Scale Bar:** 10 μm.

Having established that in flies overexpressing *TGFBI-wild type*, lumenal MFAS has an unremarkable appearance with age, I next studied the effects of overexpressed *TGFBI* amyloidogenic mutations on lumenal MFAS at the same time point. As shown in **Figure**

6.39, except for *TGFBI-R555Q*, none of these mutants significantly altered the morphology of lumenal MFAS at 18 days. In the case of *TGFBI-R555Q*, however, confirming results of an earlier experiment (**§ 6.2.7.5**, **Figure 6.37B'** and **Figure 6.37D**), MFAS at 18 days within the gland lumen assumed a distinctive appearance. With this particular mutation, rather than displaying the amorphous appearance common to the other mutant lines, the MFAS appeared more organised in the form of small floccules (**Figure 6.37D** and **6.39C**). As alluded to earlier, *TGFBI-R555Q* causes a pernicious form of CD (Thiel-Behnke CD) (Thiel and Behnke, 1967), which, appearing as early as infancy, causes painful, persistent, recurrent corneal ulcerations, and even affects transplanted cornea tissue. The roots of this clinical intransigence are revealed in studies of its molecular properties, showing that the two *TGFBI* domain-4 arginine mutations *R555W* and *R555Q* are amongst the most stable in the TGFBI protein. Furthermore, it was found that these two particular arginine point mutations had a propensity to generate amorphous deposits *in vivo*. Finally, it was found that unlike domain-4 mutations, domain-1 point mutations did not affect the stability of TGFBIp (Runager *et al.,* 2011). The authors concluded that variations 'in the stability of FAS1-4 (domain-4, parenthetical clarification added by me) may unleash a disease mechanism' (Runager, K., *et al.,* J. Biol. Chem., 286:7, pg. 4951). Thus the amorphous MFAS flocculations seen in flies overexpressing *R555Q* (**Figure 6.39C**) are in agreement with these earlier studies, and suggest that this particular TGFBIp mutation induces changes in MFAS similar to what Runager *et al.* were referring to.

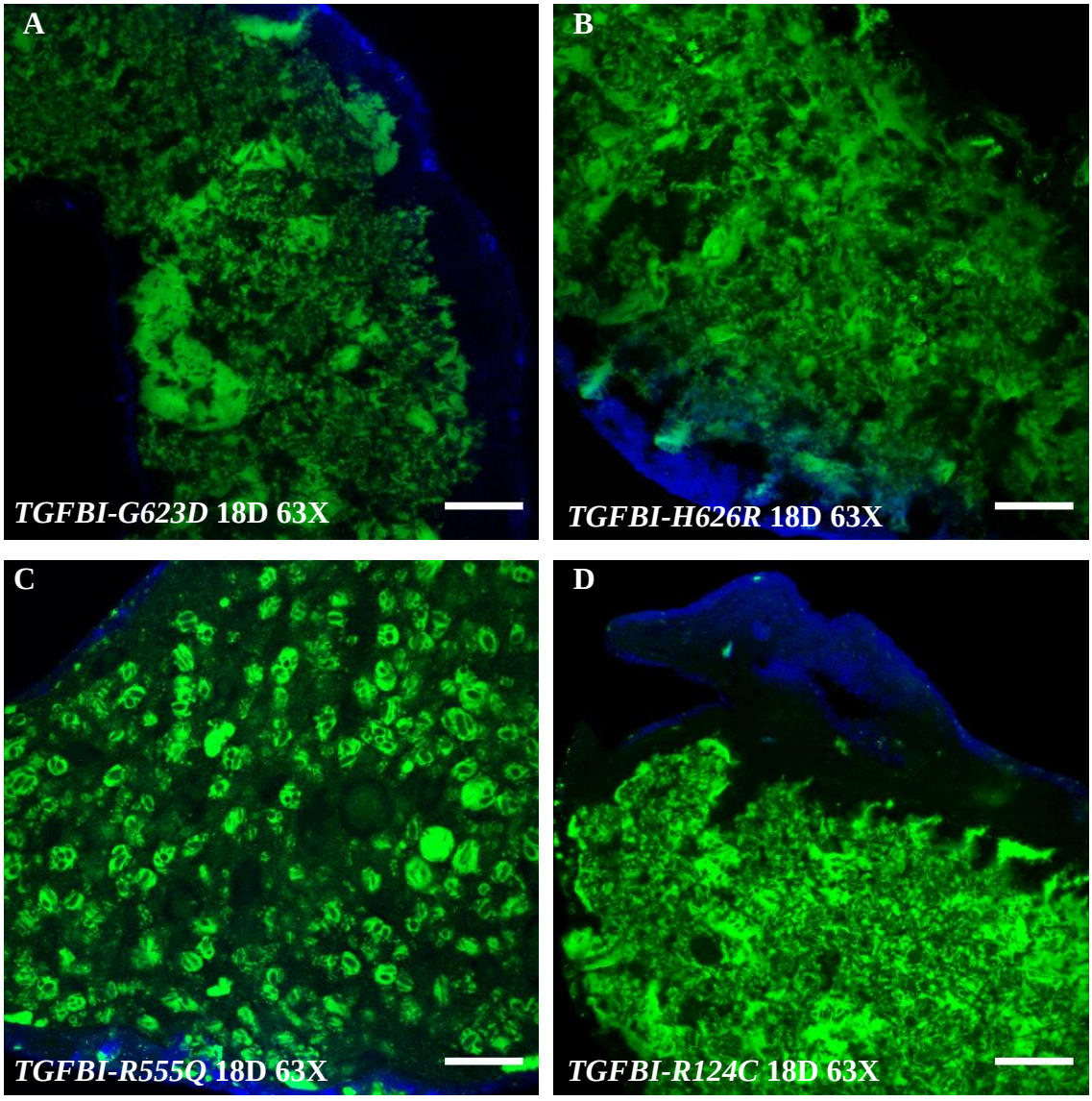

Figure 6.39: Comparison of MFAS in AG lumens at 18 days. AGs were imaged by confocal microscopy using GFP and DAPI channels. AGs from virgin males stained with DAPI and imaged with confocal microscopy using GFP and DAPI channels are depicted, showing lumenal MFAS at 63X magnification. **A)** *w^{1118}; tub-GAL80^{ts}/TGFBI-G623D; dsx-GAL4 GFP-mfas/+* at 18 days **B)** *w^{1118}; tub-GAL80^{ts}/TGFBI-H626R; dsx-GAL4 GFP-mfas/+* at 18 days **C)** *w^{1118}; tub-GAL80^{ts}/TGFBI-R555Q; dsx-GAL4 GFP-mfas/+* at 18 days **D)** *w^{1118}; tub-GAL80^{ts}/TGFBI-R124C; dsx-GAL4 GFP-mfas/+* at 18 days. The distinctive flocculations produced by the unique biophysical properties conferred by *TGFBI-R555Q* are seen in **C). Scale Bar:** 10 μm.

Thus, as seen with these ageing experiments, amyloidogenic *TGFBI* mutants produce more tenacious MFAS in DCGs when evaluated at 18 days as compared to controls, flies

transgenic for *TGFBI-wild type*, and flies with an extra copy of *mfas-wild type*. Higher resolution (63X) confirmed the relative preservation of the structural integrity of these DCGs.

Furthermore, in all cases, on examination of the AG lumen at 63X magnification, at 6 days lumenal MFAS appears less prominent. MFAS can also be seen to outline microcarriers, experimental findings first reported by Dr. Mark Wainwright (personal communication). The ageing process, however imparts a disorganised, amorphous appearance to lumenal MFAS, which at 18 days also appears much more prominent.

Aged lumenal MFAS from controls, *TGFBI-wild type*, and *TGFBI*-CD mutants appears comparable in appearance. The exception to this is 18-day-aged MFAS from *TGFBI-R555Q* mutants, which has a distinctive appearance. This is consistent with the unusually tenacious amyloid characteristics imparted by this mutation (Runager et al, 2011) and may explain the early-onset, recurrent nature of the Thiel-Behnke CD it causes. Indeed, the recurrence of *R555Q*-driven CD has even prompted searches for innovative biopolymers in place of biological grafts for this particular CD (Ulag *et al.,* 2021). The glimpse afforded here of its basic biology might explain its recrudescence, and might hopefully provide therapeutic clues against this individual keratopathy.

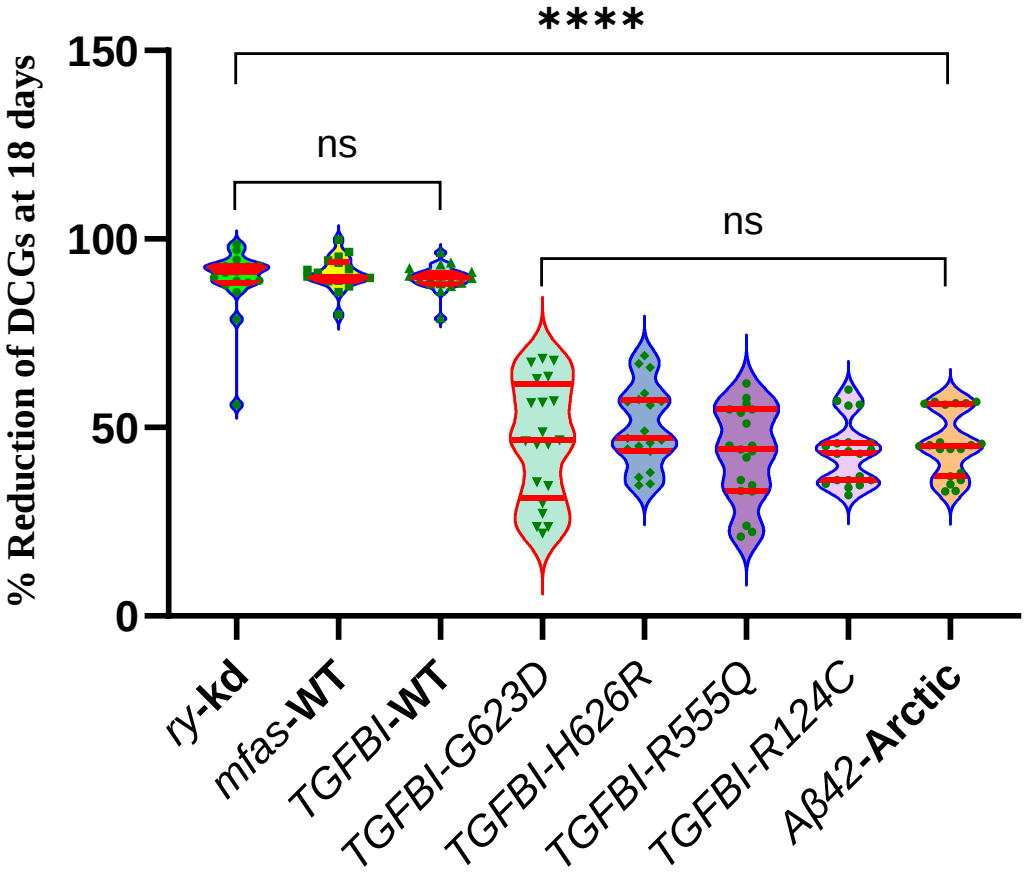

Figure 6.40: Amyloidogenic mutations, both in *TGFBI* and *Aβ*$_{42}$, result in less age-related attrition of DCGs as measured by their disintegration at 18 days. At this time point, most of the DCGs of *ry*-kd controls, *mfas-wild type* and *TGFBI-wild type* had degenerated and dissipated. All listed genotypes were driven by *w*^{1118}*; tub-GAL80*^{ts}*/CyO; dsx-GAL4 GFP-mfas/TM6B* (DTMFAS). Red lines are the mean values from different sets of experiments.

These results show that amyloid mutations are relatively tenacious over time when compared to their wild type counterparts. This is in agreement with results presented in earlier sections on rescues (**§ 5.2.4.1** to **§ 5.2.4.5,** and **§ 6.2.6.1** to **§ 6.2.6.5**), showing similar DCG-stablilising outcomes when human amyloidogenic genes were introduced into the *Drosophila* genome in a background of DCG-destablilising mutations. Specifically, this was seen in the interactions between *TGFBI* mutant lines (which

produced deformed but intact DCGs), and *APPL-RNAi* (which produced no intact DCGs, but rather mini-cores instead). In progeny from this cross, the DCG-stabilising effect of TGFBI amyloid mutations effected a partial rescue of the DCG-dispersive effect of *APPL*-kd. Similarly and more convincingly, when *$A\beta_{42}$-wild type* and *$A\beta_{42}$-Arctic* were crossed with *APPL-RNAi* and *$GAPDH_2$-RNAi*, the DCG-organising effects of the former two genotypes partially rescued the DCG-dispersive effects of the latter two. Intriguingly, the ameliorative or rescue powers of human amyloidogenic genes roughly followed their known powers of clinical amyloidogenicity. These results have prompted considerations into whether ageing experiments in this *Drosophila* system might be refined and developed into a standardized model of amyloid tenacity. The findings presented here certainly appear to support this idea, and in doing so might provide another experimental platform from which to test human amyloid diseases.

6.3 DISCUSSION

6.3.1 THE INFLUENCE OF *APP* AND *$A\beta_{42}$-WT* ON DCGs

Results in previous sections have established that *Drosophila* MFAS, which comprises the substance of DCGs and is essential for their formation, is a sensitive responder to the influence of amyloidogenic and potentially amyloidogenic molecules. DCG's reactivity to perturbations in these molecules was first demonstrated in **Section 4**, where I showed that APPL, the precursor of *Drosophila* Aβ and the homologue of human APP, influences the behaviour of MFAS in forming normal DCGs, insofar as APPL is required for the physiological fusion of MFAS particles. In the same section, I showed that GAPDH2, the *Drosophila* homologue of human GAPDH (a molecule specifically associated with amyloid neurodegenerative diseases), is also integral to the fusion process of MFAS

moeities as they form DCGs. Another surprising result was revealed in **Section 5**, where I showed that TGFBI, a human corneal amyloidogenic protein which only recently gained prominence in disease causation, also influences MFAS in its biogenesis of normal DCGs. And finally in **Section 6**, I demonstrated MFAS' susceptibility to the influence of human APP, an amyloidogenic molecule well-known because of its historical associations with Alzheimer's disease.

The value and integrity of the above-mentioned findings are strengthened by the fact that the unmanipulated versions of all these amyloid-associated molecules – APPL, GAPDH2, TGFBI and APP – had no effect on the physiological formation of normal DCGs. Thus, for *APPL* and *GAPDH2*, the DCG mini-core phenotype only appeared pursuant to their knockdown. Similarly, for *TGFBI* and *APP*, DCG abnormalities emerged only in response to the overexpression of their amyloidogenic mutations. With these discoveries, I established the *Drosophila* amyloid MFAS as an excellent barometer to report developments in interrelated amyloid molecules.

I also found that the overexpression of wild type human APP as well as overexpression of its internal, cleavage-derived fragment, wild type $A\beta_{42}$, as expected by their non-mutational status and in keeping with this tenet, led to the production of normal DCGs. However, in approximately 35 % of DCGs in SCs expressing *$A\beta_{42}$-wild type*, the central part of the core did not appear to contain any GFP-MFAS, reminiscent of the shape of a doughnut (**Figure 6.8D; Figure 6.9B**). Intriguingly, the absence of amyloidogenic mutations in these

potentially pathological precursors did not abolish their rescue properties over the mini-core phenotype of the *APPL*-knockdown (**Figure 6.30**), suggesting that these precursor molecules have innate amyloid-like properties themselves. Thus, the 'doughnut-like' central clearing seen with $A\beta_{42}$-wild type DCGs is likely a reflection of some degree of potential amyloidogenic activity seen even with this wild type version of the $A\beta_{42}$ molecule, which is directing the reorganisation of MFAS,. I therefore suggest that amyloidogenicity as we know it runs deeper than our current understanding of it allows, an idea I will expand upon in ensuing sections of this discussion.

6.3.2 THE EFFECTS OF *APP-ARCTIC, DUTCH, IOWA,* AND *SWEDISH* MUTATIONS ON DCGS

The fidelity of DCGs' reportage of the fates of various amyloids is even better demonstrated in its response to mutations. Thus, while *$A\beta_{42}$-wild type* produces normal to doughnut-shaped DCGs as noted above, the notoriously pathogenic *$A\beta_{42}$-E693G-Arctic* mutation causes a reorganisation of over 90 % of DCGs into 'targetoid' concentric circles of GFP-MFAS **(§ 6.2.1**, **Figure 6.8)**, intriguingly similar to the targetoid plaques it characteristically produces in human brains. This suggests that these peptides can play a role in organising DCGs within SCs, perhaps providing a central assembly point around which GFP-MFAS mini-cores cluster. The remarkable similarity between Aβ-Arctic's concentric-circled DCGs in *Drosophila,* and its concentric-circled plaques in humans, suggests that the organising principle of this particular amyloid mutation, however it might function, is orchestrating an identical pattern of reorganisation in two different target amyloid proteins.

Immunostaining of these targetoid amyloid plaques from patients with the *$A\beta_{42}$-E693G-Arctic* mutation showed that the outermost corona contained $A\beta_{1-42}$ peptides, the intermediate zone contained $A\beta_{17-24}$ species, while the centre of the target contained N- and C-terminal truncated $A\beta_{1-5}$ species (Kalimo *et al.,* 2013). I attempted immunostaining experiments of Artic mutation DCGs, however the delicate monolayer of AGs did not withstand the harsh alcohol washes the protocol called for.

Arctic-$A\beta_{40}$ species also have a strong propensity to form protofibrils (Nilsberth et al., 2001) as they proceed through the amyloid cycle (**Figure 1.17**), which then leads them to an accelerated phase of abundant amyloid fibril formation without the normally encountered aggregation lag phase (Hatami *et al.,* 2017, Seuma *et al.,* 2022). In addition, *Arctic* oligomers, protofibrils and protofilaments have been found to be structurally unique (Fawzi *et al.,* 2008; Gessel *et al.,* 2012). Furthermore, the E693G substitution leads to a smaller-sized side chain on each oligomer, promoting the formation of hydrogen bonds between mutant Aβ molecules, and thus further enhancing the formation of filaments (Yang *et al.,* 2023). An *in vitro* study also showed the behavioural uniqueness of $A\beta_{40}$-Arctic, in that it is induced into misfolding by wild type-$A\beta_{42}$ seeds, while wild type-$A\beta_{40}$ in the same solution remained unaffected (Yoo *et al.,* 2018). This study was pointed to as *in vitro* evidence of the prionoid crosstalk of Aβ mutants. Aβ-Arctic's toxicity has also been reported in multiple experimental systems including cultured human neuroblastoma cells (Peralvarez-Marin *et al.,* 2009) and mouse hippocampus, where it caused an increase in Tau phosphorylation and Tau-dependent neurodegeneration (Tackenberg *et al*., 2020).

Finally, its many unique qualities also extend to its clearance, since $A\beta_{40}$-Arctic was found to be resistant to neprilysin-catalysed proteolysis (Tsubuki *et al.*, 2003).

Both the *$A\beta_{42}$-E693Q-Dutch* and *$A\beta_{42}$-D694N-Iowa* FAD mutations when overexpressed in *Drosophila* SCs produce fragmented-appearing DCGs consisting of mini-cores interspersed with the occasional deformed DCG **(§ 6.2.2**, **Figure 6.10).** Biophysically, the *Aβ42-E693Q-Dutch* mutation, while not causing major side-chain alterations, does eliminate a negative charge, thus lowering the repulsion between Aβ monomers and thereby the barriers to nucleation as well, both of which enhance fibrillation (Yang *et al*., 2018, Lee *et al.*, 2021). The mutation also produces a high proportion of β-sheets which, unlike α-helical structures are known to promote aggregation. In particular, a β-turn in its midsection causes an even greater enhancement of aggregation (Miravelle *et al.*, 2000; Murukami *et al.*, 2003). Finally, the mutated Dutch peptide inserts itself into cell membranes, disrupting their integrity (McKnelly *et al.*, 2022), and in doing so displaces in particular normal Aβ peptides from endosomal membranes and lumens within synapses, thereby causing neuronal dysfunction (Kim and Bezprozvanny, 2023).

The biophysical upshot of the *$A\beta_{42}$-D694N-Iowa* mutation, on the other hand, has been shown *in vitro* to be the production of a turn rather than a bend motif in the resultant oligomer, which enhances fibrillogenesis and Aβ-induced toxicity (Krone *et al.*, 2008; Van Nostrand *et al.*, 2001; Van Nostrand *et al*., 2002). Interestingly, the D694N mutation lies

within an APP cholesterol-binding site although the significance of this in terms of disease causation is unclear (Barrett *et al*., 2012),

These three intra-$A\beta_{42}$ mutations (*Arctic*, *Dutch* and *Iowa*) in addition to causing FAD, cause an additional clinical syndrome within this cohort of Alzheimer's patients known as Cerebral Amyloid Angiopathy (CAA). This is characterized by the deposition of $A\beta_{40}$ in the walls of cerebral arteries, arterioles and capillaries, leading to microaneurysm formation and intracerebral hemorrhages (reviewed in DeSimone *et al.*, 2017). Despite the early onset of their Alzheimer's disease manifestations, FAD patients with CAA have the relative preservation of cognitive function. Unfortunately, however, the disease-defining recurrent intracerebral haemorrhages of CAA result in the shortening of their lifespans (Tomidokoro *et al*., 2010). In keeping with their theme of causation of a distinctive and unvaryingly lethal clinical syndrome, the overexpression of intra-$A\beta_{42}$ mutations in *Drosophila* SCs likewise also produces unmistakeable and immediately recognizable DCG phenotypes. Thus, as seen earlier, the *Aβ-Arctic* mutation produces targetoid DCGs, while the *Aβ-Dutch* and *Aβ-Iowa* mutations produce mini-cores.

The *APP-K595N/M596L-Swedish* double mutation lies just outside the $A\beta_{42}$ sequence, towards the N-terminal end of APP (Mullan *et al.*, 1992). In keeping with the axiom that only intra-$A\beta_{42}$ mutations produce CAA, the Swedish mutation does not cause this clinical syndrome. Rather, it leads to severe early cognitive impairment starting at a mean age of 53, and a rapid clinical decline punctuated by intractable seizures and myoclonic jerks in

65 % of patients (Axelman *et al.,* 1994). Regarding DCG morphology, unlike the intra-$A\beta_{42}$ mutations, the *APP-Swedish* mutation generates a lesser number of intact DCGs (about 2-6 per SC) amidst a background of tiny mini-cores (**Figure 6.12**). The constant feature of SCs with the *APP-Swedish* mutation, however, was their overall pathological appearance, heightened by the invariable presence of large lysosomes, suggesting the recruitment of a mechanism to clear pathological proteins.

The Swedish mutation increases total Aβ levels by increasing BACE-1 cleavage of APP at the primary β-site (M^{671}-D^{672}) rather than at the secondary β'-site (T^{681}-Q^{682}) (Kimura *et al.,* 2016). Cleavage at the β-site favours the production of amyloidogenic Aβ peptides, unlike cleavage at the β'-site, which generates amyloidolytic fragments (Kimura *et al.*, 2016; Nilsberth *et al.,* 2001). In increasing the total amount of Aβ peptides, it does so without altering the $A\beta_{40}/A\beta_{42}$ ratio, unlike other APP and Presenilin mutations, which favour the generation of larger, more aggregation-prone Aβ species (Scheuner *et al.,* 1996). This increase in total Aβ peptides in turns leads to synaptic toxicity and loss in mice, although in cultured human neurons bearing the Swedish mutation, synapse numbers and therefore synaptic transmission paradoxically increase (Zhou *et al.,* 2022). The diverse and often undefined effects of the Swedish mutation almost seem replicated in the multiple pathologies of *Drosophila* SCs in where it is overexpressed.

6.3.3 EFFECTS OF *$GAPDH_2$-RNAi, APPL-RNAi, $A\beta_{42}$-WT, $A\beta_{42}$-ARCTIC* AND *APP-SWEDISH* ON EXOSOME SECRETION

Exosomes are small extracellular vesicles (EVs) which begin as intraluminal vesicles (ILVs) in multivesicular endosomes (Möbius *et al.,* 2002; White *et al.,* 2006; Colombo *et*

al., 2014). Released by all cells, they mediate intercellular communication in a wide range of physiological and pathological processes, including neurodegeneration (Thompson *et al.,* 2016) and metastatic cancer where they reprogramme the tumour microenvironment (Becker *et al.,* 2016; Comito *et al.,* 2020; Saber *et al.,* 2020). They exist in heterogenous populations, carry diverse cargoes, and are most likely generated by different triggering influences. At least two such exosome-generating mechanisms have been identified in Multivesicular Endosomes (MVEs), one of which involves the Endosomal Sorting Complex Required for Transport (ESCRT) which plays a role in numerous processes including neurogenesis (Loncle *et al.,* 2105). In keeping with this multifaceted role, ESCRT malfunction is associated with several diseases (reviewed in Saksena and Emr, 2009). In mammals, *Chmp2b* (Charged MVB Proteins 2b) is the homologue of yeast Vacuolar Protein Sorting 2 (*VPS2*), and is associated with Frontotemporal Dementia and Amyotrophic Lateral Sclerosis, both amyloid-associated neurodegenerative diseases (Schmidt and Teis, 2012). Previously, the Wilson laboratory had demonstrated that *Chmp2b* knockdown resulted in a decrease in exosome production (Marie *et al*., 2023), and I therefore used *Chmp2b*-kd as a positive control in my experiments.

With these experiments, I demonstrated that despite the extensive links between the tested genes and neurodegeneration, neither the overexpression nor the knockdown of any of them had any effect on exosome production. The fact that *Chmp2b*-knockdown (used as a positive control) resulted in decreased exosomes confirms earlier results from our laboratory that accessory ESCRT-III proteins regulate Rab11 exosome formation through an ESCRT-dependent process, independent of the ubiquitinylation-deubiquitinylation

cycle for loading of cargoes (Marie *et al*., 2023). In these experiments, all performed on amyloid-associated genes shown to affect DCG biogenesis, I demonstrate the insularity of these connections. Specifically, while manipulations of these genes profoundly affect DCGs, they do not perturb the elemental cellular function of exosome production.

6.3.4 EFFECTS OF KNOCKDOWN OF RETROMER COMPONENTS VPS26 AND VPS39 ON DCGs

As discussed in the introductory section (**§ 6.1.2**), the retromer is a multimeric protein complex essential for recycling and retrieving protein cargoes from the endosome to the trans-Golgi network or the cell surface. Mutations or deficiencies in retromer components, by impeding this normal traffic, result in the accumulation of abnormal protein aggregates. As aberrant protein accretions are the very hallmark of amyloid neurodegenerative diseases, connections between retromer dysfunction and neurodegeneration were quickly identified. Since the results I presented earlier have shown a clear link between neurodegeneration-associated genes and DCGs, I decided to investigate any possible connections between the retromer and DCGs by knocking down *VPS26* and *VPS39*, which encode for two essential components of it's cargo-recognition core. Indeed, low levels of VPS26 and VPS39 in the entorhinal cortex are the earliest known findings of AD, far predating any clinical manifestations of the disease itself (Small *et al*., 2005).

The suggested reason for this is that the entorhinal cortex (Brodman areas 28 and 34) possesses highly specialized dendritic cells, which have unique synaptic biology, structure, function, and an unusually high dependance on endosomal transport (Moser and Moser, 2011a; Moser and Moser, 2011b; Khan *et al.,* 2014). Future experiments designed along

this line of reasoning might also prove fruitful in explaining why the substantia nigra is similarly more sensitive to the effects of VPS35 depletion in Parkinson's disease (Vilarino-Guell *et al.,* 2011), and how the additional factor of mitochondrial dysfunction fits into the PD-related endolysosomal pathology of the substantia nigra (Nalls *et al*., 2014).

The retromer is strongly associated with Alzheimer's, as initially demonstrated by microarray gene expression studies showing that VPS26 and VPS35 levels are significantly reduced in the entorhinal cortex and dentate gyrus of patients with AD (Small et al., 2005). In addition, several retromer and retromer-associated mutations have been linked to a wide array of other neurodegenerative diseases. The *D620N* missense variant in *VPS35* leads to autosomal dominant Parkinson's Disease (PD) (Zimprich *et al.,* 2011; Vilarino-Guell *et al.,* 2011) by decreasing WASH recruitment to endosomes and causing the abnormal trafficking of both ATG9A (Zavodszky *et al.,* 2014) and cathepsin D (Follett *et al.,* 2014), resulting in abnormal autophagy and decreased degradation of α-synuclein respectively. Confirming these studies, the viral-mediated gene transfer of *VPS35-D620N* led to severe degeneration of nigrostriatal dopaminergic neurons in a rat model (Tsika *et al.,* 2014). PD-associated variants in the PARK16 locus gene lead to VPS35 deficiency as well as impaired Golgi and endolysosomal trafficking, and the expression of wild type VPS35 rescues these impairments (MacLeod *et al.,* 2013). Genetic variations in retromer-related genes are also strongly related with a range of neurodegenerative disorders. Thus, the *RME-8/DNAJC13-N855S* variant is associated with essential tremor (Rajput *et al*., 2014), the loss of SNX27 by influencing glutamate receptor recycling causes excitatory synaptic dysfunction and memory loss in Down's syndrome (Wang *et al.,* 2013), genetic variants in the gene

encoding the WASH complex component strumpellin cause autosomal dominant Hereditary Spastic Paraplegia (HSP) (Freeman *et al.,* 2013), and a mutation in the *Strumpellin and WASH-Interacting Protein* (*SWIP* or *KIAA1033*) gene which reduces SWIP and destablises the entire WASH complex is linked to autosomal recessive intellectual disability (Ropers *et al.,* 2011). Rab7 regulates retromer recruitment to endosomes, and mutations therein are linked to Charcot-Marie-Tooth neuropathy (Verhoeven *et al*., 2003). Additionally, genetic variations in the retromer cargo-binding molecule SORCS2 are linked to bipolar disorder (Ollila *et al*., 2009) and schizophrenia (Christoforou *et al.*, 2011).

As shown in my knockdown experiments of retromer's cargo recognition complex components VPS26 and VPS35, the number of DCGs per SC significantly increased compared to controls. Given the preliminary nature of these experiments, designed primarily to test this *Drosophila* system on a burgeoning area of neurodegeneration research, few definitve conclusions can be drawn. A plausible mechanistic explanation is that DCG compartments are not fusing to the plasma membrane at their normal rate, quite likely because of improper maturation, which then leads to the accumulation of these compartments in SCs. The consistently-obtained results shown here thus establish a definite link between mammalian retromer cargo recognition core components and *Drosophila* MFAS, which in the preceding sections has been demonstrated to be a high-fidelity model for the study of amyloidogenic degenerative diseases. The prospect, therefore, of applying this fly model to an ever-expanding list of endolysosomal

neurodegenerative disorders caused by retromer dysfunction holds out enormous promise in studying this vast swathe of diseases.

6.3.5 INTERACTIONS BETWEEN ALZHEIMER'S GENES AND 'MINI-CORE' PRODUCING GENOTYPES

The mini-core producing genotypes are *APPL*- and *GAPDH2*-knockdowns, which, as the data so far suggest, bring about the non-fusion of MFAS particles through different underlying mechanisms. *UAS-APPL-RNAi* constructs were therefore combined with *UAS-APP*, *UAS-$A\beta_{42}$-wild type* and *UAS-$A\beta_{42}$-E693G-Arctic* constructs to test whether the amyloidogenic properties of the latter three genotypes overcame the mini-core genesis of the former. Additionally, *UAS-GAPDH2-RNAi* constructs were combined with *UAS-$A\beta_{42}$-wild type* and *UAS-$A\beta_{42}$-E693G-Arctic* constructs for similar testing.

6.3.5.1 INTERACTIONS BETWEEN HUMAN *APP*, HUMAN *$A\beta_{42}$-WILD TYPE*, AND *DROSOPHILA APPL-RNAi*

Consistent with earlier results, overexpressing *$A\beta_{42}$-wild type* resulted in normal DCGs (**Figure 6.8B** and **D**; **Figure 6.26B**), albeit with a slight central clearing which I describe as 'doughnut-shaped' or the 'doughnut' phenotype. I showed earlier that the overexpression of *APP* also produces normal DCGs (**Figure 4.29B**; **Figure 6.20B**), intriguingly, with the occasional production of the doughnut phenotype, but to a significantly lesser extent than does the overexpression of it's internal fragment, *$A\beta_{42}$-wild type* (statistical data not shown). In other words, the slightly more pronounced doughnut phenotype produced by overexpression of *$A\beta_{42}$-wild type* suggests that there is some organising activity in the cleavage product that does not emerge when it's parent molecule APP is overexpressed in its entirety.

In the case of the combination of *UAS-APP* and *UAS-APPL-RNAi*, as shown in **Figure 6.20D** the resultant phenotype has a combination of intact cores and mini-cores within the same compartment space, suggesting a partial rescue. This primarily argues that human APP can undertake the function of, or substitute for *Drosophila* APPL. This provides yet further evidence that amyloids across species are related, and, as has been suggested, can influence each other. Furthermore, this also confirms that the *APPL*-knockdown mini-core phenotype is indeed due to loss of APPL function, and not just an off-target effect.

When considering the roughly equivalent rescue outcome of *APPL-RNAi* by *Aβ42-wild type*, the results show that both APP, the potentially amyloidogenic parent molecule, as well as $A\beta_{42}$-wild type, its potentially amyloidogenic derivative, can both partially rescue *APPL-RNAi'*s mini-core phenotype. Extending the argument made above, that human APP appears to be substituting for *Drosophila* APPL, it would therefore seem that $A\beta_{42}$-wild type is doing the same thing.

The interpretation of this rescue merits further study, since there are emerging aspects to both APP and Aβ-wild type. In particular, Aβ-wild type is being shown to have roles in both health and disease (reviewed in Puzzo *et al.*, 2015; Chen *et al*., 2017; Karisetty *et al*., 2020). The seemingly physiological attributes of Aβ include the finding that it is produced in healthy brains during normal neuronal activity, and is required for memory and synaptic plasticity (Puzzo *et al*., 2015). Aβ has been found inside neurons, including infant neurons, and increases rapidly from age 4-8 years, a growth period which is characterised by high

brain plasticity. In adulthood, the majority of neurons have Aβ, while this proportion decreases by 20 % with age (Blair *et al.,* 2014). At the molecular level, it is increasingly recognized that Aβ species bind to and modulate various receptors. Examples of this include the competition between $A\beta_{40}$ and $A\beta_{42}$ for the insulin receptor (Xie *et al*., 2012), the binding of different Aβ species to hippocampal neurons and their subsequent modulation of neurotransmission depending on their concentrations (Moreth *et al*., 2013), and the interaction of $A\beta_{40}$ with cholinergic nicotinic receptors (nAChRs) – α7-nAChRs at lower picomolar concentrations, and both α7- and α4β2-nAChRs at higher nanomolar concentrations (Mura *et al.,* 2012). This aligns with other studies which show that low concentrations of a mixture of Aβ monomers and oligomers enhances long-term potentiation, synaptic plasticity, and memory, with a mechanism dependent on nAChRs (Puzzo *et al.,* 2008; Morley *et al.,* 2010), while a pathological accumulation of Aβ causes synaptic failure (Puzzo *et al.,* 2012; Puzzo and Arancio, 2013).

Numerous loss-of-function studies have also shown that Aβ is required for normal neuronal plasticity. For example, BACE-1 KO mice demonstrate dysfunction in transmission and plasticity in hippocampal neurons (Laird *et al*., 2005; Wang *et al.,* 2008), as well as numerous cognitive and behavioural abnormalities (Laird *et al.,* 2005; Savonenko *et al.,* 2008). Intriguingly, the cognitive defects in BACE1-KO mice were rescued by *APP-Swedish; Presenilin-1-ΔE9* transgenes (Laird *et al.,* 2005). PS-KO mice on the other hand, have normal neuronal transmission and plasticity, but defects in long-term spatial memory (Yu *et al*., 2001) as well as a premature progressive form of neurodegeneration appearing at the age of 4 months, which is accompanied by mitochondrial abnormalities (Wines-

Samuelson *et al*., 2010). These neurological deficits were reproduced in mice treated with inhibitors of β- and γ-secretases, and antisense or siRNA against APP. While the blockage of other APP cleavage fragments was cited in criticsm to these studies, the specific blockage of endogenous Aβ faithfully re-created these neurological abnormalities (Garcia-Osta and Alberini; Morley *et al*., 2010; Puzzo *et al*., 2011). Additionally, regardless of whether these abnormalities were induced by inhibitors of β- and γ-secretases or by Aβ antibodies, they were rescued by picomolar concentrations of Aβ (Plant *et al.*, 2003; Puzzo *et al.*, 2011), effects shown to be mediated by a highly potent agonistic action by the N-terminal end of Aβ on nicotinic recptors. This positive effect, in turn, was blunted by the co-administration of a nicotinic antagonist (Lawrence *et al.*, 2014). Finally, it has been well-established that Aβ modulates α7-nAChR function, acting either as an agonist or antagonist depending on the dose administered (Dineley *et al*., 2007; Khan *et al.*, 2010; Lawrence *et al*., 2014), a fact that is being used to devise therapeutic strategies against AD (reviewed in Karisetty *et al.*, 2020).

In light of this data suggesting a physiological role for Aβ-wild type, the fact that both APP and $A\beta_{42}$-wild type are able to rescue the mini-core-producing effect of *APPL-RNAi* takes on added significance. Furthermore, both APP and $A\beta_{42}$ when mutated, generate pathological amyloid: APP-Swedish in the case of APP, and a plethora of FAD-causing intra-$A\beta_{42}$ mutant oligomers in the case of $A\beta_{42}$. This result, therefore, lends credence to the growing conviction that amyloid precursors and their amyloid byproducts might in fact be a continuum, rather than separate entities demarcated by the boundaries of a point mutation, or constrained by a line defining their crossover into the realm of abnormal

processing. This view has the potential to explain the vagaries of amyloid diseases, which are known to defy conventional characterization. It would also support the age-old observation that amyloid neurodegeneration seems to be spurred on by comorbities like cerebrovascular disease, diabetes, inflammation, and mitochondrial dysfunction. Perhaps a perfect storm is required to move a needle that is poised to move.

6.3.5.2 INTERACTION BETWEEN *$A\beta_{42}$-E693G-ARCTIC* AND *APPL-RNAi*

The interaction between *UAS-$A\beta_{42}$-E693G-Arctic* and *UAS-APPL-RNAi* shows a much more pronounced rescue of *APPL*-knockdown's mini-core phenotype when compared with attempts using *UAS-APP* and *UAS-$A\beta_{42}$-wild type*. This seems reflective of the superior organisational properties *$A\beta_{42}$-E693G-Arctic* has previously shown in directing MFAS to reorganise into the visual appearance of concentric circles.

This result is not completely unexpected, since the *$A\beta_{42}$-E693G-Arctic* mutation is known to produce tenacious Aβ plaques in the brain. Indeed, its heft, both literally and figuratively, was shown in one of the earliest descriptions of the *$A\beta_{42}$-Arctic* mutation. Here, the extent of Aβ deposits in the brains of *Arctic* AD patients was described as 'massive', and the authors observed that the brain weights were 'considerably higher' than those seen with sporadic AD. They also noted that while AD brains were usually atrophic and smaller, no systematic studies had been undertaken comparing brain weight with amyloid burden (a lacuna in scholarship which remains true even today). Finally, they remarked: "Interestingly, the brain weights in three of the five *PS1Δ9* AD patients with large cotton wool plaques of similar abundance as Aβ plaques in our *Arctic* patients' brains were within normal limits" (Kalimo *et al*., Acta Neuropathologica Communications 2013, 1:60, pg. 13).

The same authors also found that Arctic plaques were ‘large’ and ‘embraced’ neurons, leaving the affected neocortical pyramidal and cerebellar Purkinje neurons viable despite completely engulfing them. They concluded that since *Arctic* plaques did not directly damage neurons or neuronal perikarya, their AD-inducing effects must spring from some hitherto unidentified form of neurotoxicity (Kalimo *et al*., 2013).

It is well-established that the *Arctic* mutation interferes with the processing of APP by making it less prone to α-secretase cleavage, thereby leaving more APP available for amyloidogenic β-cleavage, while also increasing the level of β-secretase cleavage itself (Sahlin *et al*., 2007). The fibrils produced by the *Arctic* mutation themselves have been shown to have at least 4 different forms, and specific post-translational modifications of each of these forms were suggested as reasons for their distinctive plaque appearance (Norlin *et al.,* 2012). While these disparate observations do not completely explain the *Arctic* mutation’s propensity to form targetoid amyloid structures, or, in these experiments, to persuasively rescue mini-core phenotypes, they certainly indicate that there are several unique aspects to this distinctive mutation.

In summary, both *APP* and it’s derivative, *$A\beta_{42}$-wild type*, have the same efficacy in rescuing *APPL-RNAi,* as judged by the shift from non-intact to intact DCGs when these genotypes were combined with *APPL-RNAi.* Thus, this percentage went from 7 % intact DCGs with *APPL-RNAi* alone, to 80 % when *APPL-RNAi* is combined with *APP, $A\beta_{42}$-wild type,* or *$A\beta_{42}$-E693G-Arctic*. Intriguingly, both *$A\beta_{42}$-wild type* and *$A\beta_{42}$-E693G-Arctic*

show the same efficacy in rescuing *APPL-RNAi*, each producing approximately 80 % intact DCGs when combined with an *APPL*-knockdown. However, the objective DCG scoring criteria belie the actual appearance of DCGs in these rescue experiments, in which *$A\beta_{42}$-E693G-Arctic* DCGs are far more well-knit than the irregular-appearing DCGs with the *APP* and *$A\beta_{42}$-wild type* rescues.

6.3.5.3 INTERACTION BETWEEN *$A\beta_{42}$-WILD TYPE* AND *GAPDH2-RNAi*

As shown earlier, *$A\beta_{42}$-wild type* is able to rescue the mini-core phenotype of *APPL-RNAi* (**Figure 6.22D** and **Figure 6.23**). Therefore, *$A\beta_{42}$-wild type* was tested for its rescue effects on *GAPDH2-RNAi*, another genotype that produces mini-cores is. However unlike the uniformly distributed mini-cores of the *APPL*-knockdowns, *GAPDH2*-kd produces mini-cores in a 'pearls-on-a-string' appearance **(§ 4.2.1, Figure 4.8B**). Furthermore, as discussed in **Section 4**, time-lapse videos of *APPL-RNAi* and *GAPDH2-RNAi* showed very different motility behaviours of the mini-cores. My time-lapse videos of *APPL-kd* mini-cores showed that they did not move, while in comparison videos of *GAPDH2-kd* made by a colleague showed that these mini-cores did move, but then did not fuse when they met or collided (Adam Wells, personal communication). Having concluded that there appears to be a fundamental mechanistic difference between the way *APPL*-kd and *GAPDH2*-kd mini-cores are produced, I attempted rescues of *GAPDH2*-kd first with *$A\beta_{42}$-wild type*, and then with *$A\beta_{42}$-E693G-Arctic.*

As seen in the results section, overexpression of *$A\beta_{42}$-wild type* does not affect normal DCG formation, other than producing a slight increase in the numbers of DCGs with a doughnut

phenotype (**Figure 6.26B**). *GAPDH2-RNAi* produces mini-cores with its distinctive 'string of pearls' appearance **Figure 6.26C**. However, the combination of *$A\beta_{42}$-wild type* and *GAPDH2-RNAi* in the same fly produced compartments which included mini-cores from the *GAPDH2-RNAi* influence, as well as a larger core from the *$A\beta_{42}$-wild type* influence (**Figure 6.26D** and **E**). It was noticeable, however, that the shapes of the *$A\beta_{42}$-wild type* DCGs in the rescue attempts were more irregular and abnormal-appearing than DCGs produced by rescue attempts driven by *$A\beta_{42}$-E693G-Arctic* (**§ 6.2.6.5**). This is consistent with the greater organising power of the *$A\beta_{42}$-E693G-Arctic* mutation as compared to its non-mutated version, *$A\beta_{42}$-wild type*, as was demonstrated in **§ 6.2.1**, **Figure 6.8D** and **E**. The apparent explanation, then, for the somewhat irrgeular shapes of the *$A\beta_{42}$-wild type* DCGs seen here would be the greater 'glueing' power that amyloidogenic transformation confers upon *$A\beta_{42}$-E693G-Arctic*, which I previously demonstrated in *$A\beta_{42}$-E693G-Arctic's* rescue of *APPL*-kd (**§ 6.2.6.3, Figure 6.24D** and **E**). Without the glueing power of a powerful amyloidogenic mutation like *$A\beta_{42}$-E693G-Arctic*, *$A\beta_{42}$-wild type* DCGs would be less likely to hold their shape when confronted with the DCG-dispersive influence of *GAPDH2*-kd. This would account for *$A\beta_{42}$-wild type's* seemingly 'weaker' rescue when compared to the more robust rescue effected by *$A\beta_{42}$-E693G-Arctic*, as is discussed below.

6.3.5.4 INTERACTION BETWEEN *$A\beta_{42}$-E693-ARCTIC* AND *GAPDH2-RNAi*

$A\beta_{42}$-E693G-Arctic is more effective in rescuing *APPL-RNAi* than in rescuing *GAPDH2-RNAi* (with the production of 80 % versus 68 % intact DCGs resulting from their combinations with *APPL-RNAi* respectively). Taken together, these data show the following: **a)** $A\beta_{42}$-wild type on its own confers some amyloidogenic adhesivity. **b)** $A\beta_{42}$-

E693G-Arctic, shown to cause greater organization of dense-cores, is nonetheless no more effective than $A\beta_{42}$-wild type in rescuing the mini-cores seen with *APPL-RNAi*. This is despite the fact that on visual inspection, DCGs from $A\beta_{42}$-E693G-Arctic rescues appear more well-knit than those from $A\beta_{42}$-wild type rescues, and **c)** $A\beta_{42}$-E693G-Arctic exerts a greater rescue effect over *GAPDH2-RNAi* than $A\beta_{42}$-wild type does over *GAPDH2-RNAi*. The last point allows for the further conclusion that the *GAPDH2*-knockdown is in some way fundamentally different from the *APPL*-knockdown. This is because with the *APPL*-kd, a rescue is effected by APPL-related molecules: specifically, by APPL's human homologue, APP, and by APP's cleavage derivates $A\beta_{42}$-wild type and $A\beta_{42}$-E693G-Arctic. With the *GAPDH2*-kd, there is already APPL in the flies, but that fails to rescue the mini-core phenotype of *GAPDH2*-kd. These differences between the MFAS-fusion-inducing or fusion-allowing properties of APPL and GAPDH2 are also reflected in the patterns of mini-cores produced by *GAPDH2* and *APPL* knockdowns, with the former producing a 'string of pearls' appearance in which MFAS adheres to the compartment membrane, while the latter produces larger mini-cores which appear to be distributed throughout the volume of the compartment, with the frequent presence of a centrally-appearing 'nidus'. These differences in mini-core biogenesis patterns, along with differences in motility patterns of these two sets of mini-cores, have been captured in time-lapse videos (Singh et al., manuscript in preparation).

The theme emerging through these experiments is that conserved amyloid proteins seemingly influence each other. This is seen firstly with the rescue of *APPL*-kd's mini-core phenotype by human APP. This tells us that conserved amyloid molecules can substitute

for each other's functions in fly SCs. It also tells us that in the rescue of an *APPL* loss-of-function phenotype, $A\beta_{42}$-E693G-Arctic's amyloidogenic activity is not required for DCG aggregation in the same way it is for the *GAPDH2*-kd, where its organising power is substituting for the loss of a completely different gene. Rather, $A\beta_{42}$-wild type and $A\beta_{42}$-E693G-Arctic proteins, both internally located segments of APP, the first physiological and the second amyloidogenic, are equally successful as their parent APP in rescuing *APPL*-kd's mini-core phenotype. This suggests that here, the rescue is not a function of amyloidogenic pathogenicity, but rather a reflection of a common ancestral amyloidogenic provenance. While my results are to the best of my knowledge the first to demonstrate a structural rescue between APP family members, a functional rescue was shown years ago by Luo, who found that transgenes encoding APPL or APP both rescue behavioural defects of *APPL* null flies (Luo 1992, Ph.D. thesis, Brandeis University). This further underscores the beauty of this *Drosophila* DCG model, which I believe going forward will corroborate previous functional studies with corresponding visible, structural underpinnings.

6.3.6 THE DURABILITY OF *$A\beta_{42}$-WT*, *$A\beta_{42}$-ARCTIC* AND *TGFBI* MUTANT DCGs AS SHOWN BY AGEING EXPERIMENTS

An established property of amyloid proteins is their durability and tenacity. Indeed, their assumption of fibrillar forms, resistance to proteolysis, and insolubility are the three characteristics common to all forms of amyloid (Rambaran and Serpell, 2008). They possess a tensile strength similar to steel, an attribute they share with silk, their structural cousin (Smith *et al.*, 2006). To test this staying power, control flies and those bearing amyloidogenic *$A\beta_{42}$* and *TGFBI* mutations were aged and analyzed using confocal microscopy. Specifically, mutants were compared with controls to assess the durability of

their MFAS-comprised DCGs, which, as shown in earlier results, undergo morphological alterations when subjected to the influence of amyloidogenic mutations in either $A\beta_{42}$ or *TGFBI*. An assessment of DCG durability, as measured by stability of numbers and structural integrity, was then made at 6 and 18 days.

6.3.6.1 THE NORMAL AGEING OF DCGs IN CONTROL FLIES

At day 6, the standard age at which all imaging in this thesis was done, DCG morphology is considered representative of young adult males, and imaging at both 10X and 40X showed normal DCGs in which MFAS-GFP was concentrated. Furthermore, the AG lumens appeared clear, without the dispersion of GFP-MFAS. When aged to 18 days, however, the GFP-MFAS in DCGs appeared to be disintegrating, being dispersed instead at high levels throughout the AG lumen in a non-homogeneous pattern (**Figure 6.32**).

This result demonstrated the age-related disintegration of DCGs as was expected in control flies, as they matured from young adults to senescent animals. The dissolution of DCGs was accompanied by the visible release of GFP-MFAS into the gland lumen, from where it was swept into the ejaculatory ducts. This temporal and visual pattern of MFAS' disassembly was used as a baseline from which to gauge the tenacity-conferring properties, if any, of mutant amyloids, on MFAS.

6.3.6.2 THE AGEING OF DCGs IN $A\beta_{42}$-*WT* AND $A\beta_{42}$-*E693G-ARCTIC* FLIES

As shown previously, *Drosophila* MFAS in control flies undergoes normal age-related attrition, as evidenced by a decline in the number of DCGs and the accumulation of amorphous-appearing MFAS in the AG lumen (**Figure 6.34A** and **A'**; **Figure 6.35A** and

A'). This attritional process remains unchanged with the introduction of human *Aβ42-wild type* to the fly genome (**Figure 6.33B** and **B'**). However, with the introduction of human *Aβ42* bearing the amyloidogenic *Arctic* mutation, the resultant DCGs become more stable, as evidenced by their relative persistence in aged flies (**Figure 6.33C** and **C'**). This is consistent with the known stability of amyloid proteins. **Figure 6.34B'**, showing flies transgenic for *Aβ42-E693G-Arctic,* also demonstrates MFAS in the lumen extending to the distal tip of the AG, which turned out to be an inconsistent feature found in both control flies and mutants.

In summary, combining the results of the *Aβ42-E693G-Arctic* experiments with the previous work on MFAS secretion done in the laboratory, the model of the fate of DCGs/MFAS in flies with the *Aβ42-E693G-Arctic* mutation is that these more stable DCGs remain for longer periods in SCs, decreasing the need of SCs to secrete MFAS. Once MFAS is secreted into the lumen however, there is no obvious phenotypic differentiation between the *Aβ42-E693G-Arctic* mutants and control flies. The interpretation of this observation, however, must be tempered by the fact that once in the luminal space, MFAS, whatever its genetic background, is diluted since it is in aqueous solution rather than in an extracellular matrix.

6.3.6.3 THE AGEING OF DCGs IN *mfas-WT* AND *TGFBI-WT* FLIES

As I showed in these experiments, both wild type-*mfas* and -*TGFBI* produced DCGs which underwent the same age-related attrition as controls, as evidenced by the fact that these DCGs were lost in equal measure with time in all lines tested. This shows that in the

absence of mutation-driven amyloidogenic mutations, the genomic insertion of *mfas* and its homologue *TGFBI* confer no more longevity on DCGs than do control lines with *UAS-ry-RNAi* insertions.

Having established time-dependent dissolution of DCGs as a gauge of their tenacity, I next tested whether the insertion of *TGFBI* constructs bearing amyloidogenic mutations causing corneal dystrophies could alter the durability of DCGs.

6.3.6.4 DCG AGEING IN CONSERVED *TGFBI-G623D* AND -*H626R* MUTANTS

The prolific CD-causing amyloidogenic mutations *G623D* and *H626R* in *TGFBI* are conserved in *mfas*, it's homologue. When *TGFBI* constructs with these conserved mutations were introduced into the fly genome, they imparted tenacity to DCGs as measured by their relative durability with age as compared to controls. This is in contrast to flies overexpressing a third copy of wild type *mfas* and flies with the insertion of wild type *TGFBI*, both of which produced normal DCGs susceptible to the normal dissipation of ageing (**§ 6.2.6.7.3**).

Amyloid deposits from the domain-4 conserved mutations H626R and G623D were found to be highly thermostable compared to the wild type protein, and contained Apolipoprotein-A4, apolipoprotein-E, and the serine protease HTRA1. HTRA1 was found to be seven-fold enriched in corneal amyloid deposits of patients as compared to controls, and is known to preferentially mediate the proteolytic processing of TGFBIp amyloid mutants, particularly those found in domain-4 (Karring *et al.,* 2012; Karring *et al*., 2013; Poulsen *et al.,* 2019).

Furthermore, the peptide sequences G^{511}DNRFSMLVAAIQSAGLTETLNR^{533} and Y^{571}HIGDEILVSGGIGALVR^{588} from domain-4 of TGFBI were also enriched in H626R and G623D corneal amyloid deposits, the significance of this finding being that these sequences have a high propensity to form amyloid fibrils (Venkatraman *et al.*, 2017). Given these biophysical data, the dissolution-resistant properties of DCGs in fly lines with the TGFBI domain-4 amyloidogenic mutations G623D and H626R might have been predicted. However, an inescapable and looming fact still remained unexplained, namely, how different amyloids clearly appeared to be orchestrating the actions of others.

6.3.6.5 DCG AGEING IN NON-CONSERVED *TGFBI-R555Q* AND *-R124C* MUTANTS

Subsequent experiments addressed the question of whether the non-conserved TGFBI mutations R555Q and R124C also conferred a similar ageing-resistant effect on DCGs as did their conserved counterparts. This having also being found to be the case in results presented earlier, the likely biophysical reasons for this phenomenon are discussed below. These two non-conserved TGFBI mutations are located at either end of the molecule (in domains -4 and -1 respectively) and both cause variants of Granular CD with similar-appearing corneal deposits. The question about how mutations at opposite ends of the TGFBI molecule could cause the same CD prompted ultrastructural studies of these pathologically mutated proteins. These showed that in Granular CD Type-2, the His^{124} in one TGFBI molecule interacts with the Arg^{555} in another, while in Granular CD Type-1, the Arg^{124} in one molecule interacts with the Trp^{555} in another. As visualised by cross-linking mass spectrometry and in-line size exclusion chromatography-small angle X-ray scattering, these FAS1-1 - FAS1-4 interactions are held together by numerous hydrophobic

interactions between surrounding residues. These hydrophobic interactions between TGFBI's N- and C-terminal domains cause dimerization of mutated TGFBI molecules in solution which is repeated indefinitely in crystal packing, producing linear chains of mutated proteins. These N- and C-terminal interfaces are not permitted by the Arg^{124} and Arg^{555} residues of wild type TGFBI, since the arginines preclude the approximation of these two domains due of their size as well as because of their mutual electrostatic repulsion (Nielsen *et al.*, 2021). This therefore suggests a molecular mechanism driving the accretion of these arginine-substitution mutations TGFBI in corneal dystrophies. Furthermore, this dimerization-driven crystal packing and subsequent aggregation of mutated TGFBIp would explain the presence of rod-shaped or crystalline deposits seen by electron microscopy in the corneas of patients with Granular CD Types 1 and 2 (Iwamoto *et al.*, 1975; Klintworth, 2009).

My results showing that fly lines with *R124C* and *R555W* constructs produce tenacious DCGs are concordant with the enhanced (and explainable) molecular aggregability conferred on TGFBI by these mutations. Interestingly, although these mutations are not conserved in MFAS, TGFBI's homologue, MFAS still responds to the heightened adhesivity they bestow. This observation can be explained by the fact that the actual dimerization of mutant TGFBI molecules is not effected by these mutated residues, which merely permit the approximation of the N- and C-terminals, but by hydrophobic interactions between surrounding residues (Krissinel and Henrick, 2007; Nielsen *et al.*, 2021). It does, however, once again invoke the spectre of amyloids (in this case, homologous ones) affecting each other's behaviour.

6.3.7 THE AGE-RELATED FATE OF MFAS IN THE AG LUMEN

Taken together, the prior ageing results show that amyloid mutations bestow relatively greater tenacity over time when compared to their wild type counterparts, as judged by the hardiness of the resultant DCGs. Therefore, as the next step in following the fate of MFAS which seemingly has been influenced by amyloidogenic transformations in cognate molecules (TGFBI and AB_{42}), I traced its time-related behaviour in the AG lumen.

When MFAS from different genetic backgrounds was examined at different time points in AG lumens, all these versions all displayed age-related dissipation. I tempered these observations, however, by the fact that in the lumen, MFAS was free-floating in an aqueous solution, unlike the more controlled environment of DCGs in SCs. Despite this important difference, MFAS from the *TGFBI-R555Q* mutants assumed distinctively-shaped flocculations (**Figure 6.39C**). In general, protein aggregation is triggered by unfolding which exposes hydrophobic moeities which normally are concealed, or by thermal fluctuations. Susceptibility to these biophysical forces are heightened by single amino acid changes, examples of which have previously been found in immunoglobulin, human superoxide dismutase, and human lysozyme (Raffen *et al.,* 1999; Stathopulous *et al*., 2003; Booth *et al.,* 1997). Subsequently, Runager *et al.* showed that only amino acid substitions in FAS1 domain-4 bring about changes in the stability of TGFBI (Runager *et al.,* 2011). Their group showed that the two domain-4 arginine mutations, *R555Q* and *R555W*, stabilise TGFBI because positively charged hydrophilic arginine is replaced by either the hydrophobic tryptophan, or the uncharged but polar glycine. The switch to tryptophan in one mutation lowers electrostatic repulsion, thereby increasing association between various

parts of the protein and decreasing its solubility. The switch to glycine in the other mutation does essentially the same thing, but to a lesser degree. Finally, other studies have shown that Arg^{555} is involved in forming salt bridges between domains-1 and -4 of TGFBI, stabilising the entire molecule, and even inducing dimerization with other mutated TGFBI molecules (Nielsen *et al.,* 2021). These experimental findings agree with corneal studies of patients with TGFBI-R555Q or R555W amyloid deposits, which show that these deposits are indeed aggregates comprised of intact or dimerized TGFBI molecules (Klintworth *et al.,* 1998). In contrast, the domain-4 mutation A546T just a few residues away results in the complete dissolution of the TGFBIp structure, and the deposition of cross-β sheet-TGFBI fragments within the cornea instead (Klintworth, 2009). Finally, Transverse Urea Gradient (TUG) gel electrophoresis and chemical denaturation followed by CD spectroscopy showed that TGFBI's Arg^{555} mutants were more stable than its A546T mutant (Runager *et al.,* 2011). My work, comparing TGFBI-R555Q to other TGFBI domain-1 and -4 mutants, shows that the distinctive lumenal flocculation of MFAS that is produced within a genetic background of *TGFBI-R555Q*, persists at 18 days. On the other hand, lumenal MFAS produced within the other genetic backgrounds (*TGFBI-R124C*, *TGFBI-G623D* and *TGFBI-H626R*), like lumenal MFAS produced in controls, has deteriorated into an amorphous morass by the 18-day time point. Furthermore, the last-mentioned mutants, as well as controls, do not have the distinctive floccular appearance to MFAS as is seen with MFAS in a *TGFBI-R555Q* background. Taken together, these findings show that there is indeed something unique about Arg^{555} mutations in TGFBI. Even more interesting is the fact that MFAS in DCGs accurately and dependably responds to it.

Amyloid, whether physiological or pathological, is known to be a durable form of protein, with a tensile strength prompting comparisons with steel and silk, the latter being considered it's structural congener (Smith *et al.,* 2006). The vaunted strength of amyloid fibres has prompted investigations into whether they could be functionalized by using them to make fusion proteins (Baldwin *et al*., 2006) or utilizing them as templates for metal-bound nano-wires (Scheibel *et al.,* 2003; Reches and Gaziet, 2003). When pathologically processed, amyloid's durability impedes normal cellular functions, while at the larger organ and organismal level, cumulative tissue injury and decreased clearance of abnormal amyloid proteins lead to premature tissue degeneration (Li *et al.,* 2022, Mawuenyega *et al.,* 2010). The experimental results I have presented here confirm amyloid's tenacity, the very attribute which either at the molecular, microscopic, or macroscopic level makes it clinically problematic. More broadly, they demonstrate that this *Drosophila* system continues to show fidelity in reporting on the behaviour of amyloids. It also further confirms the utility of *Drosophila* as an ideal model to study various aspects of human amyloid, from it's inception to it's degradation, and with the efficiency afforded by the brief life cycle of the fruit fly.

CHAPTER 7

FINAL DISCUSSION

7. FINAL DISCUSSION

Take but degree away, untune that string

And, hark, what discord follows!

(William Shakespeare, Troilus and Cressida, Act 1, Scene 3, 1602).

7.1 INTRODUCTION

In this chapter I summarize and further discuss the results from **Chapters 3** through **6**. These results yielded new discoveries about the *Drosophila* amyloid MFAS, and in doing so also seemingly confirmed historical reports and speculation about amyloid behaviour in humans. The data start in **Chapter 3** with the discovery of a new physiological role for *Drosophila* MFAS in forming DCGs, which builds upon previous work done in the Wilson laboratory showing that DCGs are functionally important in reproduction (Redhai *et al.*, 2016). The results go on to show that although central to the formation of DCGs, the absence of MFAS does not perturb the formation of Rab6 and Rab11 compartments, the fusion of which are central to the formation of DCGs, discoveries also made in the Wilson laboratory (Wells *et al.,* 2023). In **Chapter 4,** I show that two proteins strongly associated with Alzheimer's disease (GAPDH and APP) are also crucial for the formation of normal DCGs. In humans, the levels of GAPDH in the plasma and CSF correlate strongly with the advancement of Alzheimer's, while APP is the precursor of Aβ oligomers, the components of amyloid plaques in the brain. Thus *GAPDH2*, the *Drosophila* homologue of human *GAPDH*, and *APPL*, the *Drosophila* homologue of human *APP*, when knocked down,

result in distinctive patterns of abnormally formed DCGs, in which the MFAS moieties fail to coalesce into a single normal core. Time-lapse videos, which will be presented in an upcoming publication, show that the behaviour and movement of *GAPDH2-RNAi*- and *APPL-RNAi*-produced mini-cores are quite different from one another. This section also demonstrates that *mfas*- and *APPL*-knockdowns do not alter the number of non-acidic compartments containing ILVs.

In **Chapter 4,** I also examined the effects of knockdown of various portions of *APPL* on MFAS behaviour, as well as the effects of knockdown of APPL's processing secretases. Knockdown of APPL's *α*- and *γ-secretases* did not significantly affect MFAS in it's formation of DCGs. However, the deletion of APPL's extracellular portion decreased the number of DCGs, while deletion of it's intracellular portion resulted in the non-formation of DCGs. This is in keeping with what is known about human APP's much-studied intracellular portion, which is known to have a myriad of functions.

In **Chapter 5**, the effects of CD-causing *TGFBI* mutations were tested on transgenic *Drosophila*. These results confirmed that *TGFBI* mutations do indeed affect DCG morphology and formation, thus demonstrating that human TGFBI influences MFAS, it's *Drosophila* homologue. In the same chapter I also examined the interaction between *TGFBI* mutants and *APPL-RNAi*, given the fact that the latter reliably produced a mini-core phenotype, suggesting that with the removal of APPL, there was also the loss of a cohesive force which brought the MFAS moieties together. The resultant progeny from

these crosses had phenotypes intermediate between the *TGFBI* mutants and the *APPL*-knockdown. Rescues were not expected, since neither genotype produced morphologically normal DCGs.

In **Chapter 6**, the effect of the *Swedish* double mutation in *APP,* and the effects of the intra-*Aβ$_{42}$-Arctic, -Dutch* and *-Iowa* mutations on DCG formation were examined in transgenic flies. All these mutations influenced the formation of DCGs in their own unique ways, thus demonstrating that these human mutations in an amyloid parent protein were influencing *Drosophila* MFAS. To test the insularity of their actions, the effects of the *APP-Swedish* and *Aβ$_{42}$-Arctic* mutations on exosome production were measured, and neither affected exosome numbers. In conducting these exosome experiments, another previously reported result from the Wilson laboratory was confirmed: the fact that accessory ESCRT-III proteins regulate Rab11 exosome formation through an ESCRT-dependent process, independent of the ubiquitinylation-deubiquitinylation cycle for loading of cargoes (Marie *et al.*, 2023). Specifically, unlike other tested genotypes, *Chmp2b*-knockdown signficantly decreased the number of exosomes generated.

Also in **Chapter 6**, the effects of *APP* and *Aβ$_{42}$,* both wild type and mutated, were tested on *APPL*- and *GAPDH2*-knockdowns (both of which produced mini-core phenotypes). In progeny produced by these combinations, rescues of varying efficacies were seen, and an analysis of these results uncovered additional conclusions. The first was that *APPL*- and *GAPDH2*-knockdowns appeared to be fundamentally different, one of the reasons being

that they differed significantly in their response to rescue by DCG-organizing mutations. This difference had first been suggested by the differing morphologies and distributions of their respective mini-cores within DCG compartment boundaries, and the differing kinetic patterns of these mini-cores on time-lapse videos. And while both *$A\beta_{42}$-wild type* and *$A\beta_{42}$-Arctic* were equally efficacious in rescuing the *APPL*-knockdown, *$A\beta_{42}$-wild type* was less effective than *$A\beta_{42}$-Arctic* in rescuing the *GAPDH2*-knockdown. This further underscored a fundamental difference between the mini-core-generating forces in *APPL*- and *GAPDH2*-kds.

Since *$A\beta_{42}$-wild type* and *$A\beta_{42}$-Arctic* proved equally effective in rescuing the mini-core phenotype of *APPL-RNAi*, I considered the possibility that non-mutated amyloids might share some of the same properties as their mutated counterparts. Another piece of evidence in the same vein emerged with the finding that full-length, *wild type-APP* also partially rescued the mini-core phenotype of *APPL-RNAi*. This evoked the possibility that both parent and progeny amyloid proteins might have amyloid attributes, and that amyloid disorders might therefore be viewed as a continuum along which proteins in their various forms exist, rather than as a unidirectional march towards disease. The non-genetic factors which move amyloids on the spectrum between between normality and abnormality might be hypoxic insults, inflammation, or toxins. This would explain the simultaneous ascendancy of perfectly plausible, data-driven hypotheses pointing to inflammation and mitochondrial dysfunction as being equally potent drivers of amyloid neurodegeneration. An example of this from our own laboratory is that the Rab6 to Rab11 transition rapidly affects the microenvironment within the precursor compartments, so that the amyloid-

comprised cores coalesce (Wells *et al.,* 2023). Yet another highly plausible interpretation of this data would be that human APP, as the human homologue of *Drosophila* APPL with significant conservation in several domains, might be substituting or standing in for APPL function which has been reduced by its knockdown.

Finally, the effects of amyloidogenic mutations on the persistence of ageing DCGs was tested, given the commonly held maxim that amyloid proteins are tenacious and durable. This was supported by experiments examining DCGs in *Drosophila* transgenic for amyloidogenic *TGFBI* and $A\beta_{42}$ mutations. The implications of these results, as well as perspectives on amyloid and neurodegeneration research are discussed in the following subsections.

7.2 THE DISCOVERY OF A PHYSIOLOGICAL ROLE FOR THE *DROSOPHILA* 'AMYLOID' MFAS

Building on the concept briefly introduced in **Table 1.1 (§ 1.1.2)**, it is clear that throughout nature, amyloid proteins play physiological roles. More comprehensive lists of physiological amyloid functions are presented in **Tables 7.1** and **7.2**, where some of the more detailed molecular actions of amyloids are summarized. A similar functional role for a *Drosophila* 'amyloid' was corroborated in this thesis, where results in **§ 3.2.3** (**Figure 3.9**) show that MFAS is required for the protein aggregation events that lead to the formation of DCGs (I put the term 'amyloid' in quotation marks because of the scant research available on *Drosophila* MFAS). The evidence for it being an amyloid protein is circumstantial, which includes its homology to the human pre-amyloid protein TGFBI, and its role in forming DCGs which store biologically active molecules, similar to the amyloid

storage forms of hormones in mammalian neuroendocrine cells. In addition, in collaboration with Dr. Martin Jahn, of the Department of Biochemistry, Oxford University, a Raman spectroscopic analysis of MFAS was performed, which confirmed its amyloid profile (Martin Jahn and Preman Singh, unpublished results). DCGs in turn, play highly significant physiological roles. They store Decapentaplegic (Dpp), the *Drosophila* homologue of the mammalian Bone Morphogenetic Protein (BMP) ligands BMP2 and BMP4, which following mating accelerates the replenishment of new DCG compartments in preparation for the next mating (Redhai *et al.,* 2016). This process, accomplished by a combination of a Dpp-dependent autocrine feedback loop and paracrine signaling between SCs, suggests a shared mechanism in higher eukaryotic cells, thus providing an entry point for the *Drosophila* MFAS model into the extremely broad field of dysregulated secretion in the causation of human disease. This point is supported by the fact that mammalian cells use members of the widely conserved BMP family to control regulated secretion as well. For example, in response to fluctuating iron stores, BMP-2, -4, and -9 modulate the expression and secretion of the hormone hepcidin from hepatocytes via the SMAD pathway (Rishi *et al.*, 2015). Hepcidin and hemojuvelin abnormalities in turn cause the iron storage disorder hemochromatosis (Papanikolau *et al.,* 2004), a multisystem autosomal recessive disease which, because of dysregulated iron absorption, distribution and deposition leads to diabetes, arthritis, cirrhosis, cardiomyopathy, hypogonadism, hypothyroidism, adrenocortical insufficiency, and ultimately death. This places BMP signalling at the very heart of a broad clinical syndrome which in essence hinges on dysregulated secretion (Core *et al.,* 2014). Taken together with the discoveries presented in my thesis, these findings place MFAS, the structural repository of BMP, very firmly in

the group of amyloids which play a physiological role. I have therefore added MFAS to the list of functional amyloids in higher organisms (**Table 7.2**).

PHYSIOLOGICAL AMYLOIDS IN MICROBES

AMYLOID	ORGANISM	FUNCTION
Curli	*E.coli, Salmonella*	Bacterial biofilm assembly
FapC	*Pseudomonas*	Bacterial biofilm assembly
TasA	*B. subtilis*	Bacterial biofilm assembly
MTP pili	*M. tuberculosis, avium,*	Binds to laminin
P1 pili	*S. mutans*	Bacterial biofilm assembly
Phenol-soluble modulins	*S. aureus, S. epidermidis*	Biofilm integrity
Chaplins	*Streptomycetes* (bacteria)	Aerial hyphae formation
Hydrophobins	Filamentous fungi	Surface attachment, hyphae
Rodlins RdlA and RdlB	*Streptomyces*	Aerial hyphae formation
Bioemuslifier BE-AM1	*Solibacillus silvestris*	Cell surface properties
Major Sheath Protein A	Archaeal methanogens	Cell wall tubular sheaths
Biofilm-Assoc. Proteins	*Staphylococcus, Salmonella*	Intercellular adhesion
Microcin E492	Numerous bacteria	Pore-forming peptide
Flocculins	*S. cerevisiae*	Biofilm-like mat assembly
Mnemons	*S. cerevisiae*	Cell-cycle entry
Sup35	*S. cerevisiae*	Translation termination
Ure2p	*S. cerevisiae*	Nitrogen pathways regulation
PolyQ huntingtin exon-1	*S. cerevisiae*	Ure2p prion related
Rnq1p	*S. cerevisiae*	Prion inducibility enhancer
Swi1p	*S. cerevisiae*	Chromatin remodeling factor
Mot3	*S. cerevisiae*	Cell wall remodeling
Protein Als5p	*C. albicans*	Cell-to-substrate adhesion
NOD-like receptors	*P. anserina*	Amyloid oligomerization
Het-s prion	*P. anserina*	Heterokaryon incompatibility
M45	*Cytomegalovirus*	Virus-caused necroptosis
Harpins	*Ustilago maydis*	Destabilize plant membranes

Table 7.1: Cellular and molecular functions of physiological amyloids in bacteria, fungi, virsues and yeast. (Adapted and compiled from Otzen and Riek, Cold Spring Harbor Perspect. Biol. 2019, pp. 4-9).

PHYSIOLOGICAL AMYLOIDS IN HIGHER ORGANISMS

AMYLOID	ORGANISM	FUNCTION
Peptide hormones	Mammals	Storage and release of hormones
Fibrin peptides	Mammals	Plasminogen activator
Pmel17	Mammals	Melanosome melanin scaffold
Major Basic Protein (MBP)	Mammals	Membrane destabilization
RIP1/RIP3	Mammals	Signaling and cell death
TGFBI	Mammals	Keratinocyte adhesion protein
APP cleavage products	Mammals	Brain development
Zonadhesin and CRES	Mammals	Surrounds mammalian oocytes
Orb2	*Drosophila melanogaster*	Poly Q/H sequence
Adaptor Protein ImD	*Drosophila melanogaster*	NF-κB activation
Chorion	Silkmoth	Protects oocyte and embryo
Fish egg envelope protein	Fish	Resistance to dehydration
Zona pellucida proteins	Mouse, fish, silkmoth	Oocyte protection
Anionic dermaseptin	Mexican tree frog	Skin antimicrobial peptides
Xvelo	*Xenopus laevis*	Balbiani body formation
Midline fasciclin	*Drosophila melanogaster*	Dense-core granule formation

Table 7.2: Cellular and molecular functions of physiological amyloids in higher organisms. (Adapted and compiled from Otzen and Riek, Cold Spring Harbor Perspect. Biol. 2019, pp. 4-9).

7.3 EVIDENCE THAT AMYLOIDS INFLUENCE EACH OTHER

Both full-length human APP, as well as its intramembranous β-amyloid-generating sequence (Aβ) influence the behaviour of MFAS. Furthermore, APPL, the *Drosophila* homologue of APP also influences MFAS. These results are significant both from the standpoints of history as well as that of the future. Historically, over a century of clinical observation showed that amyloid neurodegenerative pathology progressed in a contiguous fashion, i.e., it seemed the amyloid proteins were communicating with each other. In

Alzheimer's disease, this is reflected in the Thal staging of β-amyloid, as well as the Braak and Braak staging of Tau progression. A similar contiguous principle of propagation seems operative in the advancement of α-synuclein and Tau in Parkinson's Disease. One of the mechanisms of spread is crosstalk, and my data provide good support for this occurring in both physiological and pathological circumstances. A list of neurodegenerative diseases characterized by the spread of brain amyloid from one adjacent zone to another is presented in **Table 7.3.**

NEURODEGENERATIVE DISEASES IN WHICH THE CONTIGUOUS PROGRESSION OF MISFOLDED AMYLOID IS HISTOLOGICALLY EVIDENT

MISFOLDED AMYLOID PROTEIN	DISEASE
β-AMYLOID	Alzheimer's Disease
TAU	Alzheimer's Disease
	Gerstmann-Sträussler-Scheinker Disease
	Pick's Disease
	Progressive Supranuclear Palsy
	British Dementia
	Danish Dementia
	Frontotemporal Dementia and Parkinsonism
	Guam Parkinsonism
	Corticobasilar Degeneration
	Argyrophilic Grain Disease
	White Matter Tauopathy
α-SYNUCLEIN	Parkinson's Disease
	Dementia with Lewy Bodies
	Multiple System Atrophy
	Lewy Body Dysphagia
	Pure Autonomic Failure
PRION PROTEIN	Creutzfeldt-Jakob Disease
	Kuru
	Gerstmann-Sträussler-Scheinker Disease
	Fatal Familial Insomnia
TDP-43	Amyotrophic Lateral Sclerosis
	Frontotemporal Dementia
FUSED IN SARCOMA	Amyotrophic Lateral Sclerosis
	Frontotemporal Dementia
HUNTINGTIN	Huntington's Disease

Table 7.3: Misfolded amyloids which visibly 'spread' in neurodegenerative diseases.

As suggested by the table above, amyloid neurodegenerative disorders behave much like prion diseases, and furthermore prion protein deposits in the brain were discovered to be comprised of amyloid (reviewed in Prusiner, 1991; and in Sabate *et al*., 2015). While APPL's influence over MFAS (since they are both *Drosophila* amyloid proteins) might have reasonably been anticipated by the historically conjectured 'crosstalk' between the human amyloid proteins α-synuclein, β-amyloid and Tau, the truly surprising result was the influence of human APP over *Drosophila* MFAS. This result demonstrates amyloid crosstalk *across* species, and once again invokes the spectre of the long-suspected prion-like properties of amyloid.

Reports of amyloid's prion-like properties have been accumulating since the late 1950s, starting with the now-discontinued practice which was in effect from 1958 to 1985, of injecting pooled cadaveric pituitary homogenates into patients to treat Growth Hormone deficiency (Will, 2003). This led to both Creutzfeldt-Jakob Disease and CAA (the version of FAD caused by intra-$A\beta_{42}$ mutations) in injection recipients, diagnosed only decades later. Retrospective analysis of these pituitary homogenates revealed that some of the original donors did indeed have intra-$A\beta_{42}$ mutations. Furthermore, mice injected with these cadaveric homogenates developed CAA (Purro *et al.*, 2018; Huynh and Holtzman, 2018) (**Figure 7.1**). The enduring biological potency of these pituitary homogenates, surprisingly stable despite having been warehoused at room temperature for decades, inadvertently demonstrated yet another putative property of amyloid: the intriguing stability of these amyloid 'seeds' (Ye *et al.*, 2015). This episode, occurring squarely during an era when excitement about 'slow viruses' was taking off and indeed when a Nobel Prize

was awarded for kuru in 1976, triggered a flurry of political and scientific action. In addition to the scientific confirmation of prions, this period in time saw the cessation of cadaveric Growth Hormone injections, the adoption of recombinant Growth Hormone as the standard of care instead, and the creation of the UK National Prion Monitoring Cohort (Thompson *et al.*, 2013).

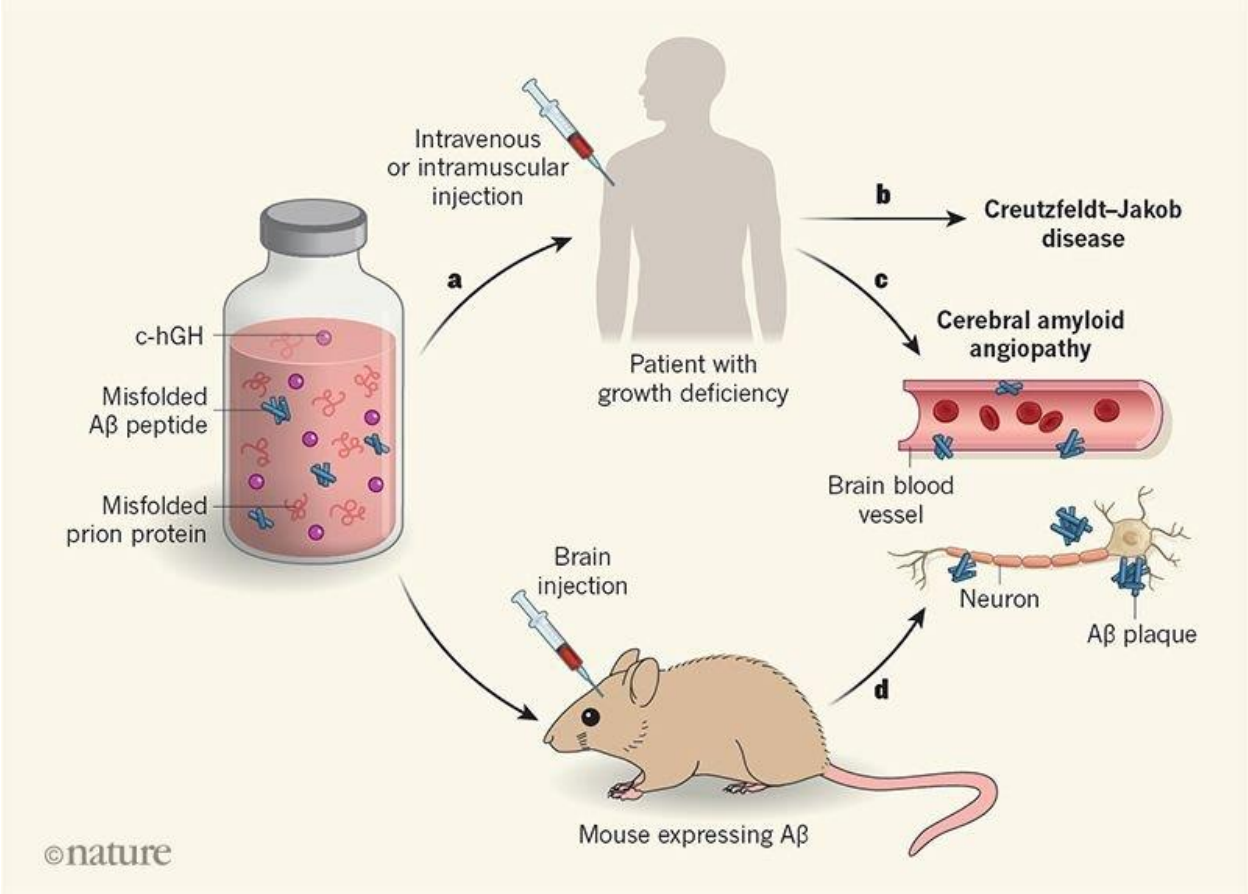

Figure 7.1: The prionoid behaviour of amyloid (Huynh and Holtzman, Nature 2018, p. 355).

Understandably, these lessons of history saw different pathways of amyloid crosstalk being postulated. First, similar amyloids were believed to communicate and influence each other: β-amyloid-to-β-amyloid, Tau-to-Tau, and α-synuclein-to-α-synuclein (as demonstrated by

clinical and post-mortem neuropathological observations in Alzheimer's disease, Parkinson's disease, Frontotemporal Dementia and Tauopathies). This mode of amyloid propogation was described as 'homologous cross-seeding'. Second, *different* amyloids were felt to influence each other: human islet of Langerhans amyloid polypeptide (hIAPP) and Aβ increase in lockstep, as shown by clinical and post-mortem observations (Bharadwaj *et al.,* 2017). Thus, the linking of hIAPP and Aβ provided an explanation for the earliest recognized association between two separate amyloid diseases: type 2 diabetes and Alzheimer's (type 2 diabetes is now considered an amyloid disease, in which replacement of the β-cells of the islets of Langerhans by hIAPP is the underlying cause of decreased insulin production). This presumed crosstalk between dissimilar amyloids was called 'heterologous cross-seeding'. Several other reports illustrating the greater-than-chance coexistence of disparate amyloid diseases subsequently emerged, making these amyloid associations axiomatic in clinical practice (Almeida and Brito, 2020). A knowledge of these simultaneously progressing amyloid syndromes within the same patients alerted me when it appeared that different amyloids in flies were influencing each other.

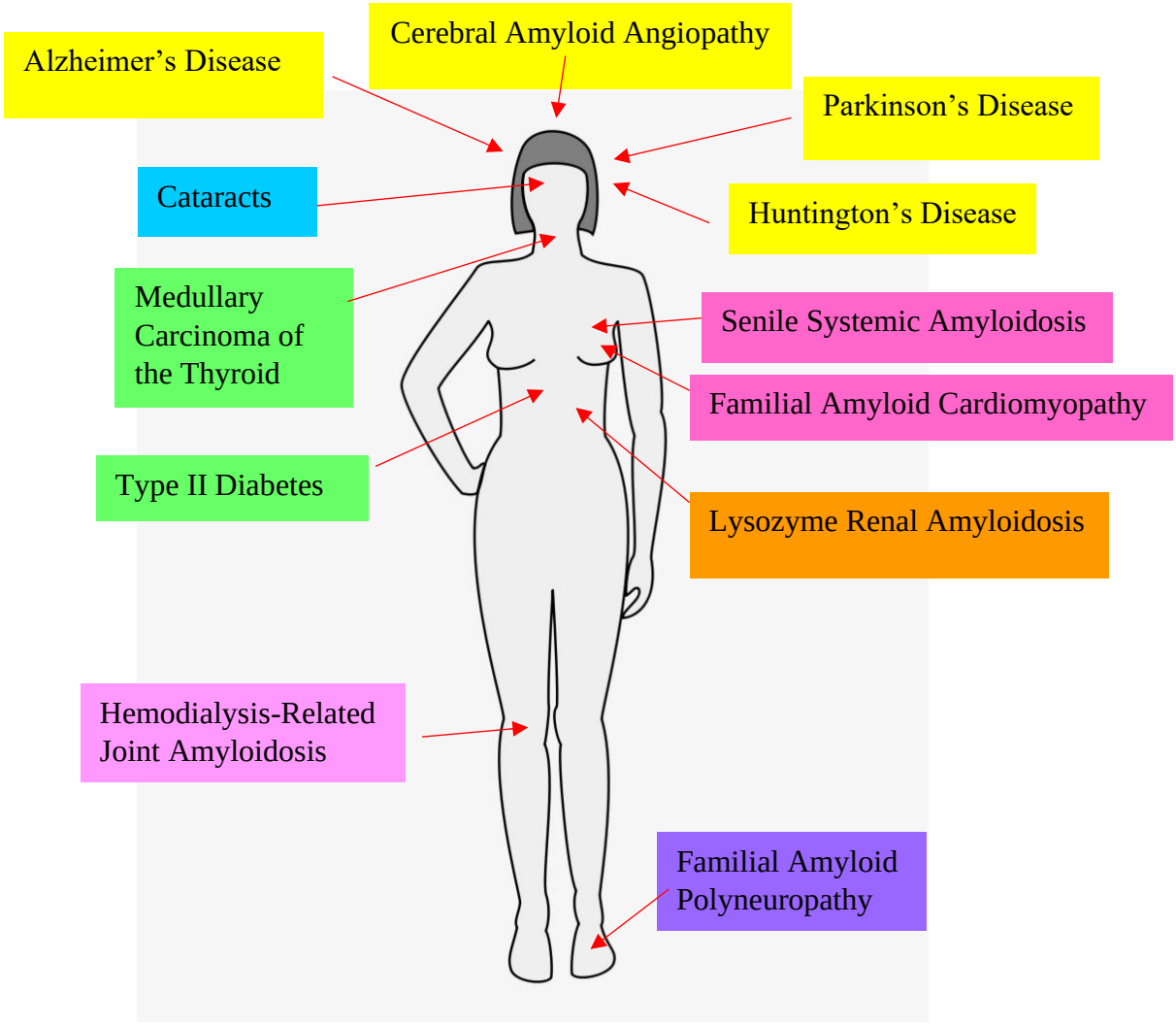

Figure 7.2: Heterologous crosstalk between different amyloids. The higher-than-chance coexistence of several amyloid diseases raised the spectre of crosstalk between different amyloids. Each of the amyloidoses depicted above are known to coexist with the others, supporting the hypothesis of heterologous amyloid crosstalk. **Yellow boxes:** CNS amyloidoses (Aβ, Huntingtin, and Tau); **Blue box:** Cataracts (γ-crystallins); **Pink boxes:** Cardiac amyloidoses (wild type transthyretin and transthyretin variants); **Green boxes:** Endocrine amyloidoses in the thyroid and pancreas (calcitonin and human inslet amyloid polypeptide); **Orange box:** Renal amyloidosis (lysozyme variants); **Mauve box:** Joint and musculoskeltal amyloidosis (wild type and β_2-microglobulin); **Purple box:** Peripheral nerve amyloidosis (transthyretin variants).

7.4 HUMAN AND *DROSOPHILA* AMYLOIDS AND AMYLOID-ASSOCIATED PROTEINS INTERACT

The studies cited above make clear, on the face of it at least, that similar and dissimilar amyloids are capable of influencing each other. In this thesis, results in **Chapter 4** demonstrate that amyloids associated with Alzheimer's disease affect *Drosophila* MFAS. Thus, the overexpression of human *GAPDH*, which encodes an enzyme closely linked with the clinical progression of AD, influences *Drosophila* MFAS into increasing the number of DCGs per SC. On the other hand, knockdown of *GAPDH2*, the *Drosophila* homologue of human *GAPDH* results in the non-formation of intact DCGs in a distinctive mini-core pattern, wherein MFAS particles cling to the limiting membrane of the DCG compartment without being able to fuse into a single intact core, a phenomenon caught on time-lapse videos. While GAPDH's best-known connection is with AD, recent studies have linked it to a rising number of amyloid neurodegenerative diseases.

Similar amyloid-to-amyloid influences are seen in experiments in **Chapter 6** wherein mutated versions of human APP and it's internal $A\beta_{42}$ segment influence the behaviour of MFAS. In **Chapter 4**, knockdown of Drosophila *APPL* also influences MFAS by preventing it's normal coalescence into physiological DCGs. Furthermore, in **Chapter 5**, MFAS is affected by numerous amyloidogenic mutations in TGFBI, it's human homologue. Also in **Chapter 6**, FAD mutations in human APP and human $A\beta_{42}$ profoundly affect *Drosophila* MFAS in its biogenesis of DCGs. Rescue experiments in the same Chapter show that an MFAS-organizing mutation in human $A\beta_{42}$ ($A\beta_{42}$-Arctic) as well as human $A\beta_{42}$-wild type can rescue the MFAS-disrupting effects of *Drosophila APPL*- and

GAPDH$_2$-knockdowns, and that human APP can also rescue the MFAS mini-cores produced by *APPL*-knockdown. A brief summary of interacting amyloids discovered in the course of this work, both within and across species, is provided below.

7.4.1 GAPDH/GAPDH2 INFLUENCE *DROSOPHILA* MFAS

GAPDH has long historical associations with Alzheimer's disease (Yankers and Lu, 2009), although explanations for these ties have been sparse. For decades, the reasons pointed to were simply GAPDH's ubiquity as a multifaceted, moonlighting glycolytic enzyme. With its newly-discovered associations with several other neurodegenerative diseases, as well as its links with autophagy, cancer. and mitochondrial disorders, more nuanced clarifications of its roles have gradually emerged (reviewed in Butera *et al.,* 2019; and Sirover, 2013). As an example, GAPDH inactivated by Huntingtin has been shown to impair mitophagy, thus perpetuating and amplifying the neuronal damage of Huntington's disease (Hwang *et al.,* 2015) (**Figure 7.3**).

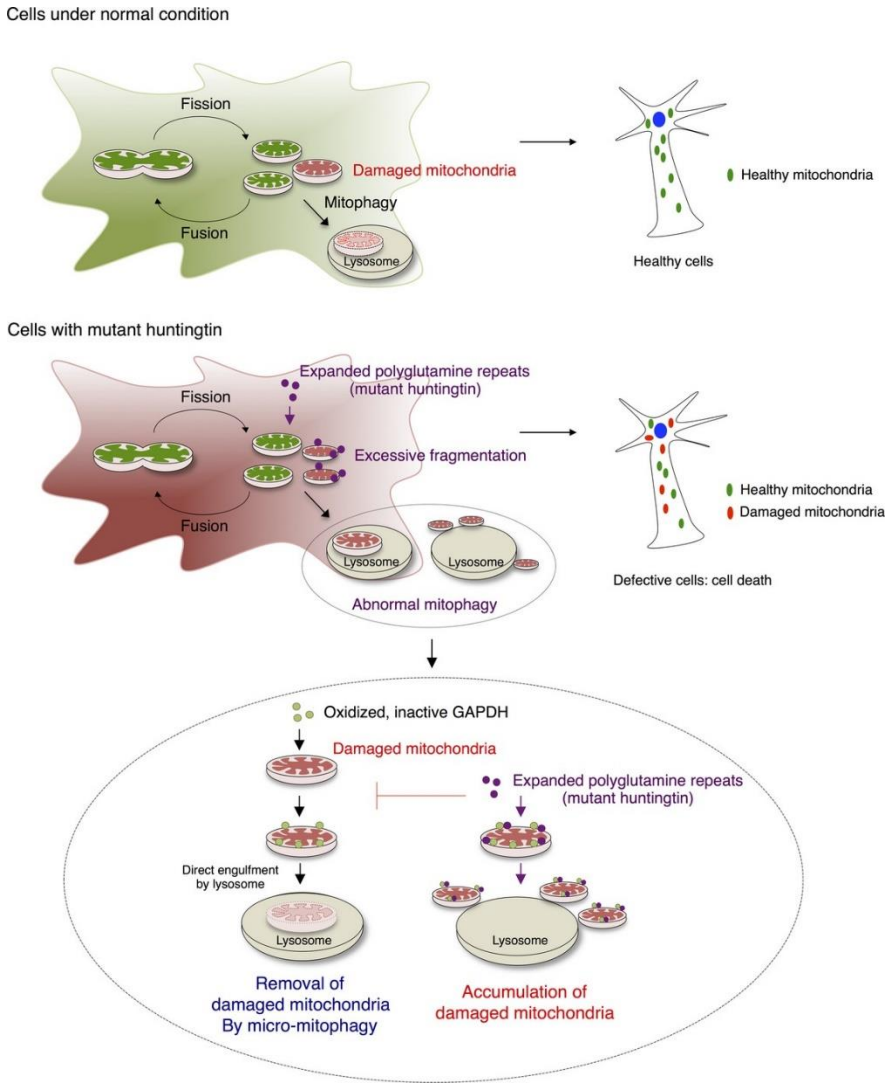

Figure 7.3: Huntingtin-inactivated GAPDH impedes mitophagy, thus further perpetuating the neuronal damage of Huntington's disease (Hwang *et al*., EMBO Mol. Med. 2015, p. 1320).

In addition, GAPDH has been found to interact with α-synuclein in Parkinson's disease (Tatton *et al.*, 2000), Ataxin-1 in Spinocerebellar Ataxia Type 1, and the androgen receptor in Spinobulbar Muscular Atrophy (Koshy *et al*., 1996). It is found in the characteristic brain lesions of each of these diseases, and rises as each of these conditions progress (reviewed in Sirover, 2013). Thus, the findings that *GAPDH* overexpression increases the number of DCGs generated (**Figure 4.8C**), and that *GAPDH2*-knockdown severely impairs the

coalescence of *Drosophila* MFAS (**Figure 4.8B**) are unsurprising results, given these long and still-emerging associations with amyloid neurodegenerative diseases. In light of what we know about GAPDH's 'moonlighting' proclivities, its production of mini-cores might well be yet another example of one of these hitherto undiscovered moonlighting actions. Thus, in its role in producing mini-cores in *Drosophila* SCs, its presumed 'moonlighting activity' would appear to be its secretion into the lumen of DCGs and other compartments, a conjecture earlier evoked by work also done in the Wilson laboratory (Dar *et al.*, 2021).

7.4.2 APP/APPL AND THE HUMAN Aβ42 SEGMENT INFLUENCE *DROSOPHILA* MFAS

The literature is replete with data on APP, its cleavage products $A\beta_{40\text{-}49}$, and the resultant Aβ plaques in Alzheimer's disease. The experimental results described here show that AD mutations in APP and $A\beta_{42}$ (but not their wild type versions), prompt MFAS into producing dysmorphic DCGs. This demonstrates that a human amyloid precursor protein (APP) as well as it's cleavage product ($A\beta_{42}$), depending on whether they are mutated or not, reliably direct the aggregation of another potentially amyloidogenic *Drosophila* protein (MFAS) towards different morphological fates. The interpretation of these results however must be tempered by the fact that wild type APPL is still present in several of these experiments, meaning that they are not looking at APPL-independent function of these mutants, and the possibility still exists that APPL may be providing some 'rescue', or other modifying effects.

Specifically, *APP's Swedish* double mutation, located just outside the *Aβ* sequence towards the N-terminal end, when overexpressed in *Drosophila*, induces MFAS to either produce normal or diminished numbers of DCGs, accompanied by the presence of giant lysosomes (**Figure 6.12B** and **C**). The *APP-K670N/M671L-Swedish* mutation is known to increase cleavage of APP by BACE-1 tenfold at the Met^{671}-Asp^{672} β-site, a scission which generates more amyloidogenic Aβ oligomers, unlike cleavage at the Thr^{681}-Gln^{682} alternative β'-site, which does not (Kimura *et al.,* 2016). This increases total $A\beta_{40}$ and $A\beta_{42}$ levels without altering the $A\beta_{40}/A\beta_{42}$ ratio (Johnston *et al.,* 1994). And while early work reported that *APP-Swedish* undergoes cleavage in the Golgi and post-Golgi vesicles (Thinakaran *et al.,* 1996), subsequent studies showed that the *APP-Swedish* mutation dramatically increased the lysosomal processing of APP (Tam *et al.,* 2014). Evidence for this includes the fact that APP-Swedish is transported to lysosomes by Adaptor Protein-3 (AP3) a heterotetrameric protein complex which is known to function as a lysosomal ferry. Furthermore, it has been found that γ-secretase function and activity (specifically presenilin-1 and nicastrin) are present in purified lysosomes, that APP's cleavage is optimized in acidic milieus, and that the majority of its cleavage occurs at the lysosomal membrane (Pasternak *et al.,* 2003), a phenomenon demonstrated for APP-Swedish in particular. My experimental findings of giant lysosomes with the *APP-Swedish* mutation are broadly in agreement with the cited studies.

Based on what I saw with several experiments, it appears that mutant DCG compartments form abnormally, and these are then targeted by lysosomal fusion. These targeted DCG compartments subsequently show diffuse GFP-MFAS within them, and small acidic

regions at their periphery. From this point on, whether mutant APP molecules are cleaved in the Golgi or the lysosomes and the delineation of precise models for various mutations will require more detailed studies. The upshot of my observations, however, is that wild type human APP does not perturb *Drosophila* MFAS in its formation of normal DCGs, whereas its clinically devastating Swedish mutant has proportionate effects on *Drosophila* MFAS, replete with the expected downstream effects of generating giant lysosomes within SCs.

The intra-*Aβ$_{42}$-Arctic* mutation, on the other hand, known in humans to produce distinctive 'targetoid' Aβ plaques, induces MFAS to reorganize into targetoid DCGs.

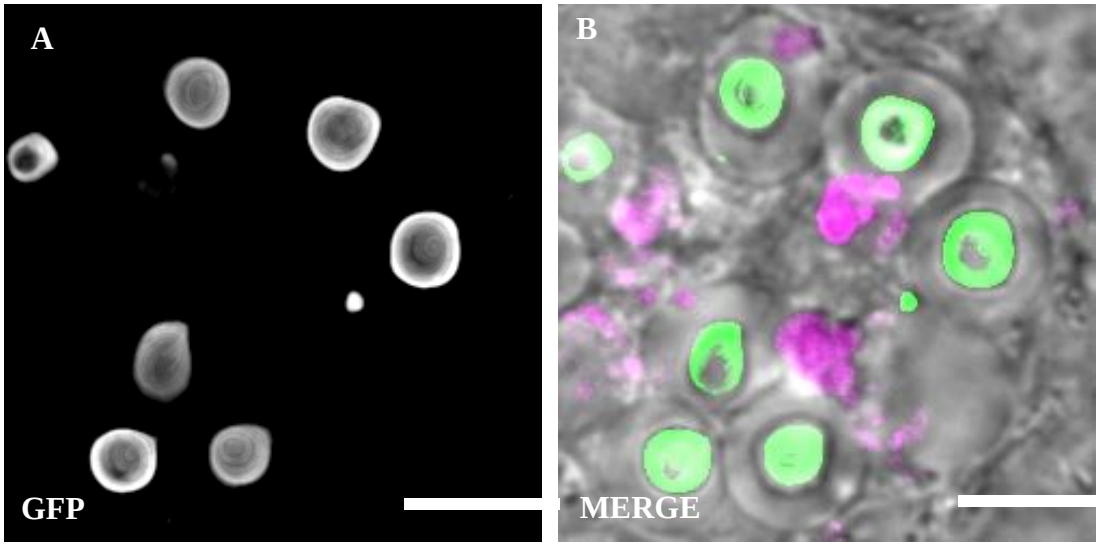

Figure 7.4: The *Aβ$_{42}$-E693G*-Arctic mutation causes re-arrangement of MFAS in DCGs into a targetoid configuration. SCs from six day-old virgin males stained with LysoTracker Red and imaged *ex vivo*, using DIC and fluorescence microscopy for GFP and LysoTracker Red. Detailed view of DCGs from *w^{1118}; GAL80^{ts}/UAS-Aβ$_{42}$-E693G-Arctic; dsx-GAL4 GFP-mfas/+* showing the targetoid appearance associated with *Aβ$_{42}$-Arctic* mutations. **A:** GFP channel. **B:** DIC, GFP and LysoTracker Red channels merged. The MFAS in DCGs is re-arranged into targetoid concentric circles. Scale bar = 5 μm.

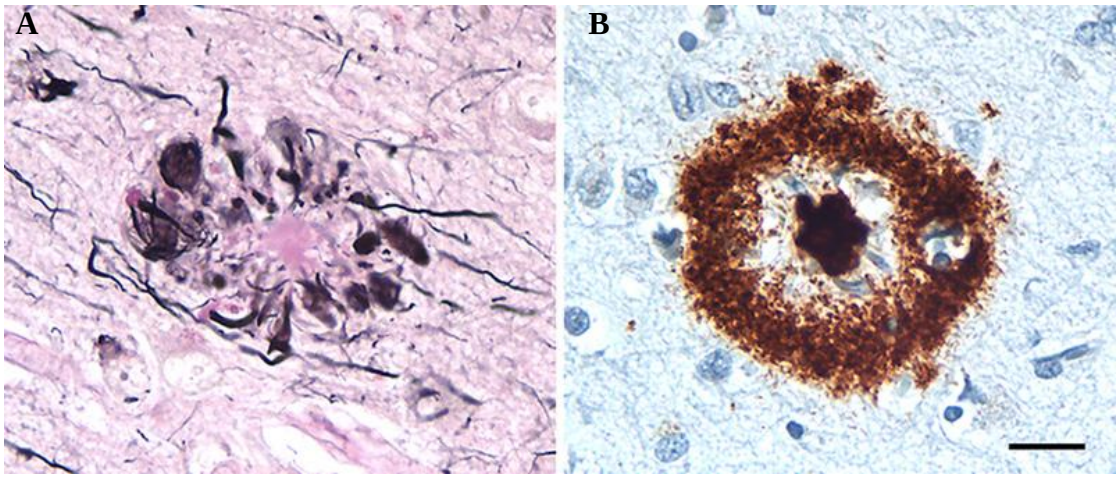

Figure 7.5: The typical targetoid plaques caused by the *Aβ$_{42}$-E693G-Arctic* mutation. Left: a conventional 'cotton wool' Aβ plaque stained with the Naoumenko-Felgin silver stain method and periodic acid-Schiff (PAS) counterstain. **Right:** a targetoid plaque casued by the *Aβ$_{42}$-E693G-Arctic* mutation with the general antibody 4G8 to Aβ with a Nissl counterstain. **Scale bar:** 20 μm. (Walker, Free Neuropathology 2020, p. 2).

As shown above, the targetoid conformation of *Aβ$_{42}$-Arctic* brain plaques is mimicked in the targetoid-appearing reorganization of MFAS in *Drosophila* in which the *Aβ$_{42}$-Arctic* mutation was overexpressed in SCs. Originally thought to be ring-shaped with Bielchowsky silver staining (Basun *et al.,* 2008), immunostaining revealed *Aβ$_{42}$-Arctic* plaques to be targetoid (Philipson *et al.,* 2012), with shorter Aβ$_{1\text{-}5}$ species in the centre, Aβ$_{17\text{-}24}$ in the midzone, and the periphery containing Aβ$_{x\text{-}42}$ (Kalimo *et al.*, 2013). Amyloid staining on these *Drosophila* samples was attempted; however they did not withstand the harsh alcohol washes required. I also hasten to add that the scales in **Figures 7.4** (showing *Drosophila* DCGs) and **7.5** (showing human brain plaques) are quite different; these images are intended to illustrate the MFAS-organisational influence of the *Aβ$_{42}$-E693G-Arctic* mutation and the resultant resemblance to human brain lesions.

The two other intra-$A\beta_{42}$ mutations studied, *Dutch* and *Iowa*, which in humans produce 'fluffy' or 'cloud-like' Aβ plaques, when overexpressed in *Drosophila* induce the dispersion of MFAS into cloud-like or diffuse-appearing mini-cores. Thus, the results show that a human amyloid, either in its entirety, or an internally located portion of it (like the situation with *APP* and $A\beta_{42}$), directs a *Drosophila* amyloid to change it's conformation into a similar appearance. While again the scales are very different, a remarkable feature of the fly assay is that it is able to distinguish the different organising activities of the different APP and Aβ mutants. Again, the overall lesson was that while wild type human $A\beta_{42}$ is virtually inconsequential in its effects on DCG biogenesis, even point mutations in the human APP or $A\beta_{42}$ molecule could prompt *Drosophila* MFAS to quite remarkably mimic the resultant conformational changes in DCGs.

7.4.3 HUMAN TGFBI INFLUENCES *DROSOPHILA* MFAS

Amyloidogenic mutations introduced into TGFBI prompt MFAS in DCGs to become dysmorphic, as shown in the data in previous sections (**Figures 5.9** and **5.10)**. This apparent communication between TGFBI and MFAS is the least surprising of the inter-amyloid crosstalk results, since these proteins are homologues of each other. The ancestral provenance of *Drosophila mfas* through the Cambrian fossil records of ancient chordate lineages stretches back to the basal chordate, Amphioxus (*Branchiostoma belcheri*) and demonstrates linkages with *TGFBI* (Song *et al.,* 2014) (**Figure 7.6**). These evolutionary linkages survive in the form of the identical structural organization of their descendants (TGFBI and MFAS) making it unsurprising that CD mutations in TGFBI direct MFAS to produce abnormal DCGs commensurate with TGFBI's pathological potential.

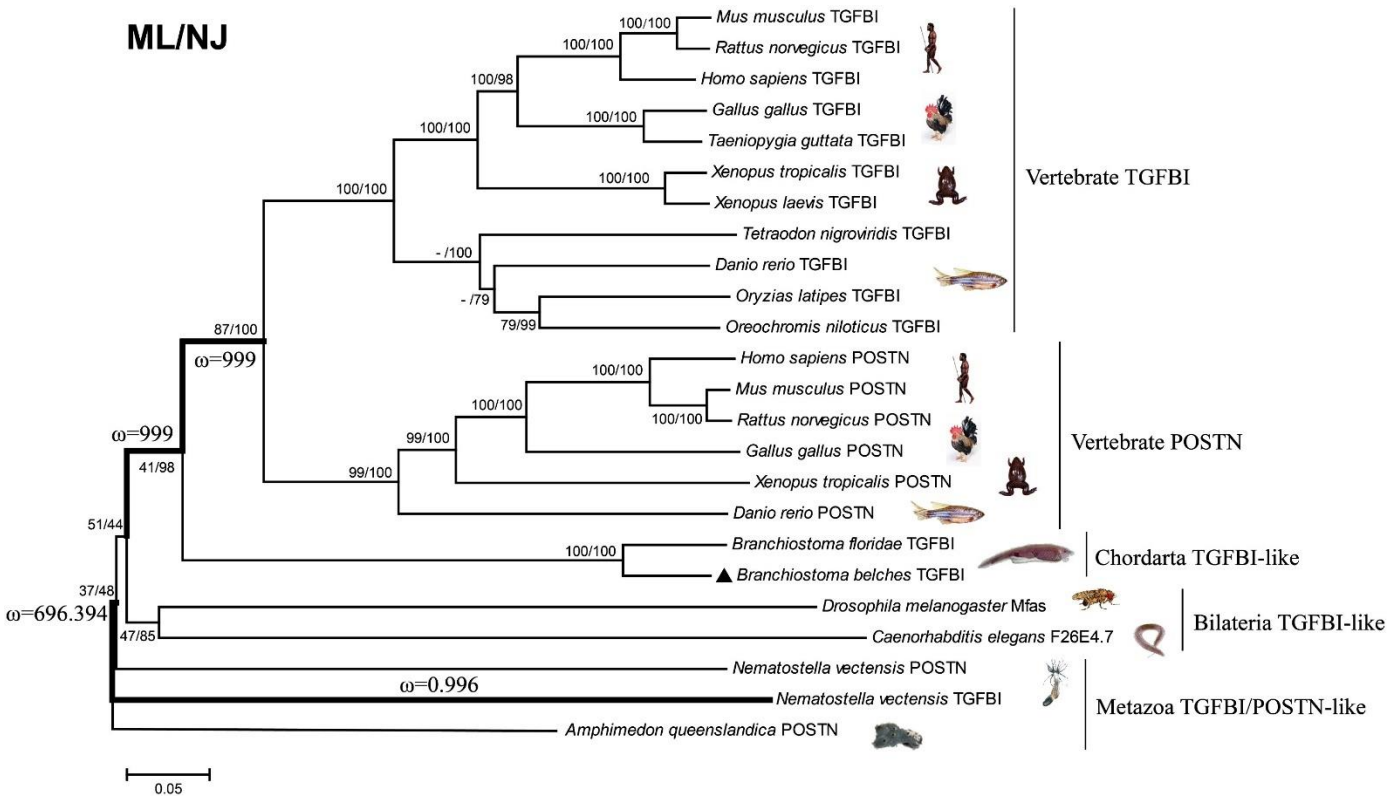

Figure 7.6: The phylogenetic tree of *TGFBI*, revealing it's ancient origins. TGFBI is the human homologue of *Drosophila* MFAS, which is also shown. The maximum likelihood **(ML)** and neighbour joining **(NJ)** analyses are identical. The *TGFBI* family includes the genes *TGFBI* and *POSTN* (periostin), which diverge in sequence only after the fourth fasciclin domain. (Song *et al.*, Genomics 2014, p. 151).

Periostin (POSTN) is the other member of *TGFBI's* gene family (Fasciclin I), and it's expression is promoted by Bone Morphogenetic Protein-2 (BMP-2) (Inai *et al.*, 2008; Snider *et al.*, 2008; Wallace *et al.*, 2008). Interestingly, as alluded to earlier, DCGs store Decapentaplegic, the *Drosophila* homologue of mammalian BMP ligands BMP-2 and BMP-4. While BMP drives the expression of *POSTN*, Decapentaplegic drives DCG-dependent reproductive responses (Redhai *et al.*, 2016). POSTN also has numerous roles in structure and development, and through it's binding to integrins, has many links with cancer. While an RGD motif is not found in POSTN (**Figure 7.8**), the RGD-similar Asp-Ile (DI) dimers conserved in fasciclin domains-2 and -4, and found both in POSTN and

TGFBI are consistent with POSTN's integrin-binding function (Hoersch and Andrade-Navarro, 2010; Park *et al.*, 2004). Among the emerging commonalities therefore which unite TGFBI, POSTN, and their ancient cousin MFAS, are prominent structural roles for all three. Fortunately, the easily witnessed disruption of MFAS' structural role in it's formation of DCGs makes the present *Drosophila* model feasible, and furnishes evidence that MFAS is influenced by yet another amyloid, this one being its human homologue, TGFBI.

7.5 HUMAN APP AND Aβ INFLUENCE MFAS IN RESCUES OF MINI-CORE-GENOTYPES: CONSIDERATIONS AND PERSPECTIVES

In *Drosophila*, the term phenotype rescue describes a phenomenon defined by FlyBase as heterologous rescue or functional complementation (Ecovoiu *et al*., 2022). In designing my rescue experiments, I considered the *a priori* validation of the functional homology of the gene pairs being tested. Given my earlier results showing that both human and fly amyloid and amyloid-associated genes informed the fate of MFAS, I believed sound reasoning lay behind my decision to test whether Aβ and its parent, APP, could provide MFAS-organising activity in two genetic backgrounds where different MFAS organisers (APPL and GAPDH2) had been reduced. Thus, the DCG-organizing mutations *$A\beta_{42}$-Arctic* and *$A\beta_{42}$-wild* type were tested against the mini-cored phenotypes produced by *APPL-RNAi* and *$GAPDH_2$-RNAi,* and the rescues were successful to varying extents. Human APP was also tested against *APPL-RNAi*, and this too resulted in a rescue of the latter's mini-core phenotype. Noticeably, the degrees of these rescues differed: rescues of *APPL-RNAi* by *APP-wild type*, *$A\beta_{42}$-wild type* and *$A\beta_{42}$-Arctic* were all equally successful in restoring 80 % of mini-core DCGs to intactness. However, rescues of *GAPDH2-RNAi* were successful

in the reversion of 68 % of mini-core DCGs to intactness when attempted by *$A\beta_{42}$-wild type*, and the reversion of 80 % of mini-core DCGs to intactness, when attempted by *$A\beta_{42}$-Arctic*. It therefore seemed that the relatedness between human APP, human $A\beta_{42}$-wild type, human $A\beta_{42}$-Arctic, and *Drosophila* APPL allowed them to substitute for the reduction of *Drosophila* APPL. On the other hand, the lower rescue rate of *Drosophila GAPDH2*-kd by human *$A\beta_{42}$-wild type*, as compared to its higher rescue rate by the potently amyloidogenic human *$A\beta_{42}$-Arctic* mutant, suggested that in rescuing the mini-core effect of the loss of a completely unrelated gene (*GAPDH2*), human *$A\beta_{42}$-wild type* was less successful than its amyloidogenic counterpart. My inference here, therefore, was that this rescue was not the result of a common amyloidogenic genetic ancestry, but rather a demonstration of $A\beta_{42}$-Arctic's 'glueing' powers. Yet again, however, the theme of an amyloid-to-amyloid influence was observed, this time in the form of a phenotype rescue.

In interpreting these rescue studies, a caveat I always bore in mind was that the genetic constructs used to create the transgenic *Drosophila* lines might have unknown effects, including the suppression of knockdown phenotypes (the culprits to be considered here would include both the *UAS* and *GAL4* constructs). Specifically, the *UAS-human DNA* might reduce the efficacy of the *RNAi* by diluting the *GAL4* which activates *UAS* elements, thus suppressing the phenotype by diluting the effect of the *RNAi* (Bellen *et al.,* 2019). These unknown effects of genetic enhancers or suppressors merit further scrutiny and will undoubtedly be increasingly flagged up as future translational work moves us ever closer to personalized therapeutics.

Other potential scenarios, germane to suboptimal rescue results, could be the possibility that the human interactome might have changed during evolution, making it unworkable within the ancient *Drosophila* genome. Put differently, homologous human genes, while working towards the same outcome, might be doing so through different molecular avenues, and in an altered molecular framework. Additionally, hidden and undiscovered mutations in the *Drosophila* pathway might obstruct the rescue. Finally, the stereochemical fit of the rescuing human protein might be unstable, loose, or otherwise inactive, making a failed rescue the observable result. Fortunately, none of these theoretical considerations had to be considered with the present set of successful experiments.

Finally, these rescue experiments are not just instructive in the context of laying the groundwork for future applicability; rather, they reveal fundamentally intriguing biological truths about which of our 'newer' human genes still function within the apparatus and framework of the older *Drosophila* genome, and within the even more ancient genomes of common ancestors of flies and humans. In that sense, as this and other studies develop, I hope they give greater clarity into who and what we are as a human species, and how we, either reposed in health or enmired in frailties, fit into natural the world without and within.

7.6 CONCLUDING REMARKS

This programme of work yielded many discoveries, many of which stood alone on their scientific merits. However, when I examined them as a whole, I found they wove a compelling narrative which, I hope, will help move the field of neurodegeneration research forward. These perspectives are presented as concluding remarks below.

7.6.1 LESSONS FROM MFAS

MFAS, a *Drosophila* amyloid protein and homologue of human TGFBI, has been found to be uniquely positioned to lend itself to the study of amyloidogenesis in humans. This is because of several unique biological properties it possesses, some of which were known prior to these studies, and which indeed which made this programme of work possible. The rest of these facts were discovered in the course of this work, and a summary of all these facts, new and known, are summarized below.

7.6.1.1 MFAS' HIGH EXPRESSION IN SCs

MFAS is the seventh-highest expressed gene in *Drosophila* SCs **(Figure 7.7)**, an attribute which makes it's examination and analysis straightforward, even with live microscopy. This finding, reported by Immarigeon *et al.*, in 2020, made my work possible by alerting me to an easily visible target.

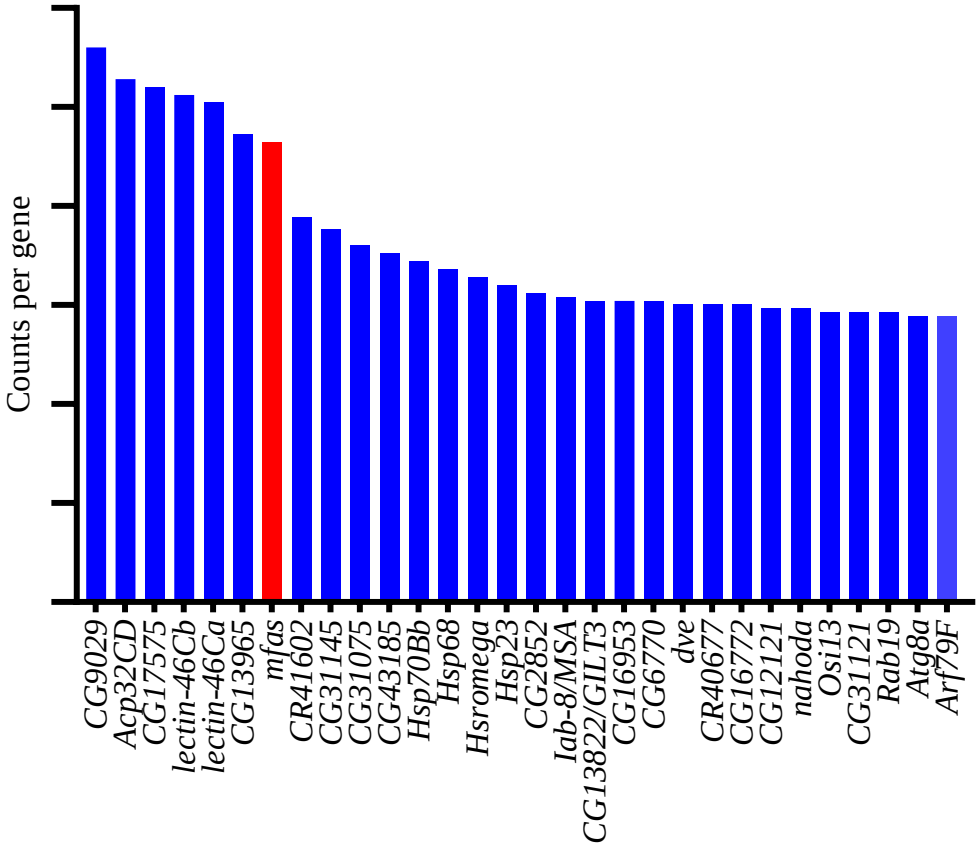

Figure 7.7: MFAS is among the top 30 most highly expressed genes in SCs Regularly-spaced tick marks on the Y-axis representing transcriptome counts per gene ranging from 1,00+00 to 1,00+06. (Adapted from Immarigeon *et al.,* Proc. Natl. Acad. Sci. USA 2020, p. 4).

7.6.1.2 MFAS IS ORGANIZATIONALLY IDENTICAL TO IT'S HOMOLOGUE TGFBI

mfas is a member of the Fasciclin I gene family, and encodes a protein consisting of four 150 amino acid repeats, characteristic of it's Fasciclin I parent family (Hu *et al.,* 1998). This organization is mirrored by it's human homologue, TGFBI (**Figure 1.13) (**Clout *et al.,* 2003; Clout and Hohenester, 2003), and also by its other family member, periostin

(Silver *et al.*, 2016; Di Vita *et al.*, 2021; Vardaki *et al.*, 2016; Balbi *et al.*, 2021) (**Figure 7.8**).

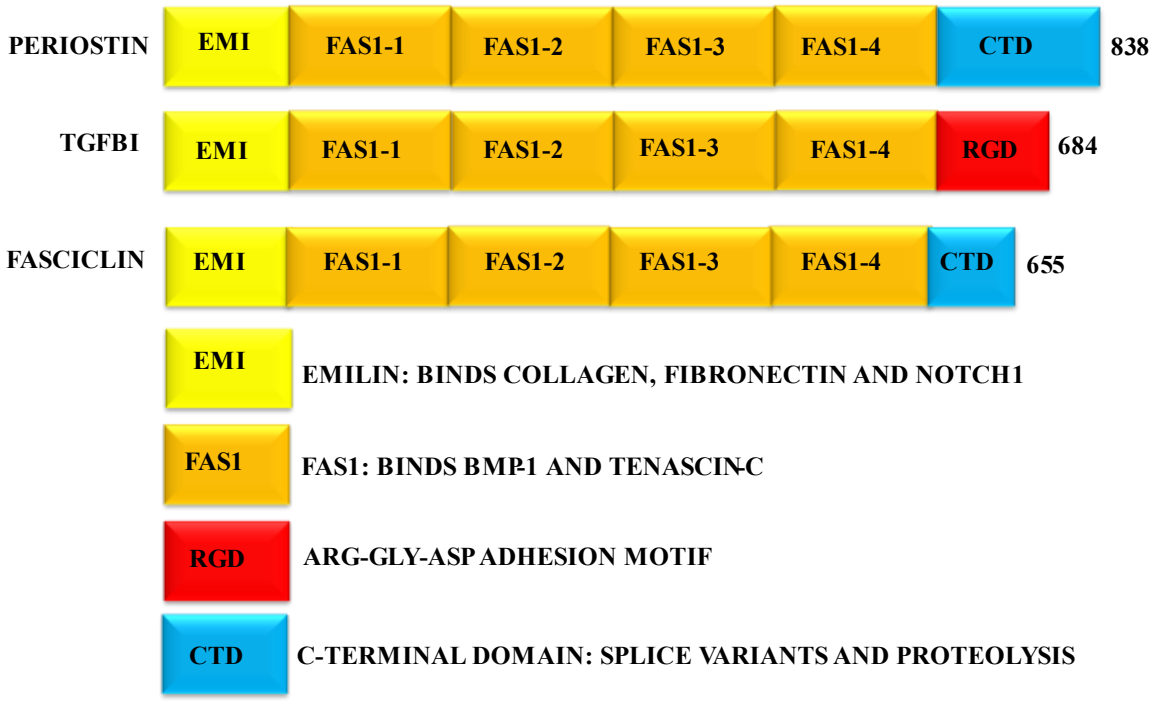

Figure 7.8: Periostin is a member of the closely-related Fasciclin I family, which includes TGFBI and *Drosophila* Fasciclin. As shown, they all share organisational similarities.

7.6.1.3 MFAS IS AN AMYLOID PROTEIN

MFAS was examined by Raman Spectroscopy, confirming it's amyloid identity (Martin Jahn and Preman Singh, 2021, unpublished results). This fact further underscores it's links to human TGFBI, which is potentially amyloidogenic, and is responsible for a wide array of debilitating corneal diseases. MFAS' amyloid properties also give it durability, allowing it to be imaged *ex vivo* without loss of structural integrity, and making possible ageing experiments which can be conducted for weeks, limited only by the lifespan of the fly.

7.6.1.4 MFAS IS CRUCIAL FOR THE FORMATION OF DCGs

My work showed that the knockdown of *mfas* leads to the complete non-formation of DCGs in all *Drosophila* lines tested (**Figure 3.9**). The discovery of so narrow and critical a function for MFAS provided focus and refinement to the task of measuring the numerous genetic manipulations that were subsequently discovered to influence MFAS and DCG biogenesis.

7.6.1.5 MFAS HAS INSULARITY OF FUNCTION

Despite it being crucial for the seemingly central and prominent function of dense-core formation in *Drosophila* SCs, I found that *mfas*-knockdown does not affect the formation of Rab6 or Rab11 compartments in SCs, or the generation of Rab6 or Rab11 exosomes. This discovery was somewhat unexpected, since Rab11, in particular, has strong associations with Alzheimer's disease as well as several other amyloidogenic neurodegenerative diseases. This underlines even further the narrowness and insularity of MFAS' role, an attribute bestowing a greater sense of precision on the experimental results which were presented here.

7.6.1.6 MFAS IS SUSCEPTIBILE TO THE INFLUENCE OF OTHER AMYLOIDS

7.6.1.6.1 MFAS IS INFLUENCED BY *DROSOPHILA* APPL

The knockdown of *Drosophila APPL* leads to the non-coalescence of MFAS, resulting in distinctive 'mini-cores'. Time-lapse videos clearly demonstrate the failure of fusion of MFAS moieties as a result of APPL's absence, strongly suggesting that the combined presence of APPL and MFAS contrive on a structural, bioenergetic, or some other combinatorial level to bring discrete particles of MFAS together.

7.6.1.6.2 MFAS IS INFLUENCED BY HUMAN FAD MUTATIONS

FAD mutations both within and outside the $A\beta_{42}$ segment of *APP* impacted the organization of MFAS in a very particular manner, depending on the individual mutation involved. Demonstrating MFAS' particularity, however, was its non-perturbation by wild type $A\beta_{42}$ and *APP*.

a) MFAS' RESPONSE TO $A\beta_{42}$-*E693Q-DUTCH* AND $A\beta_{42}$-*D694N-IOWA*

The $A\beta_{42}$-*Dutch* and $A\beta_{42}$-*Iowa* mutations, which both produce human brain plaques described as 'cloud-like' or 'diffuse', result in similarly diffuse, fragmented-appearing DCGs. This DCG appearance is also the result of non-coalescence of MFAS seen on time-lapse videos I made (not shown in this thesis), and again raises several questions about the fundamental nature of the interaction between these disparate amyloids.

b) MFAS' RESPONSE TO $A\beta_{42}$-*E693G-ARCTIC*

$A\beta_{42}$-*Arctic*, the archetypal intra-$A\beta_{42}$ mutation, uniquely produces distinctive 'targetoid' brain plaques. Intriguingly, this mutation re-organizes MFAS into a similar targetoid configuration. It is well accepted that the amyloid forms of proteins represent their most bioenergetically advantageous states (**Figure 7.9**). In particular, amyloid crystals have been identified as the base, or ground state within the protein folding and aggregation bioenergetic landscape (Adamcik and Mezzenga, 2018). These, therefore would be the amyloid crystal storage forms of peptide hormones in biologically active granules in mammals, and, quite likely, the Decapentaplegic-storing form of MFAS in *Drosophila's* DCG*s*.

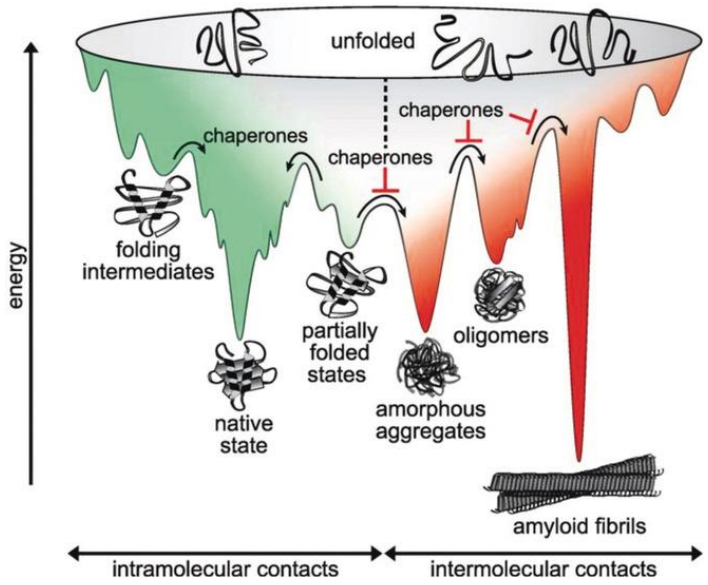

Figure 7.9: Amyloids, and specifically amyloid crystals, represent the most bioenergetically advantageous form of protein existence. In their natively folded state, intramolecular contacts dominate; however in their amyloid state, intermolecular interactions become more important. These various bioenergetic adjustments all work together to make them energy-efficient. (Adamcik and Mezzenga, Angew. Chem. Int. Ed. 2018, p. 8734).

The investigation of the basis of the concentric-circle reorganization of MFAS with the *$A\beta_{42}$-Arctic* mutation, as well as an evaluation of the unusual repulsion of *$GAPDH_2$*- and *APPL*-kd mini-cores from the point of view of bioenergetics, would undoubtedly lead to fascinating insights into some of these basic questions. With some understanding of the biophysics of amyloids, and with a live platform upon which to test them, some of these fundamental questions might be tackled using this *Drosophila* system.

c) MFAS' RESPONSE TO *APP-K670N/M671L-SWEDISH*

Amyloid Precursor Protein (*APP*), the human homologue of *Drosophila APPL* and the gene which encodes the progenitor of Aβ oligomers, has several FAD mutations along it's length. The Swedish *APP-K670N/M671L* double mutation lies just outside the β-secretase

cleavage site, and is responisble for a particularly pernicious from of FAD, characterized by an early onset, rapidly progressive dementia, and the frequent accompaniment of refractory seizures. In *Drosophila*, overexpression of the *APP-Swedish* mutation in SCs results in fewer intact DCGs, abnormal-appearing and misshapen SCs, and giant lysosomes, suggesting that the cellular machinery is likewise dealing with profoundly pathological proteins. By virtue of it's location just outside the amyloidogenic $A\beta_{42}$ sequence, the Swedish mutant provides a glimpse of the effects of an extra-$A\beta_{42}$ perturbation, and by the same token, the fidelity of the fly MFAS system. To wit, the three intra-$A\beta_{42}$ mutations (*Arctic*, *Dutch* and *Iowa*), all directed the reorganization of MFAS in patterns that correlated with their neuropathological plaque patterns in human disease. Not so with the *Swedish* mutation, which is but a single amino acid removed from the specialized $A\beta$ zone. Rather, it produces the classic, more recognizable 'cotton wool' plaques of AD. Thus, since *Swedish's* location is just outside the $A\beta$ zone, it follows the rule of not producing CAA, while in the context of SCs, it produces generally abnormal appearing SCs and a diminution in DCG numbers. Furthermore, in keeping with evidence that APP-Swedish is preferentially processed in acidic milieus, my experiments showed the consistent finding of giant lysosomes with this mutation. My hypothesis here is that the APP-Swedish mutation blocks processing in DCG compartments, but some compartments mature normally because they also express *Drosophila* APPL, and so the defective compartments are then targeted to lysosomes. My surmise is that the abnormal proteins overcome the salutary effects of APPL, and therefore go on to overwhelm the lysosomal system. Again, this particular set of experiments made it clear that MFAS was exquisitely sensitive to the human APP-Swedish double mutation as well.

7.6.1.6.3 MFAS IS INFLUENCED BY TGFBI, IT'S HUMAN HOMOLOGUE

MFAS is organizationally identical to it's homologue TGFBI, a potentially amyloidogenic protein which plays a key structural role in the mammalian cornea, as well as important roles in severeal cancers. Human *TGFBI* mutations result in vision-threatening corneal dystrophies, often requiring the drastic treatment measure of corneal transplantation. Mutated *TGFBI,* when introduced into the *Drosophila* genome, directed it's homologue MFAS into the formation of severely mishapen DCGs. As an additional test, a mutation conserved between *TGFBI* and *mfas* was introduced into *mfas* which was then introduced as an extra copy into the fly genome, and this too produced similarly abnormal DCGs. Finally, the introduction of wild type *TGFBI* as well as the introduction of an extra copy of wild type *mfas* into the fly genome produced normal DCGs. These results show that amyloidogenic TGFBI mutations influence it's homologue, MFAS, and, as shown here, in each case those mutations involved just a single nucleotide.

7.6.1.7 MFAS IS AMENABLE TO RESCUE BY OTHER AMYLOIDS

In the experiments done here, this was illustrated in the combination of *$A\beta_{42}$-E693G-Arctic* and *APPL-RNAi,* as well as in the combination of *$A\beta_{42}$-E693G-Arctic* and *$GAPDH_2$-RNAi,* in which the DCG-organizing effects of the Arctic mutation rescued the mini-core-producing effects of *APPL*- and *$GAPDH_2$*-kds. Similar effects were also seen with the combination of *TGFBI*-CD mutations and *APPL-RNAi* **(§ 5.2.4**). In the case of the *TGFBI* mutants, however, the resultant phenotypes were not considered rescued, since both parental phenotypes had abnormal DCGs to start with. Rather, the progeny emerged more as intermediates, possessing DCG characteristics from both parents. In either scenario, however, these experiments demonstrated the excellence of MFAS as an indicator of the

interplay of these physiological and pathological forces, and provided a good platform from which to measure the pathogenicity of one amyloid against another.

7.6.1.8 MFAS' OVERALL SENSITIVITY AND SPECIFICITY TO THE MANIPULATION OF OTHER AMYLOIDS

As demonstrated in the preceding experimental results, MFAS is extremely responsive to specific changes in certain amyloids. Specifically, in each of the mutants tested, the mutation involved a change in just a single nucleotide. As a cross-check, the wild type genes (*mfas, TGFBI, APP,* and $A\beta_{42}$) were all tested alongside their mutated versions, and the wild types all produced normal DCGs. Thus, the fact that MFAS' responses are both highly sensitive and specific argue against the possibility of the dysmorphic biogenesis of DCGs being merely a general reaction to a cellular insult. Put differently, this constitutes experimental evidence that a change in one amyloid protein affects other amyloid proteins in a very specific way. Fortuitously, owing to the confluence of several factors, MFAS has emerged as an excellent barometer of this phenomenon.

The historical context behind this speculative amyloid-to-amyloid influence was the century-old neuropathological observation that Alzheimers brains unfailingly showed amyloid spreading in a contiguous fashion. The inescapable conclusion was that misfolded amyloid was inducing normal protein neighbours to misfold. This observation is the basis for the Braak and Braak staging of tau (Braak and Braak, 1991), the Thal staging of Aβ (Thal *et al*., 2002), the McKeith staging of α-synuclein in Lewy Body Dementias (McKeith *et al.,* 1996; McKeith *et al.,* 2005), the Brettschneider staging of TDP-43 in Amyotrophic Lateral Sclerosis (Brettschneider *et al.,* 2013), the Parchi staging of both Creutzfeldt-Jakob

Disease (Parchi *et al.,* 1999) and Fatal Familial Insomnia (Parchi *et al.,* 1995), and the Vonsattel staging of Huntingtin in Huntington's disease as it spreads in the basal ganglia (Vonsattel *et al.,* 1985). In the wake of these clinical and pathological observations, theories such as amyloid 'seeding' or 'crosstalk' sprung up (reviewed in Subedi *et al.,* 2022). Providing further support for this hypothesis were reports that cadaveric pituitary growth hormone injections introduced Aβ pathology into otherwise healthy recipients (Purro *et al.,* 2018; Huynh and Holtman, 2018). Even more surprisingly, host-to-graft amyloid transformation was seen with the development of Lewy bodies in grafted neurons implanted in the brains of patients with Parkinson's disease (Li *et al.,* 2008; Kordower et *al.,* 2008). Similarly, the development of amyloid changes in transplanted corneas has also been reported in patients with the *TGFBI-R555Q* mutation (Gear *et al.,* 2005).

Given this history, it seems reasonable to interpret MFAS' responses to manipulation of other amyloids as evidence of this elusive inter-amyloid communication. With the decades-long time frame of amyloid neurodegeneration in living patients, this putative process of amyloid crosstalk has heretofore been impossible to observe, the barriers to it's study being temporal, technical and ethical. The experiments presented here might therefore be the first to document this process in a living organism.

7.6.2 FUTURE DIRECTIONS

The brief 16-day cycle between the creation of *Drosophila* crosses and their imaging allows for efficiency and rapid experimentation. It also enables rapid screening with modalities like stereomicroscopy and live widefield microscopy, combined with large-scale genetic

knockdown analysis. Such analyses could potentially shed light on the highly relevant question of amyloid crosstalk. Furthermore, as the section on rescue experiments suggests, unravelling the mechanisms of crosstalk holds out therapeutic promise. While it could be argued that the actual rescues are more about replacing protein aggregation activity, genetic screens to suppress amyloidogenesis are definitely possible. Specific steps being taken towards this, together with suggestions for future research, are laid out below.

7.6.2.1 CREATING A DATABASE BASED ON DCG MORPHOLOGY

Neurodegeneration research in *Drosophila* has resulted in the development of fly models for Alzheimer's disease, Parkinson's disease, Dementia with Lewy Bodies, Amyotrophic Lateral Sclerosis, Frontotemporal Dementia, Huntington's disease, Ataxia Telangiectasia, Mitochondrial Encephalomyopathies, Leigh syndrome, Traumatic Brain Injury, and neurodegeneration-linked brain tumours (McGurk *et al.,* 2015; Bolus *et al.,* 2020). These in turn have engendered several assays, both behavioural and structural, designed to objectively quantify the extent of the underlying neuropathology. Behavioural assays measure climbing ability, olfactory acuity, lifespan, fast phototaxis, negative geotaxis, eclosion percentages, bang-sensitivity, flying, locomotion, jumping, shock reactivity, odour conditioning, and learning and memory. Structural assays include eye morphology, retinal degeneration, histology for photoreceptor degeneration, histology for brain morphology, dendritic branching, photoreceptor morphology count, histological staining for vacuole quantification, adult mushroom body morphology, larval wing imaginal disc morphology, and larval neuromuscular junction morphology. Other assays include electroretinograms, measurement of various protein levels, and various immunostaining techniques applied to different parts of the nervous sytem (reviewed in Bolus *et al.,* 2020).

The work presented in this thesis has led to the idea of cataloguing DCG and SC morphologies in *Drosophila* transgenic for amyloidogenic human genes. Examples of these would be the mini-core phenotypes produced by *Aβ42-Dutch* and *Iowa* mutations, the targetoid DCG phenotype produced by the *Aβ42-Arctic* mutation, and the giant lysosome phenotype produced by the *APP-Swedish* double mutation. Indeed, *APP* is subject to numerous FAD mutations along it's length, which would be easily testable using this sytem. Examples are the *French, German, Australian, London, Indiana,* and *Florida* mutations, located towards the C-terminal of APP, and which would provide invaluable information about aberrations in the biologically active intracellular domain of APP. The above-listed mutations are analogous to the *Swedish* mutation in causing severe FAD and lying just outside the *Aβ42* sequence, but at *APP's* C-terminal end (**Figure 7.10**). Thus, this cluster might be viewed as *Swedish*'s C-terminal counterpart and a potential treasure trove of information, easily pried open with this experimental model.

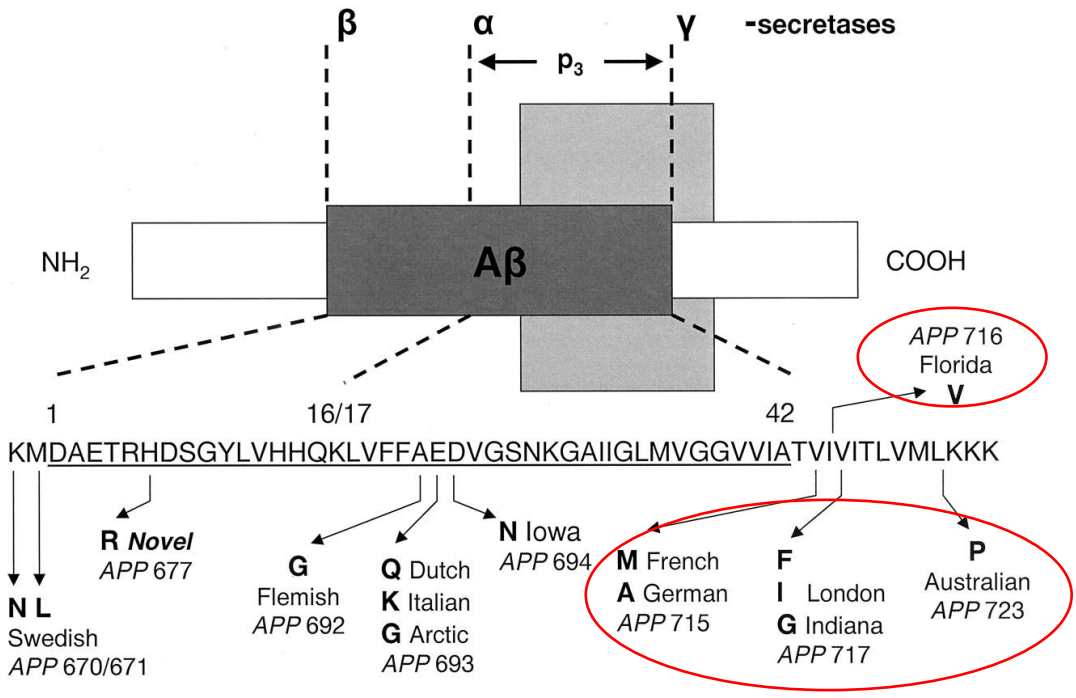

Figure 7.10: *APP's* C-terminal FAD mutations (red ovals). The *French, German, London, Indiana, Florida,* and *Australian* mutations occupy positions analogous to the *Swedish* mutation, but on the C-terminal end of *APP*. (Adapted from Janssen *et al*., Neurology 2003, p. 3).

Other notable inclusions within this database would be the various DCG deformities produced by *TGFBI*-CD mutations. The overall aim of this is data repository would be to create a new structural assay, adding to the tools available to *Drosophila* neurodegeneration researchers. Furthermore, with the morphological objectivity provided by DCGs, automation and machine-learning algorithms could easily be applied to their measurement (development of such algorithms for DCGs are currently being developed and tested in the Wilson laboratory). Precise, automated algorithms would enhance the reliability of this database, and ensure that new data could quickly be added and accurately analysed against existing information. Thus, DCG/MFAS measurements would add to the pantheon of traditional structural assays, and with their objectivity and amenability to machine learning, might hopefully become regarded as exacting standards in neurodegeneration research.

Recent work has demonstrated that endoplasmic reticulum (ER) mutations in spastin, ATL1, RTN2 and REEP1 are increasingly linked to neurodegenerative diseases like Herditary Spastic Paraplegias (HSPs). Other ER-associated mutations are linked to Alzheimer's, Parkinson's, Amyotrophic Lateral Sclerosis, Huntington's, Warburg syndrome, and Peripheral Neuropathies (reviewed in Öztürk, O'Kane and Pérez-Moreno, 2020). This points to a definite intersection between the burgeoning field of ER-related neurodegeneration and amyloid biology, which I intend to pursue with this DCG model. In

addition, there are emerging links between brain tumours and neurodegeneration, which could lend themselves to the application of this experimental system. One such link involves mouse gliomagenesis and fly synaptic dysfunction, as evidenced by the fact that mice expressing mutated isocitrate dehydrogenase (IDH) in the subventricular zone showed an expansion of cells in this area, with a pattern of gene expression mirroring that of human glioblastomas (Bardella *et al.,* 2016). IDH driver mutations are also found in acute myeloid leukaemia, cholangiocarcinoma, chondrosarcoma, and sporadically in several other cancers, making IDH an important target. Intriguingly, loss of *Drosophila* IDH causes loss of synaptic transmission, in addition to causing a reduction in the Krebs cycle metabolite α-ketoglutarate (α-KG) (Ugur *et al.,* 2017). When α-KG, which has links to neurodegeneration, is supplemented, these *Drosophila* neural defects are mitigated. This demonstrates just one of the many newly-discovered fly-mammalian neuropathological connections which could potentially be well-served with the rapid and reliable fly neurodegeneration model described here.

7.6.2.2 CREATING A DATABASE SUBSECTION COMPARING EFFICACY OF RESCUES

In addition to creating a core compendium of mutation-driven structural variants, a subsection comparing the efficacy of rescues could be included. The rescue experiments presented here, while yielding some surprises, also suggested new avenues of investigation. Insights such as these could set the stage for an array of starting points for reverse translational research. I would make a distinction, however, between overexpressing proteins, as I did here, from RNAi screens. Another distinction would be the difference between the suppression of an amyloidogenic phenotype, like mini-cores caused by

overexpressing *Aβ42-Dutch* and *Aβ42-Iowa*, from the suppression of mini-cores produced by failure of MFAS to aggregate, as seen in *GAPDH*- and *APPL*-kds.

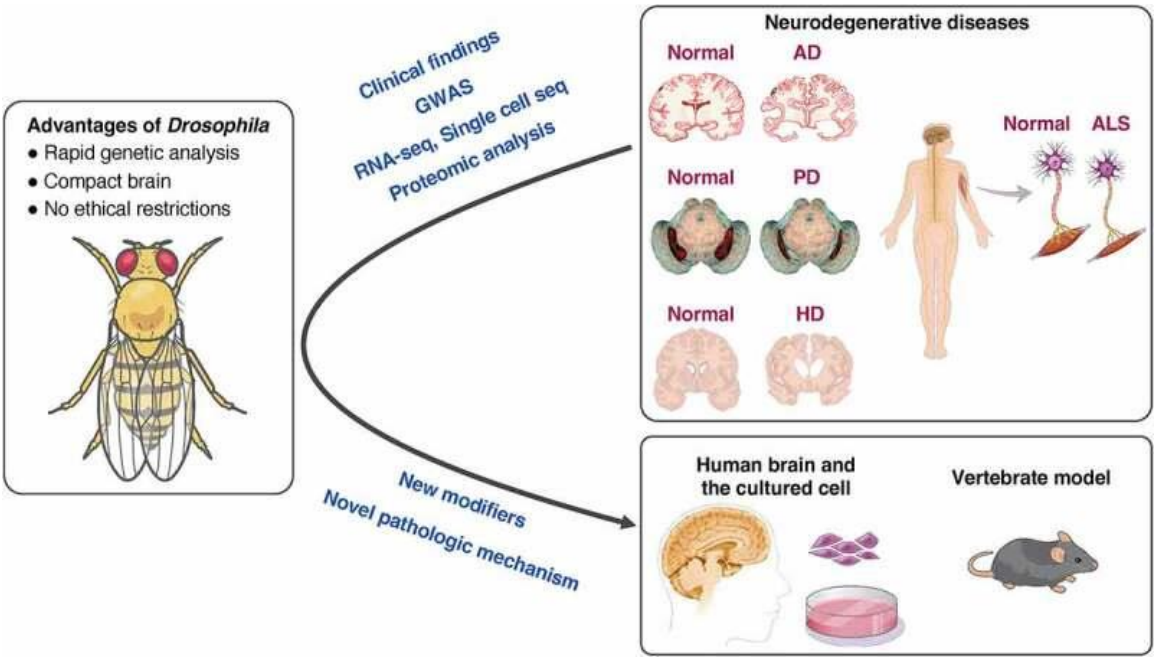

Figure 7.11: Reverse translational research using *Drosophila.* (Nitta and Sugie, Fly 2022, p. 280).

This *Drosophila* system would be an excellent forum for identifying disease-specific aberrations in MFAS in flies transgenic for the genetic disease in question, and then correlating or reverse-engineering these abnormalities back to mouse or tissue culture models. An example of such a reverse translational discovery making it's way into the neuropathological canon was the finding that expression of α-synuclein in the *Drosophila* brain resulted in the formation of rod-like actin-positive structures in neurons and abnormalities in the actin filament network (Ordonez *et al.*, 2018). Identical findings were subsequently confirmed in postmortem brains of patients with Dementia with Lewy

Bodies, and in a synucleinopathy mouse model (Sarkar *et al.,* 2021). Thus, the inkling of a new disease mechanism, first seen in *Drosophila*, when taken forward to higher organisms was found to be conserved in humans and mice. Similarly, in *Drosophila* Tauopathy models, heterochromatin was found to be relaxed, revealing increased gene transcription and the activation of normally inactive transposable elements (Frost *et al.,* 2014; Sun *et al.,* 2018). Subsequent RNA sequencing data from 636 Alzheimer's patients confirmed this pattern of heterochromatin relaxation and activation of retrotransposon transcription, enabling the identification of a new disease mechanism in Alzheimer's and Progressive Supranuclear Palsy (Guo *et al.,* 2018).

7.6.2.3 EXPLORING NEURODEGENERATION AND NEUROREGENERATION

In a rather more optimistic vein than neurodegeneration, the fly is emerging as a model to study neuroregeneration. These studies involved the recreation of scenarios of nerve crush injuries (Mishra *et al.,* 2014), the simulation of nerve transections by laser axotomies or dendriotomies (Li *et al.,* 2018), or the reproduction of traumatic brain injuries (Sanuki *et al.,* 2019). As demonstrated by the lessons of reverse translational research, we stand to learn a lot from this 'reverse neurodegeneration' approach. For example, almost two decades ago it was shown that APP promotes post-developmental neurite arborization in the *Drosophila* brain (Leyssen *et al.,* 2005). The rescue experiments included in my thesis showed that overexpression of *APP* and its internally located component, $A\beta_{42}$, rescued *APPL-RNAi,* a highly penetrant mini-core-producing genotype. Conceivably, such rescue experiments with *APP* might reveal a neuroregenerative clue which, if conserved in higher organisms, might in turn lead to therapeutic insights. Anticipating the argument that the *APP/*$A\beta_{42}$*-APPL-RNAi* rescue was in fact a fairly straightforward one without any

redeeming deeper lessons, I would counter that these interactions could at least refine our understanding of regeneration and rescues. This might be particularly true if we were to compare time-lapse videos of rescues with those of their ‘un-rescued’ pathological forms.

7.6.2.4 USING THIS FLY MODEL AS A WINDOW TO EXPLORE THE FUNDAMENTAL BIOLOGY OF AMYLOID

Finally, these results raise fundamental questions about amyloid: is its behaviour comprehensible by conventional scientific explanations, or is it a quasi-autonomous, prion-like element, governed by yet-undiscovered biological rules? If so, our view of degenerative diseases would change completely. Rather than being resigned to the inevitability of degeneration in general and neurodegeneration in particular, we might instead raise our sights and set about managing and controlling these conditions. Until recently, prions were dismissed as biological heresy. Could amyloid join them as outliers in the DNA-RNA-protein orthodoxy? If this occurs, it would be a paradigm shift in biology and medicine.

CHAPTER 8

BIBLIOGRAPHY

8. BIBLIOGRAPHY

- Adamcik, J., and Mezzenga, R. (2018). Amyloid polymorphism in the protein folding and aggregation energy landscape. Angew. Chem. Int. Ed. 57: 8370-8382.
- Afshari, N., *et al.* (2004). Discovery of a novel homozygous mutation in the TGFBI (BIGH3) gene (V624M) in a patient with unilateral lattice corneal dystrophy. Invest. Ophthalmol. Vis. Sci. 45E-abstract 1517.
- Akbergenova, Y., and Littleton, J. T. (2017). Pathogenic Huntington alters BMP signaling and synaptic growth through local disruption of endosomal compartments. J. Neurosci. 37 (12): 3425-3439.
- Akiya, S., and Brown, S. I. (1970). Granular dystrophy of the cornea. Characteristic electron microscopic lesions. Arch. Ophthalmol. 84: 179-192.
- Aldave, A. J., *et al.* (2005). A unique corneal dystrophy of Bowman's layer and stroma associated with the Gly623Asp mutation in the transforming growth factor beta-induced (TGFBI) gene. Ophthalmology. 112: 1017-1022.
- Altman, N., and Krzywinski, M. (2015). Points of significance: Sources of variation. Nat. Methods. 12: 5-6.
- Andersen, O. M., *et al.* (2005). Neuronal sorting protein-related receptor sorLA/LR11 regulates processing of the amyloid precursor protein. Proc. Natl. Acad. Sci. USA. 102: 13461-6.
- Andersen, R. B., *et al.* (2004). Purification and structural characterization of Transforming Growth Factor Beta-Induced protein (TGFBIp) from porcine and human coneas. Biochemistry. 43: 16374-16384.

- Arriagada, P. V., *et al.* (1992). Neurofibrillary tangles and not senile plaques parallel duration and severity in Alzheimer's disease. Neurology. 42: 1681-1688.
- Attrill, H., *et al.* (2016). FlyBase: establishing a gene group resource for *Drosophila melanogaster*. Nucleic Acids Res. 44: D786-D792.
- Axelman, K., *et al*. (1994). A large Swedish family with Alzheimer's Disease with a codon 670/671 Amyloid Precursor Protein mutation. Arch. Neurol. 51: 1193-1197.
- Bairati, A. (1968). Structure and ultrastructure of the male reproductive system in Drosophila melanogaster meig. 2. The genital duct and accessory glands. Monitore Zoologico Italiano (Italian Journal of Zoology). 2 (34): 105-182.
- Balbi, C., *et al.* (2021). An exosomal-carried short periostin isoform induces cardiomyocyte proliferation. Theranostics. 11 (12): 5634-5649.
- Baldwin, A. J., *et al.* (2006). Cytochrome display on amyloid fibrils. J. Am. Chem. Soc. 128: 2162-2163.
- Barbagallo, A., *et al.* (2010). Tyr (682) in the intracellular domain of APP regulates amyloidogenic APP processing *in vivo*. PLoS One. e15503.
- Bardella, C., *et al.* (2016). Expression of Idh1R132H in the murine subventricular zone stem cell niche recapitulates features of early gliomagenesis. Cancer Cell. 30: 578-594.
- Barrett, P. J., *et al.* (2012). The amyloid precursor protein has a flexible transmembrane domain and binds cholesterol. Science. 336 (6085): 1168-1171.
- Bastiani, M. J., *et al.* (1987). Expression of glycoproteins I and II on subsets of axon pathways during neuronal development in the grasshopper. Cell. 48: 745-755.

- Basun, H., *et al.* (2008). Clinical and neuropathological features of the Arctic App gene mutation causing early-onset Alzheimer's disease. Arch. Neurol. 65: 499-505.
- Becker, A., *et al.* (2016). Extracellular vesicles in cancer: cell-to-cell mediators of metastasis. Cancer Cell. 30: 836-848.
- Bécot, A., *et al.* (2020). Transmissible endosomal intoxication: a balance between exosomes and lysosomes at the basis of intracellular amyloid propagation. *Biomedicines.* 8; 272; doi:10.3390/biomedicines8080272.
- Bellen, H.J. *et al.* (2010). 100 years of *Drosophila* research and its impact on vertebrate neuroscience: a history lesson for the future. *Nature Reviews Neuroscience.* 11: 514-522.
- Bellen, H. J., *et al.* (2019). The fruit fly at the interface of diagnosis and pathogenic mechanisms of rare and common human diseases. Hum. Mol. Genet. 28 (R2): R207-R214.
- Berry, M. D. (2004). Glyceraldehyde-3-phosphate dehydrogenase as a target for small-molecule disease-modifying therapies in human neurodegenerative disorders. J. Psychiatry Neurosci. 29 (5): 337-345.
- Berry, M. D., and Boulton, A. A. (2000). Glyceraldehyde-3-phosphate dehydrogenase and apoptosis. J. Neurosci. Res. 60: 150-154.
- Berson, J. F., *et al.* (2003). Proprotein convertase cleavage liberates a fibrillogenic fragment of a resident glycoprotein to initiate melanosome biogenesis. J. Cell Biol.
- Blair, J. A., *et al.* (2014). Accumulation of intraneuronal amyloid-β is common in normal brain. Curr. Alzheimer Res. 11: 317-324.

- Bloch Qazi, M. C., and Wolfner, M. F. (2003). An early role for the Drosophila melanogaster male seminal protein Acp36DE in female sperm storage. J. Exp. Biol. 206: 3521-3528.
- Bolkan, B. J., *et al.* (2012). Beta-secretase cleavage of the fly amyloid precursor protein is required for glial survival. J. Neurosci. 32 (46): 16181-16192.
- Bolus, H., *et al.* (2020). Modeling neurodegenerative disorders in *Drosophila melanogaster*. Int. J. Mol. Sci. 21: 3055.
- Bonifacino, J., *et al.* (2003). Signals for sorting of transmembrane proteins to endosomes and lysosomes. Annu. Rev. Biochem. 395-447.
- Booth, D. R., *et al.* (1997). Instability, unfolding and aggregation of human lysozome variants underlying amyloid fibrillogenesis. Nature. 385: 787-793.
- Boulianne, G. L., *et al.* (1997). Cloning and characterization of the *Drosophila* presenilin homologue. Neuroreport. 8 (4): 1025-1029.
- Braak, H., and Braak, E. (1991). Neuropathological staging of Alzheimer-related changes. Acta Neuropathologica. 82:239-259.
- Brand, A. H., and Perrimon, N. (1993). Targeted gene expression as a means of altering cell fates and generating dominant phenotypes. Development. 118 (2): 401-415.
- Breda, C., *et al.* (2015). Rab11 modulates alpha-synuclein-mediated defects in synaptic transmission and behaviour. Hum. Mol. Genet. 24: 1077-1091.
- Brettschneider, J., *et al.* (2013). Stages of pTDP-43 pathology in Amyotrophic lateral Sclerosis. Ann. Neurol. 74 (1): 20-38.

- Brinkmalm, G., *et al.* (2019). Identification of neurotoxic cross-linked β-amyloid dimers in the Alzheimer's brain. Brain. 142: 1441-1457.
- Brunholz, A., *et al.* (2012). Axonal transport of APP and the spatial regulation of APP cleavage and function in neuronal cells. Exp. Brain Res. 353-364.
- Burd, C., and Cullen, P. J. (2014). Retromer: a master conductor of endosomal sorting. Cold Spring Harbor Perspect. Biol. 6 a016774.
- Burrough, A. M., *et al.* (2007). Small but versatile: the extraordinary functional and structural diversity of the β-grasp fold. Biol. Dir. 2: 18.
- Butera, G., *et al.* (2019). Regulation of autophagy by nuclear GAPDH and its aggregates in cancer and neurodegenerative disorders. Int. J. Mol. Sci. 20 (9): 2062.
- Cao, X., and Südhof, T. C. (2001). A transcriptional correction of a transcriptionally active complex of APP with Fe65 and histone acetyltransferase Tip60. Science. 115-120.
- Carmine-Simmen, K., *et al.* (2009). Neurotoxic effects induced by the Drosophila amyloid-beta peptide suggest a conserved toxic function. Neurobiol. Dis. 33 (2): 274-281.
- Carson, D. D., *et al.* (2002). Changes in gene expression during the early to mid-luteal (receptive phase) transition in human endometrium detected by high-density microarray screening. Mol. Hum. Reprod. 8: 871-879.
- Cassar, M., and Kretzschmar, D. (2016). Analysis of Amyloid Precursor Protein function in *Drosophila melanogaster*. Frontiers in Molecular Neuroscience. 9: 1-9.

- Castanho, I., and Lunnon, K., (2019). Epigenetic processes in Alzheimer's disease. In: Chromatin Signaling and Neurological Disorders, pp. 153-180. Academic Press, Elsevier. https://doi.org/10.1016/B978-0-12-813796-3.00008-0.
- Chakravarti, S., *et al.* (2005). TGFBI gene mutations causing lattice and granular corneal dsytrophies in Indian patients. Invest. Ophthalmol. Vis. Sci. 46: 121-125.
- Chan, C. C., *et al.* (2011). Systematic discovery of Rab GTPases with synaptic functions in *Drosophila.* Curr. Biol. 21: 1704-1715.
- Chang, C., *et al.* (2015). AMPK-dependent phosphorylation of GAPDH triggers SIRT1 activation and is necessary for autophagy upon glucose starvation. Mol. Cell. 60: 930-940.
- Chapman, M. R., *et al.* (2002). Role of *Escherichia coli* curli operons in directing amyloid fibre formation. Science. 295: 851-855.
- Chapman, T., *et al.* (2003). The sex peptide of Drosophila melanogaster. Female post-mating responses analyzed by using RNA interference. Proc. Natl. Acad. Sci. USA. 100: 9923-9928.
- Chassigneaux, S., and Allinquant, B. (2012). Functions of APP, sAAPα and sAPPβ: similarities and differences. J. Neurochem. 120 (1): 99-108.
- Chau, H. M., *et al.* (2003). H626R and R124C mutations of the TGFBI (BIGH3) gene cause lattice corneal dystrophy in Vietnamese people. Br. J. Ophthalmol. 87: 686-689.
- Chen, G., *et al.* (2017). Amyloid beta: structure, biology and structure-based therapeutic development. Acta Pharmacol. Sin. 38: 1205-1235.

- Chen, W., *et al.* (1990). A sequence found in cytoplasmic tails is required for coated-pit internalization of the low density lipoprotein receptor. J. Biol. Chem. 3116-3123.
- Chiti, F., and Dobson, C. M. (2006). Protein misfolding, functional amyloid, and human disease. Ann. Rev. Biochem. 75: 333-366.
- Choy, R. W., *et al.* (2014). Retromer mediates a discrete route of local membrane delivery to dendrites. Neuron. 82: 55-62.
- Christoforou, A., *et al.* (2011). Convergence of linkage, association and GWAS findings for a candidate region for bipolar disorder and schizophrenia on chromosome 4p. Mol. Psychiatry. 16 (3): 240-242.
- Chutna, O., *et al.* (2014). The small GTPase Rab11 co-localizes with α-synuclein in intracellular inclusions and modulates its aggregation, secretion and toxicity. Hum. Mol. Genet. 23 (25): 6732-6745.
- Cipriani, G., et al. (2011). Alzheimer and his disease: a brief history. Neurol. Sci. 32: 275-279.
- Clout, N. J., *et al.* (2003). Novel fold revealed by the structure of a FAS1 domain pair from the insect cell adhesion molecule Fasciclin I. Structure (Camb). 11: 197-203.
- Clout, N. J., and Hohenester, E. (2003). A model of FAS1 domain 4 of the corneal protein beta(ig)-h3 gives a clearer view on corneal dystrophies. *Mol. Vision*. 9: 440-448.
- Cohen, A. S., and Calkins, E. (1959). Electron microscopic observation on a fibrous component in amyloid of diverse origins. Nature. 183:1202-1203.

- Cohen, S. I. A., *et al.* (2013). Proliferation of amyloid amyloid-β_{42} aggregates occurs through a secondary nucleation mechanism. Proc. Natl. Acad. Sci. USA. 110: 9758-9763.
- Colombo, M., *et al.* (2014). Biogenesis, secretion and intracellular interactions of exosomes and other extracellular vesicles. Annu. Rev. Cell. Dev. Biol. 30: 255-289.
- Colon, W., and Kelly, J. W. (1992). Partial denaturation of transthyretin is sufficient for amyloid fibril formation in vitro. Biochemistry. 31: 8654-8660.
- Comito, G., *et al.* (2020). Nutritional exchanges within tumor microenvironment: impact for cancer aggressiveness. Front. Oncol. 10. https://doi.org/10.3389/fonc.2020.00396.
- Congdon, E. E., and Sigurdsson, E. M. (2018). Tau-targeting therapies for Alzheimer disease. Nature Reviews Neurology. 14: 399-415.
- Cooper, D. N., *et al.* (2010). Methylation-mediated deamination of 5-methylcytosine appears to give rise to mutations causing human inherited diseases in CpNpG dinucleotides. Hum. Genom. 4: 406-410.
- Core, A. B., *et al.* (2014). Hemojuvelin and bone morphogenetic protein (BMP) in iron homeostasis. Frontiers in Pharmacology. 5: 104.
- Corrigan, L., *et al.* (2014). BMP-regulated exosomes from *Drosophila* male reproductive glands reprogram female behavior. *J. Cell Biol*. 206: 671-688.
- Dahm, R. (2006). Alzheimer's discovery. Curr. Biol. 16 (21): R906-R910.

- Dar, G.H., *et al*. (2021). GAPDH controls extracellular vesicle biogenesis and enhances the therapeutic potential of EV mediated siRNA delivery to the brain. Nat. Commun. 12, 6666 https://doi.org/10.1038/s41467-021-27056-3.
- Day, R., and Gorr, S. U. (2003). Secretory granule biogenesis and chromogranin A: master gene, on/off switch, or assembly factor? Trends Endocrinol. Metab. 14 (1): 3-10.
- Dawkins, E., and Small, D. H. (2014). Insights into the physiological function of the β-amyloid precursor protein: beyond Alzheimer's Disease. Journal of Neurochemistry. 129: 756-769.
- Deshpande, M., *et al.* (2016). Role of BMP receptor traffic in synaptic growth defects in an ALS model. Mol. Biol. Cell. 27: 2898-2910.
- DeSimone, C.V., *et al.* (2017). Cerebral Amyloid Angiopathy: diagnosis, clinical implications and management strategies in atrial fibrillation. J. *Amer. Coll. Cardiol.* 70 (9): 1173-1182.
- Di Vito, A., *et al.* (2021). Extracellular matrix in calcific aortic valve disease: architecture, dynamics and perspectives. Int. J. Mol. Sci. 22 (2): 913.
- Dineley, K. T. (2007). Beta-amyloid peptide – nicotinic acetylcholine receptor interaction: the two faces of health and disease. Front. Biosci.12: 5030-5038.
- Eanes, E. D., and Glenner, G. G. (1968). X-ray diffraction studies on amyloid filaments. J. Histochem. Cytochem. 16: 673-677.
- Ecovoiu, A. A., *et al.* (2022). Inter-species rescue of mutant phenotype-the standard for genetic analysis of human genetic disorders in *Drosophila* melanogaster model. Int. J. Mol. Sci. 23: 2613.

- Edbauer, D., *et al.* (2002). Insulin-degrading enzyme rapidly removes the beta-amyloid precursor protein intracellular domain (AICD). J. Biol. Chem. 277: 13389-13393.
- Eisenberg, D, and Jucker, M. (2012). The amyloid state of proteins in human diseases. Cell. 148 (6): 1188-1203.
- Enehalt, R., *et al.* (2003). Amyloidogenic processing of the Alzheimer β-amyloid precursor protein depends on lipid rafts. J. Cell Biol. 160: 113-123.
- Escribano, J., *et al.* (1994). cDNA from human ocular ciliary epithelium homologous to beta ig-h3 is preferntiall expressed as an extracellular protein in the corneal epithelium. J. Cell. Physiol. 160: 511-521.
- Evans, C.J., *et al.* (2016). Genotype-phenotype correlation for TGFBI Corneal Dystrophies identifies p.(G623D) as a novel cause of Epithelial Basement Membrane Dystrophy. *Invest. Ophthalmol. Vis. Sci.* 57: 5407-5414.
- Fan, Y., *et al.* (2014). TGF-beta-induced upregulation of malat1 promotes bladder cancer metastasis by associating with suz12. Clin. Cancer Res. Off. J. Am. Assoc. Cancer Res. 20: 1531-1541.
- Farg, M. A., *et al.* (2014). C9ORF72, implicated in amyotrophic lateral sclerosis and frontotemporal dementia, regulates endosomal trafficking. Hum. Mol. Genet. 23: 3579-3595.
- Fawzi, N. L., *et al.* (2008). Protofibril assemblies of the Arctic, Dutch, and Flemish mutants of the Alzheimer's Abeta1-40 peptide. Biophys. J. 94 (6): 2007-2016.
- Feldman, R. G., *et al.* (1963). Familial Alzheimer's Disease. Neurology. 13 (10): 811-824.

- Follett, J., *et al.* (2014). The VPS35 D620N mutation linked to Parkinson's disease disrupts the cargo-sorting function of retromer. Traffic. 15 (2): 230-244.
- Fowler, D. M., *et al*. (2007). Functional amyloid – from bacteria to humans. Trends in Biochemical Sci. 32 (5): 1-8.
- Freeman, C., *et al.* (2013). The hereditary spastic paraplegia protein strumpellin: characterisation in neurons and of the effect of disease mutations on WASH complex assembly and function. Biochim. Biophys. Acta. 1832 (1): 160-173.
- Freude, K. K., *et al.* (2011). Soluble amyloid precursor protein induces rapid neural differentiation of human embryonic stem cells. J. Biol. Chem. 286: 24264-24274.
- Frost, B., *et al.* (2014). Tau promotes neurodegeneration through global chromatin relaxation. Nat. Neurosci. 17 (3): 357-366.
- Garcia-Osta, A., and Alberini, C. M. (2009). Amyloid beta mediates memory formation. Learn. Mem. 16: 267-272.
- Gear, H. C., *et al.* (2005). Recurrence of Thiel-Behnke corneal dystrophy: an electron microscopic study. Br. J. Ophthalmol. 89: 518-519.
- Gellermann, G. P., *et al.* (2005). Raft lipids as common components of human extracellular amyloid fibrils. Proc. Natl. Acad. Sci. USA. 102 (18): 6297-6302.
- Gessel, M. M., *et al.* (2012). Familial Alzhiemer's disease mutations differentially alter amyloid-beta protein oligomerization. ACS Chem. Neurosci. 3 (11): 909-918.
- Glenner, G. G., *et al.* (1971). Amyloid fibril proteins: proof of homology with immunoglobulin light chains by sequence analyses. Science. 172: 1150-1151.
- Goedert, M. (2010). The propogation of prion-like protein inclusions in neurodegenerative diseases. *Trends in Neurosciences.* 33: 317-325.

- Gondré-Lewis, M. C., *et al.* (2012). Cellular mechanisms for the biogenesis and transport of synaptic and dense-core vesicles. Int. Rev. Cell. Mol. Biol. 299: 27-115.
- Goodman, Y., *et al.* (1994). Secreted forms of beta-amyloid precursor protein protect hippocampal neurons against amyloid beta-peptide-induced oxidative injury. Exp. Neurol. 128: 1-12.
- Goold, C. P., and Davis, G. W. (2007). The BMP ligand Gbb gates the expression of synaptic homeostasis independent of synaptic growth control. Neuron. 56 (1): 109-123.
- Goulley, J., *et al.* (2007). BMP4-BMPR-1A signaling in beta cells is required for and augments glucose-stimulated insulin secretion. Cell Metabolism. 5 (3): 207-219.
- Greenwald, J., *et al.* (2018). Peptide amyoids in the origin of life. J. Mol. Biol. 430: 3735-3750.
- Guo, C., *et al.* (2018). Tau activates transposable elements in Alzheimer's disease. Cell Reports. 23 (10): 2874-2880.
- Gouwens, L. K., *et al.* (2018). $A\beta_{42}$ protofibrils interact with and are trafficked through microglial-derived microvesicles. ACS Chem. Neurosci. 9: 1416-1425.
- Gralle, M., and Ferreira, S. T. (2007). Structure and functions of the human amyloid precursor protein: the whole is more than the sum of it's parts. Prog. Neurobiol. 82: 11-32.
- Gremer, L., *et al.* (2017). Fibril structure of amyloid-β (1-42) by cryo-electron microscopy. *Science.* 358: 116-119.

- Guo, Y. S., *et al.* (2011). Betaig-h3 regulates store-operated calcium entry and promotes the invasion of human hepatocellular carcinoma cells. Cell Biol. Int. 35: 811-817.
- Gustavsson, A., *et al.* (1991). Normal transthyretin and synthetic transthyretin fragments form amyloid-like fibrils *in vitro*. Biochem. Biophys. Res. Commun. 175: 1159-1164.
- Gustavsson, A., *et al.* (2022). Global estimates on the number of persons across the Alzheimer's Disease spectrum. Alzheimer's and Dementia. 2022: 1-13.
- Haass, C., *et al.* (2012). Trafficking and proteolytic processing of APP. Cold Spring Harb. Perspect. Med. 2.
- Han, K.E., *et al.* (2016). Pathogenesis and treatments of *TGFBI* Corneal Dystrophies. *Progr. Ret. Eye Res.* 50: 67-88.
- Han, S. B., *et al.* (2021). Genotypic heterogeneity in distinctive Transforming Growth Factor Beta-Inducing (TGFBI) protein phenotypes. Int. J. Mol. Sci. 22 (3): 1230.
- Hampel, H., *et al.* (2021). The Amyloid-β pathway in Alzheimer's Disease. Mol. Psych. 26: 5481-5503.
- Hatami, A., *et al.* (2017). Familial Alzheimer's disease mutation within the Amyloid Precursor Protein alter the aggregation and conformation of the amyloid beta-peptide. J. Biol. Chem. 292 (8): 3172-3185.
- Haussmann, I. U., *et al.* (2013). Multiple pathways mediate the sex peptide-regulated switch in female *Drosophila* reproductive behaviours. Proc. Biol. Sci. 280: 20131938.

- Herndon, L. A., and Wolfner, M. F. (1995). *Drosophila* seminal fluid protein Acp26Aa stimulates egg laying in females for 1 day after mating. Proc. Natl. Acad. Sci. USA. 92: 10114-10118.
- Hippius, H., and Neundorfer, G. (2003). The discovery of Alzheimer's disease. Dialogues in Clinical Neuroscience. 5 (1): 101-108.
- Hirano, K., *et al.* (1996). Big-h3 is synthesized by corneal epithelium and perhaps endothelium in Fuch's dystrophic corneas. Curr. Eye Res. 15: 965-972.
- Hoersch, S., and Andrade-Navarro, M. A. (2010). Periostin shows increased evolutionary plasticity in its alternatively spliced region. BMC Evol. Biol. 10: 30.
- Hof, P. R., *et al.* (1995). Neurofibrillary tangles correlate with dementia severity in Alzheimer's disease. Arch. Neurol. 52: 81-88.
- Hong, C. S., and Koo, E. H. (1997). Isolation and characterization of *Drosophila* presenilin homolog. Neuroreport. 8 (3): 665-668.
- Hong, W., *et al.* (2018). Diffusible, highly bioactive oligomers represent a minority of soluble Aβ in Alzheimer's disease brain. Acta Neuropathol. 136: 19-40.
- Howard, L., *et al.* (1996). Molecular cloning of MADM: a catalytically active mammalian disintegrin-metalloprotease expressed in various cell types. Biochem. J. 317: 45-50.
- Hu, S., *et al.* (1998). Midline Fasciclin: a *Drosophila* Fasciclin-I-related membrane protein localized to the CNS midline cells and trachea. J. Neurobiol. 35 (1): 77-93.
- Huber, O., *et al.* (1994). Isoforms of a cell adhesion moecule in embryos of the alga *Volvox* with homology to *Drosophila* fasciclin I. EMBO. 13: 4212-4222.

- Hung, M.-S., *et al.* (2015). Knockdown of Cul4A increases chemosensitivity to gemcitabine through upregulation of TGFBI in lung cancer cells. Onc. Reports. 34: 3187-3195.
- Hussain, N. K., *et al.* (2014). Sorting nexin 27 regulates basal and activity-dependent trafficking of AMPARs. Proc. Natl. Acad. Sci. USA. 111: 11840-11845.
- Huynh, T.-P.V., and Holtzman, D.M. (2018). Amyloid-β 'seeds' in old growth-hormone vials. *Nature.* 564: 354-355.
- Hwang, S., *et al.* (2015). Impaired GAPDH-induced mitophagy contributes to the pathology of Huntington's disease. EMBO Molecular Medicine. 7: 1307-1326.
- Hyman, B. T., *et al.* (2012). National Institute on Aging - Alzheimer's Association guidelines for the neuropathologic assessment of Alzheimer's Disease. Alzheimer's Dement. J. Alzheimer's Assoc. 8: 1-13.
- Immarigeon, C., *et al.* (2020). Identification of a micropeptide and multiple secondary genes that modulate *Drosophila* male reproductive success. Proc. Natl. Acad. Sci. USA. 118: 15 e2001897118.
- Inai, K., *et al.* (2008). BMP-2 induces cell migration and Periostin expression during atrioventricular valvulogenesis. Dev. Biol. 315: 383-396.
- Inoshita, T., *et al.* (2017). Vps35 in cooperation with LRKK2 regulates synaptic vesicle endocytosis through the endosomal pathway in *Drosophila.* Hum. Mol. Genetics. 26 (5): 2933-2948.
- Ishitani, R., *et al.* (2003). Proapoptotic protein glyceraldehyde-3-phosphate dehydrogenase: a possible site of action of anti-apoptotic drugs. Prog. Neuropsychopharmacol. Biol. Psychiatry. 27: 291-301.

- Iwamoto, T., *et al.* (1975). Ultrastructural variation in granular dystrophy of the cornea. Albrecht Von Graefes Arch. Klin. Exp. Ophthalmol. 194: 1-9.
- Jacobsen, K. T., and Iverfeldt, K. (2009). Amyloid precursor protein and its homologues: a family of proteolysis-dependent receptors. *Cell. Mol. Life Sci.* 66: 2299-2318.
- Janssen, J. C., *et al.* (2003). Early onset Alzheimer's disease. Mutation frequency in 31 families. Neurology. 60: 2.
- Johnston, J. A., *et al.* (1994). Increased beta-amyloid release and levels of amyloid precursor protein (APP) in fibroblast cell lines from family members with the Swedish Alzheimer's disease APP670/671 mutation. FEBS Lett. 354 (3): 274-278.
- Jucker, M., and Walker, L.C. (2013). Self-propogation of pathogenic protein aggregates in neurodgenerative diseases. Nature. 501: 45-51.
- Kakidani, H., and Ptashne, M. (1988). GAL4 activates gene expression in mammalian cells. Cell. 52 (2): 161-167.
- Kalimo, H., *et al.* (2013). The Arctic AβPP mutation leads to Alzheimer's Disease pathology with highly variable topographic deposition of differentially truncated Aβ. Acta Neuropathologica Comm. 1 (60): 1-19.
- Kang, J., *et al.* (1987). The precursor of Alzheimer's disease amyloid A4 protein resembles a cell-surface receptor. Nature. 325: 733-736.
- Kannabiran, C., and Klintworth, G. K. (2006). TGFBI gene mutations in Corneal Dystrophies. *Hum. Mutation.* 27 (7): 615-625.

- Kapur, J. N., *et al.* (1985). A new method for gray-level picture thresholding using the entropy of the histogram. Computer Vision, Graphics and Image Processing. 29 (3): 273-285.
- Karch, C.M., and Goate, A.M. (2015). Alzheimer's disease risk genes and mechanisms of disease pathogenesis. *Biol. Psychiatry*. 77: 43-51.
- Karisetty, B. C., *et al.* (2020). Amyloid-β peptide impact on synaptic function and neuroepigenetic disease control reveal new therapeutic strategies for Alzheimer's disease. Front. Mol. Neurosci. 13: 2020. fnmol. 2020 577622.
- Karring, H., *et al.* (2012). Composition and proteolytic processing of corneal deposits associated with mutations in the TGFBI gene. Exp. Eye Res. 96 (1): 163-170.
- Karring, H., *et al.* (2013). Serine protease HtrA1 accumulates in corneal transforming growth factor beta-induced protein amyloid deposits. Mol. Vis. 19: 861-876.
- Ke, P.C., *et al.* (2020). Half a century of amyloids: past, present and future. *Chem. Soc. Rev.* 49: 5473-5509.
- Keefer, K. M., *et al.* (2017). Heterologous prion-forming proteins interact to cross-seed aggregation in Saccharomyces cerevisiae. *Scientific Reports*. 7: 5853. Doi: 10.1038/s41598-017-05829-5.
- Khan, G. M., *et al.* (2010). Beta-amyloid activates presynaptic alpha7 nicotinic acetylcholine receptors reconstituted into a model nerve system; involvement of lipid rafts. Eur. J. Neurosci. 31: 788-796.

- Khan, U. A., *et al.* (2014). Molecular drivers and cortical spread of lateral entorhinal cortex dysfunction in preclinical Alzheimer's disease. Nature Neurosci. 17: 304-311.
- Kheir, V., *et al.* (2019). Mutation update: TGFBI pathogenic and likely pathogenic variants in corneal dystrophies. Human Mutation. 40: 675-693.
- Khurana, V., *et al.* (2010). Lysosomal dysfunction promotes cleavage and neurotoxicity of tau in vivo. PLoS Genet. 6:e1001026.
- Kim, D. Y., *et al.* (2011). Reduced sodium channel levels in BACE-1 null mice. J. Biol. Chem. 286: 8106-8116.
- Kim, J., and Holtzman, D.M. (2010). Prion-like behavior of Amyloid-β. *Science.* 330: 918-919.
- Kim, J. E., *et al.* (2002). Identification of motifs in the fasciclin domains of the transforming growth factor-beta-induced matrix protein betaig-h3 that interact with the alphavbeta5 integrin. J. Biol. Chem. 277: 46159-46165.
- Kim, M., and Bezprozvanny, I., (2023). Analysis of non-amyloidogenic mutations in APP supports loss of function hypothesis in Alzheimer's disease. Int. J. Mol. Sci. 24 (3).
- Kim, M. O., *et al.* (2003). Transforming growth factor-beta-inducible gene -h3 (betaig-h3) promotes cell adhesion of human astrocytoma cells in vitro: implication of alpha6beta4 integrin. Neurosci. Lett. 336: 93-96.
- Kim, Y. J., *et al.* (2010). MIPs are ancestral ligands for the sex peptide receptor. Proc. Natl. Acad. Sci. USA. 107: 6520-6525.

- Kimura, A., *et al.* (2016). Alternative selection of β-site APP-cleaving enzyme (BACE1) cleavage sites in amyloid precursor protein (APP) harboring protective and pathogenic mutations within the Aβ sequence. J. Biol. Chem. 291 (46): 24041-24053.
- Kiral, F. R., *et al.* (2018). Rab GTPases and membrane trafficking in neurodegeneration. Curr. Biol. 28: R471-R486.
- Kitahama, S., *et al.* (Expression of fibrillins and other microfibril-associated proteins in human bone and osteoblast-like cells. Bone. 27: 61-67.
- Klintworth, G. K., *et al.* (1998). Accumulation of beta ig-h3 gene product in corneas with granular corneal dystrophy. Am. J. Pathol. 152: 743-748.
- Klintworth, G. K. (2003). The molecular genetics of the corneal dystrophies - current status. Front. Biosci. 8: d687-d713.
- Klintworth, G. K. (2009). Corneal dystrophies. Orphanet J. Rare Dis. 4: 7.
- Koffie, R. M., *et al.* (2009). Oligomeric amyloid-beta associates with post-synaptic densities and correlates with excitatory synapse loss near senile plaques. Proc. Natl. Acad. Sci. USA. 106: 4012-4017.
- Komaki, K., *et al.* (2022). Lemur tail kinase 1 (LMTK1) regulates the endosomal localization of β-secretase BACE1. J. Biochemistry. 170 (6): 729-738.
- Koo, E. H., *et al.* (1990). Precursor of amyloid protein in Alzheimer disease undergoes fast anterograde axonal transport. Proc. Natl. Acad. Scie. USA. 87: 1561-1565.
- Kopan, R., and Ilagan, M. X. (2009). The canonical Notch signaling pathway: unfolding the activation mechanism. Cell. 137: 216-233.

- Kordower, J. H., *et al.* (2008). Lewy body-like pathology in long-term embryonal nigral transplants in Parkinson's disease. Nat. Med. 14: 504-506.
- Kornfeld, S., and Mellman, I. (1989). The biogenesis of lysosomes. Annu. Rev. Cell Biol. 483-525.
- Koshy, B., *et al.* (1996). Spinocerebellar ataxia type-1 and Spinomuscular atrophy gene products interact with GAPDH. Hum. Mol. Genet. 5: 1311-1318.
- Kroeger, B. R. (2017). The genetic regulation and subcellular dynamics of secretory and endolysosomal organelles of *Drosophila* secondary cells. DPhil thesis, University of Oxford.
- Krissinel, E., and Henrick, K. (2007). Inference of macromolecular assemblies from crystalline state. J. Mol. Biol. 372: 774-797.
- Krone, M. G., *et al.* (2008). Effects of familial Alzheimer's disease mutations on the folding nucleation of the amyloid beta protein. J. Mol. Biol. 381 (1): 221-228.
- Kubli, E. (2003). Sex-peptides, seminal peptides of the *Drosophila* male. Cell Mol. Life Sci. 60: 1669-1704.
- Kubli, E., and Bopp, D. (2010). Sex bei den Insekten. Von Jungfrauen, Liebesgesangen, chemischen Keuschheitsgurtein und Hermaphroditen. Hsg Naturforschende Ges. Zurich, Jg. 155: 1-82.
- Kubli, E., and Bopp, D. (2012). Sexual behaviour: how sex peptide flips the postmating switch of female flies. Curr. Biol. 22 (13): R520-R522.
- Kumar-Singh., S., *et al.* (2002). Dense-core senile plaques in the Flemish variant of Alzheimer's Disease are vasocentric. Am. J. Pathol. 161 (2): 507-520.

- Kuperstein, I., *et al.* (2010). Neurotoxicity of the Alzheimer's disease Abeta peptides is induced by small changes in the Abeta42 to Abeta40 ratio. EMBO J. 29: 3408-3420.
- La Voie, M.J., *et al.* (2003). Assembly of the γ-secretase complex involves early formation of an intermediate subcomplex of Aph-1 and nicastrin. *J. Biol. Chem.* 278: 37213-37222.
- Lacor, P. N., *et al.* (2007). Abeta oligomer-induced aberrations in synapse composition, shape and density provide a molecular basis for loss of connectivity in Alzheimer's disease. J. Neurosci. 27: 796-807.
- Lai, A., *et al.* (1995). Characterization of sorting signals in the beta-amyloid precursor protein cytoplasmic domain. J. Biol. Chem. 270: 3565-3573.
- Lai, A., *et al.* (1998). Signal-dependent trafficking of beta-amyloid precursor protein-transferrin receptor chimeras in Madin-Darby Canine Kidney cells. J. Biol. Chem. 3732-3739.
- Laird, F. M., *et al.* (2005). BACE1, a major determinant of selective vulnerability of the brain to amyloid beta amyloidogenesis, is essential for cognitive, emotional, and synaptic functions. J. Neurosci. 25: 11693-11709.
- Lauritzen, I., *et al.* (2019). Targeting γ-secretase triggers the selective enrichment of oligomeric APP-CTFs in brain extracellular vesicles from Alzheimer cell and mouse models. *Transl. Neurodegen.* 8: 35.
- Lawrence, J. L., *et al.* (2014). Regulation of presynaptic Ca^{2+}, synaptic plasticity and contextual fear conditioning by an N-terminal beta-amyloid fragment. J. Neurosci. 34: 14210-14218.

- Lazarev, V. F., *et al.* (2021). Extracellular GAPDH promotes Alzheimer disease by enhancing amyloid-β aggregation and cytotoxicity. Aging Dis. 12 (5): 1223-1237.
- Lee, M. C., *et al.* (2021). Amyloid-β40 E22K fibril in familial Alzheimer's disease is more thermostable and susceptible to seeding. IUBMB Life. 74 (8): 739-747.
- Lee, S. H., *et al*. (2003). Expression of TGF-beta-induced matrix protein betaig-h3 is up-regulated in the diabetic rat kidney and human proximal tubular epithelial cells treated with high glucose. Kidney Int. 64: 1012-1021.
- Leiblich, A., *et al.* (2019). Mating induces switch from hormone-dependent to hormone-independent steroid recptor-mediated growth in *Drosophila* secondary cells. *PLoS Biol.* 17(10): e3000145.
- Leiden Open Variation Database. databases.lovd.nl/shared/genes/TGFBI.
- Leysson, M., *et al.* (2005). Amyloid precursor protein promotes post-developmental neurite arborization in the Drosophila brain. EMBO J. 24: 2944-2955.
- Li, C., *et al.* (2016). Role of the retromer complex in neurodegenerative diseases. Front. Aging Neurosci. https://doi.org/10.3389/fnagi.2016.00042.
- Li, D., *et al.* (2018). A *Drosophila* in vivo injury model for studying neuroregeneration in the peripheral and central nervous system. JoVE J. Vis. Exp. 135: e57557.
- Li, J. Y., *et al.* (2008). Lewy bodies in grafted neurons in subjects with Parkinson's disease suggests host-to-graft disease propogation. Nat. Med. 14: 501-503.
- Li, X., *et al.* (2008). A function of huntingtin in guanine nucleotide exchange on Rab11. Neuroreport. 19 (16): 1643-1647.

- Li, X., *et al.* (2009). Disruption of Rab11 activity in a knock-in mouse model of Huntington's disease. Neurobiol. Dis. 36: 374-383.
- Li, Y., *et al.* (2004). Association of late-onset Alzheimer's disease with genetic variation in multiple members of the GAPD gene family. Proc. Natl. Acad. Sci. USA. 101: 15688-15693.
- Li, Y., *et al.* (2014). Structural biology of presenilin 1 complexes. Mol. Neurodegeneration. 9: 59.
- Li, Y., *et al.* (2022). Decreased CSF clearance and increased brain amyloid in Alzheimer's Disease. Fluids and Barriers of the CNS. 19 (21): 1-9.
- Lichtenthaler, S. F., *et al.* (2011). Regulated intramembrane proteolysis – lessons from amyloid precursor protein processing. J. Neurochem. 117: 779-796.
- Lim, K.H. (2019). Diverse misfolded conformational strains and cross-seeding of misfolded proteins implicated in neurodegenerative diseases. *Front. Mol. Neurosci.* 12: 158. Doi: 10: 3389/fnmol.2019.00158.
- Liu, H., and Kubli, E. (2003). Sex-peptide is the molecular basisi of the sperm effet in Drosophila melanogaster. Proc. Natl. Acad. Sci. USA. 100: 9929-9933.
- Loncle, N., *et al.* (2015). An ESCRT module is required for neuron pruning. Sci. Rep. 5, 8461. https://doi.org/10.1038/srep08461.
- Lord, S. J., *et al.* (2020). SuperPlots: Communicating reproducibility and variability in cell biology. J. Cell Biol. 219 (6): e202001064.
- Lu, D., *et al.* (2003). Caspase cleavage of the amyloid precursor protein modulates amyloid beta-protein toxicity. J. Neurochem. 733-741.

- Lucin, K. M., *et al.* (2013). Microglial beclin 1 regulates retromer trafficking and phagocytosis and is impaired in Alzheimer's disease. Neuron. 79: 873-886.
- Lund, V. K., *et al.* (2018). *Drosophila* Rab2 controls endosome-lysosome fusion and LAMP delivery to late endosomes. Autophagy. 14 (9): 1520-1542.
- Luo, L. (1992). Functional analysis of APPL, the *Drosophila* homologue of human amyloid precursor protein associated with Alzheimer's disease. PhD thesis, Brandeis University.
- Luo, L. Q., *et al.* (1990). Identification, secretion and neural expression of APPL, a *Drosophila* protein similar to human amyloid protein precursor. J. Neurosci. 10: 3849-3861.
- Luo, Y., *et al.* (2001). Mice deficient in BACE-1, the Alzheimer's β-secretase, have normal phenotype and abolished β-amyloid generation. Nat. Neurosci. 4: 231-232.
- Maekawa, T., *et al.* (2016). Leucine-rich repeat kinase 2 (LRKK2) regulates α-synuclein clearance in microglia. BMC Neuroscience. 17 (1): 77.
- MacLeod, D. A., *et al.* (2013). RAB7L1 interacts with LRRK2 to modify intraneuronal protein sorting and Parkinson's disease risk. Neuron. 77 (3): 425-439.
- Maji, S. K., *et al.* (2008). Amyloid as a depot for the formulation of long-acting drugs. PLoS Biol. 6: e17.
- Maji, S. K. *et al.* (2009). Functional amyloids as natural storage of peptide hormones in pituitary secretory granules. *Science*. 325 (5938): 328-332.
- Marie, P. P., *et al.* (2023). Accessory ESCRT-III proteins are conserved and selective regulators of Rab11a-exosome formation. J. Extracellular Vesicles. https://doi.org/10.1002/jev2.12311.

- Martin-Morris, L. E., and White, K. (1990). The *Drosophila* transcript encoded by the beta-amyloid protein precursor-like gene is restricted to the nervous system. Development. 110 (1) pmid 2127912.
- Masters, C.L., *et al.* (2015). Alzheimer's Disease. Nat. Rev. Dis. Primers 1, 15056 https://doi.org/10.1038/nrdp.2015.56.
- Mawuenyega, K. G., *et al.* (2010). Decreased clearance of CNS beta-amyloid in Alzheimer's Disease. Science. 330:1774.
- Mazzola, J. L. (1999). New insights into an old protein: the functional diversity of mammalian glyceraldehyde-3-phosphate dehydrogenase. Biochim. Biophys. Acta. 1432: 159-184.
- Mazzola, J. L., and Sirover, M. A. (2002). Alteration of intracellular structure and function of glyceraldehyde-3-phosphate dehydrogenase: a common phenotype of neurodegenerative disorders? Neurotoxicology. 23: 603-609.
- Mazzola, J. L., and Sirover, M. A. (2002). Alteration of nuclear glyceraldehyde-3-phosphate dehydrogenase structure in Huntington's disease fibroblasts. Mol. Brain Res.100: 95-101.
- McConlogue, L., *et al.* (1996). Differential effects of a Rab6 mutant on secretory versus amyloidogenic processing of Alzheimer's β-amyloid precursor protein. J. Biol. Chem. 271: 1343-1348.
- McGuire, S. E., *et al.* (2003). Spatiotemporal rescue of memory dysfunction in *Drosophila.* Science. 302 (5651): 1765-1768.

- McGuire, S. E., *et al.* (2003). Spatiotemporal rescue of memory dysfunction in *Drosophila.* Science. 302 (5651): 1765-1768.

- McGurk, L., *et al.* (2015). *Drosophila* as an in vivo model for human neurodegenerative disease. Genetics. 201: 377-402.
- McKeith, I. G., *et al.* (1996). Consensus guidelines for the clinical and pathologica diagnosis of dementia with Lewy bodies: report of the consortium on DLB international workshop. Neurology. 47: 1113-1124.
- McKeith, I. G., *et al.* (2005). Diagnosis and mangement of dementia with Lewy bodies: third report of the DLB consortium. Neurology. 65: 1863-1872.
- McKnelly, K. J., *et al.* (2022). Effects of Familial Alzheimer's disease mutations on the assembly of a beta-hairpin peptide derived from Aβ16-36. Biochemistry 61 (6): 446-454.
- Messenger, S. W., *et al*. (2014). Calcium-regulated secretory granule exocytosis in pancreatic and parotid acinar cells. Cell Calcium. 55 (6): 369-375.
- Miravelle, L., *et al.* (2000). Substitutions at codon 22 of Alzheimer's Abeta peptide include diverse conformational changes and apoptotic effects in human cerebral endothelial cells. J. Biol. Chem. 275 (35): 27110-27116.
- Mirra, S. S., *et al.* (1991). The Consortium to Establish a Registry for Alzheimer's Disease (CERAD), Part II. Standardization of the neuropathological assessment of Alzheimer's Disease. Neurology. 41: 479-486.
- Mishra, B., *et al.* (2014). Using microfluidics chips for live imaging and study of injury responses in *Drosophila* larvae. JoVE J. Vis. Exp. 84: e50998.
- Mitra, J., *et al.* (2019). Loss of endosomal recycling factor RAB11 coupled with complex regulation of MAPK/ERK/AKT signaling in postmortem spinal cord specimens of amyotrophic lateral sclerosis patients. Mol. Brain. 12 (1): 55.

- Miura, E., *et al*. (2014). VPS35 dysfunction impairs lysosomal degradtion of alpha-synuclein and exacerbates neurotoxicity in a *Drosophila* model of Parkinson's disease. Neurobiol. Dis. 71: 1-13.
- Miyazaki, Y., *et al.* (2007). The fruiting-specific *LeFlp1* gene, encoding a novel fungal fasciclin-like protein, of the basidomycetous mushroom *Lentinula edodes*. Curr. Genet. 51: 367-375.
- Möbius, W. *et al.* (2002). Immunoelectron microscopic localization of cholesterol using biotinylated and non-cytolytic Perfringolysin. Histochem. Cytochem. 50: 43-55.
- Modarresi, F., *et al.* (2011). Knockdown of BACE1-AS nonprotein-coding transcript modulates beta-amyloid-related hippocampal neurogenesis. Int. J. Alz. Dis. doi:10.4061/2011/929042.
- Molnár, Z., *et al.* (2019). New insights into the development of the human cerebral cortex. J. Anatomy. 235: 432-451.
- Moreth, J., *et al.* (2013). Globular and protofibrillar Aβ aggregates impair neurotransmission by a different mechanism. Biochem. 52: 1466-1476.
- Morley, J. E., *et al.* (2010). A physiological role for amyloid-beta protein: enhancement of learning and memory. J. Alz. Dis. 19: 441-449.
- Moser, E. I., and Moser, M.-B. (2011a). Crystals of the brain. EMBO Mol. Med. 3: 1-4.
- Moser, E. I., and Moser, M.-B. (2011b). Seeing into the future. Nature. 469: 303-304.

- Moya, K. L., *et al.* (1994). The amyloid precursor protein is developmentally regulated and correlated with synaptogenesis. Dev. Biol. 161: 597-603.
- Mueller, H. T., *et al.* (2000). Modulation of amyloid precursor protein metabolism by X11alpha/Mint-1. A deletion analysis of protein-protein interaction domains. J. Biol. Chem. 39302-39306.
- Mullan, M., *et al.* (1992). A pathogenic mutation for probable Alzheimer's Disease at the N-terminus of β-amyloid. Nature Genet. 1: 345-347.
- Müller, U., and Wild, K. (2013). Structure and Function of the APP Intracellular Domain in Health and Disease. From: Understanding Alzheimer's Disease. Ed: Inga Zerr. Augusta University, Augusta, GA, USA.
- Munier, F. L., *et al.* (1997). Kerato-epithelin mutations in four 5q31-linked corneal dystrophies. Nat. Genet. 15: 247-251.
- Munsie, L. N., *et al.* (2015). Retromer-dependent neurotransmitter receptor trafficking to synapses is altered by the Parkinson's Disease VPS35 mutation pD620N. Hum. Mol. Genet. 24: 1691-1703.
- Mura, E., *et al.* (2012). Dual effect of beta-amyloid on α7 and α4β2 nicotinic receptors controlling the release of glutamate, aspartate and GABA in rat hippocampus. PLoS One. 7e:29661.
- Murukami, K., *et al.* (2003). Neurotoxicity and physicochemical properties of Abeta mutant peptides from cerebral amyloid angiopathy: implications for the pathogenesis of cerebral amyloid angiopathy and Alzheimer's disease. J. Biol. Chem. 278 (46): 46179-46187.

- Myerowitz, R., *et al.* (2021). Impaired autophagy: the collateral damage of lysosomal storage disorders. eBioMedicine. 63: 103166.
- Nagarkar-Jaiswal, S. *et al.* (2015). A library of MiMICs allows tagging of genes and reversible, spatial and temporal knockdown of proteins in *Drosophila. eLife* 2015;4:e05338 DOI: 10.7554/eLife.05338.
- Nalls, M. A., *et al.* (2014). Large-scale meta-analysis of genome-wide association data identifies six new risk loci for Parkinson's disease. Nat. Genet. 46: 989-993.
- Nam, E. J., *et al.* (2006). Up-regulated transforming growth factor beta-inducible gene h3 in rheumatoid arthritis mediates adhesion and migration of synoviocytes through alpha v beta 3 integrin: regulation by cytokines. Arth. Rheumat. 54: 2734-2744.
- Narayanan, A.S. and Rothenfluh, A. (2016). I believe I can Fly! Use of *Drosophila* as a model organism in Neuropsychopharmacology research. *Neuropsychopharmacology.* 41: 1439-1446.
- Neuman, S.D., *et al.* (2021). Mistargeting of secretory cargo in retromer-deficient cells. *Dis. Model. Mech.* 14:dmm046417. https://doi.org/10.1242/dmm.046417.
- Ni, J. Q., *et al.* (2009). A *Drosophila* resource of transgenic lines for Neurogenetics. Genetics. 182(4): 1089-1100.
- Nielsen, N. S., *et al.* (2020). Biochemical mechanisms of aggregation in *TGFBI*-linked corneal dystrophies. Progr. Ret. Eye Res. 77: 100843: 1-21.

- Nielsen, N. S., *et al.* (2021). Mutation-induced dimerization of transforming growth factor-β-induced protein may drive protein aggregation in granular corneal dystrophy. J. Biol. Chem. 297 (1): 100858.
- Nikolaev, A., *et al.* (2009). APP binds DR6 to trigger axonal pruning and neuron death via distinct caspases. Nature. 457: 981-989.
- Nilsberth, C., *et al.* (2001). The 'Arctic' mutation (E693G) causes Alzheimer's Disease by enhanced Aβ profibril formation. Nature Neuroscience. 4 (9): 887-893.
- Nitta, Y., and Sugie, A. (2022). Studies of neurodegenerative diseases using *Drosophila* and the development of novel approaches for their analysis. Fly. 16 (1): 275-298.
- Norlin, N., *et al.* (2012). Aggregation and fibril morphology of the Arctic mutation of Alzheimer's Abeta peptide by CD, TEM, STEM and in situ AFM. J. Struct. Biol. 180: 174-189.
- Nyitrai, H., *et al.* (2020). ELKS1 captures Rab6marked vesicular cargo in presynaptic nerve terminals. Cell Rep. 31: 107712.
- Obregon, D., *et al.* (2012). Soluble amyloid precursor protein-α modulates β-secretase activity and amyloid-β generation. Nature Commun. 3: 77.
- Ollila, H. M., *et al.* (2009). Findings from bipolar disorder genome-wide association studies replicate in a Finnish bipolar family-cohort. Mol. Psychiatry. 14 (4): 351-353.
- Olsen, O., *et al*. (2014). Genetic analysis reveals that amyloid precursor protein and death receptor 6 function in the same pathway to control axonal pruning independent of β-secretase. J. Neurosci. 34: 6438-6447.

- Opdam, F. J., *et al.* (2000). The small GTPase Rab6, a novel Rab6 subfamily member, is cell-type specifically expressed and localized to the Golgi apparatus. J. Cell Sci. 113: 2725-2735.
- Ordonez, D. G., *et al.* (2018). α-synuclein induces mitochondrial dysfunction through spectrin and the actin cytoskeleton. Neuron. 97 (1): 108-124.e6.
- Otzen, D., and Riek, R. (2019). Functional Amyloids. Cold Spring Harb. Perspect. Biol. 11: a033860.
- Öztürk, Z., *et al.* (2020). Axonal endoplasmic reticulum dynamics and its role in neurodegeneration. Frontiers in Neuroscience. 14 (48): 1-33.
- Padgett, R. W., *et al.* (1993). Human BMP sequences can confer normal dorsal-ventral patterning in the *Drosophila* embryo. Proc. Natl. Inst. Sci. USA. 90: 2905-2909.
- Paisan-Ruiz, C., *et al.* (2004). Cloning of the gene containing mutations that cause PARK8-linked Parkinson's disease. Neuron. 44 (4): 595-600.
- Pannen, H., *et al.* (2020). The ESCRT machinery regulates retromer-dependent transcytosis of septate junction components in *Drosophila.* eLife 9: e61866.
- Papanikolau, G., *et al.* (2004). Mutations in HFE2 cause iron overload in chromosome 1q-linked juvenile hemochromatosis. Nat. Genet. 36 (1): 77-82.
- Parchi, P., *et al.* (1999). Classification of sporadic Creutzfeldt-Jakob disease based on molecular and phenotypic analysis of 300 subjects. Ann. Neurol. 46: 224-233.
- Parchi, P., *et al.* (1995). Regional distribution of protease-resistant prion protein in Fatal Familial Insomnia. Ann. Neurol. 38: 21-29.

- Pardossi-Picard, R., and Checler, F. (2012). The physiology of the β-amyloid precursor protein intracellular domain AICD. J. Neurochem. 120 (1): 109-124.
- Park, S. J., *et al.* (2004). Conformational resemblance between the structures of integrin-inactivating pentapeptides derived from betaig-h3 and RGD peptide analogues in a membrane environment. Peptides. 25: 199-205.
- Park, S. Y., *et al.* (2009). Stabilin-2 mediates homophilic cell-cell interactions via its FAS1 domains. FEBS Lett. 583: 1375-1380.
- Pardossi-Picard, R., *et al.* (2005). Presenilin-dependent transcriptional control of the Abeta-degrading enzyme neprilysin by intracellular domains of betaAPP and APLP. Neuron. 46: 541-554.
- Pasternak, S. H., *et al.* (2003). Presenilin-1, nicastrin, amyloid precursor protein and gamma-secretase activity are co-localized in the lysosomal membrane. J. Biol. Chem. 278: 26687-26694.
- Pastorino, L., *et al.* (2006). The prolyl isomerase Pin1 regulates amyloid precursor protein processing and amyloid-beta production. Nature. 528-534.
- Peralvarez-Marin, A., *et al.* (2009). Infleunce of residue 22 on the folding, aggregation profile and toxicity of the Alzheimer's beta-amyloid peptide. Biophys. J. 97 (1): 277-285.
- Perez, R. G., *et al.* (1999). Mutagenesis identifies new signals for beta-amyloid precursor protein endocytosis, turnover, and generation of secreted fragments including Abeta42. J. Biol. Chem. 274: 18851-18856.
- Perkins, L. A., *et al.* (2015). The Transgenic RNAi Project at Harvard Medical School: resources and validation. Genetics. 201 (3): 843-852.

- Perl, D. P. (2010). Neuropathology of Alzheimer's Disease. Mt. Sinai J. Med. 77: 32-42.
- Petkova, A. V., *et al.* (2005). Self-propagating, molecular-level polymorphism in Alzheimer's beta-amyloid fibrils. Science. 307: 262-265.
- Philipson, O., *et al.* (2012). The Arctic amyloid-beta precursor protein (AbetaPP) mutation results in distinct plaques and accumulation of N- and C-trunacted Abeta. Neurobiol. Aging. 33 (10): e1011-e1013.
- Philstrøm, L., *et al.* (2018). Genetics of neurodegenerative diseases: an overview. Handbook of Clinical Neurology. Vol. 145 (3rd series): 309-323, Elsevier.
- Plant, L. D., *et al.* (2003). The production of amyloid beta peptide is a critical requirement for the viability of central neurons. J. Neurosci. 23: 5531-5535.
- Politz, O., *et al.* (2002). Stabilin-1 and -2 constitute a novel family of fasciclin-like hyaluronan receptor homologues. Biochem. J. 362: 155-164.
- Poulsen, E. T., *et al.* (2019). The serine protease HtrA1 cleaves misfolded transforming growth factor β-induced protein (TGFBIp) and induces amyloid formation. J. Biol. Chem. 294 (31): 11817-11828.
- Preat, T., and Goguel, V. (2016). Role of *Drosophila* amyloid precursor protein in memory formation. Front. Mol. Neurosci. 9: 142.
- Prince, E., *et al.* (2019). Rab-mediated trafficking in the secondary cells of *Drosophila* male accessory glands and its role in fecundity. Traffic. 20 (2): 137-151.
- Prusiner, S. B. (1991). Molecular biology of prion diseases. Science. 252 (5012): 1515-1522.

- Purro, S., *et al.* (2018). Transmission of amyloid-β protein pathology from cadaveric pituitary growth hormone. Nature. 564: 415-419.
- Puzzo, D., *et al.* (2005). Amyloid-beta peptide inhibits activation of the nitric oxide/cGMP/cAMP-responsive element-binding protein pathway during hippocampal synaptic plasticity. J. Neurosci. 25: 6887-6897.
- Puzzo, D., *et al.* (2008a). Picomolar amyloid-beta positively modulates synaptic plasticity and memory in hippocampus. J. Neurosci. 28: 14537-14545.
- Puzzo, D., *et al.* (2008b). Picomolar amyloid-beta positively modulates synaptic plasticity and memory in hippocampus. J. Neurosci. 28: 14537-14545.
- Puzzo, D., *et al.* (2012). Hormetic effect of amyloid-beta peptide in synaptic plasticity and memory. Neurobiol. Aging. 33: 1484: e15-e24.
- Puzzo, D., *et al.* (2015). The keystone of Alzheimer pathogenesis might be sought in A-beta physiology. Neuroscience. 307: 26-36.
- Querfurth, H. W., and LaFerla, F. (2010). Alzheimer's Disease. N. Engl. J. Med. 362 (4): 329-344.
- Raffen, R., *et al.* (1999). Physicochemical consequences of amino acid variations that contribute to fibril formation by immunoglobulin light chains. Protein Sci. 8 (3): 509-517.
- Rai, P., and Roy, J. K. (2022). Endosomal recycling protein Rab11 in Parkin and Pink1 signalling in *Drosophila* model of Parkinson's disease.
- Rajput, A., *et al.* (2014). VPS35 and DNAJC13 disease-causing variants in essential tremor. Eur. J. Hum. Genet. 23 (6): 887-888.

- Ramaker, J., and Copenhaver, P. (2017). Amyloid Precursor Protein family as unconventional Go-coupled receptors and the control of neuronal motility. Neurogenesis. 4 (1): e1288510.
- Rambaran, R. N., and Serpell, L. C. (2008). Amyloid fibrils. Prion. 2 (3): 112-117.
- Ravi Ram, K., and Wolfner, M. F. (2007). Sustained post-mating response in Drosophila melanogaster requires multiple semial fluid proteins. PLoS Genetics. 3:e238.
- Rawe, I. M., *et al.* (1997). Beta-ig. Molecular cloning and in-situ hybridization in corneal tissues. Invest. Ophthalmol. Vis. Sci. 38: 893-900.
- Reches, M., and Gazit, E. (2003). Casting metal nanowires within discrete self-assembled nanotubes. Science. 300: 625-627.
- Redhai, S., *et al.* (2016). Regulation of dense-core replenishment by autocrine signalling in *Drosophila* secondary cells. *PLoS Genet.* 12: e1006366.
- Reitz, C. (2018). Retromer dysfunction and neurodegenerative disease. Curr. Genomics. 19: 279-288.
- Rice, H. C., *et al.* (2019). Secreted amyloid-β precursor protein acts as a GABA(B)R1a ligand to modulate synaptic transmission. Science. 363: eaao4827.
- Richards, P., *et al.* (2011). Dendritic spine loss and neurodegeneration is rescued by Rab11 in models of Huntington's disease. Cell Death and Differentiation. 18 (2): 191-200.
- Rideout, E. J., *et al.* (2010). Control of sexual differentiation and behaviour by the doublesex gene in *Drosophila melanogaster*. Nat. Neurosci. 13 (4): 458-466.

- Rieche, F., *et al.* (2018). *Drosophila* full-length amyloid precursor protein is required for visual working memory and prevents age-related memory impairment. Curr. Biol. 28: 817-823.
- Ring, S., *et al.* (2007). The secreted beta-amyloid precursor protein ectodomain APPs alpha is sufficient to rescue the anatomical, behavioural and electrophysiological abnormalities of APP-deficient mice. J. Neurosci. 27: 7817-7826.
- Rishi, G., *et al.* (2015). Hepcidin: regulation of the master iron regulator. Bioscience Reports. 35: 3
- Roberds, S. L., *et al.* (2001). BACE knockout mice are healthy despite lacking the primary β-secretase activity in the brain: implications for Alzheimer's disease therapeutics. Hum. Mol. Genet. 10: 1317-1324.
- Roberts, R. C., *et al.* (2010). Mistargeting of SH3TC2 away from the recycling endosome cuase Charcot-Marie-Tooth disease type 4C. Hum. Mol. Genet. 19: 1009-1018.
- Roberts, S. B., *et al.* (1994). Non-amyloidogenic cleavage of the β-amyloid precursor protein by an integral membrane metalloendopeptidase. J. Biol. Chem. 269: 3111-3116.
- Roncarati, R., *et al.* (2002). The gamma-secretase-generated intracellular domain of beta-amyloid precursor protein binds Numb and inhibits Notch signaling. Proc. Natl. Acad. Sci. USA. 7102-7107.
- Rooke, J., *et al.* (1996). KUZ, a conserved metalloprotease-disintegrin protein with two roles in *Drosophila* neurogenesis. Science. 273 (5279): 1127-1231.

- Ropers, F., *et al.* (2011). Identification of a novel candidate gene for non-syndromic autosomal recessive intellectual disability: the WASH complex member SWIP. Hum. Mol. Genet. 20 (13): 2585-2590.
- Rorsman, P., and Ashcroft, F. M. (2018). Pancreatic β-cell electrical activity and insulin secretion: of mice and men. Physiol. Rev. 98: 117-214.
- Rosen, D. R., *et al.* (1989). A *Drosophila* gene encoding a protein resembling the human beta-amyloid protein precursor. Proc. Natl. Acad. Sci. USA. 86: 2478-2482.
- Rufo, C. M., *et al.* (2014). Short peptides self-assemble to produce catalytic amyloids. Nat. Chem. 6: 303-309.
- Runager, K., *et al.* (2011). Human phenotypically distinct corneal dystrophies are linked to the stability of the fourth FAS1 domain of TGFBIp. J. Biol. Chem. 286 (7): 5951-4958.
- Runager, K., et al. (2013). The insoluble TGFBIp fraction of the cornea is covalently linked via a disulfide bond to type XII collagen. Biochemistry. 52: 2821-2827.
- Rylett, C. M., *et al.* (2007). Male accessory glands of *Drosophila melanogaster* make a secreted angiotensin-I converting enzyme (ANCE), suggesting a role for the peptide-processing enzyme in seminal fluid. J. Exp. Biol. 210: 3601-3606.
- Sabate, R., *et al*. (2015). Amyloids or prions? That is the question. Prion. 9 (3): 200-206.
- Saber, S. H., *et al*. (2020). Exosomes are the driving force in preparing the soil for the metastatic seeds: lessons from prostate cancer. Cells 9. https://doi.org/10.3390/cells9030564.

- Sahlin, C., *et al.* (2007). The Arctic Alzheimer mutation favors intracellular amyloid-beta production by making amyloid precursor protein less available to alpha-secretase. J. Neurochem. 101: 854-862.
- Saksena, S., and Emr, S. D. (2009). ESCRTs and human disease. Biochem. Soc. Trans. 37: 167-172.
- Sanuki, R., *et al.* (2019). Normal aging hyperactivates innate immunity and reduces the medical efficacy of minocycline in brain injury. Brain Behav. Immun. 80: 427-438.
- Sarkar, S., *et al.* (2021). Oligomerization of Lrrk controls actin severing and α-synuclein neurotoxicity in vivo. Mol. Neurodegeneration. 16 (33): https://doi.org/10.1186/s13024-021-00454-3.
- Sato, C., *et al.* (2006). Structure of the catalytic pore of γ-secretase probed by the accessibility of substituted cysteines. J. Neurosci. 26: 12081-12088.
- Savovenko, A. V., *et al.* (2008). Alteration of BACE1-dependent NRG1/ErbB4 signaling and schizophrenia-like phenotypes in BACE1-null mice. Proc. Natl. Acad. Sci. USA. 105: 5585-5590.
- Sawaya, M. R., *et al.* (2021). The expanding amyloid family: structure, stability, function and pathogenesis. Cell. 184: 4857-4873.
- Scheibel, T., *et al.* (2003). Conducting nanowires built by controlled self-assembly of amyloid fibers and selective metal deposition. Proc. Natl. Acad. Sci. USA. 100: 4527-4532.
- Scheper, W., *et al.* (2004). Rab6 membrane association is dependent on *Presenilin-1* and cellular phosphorylation events. Brain Res. Mol. Brain Res. 122: 17-23.

- Scheper, W., *et al.* (2007). Rab6 is increased in Alzheimer's disease brain and correlates with endoplasmic reticulum stress. Neuropathol. Appl. Neurobiol. 33: 523-532.
- Scheuner, D., *et al.* (1996). Secreted amyloid-beta protein similar to that in the senile plaques of Alzheimer's disease is increased in vivo by the Presinilin 1 and 2 and APP mutations linked to familial Alzheimer's disease. Nat. Med. 2 (8): 864-870.
- Schmid, L. C., *et al.* (2016). Dysfunction of somatostatin-positive interneurons associated with memory deficits in an Alzheimer's disease model. Neuron. 92: 114-125.
- Schmidt, O., and Teis, D. (2012). The ESCRT machinery. Curr. Biol. 22 (4): R116-R120.
- Schultz, C. J., *et al.* (2002). The classical arabinogalactan protein gene family of *Arabidopsis.* Plant Cell. 12; 1751-1768.
- Schulze, H., *et al.* (1993). Rat brain glyceraldehyde-3-phosphate dehydrogenase interacts with recombinant cytoplasmic domain of Alzheimer's β-amyloid precursor protein. J. Neurochem. 60: 1915-1922.
- Seaman, M.N.J. (2021). The Retromer Complex: from genesis to revelations. *Trends Biochem. Sci.* S0968-0004 (20) 30321-2. https://doi.org/10.1016/j.tibs.2020.12.009.
- Seaman, M. N., *et al.* (1998). A membrane coat complex essential for endosome-to-Golgi retrograde transport in yeast. J. Cell Biol. 142: 665-681.

- Sekar, A., *et al.* (2021). Rbf/E2F1 control growth and endoreplication via steroid-independent Ecdysone Receptor signalling in *Drosophila* prostate-like secondary cells. https://doi.org/10.1101/2021.03.27.437310.
- Selkoe, D.J., and Hardy, J. (2016). The amyloid hypothesis of Alzheimer's disease at 25 years. *EMBO Mol. Med*. 8: 595-608.
- Seuma, M., *et al.* (2022). An atlas of amyloid aggregation: the impact of substitutions, insertions, deletions and truncations on amyloid beta fibril nucleation. Nat. Commun. 13 (1): 7084.
- Shah, S., *et al.* (2005). Nicastrin functions as a gamma-secretase substrate receptor. Cell. 122: 435-447.
- Sharma, M., *et al.* (2012). A multi-center clinico-genetic analysis of the VPS35 gene in Parkinson's disease indicates reduced penetrance for disease-associated variants. J. Med. Genet. 49 (11): 721-726.
- Sharples, R.A., *et al.* (2008). Inhibition of γ-secretase causes increased secretion of amyloid precursor protein C-terminal fragments in association with exosomes. *FASEB J*. 22: 1469-1478.
- Sidhanta, A., *et al.* (2000). Inhibition of phophatidic acid synthesis alters the structure of the Golgi apparatus and inhibits secretion in endocrine cells. J. Biol. Chem. 275 (16): 12023-12031.
- Silver. C. R., *et al.* (2016). Identification of extracellular vesicle-borne periostin as a feature of muscle-invasive bladder cancer. Oncotarget. 7 (17): 23335-23345.
- Singh, P. J., *et al.* (2022). Homologues of the human disease-associated amyloidogenic proteins APP and TGFBI are required for physiological protein

aggregation in *Drosophila* secondary cells. Poster presented at the 63rd Annual *Drosophila* Research Conference, Genetics Society of America, San Diego, CA, April 6-10, 2022.

- Singh, S. K., *et al.* (2017). Knockdown of APPL mimics transgenic Aβ induced neurodegenerative phenotypes in *Drosophila*. Neurosci. Lett. 648: 8-13.
- Sirover, M. A. (2013). Studies on Alzheimer's Disease: oxidative stress in applied basic research and clinical practice. Humana Press, Totowa, NJ.
- Skonier, J., *et al.* (1992). cDNA cloning and sequence analysis of βig-h3, a novel gene induced in a human adenocarcinoma cell line after treatment with transforming growth factor-β. DNA Cell Biol. 11: 511-522.
- Small, D. (1994). A heparin-binding domain in the amyloid protein precursor of Alzheimer's disease is involved in the regulation of neurite outgrowth. J. Neurosci. 14: 2117-2127.
- Small, S. A., *et al.* (2005). Model-guided microarray implicates the retromer complex in Alzheimer's disease. Ann. Neurol. 58: 909-919.
- Small, S. A., and Petsko, G. A. (2015). Retromer in Alzheimer's disease, Parkinson's disease and other neurological disorders. Nat. Rev. Neurosci. 16: 126-132.
- Smith, J. F., *et al.* (2006). Characterization of the nanoscale properties of individual amyloid fibrils. Proc. Natl. Acad. Sci. USA. 103: 15806-15811.
- Snider, P., *et al.* (2008). Periostin is required for maturation and extracellular matrix stabilization of noncardiomyocyte lineages of the heart. Circ. Res. 102: 752-760.

- Snow, P. M., et al. (1988). Characterization and cloning of fasciclin I and II glycoproteins in the grasshopper. Proc. Natl. Acad. Sci. USA. 85: 5291-5295.
- Soejima, N., *et al.* (2013). Intracellular accumulation of toxic turn amyloid-beta is associated with endoplasmic reticulum stress in Alzheimer's disease. Curr. Alzheimer Res. 10: 11-20.
- Söllvander, S., *et al.* (2015). Increased number of plasma B cells producing autoantibodies against protofibrils $A\beta_{42}$ in Alzheimer's disease. J. Alzheimers Dis. 48: 63-72.
- Song, X., *et al.* (2014). Identification and characterization of Transforming Growth Factor Beta-Induced gene (TGFBIG) from *Branchiostoma belcheri*: insights into evolution of the TGFBI family. Genomics. 103: 147-153.
- Song, Z., *et al.* (2020). Brain derived exosomes are a double-edged sword in Alzheimer's Disease. Front. Mol. Neurosci. 13: 79. https://doi.org/10.3389/fnmol.2020.00079.
- Sosa, L. J., *et al.* (2017). The physiological role of the amyloid precursor protein as an adhesion molecule in the developing nervous system. J. Neurochem. 143: 11-29.
- Southwell, A. L., *et al.* (2012). Antisense oligonucleotide therapeutics for inherited neurodegenerative disease. Trends in Mol. Med. 18 (11): 634-643.
- Spalton, D. J., *et al.* (2004). Atlas of Clinical Ophthalmology. Elsevier Health Sciences.

- Stamnes, M. A., and Rothman, J. E. (1993). The binding of AP-1 clathrin-adaptor particles to Golgi membranes requires ADP-ribosylation factor, a small GTP-binding protein. Cell. 73 (5): 999-1005.
- Stathopoulus. P. B., *et al.* (2003). Cu/Zn superoxide dismutase mutants associated with amyotrophic lateral sclerosis show enhanced formation of aggregates *in vitro*. Proc. Natl. Acad. Sci. USA. 100 (12): 7021-7026.
- Steiner, H., *et al.* (2018). Making the final cut: pathogenic amyloid β-peptide generation by γ-secretase. Cell Stress. 2 (11): 292-310.
- Stempfle, D., *et al*. (2010). In vivo reconstitution of gamma-secretase in *Drosophila* results in substrate specificity. Mol. Cell. Biol. 30: 3165-3175.
- Subedi, S., *et al.* (2022). Amyloid cross-seeding: mechanism, implication and inhibition. Molecules. 27 (6): 1776.
- Sullivan, C.P., *et al.* (2011). Retromer disruption promotes amyloidogenic APP processing. *Neurobiol. Dis.* 43: 338-345.
- Sultana, P., and Novotny, J. (2022). Rab11 and it's role in neurodegenerative diseases. Am. Soc. Neurochem. Neuro. 14: 1-19.
- Sumioka, A., *et al.* (2005). Role of 14-3-3 gamma in FE65-dependent gene transactivation mediated by the amyloid beta-protein precursor cytoplasmic fragment. J. Biol. Chem. 42364-42374.
- Sun, L. L., *et al.* (2013). Global analysis of fission yeast mating genes reveals new autophagy factors. PLoS Genet. 9: e1003715.

- Sun, W., *et al.* (2018). Pathogenic tau-induced piRNA depletion promotes neuronal death through transposable element dysregulation in neurodegenerative tauopathies. Nat. Neurosci. 18: 1-16.
- Sunaga, K., *et al.* (1995). Glyceraldehyde-3-phosphate dehyrdogenase is overexpressed during apoptotic death of neuronal culture and is recognized by a monoclonal antibody against amyloid plaques from Alzheimer's disease. Neurosci. Lett. 200: 133-136.
- Swanson, T. L., *et al.* (2005). The insect homologue of the amyloid precursor protein interacts with the heterotrimeric G protein go alpha in an identical population of migratory neurons. Dev. Biol. 288: 160-178.
- Swarbrick, S., *et al.* (2019). Systematic review of miRNAs as biomarkers in Alzheimer's Disease. Mol. Neurobiol. 56 (7): 6156-6167.
- Szodorai, A., *et al.* (2009). APP anterograde transport requires Rab3A GTPase activity for assembly of the transport vesicle. J. Neurosci. 14534-14544.
- Tackenberg, C., *et al.* (2020). Alzheimer's disease mutations at position 22 of the amyloid-beta peptide sequence differentially affect synaptic loss, Tau phosphorylation, and neuronal cell death in an *ex vivo* system. PLoS One. 15 (9): e0239584.
- Takeshita, S., *et al.* (1993). Osteoblast-specific factor-2: cloning of a putative bone adhesion protein with homology with the insect protein fsaciclin I. Biochem. J. 294: 271-278.

- Tam, J. H. K., *et al*. (2014). The amyloid precursor protein is rapidly transported from the Golgi apparatus to the lysosome where it is processed into beta-amyloid. Molecular Brain. 7: 54.
- Tan, J. Z. A., and Gleeson, P.A. (2019). The role of membrane trafficking in the processing of amyloid precursor protein and production of amyloid peptides in Alzheimer's disease. Biochim. Biophys. Acta Biomembr. 1861: 697-712.
- Tatton, N. A. (2000). Increased caspase 3 and Bax immunoreactivity accompany nuclear GAPDH translocation and neuronal apoptosis in Parkinson's disease. Exp. Neurol. 166: 29-43.
- Thal, D. R., *et al.* (2002). Phases of amyloid beta deposition in the human brain and its relevance for the development of AD. Neurology. 58: 1791-1800.
- Thiel, H. J., and Behnke, H. (1967). A hitherto unknown subepithelial hereditary corneal dystrophy. Klin. Monatsblatter für Augenheilkd. 150: 862-874.
- Thinakaran, G., *et al.* (1996). Metabolism of the 'Swedish' amyloid precursor protein variant in neuro2a cells. Evidence that cleavage at the 'beta-secretase' site occurs in the Golgi apparatus. J. Biol. Chem. 271: 9390-9397.
- Thompson, A. G., *et al.* (2016). Extracellular vesicles in neurodegenerative diseases – pathogenesis to biomarkers, Nat. Rev. Neurol. 12: 346-357.
- Tolia, A., *et al.* (2006). Contribution of presenilin transmembrane domains 6 and 7 to a water-containing cavity in the γ-secretase complex. J. Biol. Chem. 281: 27633-27642.
- Tomidokoro, Y., *et al.* (2010). Iowa variant of familial Alzheimer's Disease. Am. J. Pathol. 176 (4): 1841-1854.

- Tong, C., *et al.* (2011), Rich regulates traget specificity of photoreceptor cells and N-cadherin trafficking in the *Drosophila* visual system via Rab6. Neuron. 71: 447-459.
- Torroja, L., *et al.* (1999). The *Drosophila* beta-amyloid precursor protein homolog promotes synapse differentiation at the neuromuscular junction. *J. Neurosci.* 19: 7793-7803.
- Traub, L. M., *et al.* (1993). Biochemical dissection of AP-1 recruitment onto Golgi membranes. J. Cell Biol. 123 (3): 561-573.
- Tsai, C. W., *et al.* (2020). An investigation of the correlation between S-glutathionylyted GAPDH levels in blood and Alzheimer's disease progression. PLoS ONE 15(5): e0233289. https://doi.org/10.1371/journal.pone.0233289.
- Tsika, E., *et al.* (2014). Parkinson's disease-linked mutations in VPS35induce dopaminergic neurodegeneration. Hum. Mol. Genet. 23 (17): 4621-4638.
- Tsubuki, S., *et al.* (2003). Dutch, Flemish, Italian and Arctic mutations of APP and resistance of Abeta to physiologically relevant proteolytic degradation. Lancet. 361 (9373): 1957-1958.
- Tsuchiya, M., *et al.* (2010). Cholesterol biosynthesis pathway intermediates and inhibitors regulate glucose-stimulated insulin secretion and secretory granule formation in pancreatic beta-cells. Endocrinology. 151 (10): 4705-4716.
- Udayar, V., *et al.* (2013). A paired RNAi and RabGAP overexpression screen identifies Rab11 as a regulator of β-amyloid production. Cell Reports. 5 (6): 1536-1551.

- Ugur, B., *et al.* (2017). The Krebs cycle enzyme isocitrate dehydrogenase 3A couples mitochondrial metabolism to synaptic transmission. Cell Reports. 21: 3794-3806.
- Ulag, S., *et al.* (2021). A novel approach to treat the Thiel-Behnke corneal dystrophy using 3D printed honeycomb shaped polymethylmethacrylate (PMMA)/Vancomycin (VAN) scaffolds. Bioprinting. 24: e00173.
- Ullrich, O., *et al.* (1996). Rab11 regulates recycling through the pericentriolar recycling endosome. J. Cell Biol. 135 (4): 913-924.
- Ulstrup, J. C., *et al.* (1995). Relationship of secretion pattern and Mbp70 homology with osteoblast-specific factor to osteitis following *Mycobacterium bovis* BCG vaccination. Infect. Immun. 63: 672-675.
- Vagnozzi, A. N., and Pratico, D. (2019). Endosomal sorting and trafficking, the retromer complex and neurodegeneration. *Mol. Psychiatry.* 24: 857-868.
- Valdmanis, P. N., *et al.* (2007). Mutations in the *KIAA0196* gene at the SPG8 locus causes hereditary spastic paraplegia. Am. J. Hum. Genet. 80: 152-161.
- Van der Kant, R., and Goldstein, L. S. B. (2015). Cellular functions of the amyloid precursor protein from development to dementia. Developmental Cell. 32: 502-515.
- Van Niel, G., *et al.* (2018). Shedding light on the cell biology of extracellular vesicles. *Nat. Rev. Mol. Cell Biol.* 19: 213-228.
- Van Nostrand, W. E., *et al.* (2001). Pathogenic effects of D23N Iowa mutant amyloid-beta protein. J. Biol. Chem. 276 (35): 32860-32866.

- Van Nostrand, W. E., *et al.* (2002). Pathogenic effects of cerebral amyloid angiopathy mutations in the amyloid-beta protein precursor. Ann. NY. Acad. Sci. 977: 258-265.
- Vardaki, I., *et al.* (2016). Periostin is identified as a putative metastatic marker in breast-cancer derived exosomes. Oncotarget. 7 (46): 74966-74978.
- Vardarajan, B.N., *et al.* (2012). Identification of Alzheimer disease-associated variants in genes that regulate retromer function. *Neurobiol. Aging*. 33: 2231.e15-2231.e30. https://doi.org/10.1016/j.neurobiolaging.2012.04.020.
- Varsarajan, B.N., *et al.* (2012). Identification of Alzheimer disease-associated variants in genes that regulate retromer function. *Neurobiol. Aging.* 33: 2231.e15-2231.e30.
- Vassar, R., *et al.* (1999). β-secretase cleavage of Alzheimer's amyloid precursor protein by the transmembrane aspartic protease BACE. Science. 286: 735-741.
- Venkatraman, A., *et al.* (2017). Proteomic analysis of amyloid corneal aggregates from TGFBI-H626R lattice corneal dystrophy patient implicates serine-protease HTRA1 in mutation-specific pathogenesis of TGFBIp. J. Proteome Res. 16: 2899-2913.
- Venken, K. J. T., *et al.* (2011). MiMIC: a highly versatile transposon insertion resource for engineering *Drosophila melanogaster* genes. Nat. Methods. 8 (9): 737-743.
- Venugopal, C., *et al.* (2007). Insulysin cleaves the APP cytoplasmic fragment at multiple sites. Neurochem. Res. 32: 2225-2234.

- Verdile, G., *et al.* (2006). The role of presenilin and its interacting proteins in the biogenesis of Alzheimer's beta amyloid. Neurochem. Res. 32: 609-623.
- Verhoeven, K., *et al.* (2003). Mutations in the small GTP-ase late endosomal protein RAB7 cause Charcot-Marie-Tooth type 2B neuropathy. Am. J. Hum. Genet. 72 (3): 722-727.
- Vilarino-Guell, C., *et al.* (2011). *VPS35* mutations in Parkinson's disease. Am. J. Hum. Genet. 89: 162-167.
- Villeneuve, S., *et al*. (2015). Existing Pittsburgh Compound-B positron emission tomography levels are too high: statistical and pathological evaluation. Brain. 138: 2020-2033.
- Vonsattel, J. P., *et al.* (1985). Neuropathological classification of Huntington's disease. J. Neuropathol. Exp. Neurol. 44: 559-577.
- Wainwright, S. M., *et al.* (2021). *Drosophila* sex peptide controls the assembly of lipid microcarriers in seminal fluid. *PNAS* 118: e2019622118.
- Walsh, R. B., *et al.* (2021). Opposing functions for retromer and Rab11 in extracellular vesicle traffic at presynaptic terminals. *J. Cell Biol.* 220 (8): https://doi.org.10.1083/jcb.202012034.
- Wallace, D. P., *et al.* (2008). Periostin induces proliferation of human autosomal dominant polycystic kidney cells through alphaV-integrin receptor. Am. J. Physiol. Renal Physiol. 295: F1463-F1471.
- Walker. L. (2020). Aβ plaques. Free Neuropathology. 1:31.
- Walsh, D. M., *et al.* (1997). Amyloid beta-protein fibrillogenesis: detection of a protofibrillar intermediate. J. Biol. Chem. 272: 22364-22372.

- Walsh, R. B., *et al.* (2021). Opposing functions for retromer and Rab11 in extracellular vesicle traffic at presynaptic terminals. J. Cell Biol. 220 (8): e202012034.
- Wandinger-Ness, A., and Zerial, M. (2014). Rab proteins and the compartmentalization of the endosomal system. Cold Spring Harb. Perspect. Biol. 6 (11): a022616.
- Wang, H., *et al.* (2008). BACE1 knockouts display deficits in activity-dependent potentiation of synaptic transmission at mossy fiber to CA3 synapses in the hippocampus. J. Neurosci. 28: 8677-8681.
- Wang, Q., *et al.* (2005). Proteomic analysis of neurofibrillary tangles in Alzheimer disease identifies GAPDH as a detergent-insoluble paired helical filament tau binding protein. FASEB J. 19 (7): 869-871.
- Wang, W., *et al.* (2014). Amyloid precursor protein α- and β-cleaved ectodomains exert opposing control of cholesterol homeostasis via SREBP2. FASEB J. 28: 849-860.
- Wang, X., *et al.* (2013). Loss of sorting nexin 27 contributes to excitatory synaptic dysfunction by modulating glutamate receptor recycling in Down's syndrome. Nature Med. 19: 473-480.
- Wang, Y., and Mandelkow E. (2016). Tau in physiology and pathology. Nat. Rev. Neurosci. 17: 5-21.
- Wang, Z., *et al.* (2009). Presynaptic and postsynaptic interaction of the amyloid precursor protein promotes peripheral and central synaptogenesis. J. Neurosci. 10788-10881.

- Wasco, W., *et al*. (1992). Identification of a mouse brain cDNA that encodes a protein related to the Alzheimer's disease-associated amyloid beta protein precursor. Proc. Natl. Acad. Sci. USA. 89: 10758-10762.
- Wasco, W., *et al.* (1993). Isolation and characterization of APLP2 encoding a homologue of Alzheimer's associated amyloid beta protein precursor. Nat. Genet. 5: 95-100.
- Webster, N., *et al.* (1988). The yeast UASG is atranscription enhancer in human HeLa cells in the presence of the GAL4 trans-activator. Cell. 52 (2): 169-178.
- Ween, M. P., *et al.* (2012). Transforming Growth Factor Beta-Induced Protein: a matrix protein with dual functions in ovarian cancer. Int. J. Mol. Sci. 13: 10461-10477.
- Weidle, E., and Lisch, W. (1984). Various forms of opacities of granular corneal dystrophy. Klin. Monbl. Augenheilkd. 185: 167-173.
- Weiss, J. S., *et al. (*2015). IC3D classification of corneal dystrophies. Edition 2. Cornea. 34: 117-159.
- Wells, C. *et al.* (2021). The role of amyloid oligomers in neurodegenerative pathologies. Int. J. Biol. Macromolecules. 181: 582-604.
- Wen, L., *et al.* (2011). VPS35 haploinsufficiency increases Alzheimer's disease neuropathology. *J. Cell Biol.* 195: 765-779.
- West-Mays, J., and Dwivedi, D. (2006). The keratocyte: corneal stromal cell with variable repair phenotypes. 38 (10): 1625-1631.
- White, I. J., *et al.* (2006). EGF stimulates annexin-1 dependent inward vesiculation in a multivesicular subpopulation. EMBO J. 25: 1-12.

- Wilson, C., *et al.* (2017). The *Drosophila* accessory gland as a model for prostate cancer and other pathologies. *Curr. Top. Dev. Biol*. 121:339-375.
- Wines-Samuelson, M. I., *et al.* (2010). Characterization of age-dependent and progressive cortical neuronal degeneration in presnilin conditional mutant mice. PLoS One. 5e:10195.
- Wolfe, M. S. (2006). The γ-secretase complex: membrane-embedded proteolytic ensemble. Biochemistry. 45: 7931-7939.
- Wolfe, M. S., *et al.* (1999). Two transmembrane aspartates in presenilin-1 required for presnilin endoproteolysis and γ-secretase activity. Nature. 398: 513-517.
- Wu, M. M., *et al.* (2001). Mechanisms of pH regulation in the regulated secretory pathway. J. Biol. Chem. 276 (35): 33027-33035.
- Xie, L., *et al.* (2002). Alzheimer's beta-amyloid peptides compete for insulin binding to the insulin receptor. J. Neurosci. 22:RC221.
- Xu, X. (2009). Gamma-secretase catalyzes sequential cleavages of the AβPP transmembrane domain. J. Alzheimers Dis. 16 (2): 211-224.
- Yang, Y., *et al.* (2023). Cryo-EM structures of amyloid-beta filaments with the Arctic mutation (E22G) from human and mouse brains. Acta Neuropathol. 145 (3): 325-333.
- Yankers, B. A., and Lu, T. (2009). Amyloid-β protein toxicity and the pathogenesis of Alzheimer's disease. J. Biol. Chem. 284: 4755-4759.
- Yang, T., *et al.* (2017). Large soluble oligomers of amyloid-β protein from Alzheimer brain are far less neuroactive than the smaller oligomers to which they dissociate. J. Neurosci. 37: 152-163.

- Yang, X., *et al.* (2018). On the role of sidechain size and charge in the aggregation of $A\beta_{42}$ with familial mutations. Proc. Natl. Acad. Sci. USA. 115 (26): E5849-E5858.
- Ye, H., *et al*. (2020). Retromer subunit VPS29, regulates synaptic transmission and is required for enolysosomal function in the aging brain. *eLife.* 9:e51977. https://doi.org/10.7554/eLife.51977.
- Yin, J., *et al.* (2020). Comprehensively investigating the expression levels and prognostic role of transforming growth factor beta-induced (TGFBI) in glioblastoma multiforme. Transl. Cancer Res. 9 (10): 6487-6504.
- Yong, X., *et al.* (2020). Mechanism of cargo recognition by retromer linked SNX BAR proteins. *PLoSBiology* 18:e3000631. https://doi.org/10.1371/journal.pbio.3000631.
- Young-Pearse, T. L., *et al.* (2007). A critical function for beta-amyloid precursor protein in neuronal migration revelaed by in utero RNA interference. J. Neurosci. 27: 14459-14469.
- Ysselstein, D., *et al.* (2019). Emerging links between lysosomal storage diseases and adult parkinsonism. Movement Disorders. 34: 614-624.
- Yu, H., *et al.* (2001). APP processing and synaptic plasticity in presnilin-1 conditional knockout mice. Neuron. 31: 713-726.
- Zavodszky, E., *et al.* (2014). Mutation in VPS35 associated with Parkinson's disease impairs WASH complex association and inhibits autophagy. Nature Commun. 5: 3828.

- Zhang, D., *et al.* (2012). Rab-6.2 and retromer regulate glutamate receptor recycling through a retrograde pathway. J. Cell Biol. 196: 85-101.
- Zhang, J., *et al.* (2007). Thirty-one flavors of *Drosophila* Rab proteins. Genetics. 176: 1307-1322.
- Zhang, Q., *et al.* (2021). Supermeres are functional extracellular nanoparticles replete with disease biomarkers and therapeutic targets. *Nature Cell Biology*. 23: 1240-1254.
- Zhang, T., *et al.* (2020). Phosphorylation signalling in APP processing in Alzheimer's Disease. Int. J. Mol. Sci. 21 (1): 209.
- Zhang, X., *et al.* (2019). Role of Rab GTPases in Alzheimer's Disease. ACS Chem. Neurosci. 10: 828-838.
- Zhao, G., *et al.* (2004). Identification of a new presenilin-dependent ζ-cleavage site within the transmembrane domain of the amyloid precursor protein. J. Biol. Chem.279 (49): P50647-P50650.
- Zhou, B., *et al.* (2022). Synaptogenic effect of *APP-Swedish* mutation in familial Alzheimer's disease. Sci. Transl. Med. 14 (667): eabn9380.
- Zilka, N., and Novak, M. (2006). The tangled story of Alois Alzheimer. Bratisl Lek Listy. 107 (9-10): 343-345.
- Zimprich, A., *et al.* (2004). Mutations in LRRK2 cause autosomal-dominant parkinsonism with pleomorphic pathology. Neuron. 44 (4): 601-607.
- Zimprich, A., *et al.* (2011). A mutation in VPS35, encoding a subunit of the retromer complex, causes late-onset Parkinson's disease. Am. J. Hum. Genet. 89 (1): 168-175.

- Zinn, K., *et al.* (1988). Sequence analysis and neuronal expression of fasciclin I in grasshopper and *Drosophila*. Cell. 53: 577-587.

CHAPTER 9

APPENDIX

9. APPENDIX

9.1 SEQUENCES FOR CONSTRUCTS

1. Full-length wt-TGFBI sequence with 15 added bases at either end
2. TGFBI with the non-conserved domain-1 R124C mutation (CGC→TGT)
3. TGFBI with the non-conserved domain-4 R555Q mutation (CGC→CAA)
4. TGFBI with the conserved domain-4 G623D mutation (GGC→GAT)
5. TGFBI with the conserved domain-4 H626R mutation (CAT→CGC)
6. TGFBI with the GFP coding sequence added at C-terminus just before TAG
7. Full-length mfas RK sequence
8. Full-length mfas RK sequence with GFP added just before the stop
9. Mfas RK with the conserved domain-4 G623D mutation (GGT→GAC)
10. Mfas RK with the conserved domain-4 H626R mutation (CAC→CGA)

9.1.1 *TGFBI*-WILD TYPE

5’-GCGTCGTCCCGCTCC
ATGGCGCTCTTCGTGCGGCTGCTGGCTCTCGCCCTGGCTCTGGCCCTGGGCCCCGCCGCGACCCTGGCGG
GTCCCGCCAAGTCGCCCTACCAGCTGGTGCTGCAGCACAGCAGGCTCCGGGGCCGCCAGCACGGCCCCAA
CGTGTGTGCTGTGCAGAAGGTTATTGGCACTAATAGGAAGTACTTCACCAACTGCAAGCAGTGGTACCAA
AGGAAAATCTGTGGCAAATCAACAGTCATCAGCTACGAGTGCTGTCCTGGATATGAAAAGGTCCCTGGGG
AGAAGGGCTGTCCAGCAGCCCTACCACTCTCAAACCTTTACGAGACCCTGGGAGTCGTTGGATCCACCAC
CACTCAGCTGTACACGGACCGCACGGAGAAGCTGAGGCCTGAGATGGAGGGGCCCGGCAGCTTCACCATC
TTCGCCCCTAGCAACGAGGCCTGGGCCTCCTTGCCAGCTGAAGTGCTGGACTCCCTGGTCAGCAATGTCA
ACATTGAGCTGCTCAATGCCCTCCGCTACCATATGGTGGGCAGGCGAGTCCTGACTGATGAGCTGAAACA
CGGCATGACCCTCACCTCTATGTACCAGAATTCCAACATCCAGATCCACCACTATCCTAATGGGATTGTA
ACTGTGAACTGTGCCCGGCTGCTGAAAGCCGACCACCATGCAACCAACGGGGTGGTGCACCTCATCGATA
AGGTCATCTCCACCATCACCAACAACATCCAGCAGATCATTGAGATCGAGGACACCTTTGAGACCCTTCG
GGCTGCTGTGGCTGCATCAGGGCTCAACACGATGCTTGAAGGTAACGGCCAGTACACGCTTTTGGCCCCG
ACCAATGAGGCCTTCGAGAAGATCCCTAGTGAGACTTTGAACCGTATCCTGGGCGACCCAGAAGCCCTGA
GAGACCTGCTGAACAACCACATCTTGAAGTCAGCTATGTGTGCTGAAGCCATCGTTGCGGGGCTGTCTGT
AGAGACCCTGGAGGGCACGACACTGGAGGTGGGCTGCAGCGGGGACATGCTCACTATCAACGGGAAGGCG
ATCATCTCCAATAAAGACATCCTAGCCACCAACGGGGTGATCCACTACATTGATGAGCTACTCATCCCAG
ACTCAGCCAAGACACTATTTGAATTGGCTGCAGAGTCTGATGTGTCCACAGCCATTGACCTTTTCAGACA
AGCCGGCCTCGGCAATCATCTCTCTGGAAGTGAGCGGTTGACCCTCCTGGCTCCCCTGAATTCTGTATTC
AAAGATGGAACCCCTCCAATTGATGCCCATACAAGGAATTTGCTTCGGAACCACATAATTAAAGACCAGC
TGGCCTCTAAGTATCTGTACCATGGACAGACCCTGGAAACTCTGGGCGGCAAAAAACTGAGAGTTTTTGT
TTATCGTAATAGCCTCTGCATTGAGAACAGCTGCATCGCGGCCCACGACAAGAGGGGGAGGTACGGGACC
CTGTTCACGATGGACCGGGTGCTGACCCCCCCAATGGGGACTGTCATGGATGTCCTGAAGGGAGACAATC
GCTTTAGCATGCTGGTAGCTGCCATCCAGTCTGCAGGACTGACGGAGACCCTCAACCGGGAAGGAGTCTA
CACAGTCTTTGCTCCCACAAATGAAGCCTTCCGAGCCCTGCCACCAAGAGAACGGAGCAGACTCTTGGGA
GATGCCAAGGAACTTGCCAACATCCTGAAATACCACATTGGTGATGAAATCCTGGTTAGCGGAGGCATCG
GGGCCCTGGTGCGGCTAAAGTCTCTCCAAGGTGACAAGCTGGAAGTCAGCTTGAAAAACAATGTGGTGAG
TGTCAACAAGGAGCCTGTTGCCGAGCCTGACATCATGGCCACAAATGGCGTGGTCCATGTCATCACCAAT
GTTCTGCAGCCTCCAGCCAACAGACCTCAGGAAAGAGGGGATGAACTTGCAGACTCTGCGCTTGAGATCT

TCAAACAAGCATCAGCGTTTTCCAGGGCTTCCCAGAGGTCTGTGCGACTAGCCCCTGTCTATCAAAAGTT
ATTAGAGAGGATGAAGCATTAGCTTGAAGCACTACAG-3′

Figure 9.1: Sequence of TGFBI wild type. Areas mutated in the CDs studied in this thesis are highlighted in red and yellow (source: Genscript, personal communication).

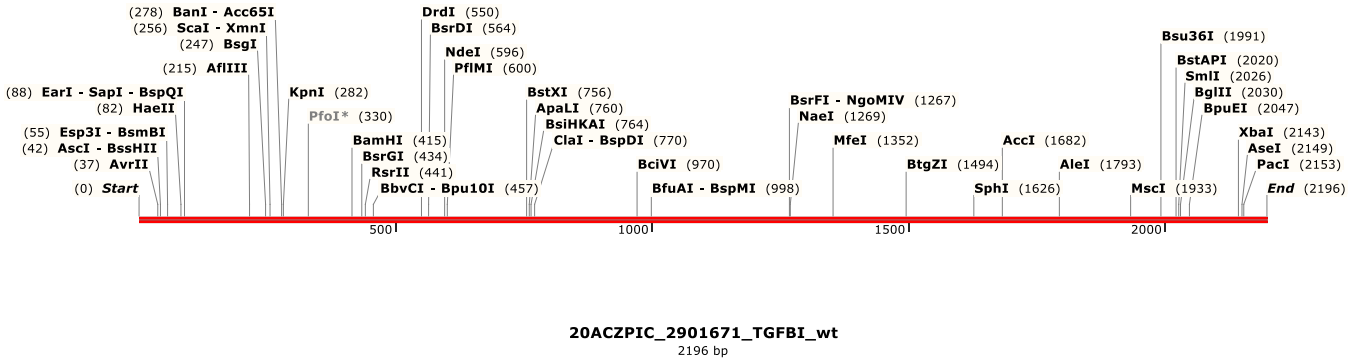

Figure 9.2: TGFBI wild type (2196 bp) showing it's restriction cleavage sites. EcoRI and XbaI restriction sites were introduced at the 5'- and 3'- ends respectively for the purposes of cloning and subcloning (source: Genscript, personal communication).

Created with SnapGene®

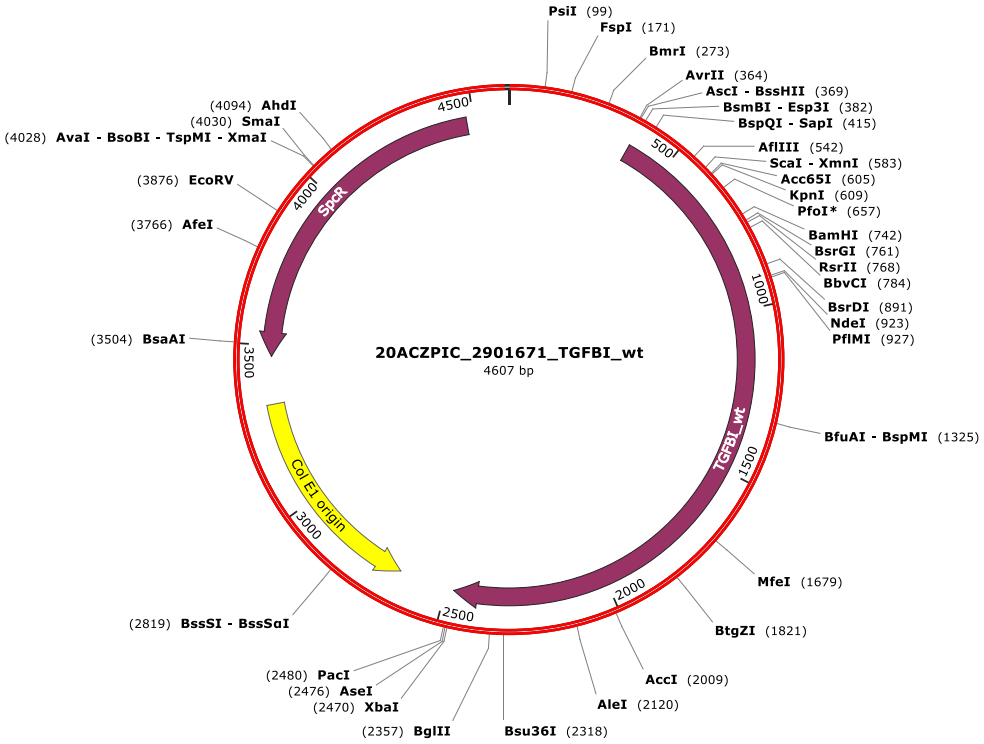

Figure 9.3: TGFBI wild type cloned into plasmid construct 20AZCPIC. It was subsequently excised and subcloned into *Drosophila*-specific plasmid pUASTattB_AN230 at the previously mentioned 5'- EcoRI and 3'- XbaI sites (source: Genscript, personal communication). For the final pUASTattB_AN230-TGFBI-wild type construct please see **Figure 2.5.**

9.1.2 *TGFBI-R124C* (CGC→TGT)

5'-GCGTCGTCCCGCTCC

ATGGCGCTCTTCGTGCGGCTGCTGGCTCTCGCCCTGGCTCTGGCCCTGGGCCCCGCCGCGACCCTGGCGG
GTCCCGCCAAGTCGCCCTACCAGCTGGTGCTGCAGCACAGCAGGCTCCGGGGCCGCCAGCACGGCCCCAA
CGTGTGTGCTGTGCAGAAGGTTATTGGCACTAATAGGAAGTACTTCACCAACTGCAAGCAGTGGTACCAA
AGGAAAATCTGTGGCAAATCAACAGTCATCAGCTACGAGTGCTGTCCTGGATATGAAAAGGTCCCTGGGG
AGAAGGGCTGTCCAGCAGCCCTACCACTCTCAAACCTTTACGAGACCCTGGGAGTCGTTGGATCCACCAC
CACTCAGCTGTACACGGAC**TGT**ACGGAGAAGCTGAGGCCTGAGATGGAGGGGCCCGGCAGCTTCACCATC
TTCGCCCCTAGCAACGAGGCCTGGGCCTCCTTGCCAGCTGAAGTGCTGGACTCCCTGGTCAGCAATGTCA
ACATTGAGCTGCTCAATGCCCTCCGCTACCATATGGTGGGCAGGCGAGTCCTGACTGATGAGCTGAAACA
CGGCATGACCCTCACCTCTATGTACCAGAATTCCAACATCCAGATCCACCACTATCCTAATGGGATTGTA
ACTGTGAACTGTGCCCGGCTGCTGAAAGCCGACCACCATGCAACCAACGGGGTGGTGCACCTCATCGATA
AGGTCATCTCCACCATCACCAACAACATCCAGCAGATCATTGAGATCGAGGACACCTTTGAGACCCTTCG
GGCTGCTGTGGCTGCATCAGGGCTCAACACGATGCTTGAAGGTAACGGCCAGTACACGCTTTTGGCCCCG
ACCAATGAGGCCTTCGAGAAGATCCCTAGTGAGACTTTGAACCGTATCCTGGGCGACCCAGAAGCCCTGA
GAGACCTGCTGAACAACCACATCTTGAAGTCAGCTATGTGTGCTGAAGCCATCGTTGCGGGGCTGTCTGT
AGAGACCCTGGAGGGCACGACACTGGAGGTGGGCTGCAGCGGGGACATGCTCACTATCAACGGGAAGGCG

ATCATCTCCAATAAAGACATCCTAGCCACCAACGGGGTGATCCACTACATTGATGAGCTACTCATCCCAG
ACTCAGCCAAGACACTATTTGAATTGGCTGCAGAGTCTGATGTGTCCACAGCCATTGACCTTTTCAGACA
AGCCGGCCTCGGCAATCATCTCTCTGGAAGTGAGCGGTTGACCCTCCTGGCTCCCCTGAATTCTGTATTC
AAAGATGGAACCCCTCCAATTGATGCCCATACAAGGAATTTGCTTCGGAACCACATAATTAAAGACCAGC
TGGCCTCTAAGTATCTGTACCATGGACAGACCCTGGAAACTCTGGGCGGCAAAAAACTGAGAGTTTTTGT
TTATCGTAATAGCCTCTGCATTGAGAACAGCTGCATCGCGGCCCACGACAAGAGGGGGAGGTACGGGACC
CTGTTCACGATGGACCGGGTGCTGACCCCCCCAATGGGGACTGTCATGGATGTCCTGAAGGGAGACAATC
GCTTTAGCATGCTGGTAGCTGCCATCCAGTCTGCAGGACTGACGGAGACCCTCAACCGGGAAGGAGTCTA
CACAGTCTTTGCTCCCACAAATGAAGCCTTCCGAGCCCTGCCACCAAGAGAACGGAGCAGACTCTTGGGA
GATGCCAAGGAACTTGCCAACATCCTGAAATACCACATTGGTGATGAAATCCTGGTTAGCGGAGGCATCG
GGGCCCTGGTGCGGCTAAAGTCTCTCCAAGGTGACAAGCTGGAAGTCAGCTTGAAAAACAATGTGGTGAG
TGTCAACAAGGAGCCTGTTGCCGAGCCTGACATCATGGCCACAAATGGCGTGGTCCATGTCATCACCAAT
GTTCTGCAGCCTCCAGCCAACAGACCTCAGGAAAGAGGGGATGAACTTGCAGACTCTGCGCTTGAGATCT
TCAAACAAGCATCAGCGTTTTCCAGGGCTTCCCAGAGGTCTGTGCGACTAGCCCCTGTCTATCAAAAGTT
ATTAGAGAGGATGAAGCATTAGCTTGAAGCACTACAG-3’

Figure 9.4: Sequence of TGFBI-R124C. The CD mutation studied in this thesis is highlighted in red and yellow (source: Genscript, personal communication).

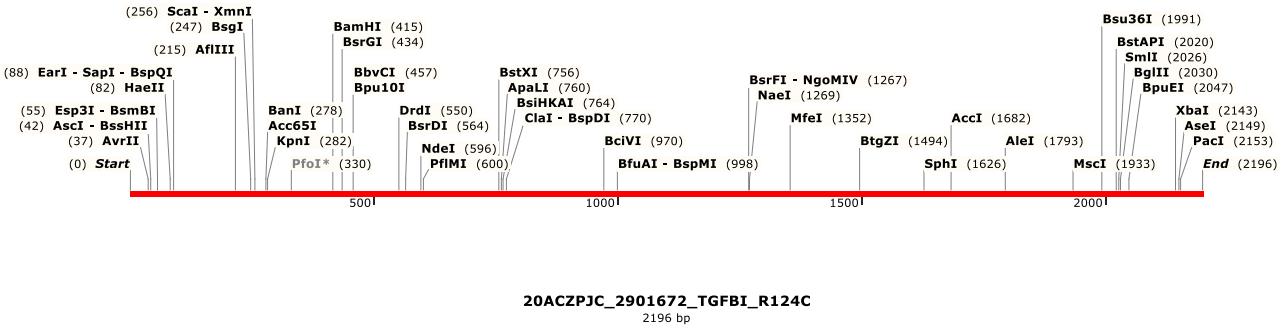

Figure 9.5: TGFBI-R124C (2196 bp) showing it’s restriction cleavage sites. EcoRI and XbaI restriction sites were introduced at the 5’ and 3’ ends respectively for the purposes of cloning and sub-cloning (source: Genscript, personal communication).

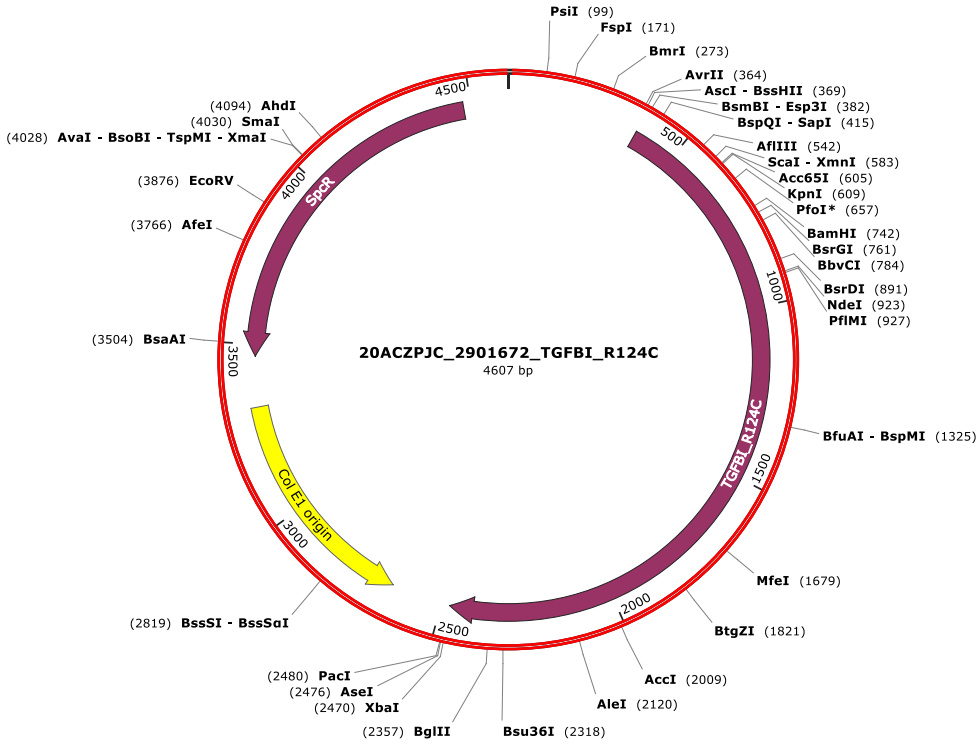

Figure 9.6: TGFBI-R124C cloned into plasmid construct 20ACZPJC. It was subsequently excised and subcloned into *Drosophila*-specific plasmid pUASTattB_AN230 at the previously mentioned 5'- EcoRI and 3'- XbaI sites (source: Genscript, personal communication). For the final pUASTattB_AN230-TGFBI-R124C construct please see **Figure 2.9**

9.1.3 *TGFBI-R555Q* (CGC→CAA)

5'-GCGTCGTCCCGCTCC

ATGGCGCTCTTCGTGCGGCTGCTGGCTCTCGCCCTGGCTCTGGCCCTGGGCCCCGCCGCGACCCTGGCGG
GTCCCGCCAAGTCGCCCTACCAGCTGGTGCTGCAGCACAGCAGGCTCCGGGGCCGCCAGCACGGCCCCAA
CGTGTGTGCTGTGCAGAAGGTTATTGGCACTAATAGGAAGTACTTCACCAACTGCAAGCAGTGGTACCAA
AGGAAAATCTGTGGCAAATCAACAGTCATCAGCTACGAGTGCTGTCCTGGATATGAAAAGGTCCCTGGGG
AGAAGGGCTGTCCAGCAGCCCTACCACTCTCAAACCTTTACGAGACCCTGGGAGTCGTTGGATCCACCAC
CACTCAGCTGTACACGGACCGCACGGAGAAGCTGAGGCCTGAGATGGAGGGGCCCGGCAGCTTCACCATC
TTCGCCCCTAGCAACGAGGCCTGGGCCTCCTTGCCAGCTGAAGTGCTGGACTCCCTGGTCAGCAATGTCA
ACATTGAGCTGCTCAATGCCCTCCGCTACCATATGGTGGGCAGGCGAGTCCTGACTGATGAGCTGAAACA
CGGCATGACCCTCACCTCTATGTACCAGAATTCCAACATCCAGATCCACCACTATCCTAATGGGATTGTA
ACTGTGAACTGTGCCCGGCTGCTGAAAGCCGACCACCATGCAACCAACGGGGTGGTGCACCTCATCGATA
AGGTCATCTCCACCATCACCAACAACATCCAGCAGATCATTGAGATCGAGGACACCTTTGAGACCCTTCG
GGCTGCTGTGGCTGCATCAGGGCTCAACACGATGCTTGAAGGTAACGGCCAGTACACGCTTTTGGCCCCG

ACCAATGAGGCCTTCGAGAAGATCCCTAGTGAGACTTTGAACCGTATCCTGGGCGACCCAGAAGCCCTGA
GAGACCTGCTGAACAACCACATCTTGAAGTCAGCTATGTGTGCTGAAGCCATCGTTGCGGGGCTGTCTGT
AGAGACCCTGGAGGGCACGACACTGGAGGTGGGCTGCAGCGGGGACATGCTCACTATCAACGGGAAGGCG
ATCATCTCCAATAAAGACATCCTAGCCACCAACGGGGTGATCCACTACATTGATGAGCTACTCATCCCAG
ACTCAGCCAAGACACTATTTGAATTGGCTGCAGAGTCTGATGTGTCCACAGCCATTGACCTTTTCAGACA
AGCCGGCCTCGGCAATCATCTCTCTGGAAGTGAGCGGTTGACCCTCCTGGCTCCCCTGAATTCTGTATTC
AAAGATGGAACCCCTCCAATTGATGCCCATACAAGGAATTTGCTTCGGAACCACATAATTAAAGACCAGC
TGGCCTCTAAGTATCTGTACCATGGACAGACCCTGGAAACTCTGGGCGGCAAAAAACTGAGAGTTTTTGT
TTATCGTAATAGCCTCTGCATTGAGAACAGCTGCATCGCGGCCCACGACAAGAGGGGGAGGTACGGGACC
CTGTTCACGATGGACCGGGTGCTGACCCCCCCAATGGGGACTGTCATGGATGTCCTGAAGGGAGACAATC
GCTTTAGCATGCTGGTAGCTGCCATCCAGTCTGCAGGACTGACGGAGACCCTCAACCGGGAAGGAGTCTA
CACAGTCTTTGCTCCCACAAATGAAGCCTTCCGAGCCCTGCCACCAAGAGAA**CAA**AGCAGACTCTTGGGA
GATGCCAAGGAACTTGCCAACATCCTGAAATACCACATTGGTGATGAAATCCTGGTTAGCGGAGGCATCG
GGGCCCTGGTGCGGCTAAAGTCTCTCCAAGGTGACAAGCTGGAAGTCAGCTTGAAAAACAATGTGGTGAG
TGTCAACAAGGAGCCTGTTGCCGAGCCTGACATCATGGCCACAAATGGCGTGGTCCATGTCATCACCAAT
GTTCTGCAGCCTCCAGCCAACAGACCTCAGGAAAGAGGGGATGAACTTGCAGACTCTGCGCTTGAGATCT
TCAAACAAGCATCAGCGTTTTCCAGGGCTTCCCAGAGGTCTGTGCGACTAGCCCCTGTCTATCAAAAGTT
ATTAGAGAGGATGAAGCATTAGCTTGAAGCACTACAG-3’

Figure 9.7: Sequence of TGFBI-R555Q. The CD mutation studied in this thesis is highlighted in red and yellow (source: Genscript, personal communication).

Created with SnapGene®

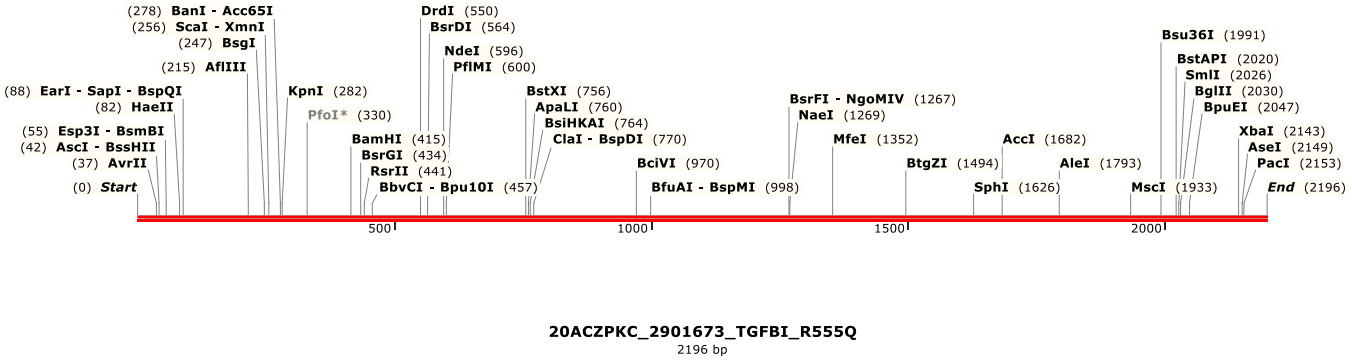

Figure 9.8: TGFBI-R555Q (2196 bp) showing it’s restriction cleavage sites. EcoRI and XbaI restriction sites were introduced at the 5’ and 3’ ends respectively for the purposes of cloning and sub-cloning (source: Genscript, personal communication).

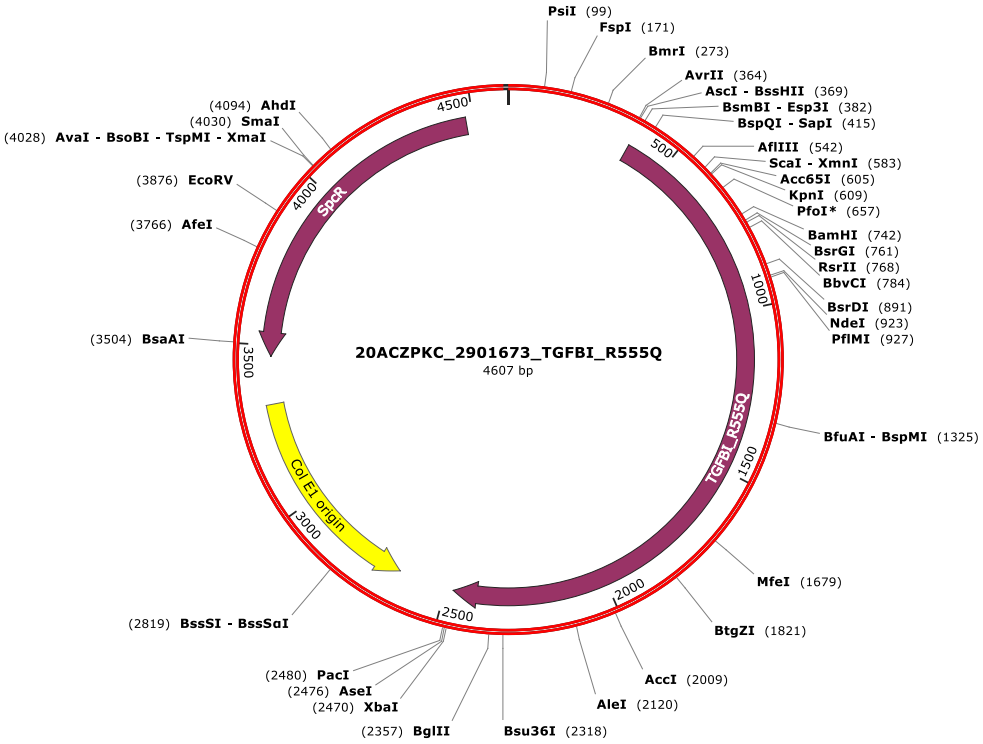

Figure 9.9: TGFBI-R555Q cloned into plasmid construct 20ACZPKC. It was subsequently excised and subcloned into *Drosophila*-specific plasmid pUASTattB_AN230 at the previously mentioned 5'- EcoRI and 3'- XbaI sites (source: Genscript, personal communication). For the final pUASTattB_AN230-TGFBI-R555Q construct please see **Figure 2.8.**

9.1.4 *TGFBI-G623D* (GGC→GAT)

5'-GCGTCGTCCCGCTCC

ATGGCGCTCTTCGTGCGGCTGCTGGCTCTCGCCCTGGCTCTGGCCCTGGGCCCCGCCGCGACCCTGGCGG
GTCCCGCCAAGTCGCCCTACCAGCTGGTGCTGCAGCACAGCAGGCTCCGGGGCCGCCAGCACGGCCCCAA
CGTGTGTGCTGTGCAGAAGGTTATTGGCACTAATAGGAAGTACTTCACCAACTGCAAGCAGTGGTACCAA
AGGAAAATCTGTGGCAAATCAACAGTCATCAGCTACGAGTGCTGTCCTGGATATGAAAAGGTCCCTGGGG
AGAAGGGCTGTCCAGCAGCCCTACCACTCTCAAACCTTTACGAGACCCTGGGAGTCGTTGGATCCACCAC
CACTCAGCTGTACACGGACCGCACGGAGAAGCTGAGGCCTGAGATGGAGGGGCCCGGCAGCTTCACCATC
TTCGCCCCTAGCAACGAGGCCTGGGCCTCCTTGCCAGCTGAAGTGCTGGACTCCCTGGTCAGCAATGTCA
ACATTGAGCTGCTCAATGCCCTCCGCTACCATATGGTGGGCAGGCGAGTCCTGACTGATGAGCTGAAACA
CGGCATGACCCTCACCTCTATGTACCAGAATTCCAACATCCAGATCCACCACTATCCTAATGGGATTGTA
ACTGTGAACTGTGCCCGGCTGCTGAAAGCCGACCACCATGCAACCAACGGGGTGGTGCACCTCATCGATA
AGGTCATCTCCACCATCACCAACAACATCCAGCAGATCATTGAGATCGAGGACACCTTTGAGACCCTTCG
GGCTGCTGTGGCTGCATCAGGGCTCAACACGATGCTTGAAGGTAACGGCCAGTACACGCTTTTGGCCCCG
ACCAATGAGGCCTTCGAGAAGATCCCTAGTGAGACTTTGAACCGTATCCTGGGCGACCCAGAAGCCCTGA
GAGACCTGCTGAACAACCACATCTTGAAGTCAGCTATGTGTGCTGAAGCCATCGTTGCGGGGCTGTCTGT
AGAGACCCTGGAGGGCACGACACTGGAGGTGGGCTGCAGCGGGGACATGCTCACTATCAACGGGAAGGCG

ATCATCTCCAATAAAGACATCCTAGCCACCAACGGGGTGATCCACTACATTGATGAGCTACTCATCCCAG
ACTCAGCCAAGACACTATTTGAATTGGCTGCAGAGTCTGATGTGTCCACAGCCATTGACCTTTTCAGACA
AGCCGGCCTCGGCAATCATCTCTCTGGAAGTGAGCGGTTGACCCTCCTGGCTCCCCTGAATTCTGTATTC
AAAGATGGAACCCCTCCAATTGATGCCCATACAAGGAATTTGCTTCGGAACCACATAATTAAAGACCAGC
TGGCCTCTAAGTATCTGTACCATGGACAGACCCTGGAAACTCTGGGCGGCAAAAAACTGAGAGTTTTTGT
TTATCGTAATAGCCTCTGCATTGAGAACAGCTGCATCGCGGCCCACGACAAGAGGGGGAGGTACGGGACC
CTGTTCACGATGGACCGGGTGCTGACCCCCCCAATGGGGACTGTCATGGATGTCCTGAAGGGAGACAATC
GCTTTAGCATGCTGGTAGCTGCCATCCAGTCTGCAGGACTGACGGAGACCCTCAACCGGGAAGGAGTCTA
CACAGTCTTTGCTCCCACAAATGAAGCCTTCCGAGCCCTGCCACCAAGAGAACGGAGCAGACTCTTGGGA
GATGCCAAGGAACTTGCCAACATCCTGAAATACCACATTGGTGATGAAATCCTGGTTAGCGGAGGCATCG
GGGCCCTGGTGCGGCTAAAGTCTCTCCAAGGTGACAAGCTGGAAGTCAGCTTGAAAAACAATGTGGTGAG
TGTCAACAAGGAGCCTGTTGCCGAGCCTGACATCATGGCCACAAAT**GAT**GTGGTCCATGTCATCACCAAT
GTTCTGCAGCCTCCAGCCAACAGACCTCAGGAAAGAGGGGATGAACTTGCAGACTCTGCGCTTGAGATCT
TCAAACAAGCATCAGCGTTTTCCAGGGCTTCCCAGAGGTCTGTGCGACTAGCCCCTGTCTATCAAAAGTT
ATTAGAGAGGATGAAGCATTAGCTTGAAGCACTACAG-3’

Figure 9.10: Sequence of TGFBI-G623D. The CD mutation studied in this thesis is highlighted in red and yellow (source: Genscript, personal communication).

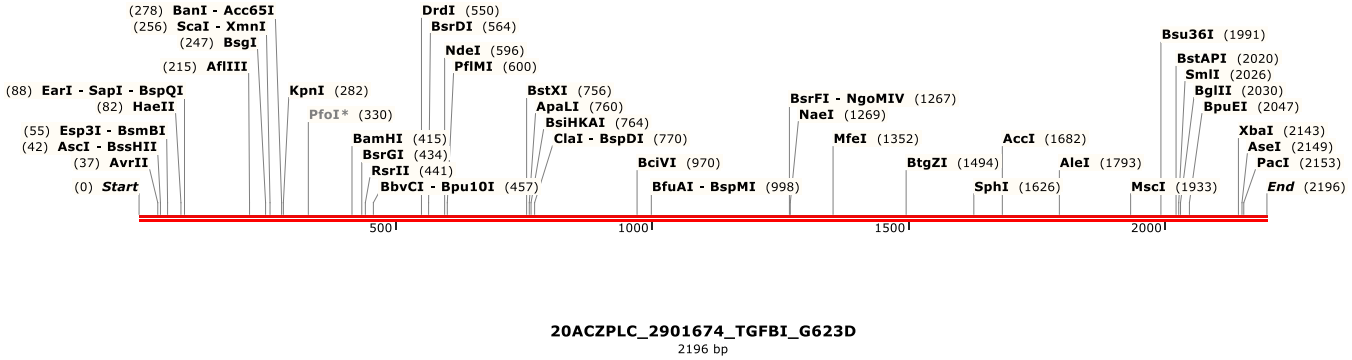

Figure 9.11: TGFBI-G623D (2196 bp) showing it’s restriction cleavage sites. EcoRI and XbaI restriction sites were introduced at the 5’ and 3’ ends respectively for the purposes of cloning and sub-cloning (source: Genscript, personal communication).

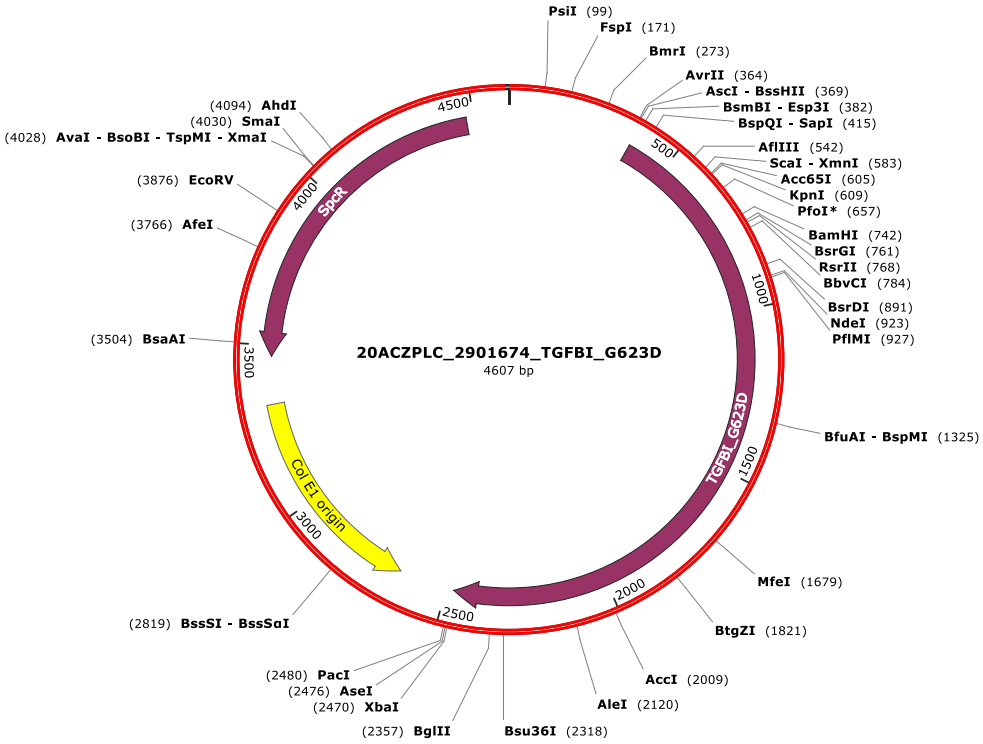

Figure 9.12: TGFBI-G623D cloned into plasmid construct 20ACZPLC. It was subsequently excised and subcloned into *Drosophila*-specific plasmid pUASTattB_AN230 at the previously mentioned 5'- EcoRI and 3'- XbaI sites (source: Genscript, personal communication). For the final pUASTattB_AN230-TGFBI-R555Q construct please see **Figure 2.7.**

9.1.5 *TGFBI-H626R* (CAT→CGC)

5'-GCGTCGTCCCGCTCC

ATGGCGCTCTTCGTGCGGCTGCTGGCTCTCGCCCTGGCTCTGGCCCTGGGCCCCGCCGCGACCCTGGCGG
GTCCCGCCAAGTCGCCCTACCAGCTGGTGCTGCAGCACAGCAGGCTCCGGGGCCGCCAGCACGGCCCCAA
CGTGTGTGCTGTGCAGAAGGTTATTGGCACTAATAGGAAGTACTTCACCAACTGCAAGCAGTGGTACCAA
AGGAAAATCTGTGGCAAATCAACAGTCATCAGCTACGAGTGCTGTCCTGGATATGAAAAGGTCCCTGGGG
AGAAGGGCTGTCCAGCAGCCCTACCACTCTCAAACCTTTACGAGACCCTGGGAGTCGTTGGATCCACCAC
CACTCAGCTGTACACGGACCGCACGGAGAAGCTGAGGCCTGAGATGGAGGGGCCCGGCAGCTTCACCATC
TTCGCCCCTAGCAACGAGGCCTGGGCCTCCTTGCCAGCTGAAGTGCTGGACTCCCTGGTCAGCAATGTCA
ACATTGAGCTGCTCAATGCCCTCCGCTACCATATGGTGGGCAGGCGAGTCCTGACTGATGAGCTGAAACA
CGGCATGACCCTCACCTCTATGTACCAGAATTCCAACATCCAGATCCACCACTATCCTAATGGGATTGTA
ACTGTGAACTGTGCCCGGCTGCTGAAAGCCGACCACCATGCAACCAACGGGGTGGTGCACCTCATCGATA
AGGTCATCTCCACCATCACCAACAACATCCAGCAGATCATTGAGATCGAGGACACCTTTGAGACCCTTCG
GGCTGCTGTGGCTGCATCAGGGCTCAACACGATGCTTGAAGGTAACGGCCAGTACACGCTTTTGGCCCCG
ACCAATGAGGCCTTCGAGAAGATCCCTAGTGAGACTTTGAACCGTATCCTGGGCGACCCAGAAGCCCTGA
GAGACCTGCTGAACAACCACATCTTGAAGTCAGCTATGTGTGCTGAAGCCATCGTTGCGGGGCTGTCTGT

AGAGACCCTGGAGGGCACGACACTGGAGGTGGGCTGCAGCGGGGACATGCTCACTATCAACGGGAAGGCG
ATCATCTCCAATAAAGACATCCTAGCCACCAACGGGGTGATCCACTACATTGATGAGCTACTCATCCCAG
ACTCAGCCAAGACACTATTTGAATTGGCTGCAGAGTCTGATGTGTCCACAGCCATTGACCTTTTCAGACA
AGCCGGCCTCGGCAATCATCTCTCTGGAAGTGAGCGGTTGACCCTCCTGGCTCCCCTGAATTCTGTATTC
AAAGATGGAACCCCTCCAATTGATGCCCATACAAGGAATTTGCTTCGGAACCACATAATTAAAGACCAGC
TGGCCTCTAAGTATCTGTACCATGGACAGACCCTGGAAACTCTGGGCGGCAAAAAACTGAGAGTTTTTGT
TTATCGTAATAGCCTCTGCATTGAGAACAGCTGCATCGCGGCCCACGACAAGAGGGGGAGGTACGGGACC
CTGTTCACGATGGACCGGGTGCTGACCCCCCCAATGGGGACTGTCATGGATGTCCTGAAGGGAGACAATC
GCTTTAGCATGCTGGTAGCTGCCATCCAGTCTGCAGGACTGACGGAGACCCTCAACCGGGAAGGAGTCTA
CACAGTCTTTGCTCCCACAAATGAAGCCTTCCGAGCCCTGCCACCAAGAGAACGGAGCAGACTCTTGGGA
GATGCCAAGGAACTTGCCAACATCCTGAAATACCACATTGGTGATGAAATCCTGGTTAGCGGAGGCATCG
GGGCCCTGGTGCGGCTAAAGTCTCTCCAAGGTGACAAGCTGGAAGTCAGCTTGAAAAACAATGTGGTGAG
TGTCAACAAGGAGCCTGTTGCCGAGCCTGACATCATGGCCACAAATGGCGTGGTCCGCGTCATCACCAAT
GTTCTGCAGCCTCCAGCCAACAGACCTCAGGAAAGAGGGGATGAACTTGCAGACTCTGCGCTTGAGATCT
TCAAACAAGCATCAGCGTTTTCCAGGGCTTCCCAGAGGTCTGTGCGACTAGCCCCTGTCTATCAAAAGTT
ATTAGAGAGGATGAAGCATTAGCTTGAAGCACTACAG-3’

Figure 9.13: Sequence of TGFBI-H626R. The CD mutation studied in this thesis is highlighted in red and yellow (source: Genscript, personal communication).

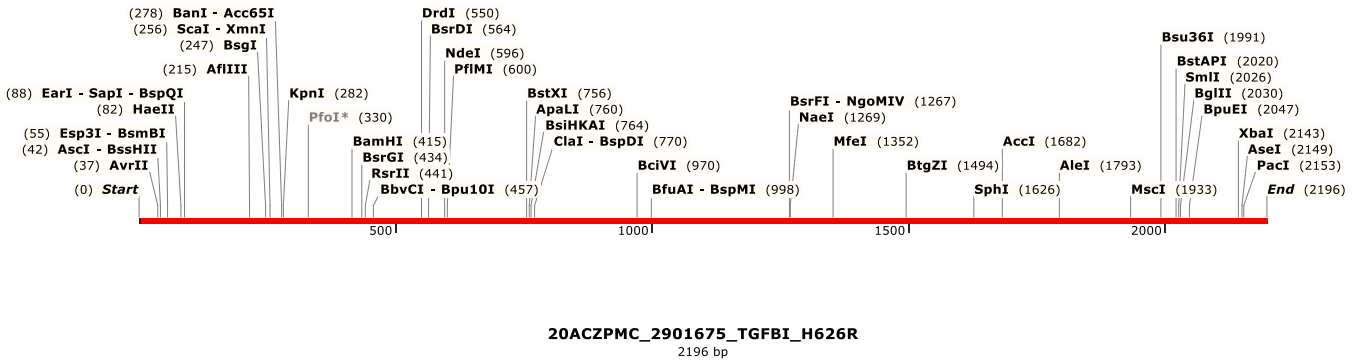

Figure 9.14: TGFBI-H626R (2196 bp) showing it’s restriction cleavage sites. EcoRI and XbaI restriction sites were introduced at the 5’ and 3’ ends respectively for the purposes of cloning and sub-cloning (source: Genscript, personal communication).

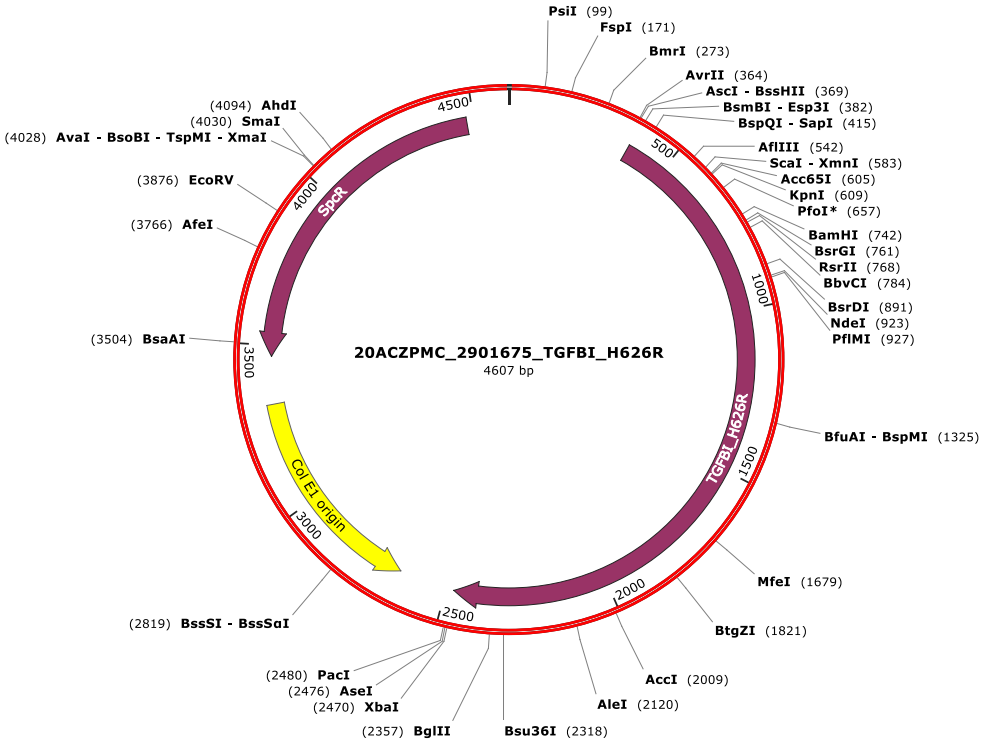

Figure 9.15: TGFBI-H626R cloned into plasmid construct 20ACZPMC. It was subsequently excised and subcloned into *Drosophila*-specific plasmid pUASTattB_AN230 at the previously mentioned 5'- EcoRI and 3'- XbaI sites (source: Genscript, personal communication).

9.1.6 *TGFBI*-WT WITH GFP cDNA ADDED BEFORE THE TAG STOP CODON

5'-GCGTCGTCCCGCTCC

ATGGCGCTCTTCGTGCGGCTGCTGGCTCTCGCCCTGGCTCTGGCCCTGGGCCCCGCCGCGACCCTGGCGG
GTCCCGCCAAGTCGCCCTACCAGCTGGTGCTGCAGCACAGCAGGCTCCGGGGCCGCCAGCACGGCCCCAA
CGTGTGTGCTGTGCAGAAGGTTATTGGCACTAATAGGAAGTACTTCACCAACTGCAAGCAGTGGTACCAA
AGGAAAATCTGTGGCAAATCAACAGTCATCAGCTACGAGTGCTGTCCTGGATATGAAAAGGTCCCTGGGG
AGAAGGGCTGTCCAGCAGCCCTACCACTCTCAAACCTTTACGAGACCCTGGGAGTCGTTGGATCCACCAC
CACTCAGCTGTACACGGACCGCACGGAGAAGCTGAGGCCTGAGATGGAGGGGCCCGGCAGCTTCACCATC
TTCGCCCCTAGCAACGAGGCCTGGGCCTCCTTGCCAGCTGAAGTGCTGGACTCCCTGGTCAGCAATGTCA
ACATTGAGCTGCTCAATGCCCTCCGCTACCATATGGTGGGCAGGCGAGTCCTGACTGATGAGCTGAAACA
CGGCATGACCCTCACCTCTATGTACCAGAATTCCAACATCCAGATCCACCACTATCCTAATGGGATTGTA
ACTGTGAACTGTGCCCGGCTGCTGAAAGCCGACCACCATGCAACCAACGGGGTGGTGCACCTCATCGATA
AGGTCATCTCCACCATCACCAACAACATCCAGCAGATCATTGAGATCGAGGACACCTTTGAGACCCTTCG
GGCTGCTGTGGCTGCATCAGGGCTCAACACGATGCTTGAAGGTAACGGCCAGTACACGCTTTTGGCCCCG
ACCAATGAGGCCTTCGAGAAGATCCCTAGTGAGACTTTGAACCGTATCCTGGGCGACCCAGAAGCCCTGA
GAGACCTGCTGAACAACCACATCTTGAAGTCAGCTATGTGTGCTGAAGCCATCGTTGCGGGGCTGTCTGT
AGAGACCCTGGAGGGCACGACACTGGAGGTGGGCTGCAGCGGGGACATGCTCACTATCAACGGGAAGGCG

ATCATCTCCAATAAAGACATCCTAGCCACCAACGGGGTGATCCACTACATTGATGAGCTACTCATCCCAG
ACTCAGCCAAGACACTATTTGAATTGGCTGCAGAGTCTGATGTGTCCACAGCCATTGACCTTTTCAGACA
AGCCGGCCTCGGCAATCATCTCTCTGGAAGTGAGCGGTTGACCCTCCTGGCTCCCCTGAATTCTGTATTC
AAAGATGGAACCCCTCCAATTGATGCCCATACAAGGAATTTGCTTCGGAACCACATAATTAAAGACCAGC
TGGCCTCTAAGTATCTGTACCATGGACAGACCCTGGAAACTCTGGGCGGCAAAAAACTGAGAGTTTTTGT
TTATCGTAATAGCCTCTGCATTGAGAACAGCTGCATCGCGGCCCACGACAAGAGGGGGAGGTACGGGACC
CTGTTCACGATGGACCGGGTGCTGACCCCCCCAATGGGGACTGTCATGGATGTCCTGAAGGGAGACAATC
GCTTTAGCATGCTGGTAGCTGCCATCCAGTCTGCAGGACTGACGGAGACCCTCAACCGGGAAGGAGTCTA
CACAGTCTTTGCTCCCACAAATGAAGCCTTCCGAGCCCTGCCACCAAGAGAACGGAGCAGACTCTTGGGA
GATGCCAAGGAACTTGCCAACATCCTGAAATACCACATTGGTGATGAAATCCTGGTTAGCGGAGGCATCG
GGGCCCTGGTGCGGCTAAAGTCTCTCCAAGGTGACAAGCTGGAAGTCAGCTTGAAAAACAATGTGGTGAG
TGTCAACAAGGAGCCTGTTGCCGAGCCTGACATCATGGCCACAAATGGCGTGGTCCATGTCATCACCAAT
GTTCTGCAGCCTCCAGCCAACAGACCTCAGGAAAGAGGGGATGAACTTGCAGACTCTGCGCTTGAGATCT
TCAAACAAGCATCAGCGTTTTCCAGGGCTTCCCAGAGGTCTGTGCGACTAGCCCCTGTCTATCAAAAGTT
ATTAGAGAGGATGAAGCAT**ATG**GTGAGCAAGGGCGAGGAGCTGTTCACCGGGGTGGTGCCCATCCTGGTC
GAGCTGGACGGCGACGTAAACGGCCACAAGTTCAGCGTGTCCGGCGAGGGCGAGGGCGATGCCACCTACG
GCAAGCTGACCCTGAAGTTCATCTGCACCACCGGCAAGCTGCCCGTGCCCTGGCCCACCCTCGTGACCAC
CCTGACCTACGGCGTGCAGTGCTTCAGCCGCTACCCCGACCACATGAAGCAGCACGACTTCTTCAAGTCC
GCCATGCCCGAAGGCTACGTCCAGGAGCGCACCATCTTCTTCAAGGACGACGGCAACTACAAGACCCGCG
CCGAGGTGAAGTTCGAGGGCGACACCCTGGTGAACCGCATCGAGCTGAAGGGCATCGACTTCAAGGAGGA
CGGCAACATCCTGGGGCACAAGCTGGAGTACAACTACAACAGCCACAACGTCTATATCATGGCCGACAAG
CAGAAGAACGGCATCAAGGTGAACTTCAAGATCCGCCACAACATCGAGGACGGCAGCGTGCAGCTCGCCG
ACCACTACCAGCAGAACACCCCCATCGGCGACGGCCCCGTGCTGCTGCCCGACAACCACTACCTGAGCAC
CCAGTCCGCCCTGAGCAAAGACCCCAACGAGAAGCGCGATCACATGGTCCTGCTGGAGTTCGTGACCGCC
GCCGGGATCACTCTCGGCATGGACGAGCTGTACAAG**TAG**CTTGAAGCACTACAG-3’

Figure 9.16: Sequence of TGFBI-WT-GFP. cDNA for GFP was added before the TAG stop codon (source: Genscript, personal communication).

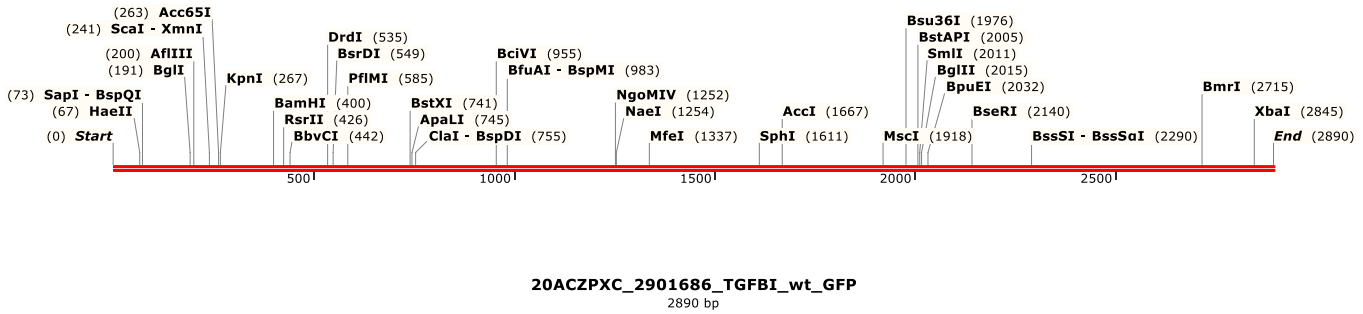

Figure 9.17: TGFBI-H626R (2196 bp) showing it's restriction cleavage sites. EcoRI and XbaI restriction sites were introduced at the 5' and 3' ends respectively for the purposes of cloning and sub-cloning (source: Genscript, personal communication).

Created with SnapGene®

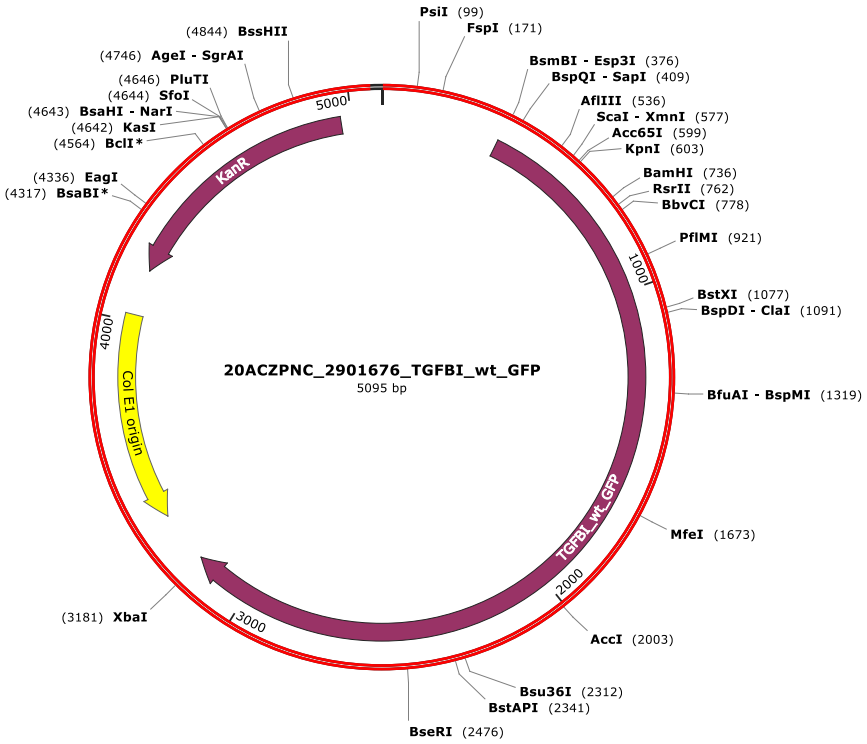

Figure 9.18: TGFBI-WT-GFP cloned into plasmid construct 20ACZPNC. It was subsequently excised and subcloned into *Drosophila*-specific plasmid pUASTattB_AN230 at the previously mentioned 5'- EcoRI and 3'- XbaI sites (source: Genscript, personal communication). For the final pUASTattB_AN230-TGFBI-WT-GFP construct please see **Figure 2.5.**

9.1.7 *mfas*-WILD TYPE ISOFORM K

```
                                                          ATTGTG
ATACCAAACA TGCTACGGCT GTGGGCCTGC CTGCTCCTCC TGGGATCAAT CCAGATCCAG
GCGGTTCCAT TCTACGGCGA CTTTATGCCA CATTTAACCC ACCCATTGCC GGCGCATCGC
AATCTGTTCG CGCCCCTGCC CTTCGCACCA CTCGCACCGC TCGAGCCCCA AGATCCACTG
CATGCCCAGG CCTCGCAGCG GATGGCGAGC GTCTGGAACG GACCCGCCCC GTTGGCGCCG
CAACTCCACT CATCTCACCT GTTGCCCCTC TTCAGCAGCG GATACGACAC CGAGTTCGTG
CCACTGGAGC ACCAGCAGCA GCCGCAGGGA CGCCAGGAGA CGGCGGCCAC CGTTCCCGCT
CAAACCCCCA GCGGTGTGGA GCAGAAGCCG TTCAATGTGG ACACCATCAC CACGGATGTG
AATTCCCCAA ATCCGGCCAT CTTCTTCCAG CAATCGTTCC CCTTCTTTGG CAATGAGTTC
TTCAATTCGT TCGGAGGCTT TGGCTTTGGA GCTGCCCAGG AGCCCTGGTG GAAGGGACCC
AATGTGTGCA CCGAAAAGGA GGAAGACGAG ACTGTGGCCA GTGAAACGGA GGCAGAAGAA
ACCGTGGACA CCTTTGGCCA GGAACGTGAT GGCGTTACCA ACGTGGTGCG ATCCCCACTC
TTTGGCCAGT TCCAGTTCAG CGTTAACTCC TGCGCCGAGA AGCCCAACAA GCACGTCTGC
ACCAAGATCG TGAATCAAAA TGGCAAGAAG AAAACGCTGA CGCTGACCCG CCAGTGCTGC
```

TATGGATATG GACGCCCCAG AAACGCTGAC TTCACAACGC CCTGCGAGAA GATCGACATC
AAGGACGTGG AGGCCACGGC CAGTGACATG GGTGCCAAGC AGTTCCTGGA GAGTGCACGC
ACCGCCGGTG AGCTGGCCGA TATGCTCGGA GCAGGCAGTG GCAAGAAGGT GACCCTCTTC
GTGCCCAACG ACGCCGCCTT CATGGAGTAC CGTGGTCATC ATCAGCAGGA GAATAATGTG
GAAGATGCCA AGGCCGAGGC TTCCAAGCCA TCCATCTACA AACTGCACGC TGTTCTCGGC
GAAGTTCAGC TGGAGGATGT GCCCAATGAG AAGCTTCTGC AGACGGAGCT GCCTGACCAG
AAGATCCGCA TCAACAGCTA CCAGCTGCCT GCGGCTTTGG GCCTGGAACC CTACCGCTTT
GCCGCCAACT GTGTGCCCAT CGAGAAGCAC GACAAGCTCT CGGAGCAGGC CCTTGTCCAC
ACTCTGGGCG GAGTCCTGAA GCCGCTGACC AAGAACCTTA TGGATATCAT CAGGGAGCGT
GCGGATATGT CCATTATGCG CACCGTTCTG GAGAAGACCA ACCTGAGCGC CATGCTAGAG
GATGACAAGC CAGTGACCAT CTTTGTGCCC ACCGATGCCG CCTTCGACAA GTTGGAACCT
CATCTGCGTC GAGCCCTCAA GGAAGGTCGC GGTTGTGCCT CCAACATCCT GAAGAACCAT
TTGCTGGACC TCACCTTCTG CTCGCTGGCC ACTGTTCCGG GTGCCAAGAC GACGGCCTAC
AATCTACTGG GAGAACCCCT GCTCCTCAAC CGAACCCACC GCGCTGCGAA TCAGACTGGA
CCGACTCCCA TCTACATCAA TAACTTGGCC AAAATCATTG ATGCCGATAT CATGGGCACC
AATGGTGTGC TGCACGTAAT CGACACCATC CTGCCCACCG AATCGGCTCT GCCCATGACC
TCGCTGATGT CGCAAAAGAA CCTGACCATC TTCCAGCGAT TGCTGGAGGC CTCCGGCTAC
GATGATCAGT TCGACGATCT GGACAACGTG ACCATCTTTG CACCAACTGA CAAGGCTCTG
CAGAATACGG AATGGGCTCG CATGCTCAAG GAACAGCCGG AGCTGCTGAA TCATAACTTG
GATCTGCTGG AGTTCCTTAA CTACCATGTG GTCAAGCCCA TGATCAAGAC CTGTGACCTG
TCGGAGAAGT CCCTGCCCAC GGTTGCTGGA TCTAGTGTGC GTCTGAACCT GTACTCCACC
CATGCTCTCT TCTCGGACGT GATGAACCGG GCAACGGTAA ACTGTGCCCG TTTGGTGCAC
TTCGATGACG AGAGCTGCGG ATCCGTTCTC CACCAGGTGG ATCGTGCCTT GGCGCCTCCC
AAGAATAACA TGCTTAAGCT GCTGGAGGCT AATCCCAACT ACAGCAAGTT CCTGGAGCTG
GTTCGTAAGG CTAATCTTAC ACAGCTGCTG TCCAACGATT CGAGGAGTCT CACCCTGCTG
GTGCCAAAGA ACGATATCTT CGAGGAGCTG AACGAGTCCG GTGAGGGTTC AAAGCCCGCC
GATCCCATGG CCTTGGTCAA AACCCATATC GTTGAGGATG TTGTCTGCTG TGCCGGCATT
ATCCCAACCA ACTGGCCATT TGTCCGCTCC ATCGAGTCCA TCTCTGGCCA GCATCTGCGT
ATCACCCGCG ATCGTCGTCC CAAGATCGAG AACGCCGGCG TCACCAAGTG CGATGTGGTG
GCCACCAATG GAATTCTCCA TGAGATCAAC GACATCATCG TGCCACGCCC ACAGCGCCAG
CAACAGCAGC GACCCCAGCT GATCCCGCCC GGAGCTGGCT ATCAGCCACA GGGCGATTTC
GATGTCTTCT TCTGAGCGGT GCTCGTCCCC

Figure 9.19: Sequence of MFAS-wild type (source: Genscript, personal communication).

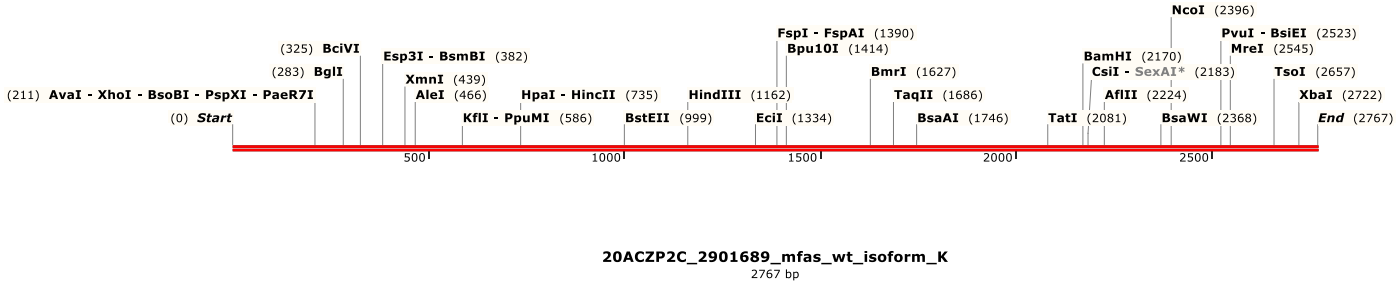

Figure 9.20: MFAS wild type isoform K (2767 bp) showing it's restriction cleavage sites. EcoRI and XbaI restriction sites were introduced at the 5' and 3' ends respectively for the purposes of cloning and sub-cloning (source: Genscript, personal communication).

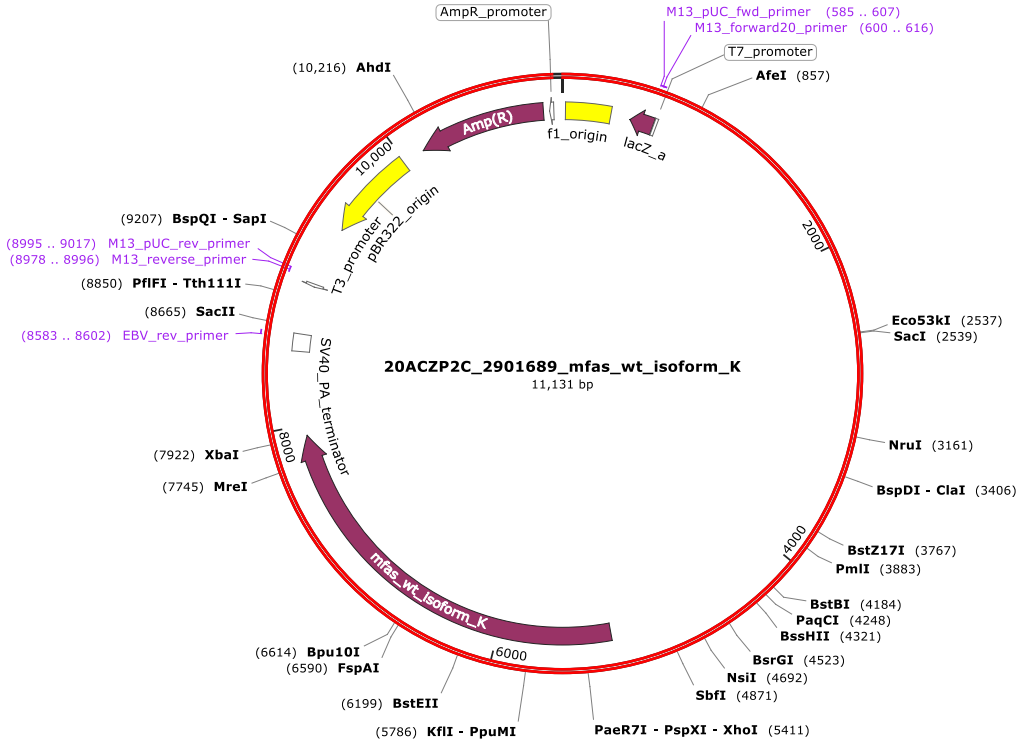

Figure 9.21: MFAS-wild type cloned into plasmid construct 20ACZP2C. It was subsequently excised and subcloned into *Drosophila*-specific plasmid pUASTattB_AN230 at the previously mentioned 5'- EcoRI and 3'- XbaI sites (source: Genscript, personal communication). For the final pUASTattB_AN230-MFAS-WT construct please see **Figure 2.2.**

9.1.8 *mfas*-WILD TYPE ISOFORM K PLUS GFP

```
                                                            ATTGTG
ATACCAAACA TGCTACGGCT GTGGGCCTGC CTGCTCCTCC TGGGATCAAT CCAGATCCAG
GCGGTTCCAT TCTACGGCGA CTTTATGCCA CATTTAACCC ACCCATTGCC GGCGCATCGC
AATCTGTTCG CGCCCCTGCC CTTCGCACCA CTCGCACCGC TCGAGCCCCA AGATCCACTG
CATGCCCAGG CCTCGCAGCG GATGGCGAGC GTCTGGAACG GACCCGCCCC GTTGGCGCCG
CAACTCCACT CATCTCACCT GTTGCCCCTC TTCAGCAGCG GATACGACAC CGAGTTCGTG
CCACTGGAGC ACCAGCAGCA GCCGCAGGGA CGCCAGGAGA CGGCGGCCAC CGTTCCCGCT
CAAACCCCCA GCGGTGTGGA GCAGAAGCCG TTCAATGTGG ACACCATCAC CACGGATGTG
AATTCCCCAA ATCCGGCCAT CTTCTTCCAG CAATCGTTCC CCTTCTTTGG CAATGAGTTC
TTCAATTCGT TCGGAGGCTT TGGCTTTGGA GCTGCCCAGG AGCCCTGGTG GAAGGGACCC
AATGTGTGCA CCGAAAAGGA GGAAGACGAG ACTGTGGCCA GTGAAACGGA GGCAGAAGAA
ACCGTGGACA CCTTTGGCCA GGAACGTGAT GGCGTTACCA ACGTGGTGCG ATCCCCACTC
TTTGGCCAGT TCCAGTTCAG CGTTAACTCC TGCGCCGAGA AGCCCAACAA GCACGTCTGC
ACCAAGATCG TGAATCAAAA TGGCAAGAAG AAAACGCTGA CGCTGACCCG CCAGTGCTGC
TATGGATATG GACGCCCCAG AAACGCTGAC TTCACAACGC CCTGCGAGAA GATCGACATC
```

```
AAGGACGTGG AGGCCACGGC CAGTGACATG GGTGCCAAGC AGTTCCTGGA GAGTGCACGC
ACCGCCGGTG AGCTGGCCGA TATGCTCGGA GCAGGCAGTG GCAAGAAGGT GACCCTCTTC
GTGCCCAACG ACGCCGCCTT CATGGAGTAC CGTGGTCATC ATCAGCAGGA GAATAATGTG
GAAGATGCCA AGGCCGAGGC TTCCAAGCCA TCCATCTACA AACTGCACGC TGTTCTCGGC
GAAGTTCAGC TGGAGGATGT GCCCAATGAG AAGCTTCTGC AGACGGAGCT GCCTGACCAG
AAGATCCGCA TCAACAGCTA CCAGCTGCCT GCGGCTTTGG GCCTGGAACC CTACCGCTTT
GCCGCCAACT GTGTGCCCAT CGAGAAGCAC GACAAGCTCT CGGAGCAGGC CCTTGTCCAC
ACTCTGGGCG GAGTCCTGAA GCCGCTGACC AAGAACCTTA TGGATATCAT CAGGGAGCGT
GCGGATATGT CCATTATGCG CACCGTTCTG GAGAAGACCA ACCTGAGCGC CATGCTAGAG
GATGACAAGC CAGTGACCAT CTTTGTGCCC ACCGATGCCG CCTTCGACAA GTTGGAACCT
CATCTGCGTC GAGCCCTCAA GGAAGGTCGC GGTTGTGCCT CCAACATCCT GAAGAACCAT
TTGCTGGACC TCACCTTCTG CTCGCTGGCC ACTGTTCCGG GTGCCAAGAC GACGGCCTAC
AATCTACTGG GAGAACCCCT GCTCCTCAAC CGAACCCACC GCGCTGCGAA TCAGACTGGA
CCGACTCCCA TCTACATCAA TAACTTGGCC AAAATCATTG ATGCCGATAT CATGGGCACC
AATGGTGTGC TGCACGTAAT CGACACCATC CTGCCCACCG AATCGGCTCT GCCCATGACC
TCGCTGATGT CGCAAAAGAA CCTGACCATC TTCCAGCGAT TGCTGGAGGC CTCCGGCTAC
GATGATCAGT TCGACGATCT GGACAACGTG ACCATCTTTG CACCAACTGA CAAGGCTCTG
CAGAATACGG AATGGGCTCG CATGCTCAAG GAACAGCCGG AGCTGCTGAA TCATAACTTG
GATCTGCTGG AGTTCCTTAA CTACCATGTG GTCAAGCCCA TGATCAAGAC CTGTGACCTG
TCGGAGAAGT CCCTGCCCAC GGTTGCTGGA TCTAGTGTGC GTCTGAACCT GTACTCCACC
CATGCTCTCT TCTCGGACGT GATGAACCGG GCAACGGTAA ACTGTGCCCG TTTGGTGCAC
TTCGATGACG AGAGCTGCGG ATCCGTTCTC CACCAGGTGG ATCGTGCCTT GGCGCCTCCC
AAGAATAACA TGCTTAAGCT GCTGGAGGCT AATCCCAACT ACAGCAAGTT CCTGGAGCTG
GTTCGTAAGG CTAATCTTAC ACAGCTGCTG TCCAACGATT CGAGGAGTCT CACCCTGCTG
GTGCCAAAGA ACGATATCTT CGAGGAGCTG AACGAGTCCG GTGAGGGTTC AAAGCCCGCC
GATCCCATGG CCTTGGTCAA AACCCATATC GTTGAGGATG TTGTCTGCTG TGCCGGCATT
ATCCCAACCA ACTGGCCATT TGTCCGCTCC ATCGAGTCCA TCTCTGGCCA GCATCTGCGT
ATCACCCGCG ATCGTCGTCC CAAGATCGAG AACGCCGGCG TCACCAAGTG CGATGTGGTG
GCCACCAATG GAATTCTCCA TGAGATCAAC GACATCATCG TGCCACGCCC ACAGCGCCAG
CAACAGCAGC GACCCCAGCT GATCCCGCCC GGAGCTGGCT ATCAGCCACA GGGCGATTTC
GATGTCTTCT TCATGGTGAG CAAGGGCGAG GAGCTGTTCA CCGGGGTGGT GCCCATCCTG
GTCGAG     CTGGACGGCG ACGTAAACGG CCACAAGTTC AGCGTGTCCG GCGAGGGCGA
GGGCGATGCC ACCTACGGCA AGCTGACCCT GAAGTTCATC TGCACCACCG
GCAAGCTGCC CGTGCCCTGG CCCACCCTCG TGACCACCCT GACCTACGGC GTGCAGTGCT
TCAGCCGCTA CCCCGACCAC ATGAAGCAGC ACGACTTCTT CAAGTCCGCC ATGCCCGAAG
GCTACGTCCA GGAGCGCACC ATCTTCTTCA AGGACGACGG CAACTACAAG ACCCGCGCCG
AGGTGAAGTT CGAGGGCGAC ACCCTGGTGA ACCGCATCGA GCTGAAGGGC ATCGACTTCA
AGGAGGACGG CAACATCCTG GGGCACAAGC TGGAGTACAA CTACAACAGC CACAACGTCT
ATATCATGGC CGACAAGCAG AAGAACGGCA TCAAGGTGAA CTTCAAGATC CGCCACAACA
TCGAGGACGG CAGCGTGCAG CTCGCCGACC ACTACCAGCA GAACACCCCC ATCGGCGACG
GCCCCGTGCT GCTGCCCGAC AACCACTACC TGAGCACCCA GTCCGCCCTG AGCAAAGACC
CCAACGAGAA GCGCGATCAC ATGGTCCTGC TGGAGTTCGT GACCGCCGCC GGGATCACTC
TCGGCATGGA CGAGCTGTAC AAGTGAGCGG TGCTCGTCCCC
```

Figure 9.22: Sequence of MFAS-WT-GFP. cDNA for GFP was added before the TAG stop codon (source: Genscript, personal communication).

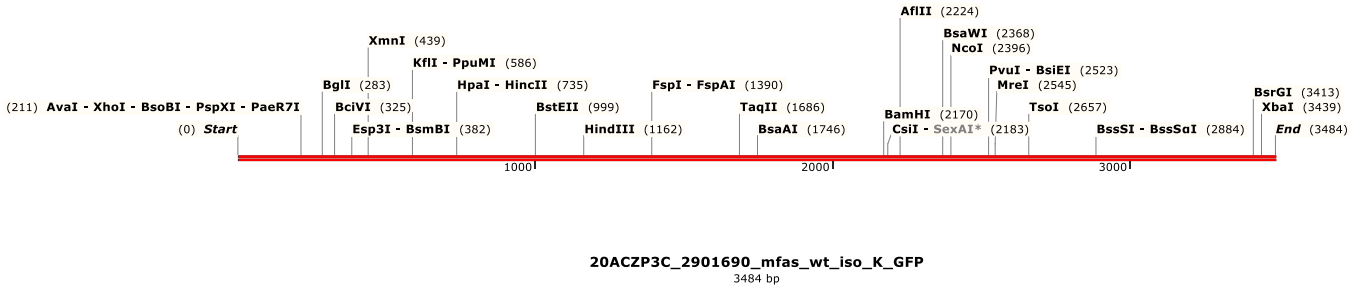

Figure 9.23: MFAS-WT-GFP (3484 bp) showing it's restriction cleavage sites. EcoRI and XbaI restriction sites were introduced at the 5' and 3' ends respectively for the purposes of cloning and sub-cloning (source: Genscript, personal communication).

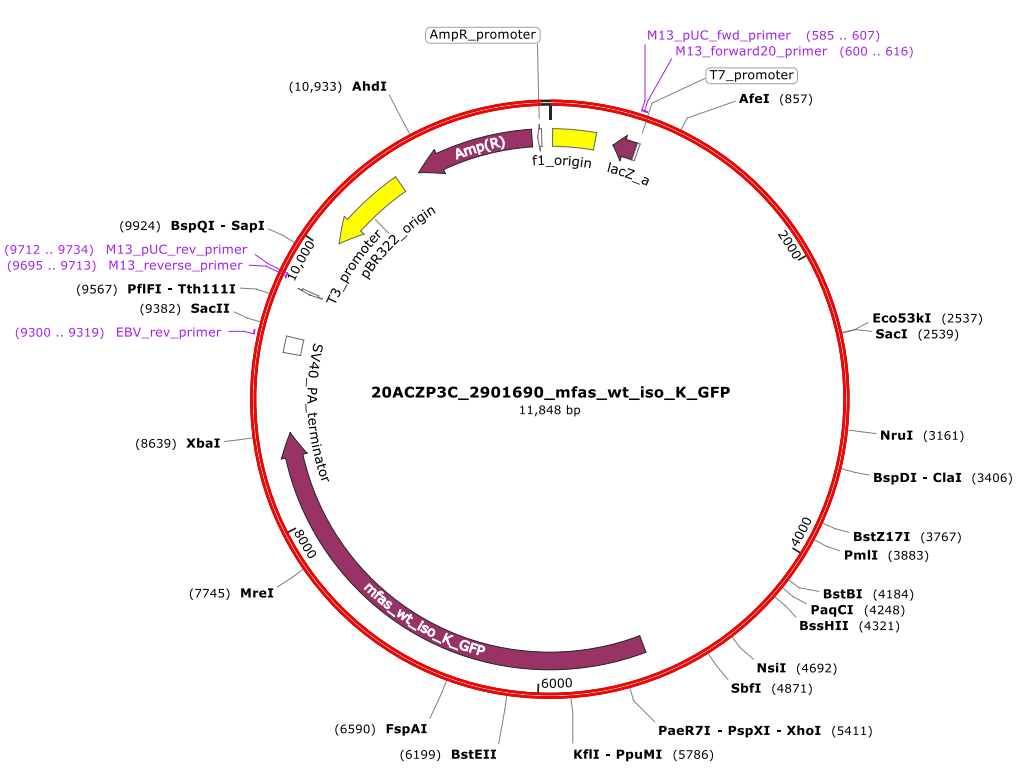

Figure 9.24: *mfas*-WT-GFPcloned into plasmid construct 20ACZP3C. It was subsequently excised and subcloned into *Drosophila*-specific plasmid pUASTattB_AN230 at the previously mentioned 5'- EcoRI and 3'- XbaI sites (source: Genscript, personal communication). For the final pUASTattB_AN230-MFAS-WT-GFP construct please see **Figure 2.3.**

9.1.9 *mfas* ISOFORM-K-G623D (GGT→GAT)

```
GCAGTTAGTT TTAAACTGCG ACTTGAAGCG GCAACATCGT CGGATCAAGC AACATATAAC
AACTTTCCTT GTCTCGTTCA TTTACTTAGC TCCCAACCGA GGCTCCAGAT TAAAATTGTG
ATACCAAACA TGCTACGGCT GTGGGCCTGC CTGCTCCTCC TGGGATCAAT CCAGATCCAG
GCGGTTCCAT TCTACGGCGA CTTTATGCCA CATTTAACCC ACCCATTGCC GGCGCATCGC
AATCTGTTCG CGCCCCTGCC CTTCGCACCA CTCGCACCGC TCGAGCCCCA AGATCCACTG
CATGCCCAGG CCTCGCAGCG GATGGCGAGC GTCTGGAACG GACCCGCCCC GTTGGCGCCG
CAACTCCACT CATCTCACCT GTTGCCCCTC TTCAGCAGCG GATACGACAC CGAGTTCGTG
CCACTGGAGC ACCAGCAGCA GCCGCAGGGA CGCCAGGAGA CGGCGGCCAC CGTTCCCGCT
CAAACCCCCA GCGGTGTGGA GCAGAAGCCG TTCAATGTGG ACACCATCAC CACGGATGTG
AATTCCCCAA ATCCGGCCAT CTTCTTCCAG CAATCGTTCC CCTTCTTTGG CAATGAGTTC
TTCAATTCGT TCGGAGGCTT TGGCTTTGGA GCTGCCCAGG AGCCCTGGTG GAAGGGACCC
AATGTGTGCA CCGAAAAGGA GGAAGACGAG ACTGTGGCCA GTGAAACGGA GGCAGAAGAA
ACCGTGGACA CCTTTGGCCA GGAACGTGAT GGCGTTACCA ACGTGGTGCG ATCCCCACTC
TTTGGCCAGT TCCAGTTCAG CGTTAACTCC TGCGCCGAGA AGCCCAACAA GCACGTCTGC
```

ACCAAGATCG TGAATCAAAA TGGCAAGAAG AAAACGCTGA CGCTGACCCG CCAGTGCTGC
TATGGATATG GACGCCCCAG AAACGCTGAC TTCACAACGC CCTGCGAGAA GATCGACATC
AAGGACGTGG AGGCCACGGC CAGTGACATG GGTGCCAAGC AGTTCCTGGA GAGTGCACGC
ACCGCCGGTG AGCTGGCCGA TATGCTCGGA GCAGGCAGTG GCAAGAAGGT GACCCTCTTC
GTGCCCAACG ACGCCGCCTT CATGGAGTAC CGTGGTCATC ATCAGCAGGA GAATAATGTG
GAAGATGCCA AGGCCGAGGC TTCCAAGCCA TCCATCTACA AACTGCACGC TGTTCTCGGC
GAAGTTCAGC TGGAGGATGT GCCCAATGAG AAGCTTCTGC AGACGGAGCT GCCTGACCAG
AAGATCCGCA TCAACAGCTA CCAGCTGCCT GCGGCTTTGG GCCTGGAACC CTACCGCTTT
GCCGCCAACT GTGTGCCCAT CGAGAAGCAC GACAAGCTCT CGGAGCAGGC CCTTGTCCAC
ACTCTGGGCG GAGTCCTGAA GCCGCTGACC AAGAACCTTA TGGATATCAT CAGGGAGCGT
GCGGATATGT CCATTATGCG CACCGTTCTG GAGAAGACCA ACCTGAGCGC CATGCTAGAG
GATGACAAGC CAGTGACCAT CTTTGTGCCC ACCGATGCCG CCTTCGACAA GTTGGAACCT
CATCTGCGTC GAGCCCTCAA GGAAGGTCGC GGTTGTGCCT CCAACATCCT GAAGAACCAT
TTGCTGGACC TCACCTTCTG CTCGCTGGCC ACTGTTCCGG GTGCCAAGAC GACGGCCTAC
AATCTACTGG GAGAACCCCT GCTCCTCAAC CGAACCCACC GCGCTGCGAA TCAGACTGGA
CCGACTCCCA TCTACATCAA TAACTTGGCC AAAATCATTG ATGCCGATAT CATGGGCACC
AATGATGTGC TGCACGTAAT CGACACCATC CTGCCCACCG AATCGGCTCT GCCCATGACC
TCGCTGATGT CGCAAAAGAA CCTGACCATC TTCCAGCGAT TGCTGGAGGC CTCCGGCTAC
GATGATCAGT TCGACGATCT GGACAACGTG ACCATCTTTG CACCAACTGA CAAGGCTCTG
CAGAATACGG AATGGGCTCG CATGCTCAAG GAACAGCCGG AGCTGCTGAA TCATAACTTG
GATCTGCTGG AGTTCCTTAA CTACCATGTG GTCAAGCCCA TGATCAAGAC CTGTGACCTG
TCGGAGAAGT CCCTGCCCAC GGTTGCTGGA TCTAGTGTGC GTCTGAACCT GTACTCCACC
CATGCTCTCT TCTCGGACGT GATGAACCGG GCAACGGTAA ACTGTGCCCG TTTGGTGCAC
TTCGATGACG AGAGCTGCGG ATCCGTTCTC CACCAGGTGG ATCGTGCCTT GGCGCCTCCC
AAGAATAACA TGCTTAAGCT GCTGGAGGCT AATCCCAACT ACAGCAAGTT CCTGGAGCTG
GTTCGTAAGG CTAATCTTAC ACAGCTGCTG TCCAACGATT CGAGGAGTCT CACCCTGCTG
GTGCCAAAGA ACGATATCTT CGAGGAGCTG AACGAGTCCG GTGAGGGTTC AAAGCCCGCC
GATCCCATGG CCTTGGTCAA AACCCATATC GTTGAGGATG TTGTCTGCTG TGCCGGCATT
ATCCCAACCA ACTGGCCATT TGTCCGCTCC ATCGAGTCCA TCTCTGGCCA GCATCTGCGT
ATCACCCGCG ATCGTCGTCC CAAGATCGAG AACGCCGGCG TCACCAAGTG CGATGTGGTG
GCCACCAATG GAATTCTCCA TGAGATCAAC GACATCATCG TGCCACGCCC ACAGCGCCAG
CAACAGCAGC GACCCCAGCT GATCCCGCCC GGAGCTGGCT ATCAGCCACA GGGCGATTTC
GATGTCTTCT TCTGAGCGGT GCTCGTCCCC ATCTCATGCA TATTGATATA TAAAGCAGAT
ATTTATATTT ACTCTTAACG ATTTGTCAAC TGATTGGAAG CCGCAAAAAG CTCAGAATCT
CCTCTGATAA ATAAAATAAA TAGTATTAAA AC

Figure 9.25: Sequence of MFAS-G623D. The CD mutation studied in this thesis is highlighted in red and yellow (source: Genscript, personal communication).

Created with SnapGene®

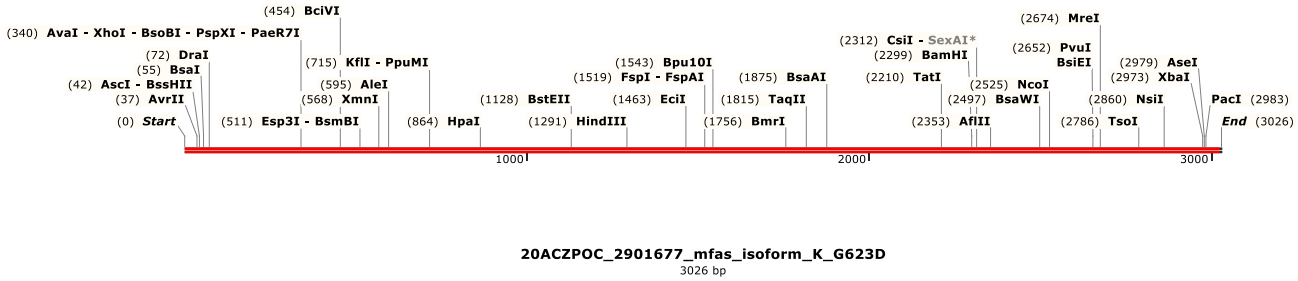

Figure 9.26: *mfas*-G623D (3026 bp) showing it's restriction cleavage sites. EcoRI and XbaI restriction sites were introduced at the 5' and 3' ends respectively for the purposes of cloning and sub-cloning (source: Genscript, personal communication).

Created with SnapGene®

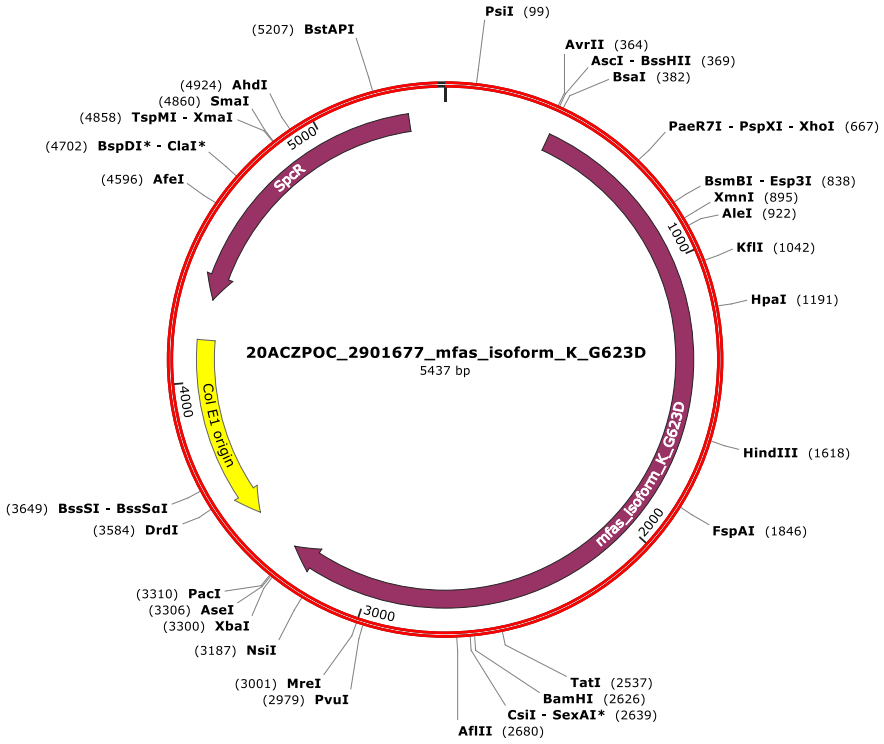

Figure 9.27: MFAS-G623D cloned into plasmid construct 20ACZPOC. It was subsequently excised and subcloned into *Drosophila*-specific plasmid pUASTattB_AN230 at the previously mentioned 5'- EcoRI and 3'- XbaI sites (source: Genscript, personal communication). For the final pUASTattB_AN230-MFAS-G623D construct please see **Figure 2.4.**

9.2 SEQUENCE ALIGNMENT OF TGFBI AND MFAS

```
CLUSTAL multiple sequence alignment by Kalign (3.3.1)

tgf       ------------------------------------------------------------
mfas      MLRLWACLLLLGSIQIQAVPFYGDSSSEEVAEFDDSSDSTHESSDNSSFMPHLTHPLPAH

tgf       ------------------------------------------------------------
mfas      RNLFAPLPFAPLAPLEPQDPLHAQASQRMASVWNGPAPLAPQLHSSHLLPLFSSGYDTEF

tgf       ------------------------------------------------------------MA
mfas      VPLEHQQQPQGRQETAATVPAQTPSGVEQKPFNVDTITTDVNSPNPAIFFQQSFPFFGNE

tgf       LFVRLLALALALALGPAATLAGPA----KSPYQLVLQHSRLR------GRQH-GPNVCAV
mfas      FFNSFGGFGFGAAQEP--WWKGPNVCTEKEEDETVASETEAEETVDTFGQERDGVTNVVR

tgf       QKVIGTNRKYFTNCKQWYQRKIC-------GKSTVISY--ECCPGYEKVPGEK---GCPA
mfas      SPLFGQFQFSVNSCAEKPNKHVCTKIVNQNGKKKTLTLTRQCCYGYGRPRNADFTTPCE-

tgf       ALPLSNLYETLGVVGSTTTQLYTDRTEKLRPEMEGPGS---FTIFAPSNEAWASLPA-EV
mfas      KIDIKDVEATASDMGA-KQFLESARTAGELADMLGAGSGKKVTLFVPNDAAFMEYRGHHQ

tgf       LDSLVSNVNIELLNALRY--HMVGRRVLTDELKHGMTLTSMYQNSNIQIHHY--PNGI--
mfas      QENNVEDAKAEASKPSIYKLHAVLGEVQLEDVPNEKLLQTELPDQKIRINSYQLPAALGL

tgf       ----VTVNCARLLKADHHATNGVVHLIDKVISTITNNIQQIIEIEDTFETLRAAVAASGL
mfas      EPYRFAANCVPIEKHDKLSEQALVHTLGGVLKPLTKNLMDIIRERADMSIMRTVLEKTNL

tgf       NTMLEGNGQYTLLAPTNEAFEKIPSETLNRILGDPEA-LRDLLNNHILKSAMCAEAIVAG
mfas      SAMLEDDKPVTIFVPTDAAFDKLEP-HLRRALKEGRGCASNILKNHLLDLTFCSLATVPG

tgf       LSVET---------LEGTTLEVGCSGDM-LTINGKAIISNKDILATNGVIHYIDELLIPD
mfas      AKTTAYNLLGEPLLLNRTHRAANQTGPTPIYINNLAKIIDADIMGTNGVLHVIDTILPTE

tgf       SAKTLFELAAESDVSTAIDLFRQAGLGNHLSGSERLTLLAPLNSVFKDG--------TPP
mfas      SALPMTSLMSQKNLTIFQRLLEASGYDDQFDDLDNVTIFAPTDKALQNTEWARMLKEQPE

tgf       IDAHTRNLLR---NHIIKDQLASKYLYHGQTLETLGGKKLRVFVYRNSLCIEN-------
mfas      LLNHNLDLLEFLNYHVVKPMIKTCDL-SEKSLPTVAGSSVRLNLYSTHALFSDVMNRATV

tgf       SCIA-AH-DKRGRYGTLFTMDRVLTPPMGTVMDVLKGDNRFSMLVAAIQSAGLTETLNRE
mfas      NCARLVHFDDESCGSVLHQVDRALAPPKNNMLKLLEANPNYSKFLELVRKANLTQLLSND

tgf       G-VYTVFAPTNEAFRALPPRERSRLLGDAKELANILKYHIGDEILVSGGI----GALVR-
mfas      SRSLTLLVPKNDIFEEL--NESGEGSKPADPMA-LVKTHIVEDVVCCAGIIPTNWPFVRS
```

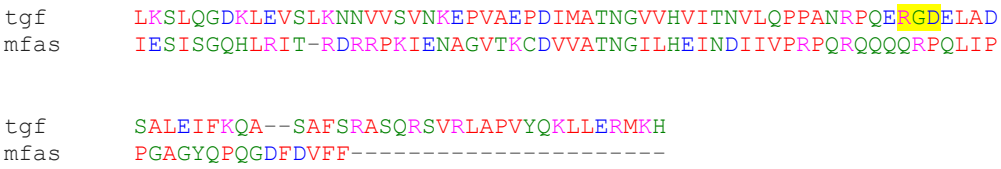

Figure 9.28: Amino acid sequence alignment of human TGFBI and *Drosophila* MFAS. MFAS lacks the C-terminal RGD adhesion sequence found in TGFBI (highlighted in yellow in TGFBI) (accessed on Kalign, European Bioinformatics Institute, on 11/03/2023).